ISSN 0021-9673

VOL. 657 NO. 2 DECEMBER 31, 1993

THIS ISSUE COMPLETES VOL. 657

JOURNAL OF CHROMATOGRAPHY A

INCLUDING ELECTROPHORESIS AND OTHER SEPARATION METHODS

ELSEVIER

JOURNAL OF CHROMATOGRAPHY A

INCLUDING ELECTROPHORESIS AND OTHER SEPARATION METHODS

Scope. The *Journal of Chromatography A* publishes papers on all aspects of **chromatography, electrophoresis** and related methods. Contributions consist mainly of research papers dealing with chromatographic theory, instrumental developments and their applications. In the *Symposium volumes*, which are under separate editorship, proceedings of symposia on chromatography, electrophoresis and related methods are published. *Journal of Chromatography B: Biomedical Applications* —This journal, which is under separate editorship, deals with the following aspects: developments in and applications of chromatographic and electrophoretic techniques related to clinical diagnosis or alterations during medical treatment; screening and profiling of body fluids or tissues related to the analysis of active substances and to metabolic disorders; drug level monitoring and pharmacokinetic studies; clinical toxicology; forensic medicine; veterinary medicine; occupational medicine; results from basic medical research with direct consequences in clinical practice.

Submission of Papers. The preferred medium of submission is on disk with accompanying manuscript (see *Electronic manuscripts* in the Instructions to Authors, which can be obtained from the publisher, Elsevier Science Publishers B.V., P.O. Box 330, 1000 AH Amsterdam, Netherlands). Manuscripts (in English; *four* copies are required) should be submitted to: Editorial Office of *Journal of Chromatography A*, P.O. Box 681, 1000 AR Amsterdam, Netherlands, Telefax (+31-20) 5862 304, or to: The Editor of *Journal of Chromatography B: Biomedical Applications*, P.O. Box 681, 1000 AR Amsterdam, Netherlands. Review articles are invited or proposed in writing to the Editors who welcome suggestions for subjects. An outline of the proposed review should first be forwarded to the Editors for preliminary discussion prior to preparation. Submission of an article is understood to imply that the article is original and unpublished and is not being considered for publication elsewhere. For copyright regulations, see below.

Publication information. *Journal of Chromatography A* (ISSN 0021-9673): for 1994 Vols. 652–682 are scheduled for publication. *Journal of Chromatography B: Biomedical Applications* (ISSN 0378-4347): for 1994 Vols. 652–662 are scheduled for publication. Subscription prices for *Journal of Chromatography A*, *Journal of Chromatography B: Biomedical Applications* or a combined subscription are available upon request from the publisher. Subscriptions are accepted on a prepaid basis only and are entered on a calendar year basis. Issues are sent by surface mail except to the following countries where air delivery via SAL is ensured: Argentina, Australia, Brazil, Canada, China, Hong Kong, India, Israel, Japan, Malaysia, Mexico, New Zealand, Pakistan, Singapore, South Africa, South Korea, Taiwan, Thailand, USA. For all other countries airmail rates are available upon request. Claims for missing issues must be made within six months of our publication (mailing) date. Please address all your requests regarding orders and subscription queries to: Elsevier Science Publishers, Journal Department, P.O. Box 211, 1000 AE Amsterdam, Netherlands. Tel.: (+31-20) 5803 642; Fax: (+31-20) 5803 598. Customers in the USA and Canada wishing information on this and other Elsevier journals, please contact Journal Information Center, Elsevier Science Publishing Co. Inc., 655 Avenue of the Americas, New York, NY 10010, USA, Tel. (+1-212) 633 3750, Telefax (+1-212) 633 3764.

Abstracts/Contents Lists published in Analytical Abstracts, Biochemical Abstracts, Biological Abstracts, Chemical Abstracts, Chemical Titles, Chromatography Abstracts, Current Awareness in Biological Sciences (CABS), Current Contents/Life Sciences, Current Contents/Physical, Chemical & Earth Sciences, Deep-Sea Research/Part B: Oceanographic Literature Review, Excerpta Medica, Index Medicus, Mass Spectrometry Bulletin, PASCAL-CNRS, Referativnyi Zhurnal, Research Alert and Science Citation Index.

US Mailing Notice. *Journal of Chromatography A* (ISSN 0021-9673) is published weekly (total 52 issues) by Elsevier Science Publishers (Sara Burgerhartstraat 25, P.O. Box 211, 1000 AE Amsterdam, Netherlands). Annual subscription price in the USA US$ 5132.25 (US$ price valid in North, Central and South America only) including air speed delivery. Second class postage paid at Jamaica, NY 11431. **USA POSTMASTERS**: Send address changes to *Journal of Chromatography A*, Publications Expediting, Inc., 200 Meacham Avenue, Elmont, NY 11003. Airfreight and mailing in the USA by Publications Expediting.

See inside back cover for Publication Schedule, Information for Authors and information on Advertisements.

0021-9673/93/$06.00

Printed in the Netherlands

CONTENTS

(Abstracts/Contents Lists published in Analytical Abstracts, Biochemical Abstracts, Biological Abstracts, Chemical Abstracts, Chemical Titles, Chromatography Abstracts, Current Awareness in Biological Sciences (CABS), Current Contents/Life Sciences, Current Contents/Physical, Chemical & Earth Sciences, Deep-Sea Research/Part B: Oceanographic Literature Review, Excerpta Medica, Index Medicus, Mass Spectrometry Bulletin, PASCAL-CNRS, Referativnyi Zhurnal, Research Alert and Science Citation Index)

REVIEW

REGULAR PAPERS

Column Liquid Chromatography

Gas Chromatography

(Continued overleaf)

Contents (continued)

Journal of Chromatography A, 657 (1993) 229–282
Elsevier Science Publishers B.V., Amsterdam

CHROM. 25 422

Review

Chemistry of zirconia and its use in chromatography

J. Nawrocki☆

Department of Chemistry, University of Minnesota, 207 Pleasant Street S.E., Minneapolis, MN 55455 (USA)

M.P. Rigney

Ecolab Inc., Ecolab Center, St. Paul, MN 55102 (USA)

A. McCormick

Department of Chemical Engineering and Material Science, University of Minnesota, Minneapolis, MN (USA)

P.W. Carr*

Department of Chemistry, University of Minnesota, 207 Pleasant Street S.E., Minneapolis, MN 55455 (USA)

ABSTRACT

The purpose of this review is to shed some light on the complex properties of zirconia's surface chemistry in order to better understand its behaviour under chromatographic conditions. We emphasize the great differences between the much better known chemistry of a silica surface and the chemistry of zirconia's surface. The review describes both the physical and chemical properties of zirconium dioxide from a chromatographic point of view. The chemistry of monoclinic zirconia surface is developed from its underlying crystalline structure.The paper describes the dependence of the specific surface area, pore volume, porosity and mechanical strength on thermal treatment. Methods of synthesis of chromatographically useful zirconia are outlined. The review also covers the adsorption properties of zirconia at both gas–solid and liquid–solid interfaces. Adsorption of water, carbon dioxide, carbon monoxide and ammonia are described and the controversies concerning the surface concentration of adsorption sites are presented. The complex chemistry of a zirconia surface is pointed out and the importance of ligand exchange reactions is emphasized. In contrast to a silica surface, ligand exchange plays an important role in liquid chromatographic applications of zirconia. Strong, hard Lewis acid sites, present on a zirconia surface, can interact with hard Lewis bases and these interactions, sometimes troublesome, can be successfully exploited even for protein separations. Zirconia's surface can be modified in many ways: dynamically, by addition of competing Lewis bases to the mobile phase, or permanently, by covering its surface with polymers or by depositing carbon.

The review also shows that the main difficulty in achieving a wider variety of applications is probably our lack of knowledge and poor understanding of zirconia's surface chemistry.

* Corresponding author.
☆ Permanent address: Faculty of Chemistry, A. Mickiewicz University, 60-780 Poznan, Poland.

0021-9673/93/$06.00
SSDI 0021-9673(93)E0801-Z

CONTENTS

1. INTRODUCTION

Zirconia, *i.e.* zirconium dioxide, exists in many crystallographic and amorphous forms. This material has interesting properties and it has numerous applications in modern technology [1,2]. We would like to draw attention to a new, promising application of zirconia: as a column packing material for high-performance liquid chromatography (HPLC). The ideal HPLC support particle should be energetically homogenous, have a high surface area on which a wide variety of chemical moieties can be irreversibly and inalterably deposited to provide useful selectivity for a number of separation problems. It should be physically and chemically stable over a

wide range in pressure, pH, temperature and solvent conditions. It should be available in a variety of particle diameters as well as pore sizes and volumes.

It is clear from the literature describing the deficiencies of existing supports and the extensive current interest in the development, evaluation and optimization of "new and improved" supports for HPLC that presently available supports remain far from this ideal.

Properties of the ideal chromatographic support are listed in Table 1. Although silica and modified silicas are the most widely used and most useful HPLC supports, it is well known that silica and bonded phase silicas are not stable outside the range of pH 2 to approximately 8 [3–8]. Above pH 8 silica is subject to attack by alkali and it dissolves. Below approximately pH 2, the siloxane linkages which hold bonded phases to silica are subject to hydrolytic attack and are slowly removed from the surface [9–11]. The dissolution of silica and removal of bonded phase is accelerated at high temperature, and leads to changes in retention, selectivity and peak shape, loss of column bed integrity, and contamination of product in preparative chromatography.

Because of the problems inherent in the use of silica-based chromatographic supports, a considerable amount of time and effort has been devoted to the identification and evaluation of alternative high-performance support materials. Among these supports are cross-linked polystyrene–divinylbenzene and related supports, carbonaceous phases, calcium hydroxyapatite, alumina and many more [12]. A review of the properties and limitations of each of these supports is beyond the scope of this article. It is sufficient to note that they fall far short of fulfilling the requirements of the ideal support outlined above, and so the search goes on.

A second reason for exploring the use of different support materials is to exploit the unique surface chemistry of a particular support for a specific separation. Support chemistry is often viewed as a nuisance to be overcome, for example, by adding "masking agents" to the mobile phase, but it should be more appropriately viewed as an important variable to be manipulated in optimizing a separation. In this context, the development of new support materials with unique surface chemistry gives the chromatographer access to additional tools with which to affect a separation. Since resolution in chromatography depends much more on selectivity than on efficiency there will always exist an interest in developing new, more selective (or even "tunable" selectivity —due to unique surface chemistry) supports.

This search for chromatographic supports with

TABLE 1

COMPARISON OF SILICA, ZIRCONIA AND SYNTHETIC POLYMER SUPPORTS IN TERMS OF CHROMATOGRAPHICALLY RELEVANT PROPERTIES

++ = Very good performance; + = good performance; − = fair performance.

	Silica	Zirconia	Polymeric phases
Mechanical stability	++	++	+
High surface area	++	++	++
Control of average pore diameter	++	++	+
Control of particle diameter	++	++	++
Chemically flexible	++	+[a]	+
Energetically homogeneous	−	−	+
Swelling	++	++	−
Chemical stability (acid, base)	−	++	++
Thermal stability	+	++	−

[a] If a method to produce a stable, monomolecular, bonded phase on zirconia were developed we would add an additional +.

improved physical and chemical properties has recently led to increased attention to transition metal oxides and related materials such as zirconium oxide, zirconium phosphate and titanium oxide [13–25]. One important reason for this interest is the remarkable mechanical, chemical and thermal stability of such materials [26–28]. The chemical stability of zirconia and zirconium phosphate has long been recognized, and has led to their use as ion-exchange materials for high-level radioactive waste treatment, recovery of fission products and high-temperature ion-exchange in the nuclear industry [29]. Literature on the use of zirconia for ion-exchange of inorganic compounds is vast [26–36]. We shall not cover this field in this review.

Zirconium oxide is known to be the only pure metal oxide which possesses four different chemical properties on its surface: acidic and basic[a] as well as oxidizing and reducing properties [1]. These unique properties are widely utilized in catalysis (see ref. 61 and references cited therein). The catalytic activity of zirconia makes its utility for chromatography more difficult but in liquid chromatography this activity can often be suppressed.

An enormous amount of work has been done to characterize these oxides and although the chemical stability (pH etc.) of these materials is remarkable, the amorphous precipitates and layered crystalline materials which have historically been prepared are *not at all suitable for use in HPLC*. They do not possess sufficient mechanical stability, nor have they been prepared with sufficiently high surface areas or controlled and reproducible pore geometries. Recently, spherical, porous, microparticulate zirconia and titania supports with excellent physical and mechanical properties have been prepared [24,25]. Some of the unique properties of these materials which make them attractive as chromatographic supports will be described below with a primary focus on zirconia and modified supports prepared from zirconia.

Despite its interesting chemistry, zirconia for chromatography must fulfill certain minimum physical requirements. These requirements are quite similar both for chromatographic grade zirconia and zirconia for use in catalysis [24,37]. A well developed pore structure (excluding microporosity) is necessary both for catalysis and chromatography. Particles of uniform geometry and dispersity as well as high mechanical strength are desirable. The surface should show a BET isotherm of type IV with a type H1 hysteresis loop (IUPAC [38])[a]. The only exception is the catalytic activity which is highly undesirable in chromatographic materials.

2. PHYSICAL PROPERTIES

2.1. Precipitation of zirconia —dependence of physical properties on the conditions

Zirconium dioxide can be prepared by precipitation from zirconium or zirconyl salts [1] or from zirconium alkoxides [39–43]. The method of preparation strongly influences the properties of the precipitate and many examples of this can be found in the literature (*e.g.* ref. 1).

There is some disagreement in the literature concerning the importance of pH as a factor which can influence the crystallinity of the precipitated zirconia. Davis [44] considers pH to be the most important factor and shows that the tetragonal phase is likely to form at pH values lower than 6.5 or higher than 10.4 while in the range $6.5 < pH < 10.4$ the monoclinic phase precipitates. Srinivasan *et al.* [45] made similar observations. However, the range of pH in which monoclinic zirconia formed was stated to be wider: $3 < pH < 10$. Other authors did not notice any dependence of the crystalline form on the pH [39]. Clearfield [46–48] proposed a mechanism of crystallization of zirconia depending on both pH and time. The mechanism is based on the tetrameric structure of zirconyl species found

[a] We will use the term acidity and basicity very often in this review. When the terms "acidity" or "basicity" are used we mean both in their broader sense, *i.e.* we mean Lewis acidity or Lewis basicity. When we refer to Brönsted acidity or basicity this will always be noted.

[a] The shape of isotherm and hysteresis loop will be discussed in detail in section 2.6.

in the solid state and in solution. He has shown that the slow process at extreme pH values should favor the tetragonal structure while rapid precipitation leads to amorphous precipitates or the monoclinic phase (the latter is promoted by heating). It is worth noting that tetrameric zirconium hydroxide structures contain bridged hydroxyls which will be discussed later [48–50]. We should also note that the degree of mesoporosity as well as total pore volume increases with increasing pH [37,51,52].

Zirconia can also be obtained by a thermolysis of zirconium salts. Thermal decomposition of zirconium sulphate at 1000°C leads to a mesoporous material with high (90 m^2/g) surface area [53]. Decomposition of $Zr(NO_3)_4$ at 500°C in the presence of H_3PO_4 leads to amorphous, highly acidic zirconia with a specific surface area of 290 m^2/g [54].

It is thus interesting to note that depending on the method of preparation and conditions of calcination, it is possible to prepare amorphous zirconia [24] or zirconia with a definite monoclinic crystallinity [30]. Generally, the precipitation of ZrO_2 at lower temperature leads to amorphous material while at higher temperatures crystalline phases are more likely. *It has yet to be shown whether the amorphous, tetragonal or monoclinic zirconia surfaces have different chromatographic properties.*

2.2. Crystallinity

Zirconia is available in four forms: amorphous, tetragonal, cubic and monoclinic. It has been known that the optical, thermal and electrical properties of the zirconia depend on its structure [55–57]; we do not doubt that zirconia's chromatographic properties will depend on its crystallinity. The crystallographic forms can change from one to another in the following way:

$$\text{monoclinic} \overset{1170^\circ C}{\Longleftrightarrow} \text{tetragonal} \overset{2680^\circ C}{\Longleftrightarrow} \text{cubic}$$

However, it is well known that all the above crystalline forms can be obtained at much lower temperatures, for example, by slow precipitation of hydrous zirconia and refluxing the slurry in mother liquid one obtains the monoclinic material [46]. Cubic zirconia can be obtained similarly [46]. Amorphous precipitates usually transform to the metastable tetragonal phase upon thermal treatment and then convert to the monoclinic phase [40]:

$$\text{amorphous} \rightarrow \underset{\text{(metastable)}}{\text{tetragonal}} \rightarrow \text{monoclinic}$$

The transition from the amorphous to the tetragonal form usually takes place at 420–470°C. This is easily observed as a sharp exothermal "glow" peak on a differential thermal analysis (DTA) curve (see refs. 24,39 and 51 and references cited therein). The exact temperature of the glow-exotherm depends on the preparative conditions [58]. The tetragonal phase is considered metastable [39,45]. The transition from the metastable tetragonal to the monoclinic crystalline phase proceeds in a temperature range between 400 and 1000°C [39,40,59,60]. The degree of conversion depends not only on the temperature but also on the total time of the thermal treatment. As a result most studies involve the use of polymorphous materials *i.e.* the substances were partially amorphous, partially tetragonal and partially monoclinic [1,51]. X-Ray diffraction shows that even materials with definite monoclinic crystallinity have a low yet discernible amount of tetragonal phase [61]. X-Ray diffraction is usually used for estimating the relative amount of the crystalline phases. However, Raman spectra [40,37,51] and ^{17}O magic angle spinning NMR spectra also appear to be sufficiently sensitive to enable detection of crystallites even when X-ray diffraction fails [62,63]. It is also worth noting that the relative amount of monoclinic/tetragonal phase can slowly change upon aging; Guglielminotti [64] noticed the transformation of the tetragonal form to the monoclinic material over a year's time. The point of zero charge (pzc) is another property which changes upon aging [65]. Polymorphism in zirconia increases surface heterogeneity. Obviously this has some effect on its chromatographic properties [66]. According to Tanabe [1] zirconia pretreated below 700°C is primarily amorphous with small tetragonal and monoclinic regions. The transformation of tetragonal to monoclinic

zirconia can also be brought about by pressure [67]. Prolonged mechanical treatment (grinding) gave a pure monoclinic phase from polymorphs containing various amounts of tetragonal and monoclinic materials [68].

2.2.1. *Monoclinic zirconia and the origin of the surface activity*

The chemical environment of zirconium and oxygen will influence their surface chemical properties and thus it is important to understand the crystal structure in some details. Monoclinic zirconia is a crystalline substance in which all zirconium atoms are heptacoordinated to oxygen atoms. This is shown in Fig. 1.

Two different kinds of oxygen atoms are present in monoclinic zirconia: tricoordinated oxygen is denoted O(1) and tetracoordinated oxygen is denoted O(2). The coordination spheres of both types of oxygens are illustrated in Figs. 2 and 3.

A stereoscopic picture of the 100 plane of monoclinic zirconia is shown in Fig. 4.

The crystalline structure of monoclinic zirconia was solved many years ago by McCullough and Trueblood [69], and Smith and Newkirk [70]. It is interesting to note that planes perpendicular to the x crystallographic axis are composed of sequential layers of oxygens (O1), zirconium

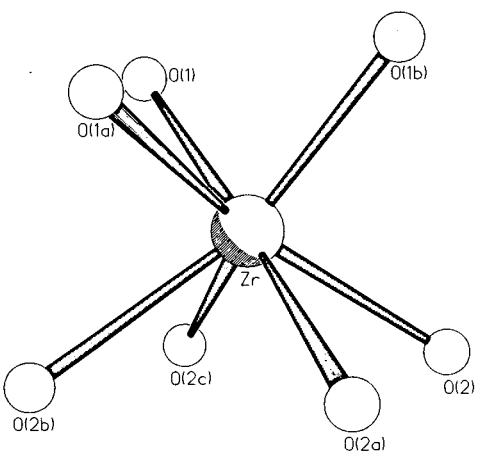

Fig. 1. Coordination sphere of zirconium atom in monoclinic zirconia. Three oxygens O1 type (O1, O1a, O1b,) and four oxygen atoms of O2 type (O2, O2a, O2b, O2c) are coordinated to each zirconium atom.

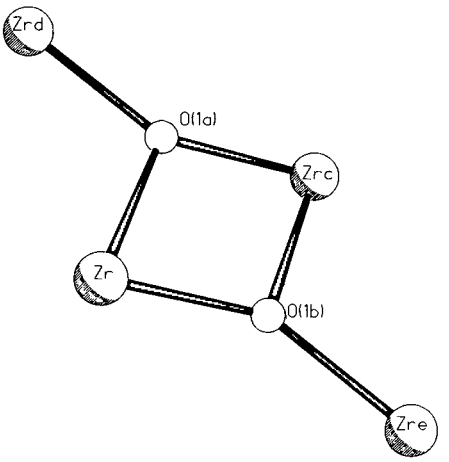

Fig. 2. Coordination sphere of O1 type oxygen atoms. Each O1 type atom is coordinated to three zirconium atoms.

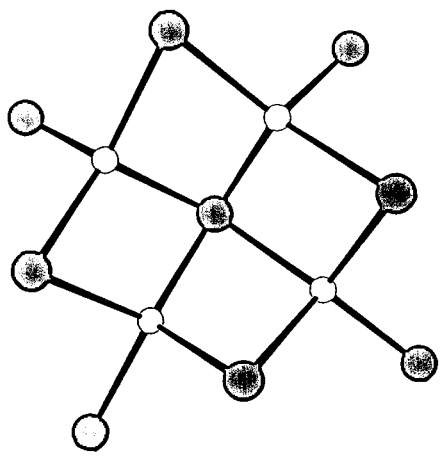

Fig. 3. Coordination sphere of O2 type oxygen atoms. Each O2 oxygen atom is coordinated to four zirconium atoms. ● = Zr; ○ = O(2).

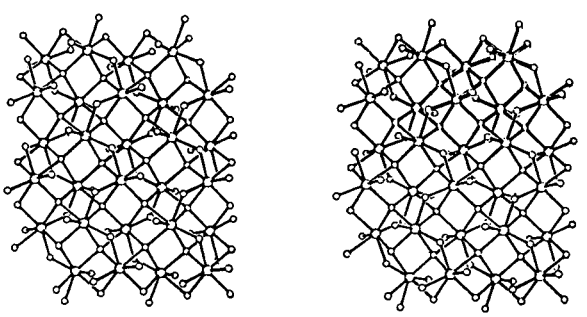

Fig. 4. Stereoscopic view of monoclinic zirconia crystal (100 plane).

atoms, oxygens (O2) and again oxygens (O1). Let us consider the structure of the zirconia surface bearing in mind this property of the oxide. First, we have to take into consideration a whole molecule of the ZrO_2 —*i.e.* we cannot "destroy" the stoichiometry of the compound.

If we illustrate the structure of monoclinic zirconia in terms of ZrO_2 molecules (Fig. 5) we will see subsequent layers of oxygen, zirconium atoms and then again oxygen. Closer inspection of the structure reveals that the oxygen atom layers inside the crystal contain twice as many oxygen atoms as does the "surface" layer. In other words Fig. 5 shows that the ratio of oxygen atoms in the surface layer to the zirconium atoms in the immediate underlayer is 1:1. Now we consider a layer of surface oxygens and a layer of zirconium atoms keeping in mind that a second layer of oxygens is below the zirconium atoms. Taking the above points into account we can identify two extreme cases: case A: the top layer is composed of O1 type oxygens or case B: the top layer is composed of O2 type oxygens.

We also assume that the atoms (Zr and O) in the surface preserve as far as possible their coordination configurations found in the bulk crystal.

In case A the zirconium atoms in layer 2 (see Fig. 5) will also be trigonally coordinated (keep in mind that the other four coordination bonds are satisfied by the type 2 oxygens (O2) in the next plane down).

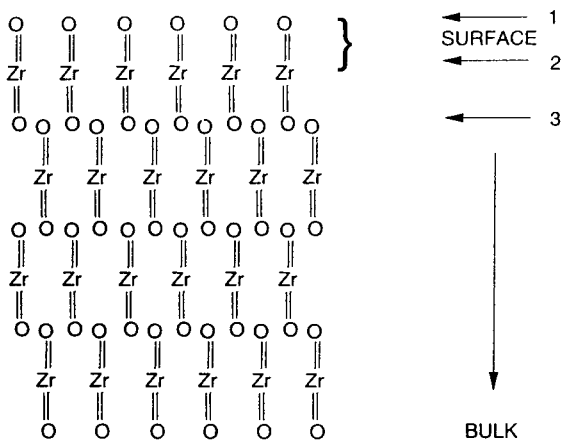

Fig. 5. Schematic view of atom layers perpendicular to *x* crystallographic axis (100 plane) in terms of zirconia molecules. 1 = surface layer of oxygen atoms; 2 = surface layer of zirconium atoms; 3 = layer of bulk oxygens.

According to our assumptions, in the layer of type 1 oxygens (O1) every second oxygen atom is coordinated by two bonds to a surface zirconium atom and every second type 1 oxygen (O1) is coordinated to only a single zirconium atom. We thus observe that some coordination valencies of both oxygen and zirconium atoms are unsatisfied. In other words the surface atoms are charged. Oxygen atoms bear a negative charge while a positive charge will accumulate on the zirconium atoms. *This is the fundamental origin of the Lewis basicity and acidity of zirconium oxide* (Fig. 7).

In case B a similar analysis can be performed. Here the top layer is comprised exclusively of O2 type oxygens. In this case four coordination valences of the zirconium atoms are projected toward the top layer of oxygen. Keeping in mind that three coordination bonds of Zr are satisfied by the subsequent layer of type 1 (O1) oxygen. According to our assumptions (that is the crystalline configuration is preserved) only two of zirconium valences can be satisfied by the type 2 (O2) oxygens. We therefore see formation of Lewis acid sites on the surface, since the unsatisfied valences are equivalent to an accumulation of a positive charge on the zirconium atoms. In the next layer the type 2 (O2) oxygens can satisfy only two (of four) coordination valences and thus a negative charge will accumulate on the oxygen atoms. This is the origin of Lewis base sites on the zirconia surface (Fig. 8).

In both cases all surface zirconium atoms are Lewis acids and all oxygen atoms Lewis bases. Indeed, it has been confirmed that basic and acid sites are contiguous [71]. The average concentration of zirconium atoms on the surface is 12.2 $\mu mol/m^2$ (calculated from data in refs. 69 and 70). In reality the surface layer is usually formed in the presence of other substances like water and oxygen. When water molecules are available the surface will be covered by hydroxyls as each surface Lewis acid–base pair will likely dissociatively adsorb a water molecule. This is in agreement with general knowledge of metal oxides [72] as well as with the observed behavior of

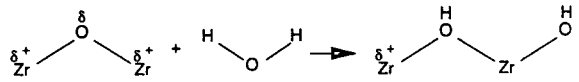

Fig. 6. Reaction of water molecule with zirconia surface.

water on thermally treated zirconia [67,73,74] (Fig. 6).

Let us note that each Zr atom bears a partial positive charge (δ^+) while the attached hydroxyl bears a full negative charge. This explains why surface hydroxyl groups on zirconia are Brönsted bases in contrast to these on silica which are Brönsted acids. The bridged hydroxyls will probably differ in basic strength as some of them bear partial (δ^-) and some of them full negative charge. Reaction of water with some acid–base pairs on zirconia surface (see Fig. 7) can lead to formation of geminal hydroxyls on the surface.

The above model leads to a surface concentration of *ca.* 25 μmol OH/m^2. The literature reports that the surface concentration of hydroxyls is higher than 20 μmol OH/m^2 [75,76]. The surface concentrations of acidic and basic sites found in the literature vary greatly. There are substantial differences between the data from various groups. The highest results show close to 5 μmol of Lewis acid sites/m^2 and about 4 μmol of Lewis base sites/m^2. These considerations

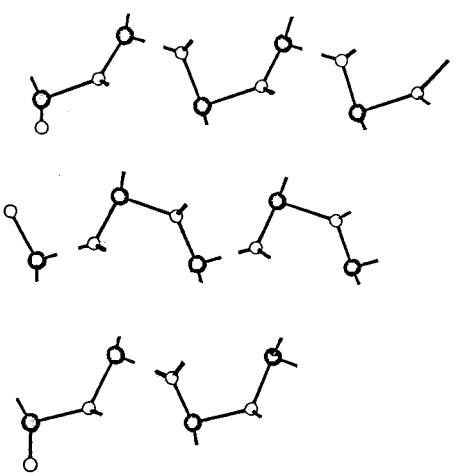

Fig. 7. Surface of zirconia (plane 100). Case A: the top layer of oxygen atoms is composed exclusively of O1 type oxygens. Note that half of the zirconium atoms have two and the other half have one unsatisfied coordination valency. The same is true for oxygen atoms. ● = Zr; ○ = O(1).

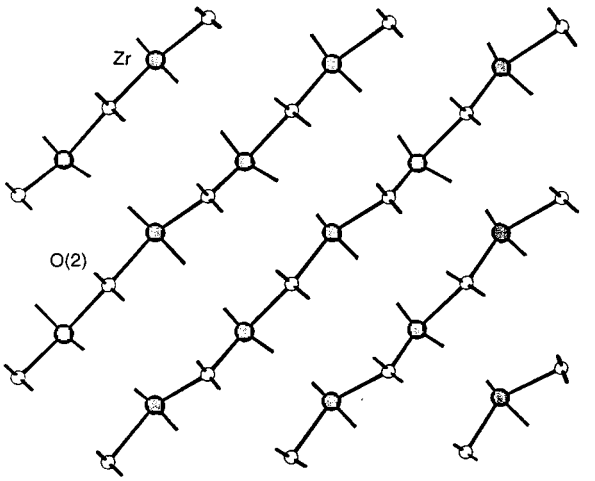

Fig. 8. Surface of zirconia (plane 100). Case B: the top layer of oxygen atoms is composed exclusively of O2 type oxygens. Note that all zirconium atoms have two coordination valencies unsatisfied. The same is true for the oxygen atoms. ● = Zr; ○ = O(1).

indicate the complexity of the zirconia surface and confirm our assumption that the surface will tend to bind any available molecule so as to satisfy its unsaturated coordination.

2.3. Surface area

The specific surface area of a support is generally accepted as one of its most important chromatographic parameters. The specific surface area of zirconia depends strongly on the sample's thermal history. This is shown in Fig. 9.

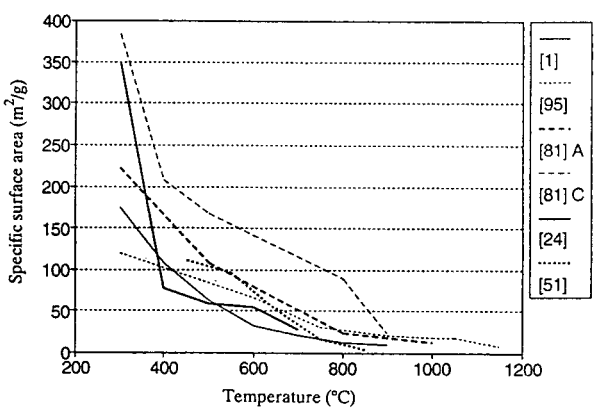

Fig. 9. The dependence of specific surface area of zirconia on temperature.

Surface area decreases sharply between 300 and 550°C. Generally, particles heated above 500°C will have a specific surface area below 100 m^2/g. Two processes are responsible for the decrease in surface area: (i) microcrystallite growth and (ii) intercrystallite sintering [51].

Fig. 9 clearly shows that we cannot expect zirconia particles to have a specific surface area comparable to that of silica. Usually zirconia thermally treated below 400°C will contain micropores. However, higher-temperature treatment means lower surface area and this trend is observed essentially for all zirconias shown in Fig. 9.

The porous structure of zirconia was studied by Sharygin *et al.* [77]. Samples of zirconia subjected to heat treatment at 150–300°C were transitionally microporous, at 300–600°C transitionally macroporous and at 700–900°C macroporous adsorbents. The authors [77] estimated (applying the Dubinin equation [78]) that part of the surface area attributable to mesopores (20 to 500 Å [38]) and compared it with the total BET surface area. This is shown in Fig. 10.

A similar estimate was made by Mercera *et al.* [51] but by a different approach (the *t*-plot method of statistical thickness [79], which is based on the observation that the ratio between the adsorbed volume and the volume of a unimolecular layer when plotted *versus* the relative pressure p/p_o can be represented by a single curve called "the standard isotherm". For a review on microporosity estimation methods see ref. 242.) This is shown in Fig. 11.

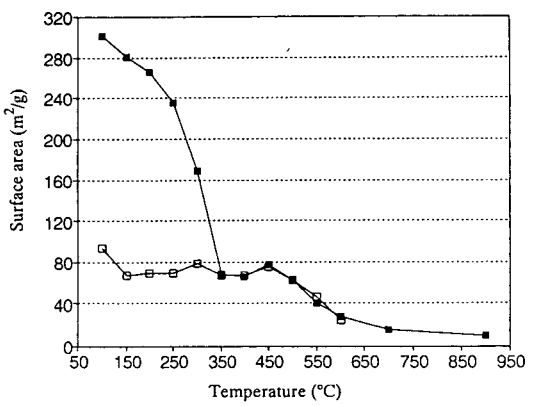

Fig. 10. Total (■) specific surface area of zirconia *vs.* surface area of mesopores (□) calculated by the Dubinin equation [77].

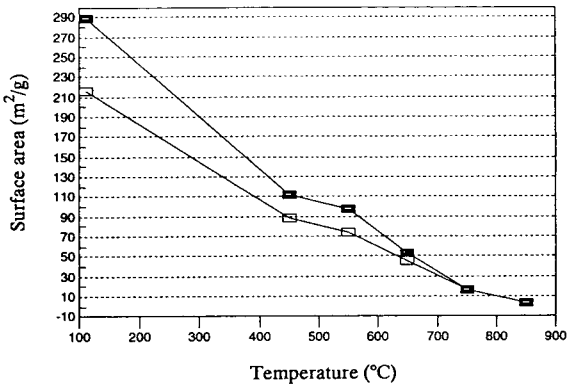

Fig. 11. Total (■) specific surface area of zirconia *vs.* surface area of mesopores (□) calculated from *t*-plot method [51].

The differences between the results (Figs. 10 and 11) may arise from the use of different experimental methods, or different adsorbates (Sharygin *et al.* used methanol while Mercera *et al.* nitrogen). The conclusion, however, is similar: zirconia when thermally treated only below 350–450°C will contain a considerable number of micropores.

The dependence of pore diameter on temperature as observed by four groups is shown in Fig. 12.

Despite the use of different definitions of the pore diameter (effective pore diameter [77], mean pore diameter [24] or most frequent pore

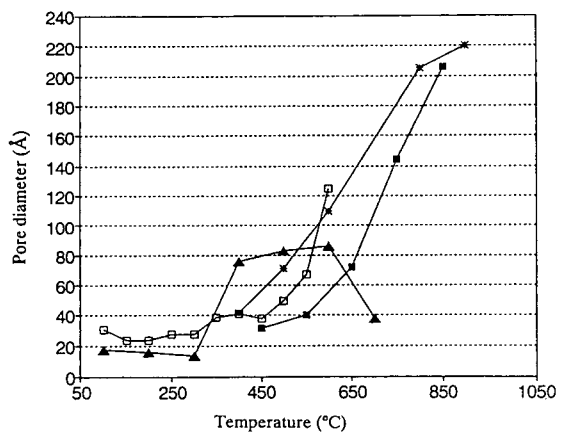

Fig. 12. Dependence of pore diameter of zirconia on thermal treatment. □ = Ref. 77; ■ = ref. 51; ▲ = ref. 24; ☆ = ref. 116.

diameter from the Barret–Joyner–Halenda (BJH) method [51] and the average pore diameter [80]) the trend observed in Fig. 12 is clear: the pore size increases with temperature.

The type of crystalline form of zirconia also seems to have an effect on the surface area. Only the tetragonal material has a surface area of 90 m^2/g after treatment at 800°C [81]. However, it is known that such high specific surface areas must be due to microporosity [51]. The surface area of monoclinic zirconia seems to be more stable than that of tetragonal zirconia. This is illustrated in Fig. 13 [51,82]

Values of the specific surface area for zirconia particles used for chromatography generally fall in the ranges shown in Fig. 11, in agreement with their thermal history [19,24]. These values are generally much lower than those for chromatographic silica [4,83]; however, the density of porous zirconia is considerably higher than that of silica. The surface areas in m^2/cm^3 of occupied bed are more comparable.

2.4. Density of zirconia

The literature indicates considerable variance in the true (bulk) density of zirconia: 5.8 g/cm^3 [19], 5.7 g/cm^3 [84], 5.85 [85], 5.56 g/cm^3 [51], 5.89 g/cm^3 [86], 5.68 g/cm^3 [87], 5.826 g/cm^3 [69,88]. Similar variation in the true density is found in older sources [89]. The densities of the tetragonal form are higher: 6.10 g/cm^3 [51,87], 6.16 g/cm^3 [90] or 6.03 g/cm^3 [86]. Cubic zirconia is reported to have the highest density: 6.27 g/cm^3 [87]. The true density of silica is reported to be 2.2 g/cm^3 [4]. The apparent density of porous zirconia depends on its degree of hydration and can vary from 0.48 g/cm^3 to 2.33 g/cm^3 [84,81]. The packing density of silica varies in the range 0.2–0.8 g/cm^3 [4]; however, most HPLC silicas have densities in the range 0.4–0.6 g/cm^3 [83]. The value of the apparent density of zirconia is important for chromatography since it allows the calculation of the available surface area per unit volume of column. The apparent densities of three different zirconia samples are shown in Fig. 14.

The value of the density strongly depends on the sample's thermal history and each sample of zirconia may have its own, specific value. The apparent density of a zirconia sample increases as the sample is subjected to increasingly higher temperature treatment. Zirconia's apparent density is about 3–4 times higher than that of silica. Taking this into account, we can compare the surface area of a zirconia column to a silica column. Due to the higher packing density a 30 m^2/g zirconia has a surface area equivalent to 90–120 m^2/g of silica.

2.5. Pore volume and porosity

The pore volume of zirconia depends strongly on its sample history. Thermal treatment at temperatures higher than 200°C gradually decreases the pore volume from 0.25 to 0.01 g/

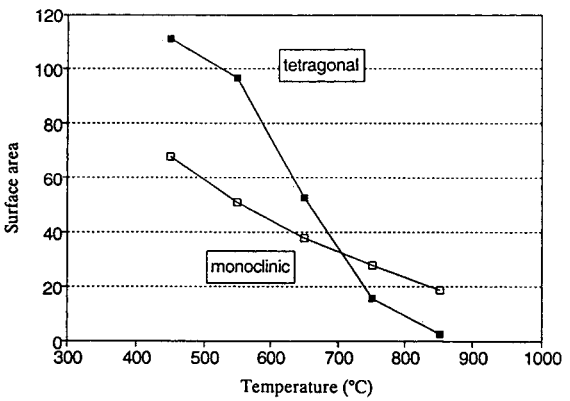

Fig. 13. Thermal stability of specific surface areas of tetragonal and monoclinic zirconias. ■ = Ref. 51; □ = ref. 82.

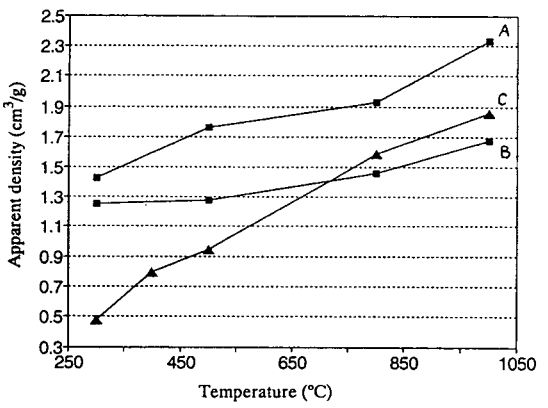

Fig. 14. Apparent density of three samples of zirconia (A [81], B [81] and C [81]) *vs.* thermal treatment.

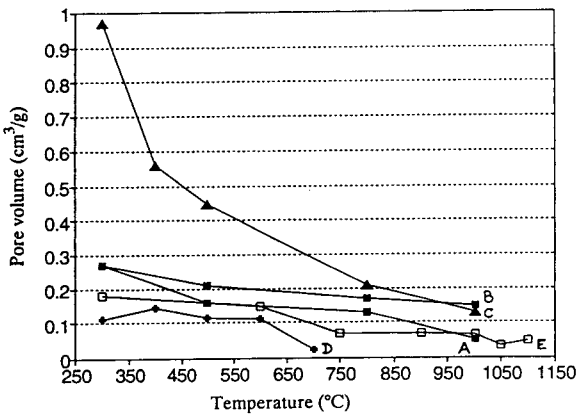

Fig. 15. Dependence of zirconia pore volume on thermal treatment (A [81], B [81], C [81], D [24], E [95]).

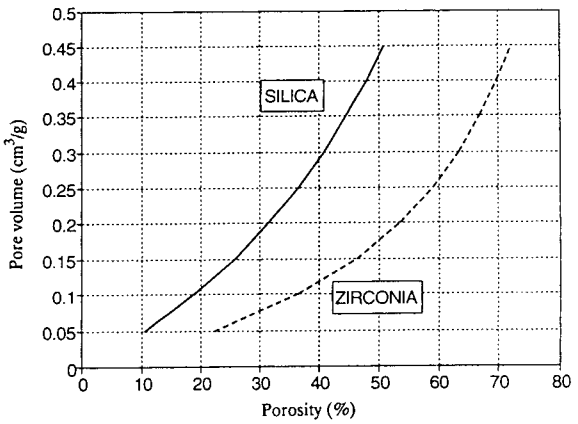

Fig. 16. Mutual dependence of pore volume and porosity for silica and zirconia.

cm^3. The pore volume of various zirconias is generally much lower than that of silicas. The pore volume of sintered zirconia particles depends on the size of the microcrystallites. The dependence of zirconia pore volume on thermal treatment is illustrated in Fig. 15.

To understand why zirconia always has a smaller pore volume (V_p) than silica, we express porosity (ϵ) as:

$$\epsilon = \rho V_p/(1 + \rho V_p)$$

Assuming $\rho_{zirconia} = 5.75$ g/cm^3 (average from all the values cited in the preceding section) and $\rho_{silica} = 2.2$ g/cm^3 [4], we can calculate pore volumes for the both materials at the same porosity (ϵ). The results are shown in Fig. 16.

As one can see, zirconia with the same porosity as silica will always have a lower pore volume than silica.

2.6. Pore size distribution and shape of the pores

The pore size distribution always provides much more information on the structure of the particle surface than either the mean or average pore diameter. Zirconia particles very often show a bimodal pore size distribution [91–93].

According to the IUPAC classification there are six types of isotherms and four types of hysteresis loops. They are shown in Fig. 17.

The type IV isotherm with H1 hysteresis loop is the most favorable for chromatographic purposes. The shape of the type IV isotherm is associated with capillary condensation taking place in mesopores and limiting uptake over a range of high p/p_o. The initial part of the type IV isotherm is attributed to monolayer–multilayer adsorption. This behavior is characteristic of materials comprised of agglomerates of approximately uniform spheres in a fairly regular array and having a narrow distribution of pore sizes [38]. Many porous adsorbents (*e.g.* inorganic oxide gels and porous glasses) tend to give type H2 loops but in such systems the distributions of pore size and shape are not well defined [38].

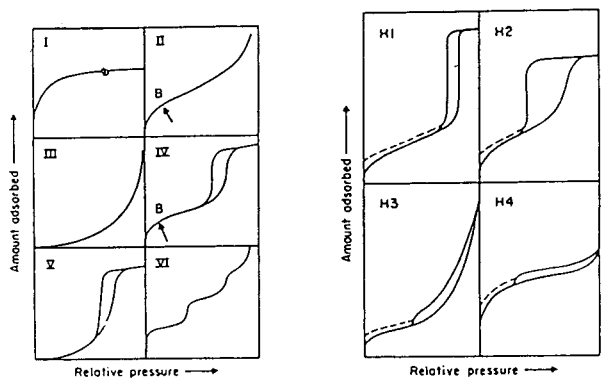

Fig. 17. Types of isotherms and types of hysteresis loops according to IUPAC classification (© 1985 IUPAC [38]).

For low temperature zirconias the pores are considered to be ink-bottle or spherical as deduced from the BET isotherm. This is unfavorable for rapid mass transfer in chromatography. Upon further treatment the pores gradually become more cylindrical [51]. Different zirconia powders can have very different adsorption isotherms and different hysteresis loops. As mentioned above, for chromatographic purposes we want a porous solid to have a type IV isotherm with a type H1 hysteresis loop. Commercial [94] and precipitated zirconias [247] often give strange type I isotherms with type H2 and H3 hysteresis loops indicative of slit-like pores. The isotherm shape improves considerably upon thermal treatment [51]. Also, use of alcohols during the preparation of the hydrogel influences the pore shape [37]. In Fig. 18 the nitrogen isotherm of a typical polymerization-induced colloid aggregation (PICA) zirconia sample [95] is shown.

The isotherm shown in Fig. 18 is of type IV with type H1 hysteresis loop. The presence of the loop in the high relative pressure range indicates mesoporosity of the solid. The pore size distribution curves (mercury porosimetry) for two PICA zirconia samples are shown in Fig. 19 [95].

The sample which was subjected to additional

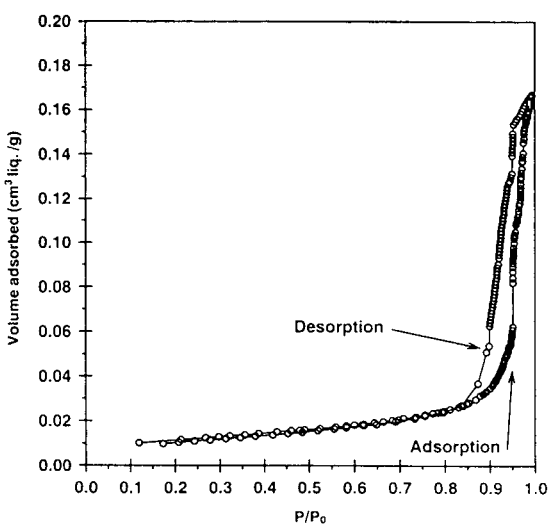

Fig. 18. Typical N_2 isotherm for PICA zirconia sintered for 6 h at 750°C and for 3 h at 900°C [95].

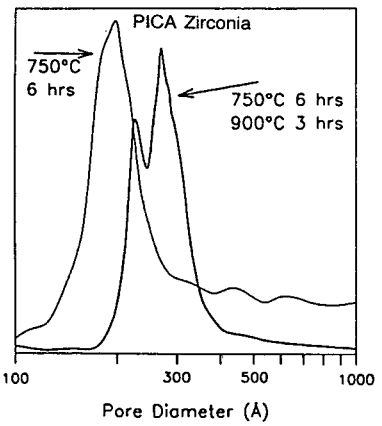

Fig. 19. Pore size distribution curves as a function of sintering conditions. (Mercury porosimetry data, [95]).

sintering at a higher temperature shows a bimodal distribution.

Two pore size distribution curves for chromatographic zirconia particles have been reported; both show unimodal pore size distribution with maximum centered at about 10 nm [19,81].

2.7. Mechanical strength

Particles in the 3–10 μm range have been routinely prepared, although size classification (due to the high density of zirconia) represents a special challenge. There are no comparable data in the literature on the mechanical strength of chromatographic-grade silica, alumina and zirconia particles. It is clear that porous microparticulate zirconias can and have been prepared with the desirable physical properties associated with other high-performance inorganic supports such as silica and alumina.

The only data available on the mechanical strength of zirconia particles for chromatography show that their strength derives from microparticle sintering during thermal treatment. This is shown in Fig. 20.

Amorphous zirconia beads have been packed at pressures up to 50 MPa without cracking [24]; commercially available, non-porous zirconia particles were safely packed at 45 MPa [15]; while monoclinic zirconia particles have been packed

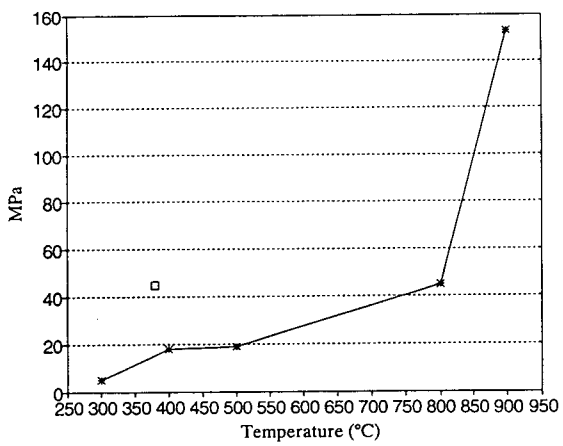

Fig. 20. Mechanical strength of zirconia particles *vs.* thermal treatment. * = Ref. 81; □ = ref. 24.

at pressures up to 9000 p.s.i. (1 p.s.i. = 6894.76 Pa) *i.e.* over 60 MPa [19].

Typical mechanical stability data for a chromatographic zirconia column bed in a pressure–flow test are shown in Fig. 21.

2.8. Purity of zirconia

In recent years the chromatographic properties of silica have been shown to depend considerably on the presence of minute metallic impurities (see refs. 83 and 97 and references cited therein). Zirconia is well known for its catalytic properties and it is also well known that certain additives can considerably increase its catalytic activity. For example incorporation of sulfate ions can generate so-called "superacid" sites on a ZrO_2 surface while the addition of SiO_2, TiO_2, Al_2O_3, SnO_2, CdO or ZnO can considerably increase the acidity of the surface. When small amounts of silica are impregnated into the zirconia matrix they considerably increase the catalytic activity by promoting acidic properties [249]. ZrO_2–TiO_2 and ZrO_2–SnO_2 also have significant basic properties [1]. Many zirconias are known to contain some hafnium: 1.6% Hf [41,98], 1.6% HfO_2 [84] or 1.8% HfO_2 [84]. Traces of Fe, Ti and Si have been reported [41,99]. Mercera *et al.* [37,51] indicated that hafnium is the main impurity in zirconia. However, traces of Cu, Fe, Ti, K and Si were also detected by X-ray fluorescence (XRF). Gimblett *et al.* [58] analyzed spectrally pure $ZrOCl_2 \cdot 8H_2O$ and found 4 ppm (w/w) Si, 3 ppm Al, 1 ppm Ca, 1 ppm Fe, and Mg and Mn both less than 1 ppm. Holmes *et al.* [74] found 100 ppm Al, 400 ppm Ca, 40 ppm Cr, 10 ppm Cu, 3000 ppm Fe, 20 ppm Mg, 50 ppm Mn, 400 ppm Si and 10 ppm Ti. Commercially available zirconia (Degussa 137) contains 0.5% Cl and 50 ppm Fe_2O_3 [99]. Three samples of zirconia were analyzed by neutron activation analysis and

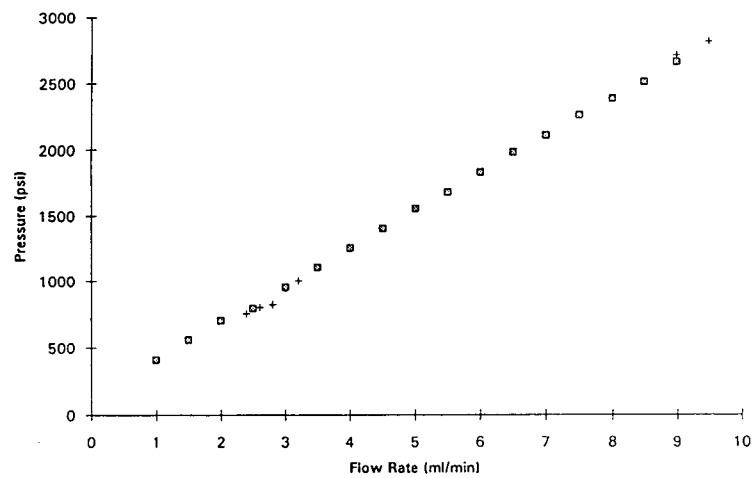

Fig. 21. Pressure-flow test of 3 μm PICA zirconia column. Mobile phase: methanol, column 50 × 0.46 cm [96]. + = Increasing flow rate; ◘ = decreasing flow rate.

various amounts of Al (4.6–364 ppm), Hf (4.1–8.7 ppm), Mn (1.3–49 ppm), Th (36.4–348 ppm) and V (1.6–4.8 ppm) were found in all samples [100]. Structural impurities substantially change the pH_{pzc} of the metal oxides [101]. *It is therefore important to pay close attention to the purity of the zirconia used to prepare chromatographic materials.*

2.9. Commercially available zirconia powders

Commercially available zirconium oxide and titanium oxide are typically irregularly shaped, low surface area, non-porous materials. Materials of this type have been used in the evaluation of the adsorption characteristics of zirconia and titania [13–15]. The literature reveals that a number of zirconia powders are commercially available (see Table 2).

Some commercially available samples (not specified) were found to be unsuitable for HPLC use [24]. A closer inspection of the above list confirms the conclusion of Trüdinger *et al.* [24] —zirconia particles with properties suitable for HPLC are not commercially available.

2.10. Requirements for and achievements in HPLC-grade zirconia technology

Porous zirconia and titania supports with many desirable properties have been prepared by sol–gel type processes [24,25]. To obtain relatively

TABLE 2

COMMERCIAL SOURCES AND PROPERTIES OF ZIRCONIA POWDERS

Manufacturer	Type	Surface area (m^2/g)	Particle size (μm)	Other data[a]	Ref.
Dynamit Nobel (Troisdorf, Germany)	Dynazircon	42	0.7	$D = 18$ nm, $V_p = 0.36\ cm^3/g$, ($\epsilon = 67\%$)	84
Aldrich		1.4	–		102
Ventron		0.66	–		102
Fisher Sci.		3	2		103
Alfa-Ventron		5.8	1–3		104
Magnesium Electron	E-10	14	–	monoclinic	105
	SC-100	32	–	amorphous	105
Magnesium Electron	S-grade	9*	10 ± 3	*after hydrothermal treatment	106
Soekawa (Tokyo, Japan)		–	3		15
INVAP-Boriloch (Argentina)		5.72	0.18	monoclinic, irregular particles, 1.5 ppm F	107
Degussa	137	63.3	–		99
A.D.Mackay	Nuclear grade	23.7	–	Hf = 0.001%	94
Tosoh	TZO grade	11.8	–	$pH_{iep} = 8.2$	108
Toyo Soda (Atlanta)	TZ-O	13.5	0.200	monoclinic, $pH_{iep} = 6.5$	109
	TZ-O	–	0.05	monoclinic, $pH_{pzc} = 6.5$	110
Industrial sample (no exact source)		2.2	–	$pH_{pzc} = 4$	111, 112

[a] D = pore diameter; ϵ = porosity.

uniform, small (2–25 μm), spherical and rigid particles, which can be used for HPLC, we can employ several different [113] methods of wet-chemical preparation of zirconia particles. Two processes are most promising: (i) sol–gel microsphere synthesis and (ii) PICA process (also called coacervation or "microencapsulation" [124,125]).

The sol–gel process can be carried out in two ways: (i) by hydrolysing zirconium compounds or (ii) by using commercially available zirconia colloids.

In the first process, the colloid must be emulsified in a water-immiscible liquid, stabilized with non-ionic surfactants and gelled by the addition of base. By adjusting the stirring velocity [24] it is possible to control the diameter of the particles. During the gelation process, colloid particles in emulsified liquid–sol droplets are converted to solid hydrogel particles. The resulting particles are subjected to a hardening process consisting of drying. The drying can be performed by: (i) conventional processes, (ii) azeotropic distillation [24] or (iii) spray-drying [92,114].

In commercially available, monoclinic [115] zirconia colloids [80,116] the size of the colloid microparticles (or core, or ultimate particles) can vary, over a relatively narrow range from 10–200 nm. The size of the colloid ultimate particles determine the final pore size of the zirconia spherule. As the water-immiscible liquid peanut oil with oleyl alcohol is commonly used [80]. Gelled spherules are separated from the reaction mixture by filtration.

The PICA process consists of the generation of: (i) a stable sol of uniformly sized colloidal particles, (ii) the addition of an organic, polymerizable and water-soluble material, (iii) initiation of polymerization of the organic material in the mixture to cause the polymerization-induced colloid aggregation into substantially spherical particles and (iv) burning off the organic material.

The PICA process produces extremely uniform zirconia particles [91]. The particle size distribution for coacervated particles of zirconia is shown in Fig. 22. For comparison the particle size distribution of coacervated silica is shown in Fig. 23 [117]. The average particle size of coacervated silica (Fig. 23) is slightly lower than the average particle size of coacervated zirconia (Fig. 22). It is probably easier to obtain narrower particle size fraction for larger particles. Fig. 24 shows a scanning electron microscopy micrograph of the PICA zirconia particles after sintering while Fig. 25 shows the surface of one particle.

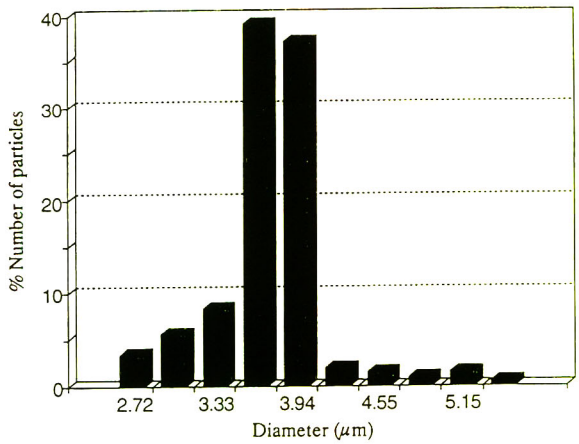

Fig. 22. Particle size distribution for coacervated zirconia [91].

According to one patent [118] it is possible to obtain zirconia particles with 582 m^2/g after sintering at 900°C or 381 m^2/g after heat treatment at 1050°C. In view of the preceding discus-

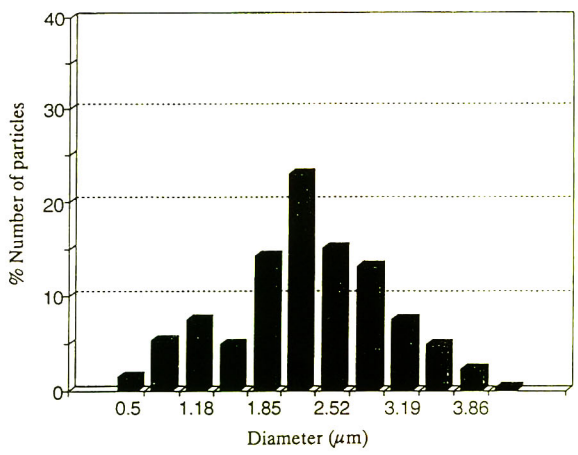

Fig. 23. Particle size distribution for PICA silica (recalculated from ref. 117).

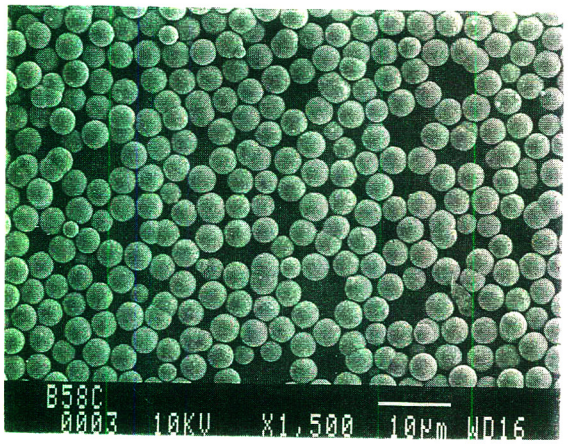

Fig. 24. SEM micrograph of coacervated zirconia particles [91].

sion concerning the surface area it is highly unlikely that such values can be realized.

Another patent claims the production of zirconia particles by simple spray-drying of sols of a zirconia colloid to which a binder is added. A binder is an active molecule which agglomerates the ultimate colloid particles and is decomposed during spray-drying. The use of zirconyl sulfate as a binder has been patented [114]. As shown below sulfates can generate superacid sites on the surface of zirconia. This will doubtless have undesirable chromatographic consequences. The patent suggests calcination at up to 800°C to remove the sulfates. This is in agreement with findings of Bensitel *et al.* [119] and Escalona Platero and Peñarroya Mentruit [53]. However, according to the work of Lunin *et al.* [120] most of the sulfate is not removed until much higher temperatures 1000–1300°C.

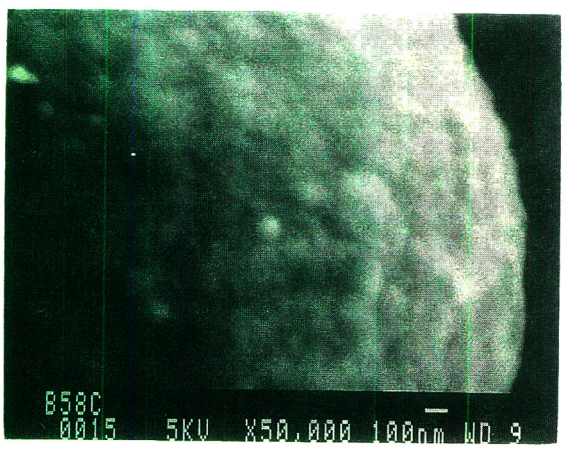

Fig. 25. SEM micrograph of the surface of a coacervated zirconia particle [91].

A chemical method of producing controlled size non-porous zirconia microspheres ($d_p < 3$ μm) has been described by Lerot *et al.* [121]. The process involves the precipitation of ZrO_2 from zirconia alkoxides by addition of propanol containing water in the presence of carboxylic acids. By controlling the amount of water added to the reaction mixture and by changing the carboxylic acids from C_6 to C_{18}, the authors were able to control the particle size in a very narrow and precise range from 0.4 to 2.7 μm. However, calcination of the product at 500°C gave particles with a very low surface area of 4 m^2/g. Such non-porous zirconia particles might be useful for rapid chromatographic separations of large molecules [122,123].

Non-porous particles can also be obtained by the oil emulsion procedure [24] and sintering of the resulting particles at 800°C for 6 h [126]. The particle size ranges from 1.5 to 2.8 μm while the specific surface area is 1.4 m^2/g.

In summary: samples of zirconia treated at low temperatures will have higher surface area, higher pore volume but will also have lower strength and lower apparent density. Moreover the higher surface areas and pore volumes result from the microporosity not mesoporosity as shown in Fig. 10. Lower treatment temperatures result in the presence of micropores [24,51,77]. We believe that materials for chromatographic purposes should be thermally pretreated at an absolute minimum of 400°C, to avoid micropores and to strengthen the particles. Such a material will then have a pore volume $V_p < 0.2$ cm^3/g and surface area < 100 m^2/g, while the apparent density will be 1.3–1.5 g/cm^3. Such materials will have a surface area per unit bed volume comparable to that of silica with *ca.* 300 m^2/g.

Oil emulsion methods [24,80,116] produce polydispersed particles which need classification before use in HPLC. PICA produces very narrow particle size distribution as shown in Fig. 22 [91]. In Table 3 we compare the physical prop-

TABLE 3

COMPARISON OF PHYSICAL PROPERTIES OF CHROMATOGRAPHIC GRADE SILICA AND ZIRCONIA PARTICLES PRODUCED BY OIL EMULSION AND COACERVATION PROCESSES

	Oil emulsion		Coacervation	
	Zirconium [24]	Zirconium [19]	Zirconium [95]	Silica [117][a]
Particle size (μm)	6	8	5	2
Specific surface area (m^2/g)	104	61	26	60
Average pore diameter (Å)	60	96	300	180
Specific pore volume (cm^3/g)	0.15	0.14	0.17	0.33
Particle porosity (%)	46	45	49	42

[a] For *n*-butylsilylated silica.

erties of chromatographic silica and zirconia produced by both methods.

Physical properties of zirconia and silica spherules produced by oil emulsion and PICA methods are similar. (However, it must be kept in mind that both zirconia materials were produced by different methods: in ref. 24 from a highly dispersed sol and in ref. 19 from monoclinic colloid particles.)

3. CHEMICAL PROPERTIES

3.1. Chemical stability

An appropriate starting point in a consideration of zirconia as an HPLC support is its chemical stability. The remarkable stability of zirconia can at least be partially understood based on the structure of monoclinic zirconia shown in Fig. 1. The strength of a zirconium–oxygen bond is comparable to that of a silicon–oxygen bond (see Table 4). However, in a monoclinic material each zirconium atom is bonded to seven oxygen atoms. In contrast in silica each silicon atom is only tetracoordinated to oxygen. These properties combine to make zirconia a chemically very stable material.

The chemical stability of zirconia and titania particles was measured under extreme pH conditions and compared to that of silica [15] and alumina [19]. The excellent chemical stability of zirconia was confirmed in both studies. The latter results are illustrated in Fig. 26. In this experiment, the stability of zirconium dioxide

TABLE 4

BOND ENERGIES (kcal/mol)

Bond	Metal coord. number	Energy of dissociation [85]	Bond strength [127]
Zr–O	7	180 ± 5	181.6 ± 2
Si–O	4	185 ± 7	193 ± 2.6
Ti–O	6	156	159.3 ± 1.5
Al–O	6	115 ± 2	121.3 ± 2.5

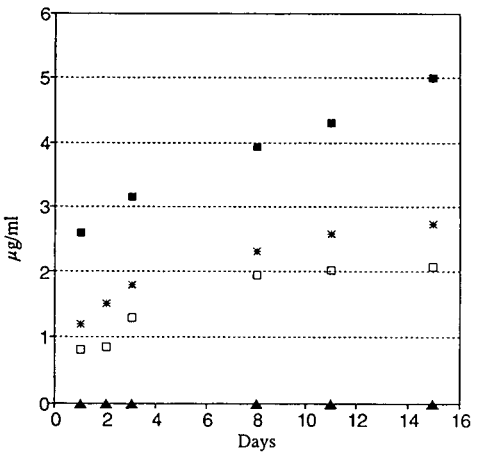

Fig. 26. Stability of zirconia and alumina over a wide pH range (replotted from ref. 19). ▲ = ZrO_2, pH 1–14; □ = Al_2O_3, pH 3; * = Al_2O_3, pH 12; ■ = Al_2O_3, pH 14.

was compared to chromatographic alumina by placing the particles in a closed container and challenging them with a variety of buffers of different pH values. Despite the fact that these static conditions are far less aggressive than those used in a chromatographic stability test where the buffer is passed continuously over the surface of the particles, Fig. 26 clearly shows that alumina dissolves at pH values greater than 12 and less than 3. In contrast, no zirconia was detected at any pH from 1 to 14 using inductively coupled plasma atomic emission spectroscopy (ICP-AES) as the detection method (zirconium detection limit = 0.03 µg/ml). It should be noted that alumina is far less soluble in aqueous media at high pH than silica, which certainly dissolves very readily under these conditions.

The stability of zirconia under alkaline conditions has been further tested by exposing a column of zirconia to a mobile phase of 1 *M* sodium hydroxide at 100°C for 3.25 h at a flow-rate of 1 ml/min. No zirconium was detected in the column effluent after this treatment. In contrast, approximately 15% of the alumina present in a comparable column was dissolved and eluted under these extreme conditions. Clearly zirconia offers a distinct advantage relative to either silica or alumina in terms of its chemical stability [19]. According to Amphlett *et al.* [26] zirconia dissolves in acid solutions (> 0.1 *M*); however, this was not confirmed in ref. 19. Zirconia will dissolve in HF, concentrated H_2SO_4 [128] and hot, concentrated H_3PO_4. Nonetheless it has been shown that zirconia is stable under acidic conditions (HCl, pH 1). It must be pointed out that it can be dissolved in very concentrated HNO_3. The solubility in nitric acid is shown in Fig. 27. However this process is very slow [129].

3.2. Adsorption properties —gas–solid interface

Zirconia surfaces have been studied very thoroughly; however, materials of various origins, crystallinity and sample histories were investigated. It is therefore difficult to generalize all prior research. It is necessary to emphasize that the surface chemistry of zirconia is much more complicated than is the better known surface chemistry of silica. Fig. 28 shows the adsorption of ammonia on SiO_2 (Rhone Poulenc MAS-100, 117.5 m^2/g) and ZrO_2 (Degussa 137, 63 m^2/g) [99].

The acid site energy distribution observed for ammonia adsorption (Fig. 29) shows two highly energetic maxima on zirconia and only one, much less energetic, maxima on silica.

These figures illustrate the greater heterogeneity of the zirconia surface. In addition to ammonia, a zirconia surface is able to adsorb CO_2 with high heats of adsorption [99]. On the basis of the CO_2 adsorption the site energy distribu-

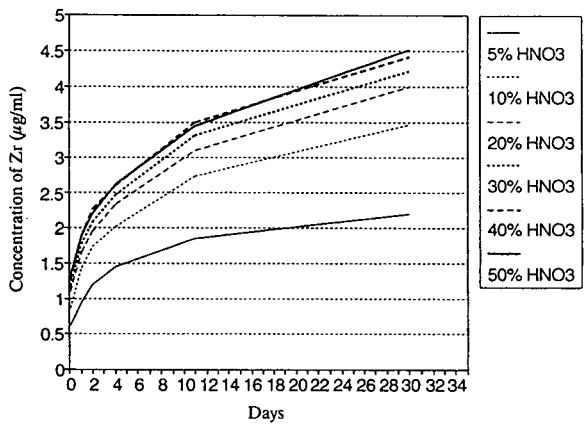

Fig. 27. Solubility of zirconia in HNO_3 [130].

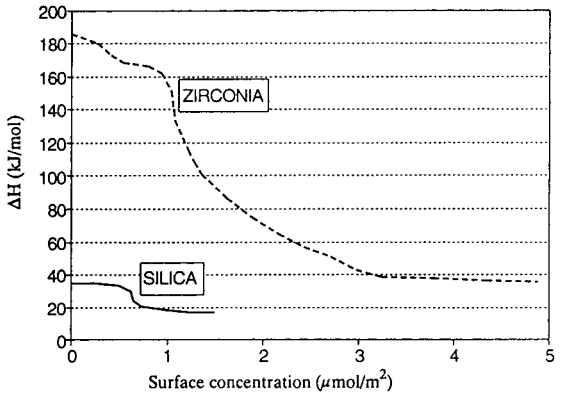

Fig. 28. Ammonia adsorption on silica and zirconia (replotted from ref. 99).

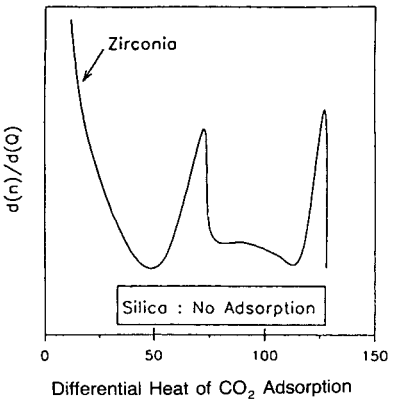

Fig. 30. Distribution of basic sites (by CO_2 adsorption) on silica and zirconia (replotted from ref. 99).

tion for basic sites was evaluated and is shown in Fig. 30 [99].

The two maxima observed for basic sites may indicate the formation of hydrogencarbonates (with basic hydroxyls) and mono- and bidentate carbonates with the basic oxygen atoms (see section 3.2.2). Another energy distribution curve for the acidic and basic sites can be found in a paper by Bibik *et al.* [131].

3.2.1. Water and hydroxyls

A zirconia surface at ambient conditions will carry a certain amount of both physically and chemically adsorbed water. This water can be partly removed at ambient temperature by vacuum, it significantly desorbs at 100°C and it is eventually eliminated at 150–200°C [73]. Desorption of water at 200°C is also reported in a paper by Xu *et al.* [132]. The elimination of water has been reported as being relatively easy [73]. However, it took 5 h of vacuum treatment at 500°C to get well resolved spectra of both–OH species on a zirconia surface [133,134]. The poor quality of some IR spectra [67,135] indicates the difficulties in removal of water from a zirconia surface.

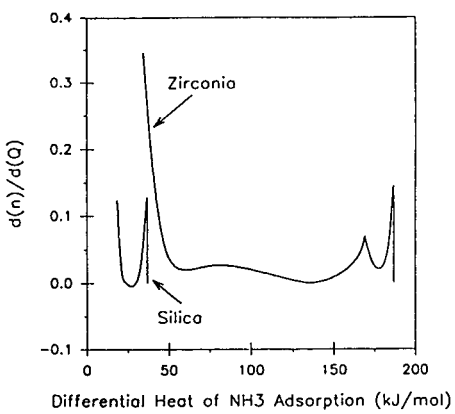

Fig. 29. Distribution of acid sites (by ammonia adsorption) on silica and zirconia (replotted from ref. 99).

When all physically adsorbed water is eliminated, IR spectra show two easily distinguished bands due to surface hydroxyls. The existence of two different surface hydroxyl groups has been confirmed in many IR studies [73,105,133]. The higher frequency band is attributed to single, isolated hydroxyl (type I; Fig. 31) while the lower frequency band is attributed to bridged hydroxyl (type II) *i.e.* hydroxyl the oxygen of which is coordinated to two zirconium atoms. These two types of hydroxyl groups are usually seen at 3770 and 3670 cm^{-1} [133]. However, Hertl [105] observed bands at 3700 and 3760 cm^{-1} for monoclinic zirconia but only one band

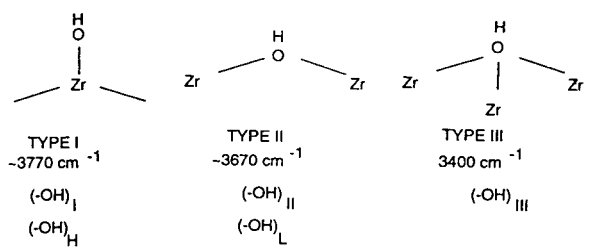

Fig. 31. Types of hydroxyl groups on zirconia surface.

at 3659 cm^{-1} for amorphous zirconia. Hydroxylated tetragonal and monoclinic zirconia show spectral differences that are associated with the crystal structure and are attributed to differences in cation–anion spacings and coordination of the surface species [67]. These two crystalline forms of zirconia were also investigated by Erkelens *et al.* [135] and clearly different IR spectra were observed.

In some papers a third lower frequency–OH band is reported and it has been ascribed [133] to the presence of bridged hydroxyl groups (type III) in which the hydroxyl oxygen is bonded to three zirconium atoms. The authors emphasized that a type III hydroxyl group cannot have proton acceptor properties since both lone pairs of oxygen are engaged in bonds to metal atoms. Tret'yakov *et al.* [136] reached the same conclusion. This was supported by the observation that only the higher frequency band disappeared upon adsorption of pyridine. Taking into account the fact that solid and dissolved zirconium compounds already have bridged hydroxyls [48–50,137–139] and the evident reactivity of the lower frequency–OH band [41,98,134] we find support for the assumption that two types of bridged hydroxyls can be present on a zirconia surface: these are denoted as hydroxyls of type II and type III according to Tsyganenko *et al.*'s classification [133]. (N.B. this agrees with Tsyganenko *et al.*'s suggestions [133]). Guglielminotti [64] observed three (–OH) bands (3780–3760; 3680–3660 and 3400 cm^{-1}) and assigned them as $(-OH)_I$, $(-OH)_{II}$ and $(-OH)_{III}$, respectively [64].

Mortera *et al.* [98] (who observed only two bands) believe that the lower frequency–OH $[(-OH)_L]$ observed at 3670–3680 cm^{-1} belongs to the $(-OH)_H$ species shifted downward by H-bonding with H_2O molecules. They observed a larger decrease in the $(-OH)_L$ band than in the $(-OH)_H$ band upon removal of water from the surface.

Fig. 32 shows the behavior of both (–OH) bands upon thermal treatment. As can be seen physically adsorbed water (see band at 1630 cm^{-1}) is easily removed from the surface [98]. However, Morterra *et al.*'s interpretation contradicts the conclusions of other groups

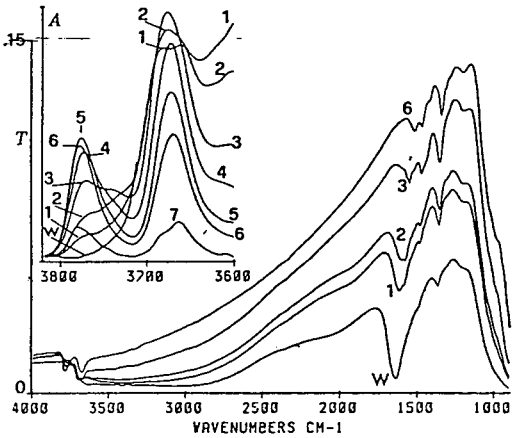

Fig. 32. IR spectrum of activation pattern of zirconia. Activation conditions: W = sample rehydrated and still in contact with 4 Torr of H_2O (1 Torr = 133.322 Pa); 1 = evacuation 5 min at 300 K; 2 = evacuation 30 min at 300 K; 3 = 30 min at 410 K; 4 = 520 K; 5 = 600 K; 6 = 670 K; 7 = 770 K. From ref. 98.

[133,134,136]. According to Yamaguchi *et al.* [134] the assignment of the $(-OH)_L$ band to hydrogen bonded species is probably incorrect because this band is narrow and symmetrical. According to Lavalley *et al.* [43] some hydroxyls (of unspecified type) are involved in H-bonding. Bensitel *et al.* [41] have shown that the IR spectrum of zirconia contains two bands of ν(OH): 3775 and 3670 cm^{-1}. These bands are easily seen upon heating at 200°C under vacuum. Vacuum treatment at higher temperatures leads to a gradual decrease in the intensity of the lower frequency band while the 3775 cm^{-1} band does not decrease as much. Both bands disappear at *ca.* 600°C. This is in agreement with the observations of Morterra *et al.* [98].

3.2.1.1. Interactions of hydroxyl groups with alcohols. Much attention has been paid to the interactions of alcohols with zirconia [37,38,41, 92,105,134,247] (Fig. 33). Sheifain and Makovskaya [247] investigated the role of several intermicellar liquids on the porous structure of zirconia. They found that the longer the alkyl

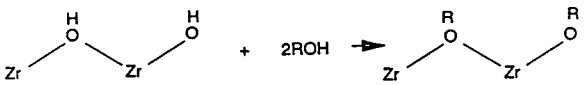

Fig. 33. Reaction of zirconia hydroxyl groups with alcohols.

chain of the alcohol the higher were the pore volume, the surface area and the mean pore diameter. Alcohol molecules form alkoxy groups on the surface of primary zirconia particles and consequently prevent (to some degree) the collapse of the porous structure of the hydrous zirconia upon formation of the xerogel [37]. In other words, alkoxy groups prevent formation of new Zr–O–Zr bonds during ageing. This should result in an increase in the mean pore diameter.

Also, washing ZrO_2 with pure ethanol after precipitation affects the properties of the calcined zirconia. The surface area, pore volume and pore radii increased significantly on washing with EtOH [37]. The BET isotherm for ethanol washed material also confirmed improvements in the pore shape. The isotherm is type IV with a H1 hysteresis loop [37,140].

Alcohols form alkoxides species with both types of hydroxyls although only the higher frequency species react with CO_2. The two types of alkoxy species were said to correspond to monodentate and bridged hydroxyls [41]. This is shown in Fig. 32.

Hertl [105] noticed that hydroxyl groups of both monoclinic and tetragonal zirconia react with alcohols but the hydroxyl groups of amorphous zirconia do not. Water can displace the –OR species [105]. On the basis of their reactivity with 2-propanol Yamaguchi *et al.* [134] state that the $(-OH)_H$ species are more reactive than $(-OH)_L$ hydroxyls. Deuteration experiments also support the hypothesis that the higher frequency band is the more reactive species [105,134].

3.2.1.2. Acidity of the surface hydroxyls. Tret'yakov and Filimonov [141] measured the Brönsted acidity of zirconia hydroxyls by applying the method of Hair and Hertl [142]. This method is based on the measurement of the dependence of $\Delta\nu_{OH}$ shift upon adsorption of benzene. According to them, the various–OH groups (single, bridged) present on an oxide surface have different acidities. The acidity is said to depend on the crystalline structure of the oxide. This agrees well with Tanabe *et al.*'s [143,144] hypothesis concerning the acidity of mixed oxides where coordination of both metals and various oxygens play a role in the development of surface acidity. The case of TiO_2 is particularly relevant, two different crystalline structures of TiO_2 (rutile, anatase) lead to two different surface acidities. As shown in Table 5 the pK_a of an anatase hydroxyl group has been spectroscopically determined to be 0.5–2.0. The pK_a value for rutile's hydroxyl group is 6.5 [141]. Similarly different acidities can be expected on the surfaces of monoclinic, tetragonal and amorphous zirconias. These were observed by Hertl [105]. In Table 5 $\Delta\nu_{OH}$ values for several oxides are compared and the relevant pK_a values are given.

The data shown in Table 5 clearly indicate the very weak acidity of zirconia's hydroxyl groups. This is also confirmed by the catalytic activity of zirconia in aldol addition reactions of acetone [146,147] where the reaction is said to take place only on basic hydroxyl groups and not on surface O^{2-} ions.

TABLE 5

$\Delta\nu_{OH}$ VALUES AND pK_a OF THE MOST COMMON OXIDES [141]

Oxide	ν_{OH} (cm^{-1})	$\Delta\nu_{OH}$ (cm^{-1})	pK_a
γ-Al_2O_3	3710	110	8.5 [145]
SiO_2	3750	120 (90)[a]	7.0 [142]
TiO_2 (anatase)	3725	190	0.5–2.0
TiO_2 (rutile)	3735	130	6.5
ZrO_2 $(-OH)_I$	3770	90 (65)[a]	10.5; 10.7[b]/11.0[a]
ZrO_2 $(-OH)_{II}$	3670	65 (47)[a]	12.8[b]/13.0[a]

[a] $\Delta\nu_{OH}$ or pK_a from deuterated hydroxyls.
[b] Calculated from data of refs. 141 and 142.

TABLE 6

ACIDITY OF ZIRCONIA SURFACE BY AN INDICATOR METHOD

The data in the table give the concentration of acidic sites (mmol/g) having an acidity higher than the pK_a given to the right but less than that directly above the entry. 0 and ± = detected but not quantified; − = not detected; + = detected.

Ref.	pK_a of zirconia surface species									
	+9.3	+7.2	+6.8	+4.8	+4.0	+3.3	+1.5	−3.0	−5.6	−8.2
148				−	0.28	0.06	0.06	0	−	−
149	0.36	−	−	−	0.29	0	0	0		
150			<0.19	±	−	−	−	−		
151	−	+	−	−	−	−	−	−	−	−

The acidity of zirconia surface was also estimated by an indicator method. The results are given in Table 6.

As seen in Table 6 it is very difficult to get reproducible surface properties. In other paper [143] the same group reports on a distribution of basic sites on a zirconia surface. Acidic sites were not detected.

Generally, however, zirconia surfaces are slightly basic. The overall concentration of the sites calculated for a sample of ZrO_2 [148] is 5.56 μmol/m^2. This is the only sample which confirms the existence of adsorption centers with $pK_a > 9.3$ which supports the observations of Tret'yakov and Filimonov [141] shown in Table 5. The values taken from ref. 149 can be recalculated to give 6.05 μmol/m^2 of sites with $pK_a =$ 4.0 and 7.51 μmol/m^2 of sites with $pK_a > 9.1$.

The higher reactivity of isolated hydroxyl groups was also observed by Tanabe and co-workers [1,134]. The isolated hydroxyl groups were selectively and irreversibly chlorinated (probably —as no adsorption product of chloroform was detected) by $CHCl_3$ while the bridged hydroxyl groups were not. Similar chlorination results were observed with CCl_4 [152]. This process was most likely responsible for the lack of elution of chloroform, dichloromethane and carbon tetrachloride in gas chromatography on zirconia particles [245]. It should be mentioned that the reaction with $CHCl_3$ changes considerably the properties (catalytic activity, basicity) of zirconia [154].

Both–OH species are completely eliminated at about 600°C [41,73] or, alternatively, according to Tret'akov *et al.* [136] at 750°C. Upon adsorption of water the higher frequency–OH band disappears. This supports the assumption that the free hydroxyls are engaged in H-bonding with water molecules [136]. On a dehydroxylated surface, both species (isolated and bridged) can interact with adsorbed molecules. This indicates that they are not H-bonded but are free [136]. However, according to Hertl [105], hydroxyls on tetragonal and amorphous phases are at least partly engaged in mutual H-bonding.

3.2.1.3. Elimination of coordinatively bonded water. Elimination of water (coordinatively bonded) and the condensation of hydroxyls leads to the development of Lewis surface acidity which first appears after activation at $T \geqslant 130$°C [73].

Rehydration of the zirconia surface proceeds by dissociative adsorption of water molecules. The heat of adsorption for this process is *ca.* 180 kJ/mol [73], which is in the range for dissociative adsorption of water (250–150 kJ/mol [153,246]). Holmes and co-workers [67,74] also indicated that a considerable part of the interaction of water with dehydrated zirconia is due to a chemical process with a very high ΔH value. Intermediate values correspond to irreversible molecular adsorption at Zr^{4+}_{cus} sites (cus = coordinatively unsaturated site) ($120 < \Delta H < 90$ kJ/mol) and to H-bonded H_20 molecules in the first hydrated layer ($90 < \Delta H < 50$ kJ/mol) [73,246]. Next is the physical adsorption of water with a heat of adsorption of *ca.* 44 kJ/mol (heat

of liquefaction). The ZrO_2 surface can adsorb about 6.6 μmol H_2O/m^2 but only about 55% of that is adsorbed irreversibly (at room temperature). However only 2.4 μmol H_2O/m^2 are needed to completely eliminate all adsorption of CO. (Note: CO is commonly used as an indicator of Lewis acid sites.) The number of Lewis acid centers revealed by CO adsorption is about 0.65 μmol/m^2 [73,153]. This means that four molecules of water are necessary to block one CO adsorption center. The dehydration process involves, from the very beginning, some σ-coordination of undissociated water molecules irreversibly held at room temperatures [153]. It must be emphasized that the process of rehydration of a zirconia surface is very different from the process of dehydration [153,155]. The differences between dehydration and rehydration are shown in dehydration and rehydration IR spectra (Figs. 34 and 35).

The very complex nature of zirconia rehydration was also noted by Holmes *et al.* [94]. According to them, zirconia irreversibly binds 11.3 μmol H_2O/m^2 at 25°C. At 300 and 400°C zirconia adsorbs 1.35 mg H_2O/g, which is equal to 6 μmol OH/m^2. At these temperatures, however, zirconia is not fully dehydroxylated and the surface concentration of hydroxyls may be higher than the numbers reported. Orio *et al.* [73] have shown that the surface Lewis acidity develops by removal of hydroxyls and not by removal of water from the surface. This is illustrated in Fig. 36.

All of the discrepancies between various observations can probably be explained by the use of different zirconias, with varying degrees of crystallinity, various contents of tetragonal/monoclinic phase resulting from various methods of synthesis and different thermal histories. This, however, indicates a need for a well defined material.

3.2.2. Carbon dioxide adsorption on the zirconia surface

Zirconia is known to form carbonate complexes with carbon dioxide upon exposure to ambient atmosphere. These complexes are very strong and thermally stable. Morterra *et al.* [98] reported that all commercially available zirconias were heavily loaded with carbonates, not only at the surface but also in bulk, due to CO_2 molecules that are trapped during the sintering process. Small amounts of such carbonates can even resist thermal treatment at 400°C [98] or 300°C [58]. Guglielminotti [64] could not eliminate many of the IR bands between 1600 and 1000 cm^{-1} even

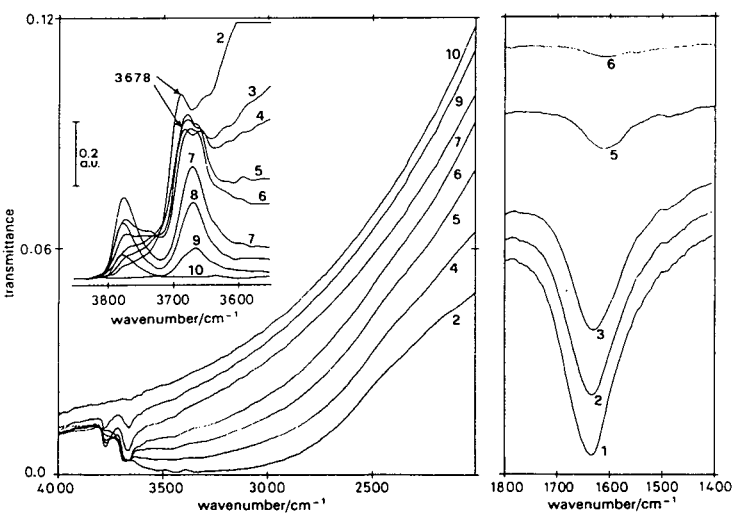

Fig. 34. IR spectra of the dehydration pattern of zirconia in the ν_{OH} and δ_{HOH} spectral regions. Conditions: 1 = in equilibrium with 3 Torr H_2O; 2–4 = evacuated at room temperature for 2, 15 and 75 min, respectively; 5–10 = activated at 100, 200, 300, 400, 500 and 600°C, respectively. From ref. 155.

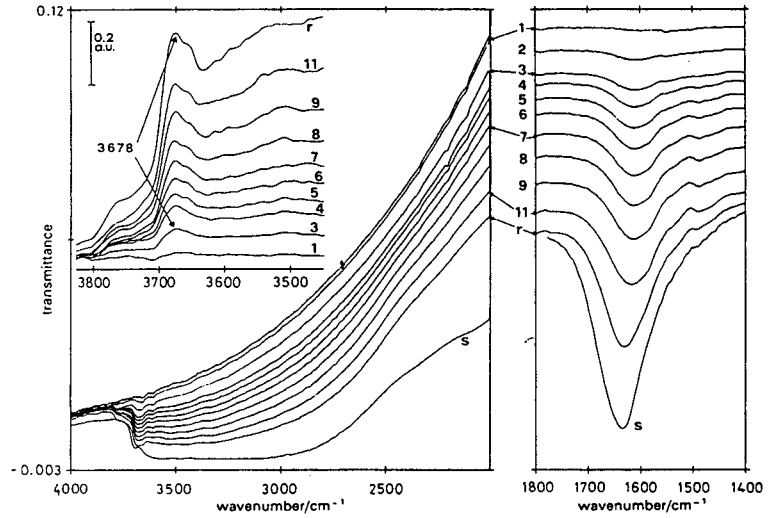

Fig. 35. IR spectra of the dehydration pattern of zirconia in the $\nu_{OH}$and δ_{HOH} spectral regions. Curves: 1–11 = after admittance of successively small doses of water vapor (equilibrium $p_{H_2O} = 0$ up to curve 9, and then $< 10^{-1}$ Torr); s = saturated with H_2O and still in equilibrium with 4 Torr H_2O; r = as in curve s after evacuation at room temperature for 110 min. From ref. 155.

by treatment at 550°C. Xu *et al.* [132] applied thermal treatment at 600°C for 3 h to remove carbonates from the surface of zirconia. Formation of carbonates was also noted for zirconia samples in equilibrium with water [98]. The

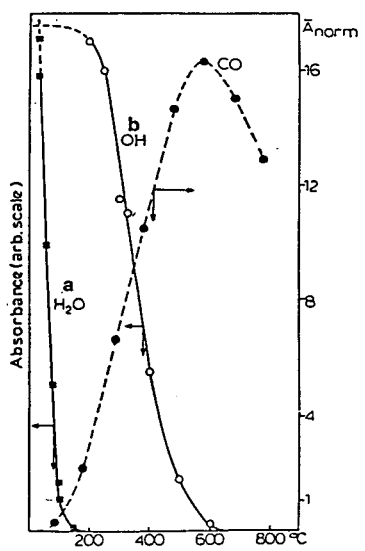

Fig. 36. Development of Lewis acidity by thermal removal of hydroxyls from zirconia surface. a = Absorbance of coordinated molecular water, b = absorbance of $(-OH)_H$ group, CO = absorbance of adsorbed CO. Reprinted from ref. 73.

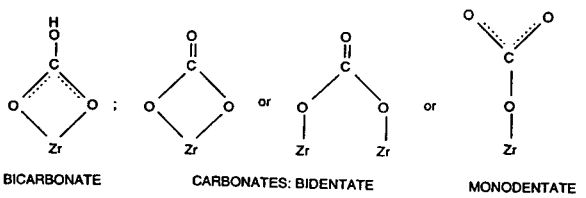

Fig. 37. Carbonate species on zirconia surface.

various carbonate species that exist on a zirconia surface are depicted in Fig. 37.

The literature suggests that carbon dioxide can chemisorb on the zirconia surface in two ways: (1) at basic sites $>B$: CO_2 (Fig. 38) and (2) at acidic sites $>A$: $O=C=O$ (Fig. 39).

This property of zirconia is very important for

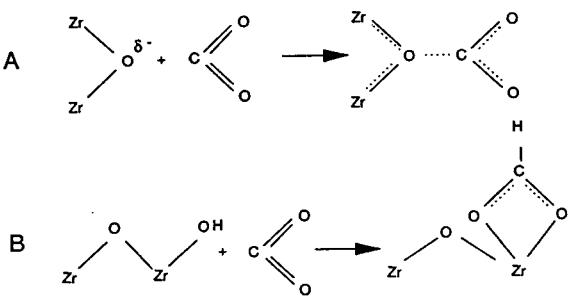

Fig. 38. Adsorption of carbon dioxide at basic sites.

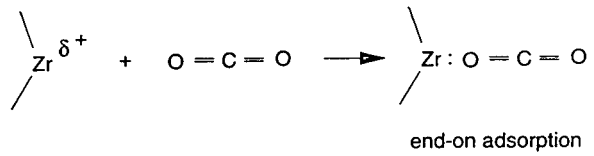

Fig. 39. Adsorption of CO_2 at Lewis acid site (end-on adsorption).

chromatography. Mobile phases must be free of CO_2 as reported by Rigney [243] and Blackwell and Carr [16–18]. The affinity of a zirconia surface for carbon dioxide and carbonates extends also to carboxylic acids which are strongly retained by the surface.

In fact CO_2 is often used in catalysis studies as an indicator of basic sites on the catalyst's surface [156]. The end-on surface adsorption of CO_2 can be used as a sensitive probe of Lewis acid sites [157]. Carbon dioxide linearly chemisorbs on a zirconia surface and gives an IR band located at 2343 cm^{-1} which moves to higher frequencies for samples activated at higher temperatures [157]. If water is present in the system, the end-on coordination does not take place [158]. Adsorption of carbon dioxide was studied in details by Morterra and co-workers [98,153,157,158]. They have shown that three kinds of Lewis acid centers on the zirconia surface are capable of linearly chemisorbing CO_2. This heterogeneity of Zr^{4+} was also confirmed by Guglielminotti [64].

The formation of carbonates upon adsorption of carbon dioxide is thought to occur on the basic sites. However, the mechanism of the hydrogencarbonate formation proposed by Morterra and Orio [158] involves a Lewis acid site

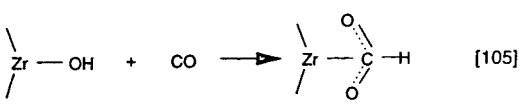

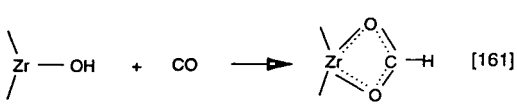

Fig. 40. Formation of formates on zirconia surface upon adsorption of carbon monoxide.

(according to them, a cation–anion pair Zr^{+}–OH^{-}). The hydrogencarbonates which form at the surface of highly hydrated zirconia are easily eliminated *in vacuo* at temperatures 100–150°C [155]. The desorption of bidentates gradually frees the coordinatively unsaturated surface sites whereas monodentates still present after evacuation at 300°C have almost no effect at all on adsorption of CO (*i.e.* they do not block Lewis acid sites) [155]. The papers of Morterra and co-workers do not give quantitative information on adsorption. Tanabe and co-workers [1,154] reported that 2.5–4 μmol CO_2/m^2 adsorbed on a zirconia surface, a similar value was observed by Wang *et al.* [149]. These results are used as a measure of the basicity of a zirconia surface [1,149,154]. In view of the papers by Morterra and co-workers, these results must reflect the concentrations of both acidic and basic sites. End-on adsorbed CO_2 can be almost entirely removed by room temperature vacuum treatment [64,158]. However, some end-on adsorbed CO_2 can withstand this treatment [158]. Traces of linearly adsorbed CO_2 after treatment at 100°C under vacuum are evident by IR spectroscopy [159].

Adsorption of carbon dioxide generates many carbonate species on the zirconia surface. It is again worth noting that there are substantial differences between monoclinic, tetragonal and amorphous zirconia [105]. CO_2 adsorption also proceeds on zirconium alkoxide surfaces to form methyl carbonates [41]. A mechanism for this reaction was proposed by Tsyganenko and Trusov [160]. Reaction of carbon dioxide with a zirconia surface were also studied by others [136,104,159,161]. CO_2 also adsorbs on TiO_2 surface; however, the adsorption seems to be much weaker than that on zirconia [162].

3.2.3. Carbon monoxide adsorption

CO interacts with exposed coordinatively unsaturated surface cations via σ-coordination. This process is used for characterizing the surface Lewis acidity [153]. According to Morterra and co-workers [98,153,163] there are two kinds of Lewis acid sites on a zirconia surface. These sites were described as two classes of Zr^{4+} ions, one likely belonging to flat (low index) faces and

the other exposed on high index planes. CO adsorption give rise to two closely overlapping IR bands located at 2182 and 2192 cm^{-1}. The complex nature of the end-on adsorption of CO on zirconia was also noticed by Guglielminotti [64]. The chemisorbed CO can be easily removed by vacuum treatment at room temperature [64].

Hertl [105] observed a substantial difference in the adsorption of CO on amorphous, tetragonal and monoclinic zirconias. The tetragonal and monoclinic forms were able to make formates upon adsorption of CO while no formates were detected on amorphous zirconia (Fig. 41).

Kondo *et al.* [159] observed a terminal CO band at 2193 cm^{-1}. Formate bands were also noted by He and Ekerdt [104] upon adsorption of CO on low surface area, monoclinic zirconia. Silver *et al.* [248] found that the adsorption of CO on zirconia depends on the time and temperature of thermal treatment. The surface concentrations of adsorbed CO were in the range 0.51–3.19 $\mu mol/m^2$.

Zr^{3+} surface centers were detected on zirconia surfaces by EPR and their existence was confirmed by IR [64,164]. Previously the signals were ascribed to Zr^{3+} ions located in the bulk of the material [165].

3.2.4. *Bases: ammonia and pyridine*

Ammonia and pyridine are often use as adsorbates to detect acid adsorption sites on surfaces.

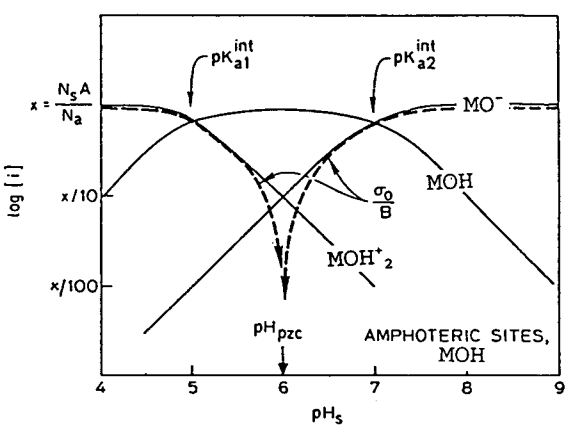

Fig. 41. Variation of charged and uncharged species concentration with the surface pH (pH_s) (after ref. 178).

Adsorption of ammonia on the oxide surface can be very complex since NH_3 can be retained on the surface in many ways: (i) through hydrogen bonding of the surface hydroxyl bond to nitrogen of ammonia, (ii) formation of NH_4^+ ion, (iii) hydrogen bonding via one of the NH_3 hydrogen atoms to a surface oxygen (or oxygen of a surface hydroxyl), (iv) coordination to an electron-deficient metal atom (Lewis acid site) and (v) dissociative adsorption with formation of M–NH_2 and a surface hydroxyl. All of these features of NH_3 adsorption are discussed in detail elsewhere [66,99].

Adsorption of ammonia on ZrO_2 was first examined by Tsyganenko *et al.* [66]. They noted that the 1190 cm^{-1} band (δ_s vibration) shifts to 1230 cm^{-1} upon desorption of ammonia. This indicated the presence of Lewis acid sites of various strengths on the surface. They also noticed that the position of the band depends on the method of sample preparation which is related to the polymorphous properties of zirconia. Dissociative adsorption of NH_3 was observed, but the formation of NH_4^+ was not. Similar surface behavior was noted by Yamaguchi *et al.* [134]. Temperature programmed desorption (TPD) profiles of NH_3 indicate that desorption of NH_3 molecules proceeds between room temperature and 500°C with a maximum at about 200°C [71]. Dual adsorption experiments carried out with CO_2 and NH_3 led to the conclusion that although independent sites are responsible for the adsorption of CO_2 and NH_3 some sites are in close proximity [71].

Hertl [105] observed that NH_3 adsorbs on Lewis acid sites on all three forms (monoclinic, tetragonal and amorphous). Very weak bands due to the presence of NH_4^+ were also observed. Dissociative adsorption of NH_3 was observed on tetragonal zirconia. Hertl also determined the amounts of ammonia adsorbed on the surface of monoclinic (1.15 $\mu mol/m^2$) and tetragonal (0.76 $\mu mol/m^2$) zirconia and considered the numbers as a measure of the "Lewis acid site concentration".

The heterogeneity of the Lewis acid sites was also confirmed by Auroux and Gervasini [99,166] who measured the differential heats of adsorp-

tion of ammonia. Two kinds of strong adsorption sites were found with strengths of over 150 kJ/mol. The total amount of NH_3 adsorbed on the surface was 5 μmol NH_3/m^2 [166] which is considerably higher than the values found by Hertl [105].

Pyridine adsorption has also been used to study the acidity of metal oxides. The complexity of its adsorption is discussed by Morterra and Cerrato [167]. As with NH_3, pyridine may be H-bonded to surface hydroxyls, coordinatively complexed with Lewis sites or may form pyridinium PyH^+ ion when it interacts with Brönsted acid sites. Tret'yakov *et al.* [136] noticed that pyridine interacts with $(-OH)_H$ species but not with $(-OH)_L$. Bands due to pyridine adsorbed on Lewis sites were also found and their positions indicated that the strength of the sites is lower than that of Al_2O_3 and TiO_2. The maximum amount of adsorbed pyridine on ZrO_2 activated at 400°C found by Nakano *et al.* [154] was very low: 0.04 μmol/m^2. Bensitel *et al.* [42] in accord with ref. 136 did not observe pyridinium ion on a ZrO_2 surface. Their quantitative results are much higher than the values given by Nakano *et al.* [154]. They found that 1.0, 0.5 and 0.13 μmol Py/m^2 adsorbed after evacuation at 100, 200 and 300°C, respectively. Hertl [105], in addition to the bands due to coordinatively adsorbed pyridine, also observed a small band of PyH^+ which indicated the presence of Brönsted acid sites. The heterogeneity of Lewis sites was also noticed by Morterra and Cerrato [167]. Pyridine adsorbs from cyclohexane solution to give a surface concentration of <1 μmol/m^2. Under the same conditions benzylamine adsorbs to give a coverage of more than 3 μmol/m^2 [108].

3.3. Surface concentration of acid and base adsorption sites in gas–solid systems

Generally the above gas–solid adsorption studies give the impression that only a rather small fraction of the zirconium ions exposed on the surface exhibit Lewis acid properties. This may be due to the use of very soft Lewis bases in these studies. These species are only able to adsorb on the strongest Lewis acid sites. Particularly low surface concentrations of Lewis acid sites are observed when CO is used as the probe. But even when stronger Lewis bases such as pyridine and ammonia are used the number of Lewis acid sites detected is still very low (Table 7). The results are not fully comparable since zirconias with various crystallinities were used, various thermal histories and various temperatures of measurement.

The exchange capacity of hydrous zirconia is 1–2 mequiv./g of ZrO_2. This value corresponds to 1–2 hydroxyl groups on eight zirconium atoms. However no surface area was provided [170].

Basicity is assessed mainly by the extent of CO_2 adsorption, however, X-ray photoelectron spectroscopy and catalytic activity in the selective dehydration of 2-alcohols to 1-olefins have also been proposed as measures of the basicity of surface oxygen atoms [143,171]. The O1s binding energy in the range 529–530.5 eV was said to be characteristic of basic surface oxygen. O1s binding energy for zirconia is reported to be 529.8 eV [172,173]. In contrast O1s binding energies for alumina and silica are 531.8 and 533.1 eV, respectively [171]. Basic oxides selectively dehydrate 2-alcohols to 1-olefins. Zirconia shows a selectivity of over 90% in such reaction while alumina produces mainly 2-olefins [1].

There are also questions of a more general nature. For example, NH_3 has a tendency to dissociate and adsorb on both acidic and basic sites [143]. According to Morterra's mechanism of hydrogencarbonate formation upon CO_2 adsorption it proceeds on acidic (coordinatively unsaturated site) Lewis sites, however, basic hydroxyl groups take part in the reaction. CO_2 is used as a basic site probe but the mechanism of carbonate species formation is not fully understood. In contrast, in liquid–solid systems, about 12 μmol/m^2 of F^- (which is very hard Lewis base) adsorb at pH 6.1 [16]. This indicates that virtually all zirconium atoms on the surface are Lewis acid sites. In liquid–solid systems (with non-polar solvents) benzoic acid can be used to detect basic sites. The concentration of the basic sites on a zirconia surface determined with a cyclohexane solution of benzoic acid was over 5 μmol/m^2 [108]. However, it is likely that the

TABLE 7

EXPERIMENTAL SURFACE CONCENTRATIONS OF ACID AND BASE SITES IN GAS–SOLID SYSTEMS

Adsorbate	Temperature of adsorption of adsorbate (°C)	Concentration of acid sites (μmol/m^2)	Ref.
Acid sites			
Pyridine	100	0.02–0.04	1, 154
Pyridine	100	1.0	42
	200	0.5	
	300	0.13	
NH_3	150	1.26 (monoclinic)	105
	150	0.76 (tetragonal)	
NH_3	22	3	149
NH_3	23	5	166
SO_3	110	2.8–7.22	248
CO	500	0.51–3.19	
CO	room temp.	1.26 (treated at 600°C)	168
	room temp.	0.93 (treated at 800°C)	
CO		1.72	153
CO	liquid N_2	3.00	169
	liquid N_2	3.84	
	liquid N_2	9.5	
Basic sites			
CO_2	100	3–4	1
CO_2	22	4	149
CO_2	23	0.85	166
Triphenyl nitroxide	100	$\approx$4 (for zirconia treated at 700°C)	1, 154

probe molecule is too bulky to detect all basic species on the surface. The Lewis acid site concentration has been estimated in liquid–solid system by an adsorption of benzylamine and pyridine. The results were over 3 μmol/m^2 and less than 1 μmol/m^2 respectively [108].

Lewis acids and bases on the surface are charged species. In gas–solid systems the species seem to be very unstable. In contrast in liquid–solid systems charged surfaces produce electrical double layers which in fact protect (stabilize) the surface charges.

The surface concentration of Lewis acid sites increase with the time and the temperature of the thermal treatment. The structures of the adsorption sites on the zirconia surface are still not very well characterized. The literature does not even provide such important data as the surface concentration of hydroxyl groups. Based on their pK_a [141,148–151] and their catalytic activity [146,147] the surface hydroxyls were found to be basic adsorption sites. The chemical (adsorption) properties also appear to be highly dependent on the crystal form of zirconia, its method of preparation, the sample's history etc. This problem is discussed by Bolis *et al.* [168] in relation not only to two ZrO_2 samples but also various samples of SiO_2 and SiC. According to them "the surface chemistry of solids having the same (nominal) composition but different origin

may be very different". In view of the previous sections this seems to be particularly true of zirconia.

3.4. Zirconia as a stationary phase in gas chromatography

There are very few papers on the use of zirconia in gas chromatography. The heats of adsorption of several hydrocarbons were determined by Lapteva *et al.* [174]. They used precipitated zirconia after thermal treatment at 900°C. However, the material was microporous. Differential heats of adsorption of pentane, hexane and heptane were reported. Djordjević *et al.* [245] used monoclinic zirconia in gas chromatography. They noticed that zirconia reacts with chlorine containing C_1 compounds. Other chloro derivatives were relatively easily eluted from the column. Specific interactions were said to increase upon increasing the temperature at which the zirconia was pretreated. Lapteva *et al.* [175] studied the adsorption of hydrocarbons on zirconia particles but the zirconia used in that paper was poorly characterized. The reported heats of adsorption for hydrocarbons differs from those reported earlier by Djordjević *et al.* [245].

Gas chromatography can be used to characterize the zirconia surface. The utility of zirconia as a column packing for gas chromatography is minor due to its high chemical and catalytic activity.

3.5. Adsorption: liquid–solid interface

3.5.1. Introduction

We now turn to liquid–solid zirconia interfaces. In liquid–solid systems (most of the systems examined were limited to water) zirconia surfaces contain an adsorbed water layer. As we have already seen from gas–solid studies, zirconia surfaces contain several types of adsorption sites. The coordination sites of zirconium are occupied by water, hydroxyl ions, and hydronium ions, depending upon the pH. These sites are electropositive and exhibit properties analogous to the coordination chemistry of transition metal ions in solution. The sites can form coordination complexes with a number of Lewis bases, particularly hard bases such as polyoxy anions (borate, sulfate, carboxylate and phosphate [72,176,177]) and fluoride [16,17,87]. Of course, a great deal of heterogeneity can exist in all of these sites because of the various geometries, surface defects and bonding types. Generally the same properties should be observed in liquid systems as seen in gas–solid interfaces. One of the striking differences (between gas–solid and liquid–solid systems) is that none of the liquid–solid systems can distinguish between the two (or even three) kinds of hydroxyls present on the surface. Another, obvious difference is the ability of zirconia to exchange ions. The surface of oxides at liquid–solid interface can be investigated by potentiometric titration, microelectrophoresis and colloid stability studies as well as by liquid chromatography. Liquid–solid equilibria differ from gas–solid equilibria in that the surface maybe charged. There are several methods of observing the accumulation of charge on the surface. These include: electrokinetic methods, conductometric titration of solids and examination of the electrical double layer of colloids. All of these methods are described by James and Parks [178]. Several catalysts were examined by Kita *et al.* [76] at the liquid–solid interface. Satisfactory correlations (between gas–solid and liquid–solid properties) were found for almost all of the oxides investigated. For zirconia, however, the results did not correlate well with those for the gas–solid interface. The amount of acid sites determined (by the titration with KOH to pH 10.5) on a ZrO_2 surface was equal to 12.1 μmol/m^2. As they considered all species whose pK_a values are less than 10.5 as acids, these results correlated quite well with those of Wang *et al.* [149] (see Table 6) where the total amount of acid was determined as 13.5 μmol/m^2. However, the distribution of acidity is quite different. In ref. 76 the acid functionality had the property: $3 < pK_a < 5$–6. However, it must be mentioned that the $pH_{pzc} = 2.7$ determined by Kita *et al.* [76] is very different from the average value of $pH_{pzc} = 6$–7 (see Table 8). According to Tanabe [179], in the presence of moisture, Lewis acids convert to Brönsted acids,

TABLE 8

VALUES OF pH FOR pzc OR iep FOR ZIRCONIA PARTICLES

pH (pzc or iep)	Method	Ref.
6.7	maximum flocculation rate	182
6–6.6	titration (5 samples)	183
4	electroosmosis	184
6.7	mobilities	185
6.7	titration	185
10	ion exchange	26,186
5.5–6.2	addition	187
12.07	calculated	188
10–11	no method specified	188
6.8	mobilities	189
6.4	titration	107
6.5	mobilities	107
6.0	addition	107
6.05	?	190
6.7	mobilities	59
8.2	titration	68
6.6	streaming potential measurements	103
8.2	commercial data	108
6.7	electrophoretic mobility	191
2.7	titration	76
4.0	titration	111
4.0	adsorption	192
5.0	mobility	110
7.5	titration	193

but hydroxyls on zirconia surfaces do not show any Brönsted acidity. Only in Hertl's work [105] were small amounts of NH_4^+ and PyH^+ ions noticed. We believe that the zirconia hydroxyls show very weak Brönsted acidity and also are fairly weak bases. The quantity of the hydroxyls on the zirconia surface was determined, by titration with Zn^{2+} [180], as 21.95 μmol/m^2 [76]. This is very close to the results of Randon *et al.* [75] obtained by a different method. A definite difference between gas–solid and liquid–solid interfaces is the lack of any basic site activity in the water–zirconia systems [76]. However, with non-polar solvents and benzoic acid as the probe over 5 μmol of basic sites/m^2 were detected [108].

As Davis *et al.* [181] pointed out, no comprehensive model exists which can simultaneously predict adsorption density and other surface properties. This is why liquid–solid systems require the number of active sites on the surface to be determined by other, independent methods. Given the site density, differences between the types of hydroxyls (*i.e.* their pK_a values) can be calculated. The electrical double layer model was derived for non-porous, crystalline oxides. Thus some monoclinic zirconia powders could fulfill these requirements.

The phenomena observed in water–zirconia systems can be classified as ion and/or ligand exchange. Zirconia is known as an ion exchanger having both cation- and ion-exchange ability due to its amphoteric nature [34,36]. The cross-over coincides with the point of zero charge. It is thus of obvious interest to know the surface equilibria which govern the ion and ligand exchange as well as the exact value of the point of zero charge or the value of pH at which the ion electrophoretic mobility (iep) is equal to zero. The adsorption properties of zirconia particles (in liquid–solid systems) will thus depend on the pH of the environment.

3.5.2. Point of zero charge

The pzc and iep values can be measured by various methods [107] in many electrolytes provided that there is no specific adsorption of the ions on the surface [178]. In simple electrolyte systems (*e.g.* $NaNO_3$, KNO_3, $KClO_4$) no net specific adsorption occurs and the pH_{pzc} equals the pH_{iep} [181]. Davis *et al.* [181] pointed out that this is rather the case for "symmetrical specific adsorption" of the electrolyte cation and anion. Specific adsorption occurs if a binding mechanism, other than a coulombic one is significantly involved [72]. Regazzoni *et al.* [107], Randon *et al.* [75], Persin *et al.* [193] and Milonjić *et al.* [192] compared the pH_{pzc} values of zirconia from various sources. They vary from 2.7 to 12.07 although most of the values were found to be between 6 and 7. The data are collected in Table 8.

pH_{pzc} values can be influenced by the degree of hydration of the surface and by impurities [101]. Even very low quantities of structural (built in the oxide matrix) and adsorbed (on the surface) impurities can substantially change pH_{pzc} values. Variation in isoelectric points for

TABLE 9

VARIATION OF pH_{pzc} UPON HYDRATION

Oxide	pH_{pzc}	Hydrous oxide	pH_{pzc}	ΔpH_{pzc}	Ref.
Fe_2O_3	6.7	Fe_2O_3 (hydrous)	8.6	1.9	101
Al_2O_3	6.7	Al_2O_3 (hydrous)	9.2	2.5	101
TiO_2	4.7	TiO_2 (hydrous)	6.2	1.5	101
ZrO_2	8.2	ZrO_2 (hydrous)	6.8	− 1.4	65,102

oxides and hydrous oxides are compared in Table 9.

It is interesting to note that according to refs. 65 and 102 the pH_{pzc} of zirconia changes in the opposite direction upon aging when compared to the behavior of other oxides. A gradual shift of the pH_{pzc} value from 8.2 to 6.8 for fresh and aged samples, respectively, was observed by Ardizzone and co-workers [65,102]. According to them [65] a partial dehydroxylation takes place at 800°C and a very slow rehydroxylation takes place in water to form a surface layer of $Zr(OH)_4$. However, as emphasized in section 3.2.1 treatment at 600°C is sufficient to remove water and all hydroxyls. The slow and very complex kinetics of rehydration were also observed by several authors [94,153]. According to Ardizzone and co-workers [68,102] the measured value of the point of zero charge is pH 6.5 which is characteristic of $Zr(OH)_4$. A similar suggestion was made by Blesa *et al.* [59]. The ZrO_2 surface becomes modified in water to give a gel-like coating only a few monolayers thick. If this hypothesis is true, structures resembling those of soluble $Zr(OH)_4$ tetramers [47,50] should exist on the zirconia surface. Then the surface would likely contain a population of geminal hydroxyls. This could be confirmed by ^{91}Zr cross-polarization magic angle spinning NMR [194]. This would also be in agreement with our hypothesis as to the presence of geminal hydroxyl sites on the zirconia surface (see section 3.2.1). Ardizzone *et al.* [68] reported that charge densities on zirconia treated at 200°C are much lower than those on materials fired at 800°C. However, the very high pore volumes of all materials investigated in that paper, except for that treated at 800°C zirconia, indicate a high degree of microporosity, which is likely to influence the equilibria during titration. Stumm *et al.* [72] emphasize that surface equilibria are attained very slowly and we usually observe only metastable states. This is even more likely in the case of microporous materials. This has also obvious implications for chromatography. Slow surface equilibria would be detrimental for chromatography. It is thus important to use zirconia particles without micropores (*i.e.* sintered at temperatures assuring the removal of micropores, see Figs. 10 and 11). This also implies that crystalline, monoclinic zirconia rather than the amorphous oxide should be used. Due to the dehydroxylation of the surface during sintering *it is necessary to rehydrate (or rehydroxylate) the surface by subsequently washing it with acid and base.*

Values of the surface charge density for the 800°C treated sample correlate well with that of a monoclinic, low surface area zirconia [107]. Regazzoni *et al.* [107] measured the pzc as pH 6.0–6.5 by three different methods. They also calculated values of pK_{a1}^{int} and pK_{a2}^{int} (see Table 10) in accordance with the Davis, James, Leckie (DJL) model [181] which is in good agreement with the data given by Amphlett *et al.* [26]. Regazzoni *et al.* [107] assumed that there are about 12 sites/ nm^2 on the zirconia surface (*i.e.* 20 $\mu mol/m^2$) but offered no experimental evidence. Randon *et al.* [191] calculated a surface concentration of sites (N_s) that can exchange protons and arrived at a value of $N_s = 14$ sites/nm^2 which is equal to 23.2 $\mu mol/m^2$ [75]. This number of sites would be possible but there would have to be one hydroxyl group on each surface zirconium atom and every bridging oxygen would have to be in the form of a bridging

TABLE 10

COMPARISON OF INTRISTIC IONIZATION CONSTANTS FOR ZIRCONIA AND OTHER OXIDE SURFACE HYDROXYL GROUPS

pK_{a1}^{int}	pK_{a2}^{int}	pH_{pzc} calc. from eqn. 1	pH_{pzc} experimental	Electrolyte	Ref.
ZrO_2					
4.2	8.6	6.4	6.4	KCl	107
4.8	10.4	7.6	7.5	water	193
4.3	9.3	6.8	7.5	NaCl	
6.2	8.3	7.25	6.7		
5.9	7.7	6.8	4.0	LiCl	192
5.8	7.2	6.5	4.0	NaCl	
5.8	6.8	6.3	4.0	KCl	
Al_2O_3					
7.89[a]	9.05	8.47	8.5	NaCl	178
8.50[b]	9.70	9.10	9.10	NaCl	
TiO_2					
5.41	6.38	5.90	6.00	$NaNO_3$	178
SiO_2					
1.34	4.6	3.00	3.00	KCl	178

[a] Data for γ-Al_2O_3.
[b] Data for α-Al_2O_3.

hydroxyl group. Milonjić *et al.* [192] also examined the interfacial properties of precipitated zirconia. This is the only paper which recognizes the diversity of hydroxyls on the ZrO_2 surface. They interpret pK_{a2I}^{int} and pK_{a2II}^{int} values (pK_{a1}^{int} and pK_{a2}^{int} values in Table 10) as the ionization constants of $(-OH)_I$ and $(-OH)_{II}$, respectively. However, these values were calculated assuming the total capacity of zirconia surface to be equal to 5 sites/nm^2 (*i.e.* 8.3 μmol/m^2) [192].

3.5.3. Surface equilibria

Yates *et al.* [195] proposed a site binding model for metal oxides and used it as the basis for explaining the differences between silica and most other oxides. The model assumes a very simplified picture of a porous oxide surface:

$$M\text{–}OH_2^+ \overset{K_{a1}^{int}}{\rightleftharpoons} M\text{–}OH \overset{K_{a2}^{int}}{\rightleftharpoons} M\text{–}O^-$$

where K_{a1}^{int} and K_{a2}^{int} are the intristic ionization constants.

Thus in the Yates model, H^+ and OH^- are the potential determining ions. The resulting surface charge depends on an excess of one type of charged site over the other and is a function of solution pH. The point of zero charge is the pH at which the number of positively charged species ($M\text{–}OH_2^+$) is equal to the number of negatively charged species ($M\text{–}O^-$) on the surface. As we can see the pH_{pzc} depends on the ionization reactions and it is related to the ionization constants by the equation [178]:

$$pH_{pzc} = 0.5(pK_{a1}^{int} + pK_{a2}^{int}) \quad (1)$$

Schematic illustration of the variation of charged species concentration with the pH_s for amphoteric surfaces is given in Fig. 41 [178].

Fig. 42 shows that: (i) at pH values between pK_{a1}^{int} and pK_{a2}^{int} the amount of undissociated hydroxyl groups is constant, (ii) the surface charge increase starting from the pH_{pzc} in both acidic and basic directions and (iii) above pK_{a1}^{int} and below pK_{a2}^{int} the surface hydroxyl groups are mainly in the ionized forms.

There have been many attempts to calculate

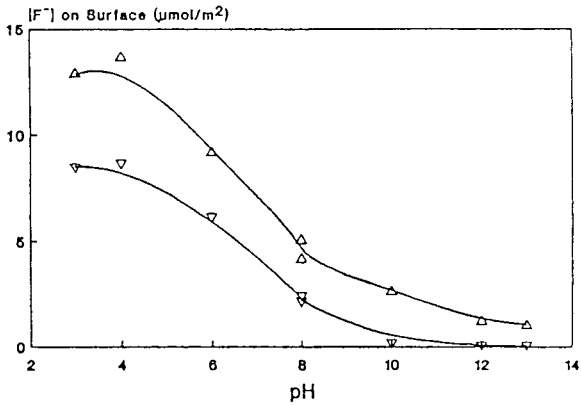

Fig. 42. Fluoride adsorption as a function of pH. △ = fluoride adsorption, ▽ = fluoride desorption at pH = 13. Buffers are all 0.1 *M* and contain 20 m*M* sodium fluoride except where noted. For pH = 3, 0.001 *M* HCl; pH = 4, acetate; pH = 6, MES; pH = 8, TAPS (top), TRIS (bottom); pH = 10, CAPS; pH = 12, 0.01 *M* NaOH; pH = 13, 0.1 *M* NaOH. From ref. 16.

the pK_{a1}^{int} and pK_{a2}^{int} values. There is also a very good correlation between the pH_{pzc} values calculated from eqn. 1 and those observed experimentally. This is shown in Table 10.

The practical meaning of the intristic ionization constants is that at $pH < pK_{a1}^{int}$ zirconia will act as a anion exchanger while at $pH > pK_{a2}^{int}$ zirconia will behave as a cation exchanger.

The intristic ionization and complexation constants of oxide surfaces were further investigated by Davies *et al.* [181] who modified the Yates model to include the formation of surface complexes. However, both of these theories, as we have pointed out above, require the number of adsorption sites from other, independent methods. Potentiometric titration can give some numbers [181], however, the results will depend on both the pH and the ionic strength of the solution during the measurement.

It is well known that cations and anions can adsorb specifically on the surface thus influencing the surface charge. In the case of simple electrolytes it is believed that there is no specific adsorption [178] or the adsorption of cations and anions is "symmetrical"[181]. Surface charge asymmetry may result when: (i) the inner layer capacitances of the interface for positively and negatively charged surfaces are different, (ii) the surface complexation strength of cation and anion are unequal or (iii) the valences of the cation and anion are unequal (*e.g.* 2:1 or 1:2 electrolytes).

These phenomena are caused by ion exchange. Hingstone *et al.* [196] have found that some anions can adsorb to a greater extent than would be predicted from their concentration when compared to non-specifically adsorbed anions. They also noted that: (i) adsorbed anions shift the pzc toward more acidic values (the surface becomes more acidic), (ii) this is due to displacement of hydroxyl ion from the inner Helmholtz layer —*i.e.* ligand exchange, (iii) specifically adsorbed anions cannot be desorbed by a solution of non-specifically adsorbed anions (at the same pH and ionic strength), (iv) to desorb specifically adsorbed anions it is necessary to make the charge on the surface more negative than the equilibrium value at which adsorption took place and (v) the same effect is accomplished by raising the pH thus increasing the adsorption of hydroxyl ion.

Stumm *et al.* [72] made similar observations and according to them the extent of adsorption (or surface coordination) will depend strongly on: (i) pH, (ii) the surface coordination constants, (iii) the surface charge, (iv) the type of the surface species (*i.e.* mono- or bidendate, protonated or deprotonated ligand etc.) and (v) the maximum amount of adsorption is likely to occur at about $pH = pK_{a\ HA}$ [72] in agreement with ref. 196. The dependencies listed by Stumm *et al.* [72] were confirmed in a study of the chromatography of benzoic acid derivatives on zirconia [176,177].

The study of these equilibria under static conditions is very difficult due to many limitations. Surface sites at edges, corners and faces are likely to posses different energies, not all surfaces sites are available due to geometric reasons and the addition of new charged groups influences the acidity of the remaining–OH groups [72]. (Similar phenomena are observed on gas–solid interfaces [1,197]).

The models of Hingstone *et al.* [196] and Stumm *et al.* [72] assume that a neutral surface site can be represented as MOH (M–metal atom of metal oxide) and ligand exchange proceeds between the OH^- and an anion. Regazzoni *et al.*

[198] argued that the metal oxide surface must contain chemisorbed (undissociated) water, the molecules of which also take part in ligand exchange. Although their discussion concerned the behavior of hematite it is most likely that the same is true of zirconia. To prove this we refer to the papers by Morterra and co-workers [73,153,155] concerning dehydration and rehydration of a zirconia surface (see section 3.2.1) where σ-coordination of water molecules at early stages of rehydration was proposed to explain the observed adsorption properties. As can be seen in Table 10 a silica surface is much more acidic and can behave as a cation exchanger. However, silica does not show any ligand-exchange behavior and it differs very much from the other oxides. Regazzoni and co-workers' hypothesis of ligand exchange of water molecules can explain the difference. The coordination number of a silicon atom in a silica matrix is low (4) and silicon never coordinates water molecules in its coordination sphere as do other oxides. This is probably why silica differs so much from other oxides. This would also mean that ligand exchange with coordinatively bonded water is more important than so far believed.

Based on the detailed theoretical and experimental work of Hingstone *et al.* [196], Yates *et al.* [195], Davis *et al.* [181] and Stumm *et al.* [72] and the papers of Regazzoni *et al.* concerning zirconia [107] and hematite [198] surfaces it is possible to write the most likely model for the ion- and ligand-exchange ability of zirconia. The following chemical equilibria have been used to describe the interaction of various species with the different sites on a zirconia surface [16]:

$$M(OH)(H_2O) + H^+ \rightleftharpoons M(H_2O)_2^+ \quad (2)$$

$$M(H_2O)_2^+ + Cl^- \rightleftharpoons M(H_2O)_2^+ \cdots Cl^- \quad (3)$$

$$M(OH)(H_2O) \rightleftharpoons M(OH)_2^- + H^+ \quad (4)$$

$$M(OH)_2^- + K^+ \rightleftharpoons M(OH)_2^- \cdots K^+ \quad (5)$$

$$M(OH)(H_2O) + L_1^- \rightleftharpoons M(H_2O)L_1 + OH^- \quad (6)$$

$$M(OH)(H_2O) + L_1^- \rightleftharpoons M(OH)L_1^- + H_2O \quad (7)$$

$$M(OH)L_1^- + L_2^- \rightleftharpoons M(OH)L_2^- + L_1^- \quad (8)$$

$$M(OH)(H_2O) + L_2^- \rightleftharpoons M(OH)L_2^- + H_2O \quad (9)$$

$$M(OH)(H_2O) + L_2^- \rightleftharpoons M(H_2O)L_2 + OH^- \quad (10)$$

where M represents the metal oxide metal and L_1 and L_2 represent a Lewis base present in the eluent and a Lewis base solute, respectively. Taken together, reactions 2 and 3 account for the presence of anion-exchange sites on the zirconia surface and the retention of non-coordinating anions (denoted $\cdots X^-$), such as chloride, nitrate and perchlorate. As the pH is increased, the anion-exchange capacity of the material decreases, as predicted by the shift to the left in process 2, and the retention of non-coordinating anions decreases. At higher pH values, processes 4 and 5 account for the presence of cation-exchange sites and the retention of non-coordinating cations (denoted $\cdots K^+$). Between these two pH limits the anion- and cation-exchange capacity of the surface varies in accord with the solution pH. Retention data suggest that the conversion from an anion exchanger at low pH to a cation exchanger at high pH occurs somewhere between pH 6 and 7, a finding consistent with the reported isoelectric point for zirconia (see Table 8). Due to the presence of coordinating Lewis acid sites on zirconia's surface, ligand-exchange processes play a role in retaining some solutes, specifically those which act as hard Lewis bases, as depicted in reactions 6–10. Processes 6 and 7 describe the modification of the surface sites which occurs when a Lewis base is present in the eluent. Processes 8–10 show the exchange of an eluent Lewis base (L_1^-) for a solute base (L_2^-). The contribution of H_2O and OH^- to ligand exchange will depend strongly on pH. At lower pH values processes 7, 8, 9 and 10 are possible. At high pH values the contribution of processes 6 and 10 to the overall ligand-exchange process is likely to be minimal as the $-OH^-$ ion is a very strong, hard Lewis base. However, we would like to emphasize the importance of coordinatively bonded water in ligand exchange. *Ligand exchange does not proceed on silica which does not contain σ-coordinated water.*

3.5.4. Borate adsorption

The predictions of Stumm *et al.* [72] were confirmed in studies of the pH dependence of the adsorption of fluoride and borate on zirconia. Fig. 42 [16] shows the effect of pH on adsorption of F^- while Fig. 43 [199] illustrates the effect on the adsorption of boric acid.

Both figures also confirm the statements of Hingstone *et al.* [196] and Stumm *et al.* [72] that the maximum adsorption is likely to occur at a $pH = pK_{a\ HA}$. Similar behavior was observed for the polymer–zirconia equilibria for polyacrylic acid adsorption [103]. Blackwell and Carr [177] have shown that the retention of benzoic acid derivatives at a given pH also depend on their pK_a values. Adsorption of boric acid on zirconia was characterized by electrokinetic measurements and potentiometric titration [199]. From the shifts in the pH_{pzc}, adsorption equilibrium constants have been derived using the site binding model [181]. Borate ion was assumed to form an ester bond with surface hydroxyl group. Calculated adsorption profile (amount adsorbed *vs.* pH) agrees well with earlier published maxima in the borate adsorption at pH *ca.* 9 on alumina [200]. The maximum amount of borate adsorption should take place at pH 9 and the surface concentration was equal to *ca.* 1 μmol/m^2 for 0.001 *M* H_3BO_3 in 0.1 *M* KNO_3. The affinity of zirconia for boric acid increases with an increase of pH (up to pH 9) but the affinity toward F^- decreases. Adsorption of boric acid from a 1 *M* solution at pH 8.4 can decrease the F^- binding capacity from 8.8 μmol/m^2 to 0.6 μmol/m^2 [16], but at pH 6.1 boric acid has much lower affinity for the ZrO_2 surface and in an eluotropic series borate is seen to be weaker than fluoride, phosphate and even sulfate [177].

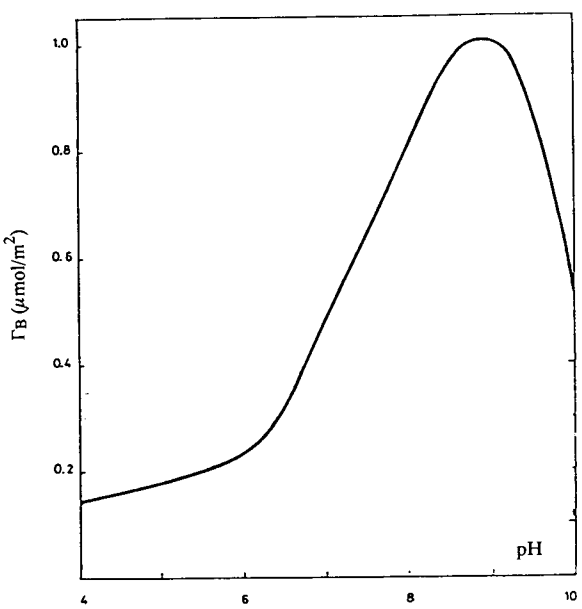

Fig. 43. Dependence of borate adsorption on pH (Γ_B = surface coverage in μmol/m^2). From ref. 199.

3.5.5. Complexes with fluoride

Zirconium forms a number of compounds with fluoride [87]. ZrF_4 exists as a stable, colorless, crystalline solid. The Zr atom is octacoordinated to fluorine and each fluorine atom is coordinated to two zirconium atoms. ZrF_4 has a tendency to form fluorozirconates in solutions containing fluorides of uni- and divalent metals. Generally Zr–F in aqueous solution is more stable than coordinatively bonded water Zr lArr; OH_2 [87]. The displacement of H_2O coordinated to Zr^{4+} by F^- ion has been observed by Blackwell and Carr [16]. The fluorozirconates are decomposed by strong alkalis and their decomposition leads to hydrous zirconia [87]. F^- ion adsorption on a zirconia surface is strongly dependent on pH which is shown in Fig. 42. A very similar curve for specific adsorption of F^- was also observed on α-FeOOH [201]. Fluoride ion is the second strongest eluent (next to phosphate) in the eluotropic series developed for zirconia at pH 6.1 [177]. Fluoride is a hard Lewis base and it is expected to interact strongly with Lewis acids. These strong interactions might be advantageous in liquid chromatography for the generation of a biocompatible zirconia stationary phase for the separation of proteins [17].

3.5.6. Complexes with phosphates

Zirconium phosphates (ZrP) are well known materials with ion-exchange properties described in several books and reviews [34–36]. Zirconium phosphates have also been used in catalysis and

chromatography. Zirconium phosphates are solid acids —the distribution of acid sites and the catalytic activity of the phosphate in alcohol dehydrogenation reactions has been investigated [35]. Applications of ZrP in chromatography are not numerous; in gas chromatography amines were separated on columns packed with a gel in the Cu^{2+}, Zn^{2+} or Mn^{2+} forms using ammonia as the gas phase [202,203]. Gas–solid chromatography was used to measure the interactions of several aromatic and aliphatic adsorbates on α-zirconium phosphate. Adsorption of hydrocarbons is said to occur at the surface and within cavities inside the structure. Oxygen-containing compounds interact strongly with the surface. This agrees with the catalytic properties of zirconium phosphate [204]. Zirconium phosphate was also tested as a gas chromatographic packing material for the separation of fatty acids [205]. Alkyl phosphate derivatives of α-ZrP have also been used in HPLC [206]. Bis(octadecylphosphate) zirconium was used as a column packing for reversed-phase chromatography and the separation of several PAHs was achieved, but the mechanical strength of the packing was very poor [207].

Zirconium phosphate was impregnated in paper and used for chromatography. This modification was used for the separation of alkaloids [208].

Zirconium phosphate has a layered crystalline structure which is responsible for its intercalation ability. The intercalation mechanism of α-ZrP was reviewed by Constantino [209].

α-Zirconium phosphate consists of zirconium layers capped on both sides by phosphate groups [36]. Granular zirconium oxide is appreciably broken down in concentrated phosphoric acid solution [26]. The strong tendency of phosphates to form layered structure is responsible for this. Schafer *et al.* [20] also noted that phosphate modification involves breaking of zirconium–oxygen bonds in the zirconia matrix.

The great affinity of zirconia for phosphate and the low solubility of zirconium phosphate in aqueous media [210] made the intentional modification of the surface of zirconia with phosphate an attractive concept. Phosphate-modified zirconia can be prepared in a straightforward fashion by refluxing zirconia particles in dilute (0.1 *M*) phosphoric acid. A simplified scheme of the likely surface species on phosphate modified zirconia is given in Fig. 44.

The resulting phosphate-modified zirconia is a cation exchanger [36] and the acidity of the bonded phosphate increases substantially. The enhancement of the acidity of the surface complexes was also described by Stumm *et al.* [72]. Similar phenomena were observed for *o*-hydroxybenzoic acid adsorption on Al_2O_3 [72,211], phosphoric acid adsorption on α-FeOOH [72,201] as well as silicic acid adsorption on α-FeOOH [72,201].

Under the "mildest" phosphating conditions, *i.e.* neutral pH, room temperature and short reaction times, phosphate physically adsorbs onto the surface of the particles (Fig. 44) especially onto the Lewis acid sites described earlier. At acidic pH and higher temperatures esterification of the phosphate with surface hydroxyls (Fig. 44) occurs. The purpose of such a modification would be to effectively block the strong

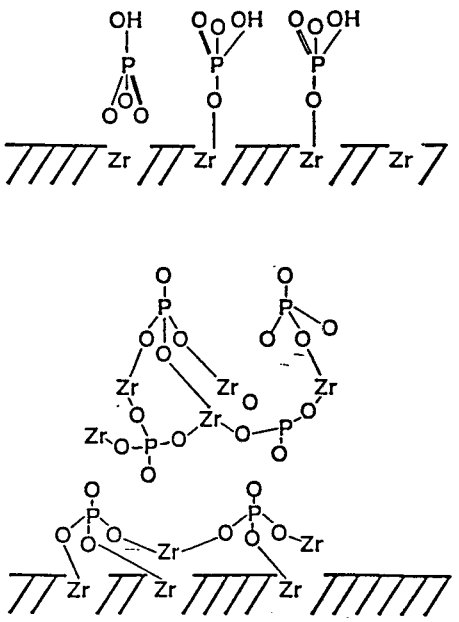

Fig. 44. Surface species on phosphate modified zirconia. Top, "mild" phosphating conditions; bottom, "rigorous" phosphating conditions. From ref. 20.

sites responsible for oxyanion interactions and thereby provide a more "bio-compatible" stationary phase. The widespread use of calcium phosphate (hydroxyapatite) in protein chromatography [212] and zirconium phosphate for transition metal ion separations [34–36] also suggested that a high-performance phosphate-modified zirconia support would be of interest as a chromatographic support.

3.6. Zirconia in liquid chromatography

Zirconia is an amphoteric material with anion-exchange properties in neutral and acid solutions, and cation-exchange properties in alkaline solutions [31–33].

The difference in the amphoteric acid–base chemistry of zirconia and titania surfaces relative to that of silica is clearly reflected in the chromatography of basic analytes. Strongly basic solutes are typically highly retained on silica and yield severely tailed peaks. By contrast, basic compounds with pK_b values as high as 11 have been separated on titania in normal-phase mode with high peak symmetry, as shown in Fig. 45 [24].

Before one starts experiments with zirconia columns, care should be taken to remove CO_2 from the mobile phase. Carbon dioxide or carbonates will block Lewis acids sites by building up on the particle surface and gradually changing the overall character of the surface. Water used to prepare mobile phase should be boiled before use and use of a scrubber or pre-column is strongly advised [17,61].

Since the zirconia surface contains many adsorption sites and is able to ion and ligand exchange, it should, in most cases, be modified. We can take advantage of the chemical reactivity of the surface to "tailor" it according to our needs. Generally there are three classes of surface modification of zirconia: (1) dynamic, chemical modification —when a mobile phase containing a strongly interacting Lewis base is used; a large variety of such systems can be imagined, (2) permanent, chemical modification —*e.g.* silylation of the surface and (3) physical screening —*e.g.* coating the zirconia surface with a polymer or carbon layer.

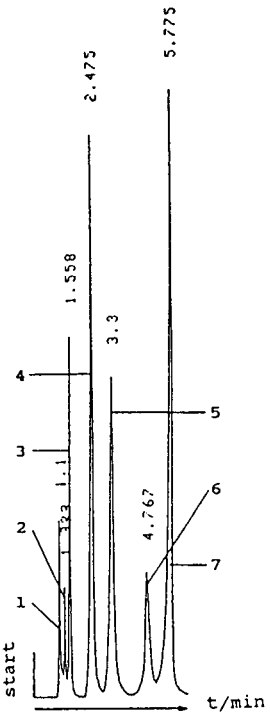

Fig. 45. Isocratic separation of basic analytes with calcined titania as a packing material; $p_d = 5$ μm; injection volume, 20 μl; eluent, dichloromethane (relative water content 100%); flow rate 1 ml/min. Peaks: 1 = N,N-dimethylaniline, 2 = N-methylaniline, 3 = *o*-toluidine, 4 = aniline, 5 = *p*-toluidine, 6 = pyridine, 7 = diazepam. From ref. 24.

3.6.1. Eluotropic series

Eluotropic series of solvents for such LC stationary phases as silica, alumina, *n*-alkyl bonded silica and carbon are well known [4,213,214]. It was of interest to develop a similar series for a zirconia surface. As shown in ref. 176, retention on ZrO_2 surface is governed primarily by the Lewis basicity of the mobile phase and the basicity of the solute. It is thus obvious that an eluotropic series of Lewis bases should be possible. It must be kept in mind that the eluotropic series developed for one pH value may substantially change upon change in pH. The eluotropic series developed for benzoic acid derivatives at pH 6.1 as probes is shown in Table 11 [177]. The eluotropic series, as given in Table 11, is *roughly* in agreement with the sequence of

TABLE 11

ELUOTROPIC SERIES BASED ON BENZOIC ACID DERIVATIVES ON ZIRCONIUM OXIDE [177]

The eluent was 20 m*M* of the Lewis bases shown below in 20 m*M* MES at pH 6.1. The flow rate was 1 ml/min at 35°C. Injections were 10 μl volumes of 10 m*M* solutions in water. Detection was at 230, 254 and 280 nm. eno = Elution not observed, na = not assessed.

Eluent species	Capacity factor at pH 6.1			
	4-Nitro benzoate	4-Cyano benzoate	4-Formyl benzoate	4-Chloro benzoate
Phosphate	0.0	0.0	0.0	0.0
Fluoride	0.0	0.0	0.0	0.0
Ethylphosphonic acid	0.2	0.2	0.2	0.4
Malic acid	0.2	0.2	0.3	0.5
Citric acid	0.3	0.2	0.2	0.6
Ethylenediaminetetra-acetate	0.3	0.3	0.4	0.9
Oxalic acid	0.5	0.5	0.5	0.8
Aspartic acid	0.7	0.6	0.7	1.5
Succinic acid	0.6	0.7	0.8	1.4
Maleic acid	0.7	0.7	0.7	na
Glutaric acid	0.6	0.7	0.9	1.5
Adipic acid	0.7	0.7	0.9	1.7
Malonic acid	0.9	1.0	1.1	2.0
Pimelic acid	0.9	1.0	1.3	2.4
Sulfate	1.5	1.6	1.8	3.0
Glycolic acid	1.7	1.8	2.0	3.4
Boric acid	1.9	2.0	2.2	3.8
Nitrilotriacetic acid	2.1	1.6	2.2	5.2
Tartaric acid	2.9	1.4	2.2	5.8
Suberic acid	2.0	2.2	3.4	7.6
Thiosulfate	3.0	3.0	3.4	5.9
Iminodiacetic acid	3.1	3.1	3.9	7.7
Sebacic acid	3.8	3.0	3.0	20.6
Acetic acid	5.6	6.3	7.6	12.7
Tris(hydroxymethyl)-aminomethane	7.6	6.7	6.0	15.6
Formic acid	8.8	9.7	9.5	20.9
Sulfamic acid	10.8	11.1	15.3	23.5
Butyric acid	13.0	15.6	18.7	34.4
Urea	17.1	17.6	24.3	37.1
Bromide	17.0	18.2	22.9	40.4
Butanesulfonic acid	23.5	22.8	29.6	45.2
Guanidine hydrochloride	20.8	22.4	27.2	eno
Nitrate	24.7	26.0	33.5	57.6
Chloride	24.7	26.6	35.1	59.9
Thiocyanate	32.3	34.3	43.3	eno
Ethylene glycol	34.1	33.6	42.3	eno
Thiourea	41.7	43.9	eno	eno

binding strengths to zirconium. The strongest eluents can be classified as hard Lewis bases.

While the eluotropic strength is in good agreement with the expectations derived from hard–soft Lewis acid–base theory [215,216], it cannot be understood solely based on this theory. For example, although bromides are certainly softer Lewis bases than chlorides they exhibit stronger eluting properties than the latter [177].

To understand the observed phenomena, the following model of retention was proposed: the zirconia surface is populated by ligands coordinated to a zirconium cation. In water these surface species are limited to bound hydroxyl, water and hydronium ion. At pH 6.1, for which an eluotropic series was developed, the concentration of surface hydronium ions can be neglected. In the mobile phase, molecules of eluent (E) and solute (S) will compete with water and hydroxide ion for the hard acid site (Zr^{4+}). The total concentration of the surface species is:

$$C_{s,TOT} = [Zr\text{–}OH^-] + [Zr\text{–}S] + [Zr\text{–}E] + [Zr\text{–}H_2O] \quad (11)$$

where the terms in square brackets denote the concentrations of surface species. On the basis of the Regazzoni *et al.* [107,198] model of adsorption we can assume a competition between the eluent and the solute molecules:

$$Zr\text{–}E + S \rightleftharpoons Zr\text{–}S + E \quad (12)$$

The solute molecules can also compete with water and hydroxyl groups:

$$Zr\text{–}H_2O + S \rightleftharpoons Zr\text{–}S + H_2O \quad (13)$$

$$Zr\text{–}OH^- + S \rightleftharpoons Zr\text{–}S + OH^- \quad (14)$$

The concentration of the solute is negligible and therefore the term [Zr–S] in eqn. 11 can be neglected.

$$k' = \frac{\text{moles of solute on the surface}}{\text{moles of solute in the mobile phase}} \quad (15)$$

Thus:

$$k' = \frac{A[Zr\text{–}S]}{V_m[S]} \quad (16)$$

where A is the surface area of the support, V_m is the volume of mobile phase in the column and [S] is the equilibrium mobile phase concentration of the solute.

Combining eqns. 11, 12 and 13:

$$k' = \frac{C_{s_{TOT}} K_s}{K_{OH}[OH^-] + K_E[E] + 1} \frac{A}{V_m} \quad (17)$$

where K_s = equilibrium constant for eqn. 13; K_E = equilibrium constant for eqn. 12; K_{OH} = equilibrium constant for eqn. 14.

Thus eqn. 17 should account for the variation of k' of a completely ionized Lewis base solute as the pH is varied and the variation in k' with a change in the concentration of a Lewis base eluting agent. All of this is based on the assumption of the homogeneity of the surface adsorption sites. It has been found [176] that the slope of a graph of k' *vs.* pH is close to -1. This can be interpreted to mean that the first term in the denominator of eqn. 8 is dominant. The dependence of log k' of *p*-cyanobenzoic acid on the concentration of Lewis base ([E]) in the mobile phase was found to decrease nearly monotonically as expected for a simple competitive displacement process. If eqn. 17 were rigorously valid then a plot of $1/k'$ *vs.* the concentration of Lewis base in mobile phase would yield a straight line. As we can see in Fig. 46 this not the case.

A small number of strong adsorption sites could be responsible for the curvature of the lines. This is in agreement with numerous reports on the gas–solid interface where the Zr^{4+}_{cus} sites were found to be heterogeneous [64,98, 153,157,158,164].

3.6.2. Chemical, dynamic modification

Despite the rather complex set of equilibria (eqns. 2–10) needed to describe zirconia's surface, we can take advantage of these for chromatography. Chromatography also appears to be a useful tool for investigating the surface chemistry of ZrO_2. Blackwell and Carr [176] examined the retention of a variety of benzoic acid derivatives with pK_a values ranging from 2.8 to 5.4 in the pH range 4.8–9.3. It should be noted that all of the acids were almost completely ionized over the entire range of pH values tested. Thus a pH dependence based on changes in the degree of

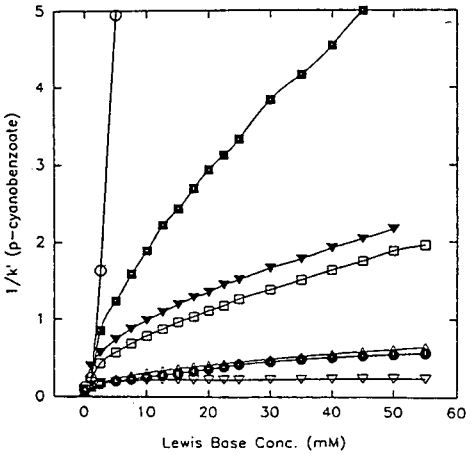

Fig. 46. (Capacity factor)$^{-1}$ *vs.* Lewis base concentration for *p*-cyanobenzoic acid. ○ = fluoride, ● = acetate, ▽ = butyrate, ▼ = succinate, □ = malonate, ■ = oxalate, ▲ = sulfate. The eluent was $(500 - X)$ m*M* sodium chloride and *X* m*M* Lewis base in 20 m*M* MES at pH 6.1. The flow rate was 1.0 ml/min at 35°C and detection was at 254 nm. From ref. 177 (© American Chemical Society).

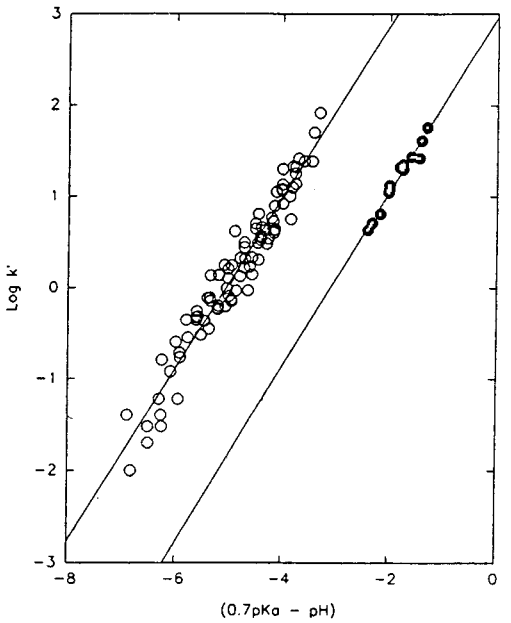

Fig. 47. Correlation of the capacity factors of *p*-benzoic acids with solute Brönsted acidity and solution pH. ○ = Aminosulfonate buffers, ● = acetate buffer. Regressions are least-squares fit. Reprinted from ref. 176.

ionization of the solute would not be expected. In a parallel study Blackwell [217] examined the retention of benzoic acid derivatives on alumina.

Capacity factors were correlated with both the pK_a of the solute and the pH of the mobile phase. When the chromatographic capacity factor is "corrected" for its pH dependence its value on a zirconia surface can be predicted from the equation:

$$\log k' = 0.67pK_a - pH + C \quad (18)$$

where C = constant.

The above relationship (eqn. 18) for benzoic acid derivatives on zirconia is shown in Fig. 47 ([176]).

Similar behavior of benzoic acid derivatives has been found on alumina [217] and the relevant equation for their retention is:

$$\log k' = 0.33pK_a - pH + C \quad (19)$$

The weaker dependence on pK_a means that Al is not as strong a Lewis acid as Zr. The higher selectivity of zirconia over alumina toward benzoic acid derivatives has been noted. Retention of these compounds on alumina was said to be more complex than on zirconia and less dependent on the pH of the mobile phase since the slope of *k' versus* pH on alumina is lower than that on zirconia [176,217]. This means that retention on alumina cannot be fully predicted by eqn. 17.

Generally we can expect that other oxides (TiO_2, Fe_2O_3) will behave similarly toward polyoxo acids. Phosphonates, benzoic acids and acetic acid are known to adsorb on TiO_2 surfaces [162].

The retention of benzoic acid derivatives is in accord with Pearson's theory [215,216] of hard and soft acids and bases and with Stumm *et al.*'s [72] postulate of ligand-exchange reactions at hydrous oxide surfaces. The results obtained on zirconia columns were compared to those on bonded phase strong anion exchangers which showed that in the range of pH values examined, no ion-exchange process was observed, and no correlation between retention and pK_a was found. Chromatographic selectivity toward the benzoic acids was much higher on zirconia surfaces than on the anion exchanger because their ionic properties do not differ significantly but their Lewis basicities differ greatly. The impor-

tance of complex formation on retention on zirconia is also reflected in zirconia's extreme sensitivity to isomerization. This has been demonstrated in the differences in retention of *ortho-*, *meta-* and *para*-hydroxy- and aminobenzoic acid isomers. The retention of the *ortho*-isomers is significantly enhanced as both functional groups can interact strongly with surface ligand-exchange sites. Isomeric selectivity was also much better for zirconia than for a conventional anion-exchange column which did not reveal any isomer selectivity. Kita *et al.* [76] could not confirm the existence of Lewis acid sites in the liquid–solid system by static methods. Lewis acidity of zirconia can, however, be confirmed by chromatography where ligand exchange at Lewis sites was observed [176,177].

In another paper, Blackwell and Carr [18] showed again that retention in aqueous media depends on the chemistry of the solute and eluent. This is shown in Table 12. Cationic solutes are not retained in chloride mobile phases. In chloride media at pH 6.1 the surface hydroxyl groups are mostly in unionized state (see Fig. 41 and Table 10 for pK_{a1}^{int} and pK_{a2}^{int} data) and the ionic strength of the eluent is high enough to displace any solute bonded by an ion exchange. When stronger Lewis bases are present (such as dicarboxylic acids) in the mobile phase, they generate a negative charge on the zirconia surface thereby causing adsorption of cations and the retention of cationic solutes change significantly. Table 12 also shows that non-electrolytes are non-retained in all buffers. This means that cationic compounds are not retained by hydrogen bonding and/or Van der Waals forces. In contrast anionic solutes were retained in chloride mobile phase but they are weakly retained when a Lewis base eluent is present in the mobile phase. This confirms again that the dominant retention process is ligand exchange [18].

TABLE 12

RETENTION AS A FUNCTION OF DISPLACING LEWIS BASE

Eluent contained 20 m*M* of displacing Lewis base with 20 m*M* MES at pH = 6.1. Flow rate was 0.5 ml/min at 35°C. Injections were 5 μl of 10 m*M* solute in 20 m*M* sodium chloride 20 m*M* MES at pH = 6.1. Detection was at 230 and 254 nm using a diode array detector. n/a = Not available, eno = elution not observed.

Solute	Capacity factor		
	Buffer		
	Sodium chloride	Malic acid	Succinic acid
Guanidine	n/a	1.6	0.7
Imidazole	0.0	0.7	0.3
Benzylamine	0.0	0.8	0.4
Benzamide	0.0	0.0	0.0
Benzyl alcohol	0.0	0.0	0.0
Benzyl mercaptan	0.1	0.1	0.1
Phenylacetic acid	eno	0.0	0.2
Benzenesulfonic acid	0.9	0.1	−0.1
Phenol	0.2	0.0	0.0
Benzenephosphonic acid	eno	eno	eno

The most interesting application of zirconia in chromatography is the separation of proteins. Zirconia as a base-stable stationary phase not only allows separation of those molecules at high pH values but also provides an easily "cleaned" surface. This stability offers many obvious chromatographic advantages. It is also significant in terms of the use of zirconia for the downstream processing of proteins because the use of hot alkaline media is a routine sanitization procedure in these applications.

Depyrogenation [218–220] especially requires vigorous conditions, for instance, 0.1 *M* sodium hydroxide in 95% aqueous ethanol or 80% aqueous dimethyl sulfoxide. In this sort of aggressive environment zirconia offers a distinct advantage since silica-based materials are destroyed under these conditions and polymer-based materials are limited by their hydrolytic, thermal and mechanical stability. Thus there is considerable interest in the development of a zirconia-based support for protein separations, hopefully without the irreversible adsorption problems common to silica-based supports and the unacceptable physical and mechanical properties of hydroxyapatite gel-type and polymer-type supports.

Initial attempts to elute proteins from bare zirconia were unsuccessful because it has a high

affinity for some functional groups, such as carboxylic acids. However, zirconia does not show the same affinity for amines that leads to irreversible protein adsorption on silica-based supports. Protein separations are possible by recognizing and taking advantage of some of the very same surface chemistry. Blackwell and Carr [221] have shown that a variety of proteins can be chromatographically separated on zirconium oxide particles. To elute the proteins, a mobile phase must contain an appropriate concentration of a hard Lewis base. The initial concentration of the base appears to be a critical parameter in achieving acceptable retention and peak shape. In practice the eluent should contain phosphate, fluoride, polyvalent carboxylates or organophosphate ligands. In a subsequent paper Blackwell and Carr [222] demonstrated an application of the ion-exchange properties of zirconia for protein separations. The zirconia surface can be loaded with Cu^{2+} ions (3.9 μmol/m^2). Providing Cu^{2+} ions remain in the mobile phase, it is possible to apply this type of copper-loaded zirconia to the separation of proteins. The solutes were said to interact with the stationary phase by a ligand-exchange mechanism.

Another example of the chemical flexibility of the zirconia surface is an application of a borate-modified zirconia surface [221] to the separation of proteins. The chromatographic behavior of this type of stationary phase correlated well with the properties of a borate-modified surface as derived from data obtained by static liquid–solid interface studies [199].

A more "universal" protein support can be produced by taking advantage of the very strong interaction of fluoride with zirconia. A protein separation on unmodified zirconia using a sodium sulfate gradient in 20 m*M* sodium fluoride is shown in Fig. 48.

There is no relationship between protein capacity factors and their isoelectric points. This is shown in Fig. 49.

Both cationic and anionic proteins are retained on zirconia in fluoride media, analogous to calcium hydroxyapatite and in contrast to the retention behavior reported for zirconium phosphate. The data in Table 13 show that the retention of proteins decreases significantly with

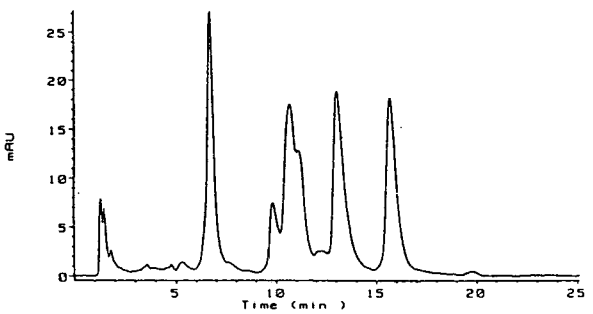

Fig. 48. Protein separation on fluoride modified zirconium dioxide. A linear gradient of 0 to 0.75 *M* Na_2SO_4 in 100 m*M* NaF and 20 m*M* MES at pH 5.5 was used. Flow rate was 0.5 ml/min at 35°C. Protein loading: 4.4 μg lysozyme, 15.4 μg α-chymotrypsin, 13.6 μg myoglobin, 15.4 μg cytochrome *c*. From ref. 17.

increasing sodium fluoride concentration in the mobile phase, suggesting that the Lewis acid–base interactions with the surface zirconium(IV) sites play an important role in retention.

The use of bare zirconia for protein separations with fluoride-containing mobile phases has the additional advantage of high loading capacity, nearly quantitative mass and activity recoveries and the aforementioned stability of unmodified zirconia.

Zirconia is well known to strongly interact

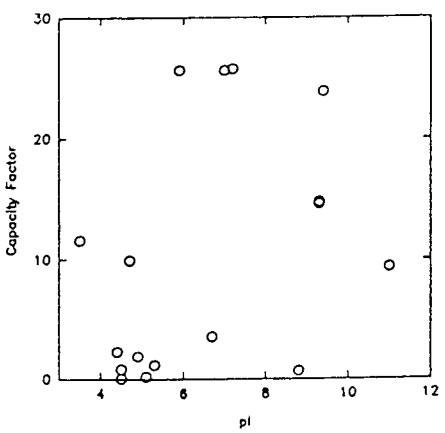

Fig. 49. Correlation of capacity factor with p*I*. Gradient elution from 0 to 0.5 *M* Na_2SO_4 in 30 min. Both buffers contained 20 m*M* NaF and 20 m*M* MES at pH 6.2 at 35°C. Flow rate was 0.5 ml/min and detection was at 280 nm. From ref. 17.

TABLE 13

PROTEIN RETENTION IN FLUORIDE MEDIA [61]

Buffers consisted of (A) sodium fluoride 20 m*M* MES pH = 5.5 and (B) buffer A with 0.5 *M* sodium sulfate added. Gradient was 0 to 100% B in 30 min then back to 0%B in 15 min with a 15-min equilibration period. Flow rate was 1 ml/min at 35°C with detection at 280 and 410 nm. Typical injections were 10 μg protein in 20 m*M* MES at pH = 5.5. eno = Elution not observed.

Protein	p*I*	Capacity factor		
		0.50 *M* NaF	0.10 *M* NaF	0.02 *M* NaF
Ovalbumin	4.7	10.6	17.3	eno
Bovine albumin	4.7, 4.9	14.2	23.1	32.5
Human albumin	4.6–5.3	17.0	25.3	34.1
Transferrin, apo	5.9	16.6	26.5	31.2
Myoglobin	6.8, 7.3	3.5	16.7	24.6
Hemoglobin	6.9–7.4	3.9	15.7	24.2
Alc. dehydrogenase	8.7–9.3	21.2	eno	eno
α-Chromotrypsin	8.8	2.3	13.2	18.1
Ribonuclease A	9.3	3.3	15.9	19.7
Ribonuclease B	9.3	3.6	6.8	11.1
Cytochrome *c*	9.4, 9.0	5.1	22.6	28.4
Lysozyme	11.0	0.2	5.2	10.3

with phosphoric acid. A phosphate-modified surface can also be utilized for the chromatography of proteins. Since phosphate-modified zirconia is a cation exchanger it can also be used for chromatography in various cationic forms: Na^+, K^+, NH_4^+ [21] or Cu^{2+} [223]. ^{31}P magic angle spinning NMR spectra [20] show the presence of covalently bonded phosphate and phosphate adsorbed on the surface. It was also proved that to bond the phosphate covalently more rigorous conditions such as lower pH, higher temperature and longer exposure time are required. The phosphated support behaves as a classical cation exchanger. It does not behave as a mixed-mode system analogous to hydroxyapatite, wherein interactions with phosphate and calcium are both involved in protein retention [212]. It is likely that phosphate ions adsorb onto and interact so strongly with surface zirconium sites that only the phosphate sites are "available" for interaction with proteins. This would explain the cation exchange behavior of ZrP rather than a hydroxyapatite-like behavior. Proteins are retained mainly by an ion-exchange process; at pH > 6 proteins with low p*I* are not retained while proteins with high p*I* are retained. Retention also decreases when the competing ion concentration is increased. That retention is due to cation exchange is also supported by the fact that the type of displacing cation has a significant effect on retention [21]. Phosphate-modified zirconia appeared to be very stable column packing, but it requires the presence of phosphate in the mobile phase. This is shown in Fig. 50.

Table 14 summarizes the retention of proteins on various chemically modified surfaces of zirconia. The table shows the chemical "tunability" of the surface. Taking advantage of the rather complex surface equilibria, it is possible to "adjust" the surface properties to the particular needs of the separation.

It should be emphasized here that Table 14 is not a comprehensive list of all possible surface modifications. For example, proteins can be also chromatographed on metal-substituted phosphate-modified zirconia [21,223]. Recovery of proteins is an important characteristic, particularly for preparative separations. Table 15 demonstrates that quantitative recovery can be obtained on both phosphate- and fluoride-modified zirconia columns.

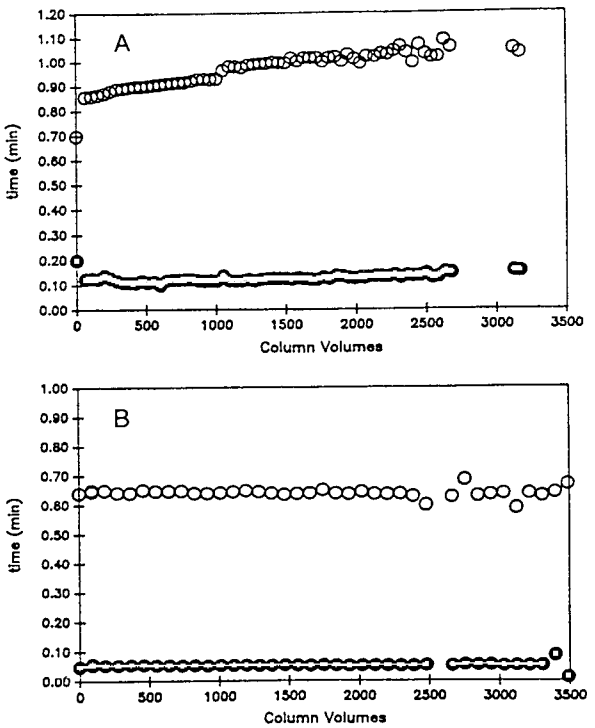

Fig. 50. Stability of phosphate-modified zirconia using benzoic acid as a probe solute. Column: 10–15 μm, 100 Å ZrP (0.1), 5 × 0.46 cm. Mobile phase: (A) 1 m*M* pH 7.0, MOPS buffer, 0.5 ml/min; (B) 20 m*M* pH 7.0, K_2HPO_4 buffer, 0.5 ml/min, detection at 254 nm. From ref. 21. ○ = retention time, ● = peak width.

3.6.3. *Chemical, permanent modification*

While the understanding of zirconia surface chemistry from the chromatographic studies described above is invaluable, it is a fact of chromatographic life that most separations are not done on highly active unmodified supports. It is reasonable to expect that the successful application of zirconia supports to a variety of chromatographic separations will require access to facile and controllable surface modification schemes. The highly developed siloxane chemistry used to tailor the surface properties of silica supports would seem a logical place to begin. The widespread use and popularity of silica-based reversed phases draw attention to the possibility of obtaining reversed phases based on zirconia. Since zirconia contains many surface hydroxyl groups, the use of silane reagents is very seductive. In fact there are a few reports in the literature concerning silanization of zirconia surfaces. Rigney [243] attempted to modify the surface with mono- and tri-functional silanes. Attempts to prepare *stable* coatings with octyldimethylchlorosilane and alkoxysilanes were unsuccessful. Although coverage up to several μmol/m^2 could be obtained the resulting phases were evidently not usefully stable under HPLC conditions. The phases were particularly unstable during extraction with methanol [243]. Modification with trifunctional octyltrichlorosilane led to a stable stationary phase with a coverage of *ca.* 3.3 μmol/m^2. Trüdinger *et al.* [24] have reported on a successful silanization of the zirconia surface with a trifunctional silane (*n*-octadecyltrimethoxysilane). The resulting phase was said to be extremely stable —withstanding 500 h at pH 12. Separation of polycyclic aromatic hydrocarbons on the phase has been reported. Yu and El Rassi [126] silanized nonporous zirconia particles with mono- and trichlorooctadecylsilanes. Monomeric octadecyl phase was very unstable in pH 2 as well as pH 12. An essentially polymeric octadecyl phase was also unstable although its properties seem to stabilize after 1000–2000 column void volumes of mobile phase. Due to extremely low surface area no coverage values are provided. Several applications of the polymeric octadecyl zirconia are provided by the authors [126]: separation of PAHs, *p*-nitrophenylmaltooligosaccharides, dansylated amino acids, peptides and proteins. Amati and Kováts [84] silanized a zirconia surface with trimethylsilyldimethylamine (TMS-A) and 3,3-dimethylbutyl–dimethylsilyldimethylamine (DMB-A) and with the corresponding silanols (TMS-O) and (DMB-O). They have obtained 3.45 μmol TMS/m^2 and 4.6 μmol TMS/m^2 with amine and silanol, respectively, as well as 2.45 μmol DMB/m^2 and 3.5 μmol DMB/m^2 with amine and silanol, respectively. However, these surfaces were not tested under chromatographic conditions. Reaction time was very long (170 h), according to the procedure developed earlier by the same group [226]. It is important to recognize that the replacement of a silicon atom in a siloxane bond by a heteroatom generally produces M–O–Si bonds which are far

TABLE 14

PROTEIN RETENTION WITH IONIC STRENGTH GRADIENTS AND CONSTANT LEWIS BASE CONCENTRATIONS [221]

Linear gradient elution from 2% B to 100% B in 15 min with a 15-min equilibration period. Flow rate was 0.5 ml/min at 35°C. Injections were 10-μl volumes of 10 mg/ml solutions of protein in 20 m*M* TABS at pH 8.4. Detection was at 280 and 410 nm. Buffer A: 20 m*M* Lewis base in 20 m*M* TABS at pH 8.4; buffer B: buffer A with 1 *M* sodium chloride. Lewis bases: A = sodium phosphate, B = sodium fluoride, C = boric acid, D = citric acid, E = aspartic acid, F = tartaric acid, G = imidodiacetic acid, H = aminomethylphosphonic acid, I = ethylphosphonic acid, J = O-phospho-DL-serine. PEP = Pepsin, GLOX = glucose oxidase, TINH = trypsin inhibitor, OVA = ovalbumin, HSA = human serum albumin, HEXO = hexokinase, βLAC = β-lactoglobulin, LIP = lipase, ATRH = apotransferrin, MYO = myoglobin, HEMO = hemoglobin, αCHY = α-chymotrypsin, CYTC = cytochrome *c*, RNA = ribonuclease A, RNB = ribonuclease B, LYS = lysozyme. eno = Elution not observed.

Protein	Capacity factors									
	A	B	C	D	E	F	G	H	I	J
PEP	−0.3	−0.3	−0.3	−0.3	−0.3	−0.3	−0.3	−0.3	−0.3	−0.3
GLOX	−0.3	–	−0.3	−0.3	1.2	−0.3	–	−0.3	−0.3	−0.3
TINH	−0.2	0.1	0.1	0.0	0.2	0.0	0.2	0.0	−0.2	−0.2
OVA	−0.2	–	–	−0.2	–	0.2	–	−0.2	−0.2	−0.2
HSA	−0.3	–	−0.3	−0.3	−0.3	−0.3	–	−0.3	−0.3	−0.3
HEXO	−0.2	1.6	1.9	0.5	1.3	1.3	3.0	0.1	−0.3	0.1
βLAC	–	–	–	–	–	–	–	−0.3	−0.3	−0.2
LIP	0.2	1.2	1.3	0.5	1.3	1.3	2.2	0.1	0.5	0.1
ATRH	12.0	–	–	0.1	–	0.0	–	−0.1	−0.2	−0.2
MYO	11.6	14.5	13.4	1.1	26.9	3.8	–	0.3	0.7	0.1
HEMO	19.4	20.0	14.4	−0.1	–	−0.1	–	−0.1	−0.2	−0.1
αCHY	13.8	–	–	12.5	22.5	14.5	–	6.3	14.2	8.8
CYTC	23.4	–	–	23.3	–	26.2	–	11.3	26.4	16.5
RNA	15.1	13.0	13.2	9.9	14.1	11.0	18.8	6.6	11.3	7.4
RNB	11.1	12.8	13.0	8.5	13.7	9.7	18.9	3.8	9.5	6.2
LYS	10.9	9.4	11.2	10.5	12.8	10.2	12.6	5.9	15.1	8.1

TABLE 15

RECOVERY OF PROTEINS FROM ZIRCONIA COLUMNS

Protein	Phosphate-modified ZrO_2 [21]	Fluoride-modified ZrO_2 [17]	
	Enhanced assay[a]	Enhanced assay	Micro assay[a]
Ribonuclease A	95% (± 5%)	–	–
Cytochrome *c*	87% (± 7%)	–	–
Lysozyme	95% (± 5%)	103.9 ± 2.5%	101.2 ± 2.2%
Myoglobin	–	107.7 ± 6.1%	95.7 ± 4.1%

[a] See refs. 224 and 225.

less stable than the Si–O–Si bond [227], and therefore the stability of silanized metal oxides will not equal that of silanized silica [228,229].

Rigney [243] discussed the instability of the Si–O and Zr–O bonds in terms of their ionic character. A siloxane bond is determined to be 50% ionic while a Zr–O bond is 67% ionic. This is in agreement with the order of hydrolytic

stability of silanized oxides established by Schindler and Schmidbaur [229]:

$$Si–O–Si–R > Zr–O–Si–R > Ti–O–Si–R > > Al–O–Si–R$$

Thus Zr–O–Si bonds should be more susceptible to hydrolysis than Si–O–Si. However, Trüdinger *et al.* [24] observed the stability of their reversed phase at pH 12 for 500 h. Since the motivation for evaluating alternatives to silica arises at least in part from the inherent instability of siloxane-bonded supports, the lower stability of silanized zirconia is of concern, and has led to a focus on modification schemes other than silanization.

Other attempts to produce reversed phase on zirconia-based surface were also only partly successful [243]. In contrast to silica, Zr–C single bonds are very uncommon and we can hardly expect a successful modification of the type Zr–O–Zr–C. Another attempt to prepare a reversed phase was also undertaken by Rigney [243] who modified the surface by adsorption of organophosphates. Octylphosphonic acid adsorbed (at a surface concentration of 2.6 μmol/m^2) on the surface did indeed exhibit reversed-phase behavior. However, the phase was not stable in alkali. Another approach to get a non-polar surface on zirconia particles was presented by Ghaemi and Wall [106]. The surface was dynamically modified with a hydrophobic quaternary amine.

3.6.4. Physically screened zirconia particles

3.6.4.1. Polybutadiene-coated zirconia. Chemically stable modification of the chromatographic performance of zirconia was accomplished by deposition and cross-linking of polybutadiene (PBD) [25] in the manner reported by Schomburg and co-workers for the modification of silica and alumina [230,231]. The result is a remarkably stable reversed-phase support. After a slight initial decrease in retention, the retention of a non-polar probe solute showed no further decrease in k' when over 30 000 column volumes of methanol–0.1 *M* sodium hydroxide (50:50) were passed throughout the column [25]. Analysis of the column effluent for zirconium by ICP-AES showed no measurable level of zirconium. It should be noted that under these same conditions, a commercial polybutadiene-modified alumina column failed due to bed collapse after 8000 column volumes. In addition to this chromatographic stability test, the stability of polybutadiene-modified zirconia and alumina was evaluated by exposing columns packed with these supports to a mobile phase of 1 *M* sodium hydroxide at 100°C. The results of ICP-AES analysis of the column effluents are given in Table 16.

No zirconium was found in the column effluent. In contrast, it is obvious from the data in Table 16 that alumina dissolves to a significant extent during the first hour of exposure to these conditions. In fact, after 3.25 h of exposure the amount of aluminum dissolved corresponded to

TABLE 16

EXPOSURE OF POLYBUTADIENE-COATED SUPPORTS TO "STERILIZING" CONDITIONS [25]

Column	Time (h)[a]	Al [μg/ml][b]	Si [μg/ml][b]	Zr [μg/ml][b]
Al_2O_3–PBD	1	680	13.6	–[c]
Al_2O_3–PBD	3.25	243	3.3	–[c]
Zirconia–PBD	1	–[c]	1.6	–[c]
Zirconia–PBD	3.25	–[c]	2.1	–[c]
Zirconia, unmodified	1	–[c]	2.4	–[c]
Blank (1 *M* NaOH)		–[c]	1.5	–[c]

[a] Time of exposure to 1 *M* NaOH at a flow rate of 1 ml/min; T = 100°C.
[b] μg/ml in column effluent as determined by ICP-AES.
[c] Less than the detection limit (0.04 μg/ml) by ICP-AES.

more than 10% of the alumina originally present in the column. Retention data for a variety of uncharged non-polar solutes on this type of reversed-phase support were comparable to data on a conventional silica bonded phase reversed-phase support. However, there was evidence of strong, irreversible interactions between certain solutes and the zirconia support. In fact these interactions were expected based on considerations of zirconia's unique surface chemistry. For example, carboxylic acids and organophosphate solutes irreversibly adsorbed. These interactions are analogous to the well known interactions of amines with an acidic silica surface. Such interactions lead to problems with peak tailing, poor efficiency, low recoveries and hysteresis effects.

These data lead us to believe that some of the surface sites are still available for interactions. By taking advantage of the strong interaction of phosphates with zirconia, the number of sites could be measured in static adsorption experiments. Even the thickest layers of PBD allowed about 2.3 μmol/m^2 of phosphate to bind to zirconia. Also chromatographic results confirm that a part of ZrO_2–PBD surface is not covered by the polymer. This leads to a mixed-mode retention mechanism.

One possible strategy for inhibiting interactions with zirconia's surface is the use of phosphate-containing mobile phases. Table 17 demonstrates the effect of various levels of inorganic phosphate on the chromatographic data of several test solutes. If these solutes were retained solely by a reversed-mode mechanism, benzoic and toluic acids should elute before benzene and toluene respectively. In 1 m*M* phosphate benzoic acid is slightly more retained than benzene. In 10 m*M* and 100 m*M* phosphate both acids elute before the related hydrocarbons. This indicates that chromatography on ZrO_2–PBD can be improved by the addition of phosphate to the mobile phase [243]. This is in contrast with the observed "substantial deactivation" of silicas coated with PBD [232]. PBD-coated zirconia was also used for several separations by Hanggi and Marks [244].

3.6.4.2. Polystyrene-coated zirconia. Particles of zirconia coated with polystyrene were used to separate several mixtures of basic compounds with mobile phases containing HNO_3 or NaOH. The separation of acidic compounds showed lower efficiency even in the presence of an acidic mobile phase [81].

3.6.4.3. Carbon-coated zirconia. Carbon-based HPLC supports have been the subject of intensive studying for the last few years [213,233–235]. Carbon packings differ substantially from other reversed-phase supports. They are commonly more retentive toward polar compounds and are often more selective for the separation

TABLE 17

EFFECT OF PHOSPHATE CONCENTRATION ON RETENTION ON ZrO_2–PBD

Column, 5 cm × 0.46 cm I.D., packed with 10–15 μm ZrO_2–PBD. Flow rate, 1 ml/min at 40°C. Injection volume 5 μl; solute concentration, 1 m*M*. eno = No elution observed at $k' < 100$.

Solute	k'		
	1 m*M* H_3PO_4 [a]	10 m*M* H_3PO_4 [b]	100 m*M* H_3PO_4 [c]
Benzene	0.58	0.60	0.47
Benzoic acid	0.64	0.53	0.24
Toluene	1.0	1.1	0.84
Toluic acid	0.90	0.72	0.40
Benzylamine	0.32	0.36	0.23
Phenylphosphonic acid	eno	eno	0.13

[a] Mobile phase MeOH–1 m*M* H_3PO_4 (50:50, v/v) adjusted to pH = 3.
[b] Mobile phase MeOH–10 m*M* H_3PO_4 (50:50, v/v) adjusted to pH = 3.
[c] Mobile phase MeOH–100 m*M* H_3PO_4 (50:50, v/v) adjusted to pH = 3.

of isomers and homologues. They also have a much greater chemical stability over a wider pH and temperature range than bonded phases. The drawbacks of carbon packings are often one or more of the following: poor mechanical stability, low surface area, a heterogeneous surface (and therefore low loading capacity) and non-uniform pore structure. Zirconia particles coated with a carbon layer developed by Funkenbush *et al.* [116] seem to be substantially different from other carbon supports. The process of carbon coating is carried out by passing organic vapors over the zirconia particles at an elevated temperature and reduced pressure. The most common conditions are: 700°C and 5–10 Torr (1 Torr = 133.322 Pa). This procedure creates a uniform carbon coating on the porous particles. It is possible to cover more than 97% of the available zirconia surface [23,116,236].

For this purpose zirconia has important advantages over silica and alumina. It can be heated to high temperatures (*i.e.* >500°C) with little change in pore structure. A variety of organic compounds have been used as the source of carbon: toluene, cyclopentane, heptane, isooctane, 1,7-octadiene and *n*-butanol. It has been found that the precursor used for the cladding has a major effect on the nature of the final support. The loading capacities of the final phases derived from saturated hydrocarbons and 1-butanol were satisfactory. Phases derived from toluene and 1,7-octadiene indicated a very strong dependence of capacity factors on the amount of polar solute injected [22,236]. Similarly, efficiencies and mass transfer characteristics of the first group of columns were better than for those packings derived from unsaturated hydrocarbons. A small number of strongly interacting adsorption sites were blamed for the behavior of carbon deposited from unsaturated hydrocarbons [236]. This situation resembles the problems observed with silica wherein a small population of strongly interacting sites causes considerable difficulties [83,97]. On carbon these sites are the cause of low linear capacity and poor efficiency for certain solutes (*e.g.*, nitroaromatics, phenols, ketones, aldehydes). This situation can be addressed to a certain extent by hydrogenation [23,236] of the surface at elevated temperatures to remove high-energy adsorption sites and/or by modifying the support by deposition and cross-linking of polybutadiene.

The resulting chemical-vapor deposited (CVD) carbon-coated material is useful as a reversed-phase support for liquid chromatography. As expected, this material demonstrates much greater selectivity for the separation of both non-polar and polar isomers than do conventional reversed phase support. This is shown in Fig. 51.

The isomers of butylbenzene are more completely resolved in less time on a carbon-clad zirconia column compared to a Hypersil ODS column, despite the greater efficiency of the Hypersil column (N_{ODS}(butylbenzene) = 2650; $N_{zirconia}$(butylbenzene) = 1665).

The separation of isomers on the carbon-zirconia column is trivial. The separation illustrated in Fig. 51 was carried out on only 16 m^2 of packing material in the column. The column can also easily separate *cis-* and *trans*-isomers. The separation of *cis-* and *trans*-stilbenes was achieved on a different carbon column by Belliardo *et al.* [237] where the available surface area exceeded 1300 m^2. Carbon-clad zirconia supports are stable at elevated temperature and pH. This is comparable to that of unmodified zirconia and polybutadiene-coated zirconia.

3.6.4.4. Polymer-coated carbon-clad zirconia. When the carbon-clad zirconia is covered by a polymer, some of the unique properties of the carbon-clad material are lost. This is due to the mechanism of retention changing from an "adsorption-like" process on the carbon surface to a more "partition-like" process in the polymer film. The resulting phase can be considered as a composite material with high chemical and mechanical stability. Polymer coating greatly alters the characteristics of carbon-clad zirconia. The solute–adsorbent interactions are significantly weakened [22,238]. However, polymer coating improves the efficiency of the packing and the mass transfer characteristics. The chemical stability has proven to be remarkable. It withstands *ca.* 2000 column volumes of methanol–water (50:50) pH 12 mobile phase at 80°C with no measurable loss of carbon [22,238]. Generally polybutadiene coating improves the performance

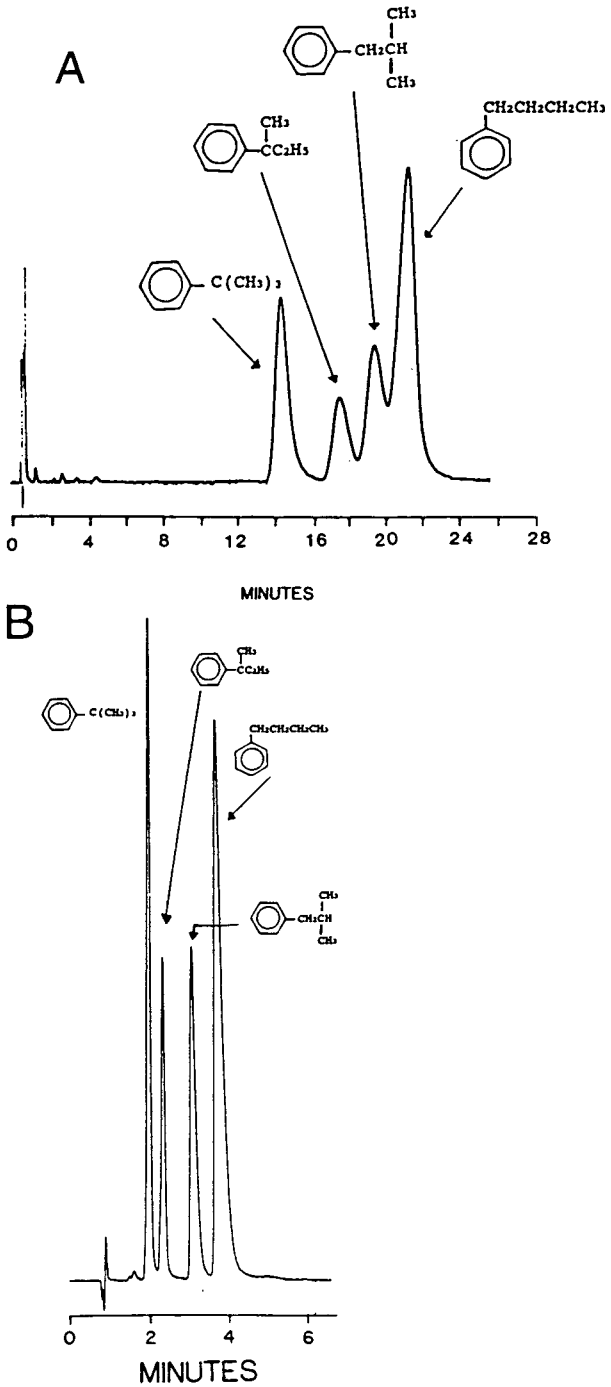

Fig. 51. Separation of butylbenzene isomers: (A) Hypersil ODS column, 10 × 0.21 cm, 5 μm particles, 0.5 ml/min, water–ACN (60:40, v/v), 254 nm detection. (B) CVD carbon-clad zirconia column, 10 × 0.21 cm, 8 μm particles, 0.4 ml/min, water–ACN (40:60, v/v), 254 nm detection. From ref. 23 (© American Chemical Society).

of the carbon-clad zirconia columns, decreases retentivity and increases loading capacity. However, some selectivity is lost [22].

3.6.5. Other zirconia applications in chromatography

Spherical particles of zirconia have also been used as the stationary phase for thin-layer chromatography [239] with diffuse reflectance Fourier transform infrared detection. Detection on zirconia was said to be better than on silica and alumina.

It is also worth mentioning applications of $Zr(OH)_4$ in paper chromatography where it has been used for the separation of amino acids [240,241].

4. CONCLUSIONS

Zirconia is a material which has many unique properties which make it attractive as a chromatographic support, notably, its excellent chemical stability and unique surface chemistry. Preparation of stable, mechanically strong particles of the desired particle and pore diameters for HPLC purposes can be provided by two modern techniques; oil emulsion and coacervation. Zirconia is expected to have lower specific surface area and pore volume compared to silica. However, due to its higher density, the surface area available in a chromatographic column and the porosity should be comparable to that of silica.

Despite many efforts to understand the surface properties of zirconia there still remains a great deal to be done so as to fully understand its complex properties. The main difficulty in achieving a wider variety of applications of zirconia in HPLC is probably a lack of knowledge and poor understanding of zirconia's surface chemistry. The main purpose of this review has been to gather as much data as possible and to shed some light on zirconia's surface chemistry. The properties of zirconia are very dependent on its synthesis. Moreover zirconia's properties are shown to change over long periods of time. To overcome all these difficulties it is decidedly better to use crystalline zirconia *i.e.* monoclinic rather than amorphous zirconia. To

assure the reproducible properties of the chromatographic zirconia a hydroxylation of the surface by washing with base and acid is recommended. Zirconia is catalytically active but this seems to be limited to cases where the surface is completely dehydroxylated. It seems that the activity can be suppressed under HPLC conditions.

Due to its unique surface chemistry zirconia offers many possibilities for use in chromatography; it can be used as a bare support, it can be dynamically modified, it may be coated with polymers or with inorganic overlayers. Stable reversed phases can be prepared by polymer deposition and cross-linking or chemical vapor deposition. Lewis acid–base interactions play an important role and can be troublesome with respect to the chromatography of some solutes, particularly oxyanions. These same interactions can be exploited to allow protein separations on the bare support. The usefulness of zirconia for protein separations and its stability under the aggressive conditions required for sanitation suggest many applications in the chromatography and purification of biomolecules. Much work remains to be done to develop a complete understanding of the complex acid–base chemistry of these supports and in producing modified surfaces for other applications. So far, no stable, monomeric, chemically bonded phase on zirconia surface has been reported and this seems to be the most serious disadvantage in comparison to silica-based HPLC packings.

5. ACKNOWLEDGEMENTS

Authors of this review wish to thank Professor Urszula Rychlewska (Faculty of Chemistry, A. Mickiewicz University, Poznan, Poland) for her substantial help in understanding the crystalline structure of monoclinic zirconia and for numerous computer images of various crystallographic planes of the zirconia.

We also thank Dr. Mike Annen for many helpful discussions and suggestions.

Financial support from National Science Foundation and National Institute of Health is gratefully acknowledged.

One of us (J.N.) acknowledges support from NSF grant CHE 9002446.

REFERENCES

1 K. Tanabe, *Mater. Chem. Phys.*, 13 (1985) 347.
2 E.C. Subbarao, in A.H. Hauer and L.W. Hobbs (Editors), *Advances in Ceramics*, Vol. 3, American Ceramic Society, Columbus, OH, 1980, p. 1.
3 R.E. Iler, *The Chemistry of Silica*, Wiley-Interscience, New York, 1979.
4 K.K. Unger, *Porous Silica* (*Journal of Chromatography Library*, Vol. 16), Elsevier, Amsterdam, 1979.
5 R.P.W. Scott, *Adv. Chromatogr.*, 20 (1982) 167.
6 C.T. Wehrli and R.E. Majors, *LC·GC*, 5 (1987) 942.
7 A. Wehrli, J.C. Hildenbrand, H.P. Keller, R. Stampeli and R.W. Frei, *J. Chromatogr.*, 149 (1978) 199.
8 K. Krummen and R.W. Frei, *J. Chromatogr.*, 132 (1977) 27.
9 J.J. Glajch, J.J. Kirkland and J. Köhler, *J. Chromatogr.*, 384 (1987) 81.
10 K.K. Unger, N. Becker and P. Roumeliotis, *J. Chromatogr.*, 125 (1976) 115.
11 Cs. Horváth, W. Melander and I. Molnár, *Anal. Chem.*, 49 (1977) 142.
12 K.K. Unger, in P.R. Brown and R.A. Hartwick (Editors), *High Performance Liquid Chromatography*, Wiley, New York, 1989, Ch. 3, p. 145.
13 M. Kawahara, H. Nakamura and T. Nakajima, *Anal. Sci.*, 4 (1988) 671.
14 M. Kawahara, H. Nakamura and T. Nakajima, *Anal. Sci.*, 5 (1989) 485.
15 M. Kawahara, H. Nakamura and T. Nakajima, *J. Chromatogr.*, 515 (1990) 149.
16 J.A. Blackwell and P.W. Carr, *J. Chromatogr.*, 549 (1991) 43.
17 J.A. Blackwell and P.W. Carr, *J. Chromatogr.*, 549 (1991) 59.
18 J.A. Blackwell and P.W. Carr, *J. Liq. Chromatogr.*, 14 (1991) 2875.
19 M.P. Rigney, E.F. Funkenbusch and P.W. Carr, *J. Chromatogr.*, 499 (1990) 291.
20 W.A. Schafer, P.W. Carr, E.F. Funkenbusch and K.A. Parson, *J. Chromatogr.*, 587 (1991) 137.
21 W.A. Schafer and P.W. Carr, *J. Chromatogr.*, 587 (1991) 149.
22 T.P. Weber, P.W. Carr and E.F. Funkenbusch, *J. Chromatogr.*, 519 (1990) 31.
23 T.P. Weber and P.W. Carr, *Anal. Chem.*, 62 (1990) 2620.
24 U. Trüdinger, G. Müller and K.K. Unger, *J. Chromatogr.*, 535 (1990) 111.
25 M.P. Rigney, T.P. Weber and P.W. Carr, *J. Chromatogr.*, 484 (1989) 273.
26 C.B. Amphlett, L.A. McDonald and M.J. Redman, *J. Inorg. Nucl. Chem.*, 6 (1958) 236.
27 N. Michael, W.D. Fletcher, D.E. Croucher and M.J. Bell, *Report CVNA-135*, Carolina-Virginia Nucl. Power Assoc., Charlotte, NC, 1961.

28 C.B. Amphlett, L.A. McDonald and M.J. Redman, *J. Inorg. Nucl. Chem.*, 6 (1958) 220.
29 E.R. Russel, A.W. Adamson, J. Schubert and G.E. Boyd, *Report CN-508*, US Atomic Energy Commission, Oak Ridge, TN, 1943.
30 J.A. Blackwell, unpublished results.
31 K.A. Kraus, T.A. Carlson, D.J. Coombe, J.S. Johnson and H.O. Phillips, *Report ORNL-2004*, US Atomic Energy Commission, Oak Ridge, TN, 1957.
32 K.A. Kraus, H.O. Phillips, T.A. Carlson and J.S. Johnson, *Ion Exchange Properties of Hydrous Oxides, Proceedings of the 2nd International Conference on the Peaceful Uses of Atomic Energy, Geneva, 1958*, United Nations, New York, 1958.
33 K.A. Kraus and H.O. Phillips, *J. Am. Chem. Soc.*, 78 (1956) 694.
34 V. Vesely and V. Pekarek, *Talanta*, 19 (1972) 219.
35 C.B. Amphlett, *Inorganic Ion Exchangers*, Elsevier, Amsterdam, 1964.
36 A. Clearfield (Editor), *Inorganic Ion Exchange Materials*, CRC Press, Boca Raton, FL, 1982.
37 P.D.L. Mercera, J.G. van Ommen, E.B.M. Doesburg, A.J. Burggraaf and J.R.H. Ross, *J. Mater. Sci.*, 27 (1992) 4890.
38 K.S.W. Sing, D.H. Everett, R.A.W. Haul, L. Moscou, R.A. Pieroti, J. Roquerol and T. Siemieniewska, *Pure Appl. Chem.*, 57 (1985) 603.
39 H.C. Wang and K.-L. Lin, *J. Mater. Sci.*, 26 (1991) 2501.
40 A. Ayral, T. Assih, M. Abenoza, J. Phalippou, A. Lecomte and A. Dauger, *J. Mater. Sci.*, 25 (1990) 1268.
41 M. Bensitel, V. Moravek, J. Lamotte, O. Saur and J.C. Lavalley, *Spectrochim. Acta Part A*, 43 (1987) 1487.
42 M. Bensitel, O. Saur, J.C. Lavalley and G. Mabilou, *Mater. Chem. Phys.*, 17 (1987) 249.
43 J.C. Lavalley, M. Bensitel, J.P. Gallas, J. Lanotte, G. Busca and V. Lorenzelli, *J. Mol. Struct.*, 175 (1988) 453.
44 B.H. Davis, *J. Am. Ceram. Soc.*, 67 (1984) c168.
45 R. Srinivasan, R. DeAngelis and B.H. Davis, *J. Mater. Res.*, 1 (1986) 583.
46 A. Clearfield, *Inorg. Chem.*, 3 (1964) 146.
47 A. Clearfield, *Rev. Pure Appl. Chem.*, 14 (1964) 91.
48 A. Clearfield, *J. Mater. Res.*, 5 (1990) 161.
49 G.H. Muha and P.A. Vaughan, *J. Chem. Phys.*, 33 (1960) 194.
50 S.L. Jones and C.J. Norman, *J. Am. Ceram. Soc.*, 71 (1988) C190.
51 P.D.L. Mercera, J.G. van Ommen, E.B.M. Doesburg, A.J. Burggraaf and J.R.H. Ross, *Appl. Catal.*, 57 (1990) 127.
52 G. Gimblett, A.A. Rahman and K.S.W. Sing, *J. Colloid Interface Sci.*, 84 (1981) 337.
53 E. Escalona Platero and M. Peñarroya Mentruit, *Mater. Lett.*, 14 (1992) 318.
54 D. Reinalda and A. Derking, *Eur. Pat.*, 0460738 A1, May 1991.
55 B. Aiken, W.P. Hsu and E. Matijevic, *J. Mater. Sci.*, 25 (1990) 1886.
56 R.C. Buchanan and S. Pope, *J. Electrochem. Soc.*, 130 (1983) 962.
57 T. Masaki, *J. Am. Ceram. Soc.*, 69 (1986) 519.
58 G. Gimblett, A.A. Rahman and K.S.W. Sing, *J. Chem. Tech. Biotechnol.*, 30 (1980) 51.
59 M.A. Blesa, A.J.G. Maroto, S.I. Passaggio, N.E. Figliolia and G. Rigotti, *J. Mater. Sci.*, 20 (1985) 4601.
60 G. Rinn and H. Schmidt, in G.L. Messing and E.R. Fuller (Editors), *Ceramic Trans. 1A*, American Ceramic Society, Westerville, OH, 1988, p. 23.
61 J.A. Blackwell, *Ph.D. Thesis*, University of Minnesota, Minneapolis, MN, 1991, p. 211.
62 T.J. Bastow, M.E. Smith and H.J. Whitfield, *J. Mater. Chem.*, 2 (1992) 989.
63 T.J. Bastow and S.N. Stuart, *Chem. Phys.*, 143 (1990) 459.
64 E. Guglielminotti, *Langmuir*, 6 (1990) 1455.
65 S. Ardizzone and M. Sarti, *Mater. Chem. Phys.*, 28 (1991) 191.
66 A.A. Tsyganenko, D.V. Pozdnyakov and V.M. Filimonov, *J. Mol. Struct.*, 29 (1975) 299.
67 P.A. Agron, E.L. Fuller and H.F. Holmes, *J. Colloid Interface Sci.*, 52 (1975) 553.
68 S. Ardizzone, G. Bassi and G. Liborio, *Colloids Surf.*, 51 (1990) 207.
69 J.D. McCullough and K.N. Trueblood, *Acta Crystallogr.*, 12 (1959) 507.
70 D.K. Smith and H.W. Newkirk, *Acta Crystallogr.*, 18 (1965) 983.
71 Bo-Qing Xu, T. Yamaguchi and K. Tanabe, *Chem. Lett.*, (1988) 1663.
72 W. Stumm, R. Kummert and L. Sigg, *Croat. Chem. Acta*, 53 (1980) 291.
73 L. Orio, V. Bolis, B. Fubini and C. Mortera, in A. Vincencini (Editor), *Ceramics Today —Tommorow's Ceramics*, Elsevier, Amsterdam, 1991, p. 1789.
74 H.F. Holmes, E.L. Fuller and R.B. Gammage, *J. Phys. Chem.*, 76 (1972) 1497.
75 J. Randon, A. Larbot, C. Guizard, L. Cot, M. Lindheimer and S. Partyka, *Colloids Surf.*, 52 (1991) 241.
76 H. Kita, N. Henmi, K. Shimazu, H. Hattori and K. Tanabe, *J. Chem. Soc. Faraday Trans. 1*, 77 (1981) 2451.
77 L.M. Sharygin, V.M. Galkin and S.P. Kurushin, *Kinet. Katal.*, 16 (1975) 1595.
78 T.I. Izotova and M.M. Dubinin, *Zh. Fiz. Chim.*, 39 (1965) 2796.
79 B.C. Lipens and J.H. de Boer, *J. Catal.*, 4 (1965) 319.
80 P.W. Carr, E.F. Funkenbush, M.P. Rigney, P.A. Coleman, D.A. Hanggi and W.A. Schafer, *US Pat.*, 5015373, May 1991.
81 L.M. Sharygin, V.M. Galkin, V.E. Moiseev, V.G. Ponomariev, V.A. Davankov, A.A. Kurganov and T.M. Ponomarieva, *Zhur. Fiz. Khim.*, 66 (1991) 2677.
82 P.D.L. Mercera, J.G. van Ommen, E.B.M. Doesburg, A.J. Burggraaf and J.R.H. Ross, *App. Catal.*, 71 (1991) 363.
83 J. Nawrocki, *Chromatographia*, 31 (1991) 177.
84 D. Amati and E.sz. Kováts, *Langmuir*, 4 (1988) 329.

85 J.E. Dean, *Lange's Handbook of Chemistry*, McGraw-Hill, New York, XIIIth ed., 1985.
86 H.Th. Rijnten, in B.G. Linsen (Editor), *Physical and Chemical Aspects of Adsorbents and Catalysts*, Academic Press, London, 1970, Ch.7, p. 315.
87 W.B. Blumenthal, *The Chemical Behaviour of Zirconium*, D. van Nostrand, New York, 1958, p. 159.
88 R.C. Garvie, in A.M. Alper (Editor), *High Temperature Oxides*, Academic Press, New York, 1970, p. 117.
89 J.W. Meller, *A Comprehensive Treatise on Inorganic and Theoretical Chemistry*, Vol. VII, Longmans, Green and Co., London, 1927, Ch. XLII, p. 98.
90 D.C. Bradley and P. Thornton, in J.C. Bailar Jr., H.J. Emeléus, R. Nyholm and A.F. Trotman-Dickenson (Editors), *Comprehensive Inorganic Chemistry*, Pergamon Press, Elmsford, NY, 1973, Ch. 33.
91 Lifang Sun, M. Annen, F. Lorenzano-Porras, P.W. Carr and A. McCormick, *J. Colloid Interface Sci.*, in press.
92 J.L. Shi, *J. Solid State Chem.*, 95 (1991) 412.
93 I.N. Yermolenko, T.M. Ulyanova, P.A. Vityaz and I.L. Fyodorova, in N. Claussen, M. Rühle and A.M. Hauser (Editors), *Advances in Ceramics*, Vol. 12, American Ceramic Society, Columbus, OH, 1983, p. 826.
94 H.F. Holmes, E.L. Fuller Jr. and R.A. Beh, *J. Colloid Interface Sci.*, 47 (1974) 365.
95 Lifang Sun, M. Annen, F. Lorenzano-Porras, P.W. Carr and A. McCormick, unpublished results.
96 P.W. Carr and Ch. Dunlap, unpublished results.
97 J. Nawrocki, *Chromatographia*, 31 (1991) 197.
98 C. Morterra, R. Aschieri and M. Volante, *Mater. Chem. Phys.*, 20 (1988) 539.
99 A. Auroux and A. Gervasini, *J. Phys. Chem.*, 94 (1990) 6371.
100 L. de O. Léllis, M. Saiki and C. Yamagata, *Publ. IPEN 293*, February 1990.
101 G.A. Parks, *Chem. Rev.*, 65 (1965) 177.
102 S. Ardizzone, G. Chidichimo, A. Golemme and M. Radaelli, *Croat. Chem. Acta*, 63(3) (1990) 545.
103 R.R. Vedula and H.G. Spencer, *Colloids Surf.*, 58 (1991) 99.
104 Ming-Yuan He and J.G. Ekerdt, *J. Catal.*, 87 (1984) 381.
105 W. Hertl, *Langmuir*, 5 (1989) 96.
106 Y. Ghaemi and R.A. Wall, *J. Chromatogr.*, 174 (1979) 51.
107 A.E. Regazzoni, M.A. Blesa and A.J.G. Maroto, *J. Colloid Interface Sci.*, 91 (1983) 560.
108 R.J. Pugh, in G.L. Messing, S. Hirano and H. Hausner (Editors), *Ceram. Trans.*, Vol. 12 (*Ceramic Powder Sci., III*), American Ceramic Society Inc., Westerville, OH, 1990, p. 375.
109 A. Bleier and C.G. Westmoreland, in Y.A. Attia, B.M. Moudgil and S. Chander (Editors), *Interfacial Phenomena in Biotechnology and Materials Processing*, Elsevier, Amsterdam, 1988, p. 217.
110 M. Hashiba, H. Okamoto, Y. Nurishi and K. Hiramatsu, *J. Mater. Sci.*, 23 (1988) 2893.
111 B. Platonov, A.A. Baran and T.A. Polischuk, *Acta Phys. Chem.*, 25 (1979) 201.
112 A.A. Baran, N.S. Mitina and B.E. Platonov, *Kolloid. Zh.*, 44 (1982) 964.
113 M.A.C.G. van de Graaf and A.J. Burggraaf, in N. Claussen, M. Rühle and A.H. Hauer (Editors), *Advances in Ceramics*, Vol. 12, American Ceramic Society, Columbus, OH, 1983, p. 744.
114 M.J. Wax and R.K. Grasselli, *Eur. Pat.*, No. 0490226 A1, June 1992.
115 Nyacol Products Inc., Ashland, MA.
116 E.F. Funkenbush, P.W. Carr, D.A. Hanggi and T.P. Weber, *US Pat.*, No. 5108597, April, 1992.
117 N.D. Danielson and J.J. Kirkland, *Anal. Chem.*, 59 (1987) 2501.
118 R.K. Iler and H.J. McQueston, *US Pat.*, 4010242, March 1977.
119 M. Bensitel, O. Saur, J.-C. Lavalley and B.A. Morrow, *Mater. Chem. Phys.*, 19 (1988) 147.
120 V.V. Lunin, E.Yu. Badina, N.N. Kuznetsova and A.O. Turakulova, *Zh. Fiz. Chem.*, 64 (1990) 2777; *Russ. J. Phys. Chem.*, 64 (1990) 1493.
121 L. Lerot, F. Legrand and P. deBruycker, *J. Mater. Sci.*, 26 (1991) 2353.
122 R. Janzen, K.K. Unger, H. Giesche, J.N. Kinkel and M.T.W. Hearn, *J. Chromatogr.*, 397 (1987) 91.
123 M.A. Rounds and F.E. Regnier, *J. Chromatogr.*, 443 (1988) 73.
124 R. Arshady, *J. Chromatogr.*, 586 (1991) 181.
125 R. Arshady, *J. Chromatogr.*, 586 (1991) 198.
126 J. Yu and Z. El Rassi, *J. Chromatogr.*, 631 (1993) 91.
127 *Handbook of Chemistry*, CRC Press, Boca Raton, FL, 67th ed., 1986/1987.
128 C.A. Hampel (Editor), *Encyclopedia of Chemical Reactions*, Vol. VIII, Reinhold Publ. Corp., New York, 1959.
129 O.A. Govorukhina, V.N. Brusentsova, T.N. Vasil'eva, N.L. Mikhailova, S.D. Nikitina, R.I. Shchegelova and V.A. Masloboev, *Zh. Neorg. Khim.*, 34 (1989) 3159; *Russ. J. Inorg. Chem.*, 34 (1989) 1807.
130 P.W. Carr and J. Nawrocki, unpublished results.
131 E.E. Bibik, N.B. Vredenskaya and A.P. Nechiporenko, *Zh. Prikl. Khim.*, 59 (1986) 2533.
132 B.-Q. Xu, T. Yamaguchi and K. Tanabe, *Mater. Chem. Phys.*, 19 (1988) 291.
133 A.A. Tsyganenko and V.M. Filimonov, *Spectrosc. Lett.*, 5 (1972) 477.
134 T. Yamaguchi, Y. Nakamo and K. Tanabe, *Bull. Chem. Soc. Jap.*, 51 (1978) 2482.
135 J. Erkelens, H.Th. Rijnten and S.H. Eggink-du Burck, *Recl. Trav. Chim. Pays-Bas*, 91 (1972) 1462.
136 N.E. Tret'yakov, D.V. Pozdnyakov, O.M. Oranskaya and V.M. Filimonov, *Russ. J. Phys. Chem.*, 44 (1970) 596.
137 M. Aberg, *Acta Chem. Scan. Ser. B*, 31 (1977) 177.
138 L.M. Zaitsev, *Russ. J. Inorg. Chem.*, 11 (1966) 900.
139 L.M. Zaitsev and G.S. Bochkarev, *Russ. J. Inorg. Chem.*, 7 (1962) 411.
140 M.S. Kaliszewski and A.H. Hauer, *J. Am. Ceram. Soc.*, 73 (1990) 1504.
141 N.E. Tret'yakov and V.N. Filimonov, *Kin. Katal.*, 13 (1972) 815.

142 M.L. Hair and W. Hertl, *J. Phys. Chem.*, 74 (1970) 91.
143 K. Tanabe in J.R. Anderson and M. Boudart, *Catalysis —Science and Technology*, Vol. 2, Springer Verlag, Berlin, 1981, Ch. 5.
144 K. Tanabe, T. Sumiyoshi, K. Shibata, T. Kiyoura and J. Kitagawa, *Bull. Chem. Soc. Jap.*, 47 (1974) 1064.
145 A.V. Kiselev and A.V. Uvarov, *Surface Sci.*, 6 (1967) 399.
146 G. Zhang, H. Hattori and K. Tanabe, *Bull. Chem. Soc. Jap.*, 62 (1989) 2070.
147 G. Zhang, H. Hattori and K. Tanabe, *Appl. Catal.*, 36 (1988) 189.
148 K. Shibata, T. Kiyoura, J. Kitagawa, T. Sumiyoshi and K. Tanabe, *Bull. Chem. Soc. Jap.*, 46 (1973) 2985.
149 Gong-Wei Wang, H. Hattori and K. Tanabe, *Bull. Chem. Soc. Jap.*, 56 (1983) 2407.
150 K. Tanabe, I. Ichikawa and H. Ikeda, *J. Res. Inst. Catal. Hokkaido Univ.*, 19 (1972) 185.
151 T. Yamaguchi, K. Tanabe and Yao Chin Kung, *Mater. Chem. Phys.*, 16 (1986) 67.
152 A.A. Tsyganenko and V.M. Filimonov, *J. Mol. Struct.*, 19 (1973) 579.
153 V. Bolis, C. Morterrra, M. Volante, L. Orio and B. Fubini, *Langmuir*, 6 (1990) 695.
154 Y. Nakano, T. Iizuka, H. Hattori and K. Tanabe, *J. Catal.*, 57 (1978) 1.
155 C. Morterra, L. Orio and C. Emanuel, *J. Chem. Soc. Faraday Trans.*, 86 (1990) 3003.
156 C. Morterra, G. Giotti, F. Boccuzzi and S. Collucia, *J. Catal.*, 51 (1978) 299.
157 C. Morterra, G. Cerrato and C. Emanuel, *Mater. Chem. Phys.*, 29 (1991) 447.
158 C. Morterra and L. Orio, *Mater. Chem. Phys.*, 24 (1990) 247.
159 J. Kondo, H. Abe, Y. Sakata, K. Maruya, K. Domen and T. Onishi, *J. Chem. Soc. Faraday Trans. I*, 84 (1988) 511.
160 A.A. Tsyganenko and E.A. Trusov, *Zh. Fiz. Khim.*, 59 (1985) 2902; *Russ. J. Phys. Chem.*, 59 (1985) 1554.
161 R.G. Silver, N.B. Jackson and J.G. Ekerdt, in W.M. Ayers (Editor), *Catalytic Activation of Carbon Dioxide (ACS Symp. Ser. No. 363)*, American Chemical Society, Washington, DC, 1988, p. 123.
162 H.P. Boehm, *Disc. Faraday Soc.*, 52 (1971) 264.
163 C. Morterra, R. Aschieri, V. Bolis, B. Fubini and M. Volante, *Gaz. Chim. Ital.*, 118 (1988) 479.
164 C. Morterra, E. Gianello, L. Orio and M. Volante, *J. Phys. Chem.*, 94 (1990) 3111.
165 M.J. Torralvo, M.A. Alario and J. Soria, *J. Catal.*, 86 (1984) 473.
166 A. Gervasini and A. Auroux, *J. Catal.*, 131 (1991) 190.
167 C. Morterra and G. Cerrato, *Langmuir*, 6 (1990) 1810.
168 V. Bolis, B. Fubini and E. Giamello, *Mater. Chem. Phys.*, 29 (1991) 153.
169 M.F. Sinilo, E.A. Stepanova and V.C. Komarov, *Kin. Kat.*, 30 (1989) 1196.
170 A. Ruvarac, in A. Clearfield (Editor), *Inorganic Ion Exchange Materials*, CRC Press, Boca Raton, FL, 1982, p. 141.
171 H. Vinek, H. Noller, M. Ebel and K. Schwarz, *J. Chem. Soc. Faraday Trans. I*, (1977) 734.
172 N.K. Huang, *J. Mat. Sci. Lett.*, 11 (1992) 681.
173 D. Majumdar and D. Chatterjee, *J. Appl. Phys.*, 70 (1991) 988.
174 T.N. Lapteva, V.V. Moskovskikh, G.D. Kharlampowich, V.P. Timakov and A.A. Pospelov, *Zh. Fiz. Khim.*, 53 (1979) 980; *Russ. J. Phys. Chem.*, 53 (1971) 551.
175 T.N. Lapteva, N.K. Bulatov, V.V. Moskovskikh and N.D. Peshekonov, *Zh. Fiz. Khim.*, 62, 980 (1988); *Russ. J. Phys. Chem.*, 62 (1988) 406.
176 J.A. Blackwell and P.W. Carr, *Anal. Chem.*, 64 (1992) 853.
177 J.A. Blackwell and P.W. Carr, *Anal. Chem.*, 64 (1992) 863.
178 R.O. James and G.A. Parks, in E. Matijević (Editor), *Surface and Colloid Science*, Vol. 12, Plenum Press, New York, 1982, p. 119.
179 K. Tanabe, private communication, Feb. 1993.
180 A. Kozawa, *J. Electrochem. Soc.*, 106 (1959) 552.
181 J.A. Davis, R.A. James and J.O. Leckie, *J. Colloid Interface Sci.*, 63 (1978) 480.
182 S. Matison and A.J. Pugh, *Soil Sci.*, 38 (1934) 299.
183 F.S. Mandel and H.G. Spencer, *J. Colloid Interface Sci.*, 77 (1980) 577.
184 E.J.W. Verwey, *Recl. Trav. Chim. Pays-Bas*, 60 (1941) 625.
185 K.C. Ray and S. Khan, *Indian J. Chem.*, 13 (1975) 577.
186 K.C. Ray and P.K. Sen, *Indian J. Chem.*, 12 (1974) 170.
187 S.M. Ahmed, *Can. J. Chem.*, 44 (1966) 1663.
188 R.H. Yoon, T. Salman and G. Donnay, *J. Colloid Interface Sci.*, 70 (1979) 483.
189 P.H. Tewari, R.H. Tuxworth and W. Lee, in R.S. Alwitt (Editor), *Proceedings of the Symposium on Oxide-Electrolyte Interfaces*, Miami, 1972, Electro-Chemical Society, Princeton, NJ, p. 91.
190 G.W. Smith and T. Salman, *Can. Met. Q.*, 5 (1966) 93.
191 J. Randon, A. Larbot, L. Cot, M. Lindheimer and S. Partyka, *Langmuir*, 7 (1991) 2654.
192 S.K. Milonjić, Z.E. Ilić and M.M. Kopečni, *Colloids Surf.*, 6 (1983) 167.
193 M. Persin, J. Randon, J. Sarrazin, A. Larbot, C. Guizard and L. Cot, *J. Colloid Interface Sci.*, 154 (1992) 416.
194 T.J. Bastow and M.E. Smith, *Solid State NMR*, in press.
195 D.E. Yates, S. Levine and T.W. Healy, *J. Chem. Soc. Faraday Trans. I*, 70 (1974) 1807.
196 F.J. Hingstone, R.J. Atkinson, A.M. Posner and J.P. Quirk, *Nature*, 215 (1967) 1459.
197 C. Morterra, R. Aschieri, V. Bolis and E. Borello, in C. Morterra, A. Zecchina and G. Costa (Editors), *Structure and Reactivity of Surfaces*, Elsevier, Amsterdam, 1989, p. 703.
198 A.E. Regazzoni, M.A. Blesa and A.J.G. Maroto, *J. Colloid Interface Sci.*, 122 (1988) 315.
199 M.A. Blesa, A.J.G. Maroto and A.E. Regazzoni, *J. Colloid Interface Sci.*, 99 (1984) 32.
200 Won-wook Choi and K.Y. Chen, *Environ. Sci. Technol.*, 13 (1979) 189.

201 L. Sigg and W. Stumm, *Colloids Surf.*, 2 (1981) 101.
202 K. Fujimura and T. Ando, *J. Chromatogr.*, 114 (1975) 15.
203 K. Fujimura and T. Ando, *Anal. Chem.*, 49 (1977) 1179.
204 A. Dyer, D. Leigh and W.E. Sharples, *J. Chromatogr.*, 118 (1976) 319.
205 G. Urbach, *Anal. Chem.*, 36 (1964) 2364.
206 L. Maya, *Inorg. Nucl. Chem. Lett.*, 15 (1979) 207.
207 L. Maya and P.O. Danis, *J. Chromatogr.*, 190 (1980) 145.
208 I.D. Coussio, G.B. Marini-Bettòlo and V. Moscatelli, *J. Chromatogr.*, 11 (1963) 238.
209 U. Constantino, in A. Clearfield (Editor), *Inorganic Ion Exchange Materials*, CRC Press, Boca Raton, FL, 1982, p. 111.
210 G. Hevesy and K. Kimura. *J. Am. Chem. Soc.*, 47 (1925) 2540.
211 R. Kummert and W. Stumm, *J. Colloid Interface Sci.*, 75 (1980) 373.
212 M.J. Gorbunoff, *Anal. Biochem.*, 136 (1984) 425.
213 J.H. Knox, K.K. Unger and H. Mueller, *J.Liq. Chromatogr.*, 6 (Suppl.) (1983) 1.
214 C.F. Poole and S.A. Schuette, *Contemporary Practice of Chromatography*, Amsterdam, Elsevier, 1984.
215 R.G. Pearson, *J. Chem. Educ.*, 45 (1968) 581.
216 R.G. Pearson, *J. Chem. Educ.*, 45 (1968) 643.
217 J.A. Blackwell, *Chromatographia*, 35 (1993) 133.
218 S.M. Lee, M.E. Gustafson, D.J. Pickle, M.C. Flickinger, G.M. Muschik and A.C. Morgan Jr., *J. Biotechnol.*, 4 (1986) 189.
219 M. Nivva, K.C. Milner and J.A. Rudbach, *J. Bacteriol.*, 97 (1969) 1069.
220 Ch.P. Prior, in C. Ho and D.I.C. Wang (Editors), *Animal Cell Bioreactions*, Butterworth-Heinemann, Boston, 1991, Ch. 17.
221 J.A. Blackwell and P.W. Carr, *J. Chromatogr.*, 596 (1992) 27.
222 J.A. Blackwell and P.W. Carr, *J. Liq. Chromatogr.*, 15 (1992) 1487.
223 J.A. Blackwell and P.W. Carr, *J. Liq. Chromatogr.*, 15 (1992) 727.
224 *BCA and BCA Protein Assay Reagent, Instructions 23230, 23225*, Pierce Chemical Company, Rockford, IL, 1986.
225 P.K. Smith, R.I. Krohn, G.T. Hermanson, A.K. Malia, F.H. Gartner, M.D. Provenzano, E.K. Fujimoto, N.M. Goecke, B.J. Olson and D.C. Klenk, *Anal. Biochem.*, 150 (1985) 76.
226 J. Gobet and E.sz. Kováts, *Adsorpt. Sci. Technol.*, 1 (1984) 111.
227 W. Noll, *Chemistry and Technology of Silicones*, Academic Press, New York, 1968.
228 P.R. Moses, L. Wier, and R.W. Murray, *Anal. Chem.*, 47 (1975) 1882.
229 F. Schindler and H. Schmidbaur, *Angew. Chem.*, 79 (1967) 697; *Angew. Chem. Int. Ed. Engl.*, 6 (1967) 683.
230 P. Kolla, J. Köhler and G. Schomburg, *Chromatographia*, 23 (1987) 465.
231 U. Bien-Vogelsang, A. Deege, H. Figge, J. Köhler and G. Schomburg, *Chromatographia*, 19 (1984) 170.
232 G. Schomburg, J. Köhler, H. Figge, A. Deege and U. Bien-Vogelsang, *Chromatographia*, 18 (1984) 265.
233 K.K. Unger, *Anal. Chem.*, 59 (1983) 361A.
234 J.H. Knox and B. Kaur, in P.R. Brown and R.A. Hartwick (Editors), *High Performance Liquid Chromatography*, John Wiley and Sons, New York 1989, Ch. 4, p. 189.
235 R. Leboda, *Mater. Chem. Phys.*, 31 (1992) 243.
236 T.P. Weber, P.W. Carr and E.F. Funkenbush, *J. Chromatogr.*, 519 (1990) 31.
237 F. Belliardo, O. Chiantore, D. Berek, I. Novak and C. Lucarelli, *J. Chromatogr.*, 506 (1990) 371.
238 E.F. Funkenbush, P.W. Carr, D.A. Hanggi and T.P. Weber, *US Pat.*, 5,182,016, Jan. 1993.
239 N.D. Danielson, J.E. Katon, S.P. Boufford and Zhaohai Zhu, *Anal. Chem.*, 64 (1992) 2183.
240 N.J. Singh Rajev and S.N. Tandon, *Ind. J. Chem.*, 15B (1977) 581.
241 A.K. Misra, D.K. Misra and V.K. Maheshwari, *J.Liq. Chromatogr.*, 14 (1991) 1469.
242 A.J. Lecloux, in J.R. Anderson and M. Boudart (Editors), *Catalysis — Science and Technology*, Vol. 2, Springer Verlag, Berlin, 1981, Ch. 4.
243 M.P. Rigney, *PhD Thesis*, University of Minnesota, Minneapolis, MN, USA, 1988.
244 D.A. Hanggi and N.R. Marks, *LC·GC*, 11 (1993) 128.
245 N.M. Djordjević, S.K. Milonjić and M.M. Kopečni, *Bull. Chem. Soc. Jap.*, 54 (1981) 3162.
246 B. Fubini, B. Volis, M. Bailes and F.S. Stone, *Solid State Ionics*, 32/33 (1989) 258.
247 R.Yu. Sheinfain and T.F. Makovskaya, *Kolloid. Zh.*, 38 (1975) 816.
248 R.G. Silver, C.J. Hou and J.G. Ekerdt, *J. Catal.*, 118 (1989) 400.
249 R. Franklin, P. Goulding, J. Haviland, R.W. Joyner, I. McAlpine, P. Moles, C. Norman and T. Nowell, *Catal. Today*, 10 (1991) 405.

Journal of Chromatography A, 657 (1993) 283–303
Elsevier Science Publishers B.V., Amsterdam

CHROM. 25 534

Hydrodynamic chromatography of polymers in packed columns

Gerrit Stegeman, Johan C. Kraak* and Hans Poppe

Laboratory for Analytical Chemistry, University of Amsterdam, Nieuwe Achtergracht 166, 1018 WV Amsterdam (Netherlands)

Robert Tijssen

Koninklijke/Shell-Laboratorium Amsterdam, Department AG/2, Badhuisweg 3, 1031 CM Amsterdam (Netherlands)

(First received June 14th, 1993; revised manuscript received August 30th, 1993)

ABSTRACT

Hydrodynamic chromatography (HDC) of linear random coil polymers in columns packed with 1.5-μm non-porous particles was investigated. For polymers with high molecular masses (10^4–10^7), the resolution appears to be almost independent of the eluent velocity. This allows for high-speed polymer separations with high efficiency. A model for the migration rate of polymers, based on the assumption that interstitial channels in a packed column can be represented by a bundle of capillary tubes, is compared with experimental elution data. The influence of polymer size and type, solvent goodness and mobile phase velocity on elution in HDC was investigated. Elution behaviour in packed columns appears to obey basically the simple migration theories developed for open tubes. The relative peak positions in the HDC trace depend slightly on the eluent velocity.

INTRODUCTION

Hydrodynamic chromatography (HDC) in packed or open-tubular columns is a technique able to separate macromolecules and particles according to size [1]. It has found application for the separation of a variety of samples in the (sub-)micrometre range such as polymer latices [2,3], flexible and rigid polymers [4–7], viruses [8], pollen [2,9], paper fibres [10,11], silica particles [9,12], proteins [4,13], DNAs [14] and liposomes [15].

DiMarzio and Guttman [16–18] were the first to give a theoretical explanation of the separation mechanism in HDC. They considered the flow of finite-sized dispersed particles through a capillary tube and concluded that the larger particles will have a higher average velocity than the smaller particles, because the particle centre cannot sample the lowest velocities on the streamlines near the wall, within a distance equal to the particle radius r_p (see Fig. 1). According to this simple exclusion model, the ratio of particle to tube radius, λ, determines to what extent the average particle velocity differs from the average solvent velocity. Despite its simplicity, this model is able to predict, at least qualitatively, the elution behaviour in capillary tubes and packed columns filled with non-porous particles.

In addition to steric exclusion, DiMarzio and Guttman also included hydrodynamic wall effects, which retard the particles with respect to the local undisturbed fluid velocity. In a refined theory by Brenner and Gaydos [19], these wall effects were described more accurately for flow in open tubes.

Small *et al.* [3,20] showed that the migration rate of polymer colloids in packed columns is

* Corresponding author.

0021-9673/93/$06.00
SSDI 0021-9673(93)E0951-P

strongly influenced by colloidal forces between the colloids and the packing particles. Colloidal forces, including electrostatic and Van der Waals forces, influence the distribution of solute particles over the cross-section of a flow channel. Because of such forces, particles do not sample the accessible streamlines in a velocity profile with equal probability. Theoretical migration models which include colloidal forces were developed for flow in open tubes by Prieve and Hoysan [21], Silebi and McHugh [22] and Buffham [23]. These models were first applied to model the migration behaviour in packed columns by representing the interstitial channels as a bundle of circular tubes. Comparison with Small *et al.*'s data showed that trends in the elution behaviour can be predicted well but no exact fit is obtained unless model parameters are adjusted. A better agreement between these models and elution data was recently obtained in capillary HDC [24].

A further complication in the treatment of the separation mechanism in HDC is the effect of solvent flow-rate on the relative particle velocity (the ratio of the average particle velocity to the average solvent velocity). In capillary HDC the relative particle velocity was reported to increase with increasing eluent flow velocity by Noel *et al.* [9] and Silebi and DosRamos [24], the increase being more pronounced for larger particles. This phenomenon has been attributed to radial particle migration due to fluid inertia such as described by Segré and Silberberg [25]. This so-called "tubular pinch" effect was recently included in theoretical migration models for capillary tubes (together with colloidal forces, hydrodynamic wall effects and wall exclusion) by DosRamos and Silebi [26] and Ploehn [27]. Comparison of these detailed models with experimental results in open tubes showed that effects of flow-rate could be described satisfactorily. More generally, these models seem to provide a fairly comprehensive analysis of the separation process in which the variables affecting the migration of particles are well understood. In packed-column HDC the situation is much more complicated. It may be argued that flow-induced lateral migration can also be of importance here. Indeed, the flow-rate has been reported to influence the relative velocity of different types of samples, but the effects on the migration rate are opposite to those observed in open tubes [12,28,29]. Whether this can be (partly) attributed to lateral migration phenomena is still unclear at present. Alternative explanations in terms of shear orientation and shear deformation have been put forward.

In the study of the transport of flexible polymers in HDC, additional difficulties emerge. Size, shape and structure of the polymer are not known accurately, nor are their effects on polymer hydrodynamics. Besides, these parameters are subject to the influence of solvent, temperature, concentration and shear rate. Tijssen and co-workers [5,30] studied the migration rate of dissolved linear polystyrenes in open microcapillary tubes and compared this with refined theoretical models for the migration of rigid impermeable and permeable spheres. They found that these models are basically obeyed and only need small modifications to describe the transport of flexible polymers. In a similar study, the migration of polystyrenes in packed columns filled with 1.5–3.5-μm particles was investigated [12]. Experimental elution data were compared with modified capillary migration models in which flow-rate effects were not accounted for. Although a slight velocity dependence of the migration rate was observed for the ultra-high molecular masses, the agreement with the theoretical models was found to be good. This finding again demonstrated the usefulness of capillary migration models in modelling the migration behavior in packed columns.

In this work, the migration of flexible polymer in packed columns was further investigated. The effect of polymer size and coil segment density on the migration rate was studied in packed columns filled with 1.5-μm solid silica packing particles. Linear polystyrenes (PS), polyisoprenes (PIP), polybutadienes (PB) and poly(methyl methacrylate)s (PMMA) in both good and poor solvents were used as test samples. The observed elution behaviour was compared with predictions from a migration model that represents the interstitial channels in a packed column by open tubes. Flow-rate-dependent migration was studied and possible explanations are sug-

gested. Further, the separation power of the columns used was demonstrated by means of some high-resolution separations of polymers.

THEORY

Polymer size

In order to describe the factors that determine the dimensions of polymer molecules in solution, an adequate model for a polymer chain is required. A useful but inaccurate model for linear polymer molecules is the random-flight chain, which is a chain of segments connected by completely flexible joints [31,32]. The modelling of a polymer chain can be made more realistic by including short-range interactions that account for fixed bond angles and hindered internal rotation. This results in a so-called ideal or unperturbed chain which has a Gaussian segment density distribution. The molecular dimensions of such a chain, called the unperturbed dimensions, can be expressed conveniently in terms of the mean square radius of gyration $\langle r_G^2 \rangle_0$, according to

$$\langle r_G^2 \rangle_0 = \frac{\sigma l^2 n}{6} \quad (1)$$

where σ is a structural parameter or "conformation factor [32]", l is the segment length and n is the number of segments in the chain. The parameter σ (which is independent of n) describes the short-range interactions and has a value ≥ 1. When $\sigma = 1$, eqn. 1 represents the dimensions of a perfectly flexible random-flight chain.

On choosing different types of polymers, we can expect σ and l to vary considerably. As a result, the size and compactness of a chain are strongly dependent on the type of polymer. This will turn out to be an important aspect in this study.

In order to improve further the modelling of a polymer chain, long-range interactions need to be considered. For example, polymer segments occupy finite volumes and therefore exclude other segments from occupying the same space at the same time. This leads to a coil that is expanded compared with the unperturbed one. Further, the polymer–solvent interactions influence the coil dimensions by either expanding or contracting the coil. In a good solvent, the polymer–solvent interactions are thermodynamically favourable and solvent molecules will be imbibed, resulting in coil expansion. With a poor solvent, the solvent molecules will be squeezed out, contracting the polymer chain. The relative goodness of a solvent depends on the temperature and the nature of the polymer–solvent system.

In most circumstances, the long-range interactions will expand the polymer coil compared with the unperturbed dimensions. Occasionally, in very poor solvents, the polymer size can be smaller than the unperturbed dimensions. Including long-range interferences, the mean square radius of gyration of a linear macromolecule is written as

$$\langle r_G^2 \rangle = \alpha^2 \langle r_G^2 \rangle_0 \quad (2)$$

where α is the linear expansion factor, which in general depends on the number of bonds n. Only when $\alpha = 1$ do long-range expansion and contraction apparently cancel, and the polymer chain behaves like an unperturbed chain. This occurs under special conditions of solvent and temperature, known as θ-conditions. Under θ-conditions, the coil dimensions are predicted to be independent of the particular solvent used. This has indeed been found experimentally for non-polar polymers in non-polar solvents, but deviations occur in case of polar polymers and solvents [33].

From the modelling of polymer chains, the radius of gyration r_G $[= (\langle r_G^2 \rangle)^{1/2}]$ logically becomes the basic size parameter. In order to test the HDC migration models, reliable relationships between r_G and the molecular mass of polymers are required. Such relationships can be derived from measurements that directly yield r_G such as light-scattering or neutron-scattering measurements. These relationships are well documented for polymers in θ-solvents [34]. With good solvents however, such relationships are only known for a limited number of polymer–solvent combinations. Alternatively, approximate r_G–M relationships can be obtained indirectly from viscometric measurements. As vis-

cosity measurements are the most commonly used way to study polymer solutions, many data are available. For good solvents, the radius of gyration can be calculated according to the Flory–Fox and Ptitsyn–Eizner relationship [35,36]:

$$r_G = \frac{1}{\sqrt{6}}\left(\frac{KM^{1+a}}{\phi_0(1-2.63\beta+2.86\beta^2)}\right)^{1/3} \quad \text{(cm)} \quad (3)$$

where the product KM^a is the polymer intrinsic viscosity, with K (in ml/g) and a being the Mark–Houwink constants, ϕ_0 is the Flory universal constant equal to $2.86 \cdot 10^{23}$ (mol^{-1}) and $\beta = (2a-1)/3$.

As stated in the Introduction, the main mechanism behind separation in HDC is the exclusion of solutes from the wall. Therefore, the size parameter of interest is the one that determines exclusion from a wall. This radius will be called r_p throughout. With rigid spherical solutes, the term "size" is unambiguous, but for polymer chains with continuously changing shapes, the relationship between any kind of radius and the extent of exclusion is less clear. Van Kreveld and Van den Hoed [37] proposed that the actual radius of a linear random coil polymer determining exclusion is half of the mean maximum cross-section of the random coil. This so-called effective radius r_{eff} is related to r_G according to

$$r_{eff} = \frac{\sqrt{\pi}}{2} \cdot r_G \quad (4)$$

r_{eff} has been used successfully in modelling the migration of random coil polymers in SEC [37] and HDC [5,12]. Still, the problem of polymer size near a solid wall has not yet been fully solved, and size parameters other than r_{eff} have been proposed (see ref. 30 for a discussion).

Other frequently used size parameters are based on a hard sphere representation of a polymer coil [38]. The equivalent sphere representation naturally originates from the spherical shape of the time-averaged random coil conformations. Hard-sphere radii such as the hydrodynamic, the viscometric or the thermodynamic radius are apparent radii equal to the radii of a hard sphere of which a given physical property is the same as that of the polymer coil. As such equivalent sphere approaches are crude and limited models, the hard-sphere radii are not exactly related to r_G. In this study, a polymer hard-sphere radius used in a general sense will be termed r_s. The hydrodynamic radius is denoted r_h.

Flow permeability of polymers

An important aspect in describing the hydrodynamic behaviour of polymers is the flow permeability of the chain. In this regard, two limits may be considered: the free-draining and the non-draining limit. In the free-draining limit, all chain segments experience the flow as if it were undisturbed by other segments. In other words, the chain is seen as an assembly of independent hydrodynamic units. In the non-free-draining limit, the solvent in the interior of the chain domain is immobilized with respect to the chain and the polymer behaves as hydrodynamically impermeable to the flow. A transition from free-draining to non-free-draining is predicted with increasing n, as chain segments in the centre are then becoming increasingly shielded.

Viscometric measurements proved that, except for a very low degree of polymerization, polymer chains behave practically as non-free-draining [32]. The same conclusions can be drawn from theoretical calculations, which showed that indeed the solvent in the interior of a polymer coil is almost stationary with respect to the coil [39]. On the other hand, the same calculations also indicated that the flow permeability of the chain increased substantially on going from the centre to the outside of the polymer.

Hence the chain as a whole can be considered as an almost impermeable hydrodynamic body, although microscopically the picture is more complicated.

Migration behaviour of polymers in packed columns

Deriving theoretical models for the migration of polymers in flowing media is complicated. Adequate modelling is actually restricted to simple flow geometries such as circular tubes. Attempts to tackle more difficult flow systems for this reason necessarily fall back on simplified

channel geometries. In this study in which polymer migration in packed columns is treated, the interstitial channels are represented by a parallel array of capillaries of equal size. Following earlier work in this field, we take as the equivalent capillary radius the hydraulic radius R_0, which is the radius of a capillary tube with equal volume-to-surface ratio as the packed bed [1,12,21]:

$$R_0 = \frac{d_p}{3} \cdot \frac{\epsilon}{1-\epsilon} \tag{5}$$

where d_p is the diameter of the packing particles and ϵ is the column porosity, which is the ratio of the interstitial liquid volume V_0 to the total column volume V_c. The simplifying assumptions on flow channel geometry allow for the use of capillary migration models. Consequently, in this section we shall focus further on the migration of polymers in open tubes.

In a tube of radius R an expression for the mean axial velocity $\langle v_p \rangle$ of a spherical particle or polymer with radius r_p is [19]

$$\langle v_p \rangle = \frac{\int_0^{R-r_p} v_p(r)\, e^{-E(r)} r\, dr}{\int_0^{R-r_p} e^{-E(r)} r\, dr} \tag{6}$$

where $v_p(r)$ is the local axial velocity of the particle and $E(r)$ is the dimensionless total potential experienced by a particle due to interactions with the capillary wall. The upper limit of integration $R - r_p$ accounts for the exclusion of the solute centre from the wall region.

In general, a non-zero value of $E(r)$ will cause the accessible radial positions in the tube to be sampled with unequal probability, leading to a radial concentration profile. $E(r)$ can contain colloidal interactions but may also include hydrodynamic forces in the form of a hydrodynamic "potential". Since in our study we focus on the migration behaviour of polymers dissolved in organic solvents, we assume that colloidal forces are absent. In capillary HDC it was shown that hydrodynamic forces cannot be omitted. A substantial influence, expressed in a flow-rate-dependent migration rate, was observed, even for solutes as small as dissolved polymers [30]. Whether hydrodynamic forces can also be significant in packed columns is not certain. Including hydrodynamic forces in migration models is very complicated. Only for flow in channels of fairly simple geometry (*i.e.*, flow in open tubes or between parallel plates), semi-empirical models have been developed [26,27,30]. Such theories, however, certainly cannot be applied directly to packed columns. In this study we shall not attempt to formulate a theory for hydrodynamic forces in packed columns. Rather, we shall neglect these forces for the moment and treat them only qualitatively in a subsequent section on flow-rate-dependent migration behaviour.

Neglecting lateral forces on the polymer molecules, we assume that all radial positions are sampled with equal probability except those in the exclusion layer (see Fig. 1). The local axial particle velocity $v_p(r)$ in a cylindrical tube can then be expressed as

$$v_p(r) = 2\langle v_m \rangle \left(1 - \frac{r^2}{R^2}\right) - v_s(r) \tag{7}$$

where $\langle v_m \rangle$ is the average velocity of the mobile phase and $v_s(r)$ is the slip velocity of the particle. The slip velocity describes the extent to which the centre of mass of a neutrally buoyant particle lags the local (unperturbed) eluent velocity. For homogeneous solid spheres, it has been found that the slip velocity depends on radial position r and on the ratio of the particle to tube radius. According to Brenner [40] and Goldman *et al.* [41], the slip velocity can be expressed as

$$v_s(r) = \gamma(r)\langle v_m \rangle \left(\frac{r_p}{R}\right)^2 = \gamma(r)\langle v_m \rangle \lambda^2 \tag{8}$$

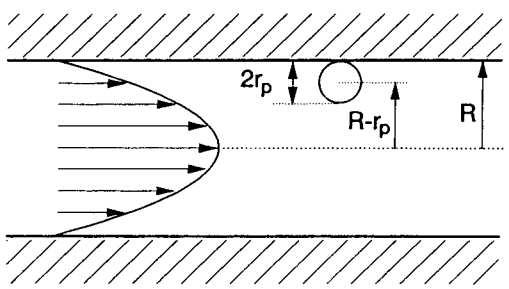

Fig. 1. Transport of a spherical particle immersed in Poiseuille flow through a cylindrical capillary.

where $\gamma(r)$ is the wall-effect parameter and λ is defined as the ratio r_p/R. $\gamma(r)$ is a function of the radial position and λ. In the centre of the tube $\gamma(r) = 4/3$.

In a pioneering effort to derive an expression for the slip velocity of free-draining polymers in Poiseuille flow through an open tube, DiMarzio and Guttman [17] represented the polymer molecule by a rigid sphere that is permeable to the solvent. They arrived at the following expression for the slip velocity:

$$v_s(r) = \gamma \langle v_m \rangle \left(\frac{r_G}{R}\right)^2 \quad (9)$$

In the approach of DiMarzio and Guttman, $\gamma = 4/3$ at every radial position and for every value of λ. Brenner and Gaydos argued that this is not entirely correct, because in this expression the hydrodynamic retardation of a sphere in the direct neighbourhood of the wall is not properly accounted for [17,19]. Strictly, eqn. 9 is not valid over the whole cross-section of the tube but only represents the slip at the axis. Keeping this in mind, there is a remarkable similarity between eqn. 9 and the expression obtained for the slip of a solid sphere in the centre of a tube (see eqn. 8). The difference between the permeable-sphere and the solid-sphere approach is apparently reflected in different radii in the expression for $v_s(r)$. For solid spheres the slip velocity is related to r_p whereas for permeable spheres a dependence on r_G is found (note that for both permeable and solid rigid spheres with a homogeneous mass distribution, $r_G = \sqrt{3/5} \cdot r_p$). Whether this means that the entire solid-sphere theory can be carried over to permeable spheres by simply replacing the solid sphere radius by r_G is not certain.

After substitution of expressions for $v_s(r)$ in eqn. 7 and carrying out the integrations in eqn. 6, a general expression for the mean particle velocity in laminar tube flow is obtained:

$$\langle v_p \rangle = \langle v_m \rangle (1 + 2\lambda - C\lambda^2) \quad (10)$$

or, in terms of a relative migration parameter τ [5],

$$\tau = \frac{\langle v_m \rangle}{\langle v_p \rangle} = (1 + 2\lambda - C\lambda^2)^{-1} \quad (11)$$

According to the basic separation mechanism (see Fig. 1 and eqn. 6), λ should be based on the size of a polymer or particle near the wall. In both the DiMarzio–Guttman and the Brenner–Gaydos model, where rigid spheres are considered, the definition of r_p (and thus λ) is enequivocal. The C value varies on choosing different expressions for v_s. In the solid-sphere model by Brenner and Gaydos, both v_s and λ are functions of r_p. The C value in this model becomes [19]

$$C_{BG} = 1 + \frac{\frac{4}{3} + 2.56}{(1-\lambda)^2} \quad (12)$$

In the permeable sphere model by DiMarzio and Guttman where the slip velocity is based on r_G rather than on the particle size near the wall, the C value is [17]

$$C_{DG} = 1 + \frac{4}{3}\left(\frac{r_G}{r_p}\right)^2 \quad (13)$$

A major reason why modelling the transport of polymers is far more complicated than that of rigid spherical particles is that size and shape of the polymer are not well defined. Even when treating polymer molecules as rigid spheres, the problem of attributing the correct size to a polymer coil remains. The polymer size of primary interest in HDC is the radius near a solid wall, r_p, or better, the distance to which the mass centre of the polymer molecule can approach the wall. This size cannot be determined accurately by experimental methods.

Further, an adequate description of the hydrodynamic structure of polymer chains is very difficult. As was discussed already, the free-draining concept of polymer chains is inconsistent with experimental results, making the permeable sphere model an unrealistic picture of a real polymer coil. The nearly impermeable interior of a polymer chain is likely to be approximated better by a solid sphere, but whether the homogeneous solid sphere is able to provide a good representation of the entire polymer coil is questionable. Yet we are left with these simplified models because more sophisticated models of polymer chains are not easily

accounted for in the analysis of transport phenomena.

Tijssen *et al.* [5] compared the Brenner–Gaydos and DiMarzio–Guttman models with the retention behaviour of dissolved polystyrenes in microcapillary tubes. They modified both models in several ways, in order to apply them to random coils polymers. For polystyrenes in a good solvent, they found that the migration behaviour agreed best with a modified DiMarzio–Guttman model, in which the polymer radius r_{eff} is substituted for r_p. In a θ-solvent, experimental data were predicted well by the same model, provided $r_p = r_G$ was chosen. Recent measurements show that also for good solvents, experimental results are best fitted when r_G is taken as the polymer radius [30].

Surprisingly, the more refined Brenner–Gaydos model, and modified versions of it, did not well fit the experimental results. All theoretical C values were obviously too high to give a good match between theory and experiment. In the modifications of the Brenner–Gaydos model, Tijssen *et al.* replaced the solid-sphere radius in the expressions for the slip velocity by r_G. As was shown by DiMarzio and Guttman [17] for solutes in the centre of the tube, this corresponds to changing the particle structure from impermeable to permeable. In view of the almost impermeable character of the polymer coil, a physically more feasible approach would be to apply the original solid-sphere model and rather define a suitable hard-sphere radius for a polymer chain. For random coil polymers, the hard-sphere radius in the expressions for the slip velocity need not necessarily be the same as the effective radius near the wall. This can be expressed in a modification of C_{BG}:

$$C_{BG} = 1 + \frac{\frac{4}{3} + 2.56}{\left(1 - \frac{r_s}{R}\right)^2} \cdot \left(\frac{r_s}{r_p}\right)^2 \qquad (14)$$

where r_s is the radius of an (equivalent) solid sphere. The term r_s/r_p accounts for the different characteristic radii upon which λ and $v_s(r)$ are based. A similar term appeared in the DiMarzio–Guttman model (eqn. 13). Obviously, eqn. 14 reduces to eqn. 12 when homogeneous solid spheres are considered, since then r_s is equal to r_p.

A suitable candidate for the hard-sphere radius of a polymer may be the hydrodynamic radius r_h. For different types of linear random coil polymers in both good and poor solvents, $r_h = 0.66–0.80\ r_G$ [38,42]. The C value obtained when substituting r_h for the hard-sphere radius r_s in eqn. 14 is lower than in Tijssen *et al.*'s modifications of the Brenner–Gaydos model. As the C values in the former modifications (and in the original model) were too high to fit experimental migration data in capillary HDC well [5], a better agreement is expected with the present approach. Our modification of the Brenner–Gaydos model yields theoretical calibration graphs close to those from the modified DiMarzio–Guttman permeable sphere model, which so far was most successful in describing the migration behaviour of polymers in open tubes.

The modified DiMarzio–Guttman model was also found to predict surprisingly well the retention behaviour in packed columns [12]. On replacing the tube radius R by the hydraulic radius R_0, the DiMarzio–Guttman model with $r_p = r_{eff}$ accurately matched the retention data for polystyrenes in tetrahydrofuran. This finding strongly encouraged further research in this area. The DiMarzio–Guttman model will be the basis for the present investigation of trends in the migration behaviour induced by polymer structure and solvent nature.

Effect of flow-rate on the migration of polymers

In the migration models discussed so far, it was assumed that all positions in a flow channel are sampled with equal probability, except those in the inaccessible exclusion layer near the wall. However, many experimental observations and theoretical considerations indicate that phenomena exist that can cause non-random sampling. In this section a survey is given of such phenomena, but only those where the distribution of polymers in the flow channel is dependent on eluent velocity will be treated (electrostatic forces will thus be neglected). A more extensive review of anomalous effects in wall-bounded

sheared flows of polymer solutions and particles can be found in refs. 43 and 44.

Stress-induced diffusion (SID). In simple laminar shear flow in a tube, high stress regions near the wall and low stress regions near the centre can be distinguished. In the high-stress regions, polymer molecules can be elongated and oriented. As a consequence, polymers near the wall have a lower entropy than polymers situated near the tube axis. This entropy gradient causes a cross-streamline migration away from the wall [44–47]. This leads to a concentration build-up in the centre of the tube and a depleted layer near the wall. Cross-streamline migration due to SID is strongly favoured by higher flow-rates, smaller tube diameters and higher molecular masses.

When a packed column with non-porous particles is considered, SID will lead to migration of polymers away from the wall, causing τ to decrease with increasing velocity. On the other hand, when porous particles are employed, it has been argued that SID is likely to cause a concentration build-up in the pores. For this reason, SID has been put forward as an explanation for observed flow-rate-dependent migration behaviour in size-exclusion chromatography (SEC) [48].

In packed-column HDC, where the velocity gradients can be sufficiently high to cause deformation of larger polymer molecules [6,8], the occurrence of SID is not unlikely. Unfortunately, a quantitative treatment of SID is difficult, especially when complicated flows such as those in packed columns are concerned. Further, the development of a lateral concentration profile in the inter-particle channels is counteracted by stream splitting around the packing particles. At present it is not clear if stream splitting can fully nullify the effect of SID under experimental conditions in HDC.

SID has been put forward as a likely cause of flow enhancement, which has been observed for flow of polymer solutions in open tubes and in various porous media including packed columns [44]. Flow enhancement means that experimentally measured flow-rates at a given stress level are much higher than predicted from cone-and-plate viscometer measurements.

Polymer deformation. When polymers are deformed in sheared flow, this may not only cause SID, but a deformation-induced change in polymer size and shape itself can also influence the migration rate. If a polymer becomes elongated the size transverse to the direction of flow decreases and thus λ decreases. When only this effect of size is considered, while further assuming random sampling of accessible positions in the flow channel, the migration behaviour will be flow-rate dependent [6,8]. At higher velocities, polymers elute at larger τ and thus mimic lower molecular masses. This flow effect is enhanced by increasing flow velocity, increasing molecular mass or decreasing flow channel dimensions.

Molecular stretching occurs only when the flow is sufficiently "strong" or, in other words, when elongating forces are no longer offset by chain relaxation [8]. A measure of the extent of deformation is the Deborah number, *De*, which is the product of the relaxation time and the elongation rate. At $De > 0.1$ the polymer is stretched to such an extent that flow-rate-dependent migration may be observed in HDC. Under the usual chromatographic conditions in HDC, *De* may well exceed 0.1 for large, flexible molecules. Experiment results have indeed shown that elution in HDC begins to shift towards a smaller apparent solute size at the onset of deformation [8,49].

Hoagland and Prud'homme [6,8] observed that the elution volume of flexible and stiff macromolecules in packed column HDC depends on the eluent velocity. They concluded that this might well be explained by shear-induced orientation and deformation. Good agreement was found between calculated cross-sectional diameters of deformed random coil polymers (modelled as deformed Rouse chains) and the dimensions calculated from HDC elution data for hydrolysed polyacrylamides. Also, for stiff xanthan molecules, the measured effect of flow-rate on τ could be predicted reasonably well using the theory of shear orientation of dumbbell type macromolecules.

The deformation-induced change in polymer size and SID affect the elution of polymers in the opposite direction. The size effect produces higher τ values with increasing eluent velocity, whereas SID does the contrary. One might argue

that they are somehow coupled to cause an overall effect on τ, which depends on the degree of deformation. Measurements of pressure drop *versus* velocity for dilute polymer solutions in porous media may point in this direction, as stated by Cohen [44]. It was found that the pressure drop was lower than expected if the flow velocity was below the point of significant polymer deformation ($De \approx 0.1$). This flow enhancement was suggested to be caused by cross-streamline migration (owing to SID). For much higher flow velocities, beyond the point of polymer deformation, flow retardation (*i.e.*, reduction) was observed, which may be indicative of shear deformation.

Inertial radial migration. A sphere under viscous flow in a tube may undergo a radial force resulting from fluid inertia. This makes particles migrate across streamlines into an annular region around the equilibrium position at about 0.6 tube radius distance from the tube axis. The influence of inertial forces becomes more pronounced with increasing flow, increasing particle diameter and decreasing radius of the tube [30].

DosRamos and Silebi [26], Ploehn [27] and Tijssen and Bos [30] incorporated radial migration by fluid inertia in residence theories for capillary HDC. Comparison with experimental results showed that this could indeed explain observed flow-rate-dependent migration. The findings in open tubes suggest that inertial effects may also affect the elution of polymers in packed columns. However, in packed columns their influence is probably less pronounced. This is in the first place because the achievement of steady-state concentration profile is prevented by the randomizing effect of stream splitting around packing particles. For flow in open tubes it was pointed out by Ploehn that a steady-state concentration profile, under normal operating conditions, requires tube lengths that are several orders of magnitude larger than the tube diameter. When the same argument applies to packed columns, a concentration build-up by inertial lateral migration will be largely undone by stream splitting and a steady-state concentration profile will certainly not be effected. Further, the flow velocities commonly employed in packed columns are lower than in capillary HDC. The influence of inertial forces on the distribution of solutes in the flow channel will therefore not be very large even if a steady state were attained in packed columns. In open tubes the inertia induced effect of flow velocity on τ can be considered insignificant when the dimensionless group $Pe\ \lambda^2 < 1$ [30], where Pe is the Péclet number ($Pe = 2\langle v_m \rangle R/D_m$, where D_m is the molecular diffusion coefficient). A comparable criterion derived by Silebi and McHugh [22] states that inertial forces are negligible unless the product of the particle Reynolds number, Re_p, and Pe exceeds 3. Under chromatographic conditions, these criteria are mostly not fulfilled. Inertial lateral migration may become significant only for the largest permitted solute sizes.

Hydrodynamically induced diffusion (HID). Several investigators have used a kinetic theory approach to describe the diffusion of bead-spring-type macromolecules in inhomogeneous flows. Aubert and Tirrell [50,51] found theoretically that such molecules with volumeless beads will migrate in the concave-side direction across curvilinear streamlines, because of the inability of the molecules to align with the flow. In this theory, lateral drift in rectilinear flow was not predicted. However, when including finite bead volume and hydrodynamic interactions, macromolecular migration is predicted across parallel streamlines in Poiseuille flow also [52–54]. The approach for parallel streamlines leads to polymer migration away from the wall, in agreement with the entropic theory of SID.

Radial migration of polymers in the concave-side direction in curved flows was confirmed experimentally in circular couette flow [55]. It was speculated that the curved streamlines in packed-column flow could also cause polymer migration towards the surface of the packing particles. Theory predicts that such migration would be enhanced by higher eluent velocities and higher molecular masses. In SEC this cross-streamline migration would tend to increase the polymer concentration in the pores with increasing velocity and this effect is expected to be more pronounced for higher molecular masses. Elution data supporting this mechanism have been reported [56].

Multi-path effect. Another mechanism able to increase the polymer concentration near the wall is the multi-path effect, described by Giddings [57]. Large molecules are forced against the wall when flow channels split around packing particles and streamlines graze within a distance r_p from the packing particles. This will lead to polymer concentrations higher than the equilibrium values near the surface. Further, polymers may become trapped in apertures between particles. Giddings speculated that escape from wall regions and apertures would depend on the polymer diffusion coefficient. He assumed that polymer retardation by the multi-path effect increases with increasing molecular mass and increasing flow-rate. The multi-path effect has not yet been proved experimentally, nor has it been expressed in theoretical models.

EXPERIMENTAL

Materials and chemicals

The solvents used were analytical-reagent grade tetrahydrofuran (THF), 1,4-dioxane, toluene, methanol and ethyl methyl ketone from Merck (Darmstadt, Germany) and acetonitrile from Janssen (Geel, Belgium). Before use the solvents were filtered through a 0.1-μm inorganic membrane filter (Anodisc 47; Anotec, Banbury, UK). Empty stainless-steel columns with dimensions 150 × 4.6 mm I.D. were obtained from Chrompack (Middelburg, Netherlands). The non-porous packing particles were a gift from Professor K.K. Unger (Johannes Gutenberg Universität, Mainz, Germany). Polystyrene (PS) standards of narrow molecular mass distribution were obtained from Merck, Machery–Nagel (Düren, Germany) and Toyo Soda (Tokyo, Japan). Polyisoprene (PIP), polybutadiene (PB) and poly(methyl methacrylate) (PMMA) standards were purchased from Polymer Laboratories (Church Stretton, Shropshire, UK). The most relevant data of these polymer fractions are summarized in Table I.

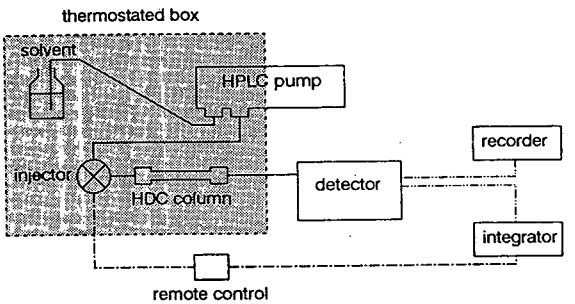

Fig. 2. Schematic representation of the experimental set-up for packed-column HDC.

Apparatus

In Fig. 2 the experimental set-up for packed-column HDC is shown schematically. Several parts of the equipment were placed in a laboratory-built air-thermostated box with polycarbo-

TABLE I

CHARACTERISTIC DATA FOR THE POLYMER STANDARDS

Polymer	Isomer composition[a] (microstructure)	M_w range ($\times 10^{-3}$)	Range of M_w/M_n ceiling values[a]	Supplier
PS		0.58–1260	1.04–1.18	Merck
PS		336–7700	1.03–1.2	Macherey-Nagel
PS		43.9 and 775	1.01	Toyo Soda
PB	45% *cis*, 49% *trans*, 6% vinyl	0.90–950	1.02–1.08	Polymer Laboratories
PIP	87% *cis*, 9% *trans*, 4% vinyl	1.35–3300	1.02–1.07	Polymer Laboratories
PMMA		2.40–1400	1.04–1.09	Polymer Laboratories

[a] Manufacturers' data.

nate walls. The temperature inside the box was registered by two calibrated electronic thermometers (Amarell, Kreuzwertheim, Germany). The HPLC pump (Spectroflow 400; ABI, Ramsey, NJ, USA) was partially thermostated, the control panel remaining outside the box. The pneumatically driven injection valve had a 1-μl internal sample loop (Ci4W; VICI, Houston, TX, USA). High-speed switching of this valve was allowed by a HSSA speed-up kit (VICI). The detector was either a variable-wavelength UV detector (Spectroflow 757; ABI) operated at 210 nm or an evaporative light-scattering detector (ELSD IIA; Varex, Burtonsville, MD, USA).

Both detectors were slightly modified to minimize their contribution to peak broadening and reduce their hold-up volume. The conventional 8-μl UV detection cell was replaced with a capillary flow cell (ABI). In this arrangement a small length of a 100 μm I.D. fused-silica capillary served as a detection cell, after removing the polymer coating. The fused-silica capillary was directly coupled to the column outlet, the length of tubing between column and detection window being 15 cm. The ELSD was connected to the column by a 75 μm I.D. fused-silica tube of length 20 cm. This capillary was directly connected to the nebulizer, after removing the original stainless-steel connection tubing. This modification reduced the equivalent liquid dead volume of the ELSD to less than 3 μl under all measuring conditions.

The retention times were measured using an integrator (Model 3390A; Hewlett-Packard, Avondale, PA, USA). Integrator runs and chromatographic runs were started simultaneously by means of a laboratory-built remote control. Chromatograms were recorded on a potentiometric recorder (Kompensograph 3; Siemens, Karlsruhe, Germany).

Column packing and characterization

Three columns were packed with non-porous silica particles according to a previously described slurry-packing procedure [12]. After evaluation of plate heights and peak shapes, one column was chosen to study the migration behaviour of polymers. Important properties of this column are summarized in Table II. The size and

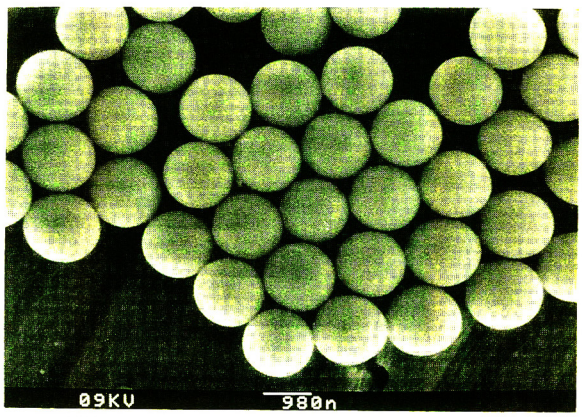

Fig. 3. Electron micrograph of 1.50-μm non-porous silica packing particles.

size distribution of the packing particles were determined using a scanning electron microscope (DS 130; ISI, Tokyo, Japan). The electron micrograph in Fig. 3 shows the very narrow size distribution of the particles. The reported particle diameter in Table II is the number-average diameter, measured for 50 particles. The mass difference between an ethanol-filled and a water-filled packed column was used to calculate V_0. This experiment was carried out in a thermostated box. A density meter (DMA 10; Paar, Graz, Austria) was used to determine accurately the density of ethanol. After emptying the column, the weighing procedure was repeated to find the total (empty) column volume. The column resistance parameter φ was calculated according to

TABLE II

COLUMN DATA

Parameter	Value
d_p (μm)	1.50 ± 0.03[b]
V_0 (μl)	1005
V_c (μl)	2550
ϵ	0.394
R_0 (μm)[a]	0.325
φ	410

[a] According to eqn. 5.
[b] Error indicates standard deviation.

$$\varphi = \frac{\Delta P d_p^2}{\langle v_m \rangle \eta L} \quad (15)$$

where ΔP is the pressure drop, η is the eluent viscosity and L is the column length.

Preparation of polymer solutions

Polymer concentrations was chosen to be as low as possible to prevent viscosity effects and to preclude effects of concentration on polymer size. When using the ELSD, the concentrations were typically around 0.05 mg/ml for the higher molecular masses and around 0.1 mg/ml for the lower molecular masses. With UV detection the concentrations were twice as high.

After adding the solvent, the polymers were allowed to swell and dissolve slowly for at least 16 h in a dark room. During this period, the polymers in good solvents were kept at room temperature, while the polymers in poor solvents were stored 5°C above the θ-temperature. Next, the solutions were homogenized by swirling slowly. Finally, they were stored at the column temperature until use. In order to prevent oxidation, PIP and PB solutions were stored under nitrogen. No solutions were used later than 2 days after preparation.

Determination of Mark–Houwink constants

For PB, PIP and PMMA, Mark–Houwink constants were determined in THF using SEC–viscometry. The SEC column used was a PLGEL Mixed D column from Polymer Laboratories. This viscosity detector was a capillary viscometer (H502; Viscotek, Porter, TX, USA). The Mark–Houwink constants were determined for molecular masses higher than 10^4.

Chromatographic measurements

All chromatographic measurements were performed at room temperature (23 ± 2°C), unless stated otherwise. For the measurements requiring careful temperature control, such as those for θ-solvents, the temperature variation was less than ±0.1°C from the desired value.

The polymer migration rate is expressed in terms of the dimensionless quantity τ; τ values are calculated as the ratio of the retention time of a polymer to that of a small unaccelerated "marker" molecule. Toluene was used as a marker when using UV detection. For the ELSD a less volatile marker was required and PS 580 was selected. All measurements using the latter marker were corrected for the small difference in migration rate between PS 580 and toluene ($\tau_{PS\ 580} = 0.9963$). This correction factor, determined for THF, was assumed to be the same in other solvents. If the polymer of interest and the marker could be baseline resolved, they were injected simultaneously, otherwise they were injected with a time interval of 2 min in between. The measured τ values, presented as points in the figures, are averages of at least three measurements.

RESULTS AND DISCUSSION

Column efficiency

In previous work, dispersion characteristics of the columns used were studied [58]. As a major result, it appeared that plate heights were virtually independent of M_w and of eluent velocity for reduced velocities over 5. For molecular masses that are of actual interest ($M_w > 10^4$), this means that plate height is virtually constant in the usual range of eluent velocities. Moreover, dispersion appeared to be very low for these polymers. Measured plate heights were found to be lower than 2.5 μm in the selected range of eluent velocities. For the three columns tested, the minimum plate heights were 2.0, 2.0 and 1.9 μm. This shows that efficient columns can be packed reproducibly with very small non-porous particles.

The flat plate height–velocity curves indicate that a high separation speed is possible without a decrease in resolution. This is in contrast to polymer separation techniques such as SEC and normal-mode field-flow fractionation, where the theoretical plate heights increase rapidly with increasing velocity [59,60]. In practice however, the analysis speed is limited by the pressure drop across the column. This limitation is not too severe for the 1.5-μm particles, because of the

low flow resistance parameter φ (see Table II). Other limitations such as shear degradation of polymers at high eluent velocities might be more restrictive in HDC [60].

An illustration of a rapid separation of PS is displayed in Fig. 4. A baseline separation in 90 s is obtained between polymers differing a factor of two in molecular mass. At this high eluent velocity, the peak shape becomes slightly tailing. We believe this to result from the higher viscosity of the sample solution. Peak tailing could be diminished by choosing either a lower polymer concentration or a lower eluent velocity.

Other examples of high-resolution separations of PB and PIP, using the ELSD, are given in Figs. 5 and 6. Owing to the high sensitivity of the ELSD, polymer concentrations could be lower than 0.1 mg/ml. The high resolving power of packed-column HDC is clearly shown by the separation of PIP fractions in Fig. 6, where the highest selectivity and thus the highest resolution, normalized on molecular mass ratio, is obtained for molecular masses between $1 \cdot 10^5$ and $5 \cdot 10^6$. Although the molecular size of the polymer fraction eluted secondly is only 1.5 times the size of fraction number 3, a very high resolution is obtained. For smaller polymers, the resolution for a given fractional difference in molecular mass is much lower. In the high-selectivity part of the chromatogram, peak widths are probably also determined by the polydispersity of the polymer fractions. The resolution might have been higher if monodisperse fractions had been used.

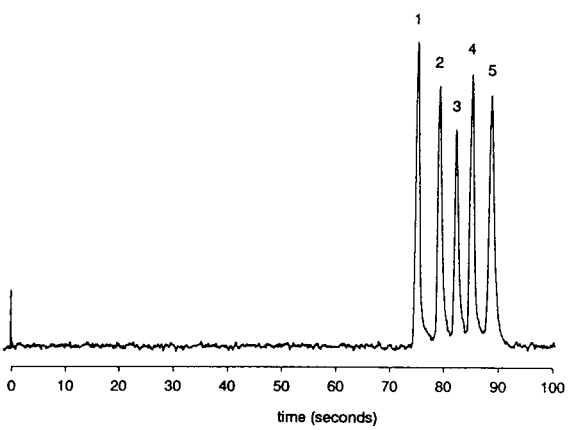

Fig. 4. High-speed hydrodynamic separation of polystyrenes dissolved in THF. Column, 150 × 4.6 mm I.D.; packing, 1.50-μm non-porous silica particles; pressure drop, 200 bar; detection, UV. Solutes: (1) PS 775 000, (2) PS 336 000, (3) PS 127 000, (4) PS 43 900 and (5) toluene, dissolved in THF (0.2 mg/ml each).

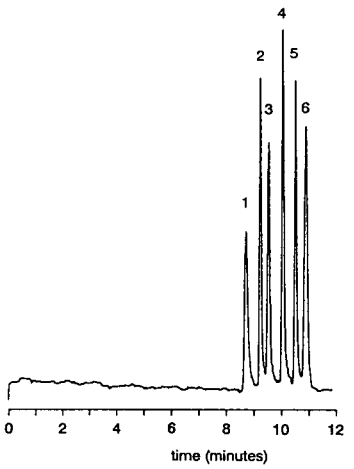

Fig. 5. Hydrodynamic separation of polybutadienes dissolved in THF. Column as in Fig. 4; pressure drop, 28 bar; detection, ELSD. Solutes: (1) PB 950 000, (2) PB 500 000, (3) PB 330 000, (4) PB 120 000, (5) PB 31 400 and (6) PB 3000 (0.06–0.10 mg/ml each).

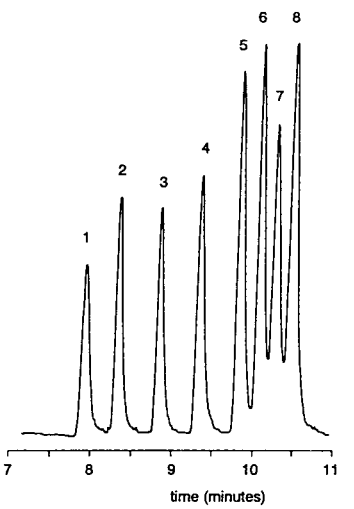

Fig. 6. Hydrodynamic separation of polyisoprenes dissolved in THF. Column as in Fig. 4; pressure drop, 29 bar; detection, ELSD. Solutes: (1) PIP 3 300 000, (2) PIP 1 200 000, (3) PIP 590 000, (4) PIP 295 000, (5) PIP 115 000, (6) PIP 60 000, (7) PIP 27 000 and (8) PIP 8000 (0.06–0.10 mg/ml each).

Effect of eluent velocity on τ

In the derivation of simple migration models, we excluded possible effects of the eluent velocity on τ. This was mainly because effects of flow velocity are not easily described in simple expressions, especially not when the flow in packed columns is considered. Moreover, a number of phenomena can be responsible for velocity-dependent τ-values. At present it is then unclear to what extent the mentioned flow effects influence τ. It is not even clear in what direction τ is predicted to alter when the eluent velocity is changed. Polymer deformation, HID and the multi-path effect predict that τ increases with increasing velocity, whereas SID and inertial migration predict the opposite. Experimental results in support of both trends have been reported. Measurements in packed-column HDC either suggest velocity-independent τ values [22] or point at an increase in τ with increasing velocity. The latter was only observed for high velocities and high molecular masses [8,12].

In order to elucidate possible effects of eluent velocity on τ further, the migration rate of polymers was studied at different eluent velocities. Velocities were chosen in a chromatographically useful range from 0.06 to 0.5 mm/s. The outcome of these experiments for PS in THF, and modified migration models, are shown in Fig. 7. The theoretical lines in this figure are drawn according to eqn. 11, using C_{DG} from eqn. 13 and C_{BG} from eqn. 14.

Starting at the lowest eluent velocity we observe a decrease in τ with increasing velocity until an apparent minimum value is reached. A further increase in eluent velocity then decreases τ. The velocity-dependent shifts in τ are largest for the highest molecular masses. In addition, the velocity at which a minimum τ value is achieved decreases with increasing molecular mass. For molecular masses below 10^6, the turnaround point for τ was not yet reached at the highest velocity.

Similar trends in the elution behaviour were also found for the other polymer types (PB, PIP and PMMA). In both good an poor solvents, the same velocity dependence of τ was observed. For a given molecular mass, the shifts in τ were approximately equal, irrespective of the polymer–solvent combination used. Apparently, the influence of polymer type and solvent on coil dimensions and coil structure is not large enough to significantly affect the observed shifts.

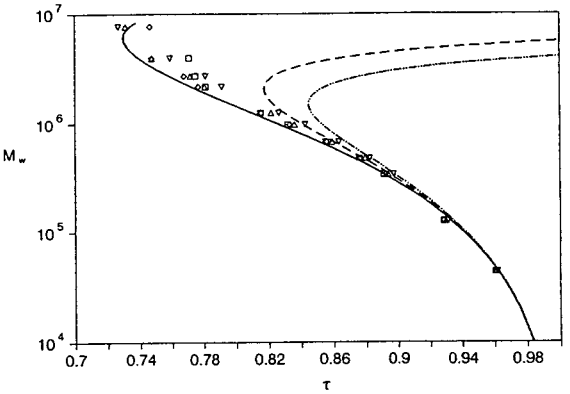

Fig. 7. Theoretical calibration graphs and experimental migration data for polystyrenes in THF. Column as in Fig. 4. Theoretical graphs: modified DiMarzio–Guttman model according to eqn. 13 with $r_p = r_{eff}$ (——), modified Brenner–Gaydos model according to eqn. 14 with $r_s = r_h = 0.7r_G$ and $r_p = r_{eff}$ (– – –) and modified Brenner–Gaydos model according to eqn. 14 with $r_s = r_h = 0.8r_G$ and $r_p = r_{eff}$ (– · · – · · –). The relationship between r_G and M_w is taken from ref. 5. Eluent velocity: (▽) 0.063, (△) 0.10, (◇) 0.22 and (□) 0.47 mm/s.

The explanation for the observed velocity-dependent migration behaviour is not straightforward. In previous work it was already found that at higher velocities τ increases with increasing $\langle v_m \rangle$. These observations could be reasonably well explained by considering the decline in transverse polymer size due to shear deformation. The opposite effect of eluent velocity on τ at low velocities has not been reported before. Possibly this effect is connected with the flow enhancement, observed in the flow of polymer solutions in porous media [44]. It has been suggested that flow enhancement may be caused by SID of polymers from the wall. Flow phenomena in packed columns are so poorly described, however, that other explanations are just as acceptable. A combination of two or more phenomena seems plausible.

In both the DiMarzio–Guttman and Brenner–Gaydos models, τ values are independent of eluent velocity, in contrast to our experimental results. In order to decide which of the models is

best we in fact require velocity-independent migration data. One may speculate that such data can be obtained only at much lower flow-rates than currently employed. Additional measurements are required to clarify this.

From a practical point of view, very low eluent velocities are not desired in HDC, because the analysis speed should be sufficiently high. We therefore have to accept a working range of eluent velocities in which τ is slightly dependent on $\langle v_m \rangle$. In the chromatographically useful range of higher velocities, the elution behaviour of polystyrenes can be described well by the DiMarzio–Guttman model.

From Fig. 7, it appears that at $\langle v_m \rangle = 0.22$ mm/s, minimum τ values are obtained for PS in THF over a wide range of molecular masses. The same was also found for other polymer–solvent combinations. In the next part, this velocity was selected to study in more detail the migration behaviour of several other polymers in different solvents. The influence of polymer type and solvent on measured τ values will be compared to predictions from the DiMarzio–Guttman model, the model that appeared to match closely the minimum τ values for PS in THF.

HDC of polymers in a good solvent

For all polymer types used (PS, PB, PIP and PMMA), THF appears to be a good solvent. In this solvent we can expect that the polymer chains are more swollen than in their unperturbed state. Because of differences in unperturbed dimensions and expansion factors, the actual polymer size for a given molecular mass is greatly dependent on polymer type. For a given molecular mass, the coil size decreases (or compactness increases) in the order PB, PIP, PS, PMMA. The difference in mass density between different polymer types finds expression in different r_G–M_w relationships. This can be seen from the relationships, summarized in Table III. For PS an r_G–M_w relationship is known from light-scattering measurements. For the other polymers, r_G–M_w relationships were obtained from eqn. 3, using the measured Mark–Houwink constants.

Applying the r_G–M_w relationships from Table III, theoretical calibration graphs according to eqn. 11, using C_{DG} and $r_p = r_{eff}$, are constructed in Fig. 8. As M_w instead of polymer size is plotted against τ, the curves for the different polymers do not overlap. Obviously, for the more tightly coiled polymer types, the calibration graph is shifted towards higher molecular mass. The good match between the theoretical curve and the experimental data, found earlier for PS, appears to hold also for other polymer types. The difference in compactness between the polymer types appears to influence migration only through its effect on coil size.

It may be argued that the difference in segment density may also influence migration through its impact on the permeability of the chain. We have already discussed that the solvent in the core of the chain is almost fully immobil-

TABLE III

RELATIONSHIPS BETWEEN r_G AND M_w FOR POLYMERS IN THF

Polymer	r_G–M_w relationship
PB	Eqn. 3; $K = 5.023 \cdot 10^{-2}$ (ml/g) and $a = 0.683$
PIP	Eqn. 3; $K = 1.25 \cdot 10^{-2}$ (ml/g) and $a = 0.775$
PS	$r_G = 1.39 \cdot 10^{-5} M_w^{0.588}$ (μm)[a]
PMMA	Eqn. 3; $K = 0.7998 \cdot 10^{-2}$ (ml/g) and $a = 0.734$

[a] Ref. 5.

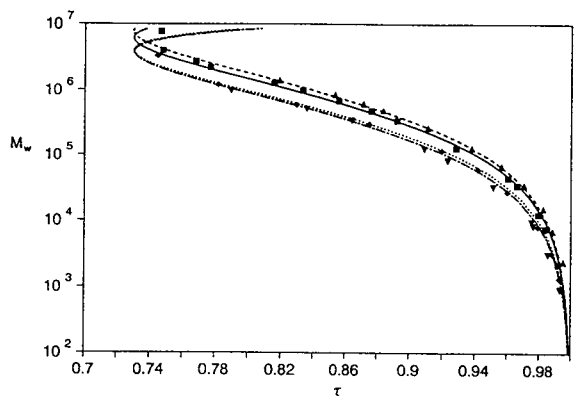

Fig. 8. Migration behaviour of different polymers in THF. Column as in Fig. 4; $\langle v_m \rangle = 0.22$ mm/s. The theoretical lines are drawn according to the modified DiMarzio–Guttman model with $r_p = r_{eff}$ and $C_{DG} = 2.698$. The experimental points and theoretical lines are for (▲, – – – –) PMMA, (□, ————) PS, (◆, ·····) PIP and (▼, – · – · – · –) PB.

ized with respect to the coil, but also that the flow permeability increases on going from the interior towards the outside of the chain. In the chain domains with partial draining, the segment density may be an important factor influencing the flow permeability. Increasing the segment density of a linear polymer coil is expected to increase the degree of solvent immobilization. In other words, the segment density of the coil affects the distance from the mass centre at which the solvent is effectively immobilized with respect to the chain. As this distance is proportional to r_h, it may be expected that the ratio r_h/r_G is dependent on the compactness of the polymer chain and thus on the type of polymer. This was indeed found experimentally, using different types of linear polymers, although the differences measured were very small. In both good and poor solvents, the ratio r_h/r_G was reported to increase slightly in the order PB, PIP, PS [41]. In our modification of the Brenner–Gaydos model (eqn. 14), a change in the r_h/r_G ratio alters C_{BG}. According to the experimental results, there is no indication that the C value should vary notably among the different polymer types.

When the calibration graphs are plotted with polymer size or λ as the abscissa and τ as the ordinate, the lines for the different polymer types in Fig. 8 will coincide. This means that a universal calibration graph is valid, just as in SEC [61]. Such a graph, drawn in Fig. 9, indeed shows that all experimental points fall on one line, which can be described accurately by the DiMarzio–Guttman model.

As the migration rate of polymers is determined by their size, it is possible to separate polymers with different segment density but equal molecular mass. In Fig. 10, this is demonstrated for a PB, PIP and PS fraction of about equal molecular mass. As predicted by theory, the polymer fractions elute in order of decreasing size.

Effect of solvent goodness on polymer migration in HDC

In the good solvent THF, the migration rate was found to be predicted well by the modified DiMarzio–Guttman model. In this section it will

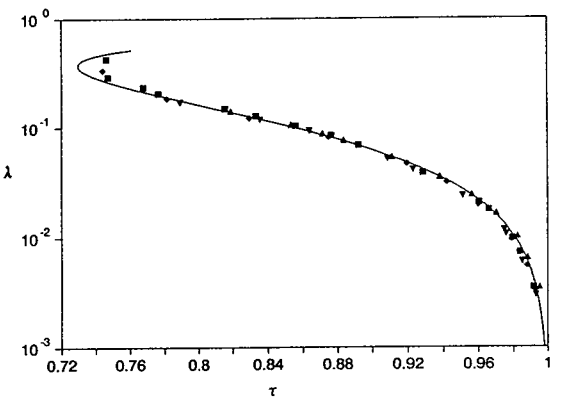

Fig. 9. Universal calibration graph for HDC. Experimental points as in Fig. 8. The theoretical line is drawn according to the modified DiMarzio–Guttman model with $r_p = r_{eff}$ and $C_{DG} = 2.698$.

be investigated whether this still holds when solvent conditions and hence the size of the coil are changed. Both good and poor solvents were used to study the effect of solvent power on the migration rate of polymers. In order to prevent adsorption of the polymers on the silica packing materials, only fairly polar solvents were regarded as suitable.

As poor solvents we selected θ-solvents

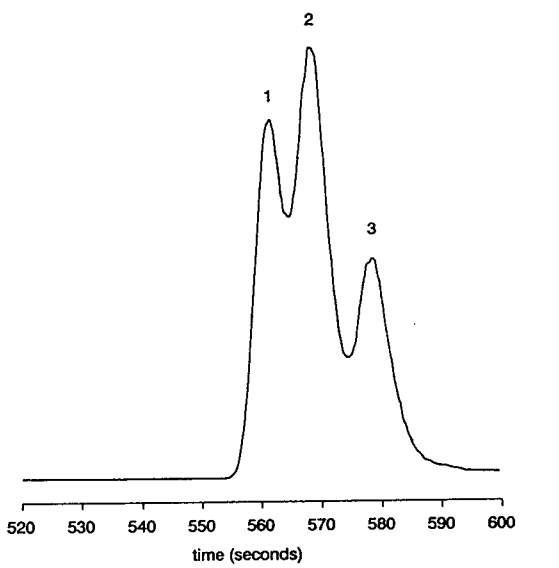

Fig. 10. Separation of different polymers of about equal molecular mass. Column as in Fig. 4; pressure drop, 28 bar; detection, ELSD. Solutes: (1) PB 330 000, (2) PIP 295 000 and (3) PS 336 000 in THF (0.10–0.15 mg/ml each).

because in that case reliable r_G–M_w relationships are known. For proper column thermostating, solvents were chosen with θ-temperatures between 20 and 45°C. The solvents used with their θ-temperatures and r_G–M_w relationships are summarized in Table IV. For PB and PIP, the literature data presented are those for polymer samples that match as closely as possible the isomer composition of our samples. For PS, a mixed solvent was used because candidate pure solvents were not suitable in the detectors used. The r_G–M_w relationships show that for the different polymers, the order of increasing compactness in a θ-solvent is the same as in THF.

Polybutadienes. When we switch from THF to a θ-solvent we may expect a substantial decrease in polymer size. This is indeed reflected in the observed migration behaviour, as shown in Fig. 11. The calibration graph for PB dissolved in dioxane at the θ-temperature is shifted towards smaller polymer sizes compared with the THF data. The theoretical calibration graph for the θ-solvent with $r_p = r_{eff}$ is in fairly good agreement with the experimental points, but the fit is not as good as for the good solvent THF. A better fit is obtained when r_G is taken as the polymer radius. As there is no physical reason to take r_G instead of r_{eff}, it is tempting to address this effect to a shortcoming of the capillary migration models in terms of their inability to describe properly flow in a packed column.

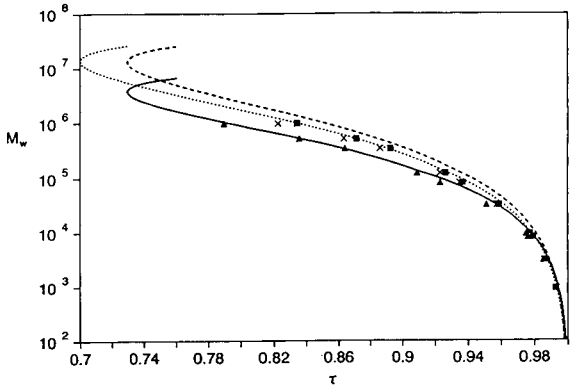

Fig. 11. Migration behaviour of PB in good and poor solvents. Column as in Fig. 4; $\langle v_m \rangle = 0.22$ mm/s. Experimental points: (▲) PB in THF, (□) PB in dioxane at 26.5°C and (×) PB in dioxane at 40.0°C. Theoretical lines are according to the modified DiMarzio–Guttman model. The lines are for PB in THF using $r_p = r_{eff}$ (———), PB in a θ-solvent using $r_p = r_{eff}$ (– – – –) and PB in a θ-solvent using $r_p = r_G$ (·····).

However, the same effect was also observed in capillary HDC of PS [5]. A possible explanation might be connected with the segment density distribution in a coil, which changes substantially when solvent conditions are changed [32].

Near the θ-point, the polymer size depends strongly on temperature. This is in contrast to good solvents where the polymer size hardly varies in a large temperature range. For PB in dioxane, we find that a temperature increment of

TABLE IV

θ CONDITIONS AND r_G–M_w RELATIONSHIPS FOR DIFFERENT POLYMERS

Polymer	Isomer composition	θ-Solvent	r_G–M_w relationship	Ref.
PB	*cis*:*trans* = 55:45–59:41; 8–11% 1,2-	Dioxane; 26.5°C	$r_G = 3.79 \cdot 10^{-5} M_w^{0.50}$ (μm)	62
PIP	70% *cis*, 23% *trans*, 7% 3,4-	Dioxane; 34.7°C	$r_G = 3.35 \cdot 10^{-5} M_w^{0.50}$ (μm)	63
	84% *cis*, 14% *trans*, 2% 1,2-	Dioxane; 34°C		34
PS		Dioxane–methanol (65.1:34.9, v/v); 34.0°C	$r_G = 2.74 \cdot 10^{-5} M_w^{0.50}$ (μm)	34
PMMA		Acetonitrile; 44.0°C	$r_G = 2.56 \cdot 10^{-5} M_w^{0.50}$ (μm)[a]	64

[a] Evaluated from data in ref. 64 for $M_w > 10^4$.

13°C above the θ-temperature yields significantly lower τ values. This is in qualitative agreement with the expected size increment. In THF a similar temperature rise resulted in a decrease in τ of less than 0.001.

Polyisoprenes. The migration behaviour of PIP in a good and a poor solvent is shown in Fig. 12. In the poor solvent dioxane, the largest PIP of molecular mass 3 300 000 could not be detected because of too low solubility. The effect of solvent on the migration behaviour of PIP is almost exactly the same as found for PB. In a θ-solvent we arrive at much higher τ values than in THF. Again we find that for a good solvent the data agree well with the graph based on r_{eff} whereas for the poor solvent r_G is a better size parameter. The strong influence of temperature on polymer size in a θ-solvent is once more demonstrated by the strong temperature dependence of τ in dioxane.

Polystyrenes. Thermodynamically, butanone is a poorer solvent for PS than THF. Consequently, the polystyrenes are smaller in butanone than in THF. From Fig. 13, it appears that this is in agreement with the experimentally observed shift in τ values when using butanone instead of THF. For the highest molecular masses, however, an unexpected reversal was found in the elution order. Further decreasing the coil dimensions by switching to a θ-solvent gives larger τ values, as expected. Similar to the results for PB and PIP, the data for the θ-solvent are best fitted when $r_p = r_G$ is substituted in the DiMarzio–Guttman model, whereas in THF, r_{eff} appears to be a more suitable size measure.

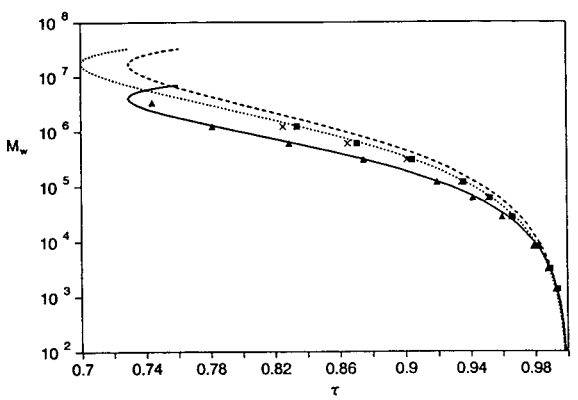

Fig. 12. Migration behaviour of PIP in good and poor solvents. Column as in Fig. 4; $\langle v_m \rangle = 0.22$ mm/s. Experimental points: (▲) PIP in THF, (□) PIP in dioxane at 34.0°C and (×) PIP in dioxane at 40.0°C. Theoretical lines are according to the modified DiMarzio–Guttman model. The lines are for PIP in THF using $r_p = r_{eff}$ (————), PIP in a θ-solvent using $r_p = r_{eff}$ (– – – –) and PIP in a θ-solvent using $r_p = r_G$ (·····).

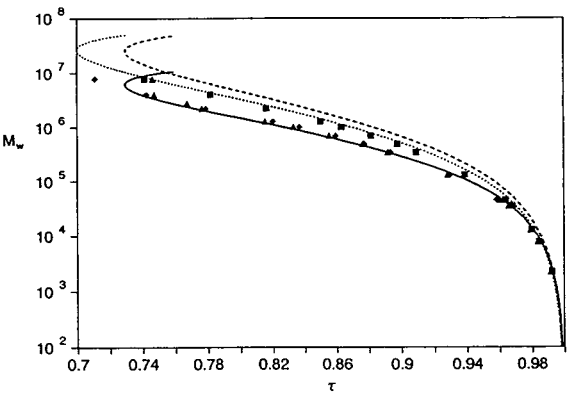

Fig. 13. Migration behaviour of PS in good and poor solvents. Column as in Fig. 4; $\langle v_m \rangle = 0.22$ mm/s. Experimental points: (▲) PS in THF, (◆) PS in butanone and (□) PS in dioxane –methanol at 34.0°C. Theoretical lines are according to the modified DiMarzio–Guttman model. The lines are for PS in THF using $r_p = r_{eff}$ (————), PS in a θ-solvent using $r_p = r_{eff}$ (– – – –) and PS in a θ-solvent using $r_p = r_G$ (·····).

Poly(methyl methacrylate)s. Also for the most compact polymer PMMA, the migration behaviour in acetonitrile at the θ-temperature is fitted best by the DiMarzio–Guttman model, provided $r_p = r_G$ is chosen in Fig. 14. The fit at low molecular masses is not very accurate, for unknown reasons. The deviations from the theoretical line are too large to be explained by the different r_G–M_w dependence that is usually found for lower molecular masses.

CONCLUSIONS

Columns packed with 1.5-μm non-porous particles are able to provide high-resolution separations for polymers having molecular masses between roughly 10^4 and $5 \cdot 10^6$. Despite the limited volume range available for peak elution, high resolution and a high peak capacity are possible owing to the very small dispersion. The dispersion being virtually independent of eluent

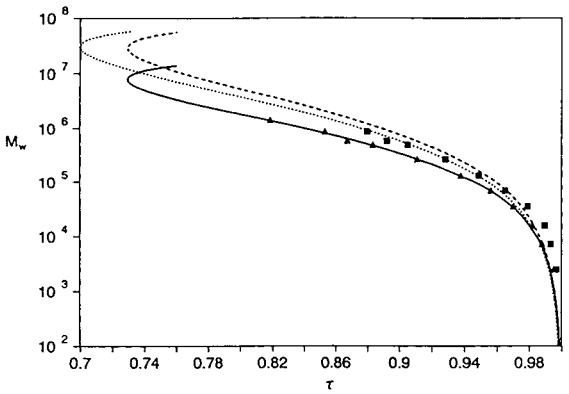

Fig. 14. Migration behaviour of PMMA in good and poor solvents. Column as in Fig. 4; $\langle v_m \rangle = 0.22$ mm/s. Experimental points: (▲) PMMA in THF and (■) PMMA in acetonitrile at 44.0°C. Theoretical lines are according to the modified DiMarzio–Guttman model. The lines are for PMMA in THF using $r_p = r_{eff}$ (————), PMMA in a θ-solvent using $r_p = r_{eff}$ (– – – –) and PMMA in a θ-solvent using $r_p = r_G$ (·····).

velocity allows for high-resolution separations in a short analysis time.

The migration behaviour for polymers of high molecular mass appears to depend slightly on eluent velocity. This phenomenon has not yet been included in the simple migration models which have been applied to packed columns so far. In a limited (but for practical use nevertheless very important) range of eluent velocities, the migration behaviour for linear random coil polymers in THF is observed to be accurately represented by the modified DiMarzio–Guttman model for open tubes. In this model the effective polymer radius is taken as the radius determining exclusion. The DiMarzio–Guttman model being successful for different types of linear polymers indicates that, at fixed eluent velocity, the migration depends on the size of the coil but not on its segment density. For this reason, a universal calibration graph was found to hold in HDC, as in SEC. Also for a very poor solvent (a θ-solvent), the DiMarzio–Guttman model was in good agreement with experimental data. However, to obtain such agreement it was necessary to take the radius of gyration as the radius determining exclusion. This has been reported before in capillary HDC. It was further shown that HDC is a suitable method for monitoring small changes in coil dimensions when, for instance, the nature of the solvent is varied.

SYMBOLS

a	Mark–Houwink constant
C	slip factor
D_m	molecular diffusion coefficient (m^2/s)
De	Deborah number
d_p	particle diameter (m)
$E(r)$	dimensionless potential working on a particle
K	Mark–Houwink constant (ml/g)
L	column length (m)
l	segment length (m)
M	molecular mass (g/mol)
M_n	number-average relative molecular mass
M_w	mass-average relative molecular mass
n	number of segment units in a chain
ΔP	pressure drop across the column (N/m^2)
Pe	Péclet number, $2\langle v_m \rangle R/D_m$
R	radius of a tube (m)
R_0	hydraulic radius of a packed column, $d_p\epsilon/3(1-\epsilon)$ (m)
Re	Reynolds number
r	radial position
r_{eff}	effective radius of a polymer chain, $0.886r_G$ (m)
r_G	radius of gyration (m)
$\langle r_G^2 \rangle$	mean square radius of gyration (m^2)
$\langle r_G^2 \rangle_0$	mean square radius of gyration of an unperturbed chain (m^2)
r_h	hydrodynamic radius (m)
r_p	particle or polymer radius determining wall exclusion (m)
r_s	radius of a (equivalent) solid sphere (m)
V_c	total column volume (m^3)
V_0	interparticle volume (m^3)
$\langle v_m \rangle$	average mobile phase velocity (m/s)
$\langle v_p \rangle$	average polymer or particle velocity (m/s)
$v_p(r)$	local axial particle velocity (m/s)
$v_s(r)$	local particle slip velocity (m/s)
α	linear expansion factor
β	solvent strength parameter
γ	wall-effect parameter
ϵ	column porosity
η	dynamic viscosity (Ns/m^2)

λ	aspect ratio, r_p/R
σ	structural parameter
τ	dimensionless migration rate, $\langle v_m \rangle / \langle v_p \rangle$
ϕ_0	Flory universal constant (mol^{-1})
φ	column resistance parameter

ACKNOWLEDGEMENTS

The authors thank Dr. F.A. Buytenhuys and H.J.F.M. van de Ven (Akzo Research Laboratories, Arnhem, Netherlands) for determining Mark–Houwink constants. This research was supported by the Netherlands Foundation for Chemical Research (SON), with financial aid from the Netherlands Organization for Scientific Research (NWO) under grant 700-344-003.

REFERENCES

1 A.J. McHugh, *CRC Crit. Rev. Anal. Chem.*, 15 (1984) 63.
2 A.W.J. Brough, D.E. Hillman and R.P. Perry, *J. Chromatogr.*, 208 (1981) 175.
3 H. Small, *J. Colloid Interface Sci.*, 48 (1974) 147.
4 J.C. Kraak, R. Oostervink, H. Poppe, U. Esser and K.K. Unger, *Chromatographia*, 27 (1989) 585.
5 R. Tijssen, J. Bos and M.E. van Kreveld, *Anal. Chem.*, 58 (1986) 3036.
6 D.A. Hoagland and R.K. Prud'homme, *J. Appl. Polym. Sci.*, 36 (1988) 935.
7 R.K. Prud'homme, G. Froiman and D.A. Hoagland, *Carbohydr. Res.*, 106 (1982) 225.
8 D.A. Hoagland and R.K. Prud'homme, *Macromolecules*, 22 (1989) 775.
9 R.J. Noel, K. Gooding, F.E. Regnier, D.M. Ball, C. Orr and H.E. Mullins, *J. Chromatogr.*, 166 (1978) 373.
10 P. Elie and M. Renaud, *Entropie*, 136 (1987) 33.
11 P. Elie and M. Renaud, *Entropie*, 115 (1984) 27.
12 G. Stegeman, R. Oostervink, J.C. Kraak, H. Poppe and K.K. Unger, *J. Chromatogr.*, 506 (1990) 547.
13 K.O. Pedersen, *Arch. Biochem. Biophys., Suppl.*, 1 (1962) 157.
14 D.A. Hoagland, K.A. Larson, R.K. Prud'homme, *Polym. Mater. Sci. Eng.*, 51 (1984) 543.
15 F.J. Molina, A.O. Vila, P. Dieguez, J.E. Figueruelo, *J. High Resolut. Chromatogr.*, 12 (1989) 560.
16 E.A. DiMarzio and C.M. Guttman, *J. Polym. Sci., Part B*, 7 (1969) 267.
17 E.A. DiMarzio and C.M. Guttman, *Macromolecules*, 3 (1970) 131 and 681.
18 E.A. DiMarzio and C.M. Guttman, *J. Chromatogr.*, 55 (1971) 83.
19 H. Brenner and L.J. Gaydos, *J. Colloid Interface Sci.*, 58 (1977) 312.
20 H. Small, F.L. Saunders and J. Solc, *Adv. Colloid Interface Sci.*, 6 (1976) 237.
21 D.C. Prieve and P.M. Hoysan, *J. Colloid Interface Sci.*, 64 (1978) 201.
22 C.A. Silebi and A.J. McHugh, *AIChE J.*, 24 (1978) 204.
23 B.A. Buffham, *J. Colloid Interface Sci.*, 67 (1978) 154.
24 C.A. Silebi and J.G. DosRamos, *J. Colloid Interface Sci.*, 130 (1989) 14.
25 G. Segré and A. Silberberg, *J. Fluid Mech.*, 14 (1962) 136.
26 J.G. DosRamos and C.A. Silebi, *J. Colloid Interface Sci.*, 133 (1989) 302.
27 H.J. Ploehn, *Int. J. Multiphase Flow*, 13 (1987) 773.
28 J. Lecourtier and G. Chauveteau, *Macromolecules*, 17 (1984) 1340.
29 M.A. Langhorst, F.W. Stanley, Jr., S.S. Cutié, J.H. Sugarman, L.R. Wilson, D.A. Hoagland, R.K. Prud'homme, *Anal. Chem.*, 58 (1986) 2242.
30 R. Tijssen and J. Bos, in F. Dondi and G. Guiochon (Editors), *Theoretical Advancement in Chromatography and Related Separation Techniques*, Kluwer, Dordrecht, 1992, pp. 397–441.
31 P.J. Flory, *Principles of Polymer Chemistry*, Cornell University Press, Ithaca, NY, 1971.
32 H. Yamakawa, *Modern Theory of Polymer Solutions*, Harper & Row, New York, 1971.
33 A. Dondos and H. Benoit, *Macromolecules*, 4 (1971) 279.
34 J. Brandrup and E.H. Immergut (Editors), *Polymer Handbook*, Wiley Interscience, New York, 3rd ed., 1989.
35 O.B. Ptitsyn and Y.E. Eizner, *Sov. Phys. Tech. Phys.*, 4 (1960) 1020.
36 W.W. Yau, J.J. Kirkland and D.D. Bly, *Modern Size Exclusion Liquid Chromatography*, Wiley, New York, 1979.
37 M.E. van Kreveld and N. van den Hoed, *J. Chromatogr.*, 83 (1973) 111.
38 J. Roovers and J.E. Martin, *J. Polym. Sci., Part B*, 27 (1989) 2513.
39 J.J.H. Mulderije and H.L. Jalink, *Macromolecules*, 20 (1987) 1152.
40 H. Brenner, *Adv. Chem. Eng.*, 6 (1966) 287.
41 A.J. Goldman, R.G. Cox and H. Brenner, *Chem. Eng. Sci.*, 22 (1967) 653.
42 S. Bantle, M. Schmidt and W. Burchard, *Macromolecules*, 15 (1982) 1604.
43 L.G. Leal, *Annu. Rev. Fluid Mech.*, 12 (1980) 435.
44 Y. Cohen, in N.P. Cheremisinoff (Editor), *Encyclopedia of Fluid Mechanics, Vol, 7, Rheology and Non-Newtonian Flows*, Gulf, Houston, TX, 1988, Ch. 14.
45 M. Tirell and M.F. Malone, *J. Polym. Sci., Polym. Phys. Ed.*, 15 (1977) 1569.
46 A.B. Metzner, Y. Cohen and C. Rangel-Nafaile, *Non-Newtonian Fluid Mech.*, 5 (1979) 449.
47 Y. Cohen and A.B. Metzner, *Chem. Eng. Commun.*, 41 (1986) 73.
48 M. Tirrell and M.F. Malone, *J. Polym. Sci., Polym. Phys. Ed.*, 15 (1977) 1569.

49 G. Stegeman, J.C. Kraak and H. Poppe, *J. Chromatogr.*, 550 (1991) 721.
50 J.H. Aubert and M. Tirrell, *J. Chem. Phys.*, 72 (1980) 2694.
51 J.H. Aubert and M. Tirrell, *Rheol. Acta*, 19 (1980) 452.
52 G. Sekhon, R.C. Armstrong and M.S. Ihon, *J. Polym. Sci., Polym. Phys. Ed.*, 20 (1982) 947.
53 P.O. Brunn, *Int. J. Multiphase Flow*, 9 (1983) 187.
54 P.O. Brunn and S. Chi, *Rheol. Acta*, 23 (1984) 163.
55 R.H. Shafer, M. Laiken and B.H. Zimm, *Biophys. Chem.*, 2 (1974) 180.
56 J.H. Aubert and M. Tirrell, *J. Liq. Chromatogr.*, 6 (1983) 219.
57 J.C. Giddings, *Sep. Sci. Technol.*, 13 (1978) 241.
58 G. Stegeman, J.C. Kraak, H. Poppe, *J. Chromatogr.*, 634 (1993) 149.
59 J.C. Giddings, *Adv. Chromatogr.*, 20 (1982) 217.
60 J.C. Giddings, M. Martin and M.N. Meyers, *J. Chromatogr.*, 158 (1978) 419.
61 H. Benoit, Z. Grubisic, P. Rempp, D. Dekker and J.G. Zilliox, *J. Chim. Phys.*, 63 (1966) 1507.
62 J. Roovers, P. Toporowski and J. Martin, *Macromolecules*, 22 (1989) 1897.
63 Y. Tsunashima, M. Hirata, N. Nemoto, K. Kajiwara and M. Kurata, *Macromolecules*, 20 (1987) 2862.
64 Y. Tamai, T. Konishi, Y. Einaga, M. Fujii and H. Yamakawa, *Macromolecules*, 23 (1990) 4075.

Journal of Chromatography A, 657 (1993) 305–326
Elsevier Science Publishers B.V., Amsterdam

CHROM. 25 535

Selection of competitive adsorption model for modelling displacement chromatography

J.C. Bellot and J.S. Condoret*

Département de Génie Biochimique et Alimentaire, UA-CNRS 544, Institut National des Sciences Appliquées, Avenue de Rangueil, F-31077 Toulouse Cédex (France)

(First received June 14th, 1993; revised manuscript received August 31st, 1993)

ABSTRACT

The influence of the model used to describe the basic competitive interactions between a stationary phase and migrating solutes was investigated to simulate reversed-phase displacement chromatography. Experimental separations of catechol–resorcinol mixtures using phenol as the displacer were compared with numerical simulations. The competitive Langmuir model, the LeVan–Vermeulen model and the quadratic model were chosen to describe the competitive adsorption equilibria. These models were related either to their non-competitive parameters or to their competitive parameters. A novel simplified experimental procedure is proposed to obtain competitive parameters for a binary mixture. The chromatographic process is described by the equilibrium-dispersive model and the calculations were performed by using a finite difference method. The results demonstrated that competitive isotherm equations with numerically fitted parameters do not lead to a good description of a displacement separation process. On the other hand, the LeVan–Vermeulen isotherm, with non-competitive Langmuir parameters, was found to be a relevant choice to the experimental conditions involved.

INTRODUCTION

Rapid and economical preparative separations of biochemical components from complex mixtures are nowadays an important challenge in the pharmaceutical and biotechnological industries. Among all the available techniques to achieve this goal, preparative liquid chromatography has proved to be an effective and promising tool. However, this technique has to be considered as completely different from the uncertain semi-empirical extrapolation of the chromatographic results. Regarded as a science in its own right, this preparative technique appears to be a difficult-to-design means of purification. Therefore, numerical modelling is a useful tool to help in understanding it. This strategy has reduced the use of experimentation where too many parameters impede an easy and correct interpretation. Besides an accurate theoretical knowledge, numerical modelling will lead to a better use of chromatographic columns, resulting in marked increases in productivity and yield [1].

All the physical phenomena encountered in chromatographic separation may be classified into two categories: the transient flow of solutes in granular media and the basic thermodynamic interactions between these migrating solutes and the stationary phase. The modelling of the former has long been the subject of many studies (for a review, see ref. 2). Different ways are proposed for describing the fluid flowing through the porous media, and the models vary from the simplest, such as the equilibrium-dispersive model, to very sophisticated, involving external and internal mass transfer resistances, radial velocity profiles, etc. Most of these models, combined with robust numerical algorithms, have proved to be very efficient tools for the

* Corresponding author.

0021-9673/93/$06.00
SSDI 0021-9673(93)E0950-Y

design of most chromatographic bioseparations in downstream processing. However, they remain useless unless they are fed with the appropriate equations describing the equilibria between the solutes and the stationary phase. This description, especially in the high concentration range, suffers from a lack of a theoretical basis, as it has not been extensively studied [3].

At high product concentrations, these basic interactions are very non-linear owing to the saturation of the support and to the concept of competition for adsorption sites that derives from it. This non-linearity and these competition effects may be of crucial importance and their influence in the modelling of the chromatographic process may exceed greatly any one of the other physical phenomena, such as the mass transfer resistances, especially when using modern HPLC columns, which are expected to be very efficient. This is why the correct choice of a model accounting for these basic interactions, even coupled with a rather simple description of the chromatographic process, deserves special attention. This tendency is nowadays observed in the scientific literature where the use of the well known competitive Langmuir isotherm appears unsuitable in too many situations [4].

As already stated in a previous paper [3], some workers have attempted to account for these various non-linear phenomena and have presented new models or adaptations of older concepts. We must emphasize, however, that only a few studies have dealt with the performances of these descriptions, especially when considering their use in dynamic simulations of a given chromatographic process. We shall consider, for instance, the work of Golshan-Shirazi *et al.* [5] and that of Jacobson *et al.* [6], but these two studies were restricted to the simulation of the elution mode in mass overload conditions.

In this paper, our purpose is to point out the difficulty of selecting a model for competitive adsorption equilibria to describe reversed-phase preparative separations. To illustrate this we chose the displacement process. This chromatographic mode was defined by Tiselius as early as 1943 [7], then fell into disuse till Horváth [8] reintroduced it in the 1980s. This is an efficient separation method that involves to a great extent all the competition phenomena for adsorption sites and therefore constitutes a good field of experimentation for testing competitive equilibria modelling. Few previous studies have undertaken the same approach but the studies by Frenz and Horváth [9] and Katti and Guiochon [10] should be mentioned.

In this study we considered an academic case, that is, the separation of common compounds such as resorcinol and catechol using phenol as the displacer. This experimental work was stimulated by that of Frenz and Horváth [9]. Three models of competitive adsorption, *i.e.*, the classical competitive Langmuir isotherm, the LeVan–Vermeulen isotherm and the quadratic isotherm, were considered and compared on the basis of either their own theoretical foundation or the choice of their parameters.

DISPLACEMENT CHROMATOGRAPHY

An outline of the principle of this chromatographic mode is necessary for familiarization with its characteristic aspects that differ from those of isocratic preparative elution. The general article by Horváth [8] covers relevant historical, experimental and theoretical studies related to this subject.

Before carrying out the separation, the chromatographic column is first equilibrated with a carrier whose affinity for the stationary phase is negligible. The mixture containing the products to be separated is then introduced, immediately followed by the feed of a solution containing the displacer. This latter is chosen in such a way that it presents an affinity for the stationary phase higher than that of the components to be separated.

When the feed mixture is introduced, a first separation process occurs in the frontal mode. Then, owing to the action of the following displacer and to competition phenomena, the components organize themselves into separated zones. Under appropriate conditions, a steady state is achieved: the components migrate, in a purified and sometimes concentrated state, at a fixed and identical velocity in the form of adjacent square waves (isotachic displacement). Fi-

nally, each component leaves the column in an order imposed by its respective affinity for the stationary phase. When all the components have been collected, the displacer must be desorbed and the column re-equilibrated with the carrier.

MODELLING SINGLE-COMPONENT ADSORPTION EQUILIBRIA

Adsorption isotherm

The amount of product adsorbed at equilibrium, per unit mass or volume of adsorbent, is essentially dependent on the concentration of this product itself in the mobile phase. This function, termed here a single-component adsorption isotherm, is the mathematical expression describing quantitatively, at a constant temperature, the relationship between these two quantities. When several components are present, interference and competition phenomena for adsorption sites occur and lead to a more complex mathematical formulation of the equilibrium. Therefore, these isotherms, termed here competitive isotherms, attempt to express relationships between the amount of one component adsorbed and the concentrations of all other constituents, either in solution or already adsorbed.

Langmuir isotherm

The simplest theoretical model and the most widely used in liquid chromatography was first developed by Langmuir [11]. It describes the adsorption of one component adsorbed as a monolayer. It was originally derived from simple kinetic considerations of gas or vapour adsorption phenomena. It may also be obtained by thermodynamic considerations that additionally lead to a more precise definition of its characteristic constants [12]. Its basic hypotheses are as follows: molecules are adsorbed on a fixed number of well localized sites; each site may accept only one molecule in such a way that they form a monolayer; all sites are energetically equivalent; there is no interaction between adsorbed molecules; and local equilibrium is assumed between the liquid phase and the support, with the equation

$$q = \frac{aC}{1 + bC} \tag{1}$$

where a and b are characteristic constants and C and q are the liquid phase and adsorbed product concentrations, respectively.

Bi-Langmuir isotherm

As indicated previously, the Langmuir adsorption isotherm is very simple, and its basic hypotheses stress its limitations. As a consequence, it may be unsuitable, especially when energetic heterogeneity of sites is present [12]. To complete the description of adsorption phenomena by taking into account the occurrence of two categories of independent and non-cooperative sites, the bi-Langmuir isotherm was derived [13–15]. This frequently used model [16–18] is expressed as follows:

$$q = \frac{aC}{1 + bC} + \frac{dC}{1 + eC} \tag{2}$$

where a, b, d and e are constants obtained by parametric identification.

MODELLING MULTI-COMPONENT ADSORPTION EQUILIBRIA

Description of the problem

The modelling of preparative separations does not simply require the precise knowledge of the specific interactions occurring between each of the encountered components and the chromatographic stationary phase. The more or less accurate understanding of the competitive equilibria involved between these mixed components and the adsorption sites is also of major importance. Numerous, and often complicated, the models have attempted to give a mathematical description of these interference and competition phenomena [3]. In addition to the arduous theoretical problems raised by this understanding of the different thermodynamic mechanisms, we would point out the difficulty in obtaining experimentally the numerical parameters of these theoretical models elaborated more or less rigorously. Among all the proposed models described in the literature, we have chosen three of them, because of the simplicity of their equations, of

their theoretical development, whose validity is suited to the experimental conditions we shall consider in our study, and also because of their widespread use. These three models are the competitive Langmuir isotherm, the quadratic isotherm and the LeVan–Vermeulen isotherm.

It is worth noting that these three competitive models have the advantage of being related either to the parameters of the individual Langmuir isotherms of each component or to correcting factors associated with the non-competitive Langmuir isotherm parameters. Within the framework of this study, we shall also consider these models as empirical equations in which all coefficients, without exception, will be obtained by parametric identification from experimental competitive adsorption data.

Competitive Langmuir isotherm

The extension of the basic Langmuir model [11] to the description of competitive adsorption phenomena was first proposed by Schwab [19], Butler and Ockrent [20] and Markham and Benton [21]. This modified model is based on the same hypotheses as for the initial one and is formulated as follows:

$$q_i = \frac{a_i C_i}{1 + \sum_{j=1}^{M} b_j C_j} \tag{3}$$

where a_i and b_i are drawn from the corresponding single Langmuir isotherms and M is the total number of components.

Quadratic isotherm

From statistical thermodynamic considerations, it has been shown that competitive adsorption isotherms may be formulated as the ratio of two polynomials of the same degree [22]. The competitive Langmuir isotherm is, for instance, the ratio of two polynomials of degree one. Better accuracy is expected when using two polynomials of degree two. Lin *et al.* [22], Zhu *et al.* [4] and Poppe [23] have used this type of isotherm, termed quadratic isotherms.

This competitive model modifies the Langmuir isotherm by assuming that the adsorption and desorption rates of each component are linear functions of the adsorbed solute and of the dissolved solute concentrations, respectively. This assumption enables one to account for molecular interactions in the two phases [22]. This isotherm is expressed here for two components:

$$q_1 = \frac{a_1 C_1 + a_{12} C_1 C_2}{1 + b_1 C_1 + b_2 C_2 + b_{12} C_1 C_2} \tag{4a}$$

$$q_2 = \frac{a_2 C_2 + a_{21} C_1 C_2}{1 + b_1 C_1 + b_2 C_2 + b_{21} C_1 C_2} \tag{4b}$$

where only the a_i and b_i are obtained from single-component Langmuir isotherms. The other parameters are correction terms.

LeVan–Vermeulen isotherm

We have also considered the use of a model based on rigorous theoretical considerations. This LeVan–Vermeulen model is derived from the I.A.S. theory (ideal adsorbed solution) and predicts in a non-intuitive manner the equilibrium relationships of solute mixtures only from data derived from single adsorption isotherms.

The I.A.S. theory, first developed by Myers and Prausnitz [24] for gaseous mixtures, is a very elaborate theory, based, as for the Langmuir model, on the concept of ideal behaviour of components in both the mobile and stationary phases. The theory has been extended to liquid–solid equilibria and applied by Radke and Prausnitz [25], Jossens *et al.* [26] and Fritz and Schluender [27]. The results may be very satisfactory in certain cases but, as emphasized by McKay and Duri [28], the mathematical complexity of the procedure, especially for more than two-component mixtures, has restricted its use among workers. Nevertheless, it must be mentioned that Golshan-Shirazi *et al.* [5] and Golshan-Shirazi and Guiochon [29] have to some extent re-established this theory by using in their numerical simulations the LeVan–Vermeulen isotherm [30], which is perhaps the simplest isotherm derived from the I.A.S. theory. Antia and Horváth [31] have also used this model to study in displacement chromatography the isotachic behaviour of components exhibiting single crossing isotherms.

The LeVan–Vermeulen model, derived from the Langmuir isotherm, has been considered in our simulations of displacement chromatography. In the case of a three-component mixture, it is written as follows:

$$q_i = \frac{b_i q_s C_i}{1 + \sum_{j=1}^{3} b_i C_i} + C_i \cdot \frac{\partial q_s}{\partial C_i} \ln\left(1 + \sum_{j=1}^{3} b_i C_i\right) \quad (5)$$

When the saturation capacities are different for each component, and when considering the two-term expansion of the LeVan–Vermeulen isotherm, always derived from the Langmuir model, q_s represents the following function [5]:

$$q_s = \frac{\sum_{j=1}^{3} q_{s,i} b_i C_i}{\sum_{j=1}^{3} b_i C_i} \quad (6)$$

where $q_{s,i} = (a_i/b_i)$ is the specific saturation capacity of the column with respect to solute i, and where the a_i and b_i are the single-component Langmuir isotherm parameters.

NUMERICAL MODEL

Within the framework of this study, we chose to use the equilibrium-dispersive model based on continuity equations whose numerical solution is achieved by the R.G.S. method (from the name of its authors, Rouchon and Golshan-Shirazi), which is a particular finite difference algorithm, used in numerous studies [32,33]. The simulation program was written in FORTRAN. A description of the model and its numerical solution have been presented previously [34].

EXPERIMENTAL

Chemicals

Catechol was purchased from Sigma (St. Louis, MO, USA) and resorcinol from Fluka (Buchs, Switzerland). Other chemicals [phenol (Rectapur), methanol (Normapur), orthophosphoric acid (Rectapur) and carbon tetrachloride and triethylamine (for HPLC analysis)] were purchased from Prolabo (Paris, France). Ultrapure water was obtained with a Milli-Q reagent water system (Millipore, Bedford, MA, USA).

Columns

Two 5-μm Nucleosil C_{18} columns (250 × 4.6 mm I.D.) (Touzart et Matignon, Vitry sur Seine, France) were used. Frontal analysis and displacement chromatographic separations were performed with the same column to ensure reliable equilibrium data characterizing the column and the chemicals. Conventionally, a microcolumn is used to obtain equilibrium data, in order to avoid excessive product consumption, but may lead to errors when actual separations are carried out and simulated in a larger column, with of course a similar stationary phase [5]. The uncertain column-to-column reproducibility may be prejudicial to simulation accuracy. HPLC analysis of the collected fractions was performed with the other column.

The column efficiency may be estimated from the Knox equation [35]:

$$h = \frac{2}{v} + v^{1/3} + \frac{v}{10} \quad (7)$$

where h is the reduced plate height ($h = H/d_p$) and v is the reduced mobile phase velocity ($v = ud_p/D_m$), d_p being the average particle diameter and D_m the molecular diffusion coefficient of the product considered; u will be taken as equal to 0.028 cm/s for frontal analysis and displacement separations and a similar diffusion coefficient (equal to 10^{-5} cm^2/s) was taken for all the small organic compounds studied in this work.

The reduced mobile phase velocity is then equal to 1.4, which corresponds to nearly 0.5 times the theoretical optimum value of this velocity ($v_{opt} = 2.71$) leading to the smallest H for the operating conditions under consideration. In this case the calculated H value is 14 μm for all products, which gives a number of theoretical plates for the column of 17 850. This corresponds to 71 420 theoretical plates per meter and indicates the very high efficiency of these columns. The columns were also experimentally tested for their efficiency by elution chromatography, and yielded the same good results.

Apparatus

A schematic diagram of the experimental apparatus used for frontal analysis and displacement separations is presented in Fig. 1. This set-up is based directly on that one of Jacobson *et al.* [36] used for measurements of competitive isotherms. It consists of a Model 420 HPLC pump (Kontron, Zurich, Switzerland) equipped with a micro-head allowing flow-rates as low as 10 μl/min. This pump was connected to an injection system composed of two sampling valves (Model 7010; Rheodyne, Cotati, CA, USA). Tubing to the two valves was fitted in such a way as to avoid significant dead volumes. The two Rheodyne loop volumes were adjusted from 5 to 10 ml by substitution. The valves were connected to the Nucleosil C_{18} column (250 × 4.6 mm I.D.) described earlier. The column effluent was monitored by a differential refractometer and its signal was recorded and processed by a data acquisition software (BOREAL; Prolabo, Paris, France). The column temperature was controlled in an oven (Sup-R5, Stabitherm; Prolabo).

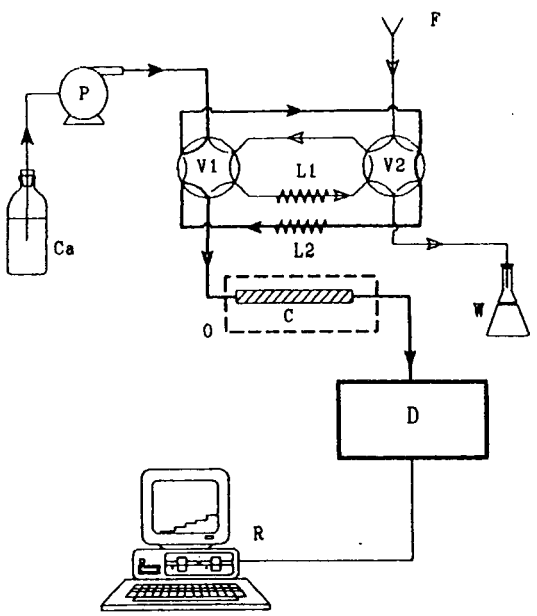

Fig. 1. Schematic diagram of the apparatus used either to perform displacement separations or to measure single-component and competitive isotherms by frontal chromatography. C = Adsorption column; Ca = carrier; D = detector; F = feed load; L1, L2 = stainless-steel sample loops; O = oven; P = pump; R = recorder; V1, V2 = sampling valves; W = waste.

Measurement of hold-up volumes

The hold-up or dead volume of the tubing (without the column) was calculated from tracer experiments, to be 0.160 ml for our set-up (Fig. 1).

The dead volume of the column itself was measured by the gravimetric method, first suggested by Riedo and Kováts [37] and used by Jacobson *et al.* [6], Frenz and Horváth [9] and Huang and Horváth [38]. With water as the carrier, the use of this method is relevant [39]. The measured hold-up volume (V_{Φ_m}) was then equal to 2.949 ml, which led to a total porosity (ε) of the column equal to 0.71.

Frontal analysis

Frontal analysis was carried out on the experimental unit shown in Fig. 1. This method was chosen as the best practical approach to obtain the single-component isotherms for resorcinol, catechol and phenol and also for the resorcinol–catechol competitive isotherm. Because of the size of the column, consumption of products is not negligible and could be a major drawback in certain situations [6].

For single-component isotherm measurement, the procedure was as follows [38]. The column was first equilibrated at 30°C with degassed ultrapure water as the mobile phase. The room temperature was also maintained at 30°C so as to allow thermally equilibrated products to be injected. The flow-rate was 0.200 ml/min. The switching valves were arranged in such a way that the mobile phase flowed through the second injection loop (circuit in thick lines in Fig. 1) while the first loop being filled, with a syringe, with a solution of the lowest product concentration. After the column had been equilibrated, the two Rheodyne valves were manually switched to apply, at the column entrance, the concentration step of the solution contained in the first loop. Frontal analysis then occurred, while the second loop was filled with a solution of product of a higher concentration than the first injected solution. When the signal of the first step was detected at the column outlet, the two

valves were rotated again. This procedure allows gradual saturation of the column with solutions of increasing concentration, sequentially introduced into the column. Finally, after the last step had been monitored, the column was washed with methanol–water mixture (50:50) and then re-equilibrated with the neat mobile phase for other measurements.

Adsorption isotherms were then calculated from the typical curve showing successive steps that have been monitored and by using a simple and accurate method based on mass balance, proposed by Jacobson *et al.* [6] and termed M.M.B. (method of mass balance). The concentration of the adsorbed compound on the stationary phase, q_i, in equilibrium with its mobile phase concentration was calculated with the following relationship:

$$q_i = [(C_i - C_{i-1})(V_{r,i} - V_D)/V_{\Phi_s}] + q_{i-1} \quad (8)$$

where C_{i-1} and C_i are the mobile phase concentrations of component i at the beginning and the end of the frontal development respectively, and q_{i-1} and q_i are the adsorbed phase concentration in equilibrium with C_{i-1} and C_i, respectively. $V_{r,i}$ is the retention volume of the concentration step corresponding to C_i, V_D is the system dead volume and V_{Φ_s} is the volume of stationary phase [38].

For competitive isotherm measurement, it is customary to operate frontal analysis in the same way as described above, by injecting mixtures of increasing concentration, with differing ratios between the various components [4,36,40–42]. Several methods are then possible for processing the results [41], but all of them require either very accurate HPLC analyses of each component concentration in all the steps, or the handling of the arduous theory of Helfferich and Klein [43].

Within the scope of this work we propose a different experimental procedure, restricted to binary mixtures. In this method, only one concentration step of the binary mixture is injected at the column entrance. During their migration, the two solutes will classify themselves as a function of their affinity for the stationary phase. Two transitions are then observed. The first is constituted by the less retained component, in a pure state, and the second by the initial mixture. After washing and re-equilibration of the column, the experiment is repeated with binary mixtures of different product ratios. Then only the monitoring of the column effluent is required to obtain the breakthrough volumes of each step.

The novelty of our approach lies in the fact that the concentration of the first step is no longer measured by HPLC but is simply estimated by the following reasoning: if the formation of the first plateau is considered to be very rapid (with regard to the total time of the frontal analysis) we may assume, for this first plateau, constituted by the pure, less retained component, that we are dealing with a simple frontal analysis of a single component. The knowledge of the single isotherm of this component, the column length and the residence time of this plateau allows a very simple determination of the concentration of this plateau to be made. By referring to the papers by Ma and Guiochon [42,44], our procedure is justified for two reasons: first, our column is characterized by a very high efficiency, and therefore may be not so different from an ideal one; and second, from Ma and Guiochon's work, the time needed for the formation and stabilization of the first front has been estimated as less than 4% of the total duration of the analysis.

Finally, our method, based only on the M.M.B. and simple experiments, may be of great interest as it can be applied to any binary system for which frontal chromatographic data can be obtained. Therefore, it is not restricted to systems whose single components exhibit Langmuir adsorption behaviour.

Displacement experiments

The set-up in Fig. 1 was also used to effect displacement separations. As mentioned previously, the column was first equilibrated with the carrier (degassed pure water). The column temperature was maintained at 30°C and the flow-rate was 0.200 ml/min. The resorcinol–catechol mixture that filled the second loop was then introduced into the column by rotating the two Rheodyne valves. After the desired volume of feed had flowed into the column, the displacing solution (phenol) contained in the first loop was

pumped to the column entrance by re-switching the two valves. Fractions of 100 μl were then manually collected throughout the emergence of the feed components. For all these experiments, the injection time of the feed containing resorcinol and catechol was 120 s. The displacer was 80 g/l of phenol in pure water, and four different mixtures corresponding to 40, 50, 60 and 70 g/l each of catechol and resorcinol were injected.

Analysis of collected fractions

Fractions collected during the displacement chromatographic runs were analysed by isocratic HPLC. First, each fraction was diluted sixfold and analysed on the previously described Nucleosil C_{18} column. The pump and the oven were the same as those used for the displacement experiments. A conventional Model 7125 sampling valve (Rheodyne) with a 20-μl sample loop was used to inject the diluted samples. The column effluent was monitored at 290 nm with a UV detector (Model 481; Waters, Milford, MA, USA). The signal was recorded by the BOREAL software already mentioned.

The temperature was 50°C and the flow-rate 0.800 ml/min. The mobile phase consisted of 10% (v/v) methanol, 0.5% orthophosphoric acid and 0.5% triethylamine in ultra-pure water [9]. This eluent was sonicated with a Vibra cell (Bioblock Scientifics, Illkirch, France).

RESULTS AND DISCUSSION

Displacement operating conditions

Experimental determination of single-component isotherms of each product (resorcinol, catechol and phenol) is justified for many reasons. First, this preliminary study allows one to characterize the kind of interaction each product has with the stationary phase and indicates the best suited model to its mathematical description. As we shall see later, this will be of major importance in the case of phenol. Second, this study allows the determination of the appropriate operating conditions for a displacement to occur and concentrations for separated products, in the case of an ideal displacement, to be predicted. Finally, this will make it possible to evaluate the error made when modelling displacement separations with single-component isotherm parameters, an evaluation that has seldom been reported in the literature.

Fig. 2 shows the single-component adsorption isotherms of resorcinol, catechol and phenol for a wide range of concentration. These curves are concave towards the abscissa; this is a necessary condition for carrying out a displacement separation, as stated by Hagdahl *et al.* [45] and Tiselius [7].

The choice of the displacer and its operating concentration is one of the most critical design parameters for obtaining a good separation efficiency. As expected [9], phenol is an adequate displacer, because its adsorption isotherm overlies the isotherms of all feed components to be displaced. An 80 g/l phenol concentration allows the operating line to intersect all the feed single-component isotherms, and thus permits a separation to occur.

Single-component isotherm

Our experimental results show that adsorption of catechol and resorcinol is perfectly well described by the Langmuir model. Concerning the adsorption of phenol, several models have been

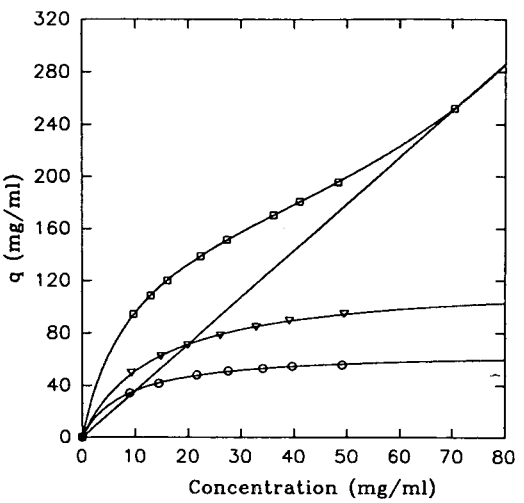

Fig. 2. Operating line for an 80 g/l phenol concentration and single adsorption isotherms for (○) resorcinol, (▽) catechol and (□) phenol measured on a 5-μm Nucleosil C_{18} column (250 × 4.6 mm I.D.) at 30°C; mobile phase, water, flow-rate, 0.2 ml/min.

TABLE I

NON-COMPETITIVE LANGMUIR ISOTHERM PARAMETERS FOR RESORCINOL AND CATECHOL

The mean relative error is the sum of the relative differences between the calculated and the experimental concentrations divided by the number of data.

Product	a	b (l/g)	$q_{s,i}$ (g/l)	k'_i	Mean relative error (%)
Resorcinol	7.937	0.120	66.08	10.45	0.69
Catechol	8.810	0.073	120.68	11.90	0.66

tested, the Langmuir, the bi-Langmuir, the Freundlich and the Langmuir–Freundlich models; it appeared that the bi-Langmuir isotherm gave the best fit. The values derived for the isotherm parameters of each product are summarized in Tables I and II. A few comments about these results are of great interest for analysing precisely the adsorption behaviour of each product.

First, considering phenol, it could be considered surprising to obtain a negative value for the parameter e in the bi-Langmuir model (see eqn. 2). This coefficient is theoretically the ratio of the adsorption rate constant to the desorption rate constant of the component concerned on one category of sites on the stationary phase. Nevertheless, when operating parametric identification on the experimental curve, two distinct phenomena, the gradual saturation of the stationary phase and solute–solute interactions between adsorbed solutes, are included in this numerical e Langmuir parameter [3]. In our case, and considering the second category of adsorption sites, we note that the complexity of the system encountered cannot be correctly, *e.g.*, physically, described by this second term of the bi-Langmuir isotherm. When fitting the experimental adsorption data of another compound, *i.e.*, 2-phenylethanol, to the bi-Langmuir model, Fallah and Guiochon [46] encountered the same problems, and preferred to use a linear function associated with the Langmuir model instead of two Langmuir equations. They specified that actually, because of the lack of physico-chemical measurements, no adequate explanation can account for such behaviour where a column seems to have an infinite saturation capacity.

TABLE II

NON-COMPETITIVE BI-LANGMUIR ISOTHERM PARAMETERS FOR PHENOL

Parameter	Value
a_3	18.218
b_3 (l/g)	0.108
d_3	0.7613
e_3 (l/g)	−0.0069
Mean relative error (%)	0.15

Nevertheless, we shall assume, in the concentration range under study, that the adsorption of phenol is well described by a "bi-Langmuir" model where the adsorption on the first category of sites is very well accounted for by a Langmuir isotherm and where the adsorption on the second category of sites is only numerically described by an empirical fitted function. This hypothesis, even though open to criticism, will not handicap our conclusions on separation modelling, as we shall see further, and will be of great use in handling our simulations.

Concerning now resorcinol and catechol, we have compared their respective retention factors (k'_i), obtained from either analytical elution experiments, and the Langmuir model:

$$k'_i = \frac{t_R - t_{R_0}}{t_{R_0}} = F \cdot \frac{\partial q_i}{\partial C_i} = Fa_i \qquad (9)$$

where F is the phase ratio and a_i the coefficient of the Langmuir isotherm that represents its slope at the origin. t_{R_0} is the residence time of an unretained component and t_R the retention time of the studied product under analytical conditions.

We have observed, as was done by Frenz and Horváth [9] and Golshan-Shirazi *et al.* [5], that the Langmuir model always underestimates this retention factor (see Table I). For these solutes in the low concentration range, Frenz and Horváth [9] came to the conclusion that the adsorption behaviour was more complex than

that given by the Langmuir isotherm. Nevertheless, the Langmuir isotherm describes very well the adsorption of the desired components in the high concentration range, which is of much greater interest when considering the simulation of a separation process based on the non-linearity of solute adsorption isotherms.

Competitive isotherms related to the individual isotherm parameters

For the sake of simplicity, when considering the modelling of displacement separations, or other preparative separation modes, it seems very attractive to use the non-competitive parameters from the single-component isotherms, more especially as the classical description we obtained for these single-component adsorptions (Langmuir or bi-Langmuir isotherms) allows us to choose two models which are easy to handle, the competitive Langmuir and the LeVan–Vermeulen isotherms.

As we have seen in the previous section, phenol is adsorbed on two categories of sites. We have assumed that only the first category of sites, which is well described by the Langmuir model (coefficients a and b in eqn. 2), is subject to competitive adsorption with resorcinol and catechol, while phenol is adsorbed alone on the second category of sites, this adsorption being described by the second term in the equation of the bi-Langmuir model (the "empirical" Langmuir function). The opposite hypothesis, catechol and resorcinol adsorbing on the second category of sites, and no longer on the first, was tested in our simulations and led to very bad results (not shown).

The phenol adsorption, partly described by an empirical fitting, may be considered as a real drawback, as we lose the physical understanding of the parameters. Nevertheless, although its adsorption is of crucial importance for displacement phenomena, it only interferes with resorcinol and catechol in a narrow zone, located near the displacer front, while competition between catechol and resorcinol, that ensures the occurrence of an efficient displacement train, is much more involved in space and time. Therefore, this empirical fitting for phenol was deemed acceptable for this work.

Competitive Langmuir isotherm. Fig. 3 shows simulations of displacement separations for the resorcinol–catechol mixture in a 1:1 ratio. These chromatograms were calculated by using the competitive Langmuir isotherm related to the non-competitive parameters of each compound. They are compared with experiments done at four different loading factors concerning the resorcinol–catechol mixture. The loading factor is the ratio of the amount of injected product to the saturation capacity of the column for this considered product [47] and is expressed as follows:

$$Lf_i = \frac{C_{i,0} V_{\text{inj}} b_i}{(1-\varepsilon) S L a_i} \tag{10}$$

where $C_{i,0}$ is the initial concentration of the injected product at the entrance of the column, V_{inj} the injection volume, ε the total porosity, S the column cross-sectional area and L its length; a_i and b_i are the parameters of the single Langmuir isotherm for component i.

Whatever the loading factor, it is obvious that no simulation accounts properly for the experimental results (see Fig. 3). Indeed, whereas all experiments achieve a more or less effective separation by displacement, simulations are only suitable in predicting the residence time of phenol but do not describe any separation between catechol and resorcinol.

We may conclude that the competitive Langmuir model, used with parameters drawn from single-component Langmuir isotherms, is really unsatisfactory. This conclusion is not surprising and has already been pointed out by other workers [29,48,49], and an attempt to explain this fact will be given below.

It must be remembered that the competitive Langmuir model, derived from the classical Langmuir model, is based on the same simplifying hypotheses, *i.e.*, an ideal behaviour of solutes in both stationary and mobile phases, without any molecular interactions between them. Golshan-Shirazi and Guiochon [29] and Jacobson *et al.* [18] specified that such ideal conditions are only seldom found, as for instance in the case of an enantiomer mixture separation. It must also be added that the competitive Langmuir

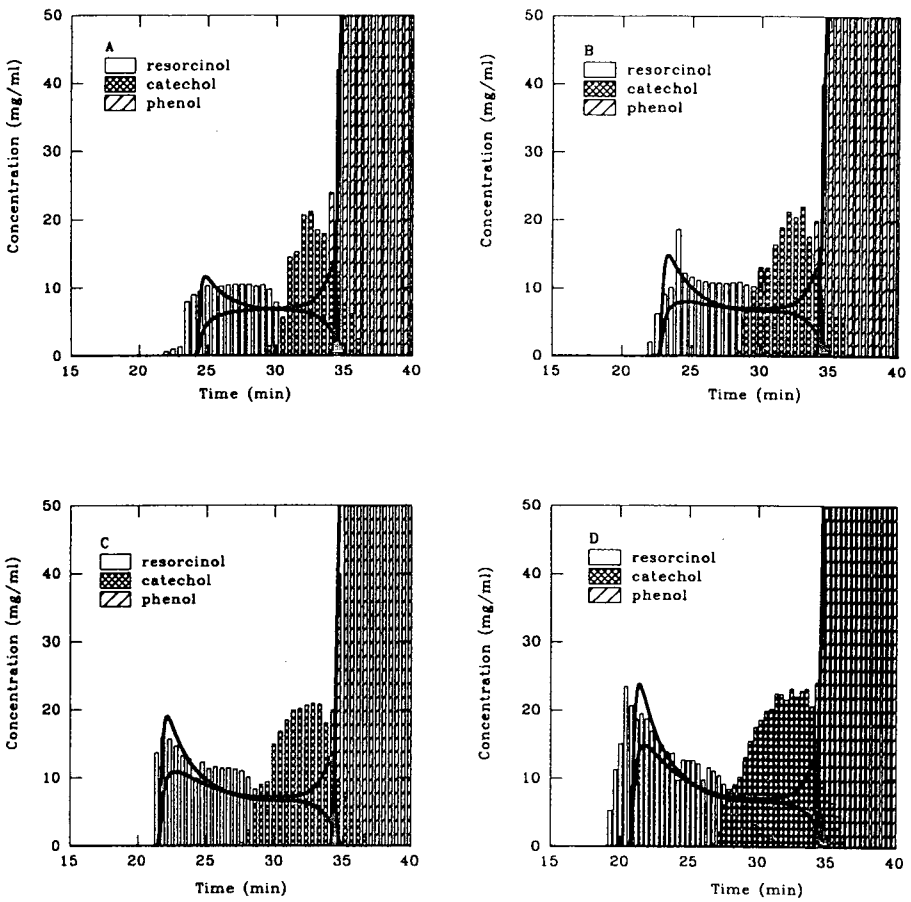

Fig. 3. Reversed-phase displacement chromatograms of a 1:1 binary mixture of resorcinol and catechol using phenol as displacer. Comparison between the band profiles (lines) calculated by using the competitive Langmuir isotherm with non-competitive parameters and the experimental data (bars). Conditions: column, 5-μm Nucleosil C_{18} (250 × 4.6 mm I.D.); phase ratio, 0.4; mobile phase, water; flow-rate, 0.2 ml/min; temperature, 30°C; V_{inj}, 0.4 ml; displacer, 80 g/l phenol in water. (A) $Lf_{res} = 20.1\%$, $Lf_{cat} = 11\%$; (B) $Lf_{res} = 25.1\%$, $Lf_{cat} = 13.7\%$; (C) $Lf_{res} = 30.1\%$, $Lf_{cat} = 16.5\%$; (D) $Lf_{res} = 35.1\%$, $Lf_{cat} = 19.2\%$.

isotherm violates the Gibbs' relationship [12] and therefore becomes thermodynamically inconsistent as soon as the saturation capacities (a_i/b_i) are different for all components [50,51]. The assumption of identical saturation capacities for products of different molecular sizes is very unrealistic because each molecule occupies on the surface of the support a space essentially dependent on its size, its three-dimensional conformation and other characteristics that cannot be applied to other molecules except in the case of enantiomers [18]. In this work, the competitive Langmuir model has been used more like a numerical description where saturation capacities may be different for every molecule than a rigorous description of the relevant thermodynamic or mechanistic phenomena encountered during the adsorption process. Besides, because of its simple and easy to handle formulation, this model remains one of the most commonly employed in the literature [10,52].

In addition, we also stress another failing of this competitive model that concerns the description of the selectivity, a parameter characterizing, for a given binary mixture of known composition, the ability of the stationary phase to

induce different migration velocities for each component and therefore its ability to separate this mixture. Selectivity is defined as follows:

$$\alpha = (q_i/C_i)/(q_j/C_j) \quad (11)$$

The competitive Langmuir isotherm predicts a constant selectivity for two components, whatever their respective concentrations, and does not take into account the influence of other components. In the present instance, it corresponds to the ratio of the initial slopes of single-component isotherms. This contradicts experimental results when the saturation capacities of the concerned products are different, and especially when the saturation capacity of the less retained component is the largest [29]. All these remarks question the validity of this model, and explain that its use, when intense competition for adsorption sites occurs, is not satisfactory. Hence a more elaborate model, such as the LeVan–Vermeulen isotherm, must be considered.

LeVan–Vermeulen isotherm. The LeVan–Vermeulen isotherm, derived from the Langmuir model, is also related to the non-competitive Langmuir parameters of each product. This model is more rigorous than the previous one because it makes use of conventional thermodynamic principles, such as the Gibbs' relationship, and can take into account the different saturation capacities of components, without problems of inconsistency. It is based, however, on simplifying hypotheses such as the ideal behaviour of solutes in both the stationary and mobile phases, a constant activity coefficient of these solutes and the absence of any molecular interaction between them [5]. Few studies have used this model to simulate separations [5,29] and our present work aims to complete these previous studies and to check the suitability of this model for our operating conditions.

Fig. 4 shows the same experimental displacement separations as in Fig. 3 and the corresponding simulations performed with the LeVan–Vermeulen model. Phenol competitive adsorption is described by this LeVan–Vermeulen isotherm plus the "empirical Langmuir" function which remained unaffected. We may note, in every situation, the very good agreement of the modelling with the actual separations. However, some mixing zones, appearing in experimental chromatograms between phenol and catechol, are not at all predicted by the calculated displacements. One explanation may be drawn from the influence of the dead volume between the column outlet and the sample collector, where hydrodynamic dispersion may degrade the separation. However, this is surely not the only reason. One may also put forward the poor and not well understood description of basic interaction phenomena with the stationary phase at low product concentrations, as previously stated for the general description of the Langmuir model. Nevertheless, one must admit the essentially good description of experimental results with this LeVan–Vermeulen model.

This model was then demonstrated to be effective for our operating conditions where products exhibit very different saturation capacities (66.08 g/l for resorcinol and 120.68 g/l for catechol), and are injected at high concentrations. Hence this difference in saturation capacities strongly influences the separation process and may be accurately taken into account by the LeVan–Vermeulen model [4,5]. In addition, as already stated by Golshan-Shirazi *et al.* [5], we can point out that the LeVan–Vermeulen model predicts a better displacement effect than that predicted by the competitive Langmuir model (see Fig. 3) when the more retained component of the binary mixture (here catechol) has the highest saturation capacity.

To complete these comments about this model, some useful information may be found in Fig. 5, which shows the competitive LeVan–Vermeulen isotherms of the two products, resorcinol and catechol, in a 1:1 ratio, and also the evolution in their selectivity. These curves are plotted as a function of the loading factor of resorcinol. The non-linearity of these isotherms is strongly marked, especially for resorcinol, which very quickly reaches it maximum concentration on the stationary phase. Resorcinol, because of strong competition for adsorption sites, cannot reach its saturation capacity on the stationary phase ($q_{s,r} = 66.08$ g/l, calculated per unit volume of particle skeleton) and its maximum adsorbed concentration is only 23 g/l. In addition, after

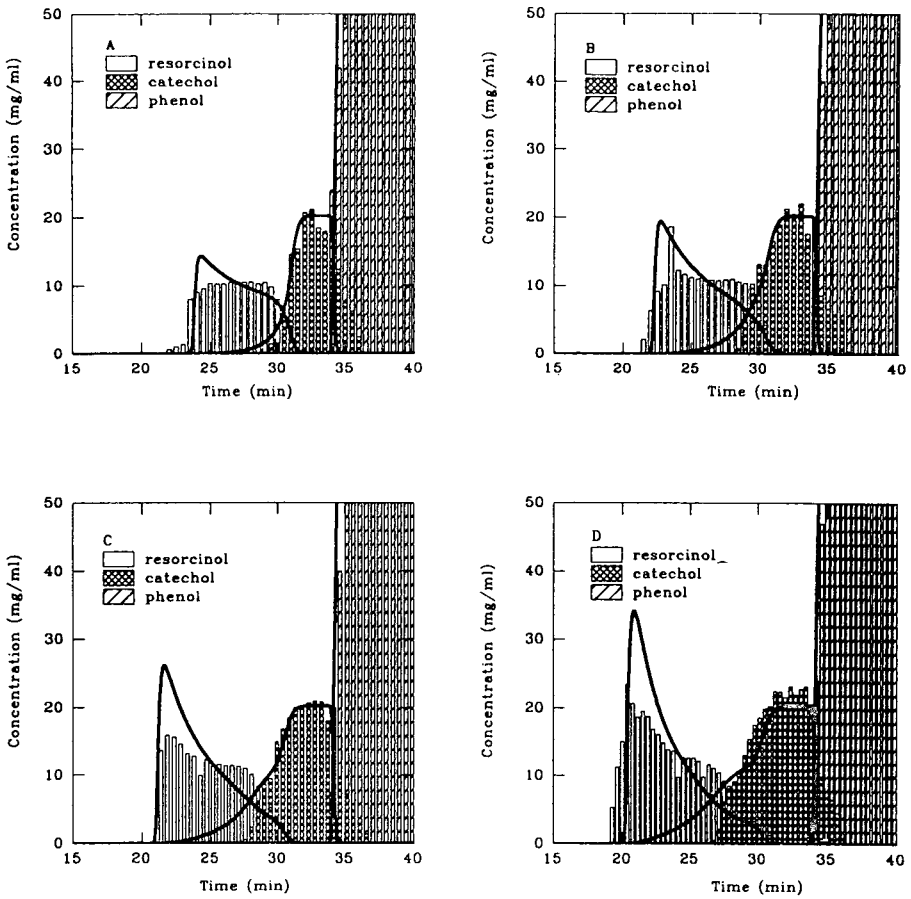

Fig. 4. Reversed-phase displacement chromatograms of a 1:1 binary mixture of resorcinol and catechol using phenol as displacer. Comparison between the band profiles (lines) calculated by using the two-term expansion LeVan–Vermeulen isotherm with non-competitive parameters and the experimental data (bars). Experimental conditions as in Fig. 4.

reaching 8% of the resorcinol loading factor, the adsorbed resorcinol concentration gradually decreases, these molecules being displaced by catechol molecules more strongly bound to the stationary phase. These latter will reach their saturation capacity only for very high loading factors because they have first to displace the adsorbed resorcinol molecules.

We observe also a continuous increase in the selectivity. This last effect is very important because it indicates that weakly resolved mixtures on an analytical scale may, under certain conditions, be separated easily on a preparative scale, and that selectivity inversions may be observed [5]. Finally, let us stress the value of this study for the LeVan–Vermeulen model, that has qualities and characteristics in common with the stoichiometric displacement model (S.D.M.) used in ion-exchange chromatography [34].

Quadratic isotherm: three floating parameters. The case of the quadratic isotherm we consider now is somewhat peculiar as this model mixes the non-competitive parameters from the single Langmuir isotherm of each component with extra correction coefficients derived from competitive experimental data. Hence great accuracy in the description of displacement effects is expected with the use of such a model, accuracy that has to justify the amount of extra experimental work required to obtain these specific competitive parameters.

From a practical point of view, we restricted

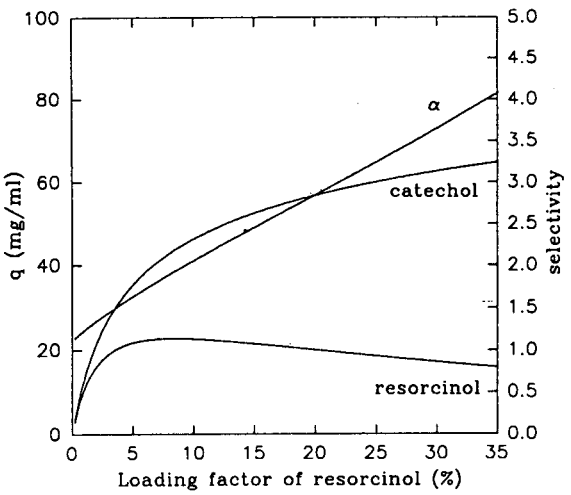

Fig. 5. Selectivity and LeVan–Vermeulen competitive isotherms with non-competitive parameters for a 1:1 binary mixture of resorcinol and catechol. Conditions: column, 5-μm Nucleosil C_{18} (250 × 4.6 mm I.D.) at 30°C; mobile phase, water.

our study to the determination of correction coefficients related only to the two products to be separated, *i.e.*, resorcinol and catechol, and we considered that the non-competitive parameters of the displacer bi-Langmuir isotherm were accurate enough. This approach may be justified in the case of displacement separations. Indeed, the displacer, *i.e.*, phenol, exerts a great influence on resorcinol and catechol but, as already stated, this influence is restricted to a narrow zone of the column, located near the displacer front. In contrast, resorcinol and catechol maintain a strong mutual competition in a broad zone. To simulate this kind of separation process it seemed to us more relevant to describe separately these competition phenomena without involving phenol and its correction factors. The experimental determination of competitive data was therefore done in an easy manner.

The problem previously encountered that arises yet again is to handle components with different adsorption models. Indeed, we use the competitive quadratic isotherm for resorcinol and catechol on the one hand, and the bi-Langmuir model characterizing the phenol adsorption on the other. To take into account the competitive influence of phenol on the adsorption of resorcinol and catechol, we modified in an intuitive manner the quadratic isotherm of these two components in the same way as the competitive Langmuir isotherm is derived from the single Langmuir isotherm. We obtained the following equations, simpler but more empirical than those derived from a quadratic model involving three components:

$$q_1 = \frac{a_1C_1 + a_{12}C_1C_2}{a + b_1C_1 + b_2C_2 + b_{12}C_1C_2 + b_3C_3} \quad (12a)$$

$$q_2 = \frac{a_2C_2 + a_{21}C_1C_2}{1 + b_1C_1 + b_2C_2 + b_{21}C_1C_2 + b_3C_3} \quad (12b)$$

where the subscripts 1 and 2 refer to resorcinol and catechol, respectively, and the coefficient b_3 is the b parameter from the Langmuir model (see eqn. 2) accounting for the adsorption of phenol on the same sites as the other two components. Let us specify again that concerning phenol, an empirical function is always associated with this Langmuir model to obtain the "semi-empirical" bi-Langmuir model introduced previously. The competitive adsorption of phenol with the other two components has been accounted for by a conventional competitive Langmuir isotherm associated with the unaffected empirical function. The latter remained unaffected because it only describes the non-competitive adsorption of phenol on specific adsorption sites.

The quadratic isotherm coefficients a_{12}, a_{21} and b_{12} were obtained by a numerical fitting of a set of competitive isotherm data. The other parameters a_i and b_i (see eqns. 12a and b) are the non-competitive Langmuir parameters. The coefficient b_{12} is set equal to b_{21} as stated by Lin *et al.* [22]. Results are summarized in Table III.

Fig. 6 shows the close agreement between the experimental displacement separations and their numerical simulations obtained with the equilibrium-dispersive model associated with the quadratic isotherms. However, a mixing zone between resorcinol and catechol, experimentally observed and also visible in the LeVan–Vermeulen-calculated profiles, is not present in the theoretical profiles presented in Fig. 6. The occurrence of a plateau for resorcinol is better

TABLE III

COMPETITIVE ISOTHERM PARAMETERS FOR THE RESORCINOL–CATECHOL MIXTURE: SUMMARY OF RESULTS

Competitive isotherm model	Parameters		Mean relative error (%)
	Resorcinol	Catechol	
Competitive Langmuir	$a_1 = 5.156$	$a_2 = 11.456$	17.50
(best-fit parameters)	$b_1 = 0.0748$ l/g	$b_2 = 0.1055$ l/g	
LeVan–Vermeulen	$a_1 = 10.746$	$a_2 = 11.3811$	10.09
(best-fit parameters)	$b_1 = 0.160$ l/g	$b_2 = 0.0989$ l/g	
Quadratic isotherm	$a_1 = 7.937$	$a_2 = 8.810$	
(three floating parameters)	$b_1 = 0.120$ l/g	$b_2 = 0.073$ l/g	8.53
	$a_{12} = -0.0622$	$a_{21} = 0.2047$	
	$b_{12} = 0.0017$ g/l	$b_{21} = b_{12}$	
Quadratic isotherm	$a_1 = 4.7253$	$a_2 = 6.476$	
(seven floating parameters)	$b_1 = 0.0358$ l/g	$b_2 = 0.0408$ l/g	4.21
	$a_{12} = -0.0537$	$a_{21} = 0.0291$	
	$b_{12} = 0.00075$ l/g	$b_{21} = b_{12}$	

accounted for in the present case than with the simulations using the LeVan–Vermeulen isotherm (see Fig. 4). Therefore, we may conclude that this quadratic model shows greater displacement effects than does the LeVan–Vermeulen model.

Fig. 7 shows the quadratic isotherms of resorcinol and catechol with a constant concentration ratio chosen as 1:1, and the evolution of their selectivity α plotted as a function of the loading factor of resorcinol. The preceding remarks about a large displacing effect may be recognized in the value of the selectivity that is always greater than that derived from the LeVan–Vermeulen model (see Fig. 5). Moreover, the increase in selectivity with increasing loading factor, observed with both the LeVan–Vermeulen and the quadratic isotherms, is much more sensitive with the latter.

Models of numerical adaptation

In this last approach, the previously mentioned models are now considered as empirical equations where all coefficients without exception are given by a parametric identification from experimental competitive adsorption data. It must be recalled that many studies have already used this concept, *e.g.*, by Jacobson *et al.* [36] and Jacobson and Frenz [41], who determined in this way the coefficients of the competitive Langmuir isotherm, Zhu *et al.* [4], who numerically identified the coefficients of the quadratic isotherm of the Fowler, Langmuir and LeVan–Vermeulen competitive models, Golshan–Shirazi *et al.* [5], who studied the LeVan–Vermeulen model, and Lin *et al.* [22], who obtained the seven floating parameters of the quadratic isotherm.

Concerning the quantitative description of the basic interaction and competitive adsorption phenomena on the stationary phase, a better accuracy is expected from this empirical approach than from that obtained with models related to non-competitive parameters, with or without correction factors [4,36]. Our study aims to show if, in the framework of our experimental displacements, other coefficients applied to the same models can lead to a better description of the separation process than that simulated by these models with their originally planned coefficients. We should mention also that modelling isotherms in a wide range of concentration, which is necessary for displacement simulations, raises some additional difficulties, as even the mobile phase concentration is no longer ideal in this instance. This can explain the agreement between calculated and experimental profiles

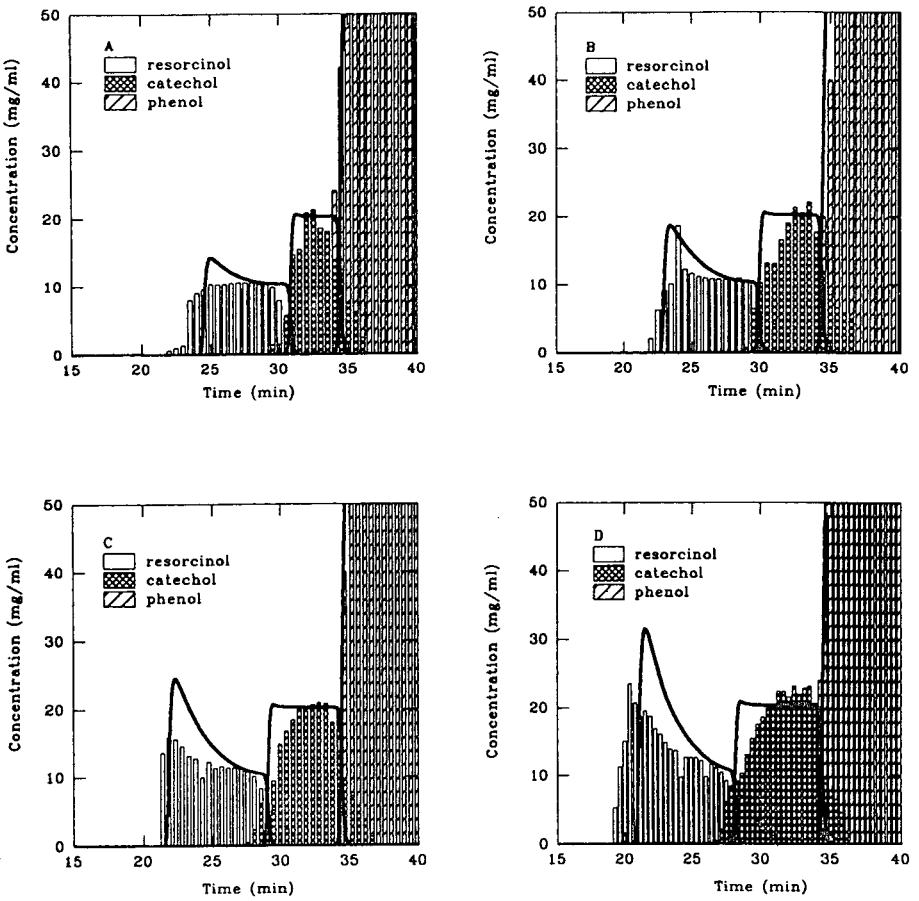

Fig. 6. Reversed-phase displacement chromatograms of a 1:1 binary mixture of resorcinol and catechol using phenol as displacer. Comparison between the band profiles (lines) calculated by using the quadratic isotherm with three floating parameters and the experimental data (bars). Experimental conditions as in Fig. 4.

being less good than in other studies dealing with elution chromatography.

As done previously, only the competitive parameters for resorcinol and catechol will be identified, and the original parameters for the phenol isotherm will again be considered as sufficiently accurate.

Competitive Langmuir isotherm. We have seen in a previous section that the competitive Langmuir isotherm related to non-competitive parameters was not at all satisfactory in describing displacement separations. This model is now considered as an empirical model for resorcinol and catechol.

First, it must be pointed out that the parametric identification used in this study led to a set of coefficients predicted with a high mean relative error (see Table III). This strong discrepancy (17.5%) highlights a poor fit of the competitive equilibrium data, and may justify the rejection of the competitive Langmuir isotherm. However, a closer study may moderate this statement. Indeed, most of the competitive frontal chromatograms were obtained with resorcinol and catechol mixtures whose total concentrations were below 80 g/l. Under these conditions we have observed that the competitive Langmuir model gave a better fit with experimental data (within a 10% mean deviation). On the other hand, when the column was more loaded, the observed deviation was larger. Relative deviations of more than 100% have been found, especially for

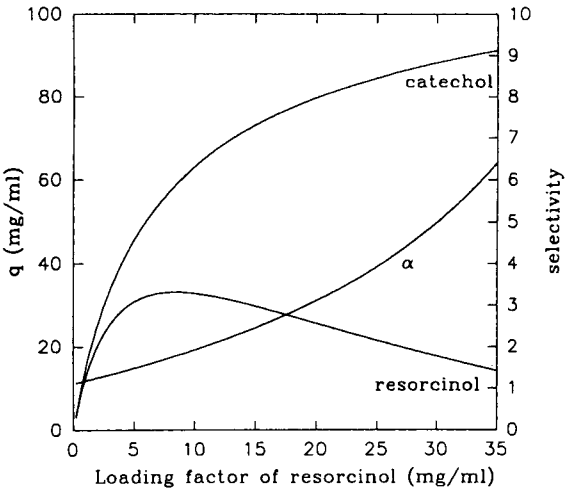

Fig. 7. Selectivity and quadratic isotherms with three floating parameters for a 1:1 binary mixture of resorcinol and catechol. Conditions: column, 5-μm Nucleosil C_{18} (250 × 4.6 mm I.D.) at 30°C; mobile phase, water.

resorcinol, whose calculated adsorbed concentration was always over-evaluated. We may conclude that, when a high limiting value of the loading factor is exceeded, the competitive Langmuir model is no longer able to account accurately for competitive adsorption of resorcinol and catechol, therefore leading to a restricted range of validity for this model. The high mean deviation is mainly due to the contribution of high concentrations and this does not exclude the use of the model in a lower concentration range.

This is illustrated in Fig. 8, where calculated displacement separations are compared with the corresponding experimental data and where a good agreement between the theoretical and actual profiles is observed. Indeed, although the initial operating conditions are not so appropriate for the use of this model (products are injected in 1:1 ratio, at concentrations higher than 40 g/l), the two products rapidly achieve a dilution that enables this model to be correct.

One can easily see that the simulations in Fig. 8 are totally different from those performed with the same competitive Langmuir model (see Fig. 2), but related to non-competitive parameters. However, this numerically adapted model still predicts a constant selectivity, independent of product concentrations, and is still as thermodynamically inconsistent as the original Langmuir model. Besides, in both models, the saturation capacities of each product are more or less similar (66.08 g/l before with non-competitive parameters and 68.93 g/l now for resorcinol, 120 g/l before and 108.58 g/l now for catechol). Therefore, it is very surprising to obtain a very poor description of the separation in one case and a fairly satisfactory one in the other.

Finally, as an attempt to understand this result, we may consider the influence of the relative retention factor of resorcinol with respect to catechol ($\alpha' = a_2/a_1$), which was studied by Ghodbane and Guiochon [53]. They observed that, when considering preparative chromatography, the larger this parameter is, the larger are the displacement effects, leading to increased yields and productivities. In our case its value is 2.22 for the numerically adapted competitive Langmuir model against a value near unity ($\alpha' = 1.11$) for the original competitive Langmuir model. This difference is certainly the explanation for the very different simulation results.

To conclude this section on the competitive Langmuir model, we must note that for two major reasons its use will nevertheless be restricted to special cases. First, as we have already mentioned, its poor description of the competitive adsorption phenomena in the high concentration range may be a real drawback in many instances.

Second, and this remark applies to all other numerically adapted models, it cannot predict suitably a totally developed displacement separation. Indeed, in the ideal case, the conventional theory of displacement enables one to predict very easily the concentrations of each product in the isotachic displacement train by the use of single-component isotherms and also the operating line. When applying this theory to the single isotherms shown in Fig. 2, it leads to the isotachic concentrations of 10.15 and 20.03 g/l for resorcinol and catechol, respectively. When using the numerically adapted Langmuir model, it is not possible to account correctly for non-competitive adsorption; indeed, we obviously do not obtain the actual single adsorption isotherm when the concentration of other components tend to zero in the equation. This is why it

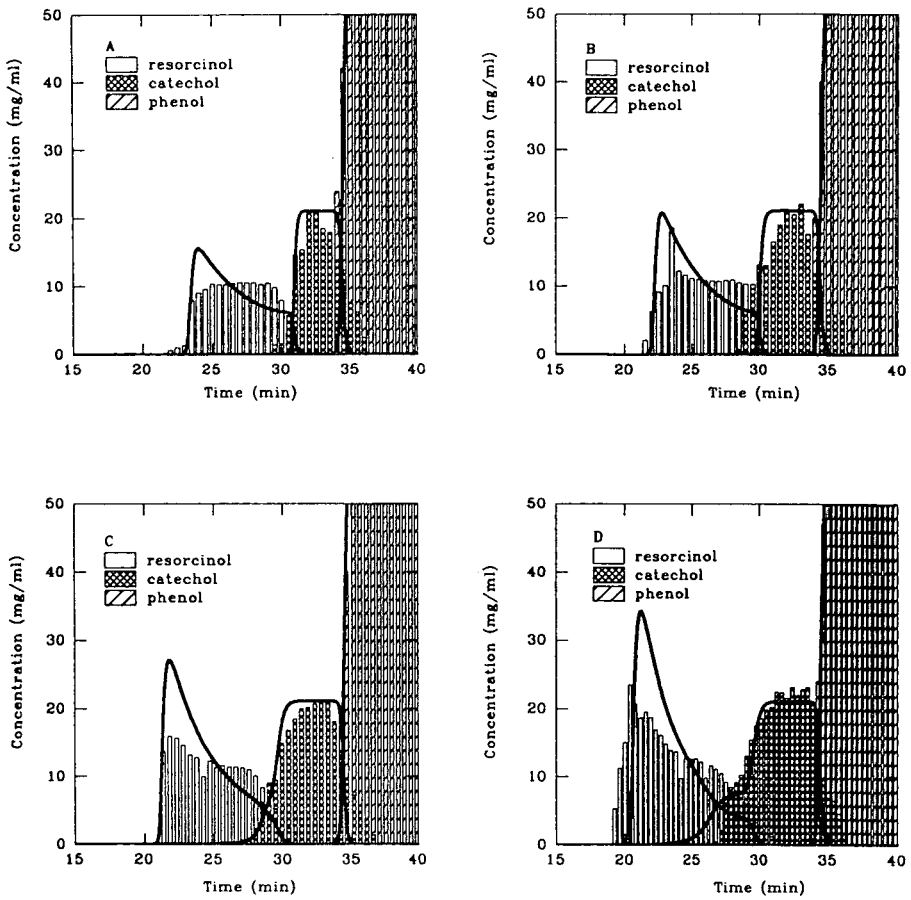

Fig. 8. Reversed-phase displacement chromatograms of a 1:1 binary mixture of resorcinol and catechol using phenol as displacer. Comparison between the band profiles (lines) calculated by using the competitive Langmuir isotherm with competitive parameters and the experimental data (bars). Experimental conditions as in Fig. 4.

cannot describe the situation where the product is migrating separately from the other one (as, for instance, when the displacement train is near to establishment). Concerning now the isotachic concentrations, we calculate with this competitive equation values of 5.90 and 20.87 g/l for resorcinol and catechol, respectively. This explains, for resorcinol, why the simulated starting plateau concentration (see Fig. 8) is much lower than the experimental value. This last conclusion may doom to failure the use of numerically adapted models to describe any developed displacement separations.

LeVan–Vermeulen isotherm and quadratic isotherm. Four parameters are now to be determined for the LeVan–Vermeulen model and seven floating parameters for the quadratic model, the coefficient b_{12} always being taken to be equal to b_{21} as stated by Lin *et al.* [22]. The results are summarized in Table III. The seven-parameter quadratic isotherm leads to the lowest mean relative deviation (4.21%) and *a priori* augurs well for the following simulations done with this model.

Figs. 9 and 10 show the results of simulations with the LeVan–Vermeulen model and the quadratic model, respectively. One can observe that these two last models, in their numerically adapted version, do not account adequately for the experimental results. For instance, the LeVan–Vermeulen model overestimates the concentration plateau for each product to be separated. Indeed, when considering the previous remark in the above section about the competi-

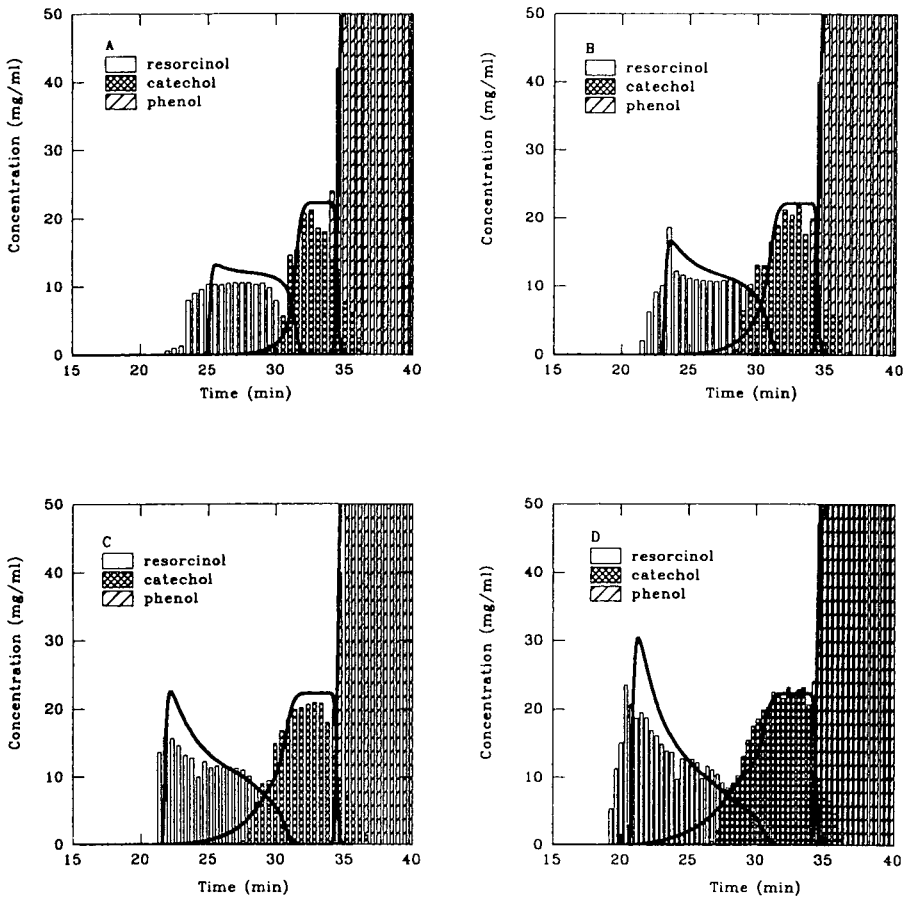

Fig. 9. Reversed-phase displacement chromatograms of a 1:1 binary mixture of resorcinol and catechol using phenol as displacer. Comparison between the band profiles (lines) calculated by using the two-term expansion LeVan–Vermeulen isotherm with competitive parameters and the experimental data (bars). Experimental conditions as in Fig. 4.

tive Langmuir model, the isotachic concentrations calculated with this LeVan–Vermeulen isotherm are 12.52 and 22.05 g/l for resorcinol and catechol, respectively, instead of the calculated values of 10.15 and 20.03 g/l according to the theory of displacement chromatography. Finally, simulations with the quadratic isotherm considered as an empirical model are the worst ones, although this model gave the best fit of the competitive adsorption experimental data (4.21% mean relative deviation).

We can therefore conclude that a competitive adsorption model, when considered as a numerical empirical equation, is not appropriate to describe the evolution of a separation process. This kind of model, which may prove to be very effective in describing competitive adsorption isotherms, could be very unsuitable when implemented in a simulation program for chromatographic separations. Indeed, after injection of products and after most of the separation process has occurred, there is no reason to consider models describing solute adsorption with competitive parameters, because products are now isolated. The use of these numerical equations will only be suitable when products remain mixed to a certain extent.

CONCLUSIONS

This work has attempted to establish a comparison between different competitive isotherms in accordance with an original criterion, more demanding than the conventional one that con-

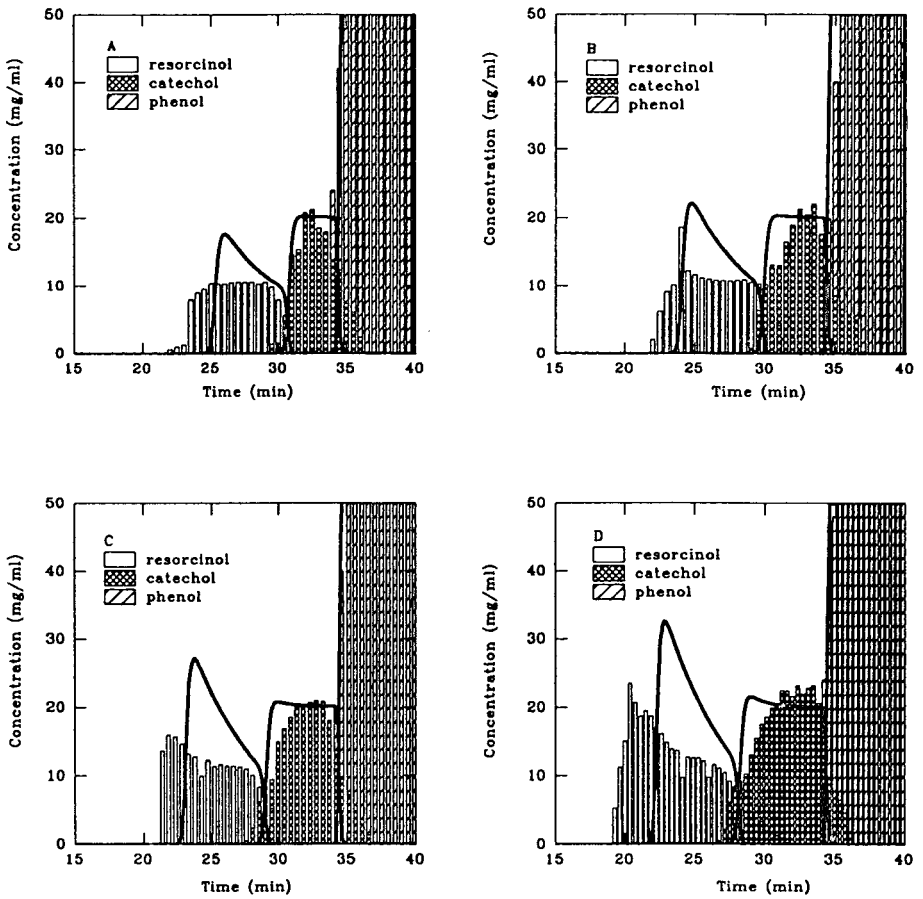

Fig. 10. Reversed-phase displacement chromatograms of a 1:1 binary mixture of resorcinol and catechol using phenol as displacer. Comparison between the band profiles (lines) calculated by using the quadratic isotherm with seven floating parameters and the experimental data (bars). Experimental conditions as in Fig. 4.

sists only in the ability of the isotherm equation to fit any set of experimental data points evaluated from competitive frontal analysis. Indeed, we have preferred to use a "dynamic" criterion which implies the implementation of the adsorption isotherm in a numerical program simulating displacement separations. This evaluation *in situ* is, in our opinion, an effective way to improve the understanding of the chromatographic process and to point out general problems directly related to the concept of separation and to the transient phenomena encountered during chromatographic separations. Three competitive adsorption models have been studied: the competitive Langmuir model, the LeVan–Vermeulen model and the quadratic model. During the past 10 years, experimental methods for obtaining competitive adsorption data have been simplified, and no longer need such tedious experiments. Nevertheless, obtaining data from single-isotherm measurements remains the simplest way [4]. Besides, in spite of the relatively good agreement of the competitive Langmuir isotherm related to competitive parameters with the experimental results, we have emphasized the limited value of competitive models considered as empirical equations in the simulation of displacement separations. This questions the usefulness of performing specific experiments to obtain these competitive parameters. Perhaps the best solution is to keep non-competitive parameters and to associate them with correction

coefficients as previously seen in the case of the quadratic isotherm with three floating parameters, or to find a numerical function describing the evolution of these correction factors with the concentration of solutes in the mobile phase. Theoretical research is also perhaps necessary to find new models or to adapt the old ones.

These conclusions have been drawn from a study that was focused on displacement separations and one may ask whether they will remain valid for other chromatographic modes, such as overloaded elution. In our opinion, in so far as a preparative separation is concerned, that means that concentrated solutions are injected, and in so far as an efficient separation process will inevitably progress from a zone of high competition for adsorption sites, to a zone of single adsorption (the aim is, of course, to obtain separated bands of migrating solutes throughout the column), all our conclusions may probably become generalized.

SYMBOLS

a_i Constant in Langmuir isotherm for component i
b_i Adsorption equilibrium constant for component i (m^3/kmol)
C_i Concentration of component i in the mobile phase (kmol/m^3)
$C_{i,0}$ Concentration of component i at the column entrance (kmol/m^3)
d_p Particle diameter (m)
$D_{i,m}$ Molecular diffusion coefficient of component i in the mobile phase (m^2/s)
F Phase ratio of the column packing $[=(1-\varepsilon)/\varepsilon]$
H Height equivalent to a theoretical plate (HETP) (m)
h Reduced plate height $(=H/d_p)$
k_i' Capacity factor for component i
L Column length (m)
M Number of components
N Number of theoretical plates $(=L/H)$
q_i Concentration of component i adsorbed on the stationary phase (calculated per unit volume of particle skeleton) (kmol/m^3)
q_s Function used for the LeVan–Vermeulen isotherm (see eqn. 6) (kmol/m^3)
$q_{s,i}$ Specific saturation value of stationary phase concentration for component i (kmol/m^3)
S Column cross-sectional area (m^2)
t Time coordinate (s)
t_R Retention time of the considered component (s)
t_{R_0} Residence time of an unretained component (s)
t_0 Beginning of a frontal analysis or a displacement chromatography (s)
u Interstitial fluid velocity (m/s)
V_D System dead volume (m^3)
V_{inj} Volume of feed injection (m^3)
V_{Φ_m} Column dead volume (m^3)
V_{Φ_s} Volume of stationary phase (m^3)
$V_{r,i}$ Retention volume of the C_i concentration step (m^3)
z Axial coordinate (m)

Greek letters

α Selectivity $[=(q_i/C_i)/(q_j/C_j)]$
α' Relative retention factor
ε Total porosity of the column packing
v Reduced mobile phase velocity $(=ud_p/D_m)$
v_{opt} Optimum reduced mobile phase velocity

REFERENCES

1 A. Felinger and G. Guiochon, *J. Chromatogr.*, 591 (1992) 31.
2 J.C. Bellot and J.S. Condoret, *Process Biochem.*, 26 (1991) 363.
3 J.C. Bellot and J.S. Condoret, *Process Biochem.*, 28 (1993) 365.
4 J. Zhu, M. Katti and G. Guiochon, *J. Chromatogr.*, 552 (1991) 71.
5 S. Golshan-Shirazi, J.-X. Huang and G. Guiochon, *Anal. Chem.*, 63 (1991) 1147.
6 J. Jacobson, J. Frenz and Cs. Horváth, *J. Chromatogr.*, 316 (1984) 53.
7 A. Tiselius, *Ark. Kemi Mineral. Geol.*, 16A (1943) 193.
8 Cs. Horváth, in F. Bruner (Editor), *The Science of Chromatography* (*Journal of Chromatography Library*, Vol. 32), Elsevier, Amsterdam, 1985, p. 179.
9 J. Frenz and Cs. Horváth, *AIChE J.*, 31 (1985) 400.
10 A. Katti and G. Guiochon, *J. Chromatogr.*, 449 (1988) 25.
11 I. Langmuir, *J. Am. Chem. Soc.*, 40 (1918) 1361.
12 D.M. Ruthven, *Principles of Adsorption and Adsorption Processes*, Wiley, New York, 1984.
13 D. Graham, *J. Phys. Chem.*, 57 (1953) 665.

14 J.D. Andrade, *Surface and Interfacial Aspects of Biomedical Biopolymers*, Plenum Press, New York, 1985, Ch. 1.
15 R.J. Laub, (*ACS Symposium Series*, No. 297), American Chemical Society, Washington, DC, 1986, p. 1.
16 A. Katti, J.-X. Huang and G. Guiochon, *Biotechnol. Bioeng.*, 36 (1990) 288.
17 J.-H. Huang, J. Schudel and G. Guiochon, *J. Chromatogr.*, 504 (1990) 335.
18 S. Jacobson, S. Golshan-Shirazi and G. Guiochon, *AIChE J.*, 37 (1991) 836.
19 G.M. Schwab, *Ergebnisse der Exakten Naturwissenschaften*, Vol. 7, Springer, Berlin, 1928, p. 276.
20 J.A.V. Butler and C. Ockrent, *J. Phys. Chem.*, 34 (1930) 2841.
21 E.C. Markham and A.F. Benton, *J. Am. Chem. Soc.*, 53 (1931) 497.
22 B. Lin, Z. Ma, S. Golshan-Shirazi and G. Guiochon, *J. Chromatogr.*, 475 (1989) 1.
23 H. Poppe, *J. Chromatogr.*, 556 (1991) 95.
24 A.L. Myers and J.H. Prausnitz, *AIChE J.*, 11 (1965) 121.
25 C.J. Radke and J.H. Prausnitz, *AIChE J.*, 11 (1972) 761.
26 L. Jossens, J.H. Prausnitz, W. Fritz, E.-U. Schluender and A.L. Myers, *Chen. Eng. Sci.*, 33 (1978) 1097.
27 W. Fritz and E.-U. Schluender, *Chem. Eng. Sci.*, 36 (1981) 721.
28 G. McKay and B.A. Duri, *Chem. Eng. J.*, 41 (1989) 9.
29 S. Golshan-Shirazi and G. Guiochon, *J. Chromatogr.*, 545 (1991) 1.
30 M.D. LeVan and T. Vermeulen, *J. Phys. Chem.*, 85 (1981) 3247.
31 F.D. Antia and Cs. Horváth, *J. Chromatogr.*, 556 (1991) 119.
32 G. Guiochon, S. Golshan-Shirazi and A. Jaulmes, *Anal. Chem.*, 60 (1988) 1856.
33 B.-C. Lin, S. Golshan-Shirazi, Z. Ma and G. Guiochon, *Anal. Chem.*, 60 (1988) 2647.
34 J.C. Bellot and J.S. Condoret, *J. Chromatogr.*, 635 (1993) 1.
35 J.H. Knox, *J. Chromatogr. Sci.*, 15 (1977) 352.
36 J. Jacobson, J. Frenz and Cs. Horváth, *Ind. Eng. Chem. Res.*, 26 (1987) 43.
37 F. Riedo and E.sz. Kováts, *J. Chromatogr.*, 239 (1982) 1.
38 J.-X. Huang and Cs. Horváth, *J. Chromatogr.*, 406 (1987) 275.
39 W. Melander, J.-F. Erard and Cs. Horváth, *J. Chromatogr.*, 282 (1983) 229.
40 X. Huang and G. Guiochon, *J. Colloid Interface Sci.*, 128 (1989) 577.
41 J. Jacobson and J. Frenz, *J. Chromatogr.*, 499 (1990) 5.
42 Z. Ma and G. Guiochon, *J. Chromatogr.*, 603 (1992) 13.
43 F. Helfferich and G. Klein, *Multicomponent Chromatography—Theory of Interference*, Marcel Dekker, New York, 1970.
44 Z. Ma and G. Guiochon, *J. Chromatogr.*, 609 (1992) 19.
45 L. Hagdahl, R.J.P. Williams and A. Tiselius, *Ark. Kemi*, 4 (1952) 193.
46 Z.El Fallah and G. Guiochon, *Anal. Chem.*, 63 (1991) 2244.
47 A.M. Katti and G. Guiochon, *Anal. Chem.*, 61 (1989) 982.
48 A.M. Katti and G. Guiochon, *J. Chromatogr.*, 499 (1990) 5.
49 S. Jacobson, S. Golshan-Shirazi and G. Guiochon, *J. Am. Chem. Soc.*, 112 (1990) 6492.
50 C. Kembal, E.K. Rideal and E.A. Guggenheim, *Trans. Faraday Soc.*, 44 (1948) 952.
51 D.B. Broughton, *Ind. Eng. Chem.*, 40 (1948) 1506.
52 M.W. Phillips, G. Subramanian and S.M. Cramer, *J. Chromatogr.*, 454 (1988) 1.
53 S. Ghodbane and G. Guiochon, *J. Chromatogr.*, 450 (1988) 27.

Journal of Chromatography A, 657 (1993) 327–335
Elsevier Science Publishers B.V., Amsterdam

CHROM. 25 531

Supercritical fluid extraction of polycyclic aromatic hydrocarbons from a marine sediment and analyte collection via liquid–solid trapping

Anja Meyer

Westfälische Wilhelms-Universität, Lehrstuhl für Analytische Chemie, Wilhelm-Klemm Strasse 8, 48149 Münster (Germany)

Wolfgang Kleiböhmer*

Institut für Chemo- und Biosensorik, Wilhelm-Klemm Strasse 8, 48149 Münster (Germany)

(First received May 17th, 1993; revised manuscript received August 26th, 1993)

ABSTRACT

A standard reference marine sediment (SRM HS-3) certified for polycyclic aromatic hydrocarbons (PAHs) was extracted with pure and toluene-modified supercritical carbon dioxide at various temperatures while the pressure was maintained at 400 atm (1 atm = 101 325 Pa). The best results were achieved with toluene-modified carbon dioxide at 140°C. Similar results were obtained when carbon dioxide was replaced with nitrous oxide. Analyte collection after off-line supercritical fluid extraction (SFE) was carried out with liquid–solid traps whereby analyte losses due to aerosol formation during the depressurization of the supercritical fluid were reduced. As the liquid–solid traps were developed from conventional clean-up systems, further clean-up steps became unnecessary in this study. Such traps yielded better PAH recoveries than SFE with analyte trapping in pure organic solvents. The results of the optimized procedure were compared with the certified PAH values, with the results obtained by Soxhlet extraction with toluene and *n*-hexane–acetone and with published SFE results. With SFE instead of conventional Soxhlet extraction, the complete time required for the extraction, evaporation and clean-up steps can be reduced from *ca.* 27 h to *ca.* 3 h per sample.

INTRODUCTION

Polycyclic aromatic hydrocarbons (PAHs) are ubiquitous environmental pollutants emitted from numerous natural and anthropogenic sources (*e.g.*, traffic, industrial processes) [1]. As PAHs comprise the largest class of known chemical carcinogens, the rapid and precise determination of these compounds in different matrices is very important. PAHs are usually recovered from soil by conventional liquid solvent extraction techniques (*e.g.*, Soxhlet extraction), although these methods are time consuming and require large amounts of organic solvents. Compared with these methods, extraction times can be reduced from hours to minutes using supercritical fluid extraction (SFE) with physiologically harmless carbon dioxide [2]. In this study, PAH extractions from a marine sediment were performed with supercritical fluids in order to determine the applicability of this technique and to improve critical steps such as analyte collection and clean-up.

The optimum extraction temperature was determined by extracting the marine sediment at different temperatures with carbon dioxide while the pressure was maintained at 400 atm. Organic modifiers can increase the extraction efficiency by reducing the affinity of the analytes for

* Corresponding author.

0021-9673/93/$06.00
SSDI 0021-9673(93)E0952-Q

sorptive sites of the matrix and by increasing their solubility in the supercritical fluid [3]. Toluene was chosen as a modifier because it yielded better results than methanol, acetone and *n*-hexane in a previous study [4].

Further increases in extraction efficiency may be obtained by using the slightly more polar nitrous oxide (N_2O) instead of CO_2 [5]. As nitrous oxide is a strong oxidant, the extraction of large amounts of organic and easily oxidizable material, particularly at elevated temperatures, should be avoided [6], so that most of the analytical SFE applications are still performed with CO_2. Nevertheless, the optimized procedure was also carried out with toluene-modified nitrous oxide at different temperatures.

Poor analyte recoveries are usually attributed to poor extraction efficiencies, although they may also be caused by incomplete analyte collection after an off-line SFE step [6–8]. The conventional collection method is depressurization of the supercritical fluid into an organic solvent. In this case, analyte losses due to aerosol formation with the expanding gas may occur [6]. Analyte collection on sorbent resins such as Tenax, C_{18}, silica gel and XAD traps has been reported [8], but the use of modifiers may influence the adsorption of the analytes or even wash them out [9]. The recently developed liquid–solid trapping method [4] allows the use of modified fluids, because washed out analytes are collected in the solvent.

PAHs are normally present in low concentrations in sample matrices spanning a wide polarity range [10]. These materials may interfere with the high-performance liquid chromatographic (HPLC) determination by causing a loss of separation reproducibility and contamination of the columns. Owing to these problems, a clean-up of the extracts is necessary but also very critical for the accurate quantification of the analytes because losses may occur if the rinse solvent is not able to overcome the solute–stationary phase interactions [7].

The aim of this work was to reduce analyte losses during analyte collection and to develop a method that combines analyte collection and clean-up in one step. Several clean-up systems were used as liquid–solid traps and the results were compared with those we had obtained by conventional analyte trapping in pure organic solvents.

Finally, the results of the optimized procedure were compared with the certified values and with the published results [11].

EXPERIMENTAL

Samples and standards

All solvents were purchased from Merck (Darmstadt, Germany) in the highest purity available. Standards of individual PAHs were obtained from Dr. Ehrenstorfer (Augsburg, Germany). The certified reference materials NIST SRM 1647b (sixteen PAHs in acetonitrile) (NIST, Gaithersburg, MD, USA) and the marine sediment HS-3 (National Research Council of Canada) were purchased from Promochem (Wesel, Germany).

The marine sediment (10 g) was treated with 1 *M* hydrochloric acid (20 ml) for 1 h, washed with distilled water (50 ml) and dried in air prior to SFE [4,12]. The aim of this pretreatment step was to reduce interactions between the analytes and the sorptive sites of the sediment. It increased the extraction efficiency by up to 20% for the PAHs investigated. For Soxhlet extractions the marine sediment was used as received because a conventional method should be employed. However, a wet sample would have to be dried only once, either prior to Soxhlet extraction or for SFE after the hydrochloric acid treatment step.

Silica gel (63–200 μm) (Merck) was heated at 500°C for 12 h and cooled in a desiccator to room temperature before addition of 3% (w/w) of water. Florisil (for residue analysis, 150–250 μm) (Merck) and alumina (neutral, for chromatography) (Baker, Gross-Gerau, Germany) were used as received.

Extraction of PAHs from marine sediment HS-3

Soxhlet extractions. A 70-ml Soxhlet extractor with 100 × 25 mm I.D. extraction thimbles and a 100-ml round-bottomed flask was used for all extractions. For each extraction 1.5 g of the sediment was mixed with 0.2 g of sodium sulphate and extracted with 80 ml of either toluene

or *n*-hexane–acetone (1:1, v/v) for 24 h in the dark. The extracts were concentrated at elevated temperatures (35–50°C) in a rotary evaporator to a volume of *ca.* 1 ml. Light petroleum (b.p. 40–60°C) (10 ml) was added and the solution was cleaned up as described below (clean-up procedure 1). Diethyl phthalate (50 μl) was added to the eluate prior to evaporation of the solvent under a gentle stream of nitrogen in order to prevent evaporation to dryness [13]. After dilution with 15 ml of acetonitrile, the extracts were analysed by HPLC.

Supercritical fluid extractions. All supercritical fluid extractions were performed with an SFE-703 supercritical fluid extraction system (Dionex, Idstein, Germany). The extraction cells (3.5 ml; 5 cm × 9.4 mm I.D.) were filled with silanized glass-fiber wadding (Macherey–Nagel, Düren, Germany) and 0.35 g of the marine sediment. Copper granules (2 g) were placed at the outlet end of the extraction cells in order to avoid restrictor plugging, which may be caused by sulphurous species that are present in marine sediments [4,7]. To modify CO_2, toluene (1 ml) was added to the sample and the loaded cell was heated at 120°C in the extraction oven for 15 min prior to dynamic extraction with pure carbon dioxide or nitrous oxide [4]. The cell pressure was set to 400 atm (1 atm = 101 325 Pa) and extractions were carried out at 60, 100 and 140°C for 75 min. A flow-rate of *ca.* 400 ml/min of gaseous CO_2 was measured after depressurization.

To prevent restrictor plugging due to frozen CO_2, the restrictor was heated to 150°C and a "dual-chamber trapping vial" [7] was used for analyte collection (Fig. 1a). This vial design prevents the heated restrictor from dipping into the analyte collection solvent (15 ml of either light petroleum or *n*-hexane placed in 5.5 × 2.5 cm I.D. vials), whereby evaporation losses were reduced. A transfer tube (Fig. 1a) was necessary to guide the expanded gas through the collection solvent, which was kept at *ca.* 3°C. For the new liquid–solid traps, the diameter of the transfer tube was reduced on the side that dips into the solvent before it was filled with silanized glass-fiber wadding and the dry solid sorbent as shown in Fig. 1b.

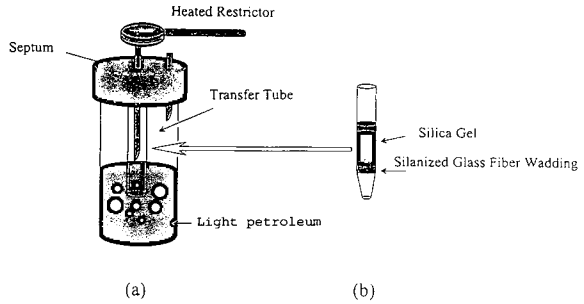

Fig. 1. Diagram of (a) the dual-chamber trapping vial and (b) the recently developed collection column, which is a modified transfer tube that is used with the dual-chamber trapping vial.

Clean-up

All clean-ups were carried out with "collection columns" that were prepared as described in Fig. 1b. The PAH recovery after the individual clean-up procedures was investigated by diluting 100 μl of the certified PAH solution SRM 1647b with 10 ml of light petroleum (clean-up procedure 1) or *n*-hexane (clean-up procedures 2–4) and transferring this solution directly on to the collection column. The sample flasks were rinsed with small amounts of the solvent (either light petroleum or *n*-hexane). For the SFE studies, the extracts were used as received from the analyte collection and handled like the standard solutions for the clean-up recovery study. The following clean-up procedures were tested.

Clean-up 1: silica gel–light petroleum–toluene. The columns were filled with 0.3 g of silica gel and washed with light petroleum (2 ml). Analyte collection during SFE and dilution of SRM 1647b for the clean-up recovery study were performed with light petroleum. PAHs were eluted with 3 ml of light petroleum–toluene (3:1, v/v) [4,14].

Clean-up 2: silica gel–n-hexane–dichloromethane. The columns were filled with 0.3 g of silica gel and washed with dichloromethane (1 ml) followed by *n*-hexane (1 ml). *n*-Hexane was used for analyte collection and dilution of SRM 1647b. PAHs were eluted with 3 ml of *n*-hexane–dichloromethane (9:1, v/v) [15].

Clean-up 3: Florisil–n-hexane–dichloromethane. The column was filled with 0.3 g of Florisil and washed with dichloromethane (1 ml) fol-

lowed by *n*-hexane (1 ml). *n*-Hexane was used for analyte collection and dilution of SRM 1647b. PAHs were eluted with 3 ml of *n*-hexane–dichloromethane (1:1, v/v) [15].

Clean-up 4: Silica gel–alumina–n-hexane–dichloromethane. The column was filled with 0.2 g of silica gel (bottom) and 0.15 g of alumina (top). It was washed with dichloromethane (1 ml) followed by *n*-hexane (1 ml). *n*-Hexane was used for analyte collection and dilution of SRM 1647b. PAHs were eluted with 3 ml of *n*-hexane–dichloromethane (3:2, v/v) [16].

To minimize evaporation losses, 50 μl of diethyl phthalate were added to each extract prior to evaporation of the solvent under a gentle stream of nitrogen. Acetonitrile (1 ml for recovery studies, 5 ml of SFE studies) was added and the extracts were analysed by HPLC [4].

HPLC analysis

For HPLC analysis, an HP Series 1050 liquid chromatograph (Hewlett-Packard) with a programmable variable-wavelength UV detector and HP ChemStation software for data analysis was used. The following wavelength programme was used: 220 nm, naphthalene, acenaphthylene, acenaphthene, fluorene; 248 nm, phenanthrene, anthracene; 234 nm, fluoranthene, pyrene; 270 nm, benz[*a*]anthracene, chrysene; 250 nm, benzo[*b*]fluoranthene, benzo[*k*]fluoranthene, benzo[*a*]pyrene; 296 nm, benzo[*ghi*]perylene, dibenz[*a*,*h*]anthracene, indeno[1,2,3-*cd*]pyrene [17]. Continuous degassing of the mobile phase was achieved with an HP Series 1050 on-line degassing system. The following acetonitrile (ACN)–water gradient was used as mobile phase: 0–6 min, 50% ACN; 35 min, 100% ACN (held until 45 min); 46 min, 50% ACN. The C_{18} HPLC column (Bakerbond Wide Pore octadecyl C_{18}, 250 × 4.6 μm I.D., 5 μm, 300 Å) (Baker) was heated to 30°C and initially equilibrated with acetonitrile–water (1:1, v/v) for 15 min prior to each run. The total flow-rate was set to 1 ml/min.

For identification of chromatographic peaks, retention times and UV spectra were compared with those of reference PAH compounds.

RESULTS AND DISCUSSION

In a first step, the PAH recoveries after different clean-up procedures were investigated using known amounts of the PAH standard solution SRM 1647b (certified for sixteen PAHs) as described above. The results (Table I) indicate that none of the clean-up procedures achieved a quantitative recovery for the most volatile PAHs (naphthalene, acenaphthylene and acenaphthene). As these components are to some extent soluble in water [18], losses may also occur during the pretreatment with hydrochloric acid and it was therefore not possible to determine these PAHs in this study. In contrast, the clean-up procedures 1, 2 and 4 achieved almost quantitative recoveries for PAHs with higher molecular masses. Only the Florisil–*n*-hexane–dichloromethane procedure (No. 3) obtained neither quantitative recoveries nor reproducible results.

Fig. 2 shows an HPLC chromatogram of an extract from SRM HS-3. Under the HPLC conditions described above, the dibenz[*a*,*h*]anthracene–benzo[*ghi*]perylene pair as well as chrysene and acenaphthene were not separated from co-eluted substances so that their accurate determination was impossible with a UV detector. Better results may be obtained by using the more sensitive fluorescence detection which, however, was not available for this study. Because of this, only the following ten PAHs were determined in the marine sediment HS-3 in this study: fluorene (Fluo), phenanthrene (Phen), anthracene (Anth), fluoranthene (F), pyrene (Py), benz[*a*]anthracene (B[*a*]A), benzo[*b*]fluoranthene (B[*b*]F), benzo[*k*]fluoranthene (B[*k*]F), benzo[*a*]pyrene (B[*a*]P) and indeno[1,2,3-*cd*]pyrene (I[*cd*]P).

To determine the optimum extraction temperature, the sediment was extracted at 400 atm and temperatures of 60, 100 and 140°C (fluid density $d = 0.89$, 0.76 and 0.64 g/cm^3) for 75 min with pure carbon dioxide. Analyte collection was carried out with light petroleum–silica gel traps. The results are presented in Fig. 3. SFE was less efficient than Soxhlet extraction with *n*-hexane–acetone for PAHs with higher molecu-

TABLE I

PAH RECOVERIES AFTER DIFFERENT CLEAN-UP PROCEDURES

A detailed description of each procedure is given in the text.

PAH	$\bar{x} \pm \sigma$ (%)			
	Clean-up 1: silica gel–light petroleum	Clean-up 2: silica gel–*n*-hexane–dichloromethane	Clean-up 3: Florisil–*n*-hexane–dichloromethane	Clean-up 4: silica gel–alumina–*n*-hexane–dichloromethane
Naphthalene	–	2.4 ± 0.1	2.3 ± 0.2	3.0 ± 0.4
Acenaphthylene	–	58.9 ± 2.6	45 ± 15	44 ± 31
Acenaphthene	40 ± 36	72.5 ± 1.8	59 ± 13	65 ± 27
Fluorene	63 ± 30	94.7 ± 0.2	74 ± 13	67 ± 9
Phenanthrene	103 ± 4	106.0 ± 1.7	101 ± 1	102 ± 3
Anthracene	97 ± 1	97.5 ± 2.7	94 ± 1	95 ± 5
Fluoranthene	103 ± 2	101.7 ± 0.3	97 ± 3	101.7 ± 0.2
Pyrene	103 ± 2	102.4 ± 0.4	98 ± 2	102.1 ± 0.5
Benz[*a*]anthracene	104 ± 2	103.0 ± 0.4	94 ± 9	102.5 ± 0.4
Chrysene	103 ± 2	102.9 ± 0.3	91 ± 13	100.0 ± 2.1
Benzo[*b*]fluoranthene	103 ± 2	103.0 ± 0.6	85 ± 19	103.0 ± 0.4
Benzo[*k*]fluoranthene	98 ± 5	100.4 ± 0.6	83 ± 26	97.9 ± 1.6
Benzo[*a*]pyrene	106 ± 5	105.0 ± 2.0	99 ± 20	90.1 ± 0.5
Dibenz[*a,h*]anthracene	100 ± 1	97.0 ± 0.9	68 ± 46	97.8 ± 0.6
Benzo[*ghi*]perylene	103 ± 2	100.8 ± 1.1	77 ± 37	102.1 ± 0.8
Indeno[1,2,3-*cd*]pyrene	102 ± 2	100.3 ± 0.7	74 ± 40	101.7 ± 0.9

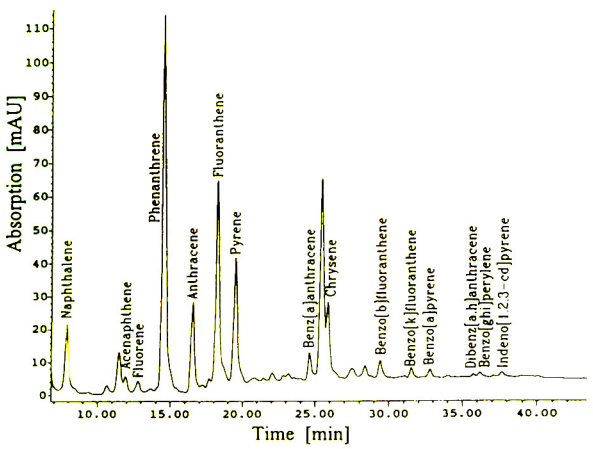

Fig. 2. Chromatogram of an extract of HS-3. Chromatographic conditions are described in the text.

lar masses (B[*b*]F, B[*k*]F, B[*a*]P, I[*cd*]P), but this discrepancy decreased with increasing temperature. The best results for these PAHs were obtained at 140°C, although the density and solvent strength of supercritical fluids decrease with increasing temperature if the pressure is held constant. This observation may be a consequence of thermal desorption effects and of increasing solute diffusivities and vapour pressures [5,6]. For PAHs with lower molecular masses, the extraction efficiency was less affected by temperature. The best results were obtained at 100°C. Both thermal desorption effects and increasing solvent strength (compared with extractions at 140°C) seem to be important in this case.

As a modifier can improve the solubility of PAHs in supercritical CO_2 and also the competition for the active sites of the sample, 1 ml of toluene was added directly to each sample. Static

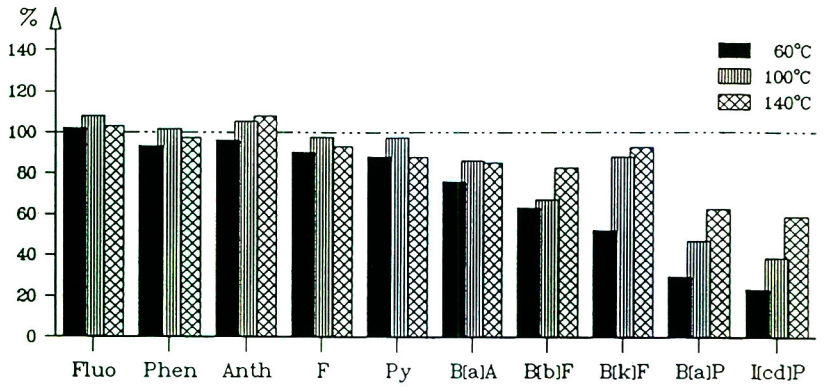

Fig. 3. Results of SFEs performed at different temperatures with pure CO_2. Fluo = fluorene; Phen = phenanthrene; Anth = anthracene; F = fluoranthene, Py = pyrene; B[*a*]A = benz[*a*]anthracene; B[*b*]F = benzo[*b*]fluoranthene; B[*k*]F = benzo[*k*]fluoranthene; B[*a*]P = benzo[*a*]pyrene; I[*cd*]P = indeno[1,2,3-*cd*]pyrene. The results are presented in comparison with those of the conventional Soxhlet extraction with *n*-hexane–acetone (100% line). Each extraction was performed in triplicate at 400 atm for 75 min.

equilibration of the system was obtained by maintaining the loaded extraction cells at 120°C for 15 min prior to dynamic extractions that were carried out at 400 atm and 100 or 140°C for 75 min. The best results were obtained at 140°C (Fig. 4). Compared with SFE with pure CO_2, the discrepancy between the SFE and Soxhlet extraction results decreased and for most of the PAHs, SFE with toluene-modified CO_2 yielded even better results than the conventional method. However, the extraction efficiency of SFE was less than that from Soxhlet extraction for PAHs with higher molecular masses.

Replacing CO_2 with the more polar N_2O should increase the SFE efficiency [2]. Because of this, extractions were performed at 100 and 140°C with toluene-modified nitrous oxide. In contrast to SFEs with toluene-modified CO_2, extractions at 100°C in most instances yielded results comparable to or even better than those which were obtained at 140°C. For safety reasons, subsequent extractions were performed with toluene-modified CO_2, as the results (Fig. 4) did not differ significantly from those obtained with CO_2 at 140°C.

To evaluate the influence of the liquid–solid trap on the collection efficiency, SFEs were performed with the following collection systems:

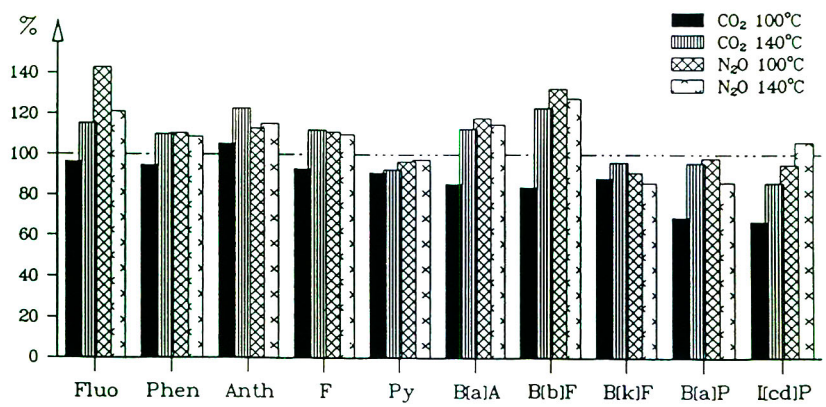

Fig. 4. Results of SFEs with toluene-modified carbon dioxide and nitrous oxide. Abbreviations as in Fig. 3. The results are presented in comparison with those of the conventional Soxhlet extraction with *n*-hexane–acetone (100% line). SFE parameters: $V_{toluene} = 1$ ml; $T_{0(equilibration)} = 120$°C; $t_0 = 15$ min; $p = 400$ atm; $t = 75$ min. Analyte collection was performed with light petroleum–silica gel traps. Each extraction was performed in triplicate.

TABLE II

COMPARISON BETWEEN ANALYTE COLLECTION VIA LIQUID–SOLID TRAPPING AND COLLECTION IN PURE ORGANIC SOLVENTS

Systems: 1 = pure *n*-hexane; 2 = silica gel–*n*-hexane–dichloromethane; 3 = silica gel–alumina–*n*-hexane–dichloromethane; 4 = Florisil–*n*-hexane–dichloromethane; 5 = pure light petroleum; 6 = silica gel–light petroleum–toluene. SFE parameters: $V_{toluene}$ = 1 ml; $T_{0(equilibration)}$ = 120°C; t_0 = 15 min; $T_{extraction}$ = 140°C; p = 400 atm; t = 75 min. Each extraction was performed in triplicate.

PAH	$\bar{x} \pm \sigma$ (μg/g)					
	System 1	System 2	System 3	System 4	System 5	System 6
Fluorene	6.3 ± 0.5	7.1 ± 0.3	6.8 ± 0.5	6.8 ± 0.8	6.1 ± 0.5	7.2 ± 0.6
Phenanthrene	74.8 ± 6.0	87.3 ± 1.1	84.5 ± 1.7	82.9 ± 6.4	75.7 ± 1.7	87.7 ± 1.7
Anthracene	8.7 ± 0.9	9.9 ± 0.3	9.8 ± 0.5	9.8 ± 0.8	8.9 ± 0.2	9.7 ± 0.1
Fluoranthene	58.2 ± 4.3	69.0 ± 1.2	67.9 ± 2.2	67.2 ± 3.8	60.1 ± 1.7	70.7 ± 1.2
Pyrene	37.7 ± 3.1	44.4 ± 1.5	42.6 ± 1.5	42.1 ± 3.7	38.2 ± 1.6	43.3 ± 1.5
Benz[*a*]anthracene	9.7 ± 1.9	10.4 ± 0.5	10.0 ± 0.4	9.5 ± 0.7	9.0 ± 0.5	10.4 ± 0.3
Benzo[*b*]fluoranthene	7.4 ± 1.0	9.0 ± 0.9	7.2 ± 0.7	7.7 ± 0.9	7.2 ± 0.6	7.6 ± 0.4
Benzo[*k*]fluoranthene	2.9 ± 0.3	3.2 ± 0.3	2.5 ± 0.3	3.1 ± 0.3	3.4 ± 0.3	3.7 ± 0.4
Benzo[*a*]pyrene	3.8 ± 0.3	4.1 ± 0.4	4.0 ± 0.2	4.5 ± 1.4	4.2 ± 0.7	4.6 ± 0.7
Indeno[1,2,3-*cd*]pyrene	2.6 ± 0.5	3.4 ± 0.4	2.4 ± 0.7	2.6 ± 0.5	3.0 ± 1.0	3.3 ± 0.4

(1) pure *n*-hexane; (2) silica gel–*n*-hexane; (3) silica gel–alumina–*n*-hexane; (4) Florisil–*n*-hexane; (5) pure light petroleum; (6) light petroleum–silica gel. Further treatment of the collection columns and solvents was carried out as described above (see clean-up procedures). Solvent exchange steps were not necessary as the solvent chosen for the clean-up (light petroleum or *n*-hexane) was already used as the collection solvent. Following procedures (1) and (5), clean-up was performed on silica gel with either *n*-hexane–dichloromethane (clean-up procedure 2) or light petroleum–toluene (clean-up procedure 1). With the liquid–solid traps, efficient analyte collection and clean-up were obtained in one step.

The results are presented in Table II. Analyte collection in pure *n*-hexane and light petroleum yielded similar results but these conventional methods were up to 50% less efficient than collection with any of the liquid–solid combinations. Langenfeld *et al.* [8] have reported that analyte collection in pure acetone yielded better results than pure *n*-hexane. However, we were not able to confirm this observation in a previous study [4]. The best recoveries were obtained with the light petroleum–silica gel traps. These results indicate that evaporation losses strongly influence the collection efficiency and that poor recoveries should not only be attributed to poor extraction efficiencies.

If our results are compared with those of other workers (Table III), the procedure presented here was more efficient for extractions of PAHs from marine sediment HS-3. The certified values and our SFE and Soxhlet extraction results are given in Table IV. There is no significant difference between SFE with toluene-modified fluids (CO_2 or N_2O) and conventional Soxhlet extraction with either *n*-hexane–acetone or toluene, but the certified values were not achieved for all compounds. However, these results are difficult to interpret because different methods may yield varying results when applied to one sample [19], and no information about the analytical procedure used for certification of HS-3 was available.

CONCLUSIONS

PAHs were extracted with supercritical carbon dioxide and nitrous oxide from the marine sediment HS-3 which was pretreated with hydrochloric acid in order to reduce interactions with the

TABLE III

COMPARISON OF RESULTS WITH THOSE OBTAINED BY OTHER WORKERS

PAH	Concentration (μg/g)			
	SFE with pure CO_2		SFE with modified CO_2	
	This work[a]	Literature [11][b]	This work[c]	Literature [11][d]
Fluorene	6.4	5.9	7.2	4.8
Phenanthrene	77.5	46.5	87.7	52.0
Anthracene	10.2	5.0	12.0	7.0
Fluoranthene	58.6	31.5	70.7	45.0
Pyrene	41.0	18.5	43.3	25.0
Benzo[*a*]anthracene	7.8	5.9	10.4	10.0
Benzo[*b*]fluoranthene	5.0	2.4	7.6	5.2
Benzo[*k*]fluoranthene	3.5	2.6	3.7	5.7
Benzo[*a*]pyrene	3.2	1.1	4.6	3.7
Indeno[1,2,3-*cd*]pyrene	1.9	0.4	3.3	2.0

[a] $T = 140$°C; $p = 400$ atm; $t = 75$ min; HS-3 was pretreated with hydrochloric acid as described and extracted in triplicate with pure CO_2.
[b] $T = 70$°C; $p = 400$ atm; $t = 25$ min; HS-3 was extracted in duplicate.
[c] $T = 140$°C; $p = 400$ atm; $t = 75$ min; HS-3 was pretreated with hydrochloric acid and extracted in triplicate with CO_2 that was modified with 1 ml of toluene.
[d] CO_2 was modified with 10% of methanol.

matrix. The extraction temperature strongly influences the SFE efficiency and the best results were obtained with toluene-modified fluids at 140°C.

For safety reasons, CO_2 was used for most of the experiments in this study, especially as the use of nitrous oxide did not increase the extraction efficiency as much as described by other

TABLE IV

RESULTS OF THE OPTIMIZED SFE PROCEDURE AND THE SOXHLET EXTRACTIONS

PAH	$\bar{x} \pm \sigma$ (μg/g)				
	Certified values	SFE with toluene-modified CO_2 [a]	SFE with toluene-modified N_2O [a]	Soxhlet extraction with toluene	Soxhlet extraction with *n*-hexane–acetone
Fluorene	13.6 ± 3.1	7.2 ± 0.6	7.5 ± 0.5	6.6 ± 0.2	6.2 ± 1.0
Phenanthrene	85 ± 20	88 ± 2	87 ± 5	78.4 ± 1.5	79.6 ± 0.5
Anthracene	13.4 ± 0.5	9.7 ± 0.1	9.1 ± 0.6	9.4 ± 0.7	7.9 ± 0.5
Fluoranthene	60 ± 9	71 ± 1	69 ± 4	62 ± 2	63 ± 1
Pyrene	39 ± 9	43 ± 2	46 ± 2	48 ± 2	47 ± 0.3
Benz[*a*]anthracene	14.6 ± 2.0	10.4 ± 0.3	10.6 ± 0.8	9.0 ± 0.3	9.2 ± 0.3
Benzo[*b*]fluoranthene	7.7 ± 1.2	7.6 ± 0.4	7.9 ± 0.6	9.1 ± 0.3	6.2 ± 0.2
Benzo[*k*]fluoranthene	2.8 ± 2.0	3.7 ± 0.4	3.3 ± 0.3	3.2 ± 0.1	3.8 ± 0.5
Benzo[*a*]pyrene	7.4 ± 3.6	4.6 ± 0.7	4.1 ± 0.4	5.8 ± 0.3	4.8 ± 0.4
Indeno[1,2,3-*cd*]pyrene	5.4 ± 1.3	3.3 ± 0.4	4.0 ± 0.4	4.2 ± 0.5	3.8 ± 0.1

[a] SFE parameters: $V_{toluene} = 1$ ml; $T_{0(equilibration)} = 120$°C; $t_0 = 15$ min; $T_{extraction} = 140$°C; $p = 400$ atm; $t = 75$ min. Each extraction was performed in triplicate.

workers. The loaded extraction cells were heated at 120°C for 15 min prior to extraction at 400 atm and 140°C for 75 min. Collection of the extracted analytes was carried out with liquid–solid traps (mostly with light petroleum–silica gel traps), which were more efficient than analyte collection in pure solvents, a fact which confirms that poor analyte recoveries are often caused by incomplete analyte collection due to aerosol losses. Further clean-up steps were unnecessary because a clean-up system was already used for the analyte collection. The advantage of the liquid–solid traps over analyte trapping via solid sorbents was their applicability for extractions with modified carbon dioxide, because washed out analytes are collected in the solvent. The results of our SFE procedure did not differ significantly from those of the conventional Soxhlet extraction with either toluene or *n*-hexane–acetone, but none of these methods reached the certified values for all compounds.

ACKNOWLEDGEMENTS

The financial support of the Bundesministerium für Forschung und Technologie (01 VQ 9003) and the Ministerium für Wissenschaft und Forschung des Landes Nordrhein-Westfalen is gratefully acknowledged.

REFERENCES

1 M.L. Lee, M. Novotny and K.D. Bartle, *Analytical Chemistry of Polycyclic Aromatic Compounds*, Academic Press, New York, 1981.
2 S.B. Hawthorne, *Anal. Chem.*, 62 (1990) 633A–642A.
3 A.T. Andrews, R.C. Ahlert and D.S. Kosson, *Environ. Prog.*, 9 (1990) 204–210.
4 A. Meyer, *Diploma Thesis*, University of Münster, Münster, 1992.
5 S.B. Hawthorne and D.J. Miller, *Anal. Chem.*, 59 (1987) 1705–1708.
6 R.W. Vannoort, J.-P. Chervet, H. Lingeman, G.J. de Jong and U.A.Th. Brinkman, *J. Chromatogr.*, 505 (1990) 45–77.
7 B.E. Richter, N.L. Porter, A.F. Rynaski, E.R. Campbell, M. Saunders, J.T. Swanson, R.B. Nielsen and B.J. Murphy, *J. Chromatogr. Sci.*, 30 (1992) 367–373.
8 J.J. Langenfeld, M.D. Burford, S.B. Hawthorne and D.J. Miller, *J. Chromatogr.*, 594 (1992) 297–307.
9 F. Höfler, *Labor Praxis*, (1992) 350–355.
10 I. Holoubek, J. Paasivirta, P. Maatela, M. Lahtiperä, I. Holoubková, P. Korínek, Z. Bohácek and J. Cáslavský, *Toxicol. Environ. Chem.*, 25 (1990) 137–154.
11 V. Lopez-Avila, N.S. Dodhiwala and W.F. Beckert, *J. Chromatogr. Sci.*, 28 (1990) 468–476.
12 F.I. Onuska and K.A. Terry, *J. High Resolut. Chromatogr.*, 14 (1991) 829–834.
13 *Die Bestimmung von Polycyclischen Aromatischen Kohlenwasserstoffen in Luftstaub*, Beschreibung des Hochdruckflüssigkeitschromatographischen Verfahrens der Landesanstalt für Immissionsschutz NRW, Essen, 1990.
14 H.G. Kicinski, S. Adamek and A. Kettrup, *GIT Fachz. Lab.*, 33 (1989) 1225–1228.
15 D.T. Kaschani and A. Brauns, *GIT Spezial Chromatographie*, 2 (1991) 66–76.
16 A. López García, E. Blanco González, J.I. García Alonso and A. Sanz-Medel, *Chromatographia*, 33 (1992) 137–154.
17 N. Hüsers, University of Münster, Münster, unpublished results, 1992.
18 Certificate of Analysis, Standard Reference Material 1647b, *Priority Pollutant Polycyclic Aromatic Hydrocarbons*, National Institute of Standards and Technology, Gaithersburg, MD, 1990.
19 H.A. Claessens, M.M. Rhemrev, J.P. Wevers, A.A.J. Janssen and L.J. Brasser, *Chromatographia*, 31 (1991) 569–574.

Journal of Chromatography A, 657 (1993) 337–343
Elsevier Science Publishers B.V., Amsterdam

CHROM. 25 541

Liquid chromatographic–mass spectrometric determination of 1-aminocyclopropane-1-carboxylic acid in tobacco

Nancy Chauvaux*

Department of Biology, University of Antwerp (UIA), Universiteitsplein 1, B-2610 Wilrijk (Belgium)

Walter Van Dongen

Department of Chemistry, University of Antwerp (RUCA), Groenenborgerlaan 171, B-2020 Antwerp (Belgium)

Eddy L. Esmans

Department of Biology, University of Antwerp (UIA), Universiteitsplein 1, B-2610 Wilrijk (Belgium) and Department of Chemistry, University of Antwerp (RUCA), Groenenborgerlaan 171, B-2020 Antwerp (Belgium)

Henri A. Van Onckelen

Department of Biology, University of Antwerp (UIA), Universiteitsplein 1, B-2610 Wilrijk (Belgium)

(First received July 8th, 1993; revised manuscript received September 7th, 1993)

ABSTRACT

Liquid chromatography–thermospray mass spectrometry was investigated as a method for determination of 1-aminocyclopropane-1-carboxylic acid (ACC) in *Nicotiana tabacum* cv. Petit Havana SR1. A stable isotope analogue of ACC ($[^2H_4]$ACC) was used as an internal standard. The internal standard was added to the plant samples prior to extraction. After solid-phase extraction both ACC and $[^2H_4]$ACC were derivatized with phenyl isothiocyanate (PITC) to the corresponding phenylthiohydantoin compounds PTH-ACC and $[^2H_4]$PTH-ACC. Selected ion monitoring of the protonated molecules $[MH]^+$ of m/z 219 and 223 was used for quantification. The method is sensitive and highly specific for the determination of ACC in plant extracts. This in contrast with the assay Lizada and Yang, which in several instances overestimated ACC in tobacco, probably owing to the presence of one or more interfering compounds.

INTRODUCTION

1-Aminocyclopropane-1-carboxylic acid (ACC) is accepted as the immediate precursor of the plant hormone ethylene [1] (Fig. 1). Not only because the availability of ACC is the most limiting step in the production of ethylene, but also because of the inducing activity of auxins on ACC-synthase, plant physiologists are more and more in need of an accurate method to de-

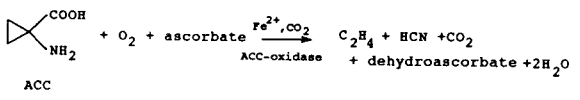

Fig. 1. Stoichiometry of ACC oxidation to ethylene by the enzyme ACC oxidase [2].

* Corresponding author.

0021-9673/93/$06.00
SSDI 0021-9673(93)E0960-3

termine ACC. For several years, the most commonly used techniques for ACC determination were based on the oxidative conversion of ACC to ethylene, followed by gas chromatographic (GC) analysis [3,4]. The main disadvantage of these techniques is that they are indirect and therefore not very specific.

More recently, some groups have been working on the development of more specific methods to determine ACC, *i.e.*, to detect ACC itself. Savidge *et al.* [5] identified ACC in Compressionwood (*Pinus contorta*) by GC–MS analysis of the 2,4-dinitrophenylmethyl ester of ACC. No attempt at quantification was made, however. McGaw *et al.* [6] determined the phthalimidomethyl ester of ACC by GC–MS. Although very sensitive, the method is very tedious, requiring several HPLC steps prior to GC–MS.

As ACC is in fact an amino acid, some groups have concentrated on the known techniques for amino acid analysis. Miller *et al.* [7] determined ACC in plasma and brain of mice by HPLC after derivatization with *o*-phthaldialdehyde and Lanneluc-Sanson *et al.* [8] used reversed phase HPLC on-line with UV detection for the determination of the phenylthiocarbamyl derivative of ACC (PTC-ACC). As some plant hormones are present in low (pmol/g fresh weight) concentrations, sensitive qualitative and quantitative techniques are needed for their measurement. Determination of underivatized ACC by combined liquid chromatography–mass spectrometry (LC–MS) using a thermospray interface (TSP) is difficult owing to the low molecular mass (101) of ACC, the protonated molecule [MH^+] of which is hard to detect amongst the intense background signals. Therefore, ACC was derivatized to the corresponding phenylthiohydantoin compound, which under LC–TSP-MS conditions produces a very intense protonated molecule at m/z 219 (relative intensity 100%). Further, the derivatives showed excellent chromatographic behaviour under conditions usually employed for LC–TSP-MS.

In this paper we present the quantitative results obtained for the determination of ACC in *Nicotiana tabacum* cv. Petit Havana SR1 by using selected ion monitoring on the ions at m/z 219 and 223 (interval time = 20 ms). The method is very specific but is less tedious than previously described GC–MS methods [5,6].

EXPERIMENTAL

Materials

ACC, [$^2H_4$]ACC (1-amino-[2,2,3,3-$^2H_4$]cyclopropane-1-carboxylic acid) and phenyl isothiocyanate (PITC) were purchased from Sigma (St. Louis, MO, USA). Methanol (gradient grade), ethanol (gradient grade), ammonia (25% solution), acetic acid (98%), trifluoroacetic acid (TFA), triethylamine and ammonium acetate were obtained from Merck (Darmstadt, Germany). RP-C_{18} solid-phase cartridges were obtained from Analytichem International (Harbor City, CA, USA) and Sephadex ion-exchange resins from Pharmacia (Uppsala, Sweden). [^{14}C]ACC was purchased from NEN (France) and hydrochloric acid (38%) from RPL (Leuven, Belgium). Water was purified by reversed osmosis with a Milli-Q water purification system (Millipore, Bedford, MA, USA).

Standard samples

Standard solutions were prepared in deionized water containing 1, 10 and 100 ng/μl ACC or [$^2H_4$]ACC. From these solutions, standard mixtures for the calibration graph were prepared by spiking 500 ng of ACC with 10, 25, 50, 100 and 250 ng of [$^2H_4$]ACC in small glass tubes (5 × 0.5 cm I.D.) or *vice versa*, in such a way that the final volume never exceeded 20 μl. After evaporation under vacuum, the standards were derivatized as described for the plant samples and analysed by LC–TSP-MS, using only one tenth of the mixture for every injection.

Plant samples

Production of plant material. Nicotiana tabacum cv. Petit Havana SR1 seeds were brought to germination in trays with soil. The trays were covered with perforated plastic foil until the plants were about 1 cm high. When they were about 5 cm tall, the plants were individually transferred to plastic pots (d = 15 cm).

The plants were germinated and grown under a light regime of 18 h/6 h (light/darkness), with a light intensity of 200 μmol s^{-1} m^{-2}, a relative

humidity of 85% and an average temperature of 25°C. At the age of 10 weeks (*ca.* twelve-leaf stage) the leaves were cut off, weighed individually and immediately frozen in liquid nitrogen. They were stored at −20°C prior to extraction.

Isolation of 1-aminocyclopropane-1-carboxylic acid. Approximately 1 g of frozen plant material was homogenized in 80% methanol, after addition of 250 ng of [$^2H_4$]ACC and 250 Bq of [^{14}C]ACC (specific radioactivity = 840 Bq/nmol) as internal standards, and kept at −20°C for 1 h during extraction. The slurry was centrifuged at 14 000 *g* for 20 min and the supernatant was diluted to 50% methanol by adding water and applied to a Bond Elut C_{18} column (2 ml). This column was immediately coupled to a column of anion-exchange resin (DEAE-Sephadex A-25, formate form, 3.0 × 1.5 cm I.D.). The last effluent was titrated to pH 2–2.5 with 1 *M* HCl and applied to a cation-exchange column (SP-Sephadex C-25, H^+ form, 3.0 × 1.5 cm I.D.). After consecutive washings with 3 m*M* HCl and water, the latter was eluted with 5% ammonia solution (5 ml). The eluate was evaporated under vacuum. One aliquot (half) was concentrated in small glass tubes prior to derivatization, while the other part was kept for analysis by Lizada and Yang's method [3].

Determination of ACC by GC. For the determination of ACC by GC the method of Lizada and Yang [3] was followed. The oxidation efficiency of ACC was monitored by spiking 100-μl aliquots of the sample with different amounts of ACC (except for the blank, to which no ACC was added). Three different concentrations of ACC were used per sample, and every measurement was carried out in duplicate. The total amount of ACC in the sample was calculated by means of linear regression. The amount of [$^2H_4$]ACC, added as an internal standard for LC–MS analysis, was subtracted from this value, to yield the initial amount of native ACC.

Derivatization with phenyl isothiocyanate. The synthesis of PTH-ACC was carried out according to Hewick *et al.* [9], with a slight change in TFA concentration and cyclization temperature in order to obtain a 100% conversion of PTC-ACC to PTH-ACC (Fig. 2). To test-tubes, 20 μl of

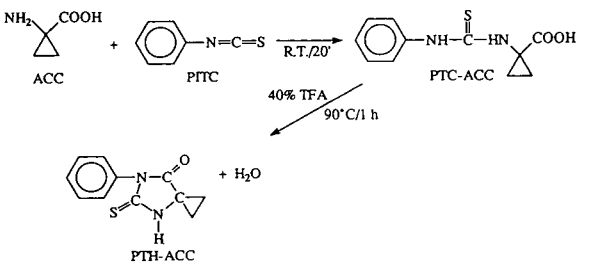

Fig. 2. Derivatization procedure of 1-aminocyclopropane-1-carboxylic acid (ACC) with phenyl isothiocyanate (PITC), resulting in the phenylthiohydantoin compound of ACC (PTH-ACC).

the derivatization solution [ethanol–water–triethylamine–phenyl isothiocyanate (7:1:1:1)] were added, and the reaction was allowed to proceed for 20 min at room temperature. After evaporation under vacuum, 50 μl of 40% TFA were added to the tubes and they were left to react at 90°C for 1 h. The reaction mixtures were evaporated to dryness under vacuum and the tubes were kept at −20°C prior to HPLC.

Preparative HPLC of PTH-amino acids. A preparative HPLC step was used to separate and isolate PTH-ACC from other PTH-amino acids and interfering products. This was done with a Spectra-Physics HPLC system, equipped with a 100-μl loop and an Alltech C_{18} (3 μm) cartridge (100 × 4.6 mm I.D.), on-line with an Applied Biosystems multi-wavelength UV detector, set at 260 nm. The mobile phase [methanol–water–acetic acid (40:59.5:0.5, v/v/v)] flow-rate was 0.5 ml/min. The eluted PTH-ACC (retention time 13 min, detected by ^{14}C analysis) was dried under vacuum and stored at −20°C for analysis by LC–TSP-MS.

Liquid chromatography–thermospray mass spectrometry of PTH-ACC

The PTH-ACC samples were injected into the HPLC system, connected to a VG TRIO-2000 mass spectrometer equipped with a thermospray interface. The HPLC system used consisted of a Waters 600-MS pump, a Waters 700 Satellite WISP autoinjector and an Alltech C_{18} (3 μm) column (100 × 4.6 mm I.D.). The mobile phase [methanol–0.1 *M* ammonium acetate (50:50, v/v)] flow-rate was 0.8 ml/min. Under these conditions, PTH-ACC had a retention time of

3.7–3.8 min. Tuning of the capillary temperature (210°C), source temperature (250°C) and the voltage on the repeller electrode (200 V) was done while introducing a standard sample in order to obtain maximum sensitivity.

Mass spectra were recorded by scanning a mass range of 150–400 u in 1 s. To improve the sensitivity, selected ion monitoring (SIM) was used for quantification. The protonated molecules at *m/z* 219 for PTH-ACC and *m/z* 223 for [$^2H_4$]PTH-ACC were monitored in the SIM chromatograms, using a dwell time of 100 ms and an interchannel delay of 20 ms.

For the quantification of the samples, the corresponding peak areas in these SIM chromatograms were used. The areas were calculated by manually selecting the start and end points of the peaks and by using Unix V6 software.

RESULTS AND DISCUSSION

Qualitative aspects of PTH-ACC analysis by LC–TSP-MS

In order to evaluate LC–TSP-MS for the determination of PTH-ACC in tobacco, a crude reaction mixture of PTH-ACC was analysed. This reaction mixture was obtained by first derivatizing pure ACC in ethanol–water–triethylamine–PITC (7:1:1:1) for 20 min at room temperature to the corresponding phenylthiocarbamyl compound. By subsequent treatment of the dried mixture with 40% TFA for 1 h at 90°C the corresponding PTH derivative was obtained. After evaporation under vacuum this mixture was analysed on an Alltech C_{18} column (3 μm, 100 × 4.6 mm I.D.) using methanol–0.1 *M* ammonium acetate (50:50, v/v) as the mobile phase at a flow-rate of 0.8 ml/min. The total ion current (TIC) chromatogram, together with the reconstructed mass chromatogram for *m/z* 219 and the UV chromatogram at 260 nm, is depicted in Fig. 3. As can be seen PTH-ACC elutes at 3.9 min.

The mass spectrum of PTH-ACC is shown in Fig. 4 together with that for the corresponding [$^2H_4$]PTH-ACC. The latter compound was obtained by an analogous derivatization procedure and analysed under the same conditions as mentioned above. The protonated molecules at

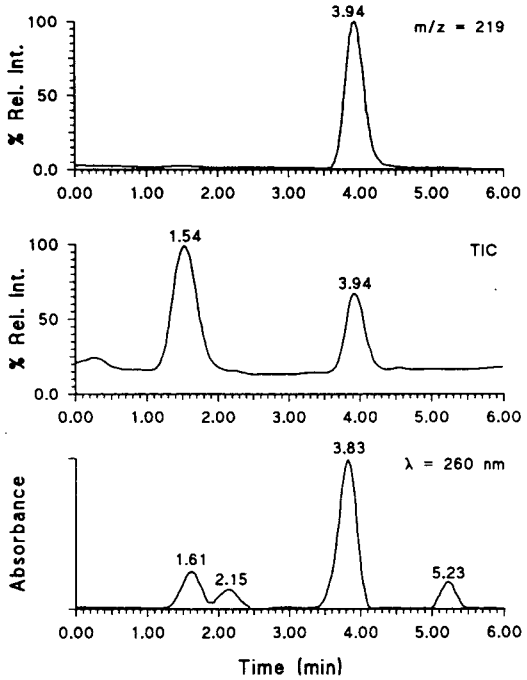

Fig. 3. Chromatograms (total scanning) of 100 ng of PTH-ACC. Column, Alltech C_{18} (3 μm, 100 × 4.6 mm I.D.); mobile phase, methanol–0.1 *M* ammonium acetate (50:50, v/v); flow-rate, 0.8 ml/min. Top, reconstructed mass chromatogram for *m/z* 219, corresponding to the protonated molecule (MH^+) of PTH-ACC; centre, TIC chromatogram (150–400 u in 1 s); bottom, UV trace at 260 nm. Rel. Int. = Relative intensity.

m/z 219 and 223 are intense and *m/z* 219 is absent in the mass spectrum of the deuterated internal standard. These features will allow the selective and highly sensitive measurement of ACC in plant material by LC–TSP-MS.

With this knowledge, several plant samples were analysed for the presence of ACC. For this purpose *Nicotiana tabacum* cv. Petit Havana SR1 leaf tissue was homogenized in 80% methanol after addition of known amounts of [^{14}C]ACC and [$^2H_4$]ACC as internal standards. After extraction for 1 h at −20°C, the ACC in the supernatants was concentrated by solid-phase extraction. The dried samples were derivatized as described for the standard mixtures. Prior to LC–TSP-MS, these samples were applied to an Alltech C_{18} column (3 μm, 100 × 4.6 mm I.D.) using methanol–water–acetic acid (40:59.5:0.5,

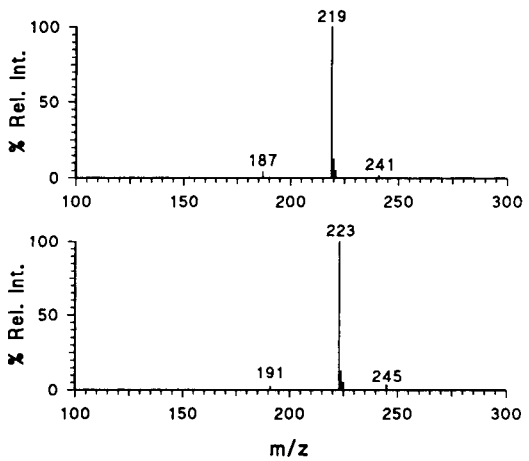

Fig. 4. Top, TSP mass spectrum of the PTH-ACC peak (retention time 3.9 min) in Fig. 3; bottom, mass spectrum of [$^2H_4$]PTH-ACC peak, obtained by an analogous procedure as for PTH-ACC. In both instances 100 ng of sample were injected.

v/v/v) as the mobile phase at a flow-rate of 0.5 ml/min. This supplementary step was used to isolate PTH-ACC from other PTH-amino acids and interfering compounds. The isolated PTH-ACC compound was analysed by LC–TSP-MS. The corresponding TIC chromatogram is shown in Fig. 5, together with the reconstructed mass chromatograms for the ions at *m/z* 219 and *m/z* 223. The PTH-ACC compound elutes at 3.8 min.

The corresponding mass spectrum is depicted in Fig. 6, where the base peak corresponds to *m/z* 207. This ion is due to another compound, however, eluting at 3.4 min (reconstructed mass chromatogram shown in Fig. 5). No contribution due to either *m/z* 219 or *m/z* 223 is expected. Compared with the standard chromatogram in Fig. 3, the analysis of the plant material shows an extra compound (*m/z* 223 at retention time 2.87 min). However, there is no contribution to $m/z = 219$. Moreover, because of the isotope dilution principle, this peak cannot be due to [$^2H_4$]PTH-ACC, but has to be due to another compound, only separated from PTH-ACC under LC–TSP-MS conditions. Therefore, this peak does not interfere with the determination of PTH-ACC. Hence LC–TSP-MS is a highly specific method for the determination of PTH-ACC.

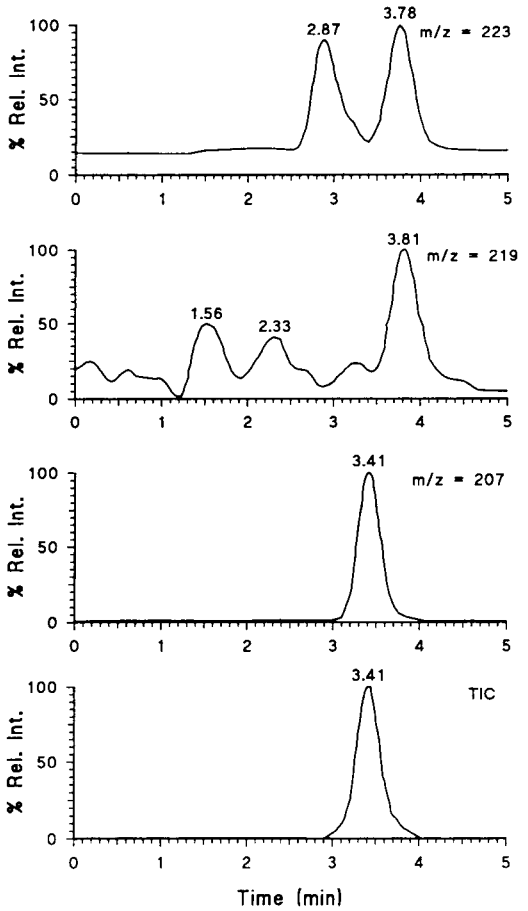

Fig. 5. Chromatograms (total scanning) of a plant sample, after preparative HPLC. Same column and mobile phase as for the standards. From top to bottom: reconstructed mass chromatograms for *m/z* 223, 219 and 207, respectively, and the TIC chromatogram. PTH-ACC elutes at 3.8 min. The peaks at *m/z* 223 and 219 correspond to *ca.* 20 and 10 ng, respectively.

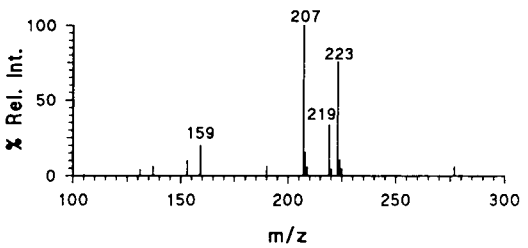

Fig. 6. TSP mass spectrum of the PTH-ACC peak (retention time 3.8 min) in Fig. 5.

Quantitative aspects of PTH-ACC analysis by LC–TSP-MS

In order to obtain the highest sensitivity possible, SIM of m/z 219 and 223 was used for the determination of PTH-ACC in both standard mixtures and unknowns. A calibration graph was obtained by spiking ACC with different amounts of [$^2H_4$]ACC and *vice versa*, resulting in a range of concentration ratios from 50:1 to 1:50 (H:^{2}H). Each concentration ratio was made up four times. These mixtures were derivatized as stated earlier and analysed by LC–TSP-MS. The area to area ratio (m/z = 219/223) was plotted against the molar ratio. The resulting calibration graph is shown in Fig. 7. For the higher ratios (H:^{2}H = 2:1 to 50:1) the inverse values were plotted. In this way, every molar ratio on the calibration graph corresponds to eight different area ratios. The regression equation for the calibration graph was $y = 0.965x + 0.004$ and the correlation coefficient was 0.99989.

With this knowledge, several plant samples were analysed by both LC–TSP-MS-SIM and the method of Lizada and Yang [3]. For this purpose, *Nicotiana tabacum* cv. Petit Havana SR1 leaf tissue was extracted with 80% methanol, after addition of known amounts of [^{14}C]ACC and [$^2H_4$]ACC as internal standards. After centrifugation and solid-phase extraction of the supernatant, one aliquot (half) of the sample was derivatized with PITC and the resulting PTH-ACC was isolated by means of a preparative HPLC step and finally determined by LC–TSP-MS using the conditions mentioned above. A typical SIM chromatogram for m/z 219 and 223 of a plant sample is depicted in Fig. 8, together with the UV trace at 260 nm. Peak areas were obtained by manually selecting the start and end points and using the Unix V6 software to calculate the areas. The initial amount of ACC in the sample was calculated by means of the regression line, using the following equation

$$\text{mol H} = (\text{area H/area } ^2\text{H} - 0.004) \cdot (\text{mol } ^2\text{H}/0.9654)$$

where (mol ^{2}H) is the amount of deuterated ACC (in moles), initially added as internal standard.

The other part of the sample was analyzed by means of the method of Lizada and Yang [3]. The amount of [$^2H_4$]ACC added as internal standard for LC–MS was subtracted from the results, yielding the initial amount of native ACC.

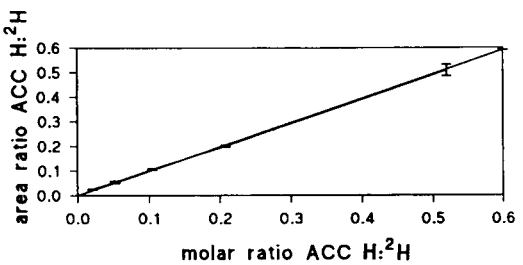

Fig. 7. Calibration graph for PTH-ACC, obtained by plotting the (m/z 219)/(m/z 223) area ratio against the injected PTH-ACC/[$^2H_4$]PTH-ACC ratio. Areas were obtained by selected ion monitoring on m/z 219 and 223. Equation: $y = 0.965x + 0.004$. Correlation coefficient = 0.99989.

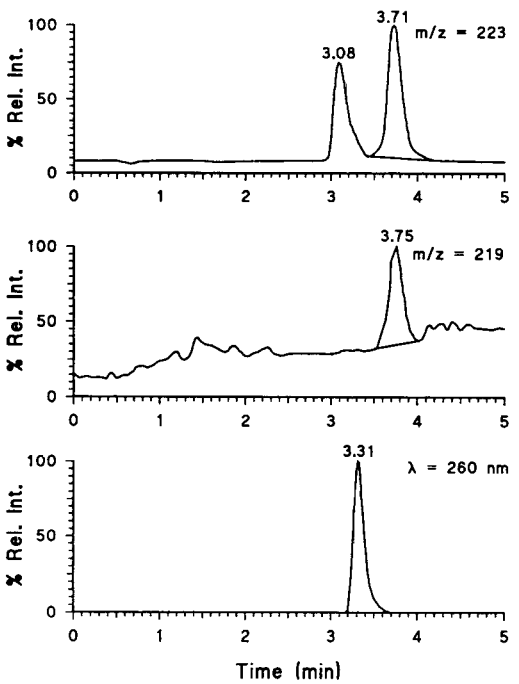

Fig. 8. Chromatogram of a plant sample (selected ion monitoring) for m/z 219 (MH^+ PTH-ACC) and m/z 223 (MH^+ [$^2H_4$]PTH-ACC), together with the UV trace at 260 nm. Conditions are the same as for the standards. The peaks at m/z 223 and 219 correspond to *ca.* 20 and 10 ng, respectively.

TABLE I

COMPARISON OF LC–TSP-MS DETERMINATION OF ACC WITH THE METHOD OF LIZADA AND YANG [3] IN THREE *NICOTIANA TABACUM* LEAF SAMPLES

Examples chosen are arbitrary (see text).

Sample No.	Endogenous ACC individual values (nmol/g fresh weight)	
	LC–MS	Lizada and Yang
1	1.46; 1.22	1.73; 1.39
2	0.63; 0.41	2.85; 1.93
3	0.73; 0.55	3.25; 2.91

Table I shows a comparison of the two methods for three tobacco leaf samples. Examples are arbitrarily chosen from a range of comparable results and, in the context of this paper, they have no physiological relevance. The values obtained from the oxidative conversion of ACC to ethylene are in several instances higher than those obtained by our method. These results are somewhat in contradiction with the reports by McGaw *et al.* [6] and Lanneluc-Sanson *et al.* [8], who compared Lizada and Yang's method with GC–MS of the phthalimido-ACC methyl ester of ACC and reversed-phase HPLC of PTC-ACC, respectively. Both groups observed an underestimation of the ACC content by Lizada and Yang's method, possibly owing to losses of ethylene during sampling.

On the other hand, it is well known that some substances may interfere with the assay according to Lizada and Yang [3]. In addition to overestimation, an underestimation of ACC can occur with this method [10,11]. For instance, treatment of senescing carnation flowers with α-aminoxyacetic acid, an inhibitor of ACC synthase, results in the production of a factor that gives rise to ethylene in the Lizada and Yang assay [10]. It is not unlikely that in tobacco one or more naturally occurring compounds are present that give rise to an overestimation of ACC owing to chemical oxidation. We can conclude that LC–TSP-MS of the phenylthiohydantoin derivative of ACC is a sensitive (detection limit = 10 pmol) and highly specific method for its determination. As ACC is usually present in plants in nanomolar concentrations, the method can be applied for the routine determination of ACC in plant tissues.

ACKNOWLEDGEMENTS

This work was supported by an FKFO grant (2.0017.92). H.A.V.O. is Research Director at the Belgian National Fund for Scientific Research. The MS equipment was sponsored by the Belgian Lotto.

REFERENCES

1 D.O. Adams and S.F. Yang, *Proc. Natl. Acad. Sci. U.S.A.*, 76 (1979) 170.
2 J.G. Dong, J.C. Fernàndez-Maculet and S.F. Yang, *Proc. Natl. Acad. Sci. U.S.A.*, 89 (1992) 9789.
3 C.C. Lizada and S.F. Yang, *Anal. Biochem.*, 100 (1979) 140.
4 T. Boller, R.C. Herner and H. Kende, *Planta*, 145 (1979) 293.
5 R.A. Savidge, G.M.C. Mutumba, J.K. Heald and P.F. Wareing, *Plant Physiol.*, 71 (1983) 434.
6 B.A. McGaw, R. Horgan and J.K. Helad, *Anal. Biochem.*, 149 (1985) 130.
7 R. Miller, J. La Grone, P. Skolnick and K.M. Boje, *J. Chromatogr.*, 578 (1992) 103.
8 D. Lanneluc-Sanson, C.T. Phan and R.L. Granger, *Anal. Biochem.*, 155 (1986) 322.
9 R.M. Hewick, M.W. Hunkapillar, L.E. Hood and W.J. Dreyer, *J. Biol. Chem.*, 256 (1981) 7990.
10 G. Bufler and Y. Mor, *Acta. Hort.*, 113 (1980) 65.
11 L.W. Coleman and C.F. Hodges, *J. Plant Physiol.*, 138 (1991) 7.

Journal of Chromatography A, 657 (1993) 345–348
Elsevier Science Publishers B.V., Amsterdam

CHROM. 25 571

Preparation and high-performance liquid chromatographic analysis of *syn* and *anti* isomers of steroidal 3-(O-carboxymethyl) oximes

Maciej Adamczyk*, Yon-Yih Chen, Jeffrey R. Fishpaugh and John C. Gebler

Divisional Chemistry, Abbott Diagnostics Division, Abbott Laboratories, Abbott Park, IL 60064 (USA)

(First received September 1st, 1993; revised manuscript received September 20th, 1993)

ABSTRACT

Syn and *anti* isomeric mixtures of methyl esters of 3-(O-carboxymethyl) oximes of progesterone, 17-α-OH-progesterone, testosterone, and cortisol were synthesized and separated on a preparative scale. The pure esters were then hydrolyzed to afford the desired *syn* or *anti* 3-(O-carboxymethyl) oximes. Analysis by HPLC was developed to determine isomeric and chemical purity of the acids and esters.

INTRODUCTION

The O-carboxymethyl oxime (CMO) functionality has been used for various conjugates for over 35 years [1,2]. Steroidal CMOs are widely used in the preparation of conjugates for immunoassays which quantify biologically important steroids. CMOs can exist as two different geometric isomers, *syn* or *anti* (Fig. 1). Most of the biologically important steroidal CMOs are commercially available from different vendors, however, the isomeric purity is never specified. Fractional crystallization has been employed to obtain a single or enriched isomer with some success, though, significant amounts of material were sacrificed [3–6]. Mappus *et al.* [7] reported on the separation of *syn* and *anti* isomers by TLC (silica gel) of several steroidal 3-CMOs using the corresponding methyl esters. Mitsuma *et al.* [8] separated the two isomers of progesterone 3-CMO N-hydroxysuccinimide esters by column chromatography (silica gel) and the resulting "active" esters were useful for direct conjugation to proteins. Both reports, however, failed to include the chemical yield and isomeric purity, and they expressed concern about racemization during ester hydrolysis and work-up to the free acid. Also, a direct chromatographic method to estimate isomeric purity of the final CMO product was not reported.

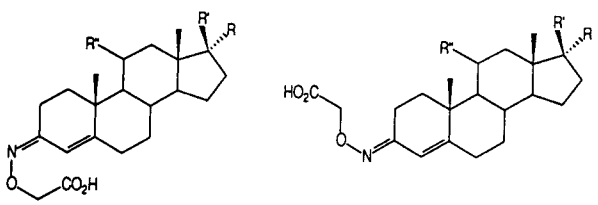

Fig. 1. *Syn* and *anti* isomers of 3-(O-carboxymethyl) oximes of progesterone (**1**), 17-α-OH-progesterone (**2**), testosterone (**3**), and cortisol (**4**). R, R′, R″: (**1**) OH, C(O)Me, H; (**2**) H, C(O)Me, H; (**3**) H, OH, H; (**4**) OH, $C(O)CH_2OH$, OH.

We needed chemically and isomerically pure (both isomers) steroidal CMOs to meet the expectations of good manufacturing practices (GMP, ISO 9000) [9,10]. Additionally, a simple

* Corresponding author.

0021-9673/93/$06.00
SSDI 0021-9673(93)E1002-H

method to directly assess the chemical and isomeric quality was required.

In this paper we report the preparation of *syn* and *anti* isomers of 3-(O-carboxymethyl) oximes of progesterone (**1**), 17-α-OH-progesterone (**2**), testosterone (**3**), and cortisol (**4**). We also describe an HPLC method to resolve and quantify the isomers.

EXPERIMENTAL

General

Solvents were HPLC grade [Fisher (Pittsburgh, PA, USA) or EM Science (Gibbstown, NY, USA)] and used without further purification. Progesterone, cortisol, 17-α-hydroxyprogesterone, testosterone 3-CMO, and N-methyl-N′-nitro-N-nitrosoguanidine were purchased from Sigma (St. Louis, MO, USA). Triethylamine, methyl chloroformate, and 4-dimethylaminopyridine were purchased from Aldrich (Milwaukee, WI, USA). HPLC analysis was performed using a custom L.C. (Custom L.C., Houston, TX, USA) C_{18}, 3 μm, 80 Å, 150 × 6.2 mm column at room temperature, eluting at flow-rate of 1 ml/min. Retention times and mobile phase are recorded in Table I.

General synthesis

O-Carboxymethyl oximes. 3-(O-Carboxymethyl) oximes of 17-α-OH-progesterone, progesterone, and cortisol (testosterone was purchased as the 3-CMO) were prepared using a previously described method [6].

Methyl esters. The crude CMO was dissolved in dry methylene chloride (100 m*M*) and cooled with an ice bath. To the clear solution was added 1.5 equivalents of triethyl amine and methyl chloroformate (added dropwise), and 0.1 equivalents of 4-dimethylaminopyridine. Upon depletion of the acid [TLC, ethyl acetate–hexane (1:3); (3:2) for cortisol] the organic layer was washed with 1 *M* sodium bicarbonate and water. The heterogeneous mixture was allowed to stand overnight and then the organic layer was collected, dried (magnesium sulfate) and concentrated by reduced pressure. Separation of the *syn* and *anti* esters was accomplished by gravity chromatography [50 × 5 cm glass column, 300 g silica gel, 230–400 mesh (40–63 μm particle size), 60 Å]. Elution was with ethyl acetate–hexane (1:3). Pure fractions of each isomer were pooled and concentrated under vacuum affording white solids. [All synthetic products gave correct analytical data (^{1}H and ^{13}C NMR, MS and HPLC)]

An alternative method was used for cortisol. The CMO was dissolved in methanol (100 m*M*) and cooled to −5°C with an ice/salt bath. Diazomethane [11], prepared just prior to use, was added in four portions (10-fold excess) as an ether solution. The yellow solution was allowed to warm to room temperature and then stirred overnight to afford a clear solution. The solvents were removed under reduced pressure to afford

TABLE I

MOBILE PHASE USED FOR HPLC ANALYSIS AND RETENTION TIMES FOR *syn* AND *anti* ISOMERS OF 3-(O-CARBOXYMETHYL) OXIMES **1–4**

CMO[a]	Retention time (min)				Mobile phase[b] water–methanol
	syn Acid	*anti* Acid	*syn* Ester	*anti* Ester	
1	15.7	17.4	32.3	36.5	25:75
2	16.4	18.1	27.5	31.6	3:7
3	15.5	16.9	28.5	32.8	3:7
4	29.8	28.5	35.6	34.9	6:4 to 3:7 in 35 min[c]

[a] See Fig. 1 for definition.
[b] Phase contains 0.1% trifluoroacetic acid.
[c] Linear gradient.

TABLE II

ISOLATED YIELD AND ISOMERIC PURITY OF *syn* AND *anti* STEROIDAL 3-(O-CARBOXYMETHYL) OXIMES **1–4**

CMO	Isolated yield (%) and isomeric purity[a]			
	syn Ester	*anti* Ester	*syn* Acid[b]	*anti* Acid[b]
1	25	46	95 (98)	92 (99)
2	26	45	94 (97)	94 (99)
3	16	47	91 (94)	88 (99)
4	7	43	60 (74)[c]	68 (98)

[a] Isomeric purity was >99% for each ester and is listed in parentheses for the acids.
[b] Yield based from pure ester.
[c] The *syn* cortisol CMO was not a stable isomer and was prone to rapid isomerization to the *anti* during work-up.

the desired 3-CMO methyl esters. Separation of the *syn* and *anti* esters was carried out as described above except elution was with ethyl acetate–hexane (3:2).

Hydrolysis

The separated esters were treated with methanolic 2 *M* sodium hydroxide (0.1 ml/mg of ester). Typical hydrolysis took 2 hours (followed by TLC) at room temperature. Upon completion the reaction mixture was made acidic (pH 4.0) with 2 *M* HCl. The CMO was extracted out with ethyl acetate and the organic layer was washed with water until neutral pH was achieved (very important to remove all residual HCl). After drying with $MgSO_4$ the solvent was removed under reduced pressure to afford the desired 3-CMO. Table II lists the isolated yield and isomeric purity.

RESULTS AND DISCUSSION

The steroidal 3-CMOs prepared herein are available from different vendors, unfortunately their isomeric purity is not specified. Based on HPLC analysis, we found the chemical purity and the *syn*:*anti* ratios to fluctuate between manufacturers and from lot to lot, even from the same company. Attempts in our lab to obtain significant amounts (>100 mg) of the pure isomers by recrystallization and/or reversed-phase HPLC separation of purchased material became costly and inefficient. Recently we reported an enzyme-mediated hydrolysis of the 3-CMO methyl esters of **1–4** using lipase from *Candida cylindracea* which resulted in 80–98% isomeric purity on an analytical (<1 mg) scale [12].

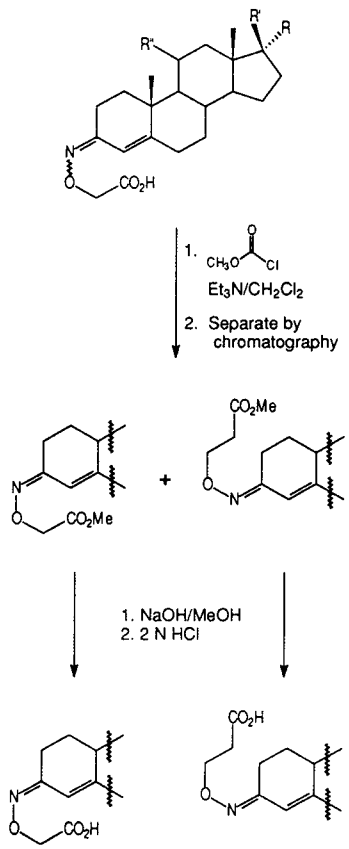

Fig. 2. General route for the preparation of *syn* and *anti* isomers of steroidal 3-(O-carboxymethyl) oximes **1–4**.

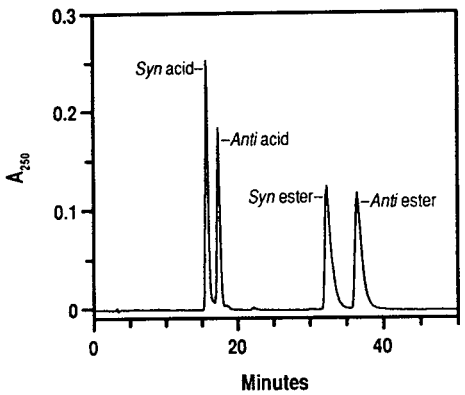

Fig. 3. HPLC of **1**, acids and esters, which is representative for all steroidal 3-CMOs **1–4**.

We were interested in obtaining each CMO isomer on a gram scale. We developed a cost effective method which involves derivatization of the parent steroid and then separation of the CMO methyl esters (Fig. 2). Preparation of the steroidal 3-CMOs was taken from literature protocols [3]. Without purification the CMOs were directly converted to methyl esters using either methyl chloroformate or diazomethane and the resulting esters were then purified by gravity chromatography on silica gel. Base hydrolysis was employed to reconstitute the steroidal CMO. Great care was taken to remove all traces of mineral acid used during the work-up to minimize acid-catalyzed racemization.

The isomers of the acids and esters could be completely resolved (Fig. 3) on a reversed-phase HPLC column using water–methanol–trifluoroacetic acid elution (Table I) affording a convenient method to determine purity.

As has been reported [6,7], the CMOs are susceptible to racemization under mild conditions (methanol). A slight loss of isomeric purity (Table II) was unavoidable and is attributed to the acid-catalyzed isomerization during work-up. It was possible to completely isomerize either isomer in methanol in approximately ten days. However, in a crystalline state, the CMOs retain stereo integrity after 6 months when stored at room temperature.

In summary, using this strategy of chemical derivatization followed by column chromatography and final hydrolysis it was possible to obtained gram quantities of isomerically pure ($\geq 94\%$) and chemically pure ($\geq 99.5\%$) steroidal 3-CMOs of **1–4** in high yield. The utility of the outlined method permits the synthesis of high quality CMOs and the ability to directly determine the chemical and isomeric purity of these important conjugate precursors.

REFERENCES

1 B.F. Erlanger, F. Borek, S.M. Beiser and S. Lieberman, *J. Biol. Chem.*, 234 (1959) 1090.
2 B.F. Erlanger, F. Borek, S.M. Beiser and S. Lieberman, *J. Biol. Chem.*, 228 (1957) 713.
3 M.G. Forest, E. Mappus and C.-Y. Cuilleron, *Steroids*, 28 (1976) 815.
4 E. Mappus and C.-Y. Cuilleron, *Steroids*, 33 (1979) 693.
5 M.T. Shipchandler, J.R. Fino, L.D. Klein and C.L. Kirkemo, *Anal. Biochem.*, 162 (1987) 89.
6 A.H. Janoski, F.C. Shulman and G.E. Wright, *Steroids*, 23 (1974) 49.
7 E. Mappus, C. Grenot, M. Forest and M. C.-Y. Cuilleron, *C.R. Acad. Sc. Paris*, 281 (1975) 247.
8 M. Mitsuma, A. Kambegawa, S. Okinaga and K. Arai, *J. Steroid Biochem.*, 28 (1987) 83.
9 *GMP (Good Manufacturing Practice), Part 820, Code of Federal Regulations*, United States Government, Washington, DC, 1992.
10 *ISO 9000 Standard—International Organization for Standardization, ANSI/ASQC Q90 ISO 9000 Guidelines*, ASQC Quality Press, Milwaukee, WI, 1992.
11 L.F. Fieser and M. Fieser, in *Reagents for Organic Synthesis*, Wiley, New York, 1967, Vol 1, p. 191.
12 M. Adamczyk, Y.-Y. Chen, J.R. Fishpaugh and J.C. Gebler, *Tetrahedron: Asymmetry*, 4 (1993) 1467.

Journal of Chromatography A, 657 (1993) 349–356
Elsevier Science Publishers B.V., Amsterdam

CHROM. 25 536

Improvement of chemical analysis of antibiotics

XX☆. Basic study on high-performance liquid chromatographic determination of four polyether antibiotics pre-derivatized with 1-bromoacetylpyrene

Hirohiko Asukabe, Hideaki Murata, Ken-Ichi Harada* and Makoto Suzuki

Faculty of Pharmacy, Meijo University, Tempaku-ku, Nagoya 468 (Japan)

Hisao Oka and Yoshitomo Ikai

Aichi Prefectural Institute of Public Health, Tsuiji-machi, Kita-ku, Nagoya 462 (Japan)

(First received June 26th, 1993; revised manuscript received August 31st, 1993)

ABSTRACT

A high-performance liquid chromatographic method for the determination of the polyether antibiotics (PEs), salinomycin (SL), monensin (MN), lasalocid (LA) and narasin (NA), based on a precolumn reaction system using 1-bromoacetylpyrene (1-BAP) as a fluorescence reagent, was established. Six standards of 1-pyrenacyl esters (PEs-PYs) including two of 1-pyrenacyl esters of internal standards, 18,19-dihydrosalinomycin (DSL) and 18,19-dihydro-20-ketosalinomycin (DKSL), were separated within 30 min on a Develosil $5C_{18}$ (5 μm) column (250 × 4.6 mm I.D.) with methanol–water (97:3) as the mobile phase at a flow-rate of 1.0 ml/min and were detected at λ_{ex} 360 nm, λ_{em} 420 nm. This system was also effective for the separation between unused 1-BAP and PEs-PYs and the simultaneous determination of SL, MN, LA and NA was achieved at concentrations from 0.2 to 100 μg/ml. At concentrations of less than 10 μg/ml a silica gel cartridge was effective in eliminating the excess of unused reagents. Four calibration graphs with the internal standard method were linear between 20 and 100 μg/ml, 2 and 10 μg/ml and 0.2 and 1.0 μg/ml. The method is applicable to feed and residue analyses.

INTRODUCTION

Polyether antibiotics (PEs) (Fig. 1) are produced by *Streptomyces* and structurally characterized as the sodium salt of a carboxylic acid ionophore and a number of cyclic ether moieties. Among them salinomycin (SL), monensin (MN), lasalocid (LA) and narasin (NA) have microbial activities against Gram-positive bacteria and fungi, and have been used all over the world as feed additives for poultry to prevent coccidiosis [1].

Many analytical method for PEs have been reported since the early 1970s. Most of them mainly involved the detection of these compounds, because most PEs have no chromophore. Several groups have performed HPLC determinations of SL, MN and NA using refractive index detection or UV detection at 214 nm [2–4]. Vanillin and *p*-dimethylaminobenzaldehyde have often been used in the conventional spectrophotometry of SL, MN and NA [5–11]. Under anhydrous acidic conditions, SL, MN,

* Corresponding author.

☆ For Part XIX, see *J. Assoc. Off. Anal. Chem.*, in press.

0021-9673/93/$06.00
SSDI 0021-9673(93)E0949-U

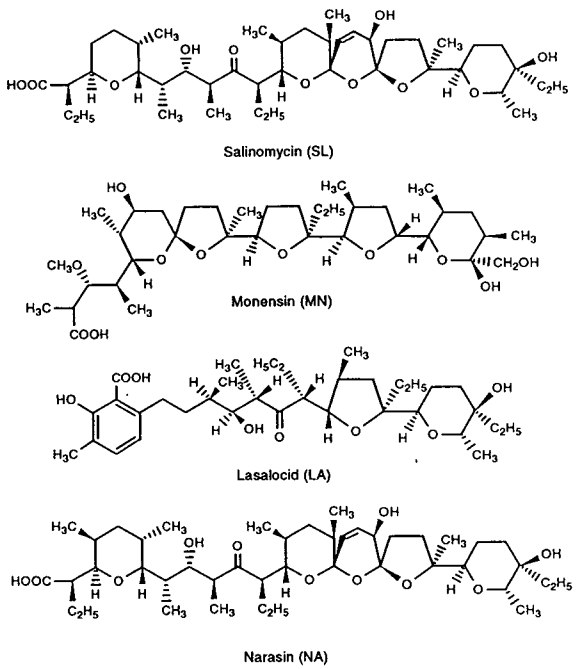

Fig. 1. Structures of polyether antibiotics (PEs).

and NA react with these reagents to form products that show strong absorption maxima in the visible region. Since Goras and Lacourse [12] reported an HPLC determination of SL using postcolumn derivatization with vanillin, many workers have used this technique for the simultaneous HPLC determination of SL, MN and NA [13–18]. LA shows significant fluorescence in various organic solvents, which has been applied in spectrofluorimetric [19–22] and HPLC with fluorescence detection methods [23–27]. However, LA is less reactive to the reagent than SL, MN and NA [28], indicating that it is difficult to determine PEs including LA simultaneously using postcolumn derivatization. Additionally, several groups tried to establish HPLC for MN with fluorescence detection using derivatization with 9-anthryldiazomethane (ADAM) [29–35], which reacts rapidly with the free carboxylic acids of PEs but it does not react with the carboxylates. Although conversion into the free carboxylic acid is possible by treatment with acidic buffer, MN is unstable during the process.

Two papers on the simultaneous determination of SL, MN, LA and NA have been published. Johannsen [16] established a sequential detection system consisting of UV detection (320 nm) for LA and postcolumn derivatization with detection at 600 nm. However, the system requires three pumps and two detectors and no actual analysis was performed using this method. Martinez and Shimoda [32] tried a multi-residue determination of these compounds, in which LA was directly esterified with ADAM, but SL, MN and NA were first acetylated followed by esterification with ADAM. It is difficult to understand why acetylation is necessary for SL, MN, and NA. Probably the method would not be directly applicable to an actual mixture of these PEs. As stated above, no practical method for the simultaneous HPLC determination of PEs including SL, MN, LA and NA has been established so far.

In a previous study, we established a high-performance thin-layer chromatographic (HPTLC) method for the simultaneous fluorodensitometric determination of SL, MN and LA based on fluorescence labelling with 1-bromoacetylpyrene (1-BAP) using 18,19-dihydrosalinomycin (DSL) and 18,19-dihydro-20-ketosalinomycin (DKSL) as internal standards (Fig. 2) [36]. Although the HPTLC method was simple and reliable, it is not always sensitive enough to allow the detection of small amounts of these compounds with good precision. Further, we have not applied the method to NA, because it has not been approved for use as a feed additive in poultry in Japan.

On the basis of the above considerations, we tried to establish an HPLC method for the determination of four PEs with fluorescence

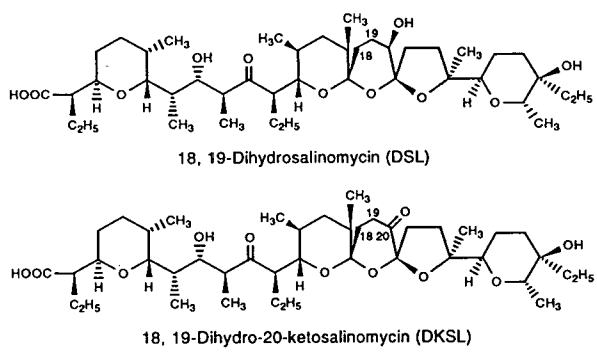

Fig. 2. Structures of internal standards (IS).

detection which is applicable to feed and residual analyses. This paper describes the optimum conditions and techniques utilized for the identification and determination of the four PEs by HPLC.

EXPERIMENTAL

Chemicals

SL and NA were supplied by Pfizer Pharmaceuticals (Tokyo, Japan), and Lilly Research Laboratories (Indianapolis, IN, USA), respectively. MN and LA were purchased from Hexyst-Japan (Tokyo, Japan) and Sigma (Tokyo, Japan), respectively. DSL and DKSL were prepared according to the procedure described in a previous paper [36]. 1-BAP [37] was prepared according to the procedure of Kawahara *et al.* [37] (1-BAP is now available from Wako, Osaka, Japan). Kryptofix 222 (K-222; 4,7,13,16,21,24-hexaoxy-1,10,diazobicyclo[8,8,8]hexacosane) was purchased from Merck (Darmstadt, Germany). A Mega Bond Elut silica gel cartridge was purchased from Varian (Harbor City, CA, USA). All other chemicals were of analytical-reagent grade.

Apparatus

An HPLC system equipped with a constant-flow pump (Trirotor; JASCO, Tokyo, Japan) was used together with a spectrofluorimetric detector (FP-210; JASCO) operated at $\lambda_{ex} = 360$ nm and $\lambda_{em} = 420$ nm. The separation was performed on Develosil $5C_{18}$ (5 μm) (Nomura Chemical, Seto, Japan) packed in a stainless-steel column (250 × 4.6 mm I.D.) using methanol–water (97:3) as the mobile phase.

Preparation of polyether pyrenacyl esters (PEs-PYs)

1-BAP (19.4 mg, 0.060 mmol) and K-222 (12.2 mg, 0.032 mmol) were added to a solution of NA (10.3 mg, 0.013 mmol) in acetonitrile (5 ml). The solution was stirred for 150 min and then concentrated under reduced pressure. The residue was chromatographed on a silica gel column (150 × 10 mm I.D.) (Merck) with benzene–acetone (9:1) to give narasin 1-pyrenacyl ester (NA-PY, 15.7 mg) as colourless needless; fast atom bombardment mass spectrometry: *m/z* 1029 $(M + Na)^+$, 1007 $(M + H)^+$ and 989 $(M + H - H_2O)^+$. The preparation of other polyether pyrenacyl esters (PEs-PYs) has been described in previous papers [36,38].

Preparation of standard and internal standard solutions

Amounts of 10 mg each of standards (SL, MN, LA and NA) and internal standards (DSL and DKSL) were accurately weighed into two 50-ml volumetric flasks and diluted to volume with methanol (200 μg/ml). In the simultaneous determination of concentrations of less than 10 μg/ml, subsequent dilutions were made with methanol to give the desired concentrations.

Preparation of 1-BAP solution

An amount of 132 mg of 1-BAP was dissolved in 25 ml of acetonitrile.

Preparation of K-222 solution

An amount of 32 mg of K-222 was dissolved in 25 ml of acetonitrile.

Clean-up procedure for elimination of reagent

After cooling a round-bottomed flask containing the reaction mixture to room temperature, the mixture was evaporated to dryness and the residue was dissolved in 5 ml of benzene–chloroform (1:1) followed by rinsing twice with 5 ml of the same solvent. After filtration of the solution, the filtrate was applied to a Mega Bond Elut silica gel cartridge activated with benzene. PEs-PYs were eluted twice with 5 ml of benzene–acetone (7:3). After evaporation of the eluate to dryness, the residue was dissolved in 10 ml of acetonitrile and the determination was carried out by HPLC.

Simultaneous determination

Volumes of 1, 2, 3, 4 and 5 ml of the standard solution (200 μg/ml) were pipetted into 20-ml round-bottomed flasks and 3 ml of internal standard solution (200 μg/ml) were added by pipette. After evaporation of the solutions to dryness, 5 ml of 1-BAP solution and 5 ml of K-222 solution were added to each flask. In this step, concentrations of standards were 20, 40,

60, 80 and 100 μg/ml, respectively, and those of internal standards (DSL and DKSL) were 60 μg/ml. The flasks were allowed to stand in an oil-bath at 50°C for 90 min. After cooling the flasks to room temperature, the reaction mixtures were subjected to HPLC.

In the simultaneous determination of concentrations ranging from 2 to 10 μg/ml and from 0.2 to 1.0 μg/ml, the concentrations of standard solution and internal standard solution were 20 and 2 μg/ml, respectively. After the derivatization, the cooled derivatizing solution was evaporated to dryness and was subjected to the clean-up procedure described above.

RESULTS AND DISCUSSION

Separation

In order to optimize the separation conditions, authentic pyrenacyl esters (PEs-PYs) of six PEs were first prepared according to our method described previously [36,38] and their structures were confirmed by mass spectrometry. Second, optimum separation conditions for the six pyrenacyl esters (SL-PY, MN-PY, LA-PY, NA-PY, DSL-PY and DKSL-PY) were sought and the separation between the derivatization reagent (1-BAP) and PEs-PYs was also investigated.

We attempted to apply our previously reported solvent system [dichloromethane–ethyl acetate–acetone–acetonitrile (15:2:1:55)] for reversed-phase HPTLC (RP-HPTLC) [36] to HPLC analysis using a C_{18} column in this work. However, sufficient resolution between 1-BAP and PEs-PYs could not be obtained, because the capacity factors were too small. The different behaviour can be explained by the assumption that the separation by RP-HPTLC is based not only on a partitioning effect but also adsorption to residual silanol groups on surface of the stationary phase. Hoshino *et al.* [30] reported that a mobile phase containing methanol gave better results than one containing acetonitrile when MN derivatized with ADAM was separated by HPLC on a C_{18} column. Therefore, various mobile phases containing methanol were tried and a satisfactory separation of the six PEs-PYs was obtained using methanol–water (97:3). There are four minor peaks in the chromatogram (Fig. 3), peaks 1, 2 and 3 between DKSL-PY and SL-PY and peak 4 behind of NA-PY. Peak 1 was identified as the pyrenacyl ester of 20-ketosalinomycin (KSL-PY), which is a minor contaminant of DKSL. The other peaks have not been identified, but peaks 2, 3 and 4 are contaminants derived from DKSL, SL and NA, respectively. However, as they do not interfere in the determination of PEs-PYs, the separation between the derivatizing reagents and the PEs-PYs was examined using this mobile phase.

After derivatization of the six PEs at concentrations of 100 μg/ml under the conditions described under Experimental, the reaction mixture was directly injected into the HPLC system. As shown in Fig. 4, new minor peaks 5 and 6 appeared and peak 1 (KSL-PY) and a minor peak derived from 1-BAP overlapped (indicated by an arrow). However, a good separation of the PEs-PYs was obtained apart from the peaks

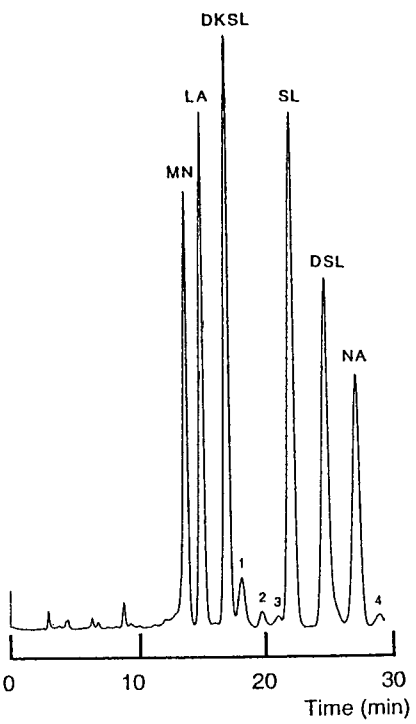

Fig. 3. HPLC separation of pyrenacyl esters of polyether antibiotics (PEs-PYs). Column, Develosil $5C_{18}$ (250 × 4.6 mm I.D.); mobile phase, methanol–water (97:3); flow-rate, 1 ml/min; detection, λ_{ex} = 360 nm and λ_{em} = 420 nm.

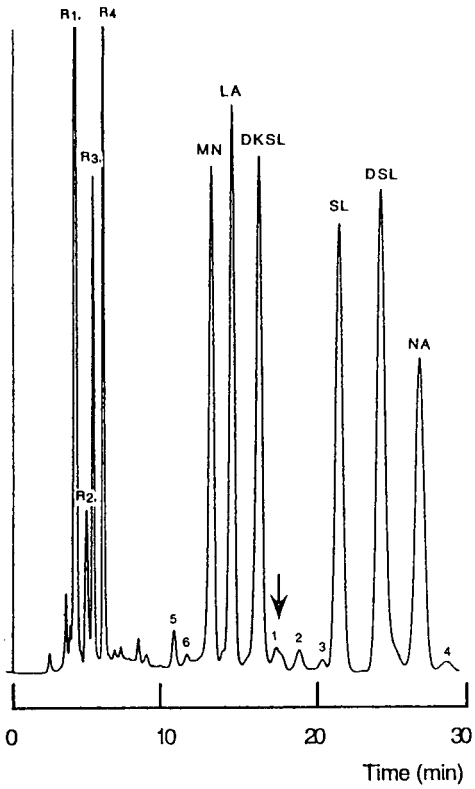

Fig. 4. Typical chromatogram of simultaneous determination (100 μg/ml).

around 5 min, which are derived from the reagent, and these minor peaks including peaks 1–6 did not interfere in the determination of PEs. These results indicate that a combination of a C_{18} column and methanol–water (97:3) as the mobile phase is suitable for the present purpose.

Derivatization

In order to determine the reaction yield of the derivatization, calibration graphs for the six PEs-PYs were constructed for concentration from 20 to 100 μg/ml, from 2 to 10 μg/ml, from 0.2 to 1.0 μg/ml and from 0.02 to 0.1 μg/ml. With the exception of the most sensitive case, the three cases showed correlation coefficients of >0.999, so the reaction yield could be calculated from these calibration graphs.

In a previous study [36], the following derivatization conditions were used: molar excess of reagent (1-BAP), 50-fold; molar excess of catalyst (K-222), 10-fold; reaction temperature, 50°C; reaction time, 90 min. We applied these conditions to the simultaneous derivatization of the six PEs at concentrations of 100, 10 and 1.0 μg/ml and calculated the reaction yields (Table I). At a concentration of 100 μg/ml, each reaction showed a yield of >90%. However, in the reaction of LA the yield decreased to <50% at a concentration of 10 μg/ml, and those of MN and LA were only 6% and 2%, respectively, at a concentration of 1 μg/ml. When the derivatization is applied to feed and residue analyses, it is necessary to have a high reaction yield even at low concentrations. We used more than 10–100-fold excesses of reagent and catalyst (100 μg/ml) to obtain higher reaction yields at analyte concentrations of 10 and 1 μg/ml, however, no peaks for the six kinds of PEs-PYs were found because of the peaks of unused reagents present on the chromatogram.

In order to eliminate the excess of reagent, the difference in the polarities of PEs-PYs and 1-

TABLE I

DERIVATIZATION CONDITIONS AND REACTION YIELD OF PEs WITH 1-BAP

Amount of PEs (μg/ml)	Molar excess (-fold)		Yield (%)[a]					
	Reagent	Catalyst	SL	MN	LA	NA	DSL	DKSL
100	50	10	96	100	94	102	101	90
10	50	10	96	85	50	105	100	91
1	50	10	80	6	2	76	72	59
10	500	100	93	98	98	104	99	94
1	5000	1000	84	85	68	85	82	80

[a] Reaction yield was calculated from calibration graphs for authentic pyrenacyl esters.

BAP was efficiently employed for a clean-up using a silica gel cartridge. When benzene was used as the mobile phase for silica gel TLC, the spots of PEs-PYs remained at the origin. Whereas 1-BAP showed an R_F value of 0.70. This chromatographic behaviour was applied with the above objective, but the amount of unused reagent was so large that the evaporated reaction mixture showed poor solubility in benzene. Although the reaction mixture was soluble in chloroform, LA was eluted first with this solvent. Therefore, chloroform–benzene (1:1) was chosen as the solvent based on the solubility of the reaction mixture and polarities of 1-BAP and PEs-PYs. Finally, the following procedure was established: after the derivatization, the rection mixture was evaporated to dryness and the residue was dissolved in 5 ml of chloroform–benzene (1:1). The solution containing PEs-PYs and 1-BAP was applied to the silica gel cartridge, followed by rinsing twice with 5 ml of the same solvent, and PEs-PYs were eluted twice with 10 ml of benzene–acetone (7:3).

To investigate the suitability of this clean-up procedure, the reaction yield of PEs was calculated at concentrations of 10 and 1 μg/ml. The reaction yield obtained is shown at bottom of Table I. Although a peak derived from 1-BAP appeared close to that of SL-PY (indicated by an arrow, Fig. 5) at the concentration of 1 μg/ml, it did not interfere in the separation of PEs-PYs. The reaction yield of LA at the concentration of 1 μg/ml was 68%, but those of the others were >80%, indicating that the derivatization system coupled with the described clean-up procedure is effective for the simultaneous determination of SL, MN, LA and NA.

Simultaneous determination of SL, MN, LA and NA by HPLC

We achieved the simultaneous determination of SL, MN, LA, and NA at concentrations ranging from 20 to 100 μg/ml, from 2 to 10 μg/ml and from 0.2 to 1.0 μg/ml under the conditions mentioned above using DSL and DKSL as internal standards. At concentrations between 20 and 100 μg/ml the reaction mixture was introduced directly into the HPLC system, and at concentrations between 2 and 10 μg/ml and between 0.2 and 1.0 μg/ml the samples were subjected to HPLC after treatment with the silica gel cartridge as described above. The data in Table II indicate a good correlation for the four PEs with the two internal standards. In a previous study [36], the internal standard DSL was effective for SL and MN and DKSL for LA. However, both internal standards were effective for the four PEs in the present study, indicating that these two internal standards can be used complementarily depending on the nature of the sample where many interfering substances may exist.

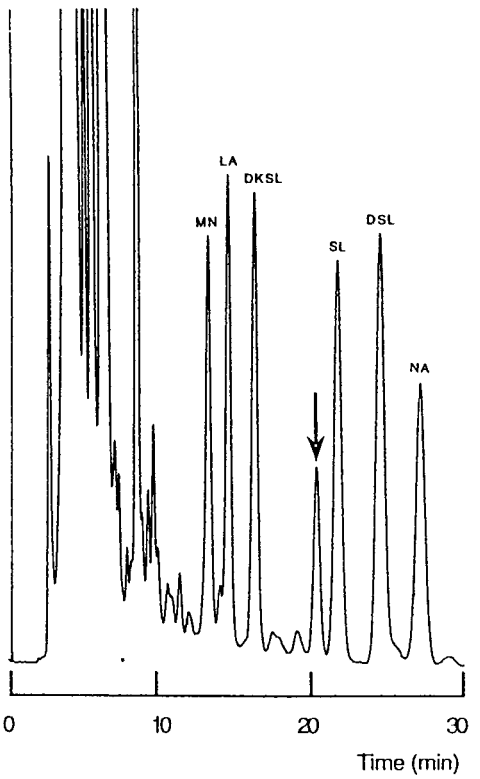

Fig. 5. Typical chromatogram of simultaneous determination (1 μg/ml).

CONCLUSIONS

A technique using HPLC with fluorescence detection and prederivatization with 1-BAP has been established for the determination of four

TABLE II

CHARACTERISTICS OF CALIBRATION GRAPHS OF POLYETHER ANTIBIOTICS (PEs) USING THE INTERNAL STANDARDS 18,19-DIHYDROSALINOMYCIN (DSL) AND 18,19-DIHYDRO-20-KETOSALINOMYCIN (DKSL)

Sample	Internal standard	20–100 μg/ml		2–10 μg/ml		0.2–1.0 μg/ml	
		Regression equation[a]	Correlation coefficient	Regression equation[a]	Correlation coefficient	Regression equation[a]	Correlation coefficient
Salinomycin (SL)	DSL	$y = 0.015x + 0.810$	0.9995	$y = 0.171x + 0.006$	1.0000	$y = 1.682x + 0.063$	0.9996
	DKSL	$y = 0.016x + 0.081$	0.9998	$y = 0.147x - 0.000$	0.9999	$y = 1.476x + 0.028$	0.9995
Monensin (MN)	DSL	$y = 0.013x + 0.015$	0.9999	$y = 0.152x - 0.091$	0.9996	$y = 1.370x + 0.030$	0.9993
	DKSL	$y = 0.015x + 0.005$	0.9998	$y = 0.131x - 0.018$	0.9997	$y = 1.202x + 0.004$	0.9993
Lasalocid (LA)	DSL	$y = 0.017x + 0.028$	0.9996	$y = 0.174x + 0.002$	0.9996	$y = 1.698x - 0.011$	0.9998
	DKSL	$y = 0.018x + 0.024$	0.9998	$y = 0.015x - 0.003$	0.9995	$y = 1.489x - 0.035$	0.9989
Narasin (NA)	DSL	$y = 0.011x + 0.032$	0.9998	$y = 0.125x + 0.018$	1.0000	$y = 1.253x + 0.044$	0.9998
	DKSL	$y = 0.012x + 0.029$	1.0000	$y = 0.108x + 0.012$	1.0000	$y = 1.099x + 0.018$	0.9994

[a] y = Ratios of peak heights of sample and I.S.; $x = \mu g/ml$.

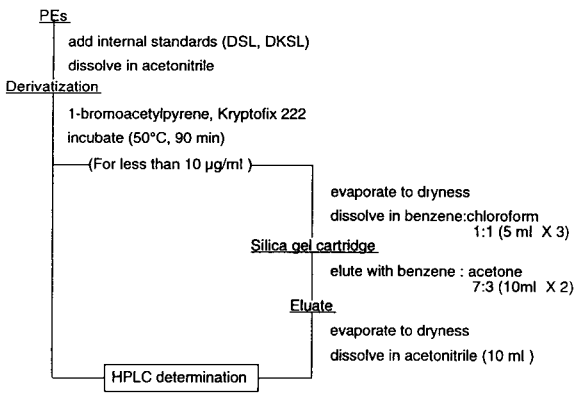

Fig. 6. Analytical procedure for PEs prederivatized with 1-BAP.

PEs. The analytical procedure is summarized in Fig. 6. We consider that this derivatization system is more reliable than that with ADAM. The established method would be a more reliable method for the determination of SL, MN, LA and NA in feed and residue analyses. We have performed feed analyses for SL, MN, and LA using this separation system and the results will be reported elsewhere [39].

ACKNOWLEDGEMENT

We are grateful to Dr. Andrew M. Dahlem (Eli Lilly, USA) for a gift of narasin.

REFERENCES

1 J.W. Westley, *Polyether Antibiotics*, Vol. 1, Marcel Dekker, New York, 1982, Ch. 6.
2 T.D. Macy and A. Loh, *J. Assoc. Off. Anal. Chem.*, 66 (1983) 284.
3 G.P. Dimenna, J.A. Creegan, L.B. Turnbull and G.J. Wright, *J. Assoc. Off. Anal. Chem.*, 70 (1987) 504.
4 M. Vuzharova, E. Tomov, I. Dorosiev and P. Papazova, *Farmatsiya (Sofia)*, 37 (1987) 7.
5 T. Golab, S.J. Barton and R.E. Scroggs, *J. Assoc. Off. Anal. Chem.*, 56 (1973) 171.
6 T. Kono and S. Yamamoto, *Shiryo Kenkyu Hokoku (Tokyo Hishiryo Kensasho)*, 5 (1979) 174.
7 G.H.W. Marten, *Ger. Offen.*, DE 3 318 597 (1983).
8 A. Kozak, *Bromatol. Chem. Toksykol.*, 17 (1984) 321.
9 T. Oyama, *Shiryo Kenkyu Hokoku (Tokyo Hishiryo Kensasho)*, 11 (1986) 209.
10 T. Suhara, *Shiryo Kenkyu Hokoku (Tokyo Hishiryo Kensasho)*, 11 (1986) 214.
11 M. Illing and B. Mueller, *Monatsh. Veterinaermed.*, 41 (1986) 854.
12 J.T. Goras and W.R. Lacourse, *J. Assoc. Off. Anal. Chem.*, 67 (1984) 701.
13 W.J. Blanchflower, D.A. Rice and J.T.G. Hamilton, *Analyst*, 110 (1985) 1283.
14 M.R. Lapointe and H. Cohen, *J. Assoc. Off. Anal. Chem.*, 71 (1988) 480.
15 F.L. Neely, *Chromatographia*, 31 (1991) 277.
16 F.H. Johannsen, *Agribiol. Res.*, 44 (1991) 79.
17 F.L. Neely, *J. Liq. Chromatogr.*, 15 (1992) 1513.
18 J.M. Rodewald, J.W. Moran, A.L. Donoho and M.R. Coleman, *J. Assoc. Off. Anal. Chem.*, 75 (1992) 272.
19 M. Osadca and M. Araujo, *J. Assoc. Off. Anal. Chem.*, 57 (1974) 636.

20 M. Osadca and M. Araujo, *J. Assoc. Off. Anal. Chem.*, 58 (1975) 507.
21 M.A. Brooks, L.D. Arconte, J.A.F. de Silva, G. Chen and C. Crowley, *J. Pharm. Sci.*, 64 (1975) 1874.
22 A.K. Mitra and M.M. Narurkar, *J. Org. Chem.*, 49 (1984) 1293.
23 M. Osadca and M. Araujo, *J. Assoc. Off. Anal. Chem.*, 61 (1978) 1074.
24 G. Weiss, N.R. Felicito, M. Kaykaty, G. Chen, A. Caruso, E. Hargroves, C. Crowley and A. Macdonald, *J. Agric. Food Chem.*, 31 (1983) 75.
25 M. Kaykaty and G. Weiss, *J. Agric. Food Chem.*, 31 (1983) 81.
26 D.R. Newkrik and C.J. Barnes, *J. Assoc. Off. Anal. Chem.*, 72 (1989) 581.
27 L.R. Frank and C.J. Barnes, *J. Assoc. Off. Anal. Chem.*, 72 (1989) 584.
28 R.L. Hamill and L.W. Crandall, in M.J. Weinstein and G.H. Wagman (Editors), *Antibiotics—Isolation, Separation and Purification (Journal of Chromatography Library*, Vol. 15), Elsevier, Amsterdam, 1978, p. 501.
29 E.E. Martinez and W. Shimoda, *J. Assoc. Off. Anal. Chem.*, 68 (1985) 1149.
30 Y. Hoshino, M. Horie, N. Nose and H. Iwasaki, *Shokuhin Eiseigaku Zasshi*, 26 (1985) 585.
31 K. Takatsuki, S. Suzuki and I. Ushizawa, *J. Assoc. Off. Anal. Chem.*, 69 (1986) 443.
32 E.E. Martinez and W. Shimoda, *J. Assoc. Off. Anal. Chem.*, 69 (1986) 637.
33 K. Gamoh and E. Okada, *Bunseki Kagaku*, 37 (1988) 324.
34 E. Okada and K. Gamoh, *Jpn. Kokai Tokkyo Koho*, JP 89 152 362 (1989).
35 K. Gamoh, *Jpn. Kokai Tokkyo Koho*, JP 89 152 363 (1989).
36 H. Asukabe, H. Yoneyama, Y. Mori, K.-I. Harada, M. Suzuki, and H. Oka, *J. Chromatogr.*, 396 (1987) 261.
37 Y. Kawahara, A. Inage, T. Morioka and Y. Shibano, *Jpn. Kokai Tokkyo Koho*, JP 81 113 728 (1981).
38 H. Asukabe, T. Sasaki, K.-I. Harada, M. Suzuki and H. Oka, *J. Chromatogr.*, 295 (1984) 453.
39 H. Asukabe, H. Murata, K.-I. Harada, M. Suzuki, H. Oka, and Y. Ikai, *J. Agric. Food Chem.*, submitted for publication.

Journal of Chromatography A, 657 (1993) 357–363
Elsevier Science Publishers B.V., Amsterdam

CHROM. 25 593

Ion-exchange–immunoaffinity purification of a recombinant baculovirus *Plasmodium falciparum* apical membrane antigen, PF83/AMA-1

David L. Narum

Department of Chronic and Infectious Diseases, Medical Biological Laboratory-TNO, Postbus 5815, 2280 HV Rijswijk (Netherlands) and Department of Microbiology and Immunology, School of Medicine, University of Maryland at Baltimore, Baltimore, MD (USA)

Gjalt W. Welling

Laboratorium voor Medische Microbiologie, Rijksuniversiteit Groningen, Oostersingel 59, 9713 EZ Groningen (Netherlands)

Alan W. Thomas*

Department of Chronic and Infectious Diseases, Medical Biological Laboratory-TNO, Postbus 5815, 2280 HV Rijswijk (Netherlands) and Department of Microbiology and Immunology, School of Medicine, University of Maryland at Baltimore, Baltimore, MD (USA)

(First received June 28th, 1993; revised manuscript received September 27th, 1993)

ABSTRACT

A two-step purification regime has been developed for a quantitatively minor, putatively transmembrane, M_r 83 000, apical membrane blood stage vaccine candidate antigen of *Plasmodium falciparum* (PF83/AMA-1), that has been expressed as a full-length baculovirus recombinant protein, PF83-7G8-1. The first step utilizes a new approach to high-performance ion-exchange chromatography (HPIEC) in which elution conditions are not only defined by charge, but also by hydrophobicity. HPIEC fractionation involves successive sodium chloride gradient anion-exchange elutions (A and B), where a change in the non-ionic detergent polyoxyethylenealkylether $C_{10}E_5$ concentration between elutions A and B (from 0.01% to 0.1% (w/v) respectively), results in a fraction that comprises from 2% to 9% PF83-7G8-1. Subsequent column immunoaffinity purification of this fraction on Q-Sepharose CL 4B-28G2dc1 mAb yields a PF83-7G8-1 preparation that is 56% pure. Rat mAb 28G2dc1 recognizes a C-terminal region that is conserved and cross reactive within the AMA-1 family, thus permitting recombinant and native full-length AMA-1 molecules from other species to be purified for molecular analysis. Immunological and molecular characterisation of the vaccine-related characteristics of purified PF83/AMA-1 are now underway.

INTRODUCTION

Malaria continues to be one of the major health problems of tropical regions. Over 40 percent of the world's population are considered at risk and, in sub-Saharan Africa alone, it is estimated that annually between 1–2 million children die from the disease. Morbidity and mortality associated with malaria are rising alarmingly as major control measures become less effective due in part to the rapid spread of resistance to chemotherapy [1]. The development of new means to combat the disease is

* Corresponding author. Address for correspondence: Department of Chronic and Infectious Diseases, Medical Biological Laboratory-TNO, Postbus 5815, 2280 HV Rijswijk, Netherlands.

0021-9673/93/$06.00
SSDI 0021-9673(93)E1018-U

imperative, and one approach is to identify parasite targets that may comprise vaccine components. A number of such targets have been identified, and rapid analysis of their potential and, where appropriate, development of these molecules as vaccines is essential. One promising vaccine molecule, PF83/AMA-1 (*P. falciparum* M_r 83 000 protein/apical membrane antigen-1), belongs to a family of quantitatively minor antigens that were originally identified in a M_r 66 000, conformation dependent, asexual blood stage merozoite antigen of the simian malaria *Plasmodium knowlesi* that was shown to be the target of inhibitory monoclonal antibodies (mAb), and that could induce protection in rhesus monkeys [2–6]. PF83/AMA-1 is a highly similar M_r 83 000 analogue of this antigen of limited variability [7–11] that has been identified in *P. falciparum*, the cause of the most severe human malaria. PF83/AMA-1 has been expressed as a full-length recombinant molecule (PF83-7G8-1) that remains associated with the cellular fraction in the eukaryotic baculovirus expression system (manuscript in preparation). We have developed a purification scheme for the preparation of recombinant PF83-7G8-1 comprising over 56% of total protein using high-performance ion-exchange chromatography (HPIEC) and immunoaffinity chromatography. Resin-based ion-exchange sorbents' main mechanism of interaction with proteins is electrostatic in nature, due to their chemical composition. In addition such ion-exchange packings may exhibit hydrophobic properties [12–15]. This may give rise to mixed-mode contributions to solute separations depending on the hydrophobic properties of the protein and the composition of the eluent, *i.e.*, salt concentration, type of salt, presence of organic solvents or detergents. The present protocol is, in part, based on the novel HPIEC strategy of Welling-Wester *et al.* [16] that achieves differential elution of integral membrane proteins by adjustment of the concentration of non-ionic detergents such as the polyoxyethylenealkylether $C_{10}E_5$. Further purification of HPIEC eluted recombinant material was obtained by passage through a Q-Sepharose CL 4B-28G2dc1 immunoaffinity column. Rat mAb 28G2dc1 recognizes, within the *Plasmodium* AMA-1 family of molecules, a highly conserved C-terminal region [17]. Recombinant material, purified as described, is currently being used for the further immunological and molecular characterisation of PF83/AMA-1.

EXPERIMENTAL

Detergent extraction of recombinant PF83-7G8-1 from Sf9 cells and sample preparation for chromatography

Full-length PF83/AMA-1 was expressed in *Spodoptera frugiperda* (Sf9) cells [18]. Batch-to-batch variation in the efficiency of expression of the recombinant malarial protein (PF83-7G8-1) resulted in starting material in which PF83-7G8-1 constituted between an estimated 0.1% and 0.5% by weight of the total cell pellet. PF83-7G8-1 was associated with the plasma membrane of infected cells. Cells expressing PF83-7G8-1 were washed in phosphate buffered saline (PBS) and cell pellets (5 min, 100 *g*) were either rapidly frozen and stored at − 70°C or were immediately extracted ($4 \cdot 10^7$ cells ml^{-1}) for 1 h on ice in extraction buffer [50 m*M* Tris–HCl pH 8.0, 1% (w/v) $C_{10}E_5$ (Kwant–Hoog Vacolie Recycling and Synthesis, Bedum, Netherlands), 5 m*M* EDTA pH 8.0, 20 m*M* iodoacetamide, 0.8 mg ml^{-1} 4-(2-aminoethyl)-benzenesulfonylfluoride (AEBSF) (Calbiochem, San Diego, CA, USA), 5 μl ml^{-1} aprotinin, 1 μg ml^{-1} pepstatin A, and 40 μg ml^{-1} chymostatin]. The cell extract was centrifuged (10 min, 10 000 *g*, 10°C), filtered through a 0.45 μm filter (Millex HA, Millipore, Bedford, MA, USA) and then either directly applied to the Mono Q column or stored at −70°C. Frozen extracts were centrifuged and refiltered prior to HPLC. Cell extracts contained between 5.6 and 8 mg ml^{-1} protein (BCA kit, Pierce, Oud Beijerland, Netherlands).

Immunoaffinity chromatography sample preparation was as follows: Mono Q 10/10 chromatography fractions containing PF83-7G8-1 were pooled and briefly dialyzed (3 h, 4°C) against 100 volumes of 20 m*M* Tris–HCl pH 7.6. Dialyzed samples were then either directly applied to the immunoaffinity column or stored at − 70°C.

Ion-exchange HPLC and immunoaffinity chromatography

Ion-exchange chromatography was performed using the micro-HPLC Smart System (Pharmacia-LKB, Uppsala, Sweden) with a Mono Q PC 1.6/5 (50 mm × 1.6 mm I.D.) column. Alternatively, a basic HPLC system with a GP-250 gradient programmer (Pharmacia-LKB) was used with a Mono Q 5/5 (50 mm × 5 mm I.D.) or a 10/10 (100 mm × 10 mm I.D.) column loaded with a 10-ml Superloop (Pharmacia-LKB). The gradient profile for the Mono Q 1.6/5 and Mono Q 5/5 columns consisted of an 8-min isocratic elution with a linear 12-min gradient from 20 m*M* Tris–HCl pH 7.6 (buffer I) to 0.5 *M* sodium chloride in the same buffer (buffer II). Buffers I and II also contained either 0.01%, or 0.1% (w/v) $C_{10}E_5$. Flow rates for the Mono Q 1.6/5 and 5/5 columns were 100 μl min^{-1} and 1 ml min^{-1}, respectively. The gradient volume used for the Mono Q 10/10 column was calculated in proportion to the relative Mono Q 5/5 and 10/10 column volumes to yield a 16-min isocratic elution followed by a linear 24-min gradient at a flow rate of 4 ml min^{-1}. All chromatography was performed at room temperature. Fraction volumes collected during elution were 100 μl (Smart system) and 4 ml (Mono Q 10/10). An initial buffer I to buffer II linear elution gradient containing 0.01% (w/v) $C_{10}E_5$ was followed by a second gradient containing 0.1% (w/v) $C_{10}E_5$ to elute the PF83-7G8-1.

Immunoaffinity resin (8 mg ml^{-1} mAb) was prepared by coupling [19] purified rat mAb 28G2dc1 (IgG2a isotype) to cyanogen bromide activated Q-Sepharose CL 4B (QS-28G2dc1) (Pharmacia LKB). A chromatography column containing 250 μl QS-28G2dc1 was equilibrated with 5 column volumes of buffer [150 m*M* NaCl, 5 m*M* EDTA pH 8.0, 0.1% (w/v) $C_{10}E_5$, 20 m*M* Tris–HCl pH 7.6, (150 m*M* NECT)]. Pooled and dialysed Mono Q 10/10 fractions containing PF83-7G8-1 were passed over the column at a flow rate of 0.5 ml min^{-1}. Fractions passing through were subsequently monitored for the presence of unbound PF83-7G8-1 by immunoblot; it appeared that saturation levels for the column were not reached. The column was washed with 15 column volumes each of 150 m*M* NECT, 500 m*M* NECT (NaCl concentration 500 m*M*), and 150 m*M* NECT. PF83-7G8-1 was eluted with Pierce Elution Buffer pH 2.8 (Pierce) into vials containing 1 *M* Tris–HCl pH 8 to rapidly neutralize the pH.

SDS-PAGE, immunoblotting, and scanning laser densitometry

Chromatography fractions were analyzed by sodium dodecyl sulfate polyacrylamide gel electrophoresis (SDS-PAGE) under reducing conditions by mixing with equal volumes of sample buffer, heating and electrophoresing essentially as previously described [20]. Duracryl (Millipore) was used to prepare gels for silver staining (Gelcode Color Silver Staining Kit, Pierce) and 10% polyacrylamide gel was used for electroblots onto nitrocellulose. The migration of prestained molecular mass markers (Gibco BRL, Bethesda, MD, USA) is noted alongside all figures. Immunoblots were stained with pooled rat mAbs, 28G2dc1 and 58F8dc1 (rat mAb 58F8dc1, isotype IgG2a, reacts with the extreme N-terminal region of PF83/AMA-1 [17], both incorporated at 5 μg ml^{-1}. All immunoblots were developed using alkaline phosphatase conjugated reagents (Pierce). The relative proportions of fractionated components were determined by scanning laser densitometry on silver stained gels using an UltraScan XL (Pharmacia LKB). Backgrounds were subtracted after being determined on adjacent tracks to which no sample had been added.

RESULTS AND DISCUSSION

Welling-Wester *et al.* [16] have reported the selective elution of Sendai virus integral membrane proteins from an anion-exchange column through a two-step elution involving manipulation of the concentration of non-ionic detergent ($C_{10}E_5$). We anticipated that this technique would also be applicable to the separation of PF83/AMA-1, a molecule which, in its mature, full length native form is an M_r 83 000, non-glycosylated protein composed of 34% non-polar and hydrophobic amino acids and contains a

predicted trans-membrane region. Initial experimentation (not shown) determined that the efficiency of PF83/AMA-1 extraction with 1.0% (w/v) $C_{10}E_5$ was comparable to that obtained with 1.0% (w/v) TX-100, the detergent we had previously used for AMA-1 extraction. PF83-7G8-1 could be eluted in a sodium chloride anion-exchange gradient containing 0.1% $C_{10}E_5$ (Fig. 1). It was detected by immunoblot as a M_r 90 000 protein of fraction 10. The observed increase in molecular mass over native PF83 is the result of N-linked glycosylation in the baculovirus system [18]. The additional bands in Fig. 1B, fractions 8, 9, and 10 at approximately M_r 55 000–60 000 are attributable to weak cross-reactions with Sf9 cell protein(s) present in large amounts (Fig. 1A fractions 8–10), as they were also detected on immunoblots of non-recombinant Sf9 preparations. Immunoblot analysis of the eluant during sample loading and isocratic elution did not reveal unbound PF83-7G8-1 (data not shown). In Fig. 2 the effect of changing detergent concentrations on the elution of PF83-7G8-1 is revealed. Although ten times less sample is loaded in tracks 8–12 (0.01% $C_{10}E_5$) than in tracks B8–B12 (0.1% $C_{10}E_5$) the total protein levels per track are comparable (panel A), showing that the bulk of the total protein is eluted during the initial, hydrophilic, 0.01% $C_{10}E_5$ elution. PF83-7G8-1 is predominantly

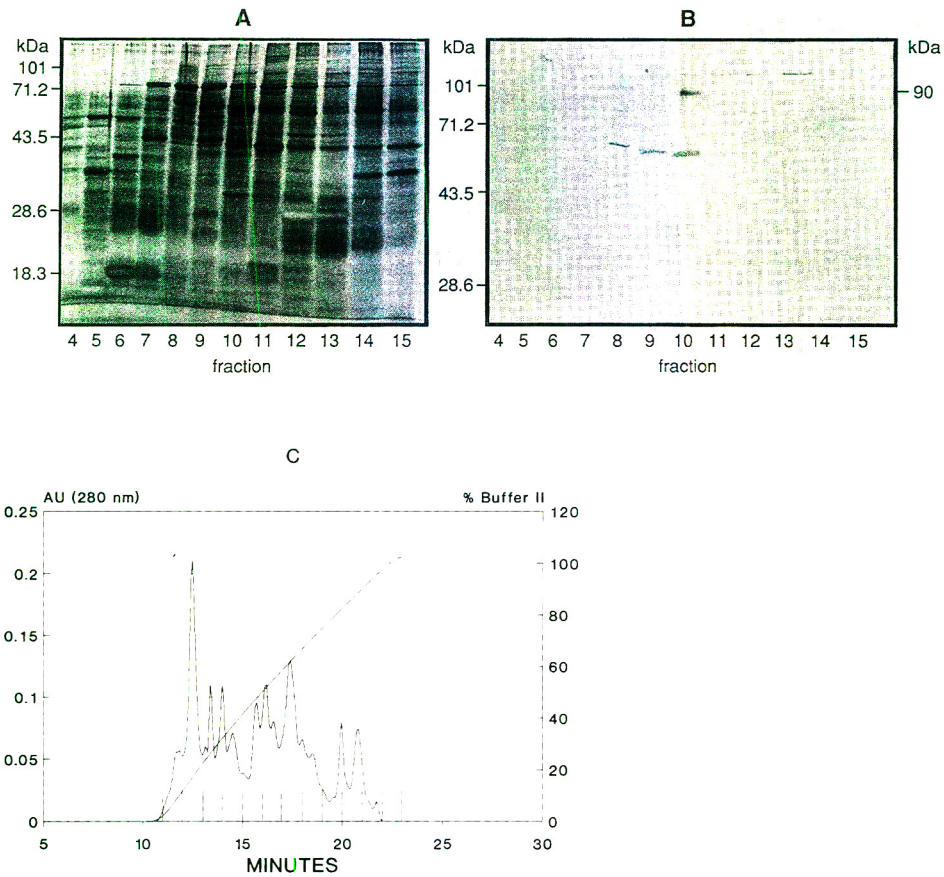

Fig. 1. SDS-PAGE silver stain with 10% Duracryl (A) and pooled mAb immunoblot analysis (B) of a Smart system anion-exchange elution of total PF83-7G8-1/Sf9 cell extract (400 μg) using a Mono Q PC 1.6/5 column. After isocratic elution retained proteins were fractionated with a sodium chloride gradient containing 0.1% (w/v) $C_{10}E_5$. Fractions 4–15 (100 μl) were prepared for SDS-PAGE and divided equally for silver stain and immunoblot. (C) Elution profile (vertical lines delineate consecutive fractions 4–15 that were collected for analysis in A and B).

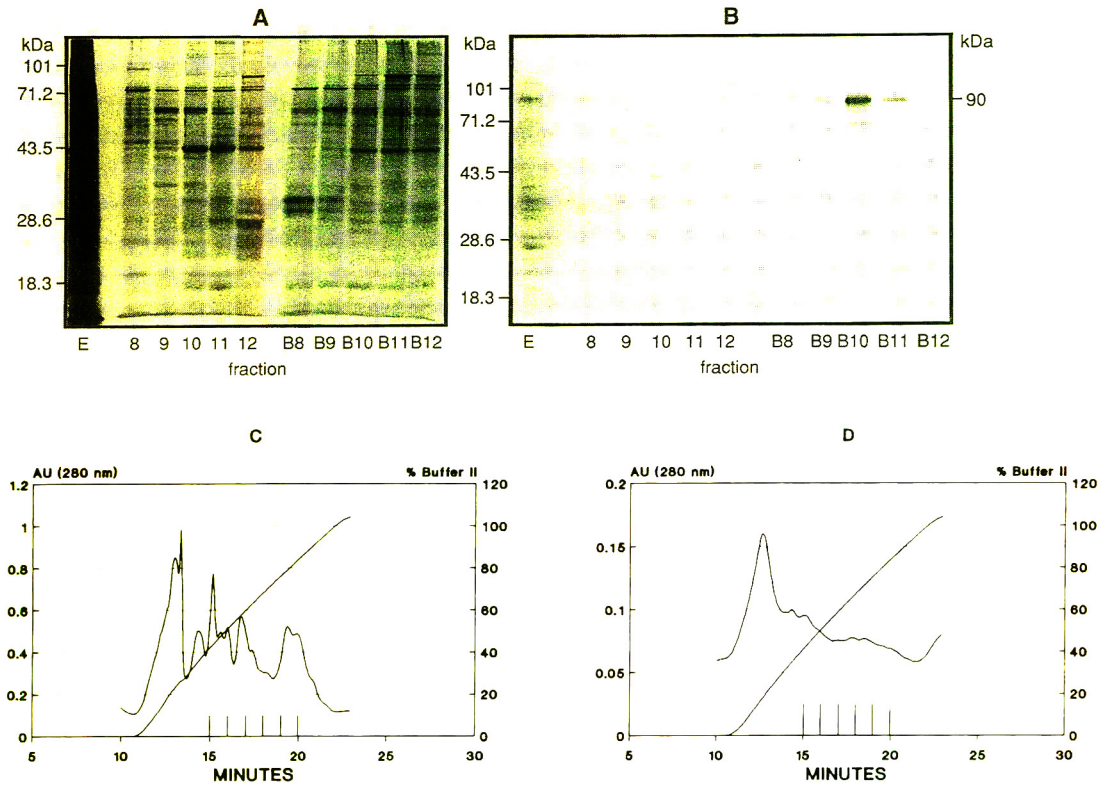

Fig. 2. Two-step $C_{10}E_5$ anion-exchange chromatography of PF83-7G8-1/Sf9 extract. Following isocratic elution a Smart system Mono Q PC 1.6/5 column loaded with 2.4 mg total extract was sequentially eluted with 0–0.5 *M* sodium chloride gradients containing 0.01% $C_{10}E_5$ (fractions 8–12, 100 μl each) and 0.1% $C_{10}E_5$ (fractions B8–B12, 100 μl each). 80 μg of total cell extract (track E) are shown alongside 5-μl samples from fractions 8–12 and 50-μl samples from fractions B8–B12 after silver stained SDS-PAGE with 10% Duracryl (A) and pooled mAb immunoblot (B). Elution profiles with 0.01% $C_{10}E_5$ (C) and 0.1% $C_{10}E_5$ (D) are marked with vertical lines to delineate consecutive fractions 8–12 (C) and B8–B12 (D) that were collected for analysis.

eluted in fraction B10 of the 0.1% $C_{10}E_5$ elution (panel B). Even when volumes of fractions 8–12 equivalent to those used for B8–B12 were analysed by immunoblot, no PF83-7G8-1 was detectable (not shown), demonstrating the selective elution of PF83-7G8-1 achieved under the higher detergent concentration. The elution profiles for anion-exchange chromatography with 0.01% $C_{10}E_5$ (panel C) and 0.1% $C_{10}E_5$ (panel D) confirm that the major protein elution occurs under low detergent conditions.

The conditions which had been defined using the Mono Q PC 1.6/5 column were predictive for scale-up to Mono Q 5/5 (data not shown) and then Mono Q 10/10 columns. The results shown in Fig. 3 derive from a Mono Q 10/10 fractionation of an PF83-7G8-1/Sf9 cell extract. Fractions were analyzed by immunoblot, and fractions eluted during the 0.1% $C_{10}E_5$ run which contained PF83-7G8-1 were pooled (28 ml) and dialyzed. Analysis of this pooled material by silver stain (Fig. 3A, track 1) and immunoblot (Fig. 3B, track 1) identified full-length PF83-7G8-1 (a), and truncated products at M_r 81 000 (b) and 72 000 (c). PF83-7G8-1 constituted 9% of this material. In other preparations the proportion of the pooled material represented by PF83-7G8-1 varied from between 2% and 9% of the pool in a manner directly dependent on the efficiency with which it was expressed in the starting material. The PF83-7G8-1 dialyzed fraction pool was then passed through a 250-μl QS-28G2dc1 immunoaffinity column. Rat mAb 28G2dc1 cross-reacts with the C-terminal

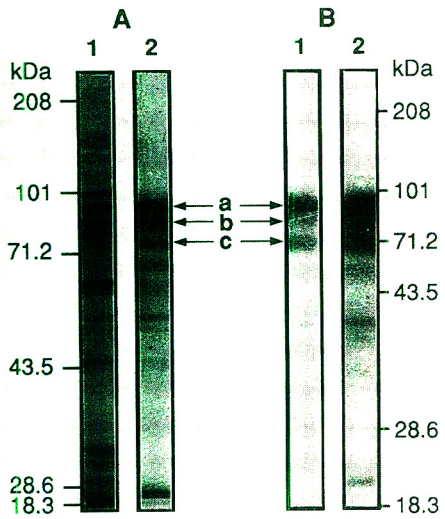

Fig. 3. Combined HPLC anion-exchange and immunoaffinity purification of PF83-7G8-1. 20 ml (6 mg ml $^{-1}$) of total PF83-7G8-1/Sf9 extract was fractionated by Mono Q 10/10 two-step detergent gradient elution at 4 ml min $^{-1}$. (A) (silver stained SDS-PAGE with 7.5% Duracryl) and (B) (immunoblot with pooled mAbs) show samples from pooled Mono Q 10/10 derived fractions containing PF83-7G8-1 before (tracks 1) and after (tracks 2) affinity purification on a Q-Sepharose CL 4B-28G2dc1 column. Arrows: (a) M_r 90 000; (b) 81 000; (c) 72 000.

region of all the molecules within the *Plasmodium* AMA-1 family studied so far and therefore provides a universal method for the purification of AMA-1 molecules from different *Plasmodium* species. The QS-28G2dc1 column was washed in a series of NECT buffers and PF83-7G8-1 was eluted with a glycine buffer, pH 2.8 (Fig. 3). By scanning laser densitometry of silver stained gels it was estimated that in the eluted fraction PF83-7G8-1 constituted 56% of total protein. This contrasts with similar immunoaffinity purification procedures using cell extracts directly, without an intervening HPIEC fractionation, where PF83-7G8-1 constituted approximately 10% of the eluted material (data not shown). The QS-28G2dc1 immunoaffinity column was rapidly re-equilibrated and reusable.

CONCLUSIONS

We have developed a two-step purification scheme that we anticipate will be of general application for molecules of the AMA-1 family of malarial proteins. The first step uses an approach to HPIEC enabling differential elution of integral membrane proteins based on their hydrophobic nature and the effect of non-ionic detergents on their solubility. This technique was initially developed with Sendai virus integral membrane proteins, and this is the first report to show a wider application for the method. The second step utilizes a QS-28G2dc1 immunoaffinity column to purify a recombinant PF83/AMA-1 molecule, PF83-7G8-1, to 56% of the total protein. MAb 28G2dc1 recognizes a C-terminal region that is conserved within the family of AMA-1 molecules of malarial parasites so far analysed. Immunological and molecular characterisation of PF83-7G8-1, made possible by this purification regime, is currently underway.

ACKNOWLEDGEMENTS

We wish to thank M. Dubbeld and J. Wubben for excellent technical assistance. We are also grateful to M.A. Braaksma and B.R.K. Douma for their willing assistance in the use of the Smart system at the Rijksuniversiteit, Groningen (Netherlands). Grant support was from the United States Agency for International Development (co-operative agreement DPE-5979-A-00-0042-00) and the STD-3 programme of the European Communities (TS3*-CT92-0147). DN was supported in part by a Graduate Research Assistantship Award from the UMAB Designated Research Initiative Fund.

REFERENCES

1 W.H. Wernsdorfer, *Parasitology Today*, 7 (1991) 297.
2 J.A. Deans, T. Alderson, A.W. Thomas, G.H. Mitchell, E.J. Lennox and S. Cohen, *Clin. Exp. Immunol.*, 49 (1982) 297.
3 A.W. Thomas, J.A. Deans, G.H. Mitchell, T. Alderson and S. Cohen, *Mol. Biochem. Parasitol.*, 13 (1984) 187
4 J.A. Deans and W.C. Jean, *Mol. Biochem. Parasitol.*, 26 (1987) 155
5 J.A. Deans, A.M. Knight, W.C. Jean, A.P. Waters, S. Cohen and G.H. Mitchell, *Parasite Immunol.*, 10 (1988) 535.
6 A.W. Thomas, L.H. Bannister and A.P. Waters, *Parasite Immunol.*, 12 (1990) 105.

7 A .W. Thomas, J.A. Deans, A.P. Waters and J. Chulay, *3rd International Congress on Malaria and Babesiosis, Annecy, France, 1987*, p. 90.
8 M.G. Peterson, V.M. Marshall, J.A. Smythe, P.E. Crewther, A. Lew, A. Silva, R.F. Anders and D.J. Kemp, *Mol. Cell. Biol.*, 9 (1989) 3151.
9 A.P. Waters, A.W. Thomas, J.A. Deans, G.H. Mitchell, D.E. Hudson, L.H. Miller, T.F. McCutchan and S. Cohen, *J. Biol. Chem.*, 265 (1990) 17974.
10 P.E. Crewther, J.G. Culvenor, A. Silva, J.A. Cooper and R.F. Anders, *Exp. Parasitol.*, 70 (1990) 193.
11 A.W. Thomas, A.P. Waters and D.A. Carr, *Mol. Biochem. Parasitol.*, 42 (1990) 285.
12 F.E. Regnier and R.M. Chicz, in K.M. Gooding and F.E. Regnier (Editors), *HPLC of Biological Macromolecules (Chromatographic Science Series*, Vol. 51), Marcel Dekker, New York, Basel, 1990, pp. 77–93.
13 K.M. Gooding and M.N. Schmuck, *J. Chromatogr.*, 327 (1985) 139.
14 M.L. Heinitz, L. Kennedy, W. Kopaciewicz and F.E. Regnier, *J. Chromatogr.*, 443 (1988) 173.
15 T.W.L. Burke, C.T. Mant, J.A. Black and R.S. Hodges, *J. Chromatogr.*, 476 (1989) 377.
16 S. Welling-Wester, M. Feijlbrief, D.G.A.M. Koedijk, M.A. Braaksma, B.R.K. Douma and G.W. Welling, *J. Chromatogr.*, 646 (1993) 37.
17 D.L. Narum and A.W. Thomas, *Mol. Biochem. Parasitol.*, submitted for publication.
18 A.W. Thomas, P. Druilhe, V. Rosario and D.L. Narum, *Infect. Immun.*, submitted for publication.
19 E. Harlow and D. Lane, *Antibodies, A Laboratory Manual*, Cold Spring Harbor Laboratory, New York, 1988.
20 J.A. Deans, A.W. Thomas and S. Cohen, *Mol. Biochem. Parasitol.*, 8 (1983) 31.

Journal of Chromatography A, 657 (1993) 365–375
Elsevier Science Publishers B.V., Amsterdam

CHROM. 25 556

Characterization of ethoxylated fatty alcohols using liquid chromatography with density and refractive index detection

I. Quantitative analysis of pure homologous series by size-exclusion chromatography

B. Trathnigg*, D. Thamer, X. Yan and B. Maier

Institute of Organic Chemistry, University of Graz, Heinrichstrasse 28, A-8010 Graz (Austria)

H.-R. Holzbauer and H. Much

Centre of Macromolecular Chemistry, Berlin (Germany)

(First received July 16th, 1993; revised manuscript received September 13th, 1993)

ABSTRACT

Ethoxylated fatty alcohols can be characterized by two-dimensional chromatography with LC under critical conditions as the first and size-exclusion chromatography (SEC) as the second dimension. The dependence of response factors on the chemical composition can be compensated by two different approaches. The results obtained are in good agreement. The SEC calibrations for the individual homologous series showed considerable differences, hence for each fraction the corresponding calibration should be used.

INTRODUCTION

Ethoxylated fatty alcohols (FAE) are in widespread use as non-ionic surfactants for various applications [1–5]. Nevertheless, their analysis is still somewhat problematic, because these products typically consist of several polymeric homologous series of polyoxyethylene with different end-groups, depending on the purity of the fatty alcohol used as the starting material, and also, in some instances, unwanted polyethylene glycols.

A complete characterization of FAE must provide information on the distributions of the chain length of the polyoxyethylene and the carbon number of the alkyl group. This can only be achieved by two-dimensional analytical methods, but the common methods are one-dimensional. Moreover, there are problems with detection, as will be pointed out later.

Lower oligomers can be analysed by GC [6–8] and for higher molecular mass products HPLC in different variations is commonly used [9–18]. Recently, high-temperature capillary GC [19] and supercritical fluid chromatography (SFC) [18] have also been applied to higher molecular mass samples. Despite the high separation ef-

* Corresponding author.

0021-9673/93/$06.00
SSDI 0021-9673(93)E0975-Z

ficiency of these techniques, quantification of the results is problematic, because the detector response for each oligomer is not predictable.

In the different modes of liquid chromatography, the separation occurs according to different criteria, as follows: size-exclusion chromatography (SEC) [20] separates according to molecular dimensions, *i.e.*, to the number of ethylene oxide units attached to the fatty alcohol; normal phase LC [9,10] also separates according to the number of ethylene oxide units; and reversed-phase LC [11–18] separates according to the alkyl end-groups.

In a special modification of liquid chromatography, called "LC at the critical point of adsorption" or "LC under critical conditions" (LCCC) [21–24], each homologous series elutes in a sharp peak, regardless of how long the polyether chain is. This allows a separation of the individual homologous series. As LCCC has been described in numerous publications [21–24], its principle will be described only briefly. The chromatographic mobility of a molecule is closely related to its distribution coefficient K_d between the stationary and mobile phases, which in turn depends on the change in free energy, ΔF, when the molecule is adsorbed:

$$K_d = \exp\left(-\frac{\Delta F}{kT}\right) \quad (1)$$

According to the second law of thermodynamics, ΔF is composed of the changes in enthalpy and entropy (ΔH and ΔS, respectively):

$$\Delta F = \Delta H + T\Delta S \quad (2)$$

where ΔH depends on the number of adsorbed segments N_a and the interaction energy ε of each segment:

$$\Delta H = -\varepsilon k T N_a \quad (3)$$

In adsorption chromatography, the retention depends on ΔH, and hence on N_a: the larger a molecule is, the later it elutes. In SEC, the opposite is true: the interaction energy here should be close to zero or at least very small, and the elution behaviour should be governed exclusively by the entropic term: smaller molecules will elute later than larger molecules.

If ε for one segment approaches a critical value ε_{cr}, ΔH and $T\Delta S$ will compensate each other, thus leading to $\Delta F = 0$. At this "critical point of adsorption" the corresponding block will become chromatographically invisible, because its chain length will have no effect on the elution volume. Hence the separation will occur only according to the end-groups, or to any groups different from the repeating unit. Applied to FAE this means, that under critical conditions for polyethylene oxide all oligomers of a homologous series (with a given alkyl end-group) will elute within a narrow peak, regardless of their chain length, thus yielding the functionality type distribution (FTD).

If LCCC is performed on a semi-preparative scale, the separated pure homologous series can be characterized using SEC with respect to their molecular mass distribution (MMD). With such a combination of LCCC as the first and SEC as the second dimension, it should be possible to obtain a "map" of these products, with the number of ethylene oxide (EO) units on the x-axis, the length of the alkyl chain on the y-axis and the amount of each oligomer on the z-axis. Even though a qualitative characterization may be fairly easy to achieve, no satisfactory quantification of the chromatograms obtained in the first or second dimension has been described up to now.

In this paper, we present a method that provides quantitative characterization of the individual homologous series in the second dimension (SEC). The quantification of the first dimension (LCCC) will be described in Part II of this series.

EXPERIMENTAL

These investigations were performed using a DDS70 density detection system (Paar, Graz, Austria), which was developed in our group and has been described in full detail in previous papers [25–27]. In SEC measurements it was combined with a SICON LCD 201 refractive index (RI) detector and in LCCC with a Bischoff 8110 RI detector. Each system was and connected to an MS-DOS computer via the serial port. Data acquisition and processing were performed using the software package CHROMA [27], which has been developed for the DDS 70.

SEC measurements were performed in chloroform (HPLC grade, Rathburn) at a constant flow-rate of 1.0 ml/min, which was maintained by a Gynkotek 300C HPLC pump. Samples were injected using a VICI injection valve equipped with a 100-μl loop; the concentration range was 4–8 g/l.

A set of four Phenogel columns, (500/500/1000/1000 Å), 30 cm each, was used for all SEC measurements. The columns were connected to an electrically switched valve (VICI WE-10-C6W) as shown in Fig. 1. When the valve is switched from position A to B before the peaks of interest leave column 4, they are sent back to column 1, and the number of columns through which they have to pass is increased by 2. By switching at appropriate intervals, the separation efficiency of a set of 10–12 columns can be achieved with only four columns. The SEC calibrations were obtained using pure oligomers of EO (from Fluka) and SEC standards from Polymer Laboratories.

In LCCC, two JASCO 880 PU pumps were used, which were equipped with Rheodyne Model 7125 injection valves with a 50- and 500-μl loop, respectively.

Reversed-phase LC was performed with methanol and methanol–water mixtures (from Merck, HPLC grade) on different analytical columns and a semi-preparative column filled with Spherisorb from Phase Separations (ODS-2, 3 μm, 100 × 4.6 mm I.D.; ODS-2, 5 μm, 250 × 4.6 mm I.D.; and ODS-2, 5 μm, 250 × 10 mm I.D.). The flow-rate was 0.5 ml/min in the analytical mea-

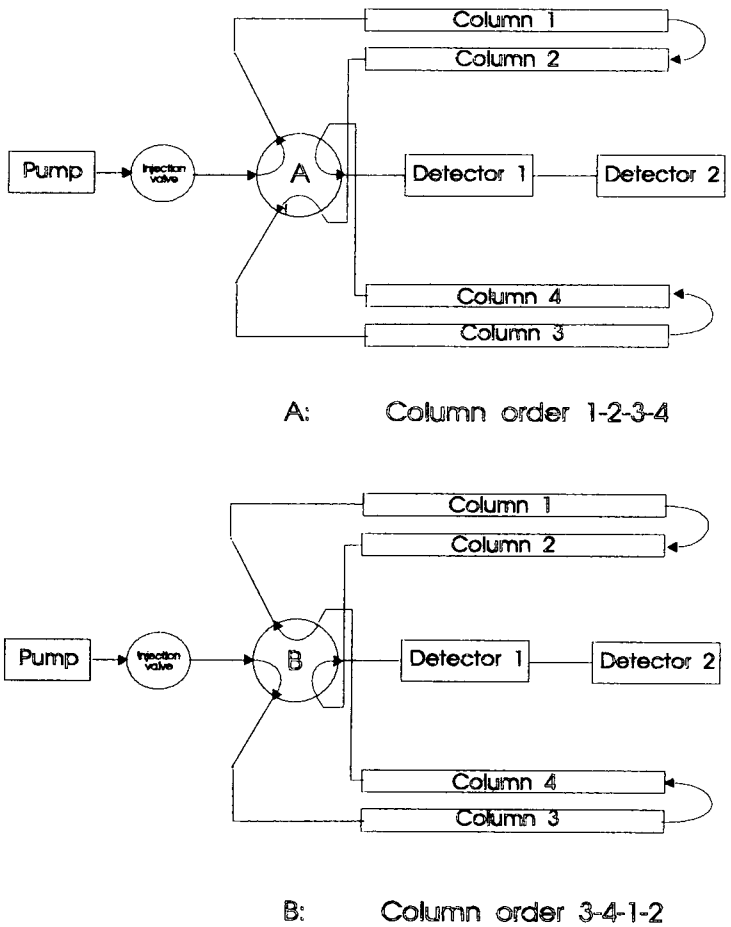

Fig. 1. Configuration used for recycling in SEC measurements.

surements and 2 ml/min in semi-preparative LCCC. An Advantec 2120 fraction collector was used in the semi-preparative separations.

The alkanols and polyoxyethylenes were purchased from Fluka and used as received. Pure homologous series were prepared by anionic ethoxylation [28] of pure 1-alkanols using standard procedures. A monodisperse oligomer octyl-$(EO)_4$ was synthesized by a modified Williamson synthesis [29–31] from 1-octyl bromide and tetraethylene glycol.

Problems in quantitative characterization of FAE

As FAE do not contain any UV-absorbing groups (unlike ethoxylated alkylphenols), different approaches have been described: some workers used derivatization (typically with 3,5-dinitrobenzoyl chloride) and subsequent UV [9] or polarographic detection [15], and others used RI [11–14] or evaporative light-scattering detectors [16]. If one wants to avoid the problems associated with derivatization, there are basically three detectors suitable for this purpose: (1) the evaporative light-scattering detector (ELSD), (2) the differential refractive index (RI) detector and (3) the density detector.

Because of its poor linearity [32], the ELSD is not the instrument of choice, even though it allows the use of gradients. Moreover, it is very likely that the response of this detector will depend on the molecular mass and composition of the sample (because they may determine the size and the transparency of the droplets or particles formed on evaporation of the mobile phase), and the nature of this dependence is not yet clear. RI and density detectors are universal detectors, which can only be used in the isocratic mode. If a separation can be achieved under isocratic conditions, both detectors perform fairly well. One has to take into account, however, that the response factors of universal detectors are closely related to specific properties, such as refractive index increment or apparent specific volume. Hence they will depend on molecular mass (in this instance on the number n of EO units) [33–39].

As has already been shown [11,20,40], this dependence can be compensated using

$$f_i = f_{i,\infty} + \frac{K}{M_i} \tag{4}$$

wherein f_i is the response factor of the oligomer with the molecular mass M_i, $f_{i,\infty}$ is the response factor of a polyether chain with infinite (or at least sufficiently high) molecular mass and K is a

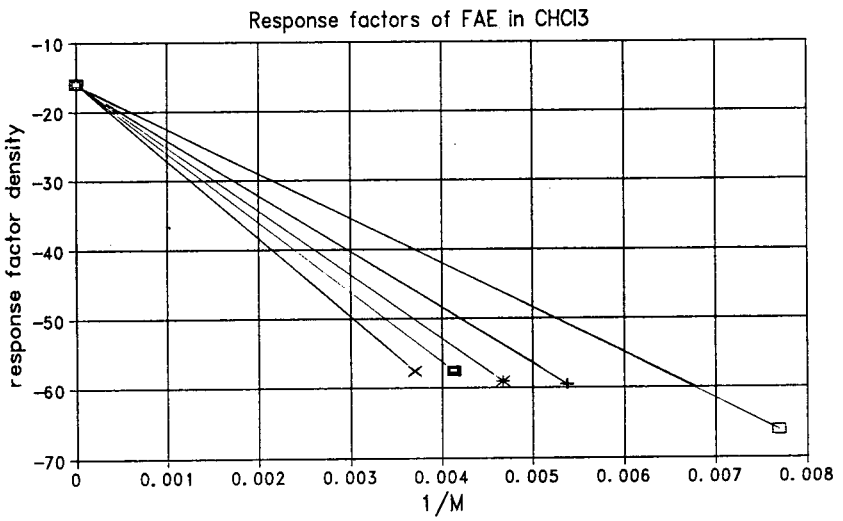

Fig. 2. Response factors (density detection) of homologous series of FAE with different end-groups, as determined by two-point calibration with PEG 3000 and the corresponding alkanols. □ = C_8; + = C_{12}; * = C_{14}; ◘ = C_{16}; × = C_{18}.

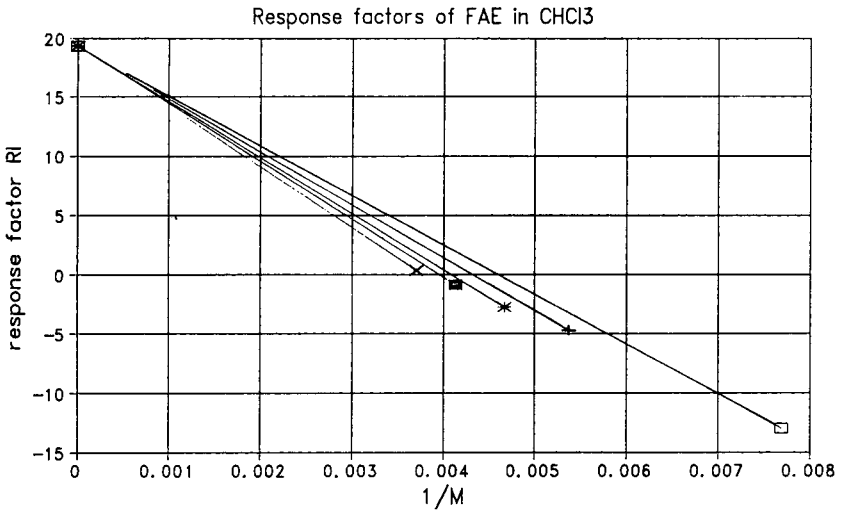

Fig. 3. Response factors (RI detection) of homologous series of FAE with different end-groups, as determined by two-point calibration with PEG 3000 and the corresponding alkanols. Symbols as in Fig. 2.

constant representing the influence of the end-groups. In a plot of f_i *vs.* $1/M_i$, K is the slope of the regression line.

As no pure oligomers are available for FAE, one can determine K from a two-point calibration using a high-molecular-mass polyoxyethylene and the fatty alcohol (with $n = 0$), or by an iteration procedure, which is provided by CHROMA.

In order to have sufficient amounts of FAE with defined end-groups available, we synthesized several samples by ethoxylation of pure *n*-alkanols and analysed them by analytical LCCC. When necessary, polyethylene glycols were removed by preparative LCCC. As can be seen from Figs. 2 and 3, the response factors of the alcohols vary considerably with their carbon number, hence different values of K are obtained, which are given in Table I.

In the analysis of pure homologous series, this approach yields satisfactory results, provided that the sign of the response factor does not change within the MWD of the sample. As can be seen from Fig. 4, which shows a separation of

TABLE I

RESPONSE FACTORS OF DIFFERENT 1-ALKANOLS IN CHLOROFORM WITH DENSITY AND RI DETECTION AND SLOPES K CALCULATED BY INTERPOLATION AND BY ITERATION (IN CHROMA)

Carbon number of PEG 3000	f_D ($f_{D,\infty} = -16.06$)	Slope for oligomers (density), K_D		f_R ($f_{R,\infty} = 19.287$)	Slope for oligomers (RI), K_R (2-point)
		2-Point	Iteration		
6	−67.07	−5202.7		−22.870	−4300.0
8	−66.11	−6505.9	−6882.9	−13.036	−4202.0
12	59.52	−8082.7	−8431.6	−4.733	−4467.7
14	59.11	−9211.3	−9211.5	−2.765	−4719.1
16	−57.60	−10051.0		−0.904	−4886.2
18	−57.67	−11232.5		0.359	−5110.6

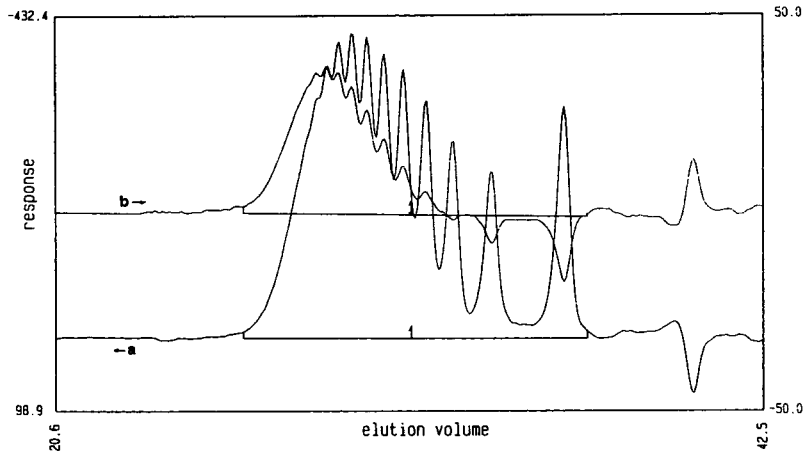

Fig. 4. Chromatogram of an ethoxylated 1-octanol, as obtained with density (a) and RI detection (b).

an ethoxylated 1-octanol by SEC in chloroform, this is fulfilled with density detection, but not with RI detection. In this case, the MWD can only be calculated from the density trace and not from the RI trace. Without compensation of the molecular mass dependence of the response factors an erroneous MWD will be found, because the lower oligomers will be overestimated. Such a compensation can be performed using eqn. 4. The results thus obtained are shown in Figs. 5 and 6.

There is, however, still the problem of the SEC calibration: the calibration line obtained with PEG standards need not necessarily be valid for the monoalkyl ethers [41]. A solution to this problem may be to use dual detection.

Determination of chemical composition using dual detection

As we have shown previously [42,43], the mass fractions m_A and m_B of the monomeric units A and B in a copolymer or a polymer mixture can be determined at any point of the MWD, by SEC with coupled density and RI detectors from the corresponding responses x_D and x_R:

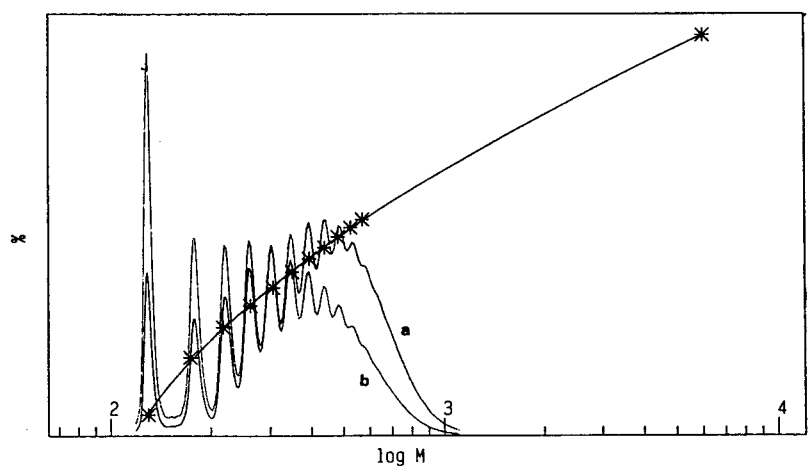

Fig. 5. MWD of the ethoxylated octanol (Fig. 4) from density detection without compensation for molecular mass dependence of response factors. a = Mass distribution; b = number distribution; *——* = calibration.

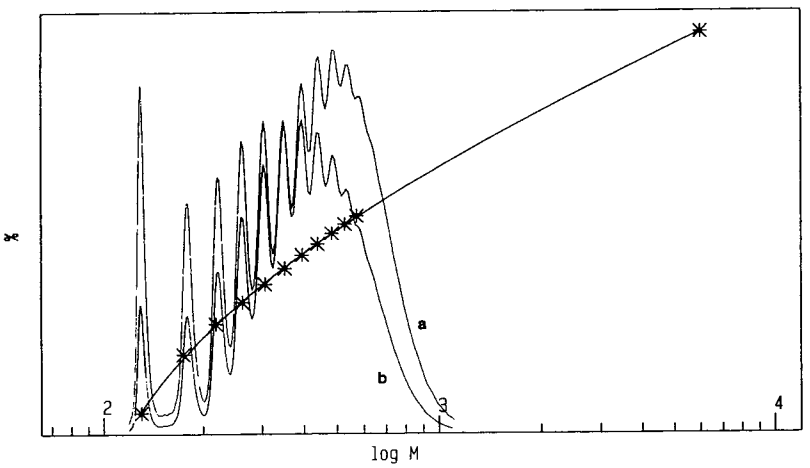

Fig. 6. MWD of the ethoxylated octanol (Fig. 4) from density detection with compensation for molecular mass dependence of response factors using eqn. 4. Curves as in Fig. 5.

$$\frac{1}{m_A} = 1 - \frac{f_{\infty,R,A} \cdot \frac{x_D}{x_R} - f_{\infty,D,A}}{f_{\infty,R,B} \cdot \frac{x_D}{x_R} - f_{\infty,D,B}} \quad (5)$$

If the parameters $f_{\infty,D}$, $f_{\infty,R}$, K_D and K_R for both components (A and B) are known, one can calculate the response factors for any point of the MWD using eqn. 4, which allows the application of these methods also to low-molecular-mass samples.

Once the mass fractions of the components for any point of the peak have been determined, the correct mass m_i eluted within each interval can be calculated using the equations

$$m_i = \frac{x_D}{m_A(f_{D,A} - f_{D,B}) + f_{D,B}} \quad (6)$$

$$m_i = \frac{x_R}{m_A(f_{R,A} - f_{R,B}) + f_{R,B}} \quad (7)$$

In the case of FAE, one may consider the

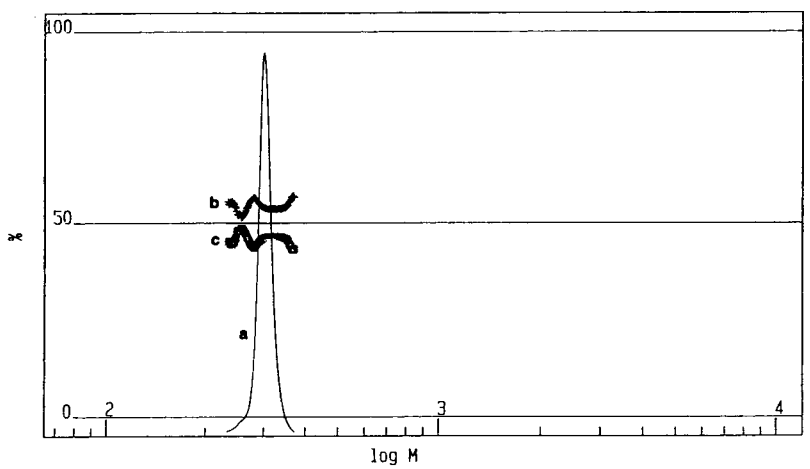

Fig. 7. MWD of octyl-tetraethylene glycol from density detection with compensation for molecular mass dependence of response factors using the mass fraction of the alkanol. a = Mass distribution; b = ethylene oxide; c = octanol.

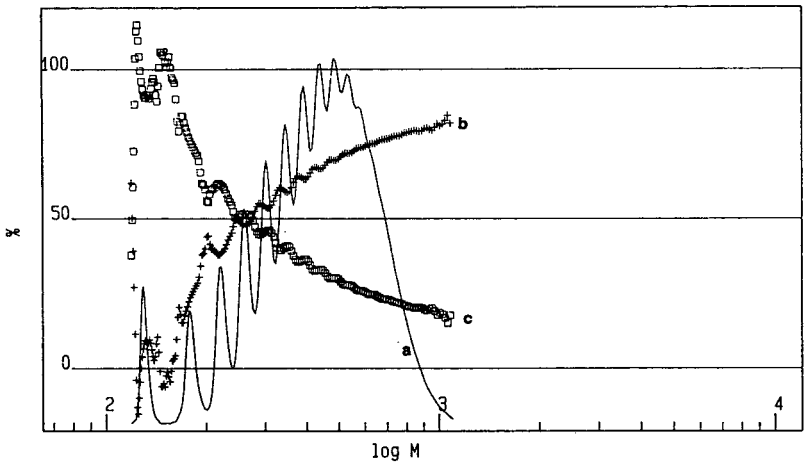

Fig. 8. MWD of the ethoxylated octanol (Fig. 4) from density detection with compensation for molecular mass dependence of response factors using the mass fraction of the alkanol; a, b and c as in Fig. 7.

polyoxyethylene chain as component A, which is inserted as a centre block between the alkyl and the hydroxy groups of component B (the fatty alcohol). In this case, no correction for the end-groups is required, because the PEO chain has no end-groups, and only the carbon number of the alkanol has to be accounted for. Using the response factors of high-molecular-mass PEG and the corresponding alkanol, one can calculate the composition and thereby the number of EO units for each fraction.

As a test of this approach, we analysed an octyl-$(EO)_4H$, which has been synthesized by condensation of tetraethylene glycol with 1-octanol, and again the ethoxylated octanol from Figs. 4 and 5. The results obtained are shown in

TABLE II

MOLECULAR MASS AVERAGES OF DIFFERENT OLIGOMERS OF OCTYL-$(EO)_n$ OBTAINED WITH TWO DIFFERENT SEC CALIBRATIONS (PEG AND OCTYL-PEO)

Correction of response factors using slope K or mass fraction of alkanol (m_A).

Sample	Parameter[a]	Calibration					
		PEG			Octyl-PEO		
		No correction	Slope	m_A	No correction	Slope	m_A
R_8EO_4	M_w	299	301	302	300	303	302
	M_n	298	300	300	299	301	301
	M_w/M_n	1.004	1.004	1.003	1.004	1.004	1.004
R_8EO_5	M_w	375	419	413	388	436	428
	M_n	288	340	331	302	352	344
	M_w/M_n	1.301	1.232	1.247	1.285	1.240	1.245
R_8EO_{10}	M_w	613	652	644	649	697	685
	M_n	507	563	533	521	587	572
	M_w/M_n	1.209	1.156	1.164	1.246	1.188	1.198

[a] M_w = Mass-average molecular mass; M_n = number-average molecular mass.

TABLE III

MOLECULAR MASS AVERAGES OF A 1-DODECYL-(EO)$_n$ OBTAINED WITH TWO DIFFERENT SEC CALIBRATIONS (PEG AND DODECYL-PEO)

Correction of response factors using slope K or mass fraction of alkanol (m_A).

Parameter	Calibration					
	PEG			Dodecyl-PEO		
	No correction	Slope	m_A	No correction	Slope	m_A
M_w	587	632	621	611	659	648
M_n	484	539	527	506	559	548
M_w/M_n	1.211	1.172	1.180	1.207	1.178	1.182

Figs. 7 and 8. Obviously, the algorithm works even in cases where the linear interpolation cannot be applied.

As soon as the mass fraction of the polyoxyethylene chain in each peak is known, one can identify each oligomer and use the maxima to establish an SEC calibration for the corresponding homologous series.

For the monodisperse oligomer, the mass fraction of the ethylene oxide chain was found to be $m_A = 53.8\%$, which agrees fairly well with the theoretical value of 57.5%. In the analysis of the ethoxylated tetradecanol, the lowest molecular peak was clearly identified as tetradecanol, and the others as the higher homologues with increasing number of EO units. In Tables II–IV the molecular mass averages for several polyoxyethylene monoalkyl ethers are given, which were obtained with different SEC calibrations (obtained as described above or with commercial PEG standards), and with two different methods of correcting the response factors (using the slope K or the chemical composition from dual detection). As can be seen, the two approaches agree fairly well. It is very important, however, to use the individual SEC calibrations instead of those for PEG.

The separation efficiency of SEC can be enhanced by a recycling technique: when the valve between the columns (Fig. 1) is switched three times during a chromatographic run, the sample has to pass ten column volumes instead of four, and the chromatogram of an octyl-(EO)$_5$ (from Fig. 4) now shows much better resolution (the

TABLE IV

MOLECULAR MASS AVERAGES OF A 1-TETRADECYL-(EO)$_n$ OBTAINED WITH TWO DIFFERENT SEC CALIBRATIONS (PEG AND TETRADECYL-PEO)

Correction of response factors using slope K or mass fraction of alkanol (m_A).

Parameter	Calibration					
	PEG			Tetradecyl-PEO		
	No correction	Slope	m_A	No correction	Slope	m_A
M_w	273	295	288	277	294	290
M_n	246	263	257	257	269	266
M_w/M_n	1.107	1.123	1.122	1.078	1.094	1.092

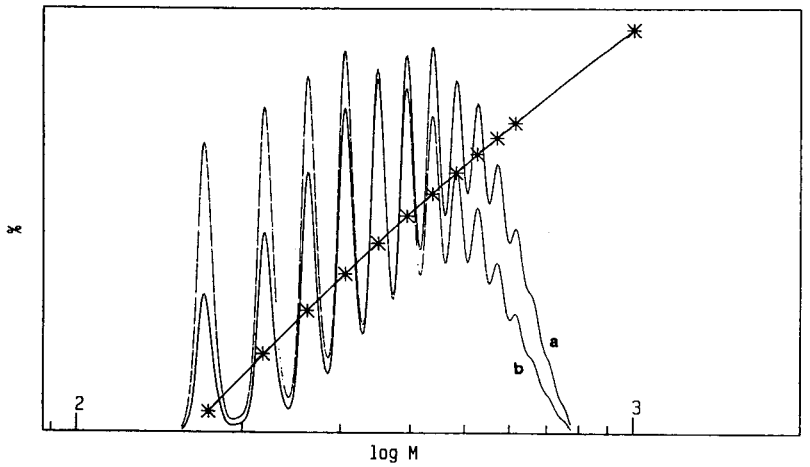

Fig. 9. MWD of the ethoxylated octanol (Fig. 4), as obtained with recycling (three switches of valve, Fig. 1), with density detection. Compensation for molecular mass dependence of response factors using the slopes (eqn. 4). a = Mass distribution; b = number distribution; *——* = calibration.

unreacted alkanol has been cut off in this separation). In Fig. 9, the MWD calculated therefrom using the slope is shown.

CONCLUSIONS

The problem of the quantitative characterization of FAE can be solved by separating the homologous series using CC (on a semi-preparative scale) as the first dimension [44] and analysing the separated homologous series in the second dimension using SEC with dual detection. The quantification of the first dimension will be described in Part II of this series [45].

ACKNOWLEDGEMENT

Financial support by the Austrian Science Foundation (Project 8253 CHE) is gratefully acknowledged.

REFERENCES

1 M. Bischoff, U. Zeidler and H. Baumann, *Fette Seifen Anstrichm.*, 79 (1977) 131.
2 H. Baumann, *GIT Fachz. Lab.*, 9 (1991) 957.
3 H.J. Richter and J. Knaut, *Parfüm. Kosmet.*, 70 (1990) 4.
4 M.F. Cox, *J. Am. Oil Chem. Soc.*, 66 (1989) 367.
5 F.E. Bailey, Jr., and J.V. Koleske (Editors), *Alkylene Oxides and Their Polymers* (*Surfactant Science Series*, Vol. 35), Marcel Dekker, New York, 1991.
6 L. Favretto and B. Stancher, *J. Chromatogr.*, 108 (1975) 183.
7 B. Stancher, L. Favretto Gabrielli and L. Favretto, *J. Chromatogr.*, 111 (1975) 459.
8 G. Czichocki, W. Gerhardt and D. Blumberg, *Tenside Surfact. Deterg.*, 25 (1988) 169.
9 H. Brüschweiler, *Mitt. Geb. Lebensmittelunters. Hyg.*, 68 (1977) 46.
10 R.H. Schreuder, A. Martijn, H. Poppe and J.C. Kraak, *J. Chromatogr.*, 368 (1986) 339.
11 M. Coupkova, K. Janes, J. Sanitrak and J. Coupek, *J. Chromatogr.*, 160 (1978) 73.
12 H. König, R. Ryschka and W. Strobel, *Fresenius' Z. Anal. Chem.*, 312 (1985) 263.
13 B. Steinbrech, D. Neugebaurer and G. Zulauf, *Fresenius' Z. Anal. Chem.*, 324 (1986) 154.
14 H. König and W. Strobel, *Fresenius' Z. Anal. Chem.*, 331 (1988) 435.
15 P.L. Desbene, B. Desmazieres, J.J. Basselier and A. Desbene-Monvernay, *J. Chromatogr.*, 465 (1989) 69.
16 Y. Mengerink, H.C.J. de Man and Sj. van der Wal, *J. Chromatogr.*, 552 (1991) 593.
17 M. Kudoh, *J. Chromatogr.*, 291 (1984) 327.
18 R.E.A. Escott and N. Mortimer, *J. Chromatogr.*, 553 (1991) 423.
19 A. Silver and H. Kalinoski, *J. Am. Oil Chem. Soc.*, 69 (1992) 599.
20 W. Heitz, B. Bohmer and H. Ullner, *Makromol. Chem.*, 121 (1969) 102.
21 B.G. Belenkii, E.S. Gankina, M.B. Tennikov and L.Z. Vilenchik, *J. Chromatogr.*, 147 (1978) 99.
22 A.V. Gorshkov, H. Much, H. Becker, H. Pasch, V.V. Evreinov and S.G. Entelis, *J. Chromatogr.*, 523 (1990) 91.
23 G. Schulz, H. Much, H. Krüger and C. Wehrstedt, *J. Liq. Chromatogr.*, 13 (1990) 1745.

24 H. Pasch, H. Krüger, H. Much and U. Just, *J. Chromatogr.*, 589 (1992) 295.
25 B. Trathnigg and Ch. Jorde, *J. Chromatogr.*, 385 (1987) 17.
26 B. Trathnigg, Ch. Jorde and B. Maier, *Chromatogr. Anal.*, (1989) 13.
27 B. Trathnigg, *GIT Fachz. Lab.*, 35 (1991) 35.
28 W. Beithan, H. Bernasch and W. Gerhardt, *Tenside Deterg.*, 19 (1982) 206.
29 W. Gerhardt and H.-R. Holzbauer, *Tenside Deterg.*, 12 (1975) 313.
30 W. Gerhardt and H.-R. Holzbauer, *Tenside Deterg.*, 14 (1977) 116.
31 H.-R. Holzbauer, A. Greiner and M. Herbst, *Tenside Deterg.*, 20 (1986) 30.
32 A.I. Hopia and V.M. Ollilainen, *J. Liq. Chromatogr.*, 16 (1993) 2469.
33 F. Candau, J. Francois and H. Benoit, *Polymer*, 15 (1974) 626.
34 G.V. Schulz and M. Hoffmann, *Makromol. Chem.*, 23 (1957) 220.
35 Y. Kobataka and H. Inagaki, *Makromol. Chem.*, 40 (1960) 118.
36 J. Francois, F. Candau and H. Benoit, *Polymer* 15 (1974) 618.
37 R. Cheng and X. Yan Xiaohu, *Acta Polym. Sin.*, 12 (1989) 647.
38 I. Géczy, *Tenside Deterg.*, 9 (1972) 117.
39 I. Géczy, *Acta Chim. Acad. Sci. Hung.*, 79 (1973) 133.
40 B. Trathnigg and X. Yan, *J. Appl. Polym. Sci., Appl. Polym. Symp.*, 52 (1993) in press.
41 J.R. Craven, H. Tyrer, S. Pok Lai Li and C. Booth, *J. Chromatogr.*, 387 (1987) 233.
42 B. Trathnigg, *J. Liq. Chromatogr.*, 13 (1990) 1731.
43 B. Trathnigg, *J. Chromatogr.*, 552 (1991) 507.
44 B. Trathnigg, D. Thamer, X. Yan and S. Kinugasa, *J. Liq. Chromatogr.*, 16 (1993) 2439.
45 B. Trathnigg, D. Thamer and X. Yan, *J. Chromatogr.*, in press.

Journal of Chromatography A, 657 (1993) 377–385
Elsevier Science Publishers B.V., Amsterdam

CHROM. 25 552

Size-exclusion chromatography of poly(ethylene terephthalate) and related polymers in methylene chloride–dichloroacetic acid

T.H. Mourey*, T.G. Bryan and J. Greener

Analytical Technology Division, Manufacturing Research and Engineering Organization B-82, Eastman Kodak Company, Rochester, NY 14650-2136 (USA)

(First received June 30th, 1993; revised manuscript received September 8th, 1993)

ABSTRACT

A solvent mixture of methylene chloride–dichloroacetic acid (DCAA) (80:20, v/v) containing 0.01 *M* tetrabutylammonium acetate is evaluated as an eluent for room temperature (30°C) size-exclusion chromatography of poly(ethylene terephthalate) (PET). Samples dissolve in less than 1 h at 70°C in 1:2 (v/v) methylene chloride–DCAA and can then be diluted at room temperature to 80% methylene chloride without polymer phase separation. There is no significant degradation of PET during sample preparation, provided the dissolution temperature is lower than 80°C and the water concentration is less than 1%. Accurate absolute molecular mass distributions are obtained using light-scattering detection with a coefficient of variation for weight-average molecular masses of *ca.* ± 2.5%.

INTRODUCTION

Several eluents have been used for size-exclusion chromatography (SEC) of poly(ethylene terephthalate) (PET). The first examples used *m*-cresol at 125–130°C [1,2], although it was later recognized that PET degrades under these conditions. More recently, *o*-chlorophenol at elevated temperatures has been successfully used as a single-component eluent [3]. Mixed eluents such as *o*-chlorophenol–chloroform [4,5], 1,1,2,2-tetrachloroethane–nitrobenzene [6] and 1,1,2,2-tetrachloroethane–phenol [7] allowed room temperature SEC operation, although the samples required extended heating for dissolution and, in at least one method [6], hot filtration. Examples of room temperature dissolution and SEC operation were given by Drott [8], using 1,1,1,3,3,3-hexafluoroisopropanol (HFIP). Some of the problems associated with calibration standards (polystyrene is insoluble in HFIP) were recently addressed by Mori [9]. Dilution of HFIP with chlorinated hydrocarbons has been more recently developed to defray the high cost of HFIP. These eluents include methylene chloride–HFIP at the azeotropic composition of 71:29 [10,11], 98:2 chloroform–HFIP [12] and 90:10 (v/v) [13]. Semi-micro SEC in 1:1 HFIP–chloroform has been proposed [14] to minimize costs further.

All of the above eluents were developed for use with a concentration-sensitive detector (either refractive index or UV) and narrow standard calibration. Most rely on methods that use Mark–Houwink constants to calculate absolute molecular mass distributions. However, constants may not be available for variants of PET, either linear or branched, or for structurally different crystalline polyesters. Absolute molecular mass distributions for these materials can be measured by SEC with molecular-mass-sensitive

* Corresponding author.

0021-9673/93/$06.00
SSDI 0021-9673(93)E0973-X

detection, such as viscometry with universal calibration or light-scattering. To date, we are aware of only one solvent system, HFIP–pentafluorophenol, that has been used with a molecular-mass-sensitive detector (low-angle laser light-scattering, LALLS) [15]. This eluent provides excellent contrast for light-scattering measurements and it is a room temperature solvent for PET samples. Unfortunately, it is quite expensive.

The limited number of applications of either light-scattering or viscometry detection to PET analysis can be partially attributed to the requirements placed by these detector systems on the SEC eluent. For example, viscometry detection is extremely difficult with the 71:29 methylene chloride–HFIP azeotrope because the low-boiling mixture (b.p. 38°C) forms bubbles in the viscometer and is difficult to pump without cavitation. Phenolic solvents are not good candidates for light-scattering detection because their refractive indices are too close to that of PET. They may also cause degradation of styrene-based SEC columns [3], which may cause particle shedding that is unacceptable for both light-scattering and viscometry detectors. Reproducible retention volumes of standards and samples has been raised as a concern for mixed solvents such as HFIP–chloroform [3], particularly for marginally soluble standards such as polystyrene. This may have a larger effect on results obtained from methods that use calibration curves (*e.g.*, viscometry detection using universal calibration) than for light-scattering. In addition, the refractive indices of these solvents differ greatly, which can lead to complications for light-scattering detection such as preferential solvation.

All of the eluents have their advantages and disadvantages. In many instances, the choice of one eluent over another may be driven by resources and requirements of a specific laboratory, *i.e.*, cost, safety, availability of light-scattering or viscometry detection, or routine *vs.* non-routine analysis. In our case, none of the eluents met all of the criteria for multidetector SEC, of which one of the detectors is molecular-mass-sensitive. These criteria are: no degradation of PET, column stability, room temperature operation, compatibility with differential refractive index (DRI) and UV spectrophotometric detection, compatibility with either light-scattering or viscometry detection, regular PET dilute solution properties (no aggregation), comparative safety and relative low cost. This has led us to investigate the properties of an alternative solvent for PET: dichloroacetic acid (DCAA). Recently, patents have issued on the use of DCAA as a sample solvent for SEC of aromatic polyesters [16] and as an SEC eluent for poly(aryl sulfones) [17]. Previous investigations of the viscosity behavior of PET in DCAA indicate that it is a good solvent for the polymer and that it does not significantly degrade PET below 80°C [18,19]. However, it is a relatively strong organic acid that can produce severe skin burns, is toxic, and can be corrosive to stainless steel. One compromise is to dilute DCAA with a common HPLC solvent of similar refractive index such that the mixture fulfils most or all of the requirements above. For this, DCAA is diluted with methylene chloride and evaluated for use as an eluent for SEC with molecular-mass-sensitive detectors.

EXPERIMENTAL

Sample preparation

PET samples were synthesized at Eastman Chemical Company (Kingsport, TN, USA). PET 39K was obtained from American Polymer Standards (Mentor, OH, USA). Typically, 25 mg of polyester sample and 3 ml of methylene chloride (J.T. Baker, HPLC grade)–DCAA (Eastman Laboratory Chemicals) (1:2, v/v) were heated for 1 h at 75°C in a sealed 10 ml volumetric flask. The volumetric flask was cooled and diluted to the mark with methylene chloride containing 0.0143 *M* tetrabutylammonium acetate (TBAA, Aldrich) to give a final concentration of quaternary ammonium salt of 0.01 *M*. A flow marker, 1-chloro-2,4-dinitrobenzene, was added at a concentration of 0.01% to each sample.

Size-exclusion chromatography

The eluent was prepared at a volumetric ratio of methylene chloride–DCAA (80:20, v/v), containing 0.01 *M* TBAA. The eluent was continuously sparged with a light stream of helium. The

nominal flow rate was 1.0 ml/min, and samples were injected in a volume of 100 μl. Three Polymer Labs. (Amherst, MA, USA) Mixed-B columns were converted from THF to methylene chloride and finally to methylene chloride–DCAA (80:20) containing 0.01 *M* TBAA at 0.5 ml/min. In order and plumbed in series after the columns were a Spectroflow 757 UV detector, an LDC Analytical KMX-6 low-angle laser light-scattering (LALLS) photometer, and a Waters Model 410 DRI detector. The SEC columns and DRI detector were thermostated to 30.0°C. The UV and LALLS detectors were operated at room-temperature. All light-scattering intensities were measured at 6–7° with an aperture of 0.15 mm.

Preliminary experiments were also conducted using a Viscotek Model 100 differential viscometry (DV) detector, connected after the UV detector and in a parallel configuration with the DRI detector. The concentration dependence of viscosity was measured at 30.0°C in a glass Ubbelohde capillary viscometer. Efflux times were long enough to ignore kinetic energy corrections.

RESULTS AND DISCUSSION

Dissolution and solution properties

PET pellets dissolve in approximately 30 min in 1:2 methylene chloride–DCAA at 70°C, depending on the molecular mass of the sample and the size of the pellet. Pulverized or crushed samples dissolve in as little as 10 min. PET samples can be diluted to 95:5 methylene chloride–DCAA containing 0.01 *M* TBAA at room temperature without polymer phase separation. A solvent mixture consisting of methylene chloride–DCAA (80:20) is a general-purpose eluent for most samples, including solid-stated PET and highly crystalline copolymers. Plots of inherent and reduced viscosities of a solid-stated PET (sample 10388) in methylene chloride–DCAA (80:20) indicated regular dilution behavior that is described by the Huggins–Kraemer equations, and an intrinsic viscosity $[\eta] = 0.882$ dl/g at 30°C. The difference in slopes of the Huggins and Kraemer plots, $k' - k'' = 0.475$ is within experimental error of the predicted value of 0.5.

Chromatography

Chromatograms obtained without TBAA added to the eluent exhibit two kinds of artifacts, neither of which is reproducible. A high-molecular-mass shoulder may appear and/or a high-molecular-mass prepeak. Both artifacts disappear completely upon addition of the quaternary ammonium salt to the eluent (Fig. 1). Preliminary investigations indicate that the TBAA breaks up PET molecular aggregates and also eliminates interactions of PET with the SEC columns. Similar results have been obtained from the addition of lithium bromide to N,N-dimethylformamide [20–23] and sodium trifluoroacetate (NAFAT) to HFIP [8]. As with NAFAT in HFIP, there are no differences in the polymer portion of chromatograms at salt concentrations between 0.01 *M* and 0.1 *M* TBAA in methylene chloride–DCAA (80:20). The tetrabutylammonium salt is used because it can be conveniently added to samples as a solution in pure methylene chloride. Tetramethyl- and tetraethylammonium acetates also eliminate prepeaks and shoulders, but they are marginally soluble in pure methylene chloride and must be added as solids to the methylene chloride–DCAA (80:20) sample solvent. It has also been observed that oxidative quaternary ammonium counterions such as nitrate and bromide can cause degradation of polystyrene samples and will cause discoloration of the methylene chloride–DCAA eluent. A peak from the quaternary ammonium

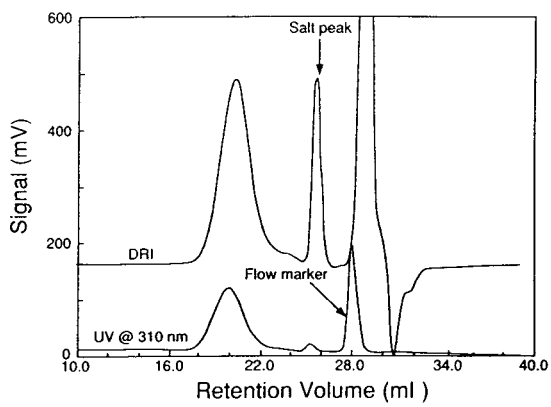

Fig. 1. UV and DRI chromatograms of PET 10388 in methylene chloride–DCAA (80:20) containing 0.01 *M* TBAA.

salt appears in the DRI chromatogram, which has implications for the calculation of the specific refractive index increment of samples (see below).

Stable baselines and reproducible PET chromatograms are obtained for both DRI and UV detection at 310 nm. The eluent absorbs ultraviolet radiation too strongly to be used at wavelengths shorter than 310 nm. Polystyrene is readily soluble in the eluent at room temperature and is detectable by DRI but not UV at 310 nm.

PET degradation

Sample preparation and analysis conditions that contribute to the degradation of PET are evaluated from normalized SEC chromatograms. Each height, $W(v)$, of a concentration detector chromatogram is divided by the total area under the chromatogram:

$$W_N(v) = \frac{W(v)}{\int_0^\infty W(v)\,dv} \quad (1)$$

Normalized chromatograms all have an area of unity, which makes them useful for comparisons.

Normalized UV chromatograms of PET injected 15 min, 24 h and 4 days after final dissolution and dilution of the sample are shown in Fig. 2. No significant differences are observed until day 4, at which time there is a minor shift in the molecular mass distribution and an increase

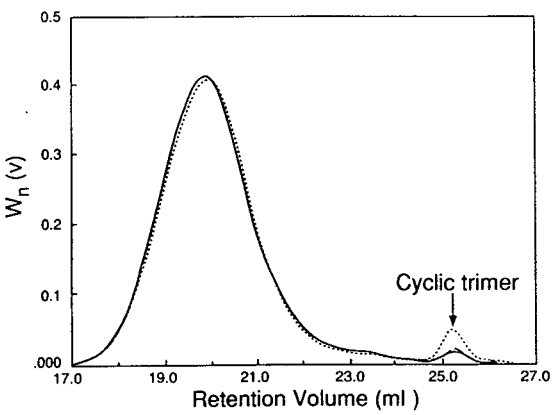

Fig. 2. Normalized UV chromatograms of PET 10388 exposed to eluent after 1 h of dissolution at 70°C. Solid = 0.25 h, dashed = 24 h, dotted = 96 h.

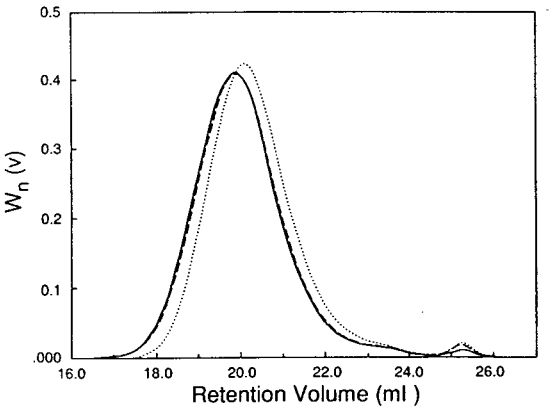

Fig. 3. Normalized UV chromatograms of PET 10388 after 1 h of dissolution at various temperatures. Solid = 70°C, dashed = 80°C, dotted = 105°C.

in cyclic trimer (peak at 25.2 ml). Normalized chromatograms of PET using sample dissolution temperatures of 70, 80 and 105°C are shown in Fig. 3. Identical chromatograms are obtained at 70 and 80°C, while a significant increase in retention time is observed at the 105°C dissolution temperature. This is consistent with the results of Tuzar *et al.* [19], who showed that PET was stable in pure DCAA at temperatures up to 80°C. Dissolution times between 0.75 and 4 h at 70°C have only minor effects on the PET size distribution. Unpublished data also indicate that some PET degradation may be expected in pure DCAA for water concentrations greater than 1.0% [24]. Chromatograms at 0.016, 1.016 and 4.016% (v/v) water concentration in the dissolution solvent confirm that degradation indeed occurs at high water concentrations (Fig. 4). No significant changes in chromatograms are observed for water concentrations in the dissolution solvent of less than 0.5%, which is considerably more than the water concentration of the eluent (0.016%) or pure DCAA (0.076%) measured by Karl Fisher titration.

In all cases, degradation of PET is recognized as a shift in the chromatogram to longer retention volumes and an increase in the concentration of cyclic trimer. This is consistent with ester interchange and hydrolysis, which in dilute solution results in an increase in cyclic trimer content [25–27].

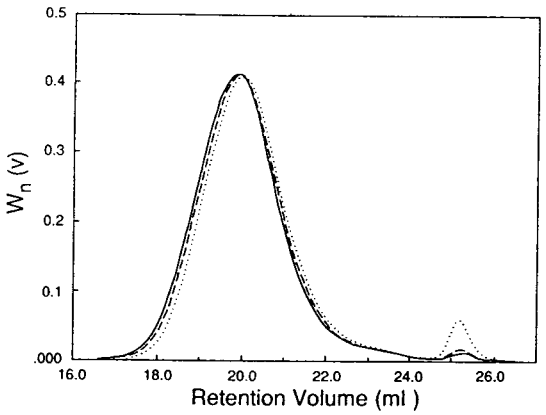

Fig. 4. Normalized UV chromatograms of PET 10388 after 1 h of dissolution at 70°C for increasing concentrations of water in the dissolution solvent. Solid = 0.016% water, dashed = 1.016%, dotted = 4.016%.

The effects of sample preparation and eluent conditions on the weight-average molecular mass ($\bar{M}_w$) of PET measured by LALLS are summarized in Table I. No significant degradation in molecular mass is observed within the following conditions: water concentrations in the dissolution solvent less than 0.5%, dissolution temperatures less than 80°C, dissolution times less than 2 h, and injection of the sample into the chromatograph less than 4 days after preparation. All of these conditions can readily be met using the procedure described in the EXPERIMENTAL section.

A comparison of the elution behavior of both PET (Fig. 5) and polystyrene (Fig. 6) at eluent compositions of methylene chloride–DCAA (80:20) and (90:10) (both containing 0.01 *M* TBAA) address the concern of reproducible retention volumes with mixed eluents. PET retention volumes increase slightly with increasing methylene chloride concentration, while polystyrene retention volumes decrease. This implies expansion of polystyrene and contraction of PET in the 90:10 methylene chloride–DCAA eluent. These shifts are consistent with the solvation of polystyrene and PET by the individual solvent components: methylene chloride is a better solvent than DCAA for polystyrene, and DCAA is a better solvent than methylene chloride for PET. The sensitivity of elution volumes to the composition of the eluent is relatively small, fortunately, and the reproducibility of chromatograms is similar to that observed in single-component solvents.

TABLE I

PET DEGRADATION STUDY

	$\bar{M}_w$
Sample preparation % water (v/v) [a]	
0.016	72 000 [b]
0.516	71 700 [b]
1.016	65 800 [b]
2.016	63 400 [b]
4.016	59 400 [b]
Sample preparation time at 70°C (h)	
0.75	70 800
1	72 000
2	71 200
3	69 400
4	68 900
Time in eluent (h)[a]	
0.25	71 600
24	71 800
96	70 000
Sample preparation temperature (°C)[c]	
60	72 000
70	72 600
85	72 800
105	57 000

[a] Samples dissolved by heating at 70°C for 1 h.
[b] Weight-average molecular masses measured by LALLS, S.D. ± 2.5%.
[c] Dissolution time 1 h.

Molecular-mass-sensitive detection: viscometry

Sudden changes in system pressure have deleterious effects on the baseline stability and calibration of viscometry detectors. Pressure changes can arise from leaks, pump failure, and bubble formation before and in the viscometry detector. The methylene chloride–DCAA eluent is prone to all of these: it is difficult to prevent bubble formation in the viscometer at room

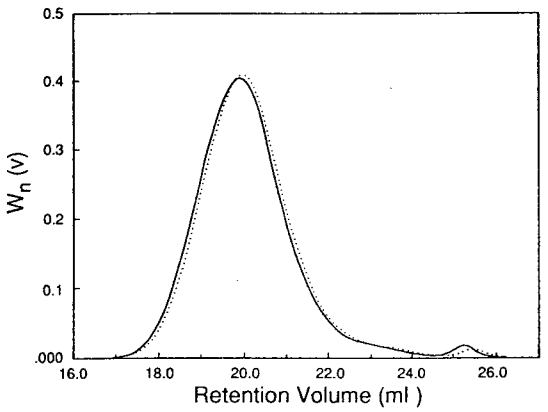

Fig. 5. Normalized UV chromatograms of PET 10388 in methylene chloride–DCAA (80:20) (solid) and methylene chloride–DCAA (90:10) (dotted). Both eluents contain 0.01 *M* TBAA.

temperature because of the low boiling point of methylene chloride, and the eluent occasionally cavitates in the pump heads, again because of its low boiling point. Also, DCAA tends to cause leaks around old stainless steel fittings, of which there are many in viscometry detectors. Passivation of stainless steel fittings with 6 *M* nitric acid minimizes this problem but does not completely eliminate it. From a practical standpoint, viscometry detection is only marginally viable with this eluent. Only relationships between viscosity and molecular mass (measured by DV detection) are presented, since they have some practical utility in the routine calculation of absolute molecular masses using only a concentration-sensitive detector. For polystyrene in methylene chloride–DCAA (80:20) containing 0.01 *M* TBAA at 30°C, and $[\eta]$ in units of dl/g,

$$[\eta] = 0.00014M^{0.70} \tag{2}$$

and for PET,

$$[\eta] = 0.00045M^{0.68} \tag{3}$$

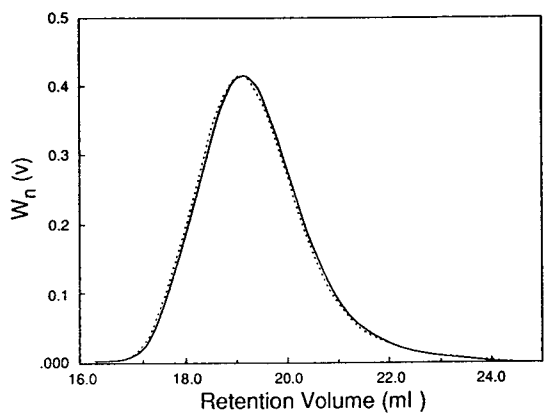

Fig. 6. Normalized chromatograms of NBS 706 in methylene chloride–DCAA (80:20) (solid) and methylene chloride–DCAA (90:10) (dotted).

Molecular-mass-sensitive detection: light-scattering

The refractive indices of methylene chloride and DCAA are 1.46 and 1.42, respectively. The refractive index of the 80:20 mixture ($n = 1.43$) is low enough to provide sufficient contrast for DRI and light-scattering detection of PET. In addition, the refractive indices of methylene chloride and DCAA are close to one another, which greatly improves DRI baseline stability. Light-scattering detection involves simpler plumbing than viscometry detection, which minimizes the problems of leaks described above. In the case of LALLS, the weight-average molecular mass at each elution slice of the SEC chromatogram, $M_{w,i}$, is obtained from the excess Rayleigh scattering at each slice, $R_{\theta,i}$,

$$\frac{Kc_i}{R_{\theta,i}} = \frac{1}{M_{w,i}P(\theta)} + 2A_2c_i + 3A_3c_i^2 + \ldots \tag{4}$$

where K is the optical constant. At the low concentrations of SEC, the concentration terms of the virial expression are negligible and at small angles the particle function $P(\theta) \sim 1.0$, thereby simplifying the calculation of $M_{w,i}$ to

$$M_{w,i} \approx \frac{R_{\theta,i}}{Kc_i} \tag{5}$$

The whole polymer $\bar{M}_w$ can be obtained from the LALLS chromatogram alone,

$$\bar{M}_w = \frac{1}{Km}\sum R_{\theta,i}\,\Delta v_i \tag{6}$$

where m is the total sample mass injected and Δv_i is the volume between adjacent data points. The parameters needed are contained in the optical constant K,

$$K = \frac{2\pi^2 n^2 (\mathrm{d}n/\mathrm{d}c)_\mu^2 (1 + \cos^2\theta)}{\lambda_0^4 N_A} \quad (7)$$

where n is the solvent refractive index, λ_0 is the wavelength of light in vacuum (632.8 nm), N_A is Avogadro's number, and $(\mathrm{d}n/\mathrm{d}c)_\mu$ is the specific refractive index increment at constant chemical potential. Only $(\mathrm{d}n/\mathrm{d}c)_\mu$ is unknown for polymer samples, but it can be measured from the multidetector SEC experiment.

Specific refractive index increment

The measurement of the specific refractive index increment in solvent mixtures at constant chemical composition, $(\mathrm{d}n/\mathrm{d}c)_c$, can lead to erroneous results if the solvents differ in refractive index and if one of the solvent components preferentially solvates the polymer. Although the refractive indices of DCAA and methylene chloride are similar, these solvents are not isorefractive and some concern must be raised about the static measurement of $(\mathrm{d}n/\mathrm{d}c)_c$ at constant chemical composition. Berkowitz [28] showed that SEC using a DRI detector can be used to measure the specific refractive index increment at constant chemical potential, $(\mathrm{d}n/\mathrm{d}c)_\mu$. Elution from the SEC column results in an exchange of solvent equivalent to exhaustive dialysis of the polymer solution. From this, the value of $(\mathrm{d}n/\mathrm{d}c)_\mu$ for a polymer of known molecular mass is determined from the LALLS response [28] for $\cos^2\theta \approx 1$.

$$(\mathrm{d}n/\mathrm{d}c)_\mu = \left[\frac{\lambda_0^4 N_A \sum R_{\theta,i}\,\Delta v_i}{4\pi^2 n^2 \bar{M}_w m}\right]^{1/2} \quad (8)$$

A value of 0.155 is obtained for polystyrene at 632.8 nm is obtained. A response factor for the DRI detector is obtained from the polystyrene chromatogram area, A_{ps}, mass injected, m, and $(\mathrm{d}n/\mathrm{d}c)_{\mu,ps} = 0.155$,

$$k_{dri} = \frac{A_{ps}}{m_{ps}} (\mathrm{d}n/\mathrm{d}c)_{\mu,ps} \quad (9)$$

which is then used to calculate refractive index increments at constant chemical potential of polyester samples, $(\mathrm{d}n/\mathrm{d}c)_{\mu,pe}$, from their SEC peak areas,

$$(\mathrm{d}n/\mathrm{d}c)_{\mu,pe} = k_{dri} \frac{m_{pe}}{A_{pe}} \quad (10)$$

The salt peak at 25.9 ml in Fig. 3 is not included in the integration.

Although the DRI detector measurement is made at a different wavelength than that used by LALLS, this method approximates $(\mathrm{d}n/\mathrm{d}c)_{\mu,pe}$ to within a few percent provided the value of $(\mathrm{d}n/\mathrm{d}c)_{\mu,ps}$ at 632.8 nm (LALLS wavelength) is used in eqn. 9.

The measured value $(\mathrm{d}n/\mathrm{d}c)_\mu = 0.148$ at 632.8 nm for PET in this solvent is higher than the value reported for PET in pure DCAA [29] ($\mathrm{d}n/\mathrm{d}c = 0.106$ at 589 nm) by an amount that is consistent with the difference in refractive indices of pure DCAA and methylene chloride–DCAA (80:20). Measurement of $(\mathrm{d}n/\mathrm{d}c)_c$ at constant chemical composition in a KMX-16 differential refractometer for polystyrene = 0.156 indicates that preferential solvation actually does not seriously affect the measurement.

Absolute molecular mass distributions

Typical LALLS and UV chromatograms used for calculating molecular masses via eqn. 5 are shown in Fig. 7. The molecular mass distribution for a PET sample obtained from SEC-LALLS is shown in Fig. 8. The polydispersity ($\bar{M}_w/\bar{M}_n$) is considerably larger than 2.0 predicted for a most probable distribution. This is not uncommon in PET because of the presence of cyclic trimer (low-molecular-mass peak in Fig. 8). The dis-

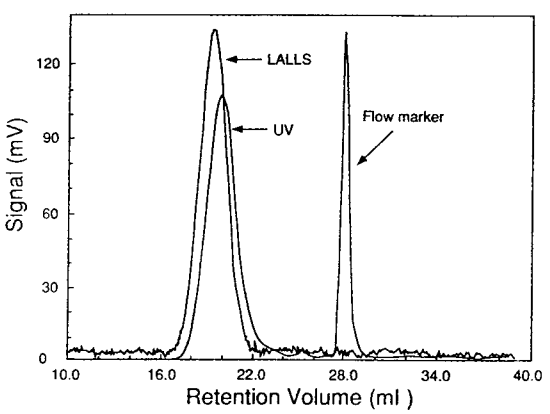

Fig. 7. UV and LALLS chromatograms of PET 10388.

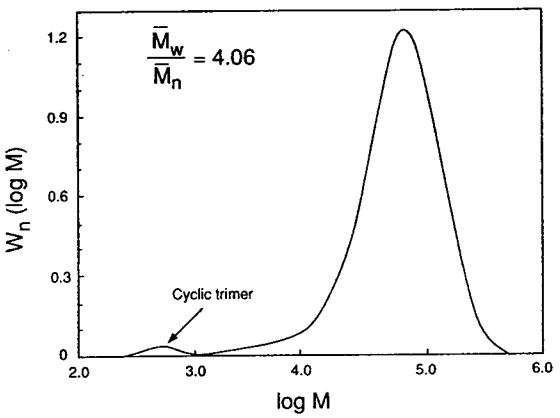

Fig. 8. Absolute molecular mass distribution of PET 10388, including cyclic trimer.

tribution obtained from excluding cyclic trimer gives the expected polydispersity for step-growth polymerization. The values for the whole polymer $\bar{M}_w$ calculated from integration of the LALLS response (eqn. 6) given in Table II are in excellent agreement with the true values (measured by light-scattering for PET 10388, 9902, 7352) and given by the vendor (PET 39K). The coefficient of variation of $\bar{M}_w$ ($\sim \pm 2.5\%$) is comparable to the precision reported for SEC-LALLS results for polystyrene in THF [30].

Application to other polyesters and polymers

This eluent has been successfully applied to the characterization of poly(ethylene 2,6-naphthalate) (PEN). PEN pellets dissolve in approximately 45 min and can be diluted to methylene chloride–DCAA (80:20, v/v) without immediate phase separation; however, some solutions form a gel at room temperature after 1–2 days and should be run within 16 h of sample preparation. The molecular mass dependence of intrinsic viscosity (units of dl/g) of PEN in methylene chloride–DCAA (80:20) at 30°C is

$$[\eta] = 0.00046M^{0.64} \quad (11)$$

From the DRI response and eqn. 9, PEN $(dn/dc)_\mu = 0.195$ at 632.8 nm. This large specific refractive index increment provides excellent LALLS response for samples of moderate ($\bar{M}_w = 40\,000$) molecular mass.

This eluent is also suitable for SEC with LALLS detection of other aromatic polyesters, both branched and linear, and readily dissolves oriented films. It also dissolves highly crystalline polycarbonates, but causes molecular mass degradation within 1–2 hours.

TABLE II

MEASURED AND CALCULATED VALUES FOR $\bar{M}_w$

Sample	Reported $\bar{M}_w$	$\bar{M}_w$ SEC-LALLS
PET 39K	39 000	36 100 ± 1000[a] (2.8%)[b]
PET 10388	69 400	72 000 ± 1800 (2.5%)
PET 9902	57 600	58 200 ± 1200 (2.1%)
PET 7352	47 200	49 700 ± 1300 (2.6%)

[a] Sample estimate of the standard deviation, s.
[b] Coefficient of variation, defined as $(s/\bar{M}_w) \times 100\%$.

CONCLUSIONS

The mixed solvent of methylene chloride–DCAA (80:20) containing 0.01 *M* TBAA has a number of desirable characteristics: it can be used at room temperature with both UV and DRI detectors, it is less expensive than eluents containing HFIP and pentafluorophenol, and degradation of PET is observed only after prolonged heating of samples at temperatures above 80°C or with water concentrations greater than 1% by volume. In addition, no loss of column efficiency and no increase in column back-pressure has been observed in nearly one year of continuous use. To its disadvantage, this eluent is difficult to use with the present design of differential capillary viscometer detectors. This disadvantage is offset by the compatibility of this eluent with light-scattering detection, which allows direct measurement of absolute molecular mass distributions.

ACKNOWLEDGEMENTS

Thanks are extended to James Cloyd and Carl Harris of Eastman Chemical Company for their comments and suggestions, and to Robert Guistina for his assistance with water analysis.

REFERENCES

1 G. Shaw, *Seventh International GPC Seminar Proceedings*, Monte Carlo, 1969, p. 309.
2 J.R. Overton, J. Rash and L.D. Moore, *Sixth International GPC Seminar Proceedings*, Miami Beach, FL, October 7–8, 1968, p. 422.
3 L. Martin, M. Lavine and S.T. Balke, *J. Liq. Chromatogr.*, 15 (1992) 1817.
4 S.A. Jabarin and D.C. Balduff, *J. Liq. Chromatogr.*, 5 (1982) 1825.
5 Ming-Min Sang, Nan-Ni Jin and Er-Fang Jiang, *J. Liq. Chromatogr.*, 5 (1982) 1665.
6 E.E. Pasche, B.A. Bidlingmeyer and J.G. Bergmann, *J. Polym. Sci., Polm. Chem. Ed.*, 15 (1977) 983.
7 C.V. Uglea, Aizicovici and S. Mihescu, *E. Polym. J.*, 21 (1985) 677.
8 E.E. Drott, in J. Cazes (Editor), *Liquid Chromatography of Polymers and Related Materials (Chromatographic Science Series, Vol. 8)*, Dekker, New York, 1976, p. 41.
9 S. Mori, *Anal. Chem.*, 61 (1989) 1321.
10 J.R. Overton and H.L. Browning, *Org. Coat. Appl. Polym. Sci. Proc.*, 48 (1983) 940.
11 J.R. Overton and H.L. Browning, in T. Provder (Editor), *Size Exclusion Chromatography (ACS Symp. Ser., Vol. 245)*, American Chemical Society, Washington, D.C., 1984, p. 219.
12 K. Weisskopf, *J. Polym. Sci.: Part A: Polym. Chem.*, 26 (1988) 1919.
13 N. Chikazumi, Y. Mukoyama and H. Sugitani, *J. Chromatogr.*, 479 (1989) 85.
14 K. Hibi, A. Wada and S. Mori, *Chromatographia*, 11 (1986) 635.
15 S. Berkowitz, *J. Appl. Polym. Sci.*, 29 (1984) 4353.
16 S. Ono, *Jpn. Kokai Tokkyo Koho JP 04 110,770*, April 13, 1992.
17 S. Ono, *Jpn. Kokai Tokkyo Koho JP 04 62,471*, February 27, 1992.
18 W.R. Moore and D. Sanderson, *Polymer*, 9 (1968) 153.
19 Z. Tuzar, V. Vošický and M. Bohdanecký, *Makromol. Chem.*, 180 (1979) 1399.
20 C.Y. Cha, *J. Polym. Sci. Part B*, 7 (1969) 343.
21 N.D. Hann, *J. Polym. Sci.*, 15 (1977) 1331.
22 P.L. Dubin, S. Koontz and K.L. Wright, III, *J. Polym. Sci.*, 15 (1977) 2047.
23 D.R. Scheuing, *J. Appl. Polym. Sci.*, 29 (1984) 2819.
24 B.W. Oliver, Jr., Eastman Chemical Company (Kingsport, TN), 1970, unpublished data.
25 H.L. Browning, Jr. and J.R. Overton, *Polym. Prepr.*, 18 (1977) 237.
26 H. Jacobson and W.H. Stockmayer, *J. Chem. Phys.*, 87 (1965) 931.
27 H. Jacobson, C.D. Beckman and W.H. Stockmayer, *J. Chem. Phys.*, 18 (1950) 1607.
28 S.A. Berkowitz, *J. Liq. Chromatogr.*, 6 (1983) 1359.
29 S. Ohoya and T. Matsuo, *Chem. Expr. (Jpn)*, 4, (1989) 761.
30 T.H. Mourey, S.M. Miller and S.T. Balke, *J. Liq. Chromatogr.*, 13, (1990) 435.

Journal of Chromatography A, 657 (1993) 387–394
Elsevier Science Publishers B.V., Amsterdam

CHROM. 25 510

Gas chromatographic separation of the enantiomers of volatile fluoroether anesthetics using derivatized cyclodextrin stationary phases. Part I

Aroonsiri Shitangkoon, Daniel U. Staerk and Gyula Vigh*

Department of Chemistry, Texas A & M University, College Station, TX 77843-3255 (USA)

(Received July 26th, 1993)

ABSTRACT

The capacity factors and chiral selectivity factors were determined as a function of temperature for the enantiomers of desflurane, enflurane and isoflurane on nine commercially available cyclodextrin derivative-coated GC capillary columns. The enantiomers could be separated with the trifluoroacetylcyclodextrin stationary phases which show good chiral selectivities coupled with modest column efficiencies. Very rapid enantiomeric trace determinations of desflurane, isoflurane and enflurane could be achieved with a trifluoroacetyl γ-cylodextrin-coated capillary column.

1. INTRODUCTION

Inhalational anesthetics are used to induce and maintain general anesthesia [1]. Several volatile compounds show anesthetic potential, including cyclopropane, nitrous oxide, halogenated hydrocarbons (*e.g.* chloroform, halothane) and ethers (*e.g.* diethyl ether and various fluoroethers). Although all of these have been used at one time or another in clinical practice, the fluoroether anesthetics are becoming favored owing to their potency, volatility, chemical stability, low toxicity and lack of flammability. The structures of the most commonly used fluoroether anesthetics (desflurane, enflurane and isoflurane) are shown in Fig. 1. Interestingly, they all are chiral compounds.

It has been commonly understood for some time that general anesthetics act on the nervous system by non-specific perturbation [2]. However, in line with the growing awareness of the biological activity differences of the enantiomerically pure drugs [3], stereoselective effects were recently observed when the interactions between the nerve ion channels and the pure enantiomers of isoflurane were studied [4]. Two recent patents suggest that the administration of the pure enantiomers of desflurane and isoflurane is more desirable than that of the racemic mixture [5,6]. Although most fluoroether anesthetics are synthesized as racemic mixtures [7], some progress has been made toward the synthesis of enantiomerically enriched materials [5,6]. Monitoring the enantiomeric purity of these materials therefore became extremely important. The recent, spectacular developments in the fields of chiral separations by capillary gas chromatography [8] allowed for the separation of the enantiomers of

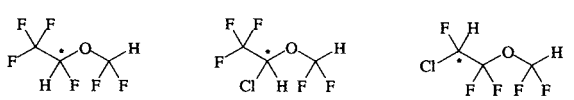

Fig. 1. Structures of desflurane, enflurane and isoflurane.

* Corresponding author.

0021-9673/93/$06.00
SSDI 0021-9673(93)E0913-F

isoflurane and enflurane on a 25-m capillary column coated with octakis(6-O-methyl-2,3-di-O-pentyl)-γ-cyclodextrin stationary phase [9].

This paper summarizes the results of a detailed investigation aimed at finding a single commercially available capillary column with sufficiently high chiral selectivity and separation efficiency that would permit the rapid separation of the enantiomers of the three fluoroether anesthetics: desflurane, enflurane and isoflurane. In order to try to elucidate possible correlations between chiral selectivity and the respective structures of the fluoroethers and the cyclodextrin-based stationary phases, the thermodynamic parameters of the enantiomers of all three anesthetics were also determined on all the stationary phases studied. The commercially available derivatized cyclodextrin-based stationary phases studied here included α-, β- and γ-dipentyl-, trifluoroacetyl- and permethyl-(*S*)-2-hydroxypropylcyclodextrins. Dipentylcyclodextrins (DAs) are synthesized [10] by treating a dimethyl sulfoxide solution of the respective cyclodextrin with excess amounts of 1-bromopentane in the presence of sodium hydroxide powder, resulting in a mixture of 2,6-di-O-pentylcyclodextrins. Permethyl-(*S*)-2-hydroxypropylcyclodextrins are then prepared by reacting the aqueous sodium hydroxide solution of the cyclodextrin with (*S*)-propylene oxide, followed by permethylation using an excess amount of methyl iodide [11]. Trifluoroacetylcyclodextrins are made by treating a solution of DAs in tetrahydrofuran with excess amounts of trifluoroacetic anhydride [12]. For most derivatized cyclodextrins, the products are mixtures of isomers and homologues [10–12].

EXPERIMENTAL

Separations were effected on a Hewlett-Packard HP 5890 series II gas chromatograph equipped with a cryostat, a septumless split/splitless injector (Microseal), a flame ionization detector and a Chemstation data collection/analysis unit. Fused-silica capillary columns (30m × 0.25mm I.D.), coated with different cyclodextrin-based stationary phases (0.25 μm film thickness) were obtained from Astec (Whippany, NJ, USA). Three types of cyclodextrin derivatives were studied: (i) DAs (commercial names ADA, BDA and GDA), (ii) permethyl-(*S*)-2-hydroxypropylcyclodextrins (PHs) (commercial names APH, BPH and GPH) and (iii) trifluoroacetylcyclodextrins (TAs) (commercial names ATA, BTA and GTA). The prefixes A, B, and G are used to describe the α-, β- and γ-cyclodextrins, respectively.

Hydrogen was used as the carrier gas at an average linear velocity of 0.5 m/s. Methane was used as an unretained compound. The injector and detector temperatures were maintained at 250°C. All separations were performed isothermally in the −10 to 70°C range as noted in the Results section. All inhalational fluoroether anesthetics were obtained from Anaquest (Murray Hill, NJ, USA), a division of BOC Health Care, and used without further purification. The anesthetics were injected either as *n*-pentane solutions or as air–vapor mixtures.

RESULTS AND DISCUSSION

All three fluoroether anesthetics have similar structures and possess an acidic proton at the chiral center. These acidic protons (the ^{1}H NMR chemical shift values are desflurane C*H*F δ = 5.925 ppm, isoflurane C*H*Cl δ = 6.031 ppm and enflurane C*H*FCl δ = 6.161 ppm) can interact with the suitable functional groups of the derivatized cyclodextrin stationary phases. Hydrogen bonding interactions and/or dipole–dipole interactions are probably the major polar interactions and might play a significant role in the chiral recognition process. Although the derivatized cyclodextrins are mixtures of isomers and homologues, and the thermodynamic parameters are average values representing a range of interactions between the solute and cyclodextrin stationary phases, it was nevertheless suggested [13] that they can be used to infer the processes which result in the eventual chiral separation of the enantiomers. Therefore, the capacity factor (k') and selectivity factor (α) values of the enantiomers of all three fluoroethers were determined as a function of temperature and analyzed as a function of the inverse absolute temperature to yield the enthalpy (ΔH^0) and entropy (ΔS^0) values according to

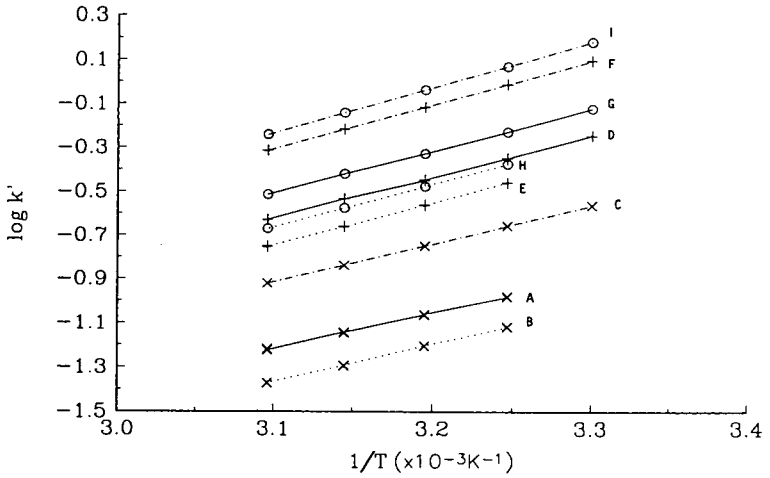

Fig. 2. Log k' *vs.* $1/T$ plots for the three fluoroethers obtained with the DA stationary phase series. A = desflurane–ADA; B = desflurane–BDA; C = desflurane–GDA; D = isoflurane–ADA; E = isoflurane–BDA; F = isoflurane–GDA; G = enflurane–ADA; H = enflurane–BDA; I = enflurane–GDA.

$$\log k' = -\frac{\Delta H^0}{2.3RT} + \frac{\Delta S^0}{2.3R} + \log \beta \qquad (1)$$

where β is the phase ratio and R is the universal gas constant. The log k' *vs.* $1/T$ plots for the more retained enantiomer of the three fluoroethers are shown in Figs. 2, 3 and 4 for the DA, PH and TA stationary phase series, respectively. The calculated enthalpy and entropy values are listed in Table I. All log k' *vs.* $1/T$ plots are linear, with the regression coefficients greater than 0.999. When the enantiomers can be separated, the corresponding $\Delta(\Delta H^0)$ and $\Delta(\Delta S^0)$ values can be calculated from the log α *vs.* $1/T$ plots as

$$\log \alpha = -\frac{\Delta(\Delta H^0)}{2.3RT} + \frac{\Delta(\Delta S^0)}{2.3R} \qquad (2)$$

The log α *vs.* $1/T$ plots for the three fluoroethers are shown in Fig. 5 for the TA stationary phase series, and the $\Delta(\Delta H^0)$ and $\Delta(\Delta S^0)$ values are listed in Table II. All log α *vs.* $1/T$ plots

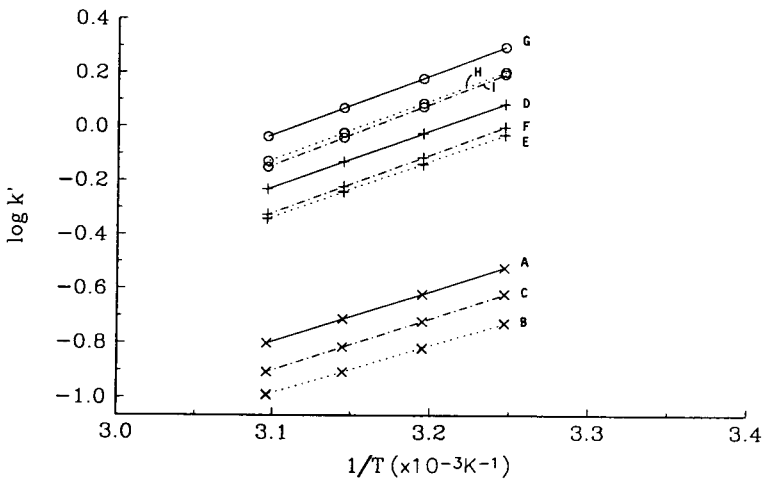

Fig. 3. Log k' *vs.* $1/T$ plots for the three fluoroethers obtained with the PH stationary phase series. A = desflurane–APH; B = desflurane–BPH; C = desflurane–GPH; D = isoflurane–APH; E = isoflurane–BPH; F = isoflurane–GPH; G = enflurane–APH; H = enflurane–BPH; I = enflurane–GPH.

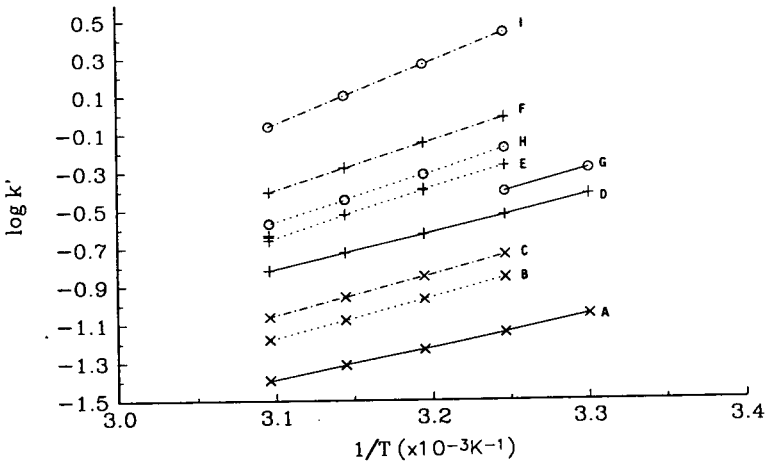

Fig. 4. Log k_2' *vs.* $1/T$ plots for the three fluoroethers obtained with the TA stationary phase series. A = desflurane–ATA; B = desflurane–BTA; C = desflurane–GTA; D = isoflurane–ATA; E = isoflurane–BTA; F = isoflurane–GTA; G = enflurane–ATA; H = enflurane–BTA; I = enflurane–GTA.

were linear with regression coefficients greater than 0.998, except for desflurane ($r^2 = 0.996$).

On the DAs, the enantiomers of the fluoroether anesthetics could not be separated. The ΔS^0 values of the different fluoroethers are the lowest on these stationary phases; they are very similar to each other with a very slight increase (about 1 entropy unit) in the order desflurane < isoflurane < enflurane. The ΔH^0 values of the different fluoroethers increase in the order desflurane < isoflurane < enflurane, following the boiling points of the fluoroethers (23.5, 48.5 and 56.5°C, respectively), and differ from each other by about 1200 cal/mol (1 cal = 4.14 J). When the ring size of the cyclodextrin is changed, the ΔH^0 values increase by about 200–300 cal/mol in the order $\alpha < \beta < \gamma$. However, the ΔS^0 values increase in the order $\alpha < \gamma < \beta$ for all three fluoroether solutes, indicating that the spatial arrangement of the active sites on the dipentyl-β-cyclodextrin is slightly more favorable for simultaneous multiple interactions.

The numerical values of ΔH^0 and ΔS^0 observed on the PHs are very similar to those observed on the DAs, indicating that the strength and specificity of the binding interac-

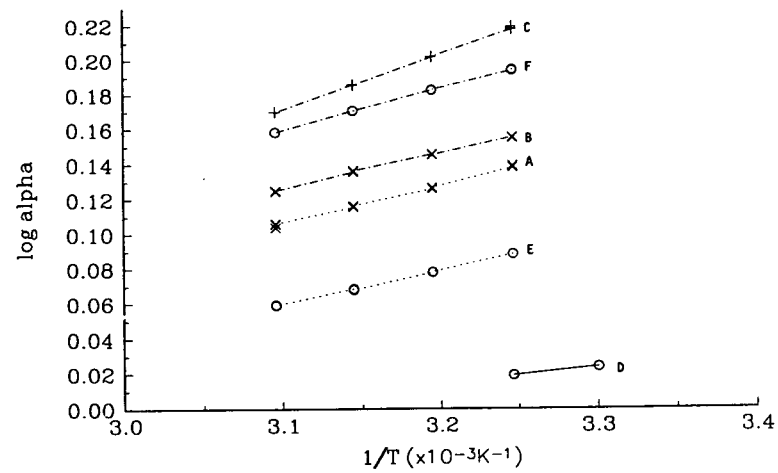

Fig. 5. Log α *vs.* $1/T$ plots for the three fluoroethers obtained with the TA stationary phase series. A = desflurane–BTA; B = desflurane–GTA; C = isoflurane–GTA; D = enflurane–ATA; E = enflurane–BTA; F = enflurane–GTA.

TABLE I

THERMODYNAMIC PARAMETERS FOR THE FLUOROETHERS CALCULATED FROM THE LOG k' *vs.* $1/T$ DATA SHOWN IN FIGS. 2–4

Phase	Desflurane		Isoflurane		Enflurane	
	ΔS^0 [cal/(mol · K)]	ΔH^0 (cal/mol)	ΔS^0 [cal/(mol · K)]	ΔH^0 (cal/mol)	ΔS^0 [cal/(mol · K)]	ΔH^0 (cal/mol)
ADA	−17.31	−7325.78	−18.27	−8514.34	−18.45	−8740.74
BDA	−19.41	−7787.91	−19.78	−8821.93	−19.73	−8923.71
GDA	−18.13	−8039.39	−18.91	−9186.77	−19.37	−9446.12
APH	−18.59	−8360.94	−19.73	−9568.32	−20.42	−10 207.93
BPH	−18.13	−7937.29	−19.69	−9395.60	−20.74	−10 052.97
GPH	−19.87	−8626.56	−20.97	−9825.79	−22.07	−10 447.42
ATA	−19.09	−7644.48	−20.10	−8819.87	−22.02	−9568.55
					−23.26	−9976.77
BTA	−22.30	−8839.96	−27.15	−11 362.59	−25.78	−10 943.74
	−24.91	−9841.49			−28.25	−11 828.34
GTA	−22.02	−8900.42	−23.21	−10 191.46	−33.05	−13 901.46
	−24.26	−9807.53	−26.92	−11 647.75	−35.66	−14 979.78

tions are very similar on both series. Both the ΔH^0 and the ΔS^0 values of the different fluoroethers increase in the order desflurane < isoflurane < enflurane, again following the boiling points. The increase is large from desflurane to isoflurane, but small from isoflurane to enflurane. When the ring size of the hydroxypropylcyclodextrins is changed, the order is $\beta < \alpha < \gamma$, different from those observed on the DAs.

The TAs are capable of chiral differentiation toward the enantiomers of the three fluoroethers, although the extent of this differentiation varies with both the type of the fluoroether and the ring size of the cyclodextrin. The enantiomers of enflurane can be separated on all three TA phases (ATA, BTA and GTA), those of desflurane on BTA and GTA, but those of isoflurane only on GTA. The interactions between the more retained enantiomers of the fluoroethers and the stationary phases (Table I) are much stronger for the TAs than for either the DAs or the PHs, and are mostly due to entropic effects (as indicated by the 2–10 entropy units increase in ΔS^0) and less to enthalpic effects (about 1.2–4 kcal/mol increase in ΔH^0). Both the ΔH^0 and the ΔS^0 values of enflurane increase with the size of the cyclodextrin ring.

The chiral selectivity factors of the fluoroethers (Fig. 5) increase with the increasing size of cyclodextrins: $\alpha < \beta < \gamma$. The $\Delta(\Delta H^0)$ and

TABLE II

THERMODYNAMIC PARAMETERS FOR THE FLUOROETHERS CALCULATED FROM THE LOG α *vs.* $1/T$ DATA SHOWN IN FIG. 5 FOR THE TA STATIONARY PHASE SERIES

Phase	Desflurane		Isoflurane		Enflurane	
	$\Delta(\Delta S^0)$ (cal/mol · K)	$\Delta(\Delta H^0)$ (cal/mol)	$\Delta(\Delta S^0)$ (cal/mol · K)	$\Delta(\Delta H^0)$ (cal/mol)	$\Delta(\Delta S^0)$ (cal/mol · K)	$\Delta(\Delta H^0)$ (cal/mol)
ATA					−1.24	−405.48
BTA	−2.61	−1001.53			−2.47	−884.60
GTA	−2.24	−907.11	−3.75	−1456.29	−2.61	−1078.27

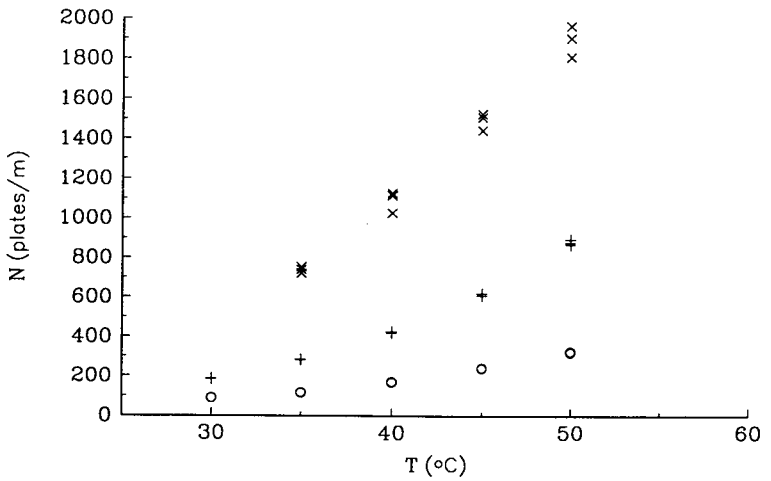

Fig. 6. Column efficiencies (plates/m) as a function of column temperature for the DA stationary phases, determined from the shape of the peak of the more retained enflurane enantiomer. + = ADA; × = BDA; ○ = GDA.

$\Delta(\Delta S^0)$ values increase regularly with the ring size of the cyclodextrin only for enflurane, which has an external stereogenic center (Fig. 1). For desflurane and isoflurane, both of which have internal stereogenic centers, there is no such clear trend: the $\Delta(\Delta H^0)$ and $\Delta(\Delta S^0)$ values for desflurane are highest on BTA and for isoflurane they are highest on GTA. Considering these trends and the fact that the molar volumes for all three solutes are similar, one cannot state that these separations are driven by an inclusion-type discrimination mechanism.

Fig. 6–8 show the column efficiencies (plates/m) for the DA, PH and TA phases, as determined from the shape of the peak of the more retained enflurane enantiomer. All three phases show a strong decrease in efficiency below 50°C. The PH columns are the least efficient and show

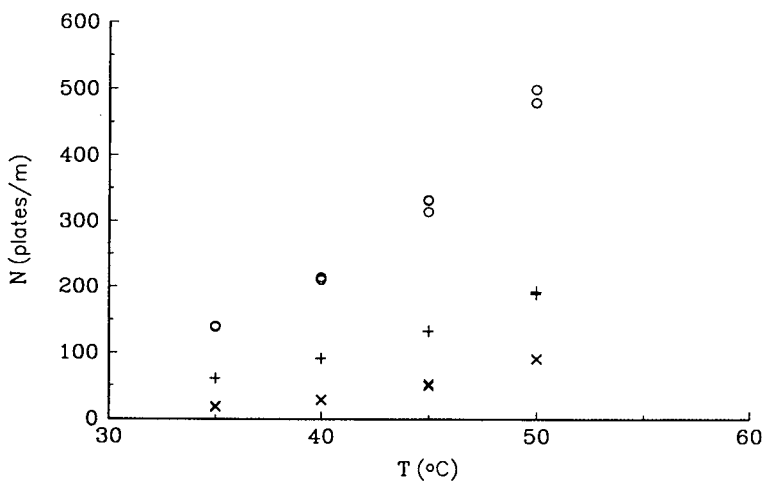

Fig. 7. Column efficiencies (plates/m) as a function of column temperature for the PH stationary phases, determined from the shape of the peak of the more retained enflurane enantiomer. + = APH; × = BPH; ○ = GPH.

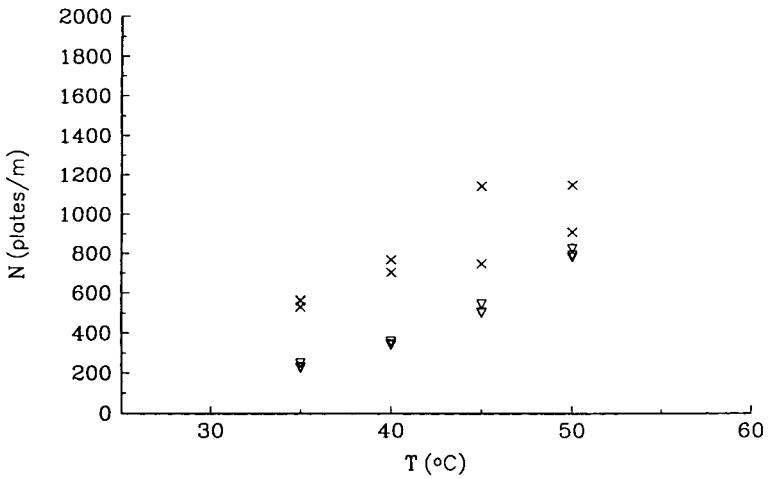

Fig. 8. Column efficiencies (plates/m) as a function of column temperature for the TA stationary phases, determined from the shape of the peak of the more retained enflurane enantiomer. × = BTA; ▽ = GTA.

no chiral selectivity for the fluoroethers; the DA columns are the most efficient, but lack chiral discrimination toward the fluoroethers. The TA columns have modest efficiencies, but their high chiral selectivities permit fast chiral separations for the fluoroethers.

From the selectivity and efficiency studies it can be concluded that the enantiomers of all three fluoroethers can be effectively separated on a single capillary, the GTA-coated column, as shown in Fig. 9. As the selectivity factors for isoflurane and enflurane are large and the capacity factors are small, good trace analyses can be performed very rapidly using short columns. The chromatograms of two enantiomerically almost pure isoflurane samples (99.97 and 98.38% enantiomeric excess, respectively, for the less retained and the more retained enantiomers) are shown in Figs. 10 and 11; the separations were obtained with a 15-m GTA column in less than 2 min.

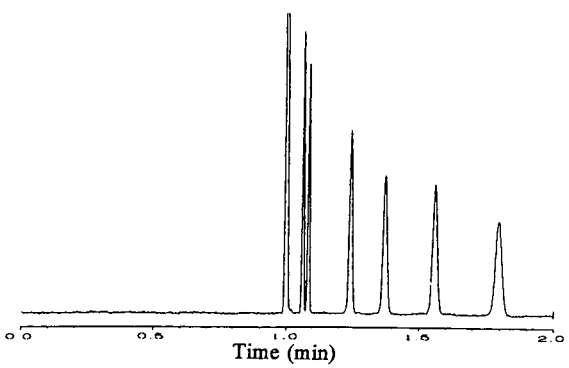

Fig. 9. Separation of the enantiomers of desflurane, isoflurane and enflurane on a 30 m × 0.25 mm I.D. fused-silica capillary, coated with a 0.25-μm thick film of GTA. Conditions: hydrogen carrier gas at a linear flow-rate of 0.5 m/s; 50°C isothermal run.

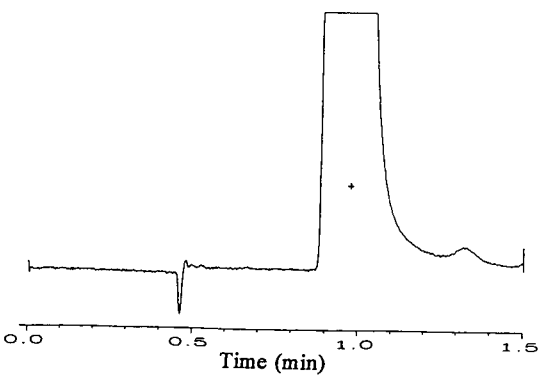

Fig. 10. Separation of the enantiomers of an enriched enflurane sample (99.95% enantiomeric excess for the less retained component) on a 15 m × 0.25 mm I.D. fused-silica capillary, coated with a 0.25-μm thick film of GTA. Conditions: hydrogen carrier gas at a linear flow-rate of 0.5 m/s; 35°C isothermal run.

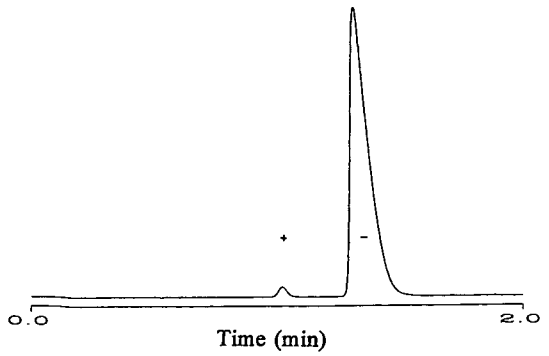

Fig. 11. Separation of the enantiomers of an enriched enflurane sample (96.82% enantiomeric excess for the more retained component) on a 15 m × 0.25 mm I.D. fused-silica capillary, coated with a 0.25-μm thick film of GTA. Conditions: hydrogen carrier gas at a linear flow-rate of 0.5 m/s; 35°C isothermal run.

CONCLUSIONS

A detailed study of commercially available cyclodextrin-based capillary columns, which do not rely on the use of a silicone stabilizing medium, indicates that very rapid enantiomeric trace determinations of desflurane, isoflurane and enflurane can be achieved with a single capillary column coated with the trifluoroacetyl-γ-cyclodextrin phase, opening the way to, among others, meaningful pharmacokinetic studies. Contrary to suggestions in the literature [13], even detailed thermodynamic studies failed to identify unequivocally the separation mechanisms that are responsible for the chiral discrimination.

ACKNOWLEDGEMENTS

Partial financial support for this project was provided by the National Science Foundation (CH-8919151), the US Department of Education (415004), Anaquest and Dow Chemical. Astec is acknowledged for providing the capillary columns used in this study.

REFERENCES

1 V.J. Collins, *Principles of Anesthesiology*, Lea & Febiger, Philadelphia, PA, 2nd ed., 1976.
2 N.P. Franks and W.R. Lieb, *Nature*, 300 (1982) 487.
3 E.J. Ariëns, *Biochem. Pharmacol.*, 37 (1988) 9.
4 N.P. Franks and W.R. Lieb, *Science*, 254 (1991) 427.
5 J.W. Young, *US Pat.*, 5 114 714 (1992).
6 J.W. Young, *US Pat.*, 5 114 715 (1992).
7 D.F. Halpern, *US Pat.*, 4 855 511 (1989).
8 W.A. König, *Gas Chromatographic Enantiomer Separation with Modified Cyclodextrins*, Hüthig, Heidelberg, 1992.
9 J. Meinwald, W.R. Thompson, D.L. Pearson, W.A. König, T. Runge and W. Francke, *Science*, 251 (1991) 560.
10 D.W. Armstrong, W. Li, A.M. Stalcup, H.V. Secor, R.R. Izac and J.I. Seeman, *Anal. Chim. Acta.*, 234 (1990) 365.
11 D.W. Armstrong, W. Li, C.D. Chang and J. Pitha, *Anal. Chem.*, 62 (1990) 914.
12 D.W. Armstrong, W. Li and H.L. Jin, *J. Chromatogr.*, 509 (1990) 303.
13 A. Berthod, W. Li and D.W. Armstrong, *Anal. Chem.*, 64 (1992) 873.

Journal of Chromatography A, 657 (1993) 395–404
Elsevier Science Publishers B.V., Amsterdam

CHROM. 25 519

Synthesis of novel tellurium containing analogues of choline and acetylcholine and their quantitation by pyrolysis–gas chromatography–mass spectrometry

S.E. Harris

Department of Chemistry and Biochemistry, University of South Carolina, Columbia, SC 29208 (USA)

L.A. Silks, III

Los Alamos National Laboratory, Biochemistry and Spectroscopy Section, INC-4: MS C346, Los Alamos, NM 87545 (USA)

R.B. Dunlap and J.D. Odom

Department of Chemistry and Biochemistry, University of South Carolina, Columbia, SC 29208 (USA)

J.W. Kosh*

College of Pharmacy, University of South Carolina, Columbia, SC 29208 (USA)

(First received March 9th, 1993; revised manuscript received August 12th, 1993)

ABSTRACT

Methods for the synthesis and quantitation of the novel choline analogues, telluronium choline and acetyltelluronium choline, are described. An assay procedure utilizing pyrolysis–gas chromatography–mass spectrometry (Py–GC–MS) with cold trapping was developed with [$^2H_4$]telluronium choline and [$^2H_4$]acetyltelluronium choline as internal standards. The telluronium compounds were ion-pair extracted from tissue with dipicrylamine, washed with 2-butanone, and pyrolyzed prior to GC–MS analysis. The compounds were monitored using selected ion monitoring at *m/z* 232 and *m/z* 190 for acetyltelluronium and telluronium choline, respectively, and at *m/z* 236 and *m/z* 194 for the analogous deuterated internal standards. The assay was linear over a range of 20 pmol–20 nmol of compound taken through the assay.

INTRODUCTION

A number of analogues of choline [$(CH_3)_3N^+CH_2CH_2OH$] and acetylcholine [$(CH_3)_3N^+CH_2CH_2OC(O)CH_3$] have been utilized to study cholinergic neurotransmission. Many of these analogues have subsequently been shown to qualify as false cholinergic neurotransmitters [1–5] and to prevent acetylcholinesterase inhibitor toxicity [6,7].

In general, alteration of the alkyl or quaternary region of the choline molecule has produced the most active choline analogues. Analogues with modified alkyl regions include homocholine, β-methylcholine [8], monoethylcholine, diethylcholine, triethylcholine and pyrolidinium choline [5]. Modifications of the quaternary nitrogen include replacement of the nitrogen with another group 15 atom to yield

* Corresponding author.

0021-9673/93/$06.00
SSDI 0021-9673(93)E0930-S

phosphocholine and arsenocholine [1] and stibocholine [2]. Replacements of the quaternary nitrogen that result in a quaternary neutral structure include carbocholine and silicocholine [9], whereas replacement of the nitrogen atom by a group 16 atom results in tertiary, positively charged structures including sulfocholine [3] and, most recently, selenonium choline [10].

Data from the recent characterization of the biological activity of selenonium choline [$(CH_3)_2Se^+CH_2CH_2OH$, TeCh] demonstrate that the compound satisfies many of the criteria of a false neurotransmitter [7,11]. It was therefore of interest to examine the tellurium-containing analogue, telluronium choline [$(CH_3)_2Te^+CH_2CH_2OH$]. Because of the structural similarity to selenonium choline, telluronium choline should be expected to behave biologically in a similar manner. The fact that tellurium occurs naturally in the earth's crust and is found in high concentrations in selected foods [12], suggests the possibility of its incorporation into biological compounds. Although tellurium-containing amino acids have not been detected in mammalian tissue, partial incorporation of telluromethionine in place of methionine in dihydrofolate reductase has been demonstrated in *Escherichia coli* [13]. Because the possibility exists that telluronium choline might occur in nature and may act as a cholinergic false transmitter, it was of interest to undertake its synthesis and to develop a method for its quantitation. The present work therefore describes the synthesis of the novel trigonal choline analogues telluronium choline and acetyltelluronium choline [$(CH_3)_2Te^+CH_2CH_2OC(O)CH_3$, ATeCh] and their quantitation using a pyrolysis–gas chromatography–mass spectrometric assay.

EXPERIMENTAL

Spectroscopic studies

NMR spectra were recorded as C^2HCl_3 or ^2H_2O solutions, unless otherwise noted, on either a Bruker AM 500, AM 300, WP-300 or AM-200 spectrometer. The resonance frequencies for ^1H, ^{13}C and ^{125}Te are 300.133, 75.427 and 94.692 MHz, respectively. Proton spectra were the result of 32 transients with a 64K data table and were referenced externally to tetramethylsilane (TMS) or as values in parts per million relative to $CHCl_3$. ^{13}C spectra were obtained with proton decoupling and were the result of 128–256 transients with a 64K data table and were either referenced to external TMS or with respect to internal C^2HCl_3 (δ-77.0). The ^{125}Te spectra were performed with proton decoupling and were the result of 1024 or 2048 transients with a 64K data table and the chemical shifts are reported as values in parts per million relative to $Te(OH)_6$ [14,15]. The concentration of ^{125}Te NMR samples was approximately 0.2 *M*. Spectra were run with a 55 kHz sweep width using a 2.8 μs tip angle (90° tip angle is 7 μs) and a 0.5 s relaxation delay. The probe was maintained at ambient temperature. All spectra were taken using 5 mm NMR tubes.

Accurate mass spectra were measured on a VG 70SQ GC–MS spectrometer using glycerin ($m/z = 185$) as a reference (Fig. 1). The exact masses for TeCh and ATeCh were 199.9853 and 241.9963, respectively, while the calculated mass for $C_4H_{11}O^{125}Te$ was 199.9854 (0.5 ppm error) and the mass for $C_6H_{13}O_2{}^{125}Te$ was 241.9960 (1.2 ppm error). Elemental analyses were performed at the Los Alamos National Laboratory and at Atlantic Microlabs. (Norcross, GA, USA).

MS analysis of the telluronium compounds was accomplished using the pyrolysis GC–MS method described by Terry *et al.* [10], with the following changes: pyrolysis temperature was 290°C, interface temperature was 190°C, and pyrolysis products were cold trapped for 6 min with an injector purge time of 6 min. The prepared samples were analyzed using a Hewlett-Packard gas chromatograph (5890)–mass spectrometer (5970) and a Stabilwax column (Restek, 30 m × 0.25 mm I.D., 0.5 μm phase). Selected ion monitoring (SIM) was employed for compound detection using m/z 232 ($[CH_3–Te–CH_2–CH_2–O–C(O)CH_3]^+$) and 236 ($[CH_3–Te–C^2H_2–C^2H_2–O–C(O)CH_3]^+$), which corresponded to the base peaks for the thermally demethylated acetyltelluronium choline (d_0) and [$^2H_4$]acetyltelluronium choline (d_4) variants, re-

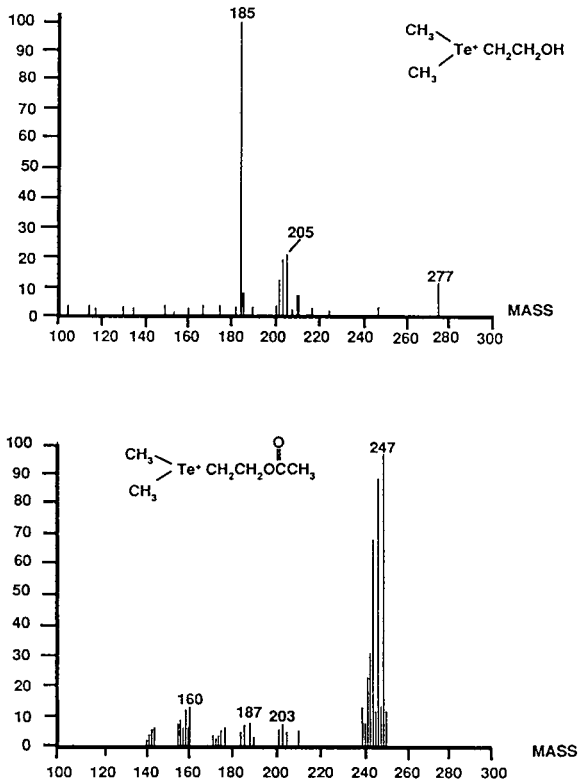

Fig. 1. Fast atom bombardment spectra (positive ion) of (top) d_0-telluronium choline$_0$- and (bottom) d_0-acetyltelluronium choline$_0$-. Spectra were obtained following a standard static procedure using a VG 705Q mass spectrometer and data system.

spectively. Similarly, d_0- and d_4-telluronium choline compounds were monitored at m/z 190 ($[CH_3-Te-CH_2-CH_2-O-H]^+$) and m/z 194 ($[CH_3-Te-C^2H_2-C^2H_2-O-H]^+$), respectively, corresponding to the base peaks of the demethylated variants. Since the Autotune function optimizes the instrument for perfluorotributylamine (PFTBA), a shift of ± 0.1 m/z is frequently observed for the ion of interest. Therefore, data collection for the telluronium compounds consisted of a three-ion bracket surrounding m/z 232 (231.9, 232.0, 232.1), m/z 236 (235.9, 236.0, 236.1), m/z 190 (189.9, 190.0, 190.1) and m/z 194 (193.9, 194.0, 194.1).

Because the ion abundances for the telluronium compounds were typically low, the areas for the ions in a three-ion bracket were summed together and used for quantitation purposes. The areas were then corrected for area spillover using a matrix based Pascal program written by one of the authors (J.W.K.). The area correction algorithm used was essentially the same as that reported by Jenden and Silverman [16] for correcting spillover between deuterated and non-deuterated variants of choline and acetylcholine. The extent of spillover for each isotope was determined using a set of three "matrix" tubes containing only d_0- or d_4-, or a mixture of both variants for each set of 12–16 experimental tubes (See Table I).

TABLE I

REPRESENTATIVE NORMALIZED AREA CONTRIBUTIONS BETWEEN IONS OF INTEREST

Tubes containing only d_0-, or only d_4-, or a mixture of d_0- and d_4-telluronium choline and acetyltelluronium choline were processed according to the assay protocol and subjected to pyrolysis–GC–MS analysis. The areas obtained during selected ion monitoring analysis for m/z 190, 194, 232 and 236 were normalized by dividing each area by the largest value obtained for that sample. The normalized areas were subsequently used in matrix calculations to provide corrected area values for the experimental samples.

	Acetyltelluronium choline, m/z		Telluronium choline, m/z	
	232	236	190	194
d_0	1.0	0.02098	1.0	0.01791
d_4	0.53969	1.0	0.54647	1.0
$d_0 + d_4$	1.0	0.74231	1.0	0.67469

Synthetic reagents

Elemental tellurium was obtained from Alfa Products as a gray powder and used without further purification. Chloroethanol was obtained from Aldrich, distilled, and stored over 4 Å molecular sieves before use. Methyl trifluoromethanesulfonate, iodomethane and ethereal solutions of methyllithium were obtained from Aldrich, and used without further purification. 2-Bromo[1-$^2H_2$,2-$^2H_2$]ethanol was obtained from Cambridge Isotopes and used without further purification. The concentration of methyllithium reagents in commercial solutions was determined by titration of diphenylacetic acid to the yellow end point [17]. Tetrahydrofuran (THF) was distilled from sodium/benzophenone prior to

Preparation of 2-(methyltellurenyl)ethanol (1)

In a flame dried and purged (nitrogen) 250-ml three-necked flask, fitted with a septum, gas inlet, ground glass stopper and magnetic stirring bar, were added 2.00 g of elemental tellurium (15.7 mmol), and 50 ml of dry THF. To the stirring tellurium–THF suspension, under nitrogen, were added dropwise, at 0°C, 11.3 ml (1.4 *M*) methyllithium. As the addition reached the end-point (1 equivalent) the dark brown suspension lightened to give a clear yellow solution. Stirring was continued for 5 min, and subsequently the temperature was lowered to −78°C. Then 1.16 ml of 2-chloroethanol (17.2 mmol) were added dropwise. Stirring was continued for 1 h at −78°C, then the mixture was allowed to warm slowly to room temperature and stirring was continued for 12 h. The reaction mixture was then filtered through a pad of SiO_2 (EM Science; 230–400 mesh; 40–200 μm) and all volatiles were removed *in vacuo*. The crude material was then subjected to flash column chromatography (SiO_2, 230–400 mesh) using $CHCl_3$ as the eluent. This gave 2.94 g (76%). NMR (in ppm): ^1H (C^2HCl_3), δ 1.87 [s, J (^1H–^{125}Te) = 20.8 Hz, 3H, CH_3Te], 2.1 (broad s, 1H, CH_2OH), 2.75 (t, J = 6.8 Hz, $TeCH_2$), 3.75 (m, 2H, CH_2OH).

Preparation of 2-(methyltellurenyl)ethyl acetate (2)

In a flame dried and purged (nitrogen) 250-ml three-necked flask, fitted with a septum, gas inlet, ground glass stopper and magnetic stirring bar, were added 2.00 g of elemental tellurium (15.7 mmol), and 50 ml of dry THF. To the stirring tellurium–THF suspension, under nitrogen, were added dropwise, at 0°C, 11.1 ml (1.4 *M*) methyllithium. As the addition reached the end-point (1 equivalent) the dark brown suspension lightened to give a clear yellow solution. Stirring was continued for 5 min, and subsequently the temperature was lowered to −78°C. Then 1.16 ml of 2-chloroethanol (17.2 mmol) were added dropwise. Stirring was continued for 1 h at −78°C then the mixture was allowed to warm slowly to room temperature and stirring was continued for 12 h. Then 2.20 ml (79 mmol) of triethylamine were added dropwise at 0°C. This was followed by the addition of 1.5 ml (79 mmol) of acetic anhydride. After 12 h the reaction was determined to be incomplete (TLC) and an additional 5 ml of acetic anhydride was added. Stirring was continued until consumption of **1** was complete as determined by TLC analysis. The reaction mixture was concentrated under reduced pressure and then chromatographed using a $CHCl_3$–heptane mixture. This gave 2.5 g (70%).

Alternatively, treatment of 0.41 g (2.18 mmol) 2-(methyltellurenyl)ethanol with 0.21 ml (2.3 mmol) of acetic anhydride, 0.185 ml (2.3 mmol) of pyridine, in 20 ml of dichloromethane for 12 h afforded a 78% yield of **2**. Data for **2**: NMR (in ppm): ^1H (C^2HCl_3), δ 1.87 (s, 3H, CH_3Te), 1.97 (s, 3H, CH_3CO), 2.70 (t, J = 7.8 Hz, 2H, $TeCH_2$), 4.25 (t, J = 7.8 Hz, 2H, CH_2OAc); ^{13}C, −22 [J (^{13}C–^{125}Te) = 157 Hz, CH_3Te], 0.9 [J (^{13}C–^{125}Te) = 166 Hz, $TeCH_2$], 20.6 (CH_3CO), 65.9 (CH_2OAc), 169.9 ($COCH_3$).

Preparation of 2-(dimethyltelluronium)-ethyl acetate trifluoromethyl sulfonate, acetyltelluronium choline (3)

To 2.5 g (10.9 mmol) of **2** in 5 ml of methylene chloride, chilled to 0°C was added 1.23 ml of methyl trifluoromethyl sulfonate (10.8 mmol) dropwise, under nitrogen. The mixture was then warmed to ambient temperature and stirred until all starting material was consumed as shown by TLC. The solution was then washed with diethyl ether. The resulting oil was then dried *in vacuo*

to give 4.29 g (97%). NMR (in ppm): ^{1}H ($^{2}H_2O$), δ 2.07 (s, 3H, CH_3CO), 2.35 [2, J (^{1}H–^{125}Te) = 25 Hz], 6H, $(CH_3)_2Te$], 3.16 (t, J = 6.0 Hz, 2H, $TeCH_2$), 4.50 (t, J = 6.0 Hz, 2H, CH_2OAc); ^{13}C, 5.0 [J (^{13}C–^{125}Te) = 152 Hz, $(CH_3)_2Te$], 21.6 (CH_3CO), 24.6 [J (^{13}C–^{125}Te) = 150 Hz, $TeCH_2$], 62.3 (CH_2OAc), 121.4 [q, H (^{13}C–^{19}F) = 318.4 Hz, $CF_3SO_3^-$], 174.5 ($COCH_3$); ^{125}Te, 493.0 (0.24 *M*). Accurate mass by positive ion fast atom bombardment gave 241.9963 (calculated mass 241.9960) with an error of 1.2 ppm. Elemental analysis calculated for $C_7H_{13}O_5F_3STe^+$: C, 21.35; H, 3.33. Found: C, 20.86; H 3.40.

*Preparation of 2-(dimethyltelluronium)-ethanol iodide, telluronium choline (**4**)*

Three ml of iodomethane (48.2 mmol) were added neat to 2.23 g of **1** (11.9 mmol) which was being rapidly stirred at 0°C. The reaction was mildly exothermic. The mixture was stirred until TLC analysis indicated **1** was consumed. The residue was taken up in water and washed with methylene chloride until the aqueous solution was clear and colorless. The solution was then dried *in vacuo* to give 3.74 g of a cream colored solid (96%). NMR (in ppm): ^{1}H ($^{2}H_2O$), δ 2.35 [s, J (^{1}H–^{125}Te) = 24 Hz, 6H, $(CH_3)_2Te$], 3.28 (t, J = 6.3 Hz, 2H, $TeCH_2$), 4.03 (m, 2H, CH_2OH); ^{13}C, 6.3 [J (^{13}C–^{125}Te) = 148 Hz, $(CH_3)_2Te$], 32.7 [J (^{13}C–^{125}Te) = 168 Hz, $TeCH_2$], 60.2 (CH_2OH); ^{125}Te, 448.1 (0.18 *M*). Accurate mass by positive ion fast atom bombardment gave 199.9853 (calculated mass 199.9854) with an error of 0.5 ppm. Elemental analysis calculated for $C_4H_{11}IOTe^+$: 14.79; H, 3.58. Found: C, 14.57; H, 3.36.

*Preparation of 2-(methyltellurenyl)-[1-$^{2}H_2$,2-$^{2}H_2$]ethanol (**5**)*

The synthesis procedure used was identical to that described for **1**, except that 11.6 ml (1.0 *M*) of methyllithium were added to 1.48 g of elemental tellurium (11.6 mmol) followed by 1.5 g of 2-bromo[1-$^{2}H_2$,2-$^{2}H_2$]ethanol (11.6 mmol). The final eluent for chromatography was $CHCl_3$–diethyl ether (95:5). Final yield was 1.65 g (74%). NMR (in ppm): ^{1}H ($C^{2}HCl_3$), δ 1.85 [s, J (^{1}H–^{125}Te) = 20.8 Hz, 3H, CH_3Te], 2.6 (broad s, 1H, CH_2OH); ^{13}C, −22 (CH_3)Te, 7 (m, $C^{2}H_2Te$), 63 (m, $C^{2}H_2OH$).

*Preparation of 2-(methyltellurenyl)-[1-$^{2}H_2$,2-$^{2}H_2$]ethyl acetate (**6**)*

The synthesis procedure used was identical to that described for **2**, except that 11.6 ml of methyllithium (1.0 *M*) were added to 1.48 g of elemental tellurium (11.6 mmol) followed by 1.5 g of 2-bromo[1-$^{2}H_2$,2-$^{2}H_2$]ethanol. Then 2.81 ml (36.3 mmol) of dry pyridine was added dropwise at 0°C followed by the addition of 3.28 ml (29.7 mmol) of acetic anhydride. Final yield was 1.5 g (55%). NMR (in ppm): ^{1}H ($C^{2}HCl_3$), δ 1.93 (s, 3H, CH_3Te), 2.04 (s, 3H, CH_3CO); ^{13}C, −22 (CH_3Te), 21 (CH_3CO), 170.6 ($COCH_3$), the deuterated carbons were not observed.

*Preparation of 2-(dimethyltelluronium)-[1-$^{2}H_2$,2-$^{2}H_2$]ethanol iodide, d_4-telluronium choline (**7**)*

The synthesis procedure used was identical to that described for **4**, except that 1.45 g of **5** (7.6 mmol) was used. The procedure yielded 1.53 g of a cream colored solid (60%). NMR (in ppm: ^{1}H ($^{2}H_2O$), 2.28 [s, J (^{1}H–^{125}Te) = 24 Hz, 6H, $(CH_3)_2Te$]; ^{13}C, 6.3 [J (^{13}C–^{125}Te) = 149 Hz, $(CH_3)_2Te$], 32.2 (m, $TeC^{2}H_2$), 59.7 ($C^{2}H_2OH$).

*Preparation of 2-(dimethyltelluronium)-[1-$^{2}H_2$,2-$^{2}H_2$]ethyl acetate trifluoromethyl sulfonate, d_4-acetyltelluronium choline (**8**)*

The synthesis procedure used was identical to that described for **3**, except that 0.73 ml of methyl trifluoromethyl sulfonate (6.5 mmol) were added to 1.5 g of **6** (6.3 mmol). Water (10 ml) was then added and the final aqueous solution was then dried *in vacuo* (the temperature was not allowed to rise above 15°C) to give 1.57 g (63%). NMR (in ppm): ^{1}H ($^{2}H_2O$), δ 1.93 (s, 3H, CH_3CO), 2.21 [s, J (^{1}H–^{125}Te) = 24 Hz, 6H, $(CH_3)_2Te$]; ^{13}C, 5.4 [J (^{13}C–^{125}Te) = 152 Hz, $(CH_3)_2Te$], 21.8 (CH_3CO), 24.0 [J (^{13}C–^{125}Te) = 150 Hz, $TeC^{2}H_2$], 61.6 ($C^{2}H_2OAc$), 121.2 [q, J (^{13}C–^{19}F) = 318.4 Hz, CF_3SO_3], 174.6 ($COCH_3$).

Storage of compounds

All pure compounds were stored under nitrogen at −70°C. Dilutions of these compounds that

were used for assay analysis were stored at either −45°C or −70°C under nitrogen. The pure compounds were stable for at least 6 months at −70°C, as were the dilutions.

Sample preparation and quantitation

The assay protocol used in the present study was based on the method of Terry *et al.* [10]. Briefly, the tissue sample to be assayed was placed in a 15-ml centrifuge tube and 2.5 nmol of deuterated (d_4-) telluronium choline and acetyltelluronium choline were then added as internal standards. A 2-ml volume of 1.0 *M* formic acid–acetonitrile solution (15:85, v/v) was added, and the sample was homogenized using a Polytron. The tube was centrifuged at 26 000 *g* for 20 min, and the supernatant was then transferred to 10-ml screw-capped centrifuge tube. A 4-ml volume of diethyl ether was then added to the tube, vortexed for 2 min, centrifuged for 2 min and the diethyl ether layer was then removed by aspiration. Traces of diethyl ether and ACN were evaporated under a vigorous stream of gaseous nitrogen for 5 min in a 25°C water bath. The telluronium compounds were then ion-pair extracted from the aqueous layer by adding 2 ml of 2 m*M* dipicrylamine (DPA) in methylene chloride, followed by 0.5 ml of 3-{[tris(hydroxymethyl)methyl]amino}-1-propanesulfonic acid (TAPS) buffer (pH 9.2). The tube was immediately vortexed for 2 min, centrifuged for 2 min, and the methylene chloride layer containing the ion-paired telluronium compounds was then transferred to a clean centrifuge tube. After evaporation of the methylene chloride layer to dryness under nitrogen at 25°C, the residue was dissolved in 250 μl of sodium acetate buffer (0.05 *M*, pH 4.0), and washed with 500 μl of 2-butanone (two times) to remove traces of DPA. The 2-butanone layer was aspirated, the aqueous layer was then evaporated to dryness under nitrogen in a 25°C water bath, and the tube stored on ice until used. Immediately prior to pyrolysis, 100 μl of acetonitrile–water (90:10) containing 250 μg of tetramethylammonium bromide [18] (TMABr) was added to the tube and then vortexed briefly. A 2-μl volume of the resulting mixture was applied to a 25 mm × 2 mm I.D. quartz tube, air dried, and then inserted into the pyrolysis interface for GC–MS analysis.

To allow quantitation, standard solutions of the d_0- and d_4-telluronium compounds were dissolved in 0.05 *M* sodium acetate (pH 4.0). Samples which contained 2.5 nmol of d_4-telluronium choline and d_4-acetyltelluronium choline as internal standards, together with known amounts (20 pmol–20 nmol) of the d_0 compounds, were then processed as described above for tissue samples. The d_0/d_4 ratios of the corrected areas (see *Spectroscopic studies)* were then plotted *versus* the d_0 analogue content to obtain a standard curve. Quantitation of "unknown" samples was accomplished by referencing the d_0/d_4 ratio to the standard curve.

RESULTS AND DISCUSSION

The present study demonstrates the successful synthesis of the novel choline analogues telluronium choline (TeCh) and acetyltelluronium choline (ATeCh). The overall synthetic yield for TeCh and ATeCh was 73 and 52%, respectively. Proof of the synthesis and purity of these analogues was provided by multinuclear NMR data, positive ion fast atom bombardment (Fig. 1), and elemental analysis (see Experimental).

Quantitation of the telluronium compounds was accomplished by modifying an existing pyrolysis–GC–MS procedure [10]. However, unlike the existing assay, telluronium choline and acetyltelluronium choline were not subjected to vacuum desiccation at any step during the assay since the related choline analogue, selenonium choline, spontaneously demethylated under these conditions. Unlike the selenonium analogues, the telluronium analogues also appeared to be thermally labile. The use of temperatures higher than 25°C during the evaporation steps resulted in significant losses of the analogues. Preliminary data (not shown) also indicate that the telluronium compounds are not stable for prolonged times at room temperature. The majority of the decomposition appeared to occur during the first 8 h and approximated 8–10% after 24 h. Because of this potential degradation, all samples were kept on ice except during the analytical processing steps.

Another major difference from the selenonium assay [10] was that propionylation of the alcohol function of TeCh was not required prior to GC–MS analysis since good peak separation was observed between ATeCh and TeCh. Further, the peak shape of the alcohol (TeCh) was symmetrical with peak widths ranging from 0.04 to 0.05 min at half-height. It was also observed that the procedure used for the propionylation of selenonium choline degraded both telluronium compounds to a significant extent, and reduced absolute recoveries.

Because the telluronium analogues were cationic, the compounds required demethylation prior to GC–MS analysis. The work of Terry *et al.* [10] previously demonstrated that it was possible to chemically demethylate the related selenonium analogues to a slight extent (*ca.* 10%) using sodium thiophenoxide. However, chemical demethylation of the telluronium compounds with this agent was ineffective. Based on the chemical similarity of the telluronium analogues to the selenonium compounds, other modes of chemical demethylation were not attempted, and thermal demethylation (pyrolysis) was selected. It was necessary to add approximately 250 μg of tetramethylammonium bromide (TMABr) to each sample prior to the final reconstitution step to aid in the pyrolysis of nanomolar quantities of the telluronium analogues. A similar approach has been used for the pyrolysis of picomolar quantities of choline and acetylcholine where only 5 μg of TMABr was sufficient [18]. The present data (not shown) indicate that the optimum pyrolysis temperature for the telluronium analogues was approximately 10–20°C lower than for the related selenonium analogues. The lower pyrolysis temperature requirement is compatible with the expected reduced stability of the tellurium–carbon bond compared to the analogous selenium–carbon bond.

Shown in Fig. 2 is a representative mass spectral "scan" for d_0- and d_4-TeCh after thermal demethylation, showing the characteristic clusters of fragments corresponding to the multiple isotopes of tellurium. As can be seen, demethylated TeCh did not fragment well, causing the molecular ion *m/z* 190 and *m/z* 194 to be

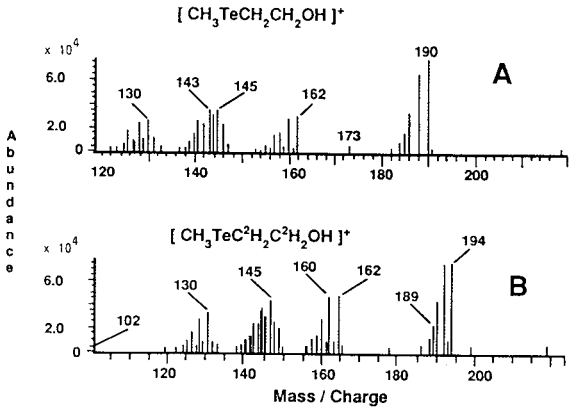

Fig. 2. Mass spectra of (A) telluronium choline and (B) [$^2H_4$]telluronium choline. The telluronium compounds were subjected to the described assay protocol and analyzed by pyrolysis–GC–MS. Data were obtained using the HP5890/5970 GC–MS system operated in the "scan" mode.

also the base peak for the d_0 and d_4 variants, respectively. Other major fragments included *m/z* 143 and 145 ($[CH_3Te]^+$) and *m/z* 130 ($[Te]^+$) which were produced by both analogues. Major fragments at *m/z* 160 and 162 appeared in both of the spectra for the TeCh analogues. Since the d_4 analogue also yielded the same fragments, this result suggested that during the fragmentation, an ethylene group was lost with the formation of a fragment corresponding to $[CH_3TeOH]^+$.

Shown in Fig. 3 is the "scan" obtained for the ATeCh analogues after thermal demethylation. The molecular ions (*m/z* 232 and 236) corresponding to the demethylated variants, were also the base peaks for the d_0 and d_4 analogues, respectively. The fragments at *m/z* 172 and 175 corresponded to $[CH_3TeCH=CH_2]^+$ and $[CH_3TeC^2H=C^2H_2]^+$ from the d_0 and d_4 spectra, respectively. The observed fragmentation patterns were significantly different from the selenonium analogues where the base peak was the fragment ($[CH_3SeCH=CH_2]^+$) common to both selenonium analogues [10]. A similar fragment (*m/z* 58, $[CH_3NCH=CH_2]^+$) was also observed for choline and acetylcholine [16].

The necessity for isotopic corrections prior to data analysis becomes evident on inspection of a representative matrix table used in the quantitation procedure (Table I). The spillover is due in

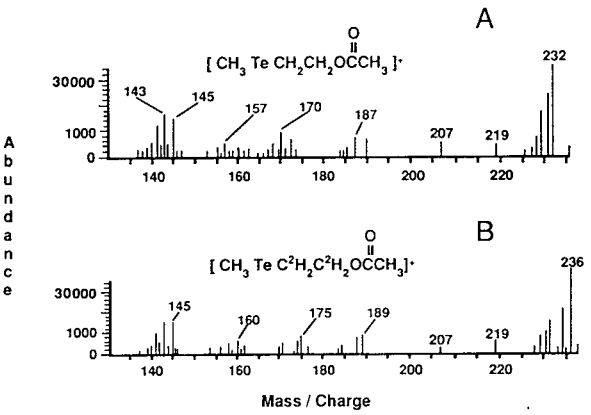

Fig. 3. Mass spectra of (A) acetyltelluronium choline and (B) [$^2H_4$]acetyltelluronium choline. The telluronium compounds were processed according to the described assay protocol and analyzed by pyrolysis–GC–MS. Data were obtained using the HP5890/5970 GC–MS system operated in the "scan" mode.

part to the large number of isotopes of tellurium and to the small difference in molecular mass between the d_0 and d_4 variants (4 u). For example, during fragmentation of demethylated d_4-ATeCh, a *m/z* 232 fragment is produced that contributes area to the base peak (*m/z* 232) of demethylated d_0-ATeCh (Fig. 3). From Table I it can be seen that the d_0 compounds contributed approximately 1–2% spillover into the areas of the d_4 analogues. However, approximately 53–55% of the d_4 areas were contributed to the area of the d_0 analogues. In comparison, the spillover of the d_4 analogues into the areas of the d_0 selenonium analogues was approximately 16–17% [10].

Fig. 4 is a representative chromatogram of 100 pmol of d_0-TeCh and d_0-ATeCh together with 2.5 nmol each of d_4-TeCh and d_4-ATeCh (internal standards). The four ions of interest were extracted from the total ion chromatogram using the "Ion Profile" software feature. The retention times for ATeCh and TeCh were approximately 14.1 and 14.7 min, respectively. For comparison, acetylselenonium choline eluted approximately 1 min earlier under the same conditions (data not shown). The abundance for the d_0 analogues was enhanced relative to the d_4 areas and, as discussed above, was due to the large spillover from the d_4 analogues.

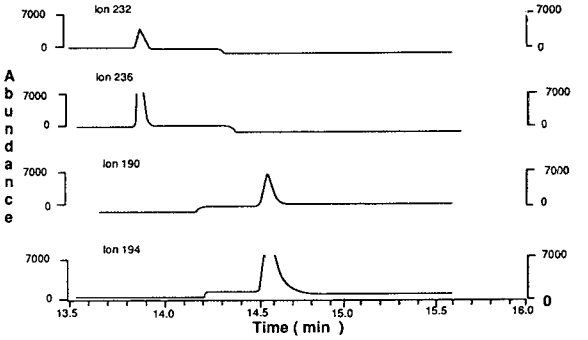

Fig. 4. Selected ion chromatogram of telluronium choline (TeCh) and acetyltelluronium choline (ATeCh). A 100-pmol amount of the d_0 analogues together with 2.5 nmol of the d_4 analogues were processed according to the described assay protocol and analyzed by pyrolysis–GC–MS. The ion chromatograms represent the ions of interest; *m/z* 232 (d_0-ATeCh), *m/z* 236 (d_4-ATeCh), *m/z* 190 (d_0-TeCh) and *m/z* 194 (d_4-TeCh).

Fig. 5 illustrates the linearity of the standard curve for 20 pmol through 20 nmol of d_0-TeCh and d_0-ATeCh. At the lowest extreme (20 pmol) and highest extreme (20 nmol), linearity appeared to fall off with increasing standard error. Since the matrix corrections were large, lack of linearity may be due to under- or overcorrection of the areas since only a single concentration (2.5 nmol) was used as the reference point for the calculations. Overcorrection of the areas also explains the negative ratio obtained for the 20

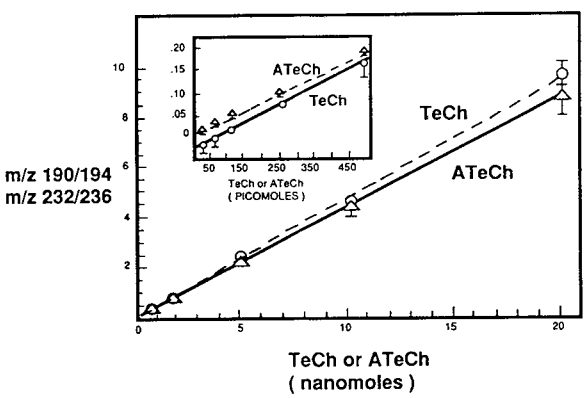

Fig. 5. Standard curves for telluronium choline (TeCh) and acetyltelluronium choline (ATeCh). Known quantities of telluronium analogues with 2.5 nmol of internal standard (d_4 telluronium variants) were processed using the described assay protocol and analyzed by pyrolysis–GC–MS. *m/z* 190/194 = TeCh, *m/z* 232/236 = ATeCh.

TABLE II

ASSAY REPRODUCIBILITY IN THE PRESENCE AND ABSENCE OF TISSUE

Known quantities of telluronium choline and acetyltelluronium choline in the presence and absence of 100 mg of mouse brain tissue were processed according to the protocol described and analyzed by pyrolysis–GC–MS.

Compound	pmol added	Observed (pmol)			
		Control	*n*	Brain tissue	*n*
Telluronium choline	100	118.3 ± 12	6	133.9 ± 17	6
	10 000	9230 ± 198	6	8970 ± 153	6
Acetyltelluronium choline	100	98.6 ± 27	6	79.9 ± 19	4
	10 000	9730 ± 169	6	9940 ± 186	6

pmol point for d_0-TeCh (Fig. 5, inset). For quantities to be analyzed at these extreme ranges of the standard curve, the use of matrix samples with quantities closer to the quantity to be measured should eliminate these problems.

Table II illustrates the recovery of the telluronium compounds in the presence of tissue. Considering the variability associated with pyrolysis methods [19], the data demonstrate a reasonable accuracy and standard error. For the TeCh data, the 100 pmol recoveries were higher than theoretical, and the 10 000 pmol quantities were lower than theoretical. The data for ATeCh were much closer to theoretical for both 100 and 10 000 pmol, but were generally lower than theoretical. All of the mean recovery values for both TeCh and ATeCh were within the standard error limits of the standard curve.

In conclusion, the compounds acetyltelluronium choline and telluronium choline have been synthesized in reasonable yield and high purity. These compounds can be quantitated in the presence of tissue by the use of pyrolysis GC–MS with linearity from 20 pmol to 20 nmol. The practical limit for the routine quantitation of these compounds using the described method is 50 pmol to 10 nmol due to the standard error experienced at concentrations outside this range.

ACKNOWLEDGEMENTS

The authors wish to thank Mrs. Emily F. Willingham for her expertise in the preparation of this manuscript, and Dr. Robert L. Beamer, Chairman of the Department of Basic Pharmaceutical Sciences, College of Pharmacy, for his generous support provided for supplies. This research was also supported by the grants NSF No. BNS-8515929 (J.W.K.) and NIH GM42907 (J.D.O.). Support of high-field NMR spectrometer purchases at the University of South Carolina by the grants NSF (CHE 84-11172) and NIH (1-S10-RR02425) is also acknowledged. We would also like to thank the National Institutes of Health (RR 02231-10) Stable Isotopes Resource (SIR) at Los Alamos National Laboratory for partial financial support for this work (L.A.S.).

REFERENCES

1 A.D. Welch and M.H. Roepke, *J. Pharmacol. Exp. Ther.*, 55 (1935) 118.
2 E.M. Meyer, R.J. Barrnett and J.R. Cooper, *J. Neurochem.*, 39 (1982) 321.
3 L. Frankenberg, G. Heimburger, C. Nilsson and B. Sorbo, *Eur. J. Pharmacol.*, 23 (1973) 37.
4 B. Hedlund, H. Norin, A. Christakopoulos, P. Alberts and T. Bartfai, *J. Neurochem.*, 39 (1982) 871.
5 B. Collier, P. Boksa and S. Lovat, in F. Tucek (Editor), *The Cholinergic Synapse* (*Progress in Brain Research*, Vol. 49), Elsevier, Amsterdam, 1979, p. 107.
6 T.A. Patterson, A.V. Terry, Jr. and J.W. Kosh, *Br. J. Pharmacol.*, 97 (1989) 451.
7 A.V. Terry, Jr., L.A. Silks III, R.B. Dunlap, J.D. Odom and J.W. Kosh, *Gen. Pharmacol.*, 23 (1992) 689.
8 R.M. Dick, J.J. Freeman and J.W. Kosh, *Life Sci.*, 36 (1985) 1183.
9 P.T. Henderson, E.J. Ariens, B.W.J. Ellenbroek and A.M. Simonis, *J. Pharm. Pharmacol.*, 20 (1968) 26.

10 A.V. Terry, Jr., L.A. Silks III, R.B. Dunlap, J.D. Odom and J.W. Kosh, *J. Chromatogr.*, 585 (1991) 101.
11 J.N. Khatri, L.A. Silks III, R.B. Dunlap, J.D. Odom and J.W. Kosh, *Life Sci.*, 51 (1992) PL213.
12 R.P. Beliles, in L.J. Casarett and J. Doull (Editors), *Toxicology: The Basic Sciences of Poisons, Metals*, Macmillan, New York, 1975, p. 493.
13 J.O. Boles, *Ph.D. Dissertation*, University of South Carolina, Columbia, SC, 1992.
14 J.M. Iriarte, L.A. Silks and J.D. Odom, presented at the *Southeastern Regional American Chemical Society Meeting, Atlanta, GA, Nov. 1988*, Inorganic Section, abstract No. 415.
15 J.M. Iriarte, *Ph.D. Dissertation*, University of South Carolina, Columbia, SC, 1990.
16 D.J. Jenden and R.W. Silverman, *J. Chromatogr. Sci.*, 11 (1973) 601.
17 W.G. Kofron and L.M. Baclawski, *J. Org. Chem.*, 41 (1976) 1879.
18 R.L. Polak and P.C. Molinar, *J. Neurochem.*, 23 (1974) 1295.
19 J.Q. Walker, *Chromatographia*, 5 (1972) 547.

Journal of Chromatography A, 657 (1993) 405–411
Elsevier Science Publishers B.V., Amsterdam

CHROM. 25 444

Determination of chlordane in air by gas chromatography–mass spectrometry with selected ion monitoring

Toshiro Yamashita*, Kimiko Haraguchi and Azuma Kido

Kitakyushu Municipal Institute of Environmental Health Sciences, Shin-ike 1-2-1, Tobata-ku, Kitakyushu-shi 804 (Japan)

Hideturu Matushita

School of Nutritional and Environmental Science, University of Shizuoka, Yata 395, Shizuoka-shi 422 (Japan)

(First received April 14th, 1993; revised manuscript received July 20th, 1993)

ABSTRACT

A gas chromatographic–mass spectrometric (GC–MS) method for the determination of chlordane in air was developed. Chlordane collected in a Tenax-TA tube was thermally desorbed into a fused-silica capillary column and determined by GC–MS with selected ion monitoring. The relative standard deviation of the peak area obtained in recovery tests ranged from 1.1 to 5.1% and the limit of detection was 5 pg (signal-to-noise ratio = 4). This method was applied to determine chlordane in indoor and ambient air samples in Kitakyushu, Japan.

INTRODUCTION

Chlordane was first prepared in the 1940s by the condensation of hexachlorocyclopentadiene with cyclopentadiene to produce chlordene, which was then chlorinated to give chlordane. Technical chlordane includes more than ten isomers and by-products, the main components being *trans*-chlordane (24%), chlordene isomers (21.5%), *cis*-chlordane (19%), heptachlor (10%) and nonachlor (7%). Chlordane had been used as an insecticide to control termites. As it is a carcinogenic substance with low degradability and high accumulation in the environment [1,2], it was specified as designated chemical substance in 1986 and its usage has been regulated since 1987 in Japan.

According to the results of a GC–MS monitoring survey performed by the Environmental Agency of Japan [3,4], chlordane was detected in sea-bottom sediment, fish and shellfish. Further, there are some reports concerning chlordane in room air and ambient air [5–14]. Suzuki *et al.* [13] measured the concentration of chlordane in atmospheric air in Kanagawa Prefecture of Japan and in the indoor air of houses that had been treated with chlordane to control termites. Even 8–9 years after the treatment, the average indoor concentration of chlordane was more than 0.4 $\mu g/m^3$. They concluded that those who spent more than 18 h per day in such houses might have inhaled more than 0.5 $\mu g/kg$ (the acceptable daily intake mass/kg specified by the FAO/WHO). This result suggests that it is necessary to carry out long-term indoor monitoring in houses treated with chlordane.

Reported methods for determining chlordane in air include the following. Chlordane in air trapped by a solid adsorbent such as silica gel or

* Corresponding author.

0021-9673/93/$06.00
SSDI 0021-9673(93)E0822-C

porous polymer beads was extracted with an organic solvent and determined by GC on a packed column with electron-capture detection. This method gave low chromatographic separation. Suzuki [15] developed a multi-dimensional GC method with MS with selected ion monitoring (GC–MS-SIM). In this method, chlordane trapped in a tube containing GC packing material (OV-17) was thermally desorbed and determined by GC–MS-SIM. However, this system is complicated and difficult to handle. Moreover, the analytical column might be polluted by bleeding of the packing material in the collection tube.

In this paper, we report a simple method for chlordane determination in which Tenax-TA is used as the trapping material and capillary GC–MS-SIM is used for analysis.

EXPERIMENTAL

Reagents

Heptachlor, oxychlorden, *cis*-nonachlor, *trans*-nonachlor, *cis*-chlordane and *trans*-chlordane were purchased from Wako. A mixed standard solution (2 ng/μl of each) was prepared in hexane.

Apparatus

Fig. 1 shows the sampling tube used in this experiment. A glass-lined stainless-steel tube (150 mm × 8 mm O.D. × 4 mm I.D.) (GL Science) was packed with 0.4 g of Tenax-TA (20–40 mesh) (GL Science) and both ends of the tube were sealed with silica-wool and connected with reducing unions (8 mm/3 mm). Before use, purified nitrogen was passed through the tube at 280°C overnight for cleaning. Air samples were collected at a flow-rate of 1 l/min by a diaphragm pump (Shibata Kagaku) equipped a needle valve to control the flow-rate. A 3 mm O.D. stainless-steel bar was used as a stopper. After sampling, the sampling tube was stored in a refrigerator until analysis. This tube was reused after the above-mentioned cleaning.

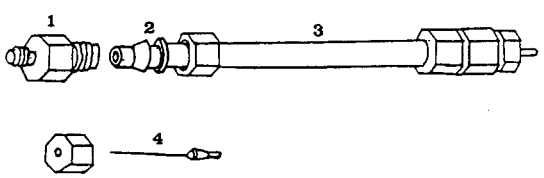

Fig. 1. Tenax-TA tube. 1 = Reducing anion; 2 = ferrule; 3 = glass lined stainless-steel tube; 4 = needle.

A thermal furnace which raises the temperature from 50 to 300°C in 2 min was purchased from the Tanaka Rikagaku Kikai.

The GC–MS system consisted of a Hewlett-Packard HP 5890J gas chromatograph and a JEOL JMS-DX 303 mass spectrometer with a DA-5000 data system.

Thermal desorption system and procedure

The thermal desorption system connected with the GC–MS system is shown in Fig. 2. A three-way tap (3) was connected with the outlet of the mass flow controller of the gas chromatograph. Another three-way tap (4) was connected to this line. Two stop valves were connected to the split and splitless vent of the gas chromatograph.

By closing these stop valves, the total flow-rate of carrier gas, most of which is usually vented to waste, passed through to the analytical column. As a result, the total flow-rate of the carrier gas

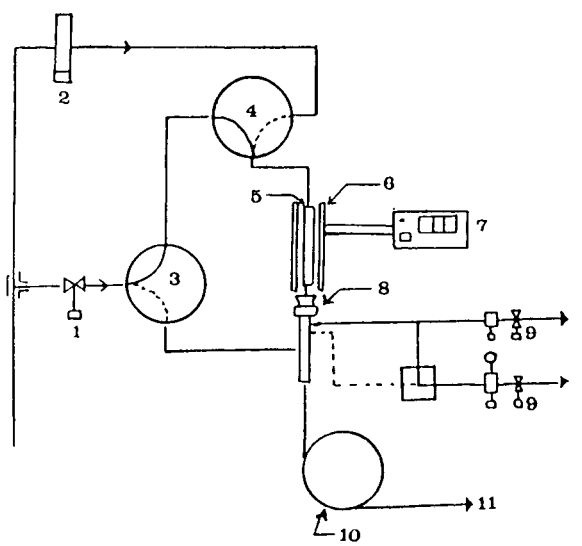

Fig. 2. Thermal desorption diagram for GC–MS analysis for chlordane. 1 = Mass flow controller valve; 2 = flow controller; 3 = three-way tap (A); 4 = three-way tap (B); 5 = Tenax-TA tube; 6 = electric furnace; 7 = control unit; 8 = injection port; 9 = stop valve; 10 = capillary column; 12 = ion source.

was 40 ml/min and the head pressure was up to *ca.* 500 kPa.

The analytical procedures were as follows. (a) After the Tenax-TA tube had been purged for 2 min by turning tap (3), it was connected to the injection port of the gas chromatograph. (b) After taps (3) and (4) had been turned, the Tenax-TA tube was heated at 300°C for 20 min by the furnace; during desorption, the GC column temperature was maintained at 50°C. (c) The two stop valves were opened and the trapped substance was measured by GC–MS. A direct coupling method is usually used for interfacing a capillary column to the MS ion source. However, it was difficult in our experiment to maintain a vacuum of the ion source, because the flow-rate of carrier gas (40 ml/min) was very high during desorption. Therefore, a capillary column was connected to the MS ion source through the quartz glass jet separator which is used to connect the GC and MS systems. The flow-rate of the make-up gas was 30 ml/min.

GC–MS-SIM procedure

The GC–MS conditions are given in Table I. The resolution of the mass spectrometer in the SIM mode was about 500 and the switching rate was 0.1 s per ion. To obtain the accuracy of the peak area, m/z values in the SIM mode were set at 271.810 and 273.810 for heptachlor, 387.800 for oxychlordane, 370.828 and 372.828 for *cis*, *trans*-chlordane and 407.790 and 408.790 for *cis*, *trans*-nonachlor.

TABLE I

GC–MS CONDITIONS FOR DETERMINATION OF CHLORDANE

Column	HP Ultra-2 (5% phenyl–95% methylsilicone) fused-silica capillary column, 25 m × 0.32 mm I.D., 0.52 μm film thickness
Temperatures:	
Column	Programmed: 1 min at 50°C, 30°C/min to 150°C, 10°C/min to 280°C, 6 min at 280°C
Injection	200°C
Inlet	250°C
Ion source	200°C
Carrier gas	Helium
Linear velocity	2 ml/min
Ionization method	Electron impact
Emission current	300 μA
Switching rate	0.1 S per ion

RESULTS AND DISCUSSION

Recovery tests of standard mixtures were carried out as follows. Three glass-lined stainless-steel tubes were connected in series. The first and third were Tenax-TA tubes and the second was packed with silica-wool. After 2 μl of standard solution containing 4 ng of each standard had been added to the second tube, the tube was heated to 100°C in the furnace. Indoor air was passed through these three tubes at a flow-rate of 2 l/min until the total flow reached 50–100 l. Impurities in room air were removed in the first tube and vaporized standard in the second tube was trapped in the third tube. Then, two kinds of thermal desorption method were performed: one was the front desorption method (FD method) in which the standard was desorbed from the sampling tube inlet; the other was the back desorption method (BD method) in which the standard was desorbed from the sampling tube outlet.

Recovery test results obtained by the FD method are given in Table II. A typical SIM chromatogram of chlordane standard mixture obtained in the recovery test is shown in Fig. 3. Most of the relative standard deviations (R.S.D.s) were less than 5%. The reproducibility

TABLE II

REPRODUCIBILITY OF PEAK AREA OBTAINED BY THE THERMAL DESORPTION METHOD (FD METHOD) ($n = 5$)

The amount added was 4 ng each.

Compound	Peak area	R.S.D. (%)
Heptachlor	1.69	3.7
Oxychlordane	0.54	1.1
trans-Chlordane	2.17	5.1
cis-Chlordane	2.25	4.8
trans-Nonachlordane	2.70	4.0
cis-Nonachlordane	2.23	4.5

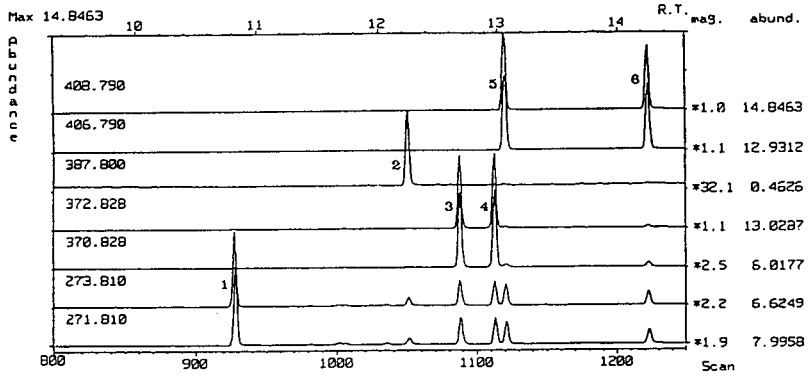

Fig. 3. SIM chromatogram of chlordane standard mixtures obtained by thermal desorption. 1 = Heptachlor; 2 = oxychlordane; 3 = *trans*-chlordane; 4 = *cis*-chlordane; 5 = *trans*-nonachlor; 6 = *cis*-nonachlor. R.T. = Retention time in min; mag. = magnification; abund. = abundance.

of the retention time of standards desorbed by the FD method is shown in Table III. The standard deviation was less than 2 s for each compound.

In our experiment, during desorption, carrier gas was passed through the capillary column at a flow-rate of 20–30 ml/min; however desorbed low-volatile components such as chlordane were retained in the inlet part of the capillary column without any cold trap. The detection limit of the method for each compound was 5 pg (signal-to-noise ratio = 4), which was estimated to represent 0.25 ng/m^3 on collecting 20 l of air.

Comparison of two kinds of desorption method

In this method, if there are no leakages in the system, all thermally desorbed substances can be introduced into the analytical GC column. It was predicted that a peak area obtained with this method would be larger than the peak area with syringe injection (syringe injection of hexane solution containing a standard by the splitless method) in GC–MS, because sample discrimination occurs in the splitless injection of low-volatile compounds. Peak areas obtained from FD method, the BD method and syringe injection were compared. The results are given in Table IV for a comparison of each method when the peak area of the splitless method is taken as 100%. The FD method was the most effective for introducing samples into the GC–MS system, because the peak area was about three times larger than that in the splitless method. This means that sample discrimination did not occur in the FD method and, as a result, a lower limit of detection can be obtained.

In the BD method, the peak areas of all

TABLE III

REPRODUCIBILITY OF RETENTION TIME BY THERMAL DESORPTION METHOD (n = 5)

′ = min; ″ = s.

Compound	Syringe injection	Thermal desorption
Heptachlor	13′36″ ± 0.5″	13′41″ ± 0.9″
Oxychlordane	15′12″ ± 0.5″	15′16″ ± 1.0″
trans-Chlordane	15′40″ ± 0.7″	15′45″ ± 0.8″
cis-Chlordane	15′59″ ± 0.5″	16′4″ ± 1.0″
trans-Nonachlordane	16′4″ ± 0.6″	16′8″ ± 1.0″
cis-Nonachlordane	17′22″ ± 0.4″	17′27″ ± 1.1″

TABLE IV

COMPARISON OF PEAK AREAS WITH THE THERMAL DESORPTION METHODS (n = 5)

Compound	BD method	FD method	BD/FD
Heptachlor	n.d.	2.5	–
Oxychlordane	1.7	2.4	0.71
trans-Chlordane	2.3	3.2	0.72
cis-Chlordane	2.3	3.1	0.74
trans-Nonachlordane	2.1	3.2	0.65
cis-Nonachlordane	2.1	3.2	0.67

compounds were relatively small and especially heptachlor was not desorbed from the Tenax-TA tube. This suggests that degradation of heptachlor was taking place in the Tenax-TA tube during desorption. In order to confirm the decomposed substance, after adding 100 ng of heptachlor the total ion chromatogram (TIC) of desorbed components from the Tenax-TA tube was obtained. However, no decomposed substances were found on the TIC. Reactions of haloganated compounds with Tenax during thermal desorption have been reported [16] and recoveries of bromotrichloromethane and pentachloroethane added to Tenax were conspicuously poor. Tri- and tetrachloroethane which were not added were desorbed from Tenax. In our experiment, although no decomposed substances were detected, there is a probability that other compounds except heptachlor are slightly decomposed in the Tenax-TA tube during desorption, because the recovery of other compounds is about 30% lower in the BD than in the FD method.

Measurement of desorption time and breakthrough volume

Desorption in the recovery test was carried out for 20 min. To determine the accurate desorption time of standard mixtures from the Tenax-TA tube at a desorption temperature 300°C, the FD and BD methods were applied. After the two stop valves had been closed and the GC column temperature was held at 280°C, the elution times of standard mixtures were measured. A SIM chromatogram obtained by the BD method is shown in Fig. 4. The elution time of *cis*-nonachlor, which was the least volatile compound tested, was about 18 min. As the elution time is equal to the desorption time at the desorption temperature, 300°C in this experiment, it takes about 18 min to desorb all the tested compounds by the BD method. On the other hand, the elution time in the FD method is about 10 min. The FD method is superior to the BD method because the desorption time is very short and no degradation occurs.

To estimate the breakthrough volume of low-volatile compounds such as chlordane, an extrapolation method has been used [17]. This is a method for the determination of retention volumes at ambient temperature by linear extrapolation of retention volumes at higher temperature. The retention volume of desorbed compounds by the above-mentioned experiment (BD method) was considered as the retention volume of the adsorbent in the Tenax-TA tube. The breakthrough point is regarded as the start of the peak on the chromatogram. We attempted to estimate the breakthrough volume of *trans*-nonachlor at ambient temperature. The breakthrough volumes of *trans*-nonachlor at eight temperatures between 200 and 340°C were obtained. These values were compensated using the equation for the corrected specific retention volume.

A linear regression equation, $\log V_r = -3.41 +$

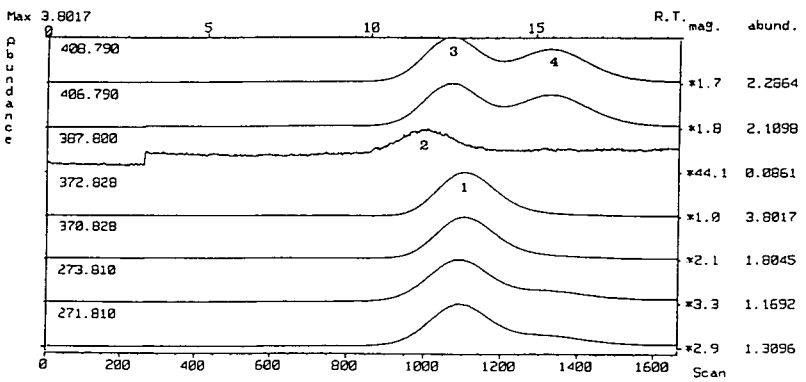

Fig. 4. Elution peak of chlordane standard mixture obtained from Tenax-TA tube by thermal desorption. 1 = Oxychlordane; 2 = *trans*-chlordane + *cis*-chlordane; 3 = *trans*-nonachlor; 4 = *cis*-nonachlor.

1.96(1/T) (where V_r is in m^3), was obtained from the relationship between log V_r and 1/T. The breakthrough volume of *trans*-nonachlor from this equation at ambient temperature (25°C) was 1.5 m^3 on the Tenax-TA tube. This value was sufficient for sampling indoor and ambient air, because the sampling volume was less than 100 l in our experiment.

Measurement of chlordane in indoor air and ambient air

The method was applied to indoor and ambient air samples. Analysis was carried out on several samples collected in the living rooms of houses that had been treated with technical chlordane and ambient air in Kitakyushu City. The volume collected was 20 l for indoor air and 100 l for ambient air for each sample. The SIM chromatograms of house 2 indoor air and ambient air are shown in Fig. 5 and the concentrations are given in Table V. Five compounds (heptachlor, *trans*-chlordane, *cis*-chlordane, *trans*-nonachlor and *cis*-nonachlor) were found in every sample except for oxychlordane, which was a metabolite. The peak patterns of both SIM chromatograms were similar to that of technical chlordane. For example, peaks 6 and 7 in Fig. 5, which are isomers in technical chlordane [18], were detected in every sample. The approximate composition of the five compounds in technical chlordane used in Japan is heptachlor 11–17%, *trans*-chlordane 32–40%, *cis*-chlordane 21–32%, *trans*-nonachlor 15–20% and *cis*-nonachlor 2–10%. The composition of the sample was similar to that of technical chlordane. The total concentration of the five compounds in house 1 that had

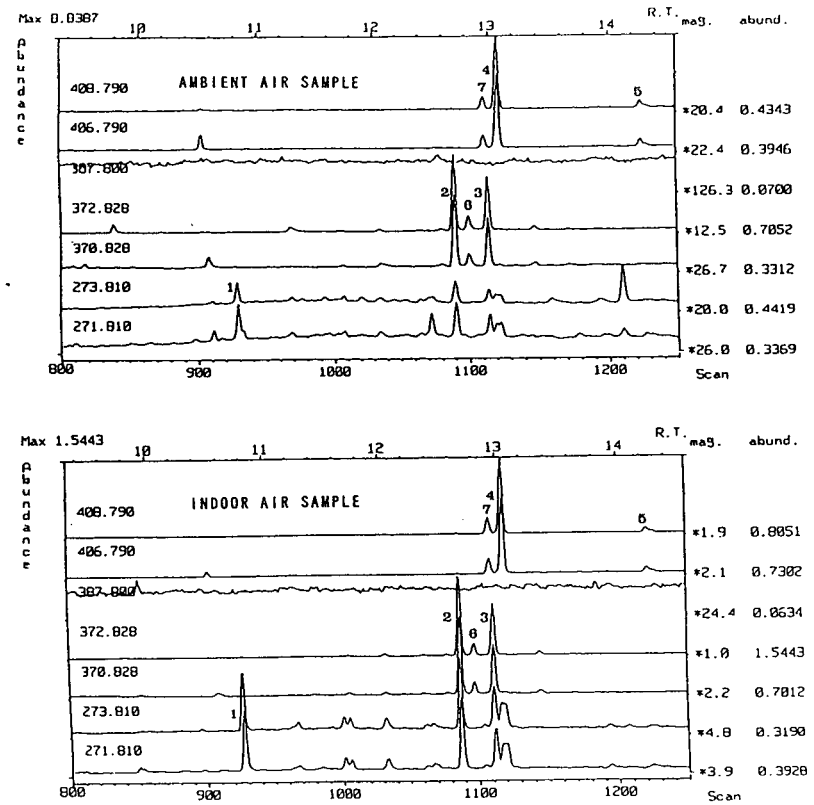

Fig. 5. SIM chromatogram of an indoor air sample (house 2) and ambient air sample in Kitakyushu City. The values following the asterisks are the magnification factors of the chromatograms. 1 = Heptachlor; 2 = *trans*-chlordane; 3 = *cis*-chlordane; 4 = *trans*-nonachlor; 5 = *cis*-nonachlor; 6, 7 = not identified.

TABLE V

CONCENTRATIONS OF CHLORDANE IN INDOOR AIR AND AMBIENT AIR IN KITAKYUSHU

Compound	Chlordane concentration (ng/m^3)		
	House 1[a]	House 2[a]	Ambient Air
Heptachlor	130	6.0	0.23
Oxychlordane	n.d.	n.d.	n.d.
trans-Chlordane	75	12.3	0.61
cis-Chlordane	61	7.6	0.45
trans-Nonachlordane	35	5.5	0.35
cis-Nonachlordane	30	0.46	0.053

[a] House 1 had been treated with technical chlordane 3 years previously and house 2 had been treated 5 years previously.

been treated with chlordane 3 years previously was more than 200 times higher than that in outdoor air.

REFERENCES

1 *IARC Monogr. Eval. Carcinog. Risk Chem. Man*, 20 (1979) 45.
2 *IARC Monogr. Eval. Carcinog. Risk Chem. Man*, 20 (1979) 129.
3 *Chemicals in the Environment*, Environmental Agency of Japan, Tokyo, 1990, p. 169.
4 *Chemicals in the Environment*, Environmental Agency of Japan, Tokyo, 1991, p. 243.
5 T.F. Bidleman and C.E. Olney, *Science*, 183 (1974) 516.
6 E. Atlas and C.S. Giam, *Science*, 211 (1981) 163.
7 J.M. Livingstone and C.R. Jones, *Bull. Environ. Contam. Toxicol.*, 27 (1981) 406.
8 C.J. Wright and R.B. Leidy, *Bull. Environ. Contam. Toxicol.*, 28 (1982) 617.
9 *Manual of Analytical Method*, NIOSH, Cincinnati, OH, 6, 1980, Method S-278.
10 O.Y. Philip and W.K. Wendell, *Bull. Environ. Contam. Toxicol.*, 33 (1984) 13.
11 F. Jitunari, F. Asakawa, T. Nakajima, Y. Manabe and A. Gotoh, *Nihon Koeisi*, 34 (1987) 302.
12 D.J. Anderson and R.A. Hites, *Environ. Sci. Technol.*, 22 (1988) 717.
13 S. Suzuki, S. Nagano and S. Satoh, *Taikiosengakkaisi*, 25 (1990) 123.
14 H. Tsuchida, Y. Hanai and T. Katou, *Taikiosengakkaisi*, 25 (1990) 133.
15 S. Suzuki, *Bunseki Kagaku*, 37 (1988) 524.
16 J.F. Walling, J.E. Bumgarner, D.J. Driscoll, C.M. Morris, A.E. Riley and L.H. Wright, *Atmos. Environ.*, 20 (1986) 51.
17 T. Tanaka, *J. Chromatogr.*, 153 (1978) 7.
18 T. Miyazaki, T. Yamagisi and M. Matsumoto, *J. Food Hyg. Soc. Jpn.*, 26 (1990) 666.

Journal of Chromatography A, 657 (1993) 413–427
Elsevier Science Publishers B.V., Amsterdam

CHROM. 25 504

Evaluation of drying agents for off-line supercritical fluid extraction

Mark D. Burford, Steven B. Hawthorne* and David J. Miller

Energy and Environmental Research Center, University of North Dakota, Box 9018, Grand Forks, ND 58202 (USA)

(First received May 18th, 1993; revised manuscript received August 11th, 1993)

ABSTRACT

Of 21 potential drying agents investigated, five (anhydrous and monohydrated magnesium sulfate, molecular sieves 3A and 5A and Hydromatrix) were able successfully to prevent restrictor plugging by water during off-line supercritical fluid extraction (*e.g.*, 400 atm CO_2 at 60°C) by retaining the majority of the water (but generally not the analytes of interest) in the extraction cell. Increasing the extraction temperature (*e.g.*, to 150°C) or adding a polar modifier [10% (v/v) methanol] to the CO_2 extraction fluid greatly reduced the amount of water the drying agents retained. However, when 10% (v/v) toluene was used for the extraction, the drying agents were able to retain the majority of the water (*ca.* 80% w/w). Polar and non-polar pollutants were quantitatively extracted from the wet drying agents (*i.e.*, water present), but nearly all of the drying agents selectively retained at least one of the polar analytes if used dry (*i.e.*, no water present), thus demonstrating the need for a spike recovery study to determine the potential for analyte loss. The successful drying agents eliminated restrictor plugging when used with moderately wet [*ca.* 20% (w/w) water at a 1:1 reagent-to-sample ratio] and very wet [*ca.* 90% (w/w) water at 4:1 reagent-to-sample ratio] samples without the need to heat the restrictor or the collection solvent.

INTRODUCTION

Supercritical fluid extraction (SFE) has become a popular alternative to conventional liquid solvent extraction methods. However, major emphasis has been placed on the application of SFE to various analytes and matrices, and less consideration has been given to some of the more practical aspects of SFE such as maintaining the supercritical fluid flow during the extraction of real samples. Most native samples contain water, and the presence of even a small amount of water (>1%, w/w) can prove problematic in SFE, as water freezes in the restrictor tip due to the Joule–Thomson cooling effect of the expanding extraction fluid at the restrictor outlet. As the cooling of the restrictor and collection solvent are very rapid (*i.e.*, the collection solvent temperature can drop to <0°C within 60 s [1]), plugging due to frozen water can occur within minutes of commencing an extraction. Maintaining the extraction flow is even more difficult with very wet samples [*ca.* >40% (w/w) water] such as fresh plant material and biosludges, as the sample matrix may compact down into the outlet of the extraction cell causing the outlet frit (rather than the restrictor) to block within seconds of pressurizing the extraction cell.

To avoid plugging from water, a number of techniques have been employed. The water can be removed from the sample prior to the extraction by air drying, oven drying (*ca.* 100°C) or freeze-drying. However, such dehydration techniques are time consuming and increase the possibility of the loss of volatile and semi-volatile analytes. Further, the presence of water can in some instances increase the extraction efficiency of the analytes from the sample matrix [2–4] so

* Corresponding author.

0021-9673/93/$06.00
SSDI 0021-9673(93)E0910-M

that removal of the water prior to SFE can be disadvantageous.

Instead of removing the water from the sample, dispersants such as sand or glass beads can be mixed with the sample matrix to stop the sample compacting and forming an impervious plug, or dispersants and/or filter-paper can be placed between the sample and the outlet frit to eliminate frit plugging [5–7]. The collection solvent can be maintained above 0°C or the restrictor can be heated to stop water freezing at the tip of the restrictor, but low collection efficiencies for volatile compounds have been associated with both techniques [1].

A recent development has been the use of drying agents to retain the water inside the extraction cell [8–14]. There are several advantages to using drying agents in that they are both sample dispersants and sorbent traps for water. As water potentially remains sorbed to the drying agent in the extraction cell during SFE, the need to control the collection solvent or restrictor temperature may be eliminated. A number of drying agents have been used in SFE with varying success, namely, Hydromatrix (pelletized diatomaceous earth) [8–10], magnesium sulfate [10,14], sodium sulfate [10–13], calcium chloride [13], molecular sieve [11] and silica [11]. However, at present a detailed survey has not been undertaken to evaluate the applicability of the drying agents with several real samples. In this study we investigated a number of conventional drying agents in terms of water retention, analyte retention and extraction flow characteristics under various SFE conditions and with several real samples.

EXPERIMENTAL

Samples and standards

Several drying agents were evaluated, including molecular sieves, water-soluble polymers, diatomaceous earth (Hydromatrix), alumina, silica and metal salts. The drying agents carboxymethylcellulose (Aldrich, Milwaukee, WI, USA), xanthan gum (Aldrich), guar gum (Aldrich), polyacrylamide gel (Aldrich), molecular sieves 3A, 4A, 5A and 13X (Alltech, Deerfield, IL, USA), 100–200-mesh (150–75 μm) chromatographic-grade alumina (Fisher Scientific, Fair Lawn, NJ, USA), 100–200-mesh chromatographic-grade silica gel (Fisher Scientific) and 60–100-mesh (250–150 μm) Florisil (Fisher Scientific) were used as received. The drying agents, Hydromatrix (diatomaceous earth received from ISCO, Lincoln, NE, USA), anhydrous sodium sulfate (Fisher Scientific), anhydrous magnesium sulfate (Fisher Scientific), anhydrous calcium sulfate (Fisher Scientific), anhydrous copper sulfate (Aldrich), anhydrous calcium oxide (Fisher Scientific), anhydrous boron trioxide (Fisher Scientific), anhydrous potassium carbonate (Fisher Scientific) and anhydrous calcium chloride (Fisher Scientific) were sieved and the 30–80-mesh (600–180 μm) fractions collected for the study. Monohydrated magnesium sulfate was made by selective dehydration of heptahydrated magnesium sulfate (Fisher Scientific) at 160°C for 2 h. The heptahydrated magnesium sulfate was initially mixed with 2-mm diameter silanized glass beads (Fisher Scientific) to prevent the reagent from forming a hard mass during dehydration. After oven drying, the drying agent was ground in a pestle and mortar and sieved to obtain the 30–80-mesh fraction used in this study.

Standards (2 mg/ml each) of eleven compounds from the Environmental Protection Agency (EPA) semi-volatile target compound list (chosen for their range of polarities) were used to determine the potential retention of analytes on the drying agents (see Table IV). The eleven compounds were prepared in methylene chloride and stored at −10°C until used. The spiking level for the semi-volatile pollutants was 20 μg of each compound.

Three real samples with different water contents and a history of extraction cell outlet frit and restrictor plugging problems were chosen to investigate the suitability of the drying agents for SFE. Petroleum waste sludge was obtained from a commercial refinery and contained *ca.* 6% (w/w) water (based on oven drying at 105°C for 2 h) and a high concentration (*ca.* 20% w/w) of extractable hydrocarbons including a complex mixture of *n*-alkanes (C_{13}–C_{40}) and polycyclic aromatic hydrocarbons (PAHs). All extractions were performed on the sample as received. The lake sediment soil was collected in the Red River

Valley, North Dakota (USA) and contained *ca.* 20% (w/w) water (as determined by oven drying at 105°C for 2 h) and <0.05% (w/w) extractable hydrocarbons. Before extraction, the sample was sieved through a 2-mm screen to remove sticks and other debris. The biosludge was obtained from a commercial refinery. Prior to extraction, the sample was centrifuged at 3000 rpm (*ca.* 1250 *g*) for 30 min to remove the suspended particles from the aqueous media. The aqueous supernatant was then discarded and the wet precipitate collected and stored at −10°C until used. The precipitate contained *ca.* 90% (w/w) water (as determined by oven drying at 105°C for 2 h) and *ca.* 0.5% (w/w) extractable hydrocarbons, the majority of which were C_{13}–C_{30} *n*-alkanes.

A fourth real sample was used to investigate the volatile analyte losses which might occur when the sample is air or oven dried or mixed with an exothermic drying agent. A wet petroleum waste sludge obtained from a commercial refinery was chosen as it contained a sufficient amount of water [*ca.* 30% (w/w) as determined by oven drying] to generate an appreciable amount of heat when mixed with magnesium sulfate. The sample also contained both volatile and semi-volatile analytes [*ca.* 4% (w/w) extractable hydrocarbons] including a complex mixture of *n*-alkanes (C_8–C_{32}), alkylbenzenes and phenols. The sample was used as received.

Supercritical fluid extraction

Two ISCO Model 260D syringe pumps were used for the SFE extractions, one containing pure SFC-grade CO_2 and the other premixed CO_2–10% (v/v) methanol or CO_2–10% (v/v) toluene (Scott Gases, Plumsteadville, PA, USA). Each pump was filled and operated independently to avoid any possible carryover of modifier. The SFE pumps were connected to 0.5- or 2.5-ml extraction cells with 1/16 in. (1.6 mm) O.D. stainless steel tubing and "Slip-free" finger-tight connectors (Keystone Scientific, Bellefonte, PA, USA). A 1-m coil of 1/16 in. (1.6 mm) O.D. tubing (placed before the extraction cell to prewarm the fluid to the extraction temperature) and the extraction cell were placed in a thermostated tube heater to maintain the extraction temperature.

The flow-rate of the supercritical fluid through the extraction cell was controlled by a 10 cm × 32 μm I.D. × 145 μm O.D. restrictor cut from fused-silica tubing (Polymicro Technologies, Phoenix, AZ, USA). However, when using CO_2–methanol as the extraction fluid it was found that the restrictor became brittle and broke within a few minutes of commencing the extraction. To eliminate the problem of restrictor breakages, the restrictor was secured inside a stainless-steel tube [10 cm long × 0.02 in. (0.5 mm) I.D. × 1/16 in. (1.6 mm) O.D.] as described elsewhere [15].

Extracted analytes were collected by inserting the outlet of the restrictor into a 7.4-ml vial (48 mm height × 14 mm I.D. neck) containing 5 ml of Fisher Optima-grade acetone. The collection vial was either free standing in air or placed in a container of water (60 ml of water in a 100-ml beaker) initially at room temperature. The collection solvent volume was maintained by small additions of solvent during SFE.

Initial experiments were performed to determine the amount of water required to plug a 10 cm × 32 μm I.D. capillary restrictor. Increasing amounts of water (HPLC grade, Fisher Scientific) were injected on to the top of 600 mg of silanized 70–80-mesh glass beads placed inside a 0.5-ml extraction cell. The cell was then immediately sealed and extracted with CO_2 at 60°C and 400 atm. A 150-μl volume of water was found to block the restrictor even when the collection vial was placed in a beaker of water to reduce the cooling of the collection solvent. As previous work had shown that maintaining the collection solvent temperature above 0°C improved the extraction flow for wet samples [16], the initial evaluation of the drying agents was carried out with the collection vial in a beaker of water. However, subsequent experiments demonstrated that a beaker of water was no longer required when the "successful" drying agents which passed the initial evaluation were used with a high temperature (*e.g.*, 150°C) or organic-modified supercritical fluid. Further, a continuous extraction flow could be obtained with pure low-temperature CO_2 (60°C) and a cooled collection solvent by increasing the amount of the "successful" drying agent used.

A 150-μl volume of water was used throughout the study to evaluate the ability of the drying agents to retain water. For consistency, all the drying agents were packed into the extraction cell and water was added to the reagents in the following manner. Silanized 70–80-mesh-glass beads (*ca.* 150 mg) were initially placed at the bottom of a 0.5-ml extraction cell to minimize plugging of the extraction cell outlet frit with fines from the drying agents. The extraction cell was then filled with drying agent (*ca.* 150–250 mg depending on the density and physical packing characteristic of the drying agent). In some instances (*i.e.*, magnesium sulfate) glass beads were also mixed with the drying agent to avoid forming a hard plug in the extraction cell during SFE. The 150-μl volume of water was injected on to the top of the reagents. The cell was then immediately sealed and placed inside the tube heater, equilibrated for 10 min and extracted for 10 min at either 60 or 150°C with pure CO_2 at 400 atm, or modified CO_2 [*i.e.*, CO_2–10% (v/v) methanol at 400 atm and 60°C or CO_2–10% (v/v) toluene at 400 atm and 80°C]. At the end of the extraction, the water content in the collection solvent was determined by Karl-Fischer titration [17].

To determine if analytes were retained on the drying agents, 10 μl of the semi-volatile pollutant mixture were spiked on to the top of *ca.* 200 mg of wet (150 μl of water added) or dry (no water added) reagents. The 0.5-ml extraction cell was then immediately sealed to prevent any loss of the volatile spike components, placed inside the tube heater, equilibrated for 10 min and then extracted for 10 min with CO_2 at 400 atm and 60°C. The extracted analytes recovered in the collection solvent were determined by GC with flame ionization detection (FID).

Three samples (petroleum waste sludge, biosludge and soil) known to cause frit and restrictor plugging problems were used to test the ability of the drying agent to retain water from real samples. Silanized 70–80-mesh glass beads (*ca.* 100 mg) were placed at the bottom of a 0.5- or 2.5-ml extraction cell to prevent plugging of the extraction cell outlet frit from sample matrix material or from fines extracted of the drying agent. The drying agent [200 mg (0.5-ml cell) or 800 mg (2.5-ml cell)] was then placed inside the extraction cell as either a "bed" of drying agent with the environmental sample (200 mg) placed on top, or the drying agent was mixed with the environmental sample [1:1 or 4:1 (w/w) drying agent-to-sample ratio] and the mixture placed inside the extraction cell (0.5 or 2.5 ml, respectively). The extraction cell was then immediately sealed, placed inside the tube heater, equilibrated for 10 min and extracted for 30 min with CO_2 at 400 atm and 60°C.

To determine the potential loss of volatile analytes when drying an environmental sample prior to extraction, a wet [30% (w/w) water] petroleum waste sludge containing both volatile and semi-volatile analytes was air dried at room temperature for 18 h or oven dried at 105°C for 1 h. The possible losses of volatile components on mixing with an exothermic drying agent (anhydrous magnesium sulfate) were also determined by comparing the components recovered when the wet petroleum waste sludge was mixed with the magnesium sulfate with those recovered when the drying agent was used as a "bed" under the wet sludge sample. The air-dried, oven-dried, and "bed" or "mixture" of petroleum waste sludge was extracted with 400 atm CO_2 at 60°C for 30 min. The extracted components were determined by GC–FID.

Gas chromatographic analysis

All GC analyses were carried out with a Hewlett-Packard Model 5890 gas chromatograph with both FID and electron-capture detection (ECD). Hydrogen was the carrier gas and nitrogen was used as the detector make-up gas for ECD. The semi-volatile pollutant extracts and the petroleum waste sludge extracts were determined by GC–FID and the drying agent extracts by GC–FID and GC–ECD. The injections were performed in the split mode with a 10:1 splitting ratio (drying agent and semi-volatile pollutant extracts) into a wide-bore (25 m × 0.32 mm I.D., 0.17 μm film thickness) HP-5 fused-silica capillary column or a 40:1 splitting ratio (real samples) into a narrow-bore (50 m × 0.2 mm I.D., 0.33 μm film thickness) HP-5 fused-silica capillary column. The injector and detector temperatures were maintained at 300°C.

GC separations of the drying agent extracts were performed with the oven temperature initially at 40°C, then programmed at 12°C/min to 320°C. For the semi-volatile pollutant extracts, the oven temperature at injection was 50°C for 1 min, then programmed at 12°C/min to 280°C. The wet petroleum waste sludge extracts were analyzed with the oven temperature set at 40°C for 2 min, then programmed at 6°C/min to 300°C. The internal standards used for GC–FID analysis of the drying agent extracts, semi-volatile pollutant extracts and the wet petroleum waste sludge extracts were phenanthrene (8 μg), fluoranthene (30 μg) and 2-phenylnaphthalene (460 μg), respectively. The internal standard used for the GC–ECD analysis of the drying agent extracts was 1,2,4-trichlorobenzene (1 μg).

RESULTS AND DISCUSSION

As the presence of water in environmental samples can cause the restrictor to plug during SFE, the simplest solution would be to air or oven dry the sample prior to extraction. However, such drying techniques are not suitable as they can result in the loss of volatile and semi-volatile analytes. For example, as shown in Fig. 1, air drying a wet petroleum waste sludge completely removed the volatile C_8–C_{11} *n*-alkanes from the sample and also reduced the amount of semi-volatile analytes present [*e.g.*, 60% of the phenol and 40% of the *m*- and *p*-cresol lost, Table I]. Oven drying the sample resulted in even greater analyte losses with only the high-molecular-mass C_{25}–C_{30} *n*-alkane recoveries remaining unaffected by the drying technique (Table I, Fig. 1).

Water retention of drying agents during extraction with CO_2 at 60 and 150°C

Table II summarizes the ability of several drying agents to eliminate restrictor plugging after adding 150 μl of water to 200 mg of reagent and extracting for 10 min with CO_2 at 400 atm and 60 or 150°C. [Note that in this initial survey (Table II) a beaker of water was required to help maintain a continuous extraction flow although, as discussed below, it was not required at high

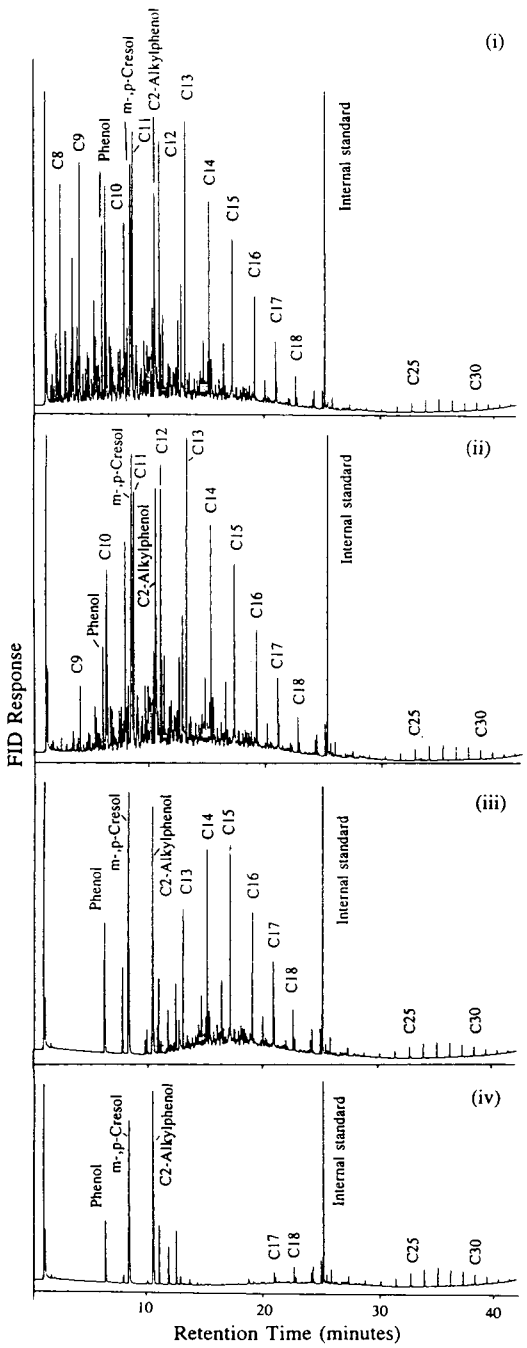

Fig. 1. GC–FID of the SFE extracts from a wet petroleum sludge: (i) wet sample placed on bed of anhydrous magnesium sulfate; (ii) wet sample mixed with anhydrous magnesium sulfate; (iii) sample air dried at room temperature for 18 h; (iv) sample oven dried at 105°C for 1 h. Extractions were performed with CO_2 at 400 atm and 60°C for 30 min.

TABLE I

LOSSES OF VOLATILE AND SEMI-VOLATILE ORGANICS FROM A WET PETROLEUM WASTE SLUDGE ON MIXING WITH $MgSO_4$ AND FROM AIR OR OVEN DRYING

Native analyte	Analyte concentration (μg/g)[a] (bed of drying agent + sample)	Recovery (%)[b]		
		Mixture of drying agent + sample (R.S.D., %)	Sample air dried for 18 h (R.S.D., %)[c]	Sample oven dried for 1 h at 105°C (R.S.D., %)[c]
n-Octane (C_8)	1499 ± 275	3 (49)	ND[d]	ND
m-, *p*-Xylene	510 ± 102	22 (51)	ND	ND
n-Nonane (C_9)	1967 ± 184	22 (12)	ND	ND
Phenol	3066 ± 573	81 (6)	44 (1)	18 (12)
n-Decane (C_{10})	1906 ± 231	49 (11)	ND	ND
m-, *p*-Cresol	5242 ± 743	81 (4)	63 (1)	39 (11)
n-Undecane (C_{11})	2125 ± 287	68 (9)	ND	ND
C_2-alkylphenol	1321 ± 183	89 (2)	109 (9)	65 (11)
n-Dodecane (C_{12})	1880 ± 257	75 (11)	17 (3)	ND
n-Tridecane (C_{13})	1598 ± 181	81 (8)	34 (8)	ND
n-Tetradecane (C_{14})	1618 ± 132	70 (7)	51 (9)	ND
n-Pentadecane (C_{15})	908 ± 117	86 (7)	82 (10)	ND
n-Hexadecane (C_{16})	536 ± 35	83 (7)	92 (10)	ND
n-Heptadecane (C_{17})	304 ± 14	81 (4)	88 (9)	12 (3)
n-Octadecane (C_{18})	138 ± 6	85 (4)	90 (9)	37 (2)
n-Nonadecane (C_{19})	115 ± 3	95 (3)	93 (8)	72 (2)
n-Pentacosane (C_{25})	31 ± 2	90 (2)	93 (2)	106 (6)
n-Hexacosane (C_{26})	41 ± 2	90 (5)	95 (2)	105 (5)
n-Heptacosane (C_{27})	44 ± 4	86 (5)	98 (7)	104 (6)
n-Octacosane (C_{28})	37 ± 5	92 (6)	111 (5)	110 (7)
n-Nonacosane (C_{29})	36 ± 4	89 (6)	103 (8)	105 (5)
n-Triacontane (C_{30})	26 ± 3	92 (8)	108 (6)	108 (4)

[a] Analyte concentration was determined from triplicate extractions with CO_2 at 400 atm and 60°C for 30 min (average value ± standard deviation).

[b] Percentage recovery relative to values obtained when bed of drying agent was used. Values in parentheses are the relative standard deviations of triplicate 30-min extractions with CO_2 at 400 atm and 60°C.

[c] Percentage recovery was normalized to wet mass.

[d] ND = Not detected. FID detection limit ≈4 μg/g as concentration in the original sample.

extraction temperatures, with modified fluids or with larger amounts of the "successful" drying agents.] Half of the drying agents investigated retained >80% of the spiked water at 400 atm CO_2 and 60°C, and a continuous extraction flow was attainable for the entire 10-min extraction. The "successful" drying agents stopped the initial removal of a large percentage of the water from the extraction cell, so that water no longer blocked the restrictor within seconds of commencing the extraction (as occurred without the drying agents). The rest of the drying agents investigated were either unable to stop water plugging the restrictor or were extracted into the collection solvent, resulting in a plugged extraction cell outlet frit and/or restrictor (Table II).

None of the reagents investigated efficiently retained all the water in the extraction cell (Table II). The poor water retention of the "unsuccessful" drying agents may be related to the temperature (60°C) of the supercritical fluid extraction. Heating the drying agent to 60°C may partially dehydrate the reagent (*e.g.*, $CaCl_2 \cdot 6H_2O$ was dehydrated to $CaCl_2 \cdot 2H_2O$ [18]) and decrease the water capacity of the drying agent. Even the "successful" drying agents which prevented restrictor plugging only retained *ca.* 80% (w/w) of the water as *ca.* 20% (w/w) of the

added water was recovered in the collection solvent. A similar amount of water was generally recovered from all the "successful" drying agents regardless of whether the water was retained by adsorption (molecular sieves, alumina and Florisil), absorption (water-soluble polymer), physical entrapment (molecular sieves) or the formation of a hydrate (metal sulfates).

The drying agents which were "successful" at maintaining an extraction flow at 60°C were also "successful" at eliminating restrictor plugging at 150°C (Table II). However, at the higher extraction temperature of 150°C all the "successful" drying agents were dehydrated [*ca.* 75% (w/w) water removed] owing to the temperature limitation of the reagents (*e.g.*, $MgSO_4 \cdot 7H_2O$ is dehydrated to $MgSO_4 \cdot H_2O$ [18]) and the order of magnitude increase in the solubility of water in CO_2 (*i.e.*, 0.008 mole fraction of water in CO_2 at 400 atm and 50°C compared with 0.06 mole fraction at 150°C [19]), which increased the extraction efficiency of water from the drying agents (Table II). The Joule–Thomson cooling effect at the restrictor tip was also decreased at the high extraction temperature (Fig. 2), so that

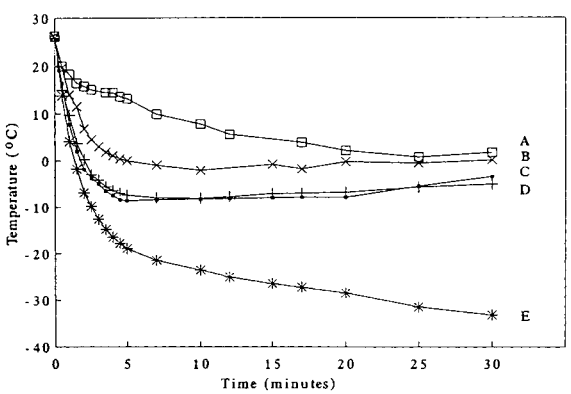

Fig. 2. Collection solvent temperature using various extraction and collection conditions. Temperature profiles are shown for the collection solvent (5 ml of acetone) in a 7.4-ml vial with a 10 cm × 32 μm I.D. restrictor using: (A) CO_2 at 400 atm and 60°C with the collection vial in a beaker of water; (B) CO_2 at 400 atm and 150°C with the collection vial free standing in air; (C) CO_2–10% (v/v) methanol at 400 atm and 60°C with the collection vial free standing in air; (D) CO_2–10% (v/v) toluene at 400 atm and 80°C with the collection vial free standing in air; and (E) CO_2 at 400 atm and 60°C with the collection vial free standing in air.

water no longer froze in the restrictor and the collection vial did not require a beaker of water to obtain a continuous extraction flow. However, the drying agents were still needed because, in their absence, liquid water quickly plugged the restrictor on commencing the extraction (Table II). Even though several of the drying agents successfully avoided restrictor plugging, only Florisil and molecular sieve 3A were able to retain a moderate amount [*ca.* 40% (w/w)] of the water at the 150°C extraction temperature.

Examination of the extraction cell and collection solvent after extracting the wet drying agents at 400 atm CO_2 and 60°C revealed that several of the reagents had precipitated in the extraction cell outlet frit, restrictor and/or collection solvent (Table II). The plugging problem associated with the extraction of the drying agents was partially related to the 60°C extraction temperature, which melted one of the hydrated reagents ($Na_2SO_4 \cdot 10H_2O$, which has a melting point of 32°C [18]), blocking the outlet frit of the extraction cell and the restrictor. Fines or small fragments removed from the drying agents during SFE also caused frit and restrictor plugging problems. These fines are probably formed as a dust during the manufacture of the reagents or from agitation of the drying agent container. However, the fines were successfully removed and the plugging eliminated from several of the reagents (*e.g.*, magnesium sulfate and Hydromatrix) by sieving the reagents prior to extraction. Unfortunately, five of the drying agents (calcium sulfate, copper sulfate, calcium oxide, potassium carbonate and calcium chloride) still plugged the frit and restrictor even after they were sieved, and small particles of drying agents were observed in the collection solvent (Table II). Impurities from some of the drying agents (*e.g.*, carboxymethylcellulose and guar gum) were also found in the supercritical fluid extracts by GC–FID (Table II), which made these reagents unsuitable for SFE.

Examination of the drying agent after SFE indicated that a number of the reagents had been compressed into a hard plug which may block the extraction cell outlet frit (Table II). For example, the water-soluble polymers (carboxymethylcellulose, guar gum and polyacrylamide

TABLE II

FLOW CHARACTERISTICS OF WET DRYING AGENTS USING CO_2 AT 400 ATM AND 60 OR 150°C

Reagent	Qualitative flow-rate[a] (CO_2, 400 atm, 60°C)	Water in collection solvent (%)[b] (CO_2, 400 atm, 60°C)	Qualitative flow-rate[a] (CO_2, 400 atm, 150°C)	Water in collection solvent (%)[b] (CO_2, 400 atm, 150°C)	Extractable components from reagents[c] (CO_2, 400 atm, 60°C)	Physical description of reagents after SFE (CO_2, 400 atm, 60°C)	Temperature of reagent on hydration[d] (°C)
Glass beads	Blocked	–	Blocked	–	–	Wet particles	21
Carboxymethylcellulose	Continuous	13	Continuous	–	Yes	Hard plug[f]	22
Xanthan gum	Continuous	13	Continuous	79	No	Rubbery strand	23
Guar gum	Intermittent	–	–	–	Yes	Rubbery strand	20
Polyacrylamide	Blocked	–	–	–	–	Hard plug[f]	23
Hydromatrix	Continuous	19	Continuous	88	No	Wet particles	21
Molecular sieve 3A	Continuous	18	Continuous	56	No	Wet particles	40
Molecular sieve 4A	Continuous	15	Continuous	74	No	Wet particles	60
Molecular sieve 5A	Continuous	14	Continuous	79	No	Wet particles	35
Molecular sieve 13X	Continuous	18	Continuous	74	No	Wet particles	85
Alumina	Continuous	17	Continuous	83	No	Wet particles	21
Silica	Intermittent	–	–	–	No	Wet particles	23
Florisil	Continuous	14	Continuous	60	No	Wet particles	21
Sodium sulfate	Blocked	–	–	–	–	White paste	25
Magnesium sulfate ($MgSO_4$)	Continuous	12	Continuous	73	No	Hard plug[f]	94
Magnesium sulfate ($MgSO_4 \cdot H_2O$)	Continuous	43	Continuous	71	No	Semi-hard plug	61
Calcium sulfate	Blocked	–	–	–	–[e]	Wet particles	26
Copper sulfate	Blocked	–	–	–	–[e]	Hard plug[f]	69
Calcium oxide	Blocked	–	–	–	–[e]	Hard plug[f]	93
Boron trioxide	Intermittent	–	–	–	–	Semi-hard plug	103
Potassium carbonate	Blocked	–	–	–	–[e]	White paste	68
Calcium chloride	Blocked	–	–	–	–[e]	White paste	91

[a] The flow was assessed as continuous (constant flow-rate ± 0.2 ml/min), intermittent (flow initially constant but within a few minutes of extraction plugging starts to occur) or blocked (no flow). Collection vial was placed in a beaker of water (initially at room temperature).

[b] Percentage of spiked water recovered in collection solvent as determined by Karl Fischer titration. Water content was only determined for agents showing a continuous flow.

[c] Extractable components from drying agent were detected in collection solvent by GC–FID.

[d] The drying agent (1 g) was placed inside a polystyrene cup and hydrated with water (3 ml). The change in temperature with the addition of water was measured with a J-thermocouple.

[e] Particles of drying agent were seen in collection solvent.

[f] Drying agent formed hard plug during extraction which proved difficult to remove from the extraction cell.

gel) form sticky hydrated gels at atmospheric pressure, but at the 400 atm extraction pressure the hydrated gels become hard or rubbery strands. On inspection of a polymer plug or strand removed from the extraction cell after depressurization, it was observed that the exterior portion of the plug had formed into a hard, clear solid, whereas the interior of the plug was dry or sticky in texture. These physical differences suggest that water preferentially flowed along the interior extraction cell wall so that "plug" flow within the cell was not achieved. Mixing a dispersant (100 μm glass beads) with the polymers did not improve the flow characteristics. However, magnesium sulfate also forms a hard plug, but mixing glass beads with the reagent made it easier to unpack the extraction cell after SFE. (Note that without glass beads a hammer and chisel were required to remove the drying agent.) Monohydrated magnesium sulfate formed a semi-hard plug which was easier to remove from the extraction cell, but the reagent retained *ca.* 30% less water than anhydrous magnesium sulfate (Table II).

Several of the drying agents also produced a large amount of heat on hydration (Table II). For example, adding water to boron trioxide increased the temperature of the mixture sufficiently to boil the water. The significant amount of heat generated from several of the drying agents may make them undesirable for use with samples containing volatile analytes (as discussed below).

Water retention of drying agents with extraction by modified CO_2

Of the 21 drying agents initially investigated, eleven "successfully" prevented restrictor plugging by water during supercritical fluid extraction with pure CO_2. The "successful" drying agents were further evaluated with a water-insoluble (toluene) and water-soluble (methanol) modified CO_2 supercritical fluid (Table III), as organic modifiers are frequently used to increase the supercritical fluid extraction efficiency of many organic pollutants from environmental matrices [20]. Hence the ideal drying agent would be expected to retain water efficiently when used with these modified fluids.

Most of the drying agents proved suitable for use with the CO_2–toluene extraction fluid, the reagents retaining >75% of the water in the

TABLE III

FLOW CHARACTERISTICS OF WET DRYING AGENTS USING CO_2–10% (v/v) TOLUENE AT 400 ATM AND 80°C AND CO_2–10% (v/v) METHANOL AT 400 ATM AND 60°C

Drying agent	Qualitative flow-rate[a]		Water in collection solvent (%)[b]		Particles of reagent in collection solvent	
	CO_2–10% (v/v) toluene	CO_2–10% (v/v) methanol	CO_2–10% (v/v) toluene	CO_2–10% (v/v) methanol	CO_2–10% (v/v) toluene	CO_2–10% (v/v) methanol
Glass beads	Blocked	Continuous	–	73	No	No
Xanthan gum	Continuous	Continuous	12	59	No	No
Hydromatrix	Continuous	Blocked	11	–	No	Yes
Molecular sieve 3A	Continuous	Continuous	20	92	No	Yes
Molecular sieve 4A	Continuous	Continuous	10	88	No	Yes
Molecular sieve 5A	Continuous	Blocked	23	–	No	Yes
Molecular sieve 13X	Continuous	Continuous	15	87	No	Yes
Alumina	Continuous	Continuous	17	76	No	Yes
Florisil	Continuous	Blocked	11	–	No	Yes
Magnesium sulfate ($MgSO_4$)	Intermittent	Blocked	22	–	Yes	Yes
Magnesium sulfate ($MgSO_4 \cdot H_2O$)	Intermittent	Blocked	24	–	Yes	Yes

[a] The flow-rates are assessed as continuous (constant flow-rate ± 0.2 ml/min), intermittent (flow initially constant but within a few minutes of extraction plugging starts to occur) or blocked (no flow). Collection vial was placed in a beaker of water (initially at room temperature).

[b] Percentage of spiked water recovered in collection solvent as determined by Karl Fischer titration. Water content was only determined for agents showing a continuous flow.

TABLE IV

RECOVERY OF SEMI-VOLATILE POLLUTANTS FROM DRYING AGENTS USING CO_2 AT 400 ATM AND 60°C

Form of drying agent	Compound	Recovery (%)[a]									
		Xanthan[b]	Hydromatrix	M.S. 3A	M.S. 4A	M.S. 5A	M.S. 13X	Alumina	Florisil	$MgSO_4$	$MgSO_4 \cdot H_2O$
Wet	2-Chlorophenol	66 (51)	92 (7)	96 (6)	97 (3)	95 (13)	99 (3)	99 (3)	95 (5)	93 (3)	105 (3)
	o-Cresol	65 (52)	93 (7)	93 (6)	95 (2)	99 (5)	96 (5)	97 (5)	95 (5)	93 (4)	102 (1)
	Nitrobenzene	72 (56)	94 (7)	94 (8)	92 (8)	98 (4)	98 (2)	97 (3)	95 (6)	94 (4)	100 (1)
	2-Chloroethoxymethane	68 (53)	95 (6)	95 (2)	98 (1)	99 (5)	98 (2)	99 (3)	96 (6)	95 (4)	100 (1)
	1,2,4-Trichlorobenzene	66 (54)	95 (8)	93 (7)	99 (1)	99 (4)	100 (1)	99 (13)	98 (5)	95 (6)	100 (2)
	4-Chloroaniline	64 (55)	98 (6)	94 (8)	99 (6)	101 (6)	100 (4)	99 (3)	96 (6)	97 (3)	96 (2)
	Tetradecane	66 (55)	95 (6)	92 (8)	98 (2)	98 (4)	98 (2)	99 (4)	95 (7)	94 (4)	96 (1)
	Dibenzofuran	65 (55)	98 (4)	96 (6)	96 (3)	96 (8)	98 (5)	98 (4)	94 (7)	93 (8)	97 (3)
	Diethyl phthalate	67 (55)	95 (4)	102 (3)	96 (1)	96 (4)	98 (2)	98 (3)	94 (6)	95 (7)	99 (1)
	Phenanthrene	66 (56)	100 (2)	103 (3)	96 (1)	98 (4)	98 (3)	98 (3)	99 (3)	96 (6)	100 (1)
	Chrysene	65 (54)	104 (5)	101 (2)	102 (2)	104 (5)	100 (4)	100 (4)	99 (3)	96 (11)	94 (6)
Dry	2-Chlorophenol		101 (8)	97 (2)	19 (57)	93 (5)	0 (0)	0 (0)	97 (7)	95 (5)	98 (5)
	o-Cresol		97 (9)	89 (3)	60 (20)	89 (4)	0 (0)	0 (0)	88 (7)	103 (1)	98 (5)
	Nitrobenzene		99 (9)	96 (3)	98 (2)	91 (4)	0 (0)	87 (3)	96 (9)	98 (9)	100 (8)
	2-Chloroethoxymethane		98 (7)	90 (2)	96 (2)	90 (5)	0 (0)	90 (1)	92 (7)	98 (2)	94 (6)
	1,2,4-Trichlorobenzene		98 (8)	94 (3)	98 (3)	91 (5)	87 (21)	93 (3)	93 (7)	102 (2)	97 (7)
	4-Chloroaniline		94 (11)	92 (2)	0 (0)	80 (5)	0 (0)	0 (0)	11 (15)	0 (0)	0 (0)
	Tetradecane		97 (8)	94 (3)	98 (1)	90 (3)	88 (21)	94 (3)	92 (7)	101 (1)	97 (6)
	Dibenzofuran		97 (8)	94 (2)	99 (2)	90 (1)	37 (48)	89 (2)	93 (7)	102 (1)	97 (6)
	Diethyl phthalate		96 (10)	12 (48)	0 (0)	89 (4)	0 (0)	2 (91)	0 (0)	99 (2)	94 (8)
	Phenanthrene		98 (9)	96 (3)	100 (0)	90 (3)	53 (37)	92 (2)	92 (7)	102 (1)	97 (6)
	Chrysene		100 (9)	96 (3)	101 (3)	90 (3)	50 (33)	71 (13)	94 (8)	102 (0)	94 (7)

[a] Values in parentheses are relative standard deviations (%) of triplicate 10-min extractions. Collection vial was in a beaker of water (initially at room temperature).

[b] Values in parentheses are relative standard deviations (%) of six 10-min extractions from xanthan gum only.

extraction cell to achieve a continuous extraction flow (Table III). However, the drying agents were unsuitable for use with the CO_2–methanol extraction fluid, as the reagents were generally co-extracted with the majority of the water, and the reagents precipitated in the extraction cell outlet frit, restrictor and collection solvent (Table III). The most severe plugging problems were with anhydrous and monohydrated magnesium sulfate, which were extracted by both the CO_2–toluene and CO_2–methanol, and irreversibly blocked the frit and restrictor (Table III). It is interesting that only xanthan gum was not extracted by either modified extraction fluid, possibly because the reagent formed a gel on hydration.

The addition of an organic modifier to CO_2 reduced the rate at which the collection solvent was cooled (Fig. 2), and a continuous extraction flow was achieved with both modified fluids without placing the collection vial in a beaker of water. The polar CO_2–methanol extracted the majority (*ca.* 80%, w/w) of the water from the drying agents, whereas the aromatic CO_2–toluene (Table III), with a low affinity for water, extracted about the same amount of water from the reagents as pure CO_2 at 60°C (Table II). Further, in contrast to the CO_2–toluene, the CO_2–methanol extraction fluid did not require a drying agent to maintain a continuous extraction flow (Table III). To confirm this observation, the 0.5-ml extraction cell was filled with water, extracted with CO_2–methanol and the extract collected in an organic solvent which was allowed to cool to below 0°C during the extraction. A liquid was observed leaving the restrictor for the first 50 s of the extraction, followed by bubbles of CO_2 typically seen during normal SFE. After 5 min of extraction all the water had been removed from the extraction cell, and no restrictor plugging had occurred during the entire extraction procedure.

Retention of semi-volatile pollutants on drying agents

Ideally, the "successful" drying agents should be able to retain selectively the extracted water from real samples but not retain the extracted analytes of interest. Therefore, the affinity of the "successful" drying agents for semi-volatile pollutants of various volatility, polarity and functional groups was investigated (Table IV). As the drying agents were intended to be used with wet samples, the semi-volatile pollutant mixture was spiked directly on to wet (150 μl of added water) drying agents. Supercritical CO_2 at 400 atm and 60°C quantitatively recovered all the analytes from the majority of the wet drying agents (Table IV). The quantitative recoveries were attributed to the deactivation of the active sites of the drying agents with water. For example, the deactivation of alumina with 5% (w/w) water prior to extraction enabled organochlorine pesticides to be recovered quantitatively from the sorbent using supercritical CO_2 [21]. However, poor analyte recoveries with high relative standard deviations were obtained with xanthan gum. The low average recoveries and poor reproducibilities obtained for all the analytes regardless of polarity were due to the "non-plug" flow or channeling of the CO_2 through the polymer, resulting in only partial hydration of the drying agent (*i.e.*, dry interior) which, as discussed below, had a significant effect on analyte retention.

The recovery of the analytes from "dry" drying agents was also evaluated (Table IV) as all the drying agents were dehydrated to some extent under SFE conditions, and a routine procedure for the extraction of environmental samples could include drying agents regardless of whether the sample is wet or dry. Without water present, a number of the drying agents proved highly retentive, completely retaining at least one of the test analytes (most often 4-chloroaniline and/or diethyl phthalate; Table IV). Poor analyte recoveries were seen for the porous molecular sieves (4A and 13X), particularly molecular sieve 13X, which has the largest pore diameter (10 Å) and adsorbed the majority of analytes regardless of polarity. As might be expected, the polar basic alumina adsorbent retained the weakly acidic phenols in addition to 4-chloroaniline and diethyl phthalate. The acidic Florisil adsorbent selectively retained diethyl phthalate and the basic 4-chloroaniline, whereas the weakly acidic magnesium sulfate retained only the 4-chloroaniline. Only Hydromatrix gave

quantitative recoveries of all the analytes investigated. As most of the drying agents retained at least one of the analytes, a spike recovery of the target analytes should always be performed to determine the appropriate drying agent for a particular set of analytes.

Thus, of the eleven drying agents investigated only five (*i.e.*, those displaying the least retention of the target analytes, namely Hydromatrix, molecular sieves 3A and 5A and anhydrous and monohydrated magnesium sulfate) proved suitable for use with environmental samples. As shown in Table II, these drying agents did not cause detectable contamination of the extracts when analyzed by GC–FID. To evaluate further the potential for contamination, extracts from each of the five drying agents were also analyzed by GC–ECD. None of the drying agents added detectable GC–ECD contaminants (compared with *ca.* 10 pg injected of 1,2,4-trichlorobenzene) to the SFE (CO_2 at 400 atm and 60°C) extracts. However, a few trace contaminants from the acetone solvent and/or CO_2 were found in the collection solvent blanks when no drying agent was present.

Evaluation of drying agents with real samples

Three real samples with different water contents and SFE-extractable components were chosen to test the ability of the drying agents to avoid restrictor plugging when using CO_2 at 400 atm and 60°C. The samples were (i) a lake sediment soil [*ca.* 20% (w/w) water] containing a very low concentration (<0.05%, w/w) of extractable hydrocarbons; (ii) a biosludge [90% (w/w) water] with *ca.* 0.5% (w/w) extractable hydrocarbons; and (iii) a petroleum waste sludge [*ca.* 6% (w/w) water] with a consistency and color similar to those of molasses and with a high concentration (*ca.* 20%, w/w) of extractable hydrocarbons. In the absence of drying agents, all three samples caused restrictor and/or frit plugging problems.

Only the drying agents that had a low affinity for the semi-volatile pollutants (*i.e.*, retained none or only one of the analytes in Table IV) were investigated with the real samples (Table V). Two extraction cell-loading procedures were used. The drying agents were placed inside the extraction cell either as a "bed" of reagent with the environmental sample placed on top, or the reagents were mixed with the environmental sample and were then placed inside the extraction cell. With both procedures, no attempt to regulate the collection solvent temperature was made. However, if restrictor plugging was still encountered when using a drying agent, the collection vial was placed in a beaker of water at room temperature to maintain the collection solvent above 0°C.

Plugging problems were encountered with all three environmental samples if just dispersants (*e.g.*, 100 μm glass beads) were used as a bed or mixed with the samples. Conversely, when a drying agent (bed or mixture) was used with the samples a good extraction flow was usually attainable, demonstrating that the reagents were not just dispersants but also sorbents which retained the water. The success of the drying agents at eliminating restrictor plugging generally depended on the nature of the sample (Table V). For the lake sediment soil, a 1:1 drying agent-to-sample ratio was sufficient to eliminate the restrictor plugging problems. Continuous extraction flows could be obtained without keeping the collection solvent above 0°C as was required when the soil sample was mixed with the glass beads. The soil contained virtually no extractable hydrocarbons but a high concentration of water (20%, w/w), hence the restrictor plugging was associated with the water. Therefore, the drying agents retained a sufficient amount of the water or slowed the rate of water removal from the extraction cell to reduce or eliminate freezing water at the restrictor tip. (Note that occasional plugging of the restrictor still occurred but that within a few seconds the flow would restart unaided.) The various cell-loading procedures using a bed or mixture of drying agent and sample (with the exception of Hydromatrix) had no observable effect on the extraction flow.

With very wet samples such as the biosludge [*ca.* 90% (w/w) water, which was equivalent to 180 μl of water], the 1:1 ratio of drying agent to sample was unable to eliminate restrictor plug-

TABLE V

FLOW CHARACTERISTICS OF REAL SAMPLES WITH DRYING AGENTS USING CO_2 AT 400 ATM AND 60°C

Drying agent	Extraction flow[a]				
	Soil (1:1)[b]	Biosludge (1:1)[b]	Biosludge (4:1)[b]	Petroleum sludge (1:1)[b]	Petroleum sludge (4:1)[b]
$MgSO_4$ (bed)	Continuous	Intermittent	Continuous	Blocked	Intermittent
$MgSO_4$ (mixed)	Continuous	Intermittent	Intermittent	Intermittent	Intermittent
$MgSO_4$ (bed, collection vial in water)	Continuous	Continuous	Continuous	Continuous	Continuous
$MgSO_4 \cdot H_2O$ (bed)	Continuous	Intermittent	Intermittent	Blocked	Intermittent
$MgSO_4 \cdot H_2O$ (mixed)	Continuous	Intermittent	Intermittent	Intermittent	Intermittent
$MgSO_4 \cdot H_2O$ (bed, collection vial in water)	Continuous	Continuous	Continuous	Continuous	Continuous
Molecular sieve 3A (bed)	Continuous	Intermittent	Continuous	Intermittent	Intermittent
Molecular sieve 3A (mixed)	Continuous	Intermittent	Intermittent	Intermittent	Intermittent
Molecular sieve 3A (bed, collection vial in water)	Continuous	Continuous	Continuous	Continuous	Continuous
Molecular sieve 5A (bed)	Continuous	Intermittent	Continuous	Intermittent	Intermittent
Molecular sieve 5A (mixed)	Continuous	Intermittent	Intermittent	Intermittent	Intermittent
Molecular sieve 5A (bed, collection vial in water)	Continuous	Continuous	Continuous	Continuous	Continuous
Hydromatrix (bed)	Intermittent	Intermittent	Intermittent	Intermittent	Intermittent
Hydromatrix (mixed)	Continuous	Intermittent	Intermittent	Intermittent	Intermittent
Hydromatrix (bed, collection vial in water)	Continuous	Continuous	Continuous	Continuous	Continuous

[a] The extraction flow was assessed as continuous (flow obtained without intervention, occasionally the flow would stop but would restart unaided), intermittent (flow required periodic gentle warming of the tip of the restrictor by placing the restrictor and ones thumb against the wall of the collection vial) or blocked (no flow).

[b] Ratio of drying agent to sample (w/w).

ging (Table V). Again, the plugging problem was associated with the high concentration of water, and a continuous extraction flow was only obtained when the collection solvent temperature was maintained above 0°C. By increasing the amount of anhydrous magnesium sulfate or molecular sieve 3A and 5A to a 4:1 drying agent-to-sample ratio, a sufficient amount of water was retained in the extraction cell to obtain a continuous extraction flow with a cooled collection solvent (*i.e.*, the beaker of water was no longer required, Table V). The cell loading procedure did have an effect on the extraction flow of the biosludge, because mixing the drying agent with the sample matrix was not as effective as using a bed of drying agent to stop water from plugging the restrictor. However, King *et al.* [22] have shown that mixing the drying agent with the sample can be advantageous for samples such as a spent bleaching clay which can become severely compacted without a reagent, so that the rate of extraction is reduced. Therefore, placing the mixture of drying agent and sample on a bed of drying agent may be more appropriate when extracting highly compressible samples.

Severe frit and restrictor plugging problems were encountered with the petroleum waste sludge (Table V). Employing a drying agent at a 1:1 or 4:1 reagent-to-sample ratio enabled a continuous extraction flow to be obtained with the sludge, although in both instances the collection vial had to be kept in a beaker of water to stop the restrictor from plugging. The need to regulate the collection solvent temperature was related to the nature of the sample matrix. The petroleum waste sludge contained a high concen-

tration (20%, w/w) of extractable hydrocarbons and a relatively low concentration (6%, w/w) of water so that the majority of the restrictor plugging appeared to be associated with the extracted hydrocarbons and not the water.

The cell-loading procedure also had an effect on the recovery of volatile analytes from a sample when mixed with an exothermic drying agent. For example, mixing anhydrous magnesium sulfate with a wet [30% (w/w) water] petroleum waste sludge caused significant losses of C_8–C_{12} *n*-alkanes, although these losses were not as severe as those produced from air or oven drying the sample (Fig. 1, Table I). During the mixing, the temperature of anhydrous magnesium sulfate and the wet sludge noticeably increased and a strong fuel odor was produced. Conversely, if the wet sludge was placed on a "bed" of anhydrous magnesium sulfate so that the physical contact between the drying agent and the sample was greatly reduced, the recovery of the volatile *n*-alkanes was significantly increased (Table I).

CONCLUSIONS

Of the 21 drying agents tested, eleven (Hydromatrix, molecular sieves, xanthan gum, carboxymethylcellulose, magnesium sulfate, alumina and Florisil) successfully prevented water from plugging a capillary restrictor during extraction with CO_2 at 400 atm and 60°C. However, none of these "successful" drying agents irreversibly retained the water. Instead, the reagents decreased the rate at which the water was removed from the cell. Increasing the extraction temperature to 150°C or adding a polar modifier (methanol) to the CO_2 greatly decreased the amount of water retained by the drying agents, whereas the addition of an aromatic modifier (toluene) resulted in no such decrease. Even though none of the drying agents retained significant amounts of polar and non-polar test analytes in the presence of water, all the reagents except Hydromatrix caused specific losses of one or more polar analytes when no water was present in the extraction cell. Therefore, a spike recovery study of the target analytes should always be undertaken to determine the appropriate drying agent for a particular set of analytes. Using the best five drying agents (*i.e.*, those displaying the least retention of polar analytes, namely Hydromatrix, molecular sieves 3A and 5A and anhydrous and monohydrated magnesium sulfate) a 1:1 (w/w) drying agent-to-sample ratio was sufficient to prevent water from plugging the restrictor when used with moderately wet samples [20% (w/w) water], but a 4:1 reagent-to-sample ratio was required with very wet samples [90% (w/w) water]. For samples containing volatile analytes, mixing the sample with exothermic drying agents (*e.g.*, magnesium sulfate) should be avoided to minimize losses of volatile analytes from the heat of hydration.

ACKNOWLEDGEMENTS

The financial support of the US Environmental Protection Agency (EMSL-LV) and the joint funding of the American Petroleum Institute and the US Department of Energy are gratefully acknowledged, as are instrument loans from ISCO.

REFERENCES

1 M.D. Burford, S.B. Hawthorne, D.J. Miller and T. Braggins, *J. Chromatogr.*, 609 (1992) 321.
2 P. Hubert and O.G. Vitzthum, *Angew. Chem., Int. Ed. Engl.*, 17 (1978) 710.
3 H.-B. Lee and T.E. Peart, *J. Chromatogr.*, 594 (1992) 309.
4 T.M. Fahmy, M.E. Paulaitis, D.M. Johnson and M.E.P. McNally, *Anal. Chem.*, 65 (1993) 1462.
5 C.A. Thomsom and D.J. Chesney, *J. Chromatogr.*, 543 (1991) 187.
6 J.A. Field, D.J. Miller, T.M. Field, S.B. Hawthorne and W. Giger, *Anal. Chem.*, 64 (1992) 3161.
7 P. Subra and P. Boissinot, *J. Chromatogr.*, 543 (1991) 413.
8 M.L. Hopper and J.W. King, *J. Assoc. Off. Anal. Chem.*, 74 (1991) 661.
9 N.L. Porter, A.F. Rynaski, E.R. Campbell, M. Saunders, B.E. Richter, J.T. Swanson, R.B. Nielsen and B.J. Murphy, *J. Chromatogr. Sci.*, 30 (1992) 367.
10 V. Lopez-Avila, J. Benedicto, N.S. Dodhiwala, R. Young and W.F. Beckert, *J. Chromatogr. Sci.*, 30 (1992) 335.
11 E.R. Campbell and B.E. Richter, in *Proceedings of the International Symposium on Supercritical Fluid Chromatography and Extraction, Park City, UT, January 14–17, 1991*, 1991, p. 105.
12 T. Greibrokk, *J. Chromatogr.*, 626 (1992) 33.

13 W.H. Griest, R.S. Ramsey, C.-H. Ho and W.M. Caldwell, *J. Chromatogr.*, 600 (1992) 273.
14 S.E. Eckert-Tilotta, S.B. Hawthorne and D.J. Miller, *Fuel*, 72 (1993) 1015.
15 M.D. Burford, S.B. Hawthorne, D.J. Miller and J. Macomber, *J. Chromatogr.*, 648 (1993) 445.
16 J.J. Langenfeld, M.D. Burford, S.B. Hawthorne and D.J. Miller, *J. Chromatogr.*, 594 (1992) 297.
17 L.F. Fieser and M. Fieser, *Reagents for Organic Synthesis,* Wiley, New York, 1967.
18 R.C. Weast (Editor), *Handbook of Chemistry and Physics*, CRC Press Cleveland, OH, 55th ed., 1974.
19 K.A. Evelein, R.G. Moore and R.A. Heidemann, *Ind. Eng. Chem., Process Des. Dev.*, 15 (1976) 423.
20 S.B. Hawthorne, *Anal. Chem.*, 62 (1990) 633.
21 J.E. France, J.W. King and J.M. Snyder, *J. Agric. Food Chem.*, 39 (1991) 1871.
22 J.W. King, G.R. List and J.H. Johnson, *J. Supercrit. Fluids*, 5 (1992) 38.

Journal of Chromatography A, 657 (1993) 429–434
Elsevier Science Publishers B.V., Amsterdam

CHROM. 25 580

Electrophoretically mediated microanalysis of ethanol

Bryan J. Harmon, Dale H. Patterson and Fred E. Regnier*

Purdue University, Department of Chemistry, West Lafayette, IN 47907-1393 (USA)

(First received July 28th, 1993; revised manuscript received September 22nd, 1993)

ABSTRACT

Capillary electrophoresis was used to determine ethanol by the methodology of electrophoretically mediated microanalysis (EMMA). In EMMA, spatially distinct analyte and analytical reagent zones of differing electrophoretic mobility are merged under the influence of an electric field, and the resulting product is transported to the detector. The enzymatic oxidation of ethanol to acetaldehyde by alcohol dehydrogenase was utilized, and the concurrent reduction of NAD^+ to NADH was monitored at 340 nm as a measure of the quantity of ethanol injected. Quantitation using an internal standard and normalization for peak migration time yielded a R.S.D. of 2.7%, and the linear range extended to that quantity of ethanol which could be reacted prior to passing by the detection window. Comparison of the EMMA technique to the Sigma spectrophotometric procedure revealed that the two methods do not yield significantly different values for the determination of ethanol. The EMMA method offered the advantages of electrophoretic mixing and miniaturization.

INTRODUCTION

Capillary electrophoresis has traditionally exploited the variability in electrophoretic mobility among charged species as a method to separate such substances. However, diversity in migration velocity under the influence of an applied electric field also offers the capability of electrophoretically mixing spatially distinct zones of chemical reagents [1–4]. As we have recently described [4], capillary electrophoretic systems offer potential for performing ultramicroassays using a methodology known as electrophoretically mediated microanalysis (EMMA). In EMMA, electrophoretic mixing is utilized to merge zones containing the analyte and analytical reagents; the reaction is then allowed to proceed either in the presence or absence of the applied electric field; and, finally, the detectable product is transported under the influence of an applied potential to the detector.

This paper demonstrates the use of EMMA as an analytical technique for the determination of substrates by enzymatic reactions. The enzymatic system chosen for this study is the catalytic oxidation of ethanol to acetaldehyde by alcohol dehydrogenase (ADH; EC 1.1.1.1):

$$CH_3CH_2OH + NAD^+ \overset{ADH}{\longleftrightarrow} CH_3CHO + NADH + H^+$$

The concurrent reduction of the coenzyme NAD^+ to NADH can be monitored by the increase in absorbance at 340 nm as a measure of the extent of reaction and, therefore, the amount

* Corresponding author.

0021-9673/93/$06.00
SSDI 0021-9673(93)E1006-L

of ethanol contained in the sample. ADH-based enzymatic methods [5] are commonly used for the determination of alcohol in many clinical laboratories. The equilibrium, which lies far to the left at neutral pH, can be forced to the right by buffering at alkaline pH and by trapping the acetaldehyde with an agent, such as hydrazine or semicarbazide.

EXPERIMENTAL

Instrumentation

All EMMA assays were performed using a BioFocus 3000 capillary electrophoresis system from Bio-Rad Labs (Hercules, CA, USA). Polyimide-coated fused-silica capillaries (Polymicro Technologies, Phoenix, AZ, USA) of 50 μm I.D. × 180 μm O.D. were utilized. The capillaries were of 24 cm total length with a separation length (distance from injection inlet to detection window) of 19.4 cm.

The spectrophotometric determinations were performed using a Spectronic 20D spectrophotometer (Milton Roy, Niagara Falls, NY, USA) operated at 340 nm.

Chemicals

Yeast alcohol dehydrogenase (YADH; 380 units/mg solid as assayed by Sigma), nicotinamide adenine dinucleotide (NAD^+), glycine buffer solution (0.5 *M*, pH 9.0) containing hydrazine trapping agent, and *p*-nitrophenol were purchased from Sigma (St. Louis, MO, USA). Absolute ethanol and mesityl oxide (neutral marker used in determination of electrophoretic mobilities) were purchased from Midwest Solvents of Illinois (Pekin, IL, USA) and Aldrich (Milwaukee, WI, USA), respectively. Glycine running buffer (50 m*M*, pH 9) was prepared by diluting the 0.50 *M* glycine buffer solution with degassed, double-distilled, deionized water. The analytical reagent/running buffer solution was prepared by dissolving YADH (200 units/ml for Figs. 1–3 and 5; 50 to 400 units/ml for Fig. 4) and NAD^+ (10 m*M*) in the running buffer solution and adjusting to pH 9.0 with 1 *M* NaOH. Ethanol standards were prepared by diluting absolute ethanol with appropriate amounts of degassed, double-distilled, deionized water and adding *p*-nitrophenol as an internal standard.

EMMA procedures

The capillaries were conditioned with 10-min rinsings of 1 *M* NaOH and running buffer prior to use. The capillary and the buffer reservoirs were filled by pressure with analytical reagent/buffer solution, and a plug of sample was then hydrodynamically injected by the application of pressure for a pressure · time constant of 1 p.s.i. · s. The assay was effected by applying an electric field (125 V/cm for Figs. 1 and 2; 300 V/cm for Figs. 3–5) and monitoring the absorbance electropherogram at 340 nm. The capillary was thermostatted by circulating water at 25°C throughout the assay. Between determinations the capillary was purged for 30 s with 0.1 *M* KOH followed by 60 s with analytical reagent/running buffer solution.

Spectrophotometric procedures

The spectrophotometric determination of ethanol was performed as described in the manual [6] contained with the Sigma Diagnostics Alcohol (Ethanol) determination kit.

RESULTS AND DISCUSSION

EMMA methodology

Conventional reaction-based chemical analysis requires four processes: (1) analyte and analytical reagent metering, (2) initiation of reaction, (3) control of reaction conditions and product formation and (4) detection of species whose production or depletion is indicative of the quantity of analyte of interest. Capillary electrophoretic systems, as employed in the EMMA determination of ethanol, are capable of executing each of these tasks [4]. In the EMMA determination of ethanol, the analytical reagents were metered by filling the capillary and the buffer reservoirs with pH 9 glycine buffer solution containing ADH and NAD^+, and the analyte was then metered by injecting a plug of ethanol solution at the anodic inlet.

Electrophoretic mixing of the analyte and analytical reagents was initiated by the application of an electric field. The reagent zones

TABLE I

ELECTROPHORETIC MOBILITIES OF CHEMICAL SPECIES AT pH 9

Chemical species	Electrophoretic mobility ($cm^2\ V^{-1}\ s^{-1}$)
Ethanol	0
YADH	$-1.6 \cdot 10^{-4}$
NAD^+	$-1.2 \cdot 10^{-4}$
NADH	$-2.3 \cdot 10^{-4}$
p-Nitrophenol (internal standard)	$-3.0 \cdot 10^{-4}$

migrated at differential rates under the influence of an electric field as dictated by their respective electrophoretic mobilities listed in Table I. Neutral ethanol migrated with the bulk electroosmotic flow toward the cathode while ADH and NAD^+ were each negatively charged at pH 9 and electrophoresed against the electroosmotic flow. Consequently, the ethanol zone interpenetrated the adjacent zones of ADH and NAD^+. Since the analytical reagents were maintained as a continuous stream within the capillary and the buffer reservoirs, upon electrophoretic mixing ethanol remained engaged with the ADH and NAD^+ zones throughout its traversal of the capillary.

The reaction phase of this assay was performed under the influence of a constant applied potential. As the ethanol zone incubated within the analytical reagent zones, NADH was produced as dictated by the kinetics of YADH [7,8]. Because NADH is negatively charged, it was continually transported from the vicinity of the reaction under the influence of the constant applied potential. However, since the magnitude of its electrophoretic mobility is less than that of the electroosmotic flow, NADH migrated toward the detection window. We have previously described the effects of kinetics and differential electrophoretic mobility upon the observed concentration profile of the NADH [4]. Typical electropherograms obtained for EMMA determinations of ethanol are depicted in Fig. 1.

Clinical substrate assays are frequently based upon end-point methods in which the reaction is allowed to essentially reach completion prior to

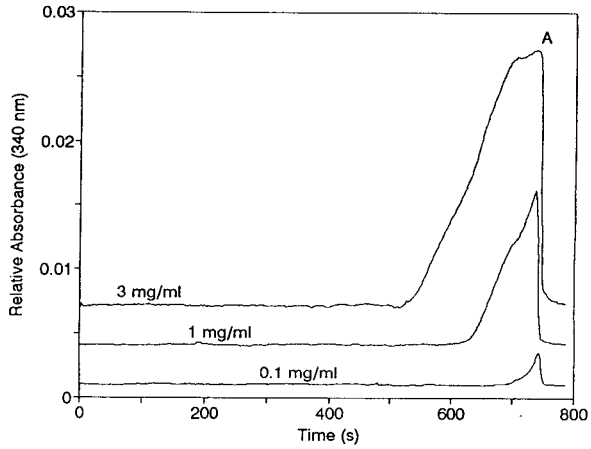

Fig. 1. EMMA determinations of 3, 1 and 0.1 mg/ml samples of ethanol; (A) NADH accumulation due to diffusional interpenetration at reagent interfaces prior to application of electric potential. For conditions see text.

taking a spectrophotometric reading. In the EMMA methodology, an end-point determination requires that all of the ethanol react prior to passing by the detection window. NADH formed after the ethanol zone passes by the detection window is not observed. This truncation effect places the upper limit on the linear range of the technique [4]. Assuming electrophoretic mixing is rapid, the total reaction time t_{rxn} available to fully deplete the substrate is equal to the time required for the ethanol to migrate from the injection point to the detection window:

$$t_{rxn} = \frac{l}{(\mu_{ep,EtOH} + \mu_{eo})E} \quad (1)$$

where l is the separation length of the capillary, $\mu_{ep,EtOH}$ is the electrophoretic mobility of ethanol, μ_{eo} is the electroosmotic flow and E is the electric field strength. Based upon the experimental electroosmotic flow of $4.4 \cdot 10^{-4}$ $cm^2\ V^{-1}\ s^{-1}$ and electric field strength of 125 V/cm, the assays depicted in Fig. 1 offered an available substrate incubation time of approximately 350 s.

Since NADH had a lower transport velocity than ethanol, the first NADH formed (due to diffusional interpretation at the interfaces of the adjacent reagent zones prior to the application of the electric field [1,4]; indicated by A in Fig. 1), was the last to be detected. The first NADH

which could be detected was that which formed as any remaining unreacted ethanol passed by the detection window. Therefore, there was a detection time window t_{det} during which NADH could be observed:

$$\frac{l}{(\mu_{ep,EtOH} + \mu_{eo})E} \leq t_{det} \leq \frac{l}{(\mu_{ep,NADH} + \mu_{eo})E} \quad (2)$$

where $\mu_{ep,NADH}$ is the electrophoretic mobility of NADH. Based upon the experimental electroosmotic flow of $4.4 \cdot 10^{-4}$ cm^2 V^{-1} s^{-1}, an electric field strength of 125 V/cm, and the electrophoretic mobilites given in Table I, the detection window for the assays depicted in Fig. 1 extended from approximately 350 to 740 s.

Reproducibility of EMMA method

Fifteen replicate determinations of a sample containing 0.5 mg/ml ethanol were made to evaluate the assay reproducibility. Quantitation based upon NADH peak area yielded a relative standard deviation (R.S.D.) of 7.0%. However, this lack of precision can be largely attributed to the irreproducibility of the hydrodynamic injection volumes (R.S.D. of injection volume was 7.1% for this study based upon peak area of internal standard). This lack of precision of sample introduction can be ascribed to the fact that we utilized the minimum possible injection volume of the BioFocus 3000's pressure injection system (pressure · time constant of 1 p.s.i. · s corresponding to an injection volume of approximately 3 nl as calculated by the Poiseuille equation). Because precision in capillary electrophoresis is largely dependent upon the reproducibility of sample introduction [9], an internal standard was used to compensate for error in injection. *p*-Nitrophenol was selected as the internal standard for this study because it exhibited high absorbance at 340 nm at alkaline pH and was sufficiently anionic at pH 9 to prevent comigration with the NADH peak. When quantitation was based upon the ratio of NADH peak area to *p*-nitrophenol peak area, R.S.D. for this study improved to 3.0%. Fig. 2 illustrates an EMMA determination of ethanol utilizing *p*-nitrophenol as the internal standard.

Temporal peak width and, consequently, peak

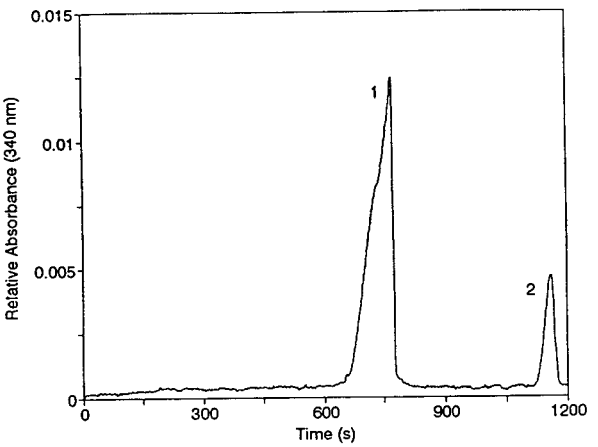

Fig. 2. EMMA determination of 1 mg/ml sample of ethanol. Peaks: 1 = NADH (analytical reaction product); 2 = *p*-nitrophenol (internal standard). For conditions see text.

area in capillary electrophoresis are inversely proportional to the instantaneous velocity of the detected species passing the detection window [10]:

$$\text{area} \propto \frac{1}{(\mu_{ep,det} + \mu_{eo})E} \quad (3)$$

where $\mu_{ep,det}$ is the electrophoretic mobility of the detected species. Thus, compensating for variability in transport velocity further improved reproducibility in our EMMA determinations of ethanol. Normalization was achieved by dividing each peak area by its migration time. The migration time of the NADH interfacial peak represents the migration velocity of the NADH because reduced cofactor in this peak traverses the entire capillary. NADH formed later in the assay travels only a portion of the length of the capillary. Although this normalization procedure actually utilizes the average migration velocity of the detected species rather than the instantaneous velocity at the detection window, quantitation based upon the ratio of NADH peak area to internal standard peak area, each normalized by dividing by their respective migration times, further reduced the R.S.D. to 2.7%.

Linearity of EMMA method

Fig. 3 depicts a typical calibration curve obtained in the EMMA determination of ethanol

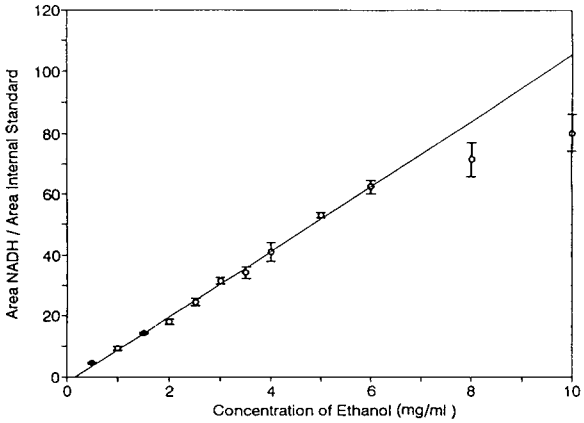

Fig. 3. Calibration curve for EMMA determination of ethanol. Points are the mean of three replicate determinations. Brackets indicate 95% confidence intervals. Line represents linear regression of 0.5 to 6 mg/ml data ($R^2 = 0.997$). For conditions see text.

samples ranging from 0.5 to 10 mg/ml. Each data point represents the mean of three replicate determinations. Quantitation was based upon the ratio of NADH and internal standard peak areas each normalized by their respective migration times. The linear range extended from 0.5 to 6 mg/ml. Linear regression of the 0.5 to 6 mg/ml data yielded $y = 10.72x - 1.844$ with a correlation coefficient of 0.997. Truncation of the NADH profile at the lower limit of the NADH detection window (eqn. 2) was observed beyond 6 mg/ml, thereby causing the response to deviate from linearity because the available reaction time (eqn. 1) was insufficient to fully deplete the ethanol. Less precision was also observed for concentrations which experienced truncation. This phenomenon was due to the fact that the internal standard was not able to compensate for the variable degree of truncation experienced with differing volumes of the same concentration. Linear regression of NADH peak areas without internal standard or migration time normalization produced a correlation coefficient of 0.969 for the 0.5 to 6 mg/ml data depicted in Fig. 3.

The linear range of the EMMA assay can be extended by increasing either the substrate incubation time or the rate of reaction. The available reaction time may be increased by decreasing the electric field strength or by increasing the separation length of the capillary (eqn. 1). However, these methods also result in a concurrent increase in the analysis time that is imposed by the upper limit of the NADH detection window (eqn. 2) or by the increased migration time of the internal standard if one is utilized. The linear range was extended without adversely affecting the analysis time by elevating the concentrations of the analytical reagents, thereby increasing the rate of reaction. Fig. 4 illustrates the effect of ADH concentration in the analytical reagent/running buffer on the upper limit of the linear range.

Comparison of EMMA to spectrophotometric method

An inter-method correlation study confirmed the validity of the EMMA technique. Eight samples contained between 0 and 4 mg/ml of ethanol were analyzed by both the EMMA procedure and the Sigma Diagnostics Alcohol (Ethanol) kit. The Sigma spectrophotometric method employs the same enzymatic system as the EMMA determination. Fig. 5 compares the results of the EMMA (x) and Sigma (y) methods. Linear regression analysis of the data yielded $y = 1.04x - 0.038$ mg/ml, with a correlation coefficient of 0.995. The paired results of the eight samples produced a paired Student's t calculation of 0.284 compared to a table value ($\alpha = 0.05$; 95% confidence interval) of 2.365. These results indicated that the two methods did

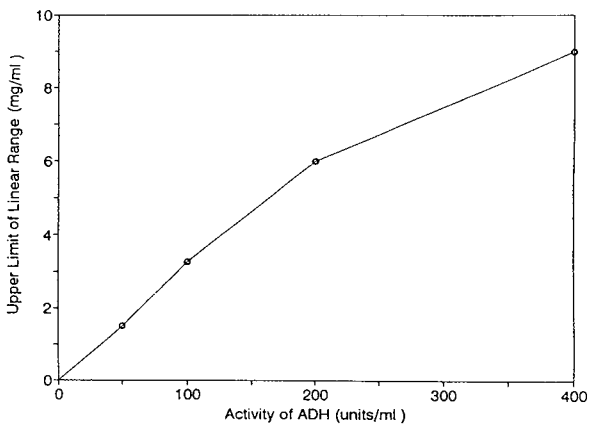

Fig. 4. Effect of concentration of alcohol dehydrogenase in analytical reagent/running buffer on the upper limit of the linear range for EMMA determination of ethanol. For conditions see text.

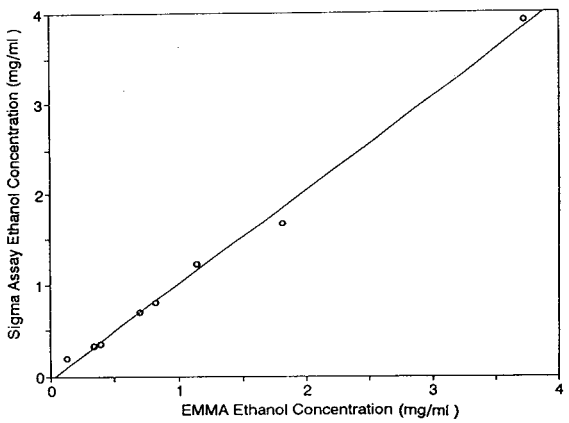

Fig. 5. Correlation of eight ethanol determinations by EMMA and Sigma spectrophotometric methods. Line represents linear regression results ($R^2 = 0.995$). Conditions stated in text.

not yield significantly different values for the determination of ethanol.

Advantages of EMMA methodology

The advantages of the EMMA methodology include those of electrophoretic mixing and miniaturization. As chemical species electrophorese essentially independently of the bulk solution, analytes can encounter many times their own volume in analytical reagents without experiencing the dilution associated with bulk mixing. In the EMMA determinations depicted in Fig. 1, the ethanol zone encountered approximately 46 and 35 times its own initial volume in ADH and NAD^+, respectively, based upon the 3 nl initial volume of the analyte plug, the differential mobilities of the reagents, and the separation length of the capillary.

The EMMA technique also requires minimal volumes of analyte. The assays shown in Fig. 1 were performed on an injection of approximately 3 nl of sample. However, the logistics of sample introduction in current capillary electrophoresis systems generally require several μl of sample actually be available. The lower limit of detection by UV absorption for the EMMA method was approximately 4 μg/ml of ethanol (300 fmol based upon an injection volume of 3 nl). However, this detection limit could be lowered by two orders of magnitude by the use of laser-induced fluorescence detection of NADH. The detection limits for EMMA determinations of substrates do not approach those reported in the analysis of enzymes [1,3] due to the non-amplifying nature of the assay. In addition to the potential for determining ultramicro samples, the EMMA method consumes very small amounts of analytical reagents. For the 13-min assays depicted in Fig. 1, only 0.8 μl of analytical reagent/running buffer solution was depleted due to the bulk electroosmotic flow.

We have performed the EMMA ethanol assay without sample preparation on beverage samples and on ultrafiltrate samples obtained from the interstitial fluid of rats dosed with ethanol. No significant interferences were observed. However, the determination of blood samples does require sample preparation (*i.e.* deproteinization) as adsorption of matrix components to the capillary's silica surface greatly diminishes reproducibility. We have not yet attempted to perform the EMMA ethanol determination on surface-modified capillaries as a method to prevent this phenomenon.

ACKNOWLEDGEMENTS

Financial support was received in part from the National Institute of Health (Grant No. GM 25431) and from the Purdue Research Foundation. We also wish to thank Michael Linhares for the rat ultrafiltrate samples.

REFERENCES

1 J. Bao and F.E. Regnier, J. *Chromatogr.*, 608 (1992) 217.
2 S. Liu and P.K. Dasgupta, *Anal. Chim. Acta*, 268 (1992) 1.
3 D. Wu and F.E. Regnier, *Anal. Chem.*, 65 (1993) 2029.
4 B.J. Harmon, D.H. Patterson and F.E. Regnier, *Anal. Chem.*, 65 (1993) 2655.
5 H.M. Redetzki and W.L. Dees, *Clin. Chem.*, 22 (1976) 83
6 *Procedure No. 332-UV*, Sigma Diagnostics, St. Louis, MO, 1990.
7 C.C. Wratten and W.W. Cleland, *Biochemistry*, 2 (1963) 935.
8 C.J. Dickenson and F.M. Dickinson, *Biochem. J.*, 147 (1975) 303.
9 D.J. Rose, Jr. and J.W. Jorgenson, *Anal. Chem.*, 60 (1988) 642.
10 X. Huang, W.F. Coleman and R.N. Zare, *J. Chromatogr.*, 480 (1989) 95.

Journal of Chromatography A, 657 (1993) 435–439
Elsevier Science Publishers B.V., Amsterdam

CHROM. 25 626

Short Communication

Study of complex-forming equilibria between divalent metal cations and some inorganic anions using ion chromatography

Pavel Janoš

Research Institute of Inorganic Chemistry, Revoluční 86, 400 60 Ústí nad Labem (Czech Republic)

(First received July 20th, 1993; revised manuscript received October 5th, 1993)

ABSTRACT

Complex-forming equilibria between some divalent metal cations (Zn^{2+}, Co^{2+}, Ni^{2+}, Fe^{2+}, Cd^{2+}, Mn^{2+}) and inorganic anions (SCN^-, SO_4^{2-}) were studied using ion chromatography on a column packed with octadecyl-bonded silica permanently coated with dodecyl sulphate. Relationships were derived describing the retention of metal cations in the presence of complexing agents. Stability constants of the complexes formed in the mobile phase were assessed from the dependences of the analyte capacity factors on ligand concentration in the mobile phase.

INTRODUCTION

Ion chromatography (IC) is frequently used for the determination of ionic substances, particularly inorganic ions. To improve the separation of metal cations, advantage is taken of complexing reactions in the mobile phase [1,2]. Relationships between the analyte retention and the composition of the mobile phase in the presence of complexing agents were derived in previous papers [3,4]; these relationships can be employed for studying the composition and stability of complexes by IC.

A detailed description of the principle of stability constant measurement was given previously and the respective mathematical relationships were derived [4]. The method was applied to the determination of the stability constants of complexes of divalent metal cations (Zn^{2+}, Co^{2+}, Ni^{2+}, Fe^{2+}, Cd^{2+}, Mn^{2+}) with the anions of simple di- and polycarboxylic acids (oxalic, tartaric, citric, pyridine-2,6-dicarboxylic and malonic). It follows from the published values of the stability constants [5] and from our previous observations [6] that some inorganic anions may also participate in the complexing reactions taking place in the mobile phase (and thus influence the retention). In this work, IC was used for studying the complex-forming equilibria between selected divalent metal cations and some inorganic anions (SCN^-, SO_4^{2-}); a more general retention model was elaborated and the respective mathematical relations were derived for this purpose.

EXPERIMENTAL

Apparatus

The measurements were conducted on the apparatus and under the conditions described in

0021-9673/93/$06.00
SSDI 0021-9673(93)E1063-6

detail previously [3,4]. The separations were carried out on a Separon SGX C_{18} (5 μm) column (Tessek, Prague, Czech Republic) dynamically coated for 2 h with a 5 mmol l^{-1} solution of sodium dodecyl sulphate (SDS) at a flow-rate of 0.1 ml min^{-1}. The preparation and properties of the separation column were described previously [6]. The measurements were carried out at room temperature (22 ± 1°C).

Chemicals

SDS solution (5 mmol l^{-1}) was prepared from the research-grade reagent (Serva, Heidelberg, Germany). NaOH, H_2SO_4 and NaSCN stock solutions (1 mol l^{-1}) were prepared. The mobile phases were prepared by combining these stock solutions in appropriate proportions and by adjusting the pH (when necessary) to 6 ± 0.05 using dilute perchloric acid.

Perchlorate solutions of the cations examined were prepared using a conventional cation-exchange column and prior to the measurements these were diluted with the mobile phase to concentrations in the range 0.01–0.1 mmol l^{-1} (constant for each run of measurements).

A 0.2 mmol l^{-1} solution of 4-(2-pyridylazo)resorcinol (PAR) containing 1 mol l^{-1} acetic acid and 3 mol l^{-1} ammonia served as the postcolumn derivatizing agent.

Unless stated otherwise, all reagents were of analytical-reagent grade (Lachema, Brno, Czech Republic). Doubly distilled water was used for preparing the solutions.

RESULTS AND DISCUSSION

It follows from our previous work [3,4,6] that the retention of metal cations on an SDS-coated C_{18} column is controlled by an ion-exchange mechanism. A retention model for metal cations participating simultaneously in the ion-exchange and complex-forming equilibria has been described, *e.g.*, by Haddad and Foley [7]; the relationships derived in our work [3,4] are also based on that model. According to that model, only "free" metal cations take part in the ion-exchange processes on the column while the remaining part of the metal in the mobile phase is present in the form of neutral or negatively charged complexes not retained by the cation exchanger. This is true with most common systems where divalent cations are separated and anions of di- or polycarboxylic acids serve as the complexing agents.

The influence of the presence of cationic complexes bearing a positive charge must not be neglected, however, in the reaction of divalent cations (M^{2+}) with some inorganic anions (and also, *e.g.*, with the commonly used 2-hydroxyisobutyric acid, HIBA [8,9]). The formation of complexes with a ligand L^- may be expressed by the following equations:

$$M^{2+} + L^- \rightleftharpoons ML^+ \quad (1a)$$

$$ML^+ + L^- \rightleftharpoons ML_2 \quad (1b)$$

$$ML_2 + L^- \rightleftharpoons ML_3^- \quad (1c)$$

etc. It may be assumed in general that both the free (*i.e.*, non-bonded in a complex) cation M^{2+} and the cationic complex ML^+ take part in the ion-exchange equilibria on a cation exchanger in accordance with

$$M_m^{2+} + 2E_s^+ \rightleftharpoons M_s^{2+} + 2E_m^+ \quad (2)$$

$$ML_m^+ + E_s^+ \rightleftharpoons ML_s^+ + E_m^+ \quad (3)$$

where E^+ is the eluting cation and the subscripts m and s refer to the mobile and stationary phase, respectively. The respective equilibrium constants (selectivity coefficients) are

$$K_M^E = \frac{[M^{2+}]_s[E^+]_m^2}{[M^{2+}]_m[E^+]_s^2} \quad (4)$$

$$K_{ML}^E = \frac{[ML^+]_s[E^+]_m}{[ML^+]_m[E^+]_s} \quad (5)$$

The capacity factor is given as the ratio of the amount of an analyte in the stationary phase to that in the mobile phase:

$$k = q \cdot \frac{[ML^+]_s + [M^{2+}]_s}{c_M} \quad (6)$$

where q is the phase ratio and c_M is the total concentration of metal in the mobile phase as given by the following relationships (for simplicity the ionic charges are omitted):

$$c_M = [M]_m + [ML]_m + [ML_2]_m + \cdots + [ML_n]_m$$
$$= [M]_m(1 + \beta_1[L] + \beta_2[L]^2 + \cdots + \beta_n[L]^n) \quad (7)$$

The following sum holds true for the column capacity:

$$Q = [E^+]_s + [ML^+]_s + 2[M^{2+}]_s \quad (8)$$

which is usually rewritten as

$$Q = [E^+]_s \quad (9)$$

On combining eqns. 4–7 and 9 the rearranging, we obtain

$$k = q \cdot \frac{K^E_{ML} Q[E^+]_m \beta_1[L] + K^E_M Q^2}{[E^+]^2_m(1 + \beta_1[L] + \beta_2[L]^2 + \cdots + \beta_n[L]^n)} \quad (10)$$

If the eluting cation concentration is kept constant and provided that only one type of complex prevails in the mobile phase, eqn. 10 can be rewritten in the following form:

$$k = \frac{A[L] + B}{1 + \beta_n[L]^n} \quad (11)$$

where all the constant terms are summed in the constants A and B. In contrast to the previously published equations [3,4], however, this simplified form cannot be transformed to a linear function.

The dependence of the capacity factor on ligand concentration in the mobile phase at constant concentration of the eluting cation was examined in a similar way as in the previous work [3,4]. The thiocyanate anion was chosen as an example of such an inorganic ligand, with which the formation of ML^+-type complexes can be presumed [5,10–12]. The mobile phases were prepared by combining the NaOH and NaSCN stock solutions in appropriate proportions ratios and adjusting their pH to a constant value of 6 ± 0.05 with dilute perchloric acid (perchlorate ions do not participate in either the complexing or the ion-exchange equilibria). On the assumption that $n = 1$ and using eqn. 11 as the basis, the method of non-linear regression was employed to calculate the values of stability constants from the experimental dependences of capacity factors on ligand concentration. The values obtained were converted to zero ionic strength with the aid of the Debye–Hückel relationship [5,12]; the results are presented in Table I.

TABLE I

STABILITY CONSTANTS (LOG β_1) OF THIOCYANATE COMPLEXES

Metal ion	IC method[a]	IC method[b]	Published data [5]
Co^{2+}	1.52 ± 0.04	1.51 ± 0.06	1.72
Ni^{2+}	1.63 ± 0.07	1.62 ± 0.06	1.76
Fe^{2+}	1.40 ± 0.02	1.44 ± 0.04	1.31
Cd^{2+}	1.80 ± 0.08	1.79 ± 0.05	1.89
Mn^{2+}	1.26 ± 0.03	1.31 ± 0.04	1.26

[a] Calculated by the non-linear regression method using eqn. 11. $n = 7$.
[b] Calculated by the linear regression method using the simplified eqn. 13 for $n = 1$. $n = 7$.

A more detailed analysis of the experimental data showed that the term corresponding to the ML^+-type complex in eqns. 10 and 11 is not very significant. It is also possible to demonstrate by calculation that under the given experimental conditions (mobile phase composition, column capacity; see ref. 6) the ratio of the selectivity coefficients K^E_{ML}/K^E_M is *ca.* 10^{-6}–10^{-5}. This implies that the cationic complexes ML^+ do not take part in ion-exchange processes on the column (analogously to neutral and anionic complexes). Therefore, the previously derived relationships [3,4] can be used for the treatment of the experimental data:

$$\frac{1}{k} = A'(1 + \beta_1[L] + \beta_2[L]^2 + \cdots \beta_n[L]^n) \quad (12)$$

On the assumption that only one type of ML_n complex is predominant in the mobile phase under certain conditions, eqn. 12 may be simplified further:

$$\frac{1}{k} = A'(1 + \beta_n[L]^n) \quad (13)$$

The dependences of the capacity factors on the thiocyanate concentration in the coordinates $1/k$ *vs.* [L] (*i.e.*, for $n = 1$) are presented in Fig. 1. As can be seen, the dependences are linear over a fairly wide concentration range and they confirm the correctness of the adopted simplifica-

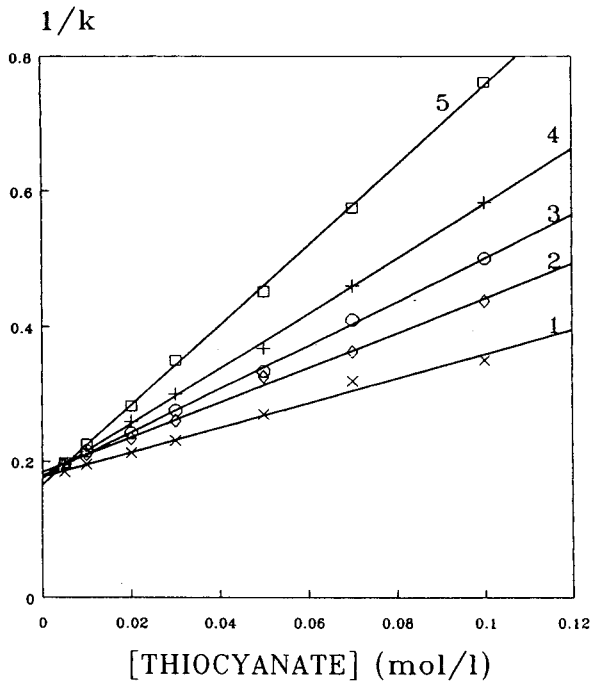

Fig. 1. Dependence of the reciprocal of the capacity factor on thiocyanate concentration in the mobile phase. Column 150 × 3 mm I.D., Separon SGX C_{18}, 5 μm, SDS coated; mobile phase, 0.1 mmol l^{-1} Na^+ + thiocyanate (pH 6 ± 0.05, adjusted with perchloric acid). 1 = Fe^{2+}; 2 = Mn^{2+}; 3 = Cd^{2+}; 4 = Co^{2+}; 5 = Ni^{2+}.

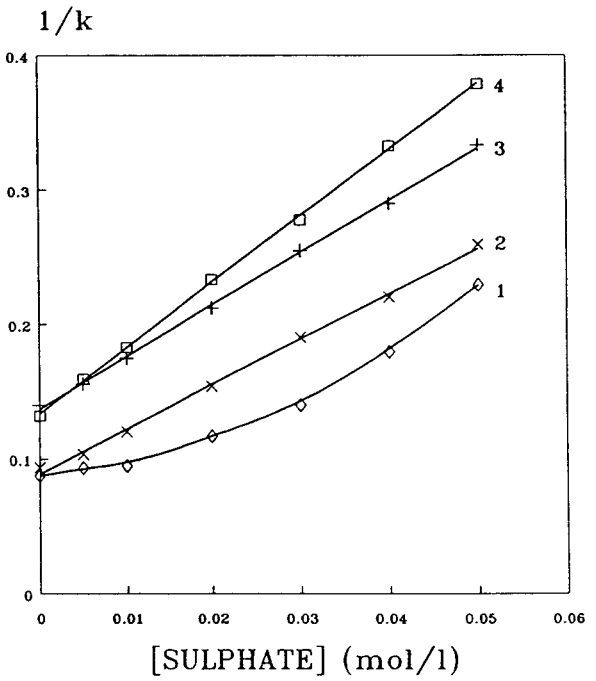

Fig. 2. Dependence of the reciprocal of the capacity factor on sulphate concentration in the mobile phase. Column as in Fig. 1; mobile phase, 0.1 mol l^{-1} Na^+ + sulphate (+ perchlorate). 1 = Cu^{2+}; 2 = Zn^{2+}; 3 = Ni^{2+}; 4 = Cd^{2+}.

tions. These dependences served as the basis for calculating the stability constants β_1; the results, converted to zero ionic strength, are presented in Table I.

A similar procedure was adopted for the study of complexing reactions of divalent metal cations with sulphate anions. Under the given conditions we need not consider the formation of cationic complexes and, therefore, eqn. 12 or, as the case may be, eqn. 13 can be employed. As can be seen from Fig. 2, the plots of $1/k$ *vs.* sulphate concentration are linear for Cd^{2+}, Ni^{2+} and Zn^{2+} (and also for Co^{2+}, Fe^{2+} and Mn^{2+}, not shown in Fig. 2). Stability constants of the sulphate complexes were calculated from these dependences and converted to zero ionic strength (Table II). For Cu^{2+}, the dependence in Fig. 2 is not linear. On the other hand, a linear dependence with a correlation coefficient close to unity ($r = 0.992$) was found when using the coordinates $1/k$ *vs.* $[L]^2$. From this dependence the value of the stability constant β_2 can be calculated (log $\beta_2 = 2.79$).

The values of the assessed stability constants of the thiocyanate complexes are in good agreement with those given in the literature. For the sulphate complexes the agreement between our results and the published data is also fairly good, except for the sulphate complexes of Cu^{2+},

TABLE II

STABILITY CONSTANTS (LOG β_1) OF SULPHATE COMPLEXES

Metal ion	IC method	Published data [5]
Zn^{2+}	2.29 ± 0.04	2.38
Co^{2+}	2.19 ± 0.04	2.36
Ni^{2+}	2.16 ± 0.03	2.32
Fe^{2+}	2.20 ± 0.04	2.2
Cd^{2+}	2.29 ± 0.06	2.46
Mn^{2+}	2.17 ± 0.03	2.26

where our results differed markedly from those published; there are only data for β_1 ($\log \beta_1 = 2.36$ for $I = 1$) in ref. 5. The reasons for this discrepancy are not clear and additional studies are needed concerning particularly those systems where higher complexes occur or where several types of complexes exist simultaneously in significant amounts.

REFERENCES

1 K. Robards, P. Starr and E. Patsalides, *Analyst*, 116 (1991) 1247.
2 P.R. Haddad and P.E. Jackson, *Ion Chromatography. Principles and Applications*. Elsevier, Amsterdam, 1990.
3 P. Janoš and M. Broul, *Fresenius' J. Anal. Chem.*, 344 (1992) 545.
4 P. Janoš, *J. Chromatogr.*, 641 (1993) 229.
5 S. Kotrlý and L. Šůcha, *Handbook of Chemical Equilibria in Analytical Chemistry*, Ellis Horwood, Chichester, 1985.
6 P. Janoš, K. Štulík and V. Pacáková, *Talanta*, 39 (1992) 29.
7 P.R. Haddad and R.C. Foley, *J. Chromatogr.*, 500 (1990) 301.
8 V. Kubáň, I. Jančářová and R. Šulová, *Fresenius' J. Anal. Chem.*, 342 (1992) 706.
9 D.E. Stijfhoorn, H. Stray and H. Hjelmseth, *Spectrochim. Acta, Part B*, 48 (1993) 507.
10 P. Senise and M. Perrier, *J. Am. Chem. Soc.*, 80 (1958) 4194.
11 T. Williams, *J. Inorg. Nucl. Chem.*, 24 (1962) 1215.
12 V.N. Kumok, *Zh. Neorg. Khim.*, 9 (1964) 362.

Journal of Chromatography A, 657 (1993) 440–444
Elsevier Science Publishers B.V., Amsterdam

CHROM. 25 564

Short Communication

Reversed-phase liquid chromatographic isolation of lubimin and solavetivone from *Hyoscyamus muticus* "hairy" root cultures

G. Ramakrishna Reddy and Mark W. Signs

Biotechnology Institute, The Pennsylvania State University, University Park, PA 16802 (USA)

H.E. Flores

Biotechnology Institute and Department of Plant Pathology, The Pennsylvania State University, University Park, PA 16802 (USA)

W.R. Curtis*

Biotechnology Institute and Department of Chemical Engineering, The Pennsylvania State University, University Park, PA 16802 (USA)

(First received March 4th, 1993; revised manuscript received September 15th, 1993)

ABSTRACT

A high-performance liquid chromatographic reversed-phase procedure was developed to estimate the concentration of sesquiterpene phytoalexins secreted into the media by *Agrobacterium* transformed root cultures of *Hyoscyamus muticus*. An isolation procedure based on solid-phase extraction (C_{18} Sep-pak) results in very rapid analysis and gives full recovery, compared to sequential chloroform extraction. A simple isocratic procedure permits quantification of sesquiterpene production by these root cultures in response to exposure to fungal elicitors. Calibration curves for lubimin and solavetivone content were obtained by fractionating sufficient material to provide a measurable weight. The identity of these compounds was confirmed by TLC, UV, GC–MS, and NMR. This experimental system is being used to examine the regulation of sesquiterpene biosynthesis, and to develop large-scale processing techniques for the production of secondary metabolites from plant roots grown in bioreactor systems.

INTRODUCTION

A wide range of plant species have the ability to perceive attack by a pathogen and respond dynamically in an attempt to stop or mitigate damage [1]. This induced defense response involves a broad range of biochemical and physiological shifts, including the production of defense chemicals referred to as phytoalexins [2]. In addition to the fundamental importance of this response to plant pathology, fungal extracts are also being used to induce the production of

* Corresponding author. Address for correspondence: Department of Chemical Engineering, 111 Fenske Laboratory, University Park, PA 16802, USA.

0021-9673/93/$06.00
SSDI 0021-9673(93)E0988-7

biologically active chemicals from plant tissues grown in culture [3,4]. Development of an understanding of phytoalexin formation has been severely hindered by the lack of knowledge of the biosynthetic pathways which produce these compounds. In this regard, the formation of fungitoxic sesquiterpenes by members of the Solanaceae is an excellent model system. Due to the agronomic importance of this plant family (which includes tomato, potato, pepper, and tobacco) there has been considerable research on the sesquiterpene biosynthetic pathway [5]. A schematic of the biosynthetic pathway of sesquiterpenes is shown in Fig. 1. A recent development of particular significance is the isolation and characterization of sesquiterpene cyclase, the enzyme responsible for diverting farnesyl pyrophosphate from sterol synthesis to the sesquiterpene pathway [6]. With the aid of antibodies to this enzyme, radioactive farnesyl pyrophosphate, and cDNA probes, it is now possible to probe induction and regulation of this pathway at a molecular level. Studies of sesquiterpene formation are revealing very interesting dynamics including translational control [7], feedback repression [3], and coordinate gene regulation [8]. To carry out further studies on sesquiterpene biosynthesis, rapid and reliable methods of sesquiterpene quantification are needed to complement the rapid advances in molecular biology. The HPLC analysis described in this paper permits easy and reliable monitoring of lubimin and solavetivone production by tissue cultures of *Hyoscyamus muticus* and other solanaceous species in response to elicitation. This will facilitate physiological studies of plant–pathogen interaction as well as technological studies focused on enhancing secondary metabolite production from cultured plant tissues.

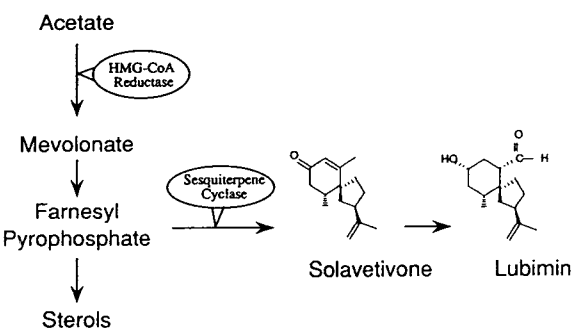

Fig. 1. Biosynthetic pathway of solanaceous sesquiterpene phytoalexins including the structure of lubimin and solavetivone: the two compounds isolated from *Hyoscyamus muticus* root cultures after exposure to extracts of pathogen *Rhizoctonia solani*.

EXPERIMENTAL

Root culture

Hyoscyamus muticus hairy root cultures were established by infection with the bacterial pathogen *Agrobacterium rhizogenes* (ATC 15834) as described previously [9] and have been maintained in culture for over 8 years. Stock cultures are maintained on liquid B5 medium [10]. Root tips are subcultured every 2 weeks into 50 ml of fresh medium in 125-ml flasks. The cultures are maintained on a gyratory shaker with a 2-in. (5-cm) stroke at 100 rpm and 25°C.

Fungal elicitor

Cultures of the fungal pathogen *Rhizoctonia solani* were maintained on SH medium [11] supplemented with 1.00 g/l myo-inositol, 2.36 g/l asparagine, 15.0 g/l pyridoxine hydrochloride, and 10 mg/l thiamine hydrochloride for 18 days on a gyratory shaker at 80 rpm and 25°C. Details on preparation of elicitor can be found elsewhere [3,4]. Briefly, the fungal mycelium is resuspended in distilled water (1 ml per 0.3 g fresh weight) and homogenized for 15 min in a blender on high speed. The homogenate is then autoclaved for 3 h to facilitate release of cell wall fragments, then centrifuged at 21000 *g* for 30 min. The final crude elicitor consists of the filter-sterilized supernatant.

Elicitation/extraction

Induction studies were carried out on root cultures grown for 14 days after inoculation with 0.2 g of root tissue in 50 ml of fresh medium. Cultures were elicited by replacing the growth media with phosphate-free media and adding 2 ml of *Rhizoctonia solani* fungal elicitor. The media was harvested 24 h after induction and extracted. Two extraction procedures were compared for isolation of lubimin and solavetivone:

chloroform partitioning and Sep-pak adsorption as shown schematically in Fig. 2.

The chloroform extraction of the media samples (*ca.* 25 ml) was carried out by partitioning twice against 25 ml of chloroform, (HPLC grade, Fisher Scientific, Pittsburgh, PA, USA). The organic layer was combined and reduced to dryness on a rotary evaporator. The residue was then dissolved in 4 ml of methanol and filtered through a 0.2-μm nylon filter syringe. The filtrate was dried under nitrogen and resuspended in acetonitrile–water (60:40, v/v) for HPLC analysis.

Isolation of lubimin and solavetivone using Sep-pak cartridges was accomplished by first passing the media through Whatman 4 filter paper, then through C_{18} Sep-pak (Waters Classic) cartridges. The cartridge was then eluted with 3 ml of methanol and filtered through 0.2-μm syringe filter. The filtrate was dried under nitrogen then resuspended in acetonitrile–water (60:40) for HPLC analysis.

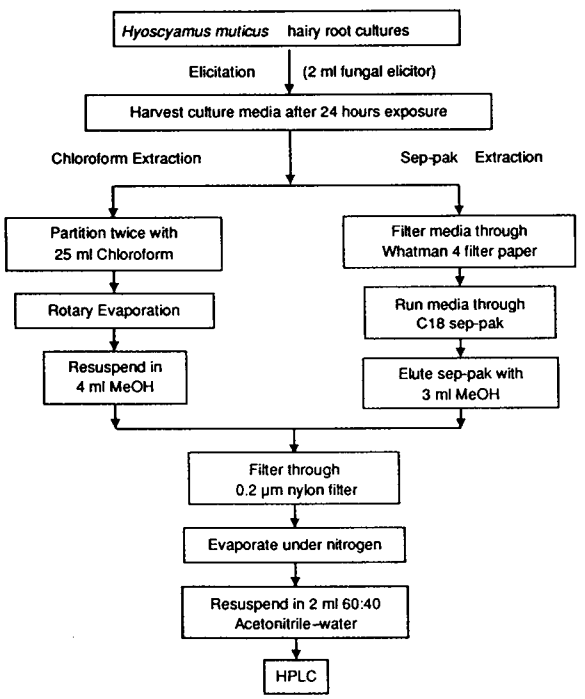

Fig. 2. Flow diagram of sample preparation for HPLC analysis of sesquiterpenes by chloroform partitioning and adsorption/elution on C_{18} cartridges.

High-performance liquid chromatography

The liquid chromatographic system consisted of a Waters Associates Model 600E multisolvent delivery system with a Model 730 data module with WISP Model 712 auto-injector, and a Model 990 photodiode array detector. The system is interfaced with a personal computer for data acquisition and control. The column used for HPLC was a 300×3.9 mm Waters μ-Bondapak C_{18} reversed-phase column. All solvents and mobile phases were of HPLC grade, and water was purified on a Millipore Milli-Q system.

The separation was undertaken isocratically with a solvent composition of acetonitrile–water (60:40) at a flow rate of 2 ml/min. A wavelength range of 195–260 nm was chosen to cover the individual λ_{max} for both lubimin and solavetivone.

Lubimin and solavetivone were purified by HPLC using repeated fraction collection, concentration and reinjection. The purified samples used for GC–MS, NMR, and calibration curves were subject to 10 cycles of fractionation and repeated chromatography at the conditions described above. To facilitate quantitative serial dilution for the calibration curves, a known quantity of acenaphthene was added to the purified samples during reconstitution. The calibration curve was constructed by plotting the peak area (absorbance × retention time) of lubimin and solavetivone against their respective weights which were calculated from initial purified sample weight and extent of dilution based on acenaphthene level.

UV spectroscopy

UV spectra of the samples in methanol (HPLC grade) were performed on Beckman, DU 7.

Thin-layer chromatography

The samples were run on silica TLC glass plates (20×20 cm) precoated with 0.3 μm thick silica gel without activation. Samples dissolved in $CHCl_3$ were spotted and developed with MeOH–$CHCl_3$ (1:19) The chromatograms were then air dried and sprayed with 5% phosphomolybdic acid solution in alcohol [12]. The spots were visualized by heating the plate at 110°C for calculation of R_F values. Both the

crude extract from the media and the purified samples were spotted to establish unambiguous R_F values for each compound.

Gas chromatography and mass spectrometry

Gas chromatography was performed on a Hewlett Packard (HP) Model 5890 Series 11 chromatograph equipped with flame ionization detectors and split injectors. Helium was used as a carrier gas. The column used was a wall-coated open tubular (WCOT) fused-silica capillary column, B-Dex 120, 30 m × 0.25 mm I.D., 0.25 μm film thickness (Supelco, Bellefonte, PA). The analysis was done isothermally at 180°C with an injector temperature of 280°C, column pressure, 18 p.s.i. (1 p.s.i. = 6894.76 Pa), and a 1:80 split ratio. GC–MS was carried out isothermally at 160°C on a Hewlett Packard 5971A mass selective detector (electron impact 70 keV) in the mass range 50–450 with a PTE-5 column, 30 m × 0.25 mm I.D., 0.25 μm film thickness, 5% phenyl, 95% methyl polysiloxane (Supelco).

NMR spectroscopy

NMR spectroscopy was performed on a Bruker WM360 Spectrometer. Solvent ([$^2H_6$]dimethyl sulfoxide) was obtained from Isotech, OH, USA.

RESULTS AND DISCUSSION

The sesquiterpenes, lubimin and solavetivone were extracted from the media of *Hyoscyamus muticus* hairy root culture by two procedures: chloroform partitioning and C_{18} adsorption cartridges (Sep-paks, Waters Assoc.) Chloroform extracts showed a greater number of background impurity peaks some of which interfered with lubimin and solavetivone, samples eluted from C_{18} cartridges provided better resolution for these sesquiterpenes. To detect and quantify lubimin and solavetivone at the highest possible resolution, different λ_{max} (200 nm and 245 nm, respectively) were chosen for multiple wavelength HPLC detection based on UV spectral data. Lubimin and solavetivone elute at retention times of 3.04 min and 5.61 min, respectively, as shown in the HPLC chromatogram of a crude media extract (Fig. 3).

Sesquiterpene analogs were not commercially available as quantitative internal standards; therefore, it was necessary to established calibration curves based on purification of sufficient material to obtain a measurable weight. Acenaphthene (λ_{max} = 220 nm) was used for determining the extent of dilution of purified lubimin and solavetivone samples since it is eluted at 6.7 min under the isocratic conditions of this separation. The calibration curves were obtained for lubimin and solavetivone over the ranges 1.26-10 μg and 0.5-4 μg, respectively. The response was linear over these ranges for both sesquiterpenes at the stated operating conditions. Regression analysis shows that the conversions factors for peak area to sesquiterpene mass at their respective λ_{max} are nearly the same.

Lubimin and solavetivone were further identified by TLC, GC–MS and NMR. GC–MS of lubimin and solavetivone showed single peaks in GC with retention times of 3.99 and 4.67 min, respectively. The mass spectra of these compounds match corresponding compounds iden-

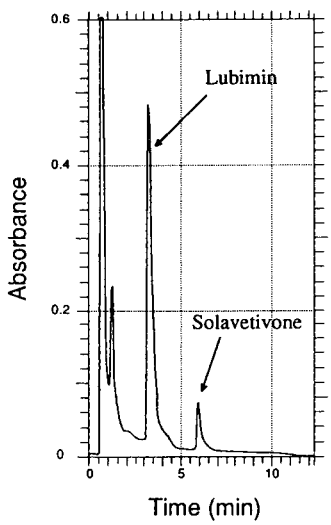

Fig. 3. HPLC chromatogram of sesquiterpenes extracted from the media of elicited root cultures using adsorption on hydrophobic C_{18} cartridges. Chromatogram was obtained from a 50-μl injection of a 25-fold media concentrate with UV detection at 200 nm. Dual wavelength detection at 245 nm provides a 2.1-fold enhancement in absorbance for solavetivone. Chromatographic conditions are given in Experimental.

tified by a mass spectral library search (NBS49K.L). The mass spectra of lubimin displayed molecular ion peak (M^+) at 236 which corresponds to the molecular formula, $C_{15}H_{24}O_2$. The mass spectra of the solavetivone showed a molecular ion peak (M^+) at 218, which corresponds to the molecular formula $C_{15}H_{22}O$. The proton NMR spectra of lubimin and solavetivone were found to display the anticipated characteristic peaks for these compounds as previously reported [13,14]. Lubimin and solavetivone showed single spots on TLC with R_F values of 0.43 and 0.65, respectively, which is also consistent with previous reports for these compounds [12].

A comparison of the chloroform extraction and Sep-pak procedures clearly shows that the Sep-pak procedure is more convenient, time saving, and cost effective. The recovery of sesquiterpenes was statistically indistinguishable (95% *t*-test) for replicated extractions performed with both procedures. Both procedures showed comparable reproducibility: the standard deviation of replicated extractions was about 1% of the response for lubimin, and 5% for solavetivone (with Sep-pak extraction displaying slightly better reproducibility due to fewer interfering peaks). The Sep-pak extraction procedure for HPLC sample preparation takes about three min. In contrast, chloroform extraction takes at least 30 min and often takes much longer due to emulsion formation caused by surface active agents in the culture medium. This means that using Sep-paks, 100 samples can easily be processed in less than a day which would require more than a week using chloroform extraction. There is a tremendous savings in solvents as well: 100 samples would require 5 l of chloroform (*ca.* US$ 95) in comparison to 500 ml of methanol (*ca.* US$ 5) which does not include disposal costs which are escalating due to environmental concerns for chlorinated hydrocarbons. This cost savings would be offset by the cost of Sep-pak cartridges (*ca.* US$ 150/100); however, since the media extracts are very "clean" (in comparison to cellular extracts for example), we found that the cartridge could be used repeatedly, as many as 50 times without degradation of recovery. Even without such repeated use, the time savings clearly makes extraction by adsorption and elution on adsorbent resins a far superior procedure for HPLC sample preparation. The speed of sample preparation will facilitate rapid evaluation of the dynamic response of induced sesquiterpene formation in response to challenge by fungal elicitors.

ACKNOWLEDGEMENTS

We are grateful to Dr. Mani Venkatachalam (Supelco, Bellefonte, PA) for carrying out GC–MS and to Dr. Adil Dhalla (The Pennsylvania State University) for performing the NMR spectroscopy. We would like to acknowledge Dr. S. Yella Reddy (The Pennsylvania State University) for his technical assistance and helpful comments during preparation of this manuscript. Finally we would like to acknowledge NSF (Grant no. BCS-9110288) for financial support.

REFERENCES

1 T. Eresek and Z. Kiraly, *Physiol. Plant.*, 68 (1986) 343.
2 C.J. Lamb, M.A. Lawton, M. Dron and R.A. Dixon, *Cell*, 56 (1989) 215.
3 P. Sachin, G.R. Reddy, D. McNeill and W.R. Curtis, *Appl. Microbiol. Biotechnol.*, 38 (1993) 550.
4 D.S. Dunlop and W.R. Curtis, *Biotech. Prog.*, 7 (1991) 434.
5 I.M. Whitehead, D.R. Threlfall and D.F. Ewing, *Phytochemistry*, 28 (1989) 775.
6 U. Vogili, J.W. Freeman and J. Chappell, *Plant Physiol.*, 93 (1990) 182.
7 P.J. Facchini and J. Chappell, *Proc. Natl. Acad. Sci.*, 89 (1992) 11088.
8 M.N. Zook and J.A. Kuć, *Physiol. Mol. Plant Path.*, 39 (1991) 377.
9 M.W. Signs and H.E. Flores, *Plant Physiol.*, 89 (1989) 135.
10 O.L. Gamborg, R.A. Miller and K. Ojima, *Exp. Cell. Res.*, 50 (1968) 151.
11 R.U. Shenk and A.C. Hildenbrandt, *Can. J. Bot.*, 50 (1972) 199.
12 A. Stoessl, J.B. Stothers and E.W.B. Ward, *Can. J. Chem.*, 53 (1975) 3351.
13 A. Stoessl, J.B. Stothers and E.W.B. Ward, *Phytochemistry*, 15 (1976) 855.
14 S.F. Osman, E.B. Kalan and R.M. Zacharius, *Tetrahedron Lett.*, 34 (1974) 2921.

Journal of Chromatography A, 657 (1993) 445–449
Elsevier Science Publishers B.V., Amsterdam

CHROM. 25 578

Short Communication

Purification of fresh cassava root polyphenols by solid-phase extraction with Amberlite XAD-8 resin

Fernando Lalaguna

Unidad de Tecnología Nuclear, Instituto Venezolano de Investigaciones Científicas, Apartado 21827, Caracas 1020-A (Venezuela)

(First received April 20th, 1993; revised manuscript received September 21st, 1993)

ABSTRACT

To obtain the polyphenolic fraction of fresh cassava root in a form amenable to analysis by thin-layer chromatography (TLC) and absorption spectroscopy, aqueous concentrates of delipidated extracts were loaded on 0.3 g (dry mass) of Amberlite XAD-8 resin, non-polyphenolics were washed off with water and polyphenols eluted with methanol–water (7:3, v/v). The resolution and purity of polyphenols were ascertained with four TLC systems. In addition, the system exhibits complete recovery and is reproducible, and the resin withstands repeated use without lost of performance, which makes it an efficient method.

INTRODUCTION

Extracts of polymeric plant polyphenols have been processed by solid-phase extraction with C_{-18} cartridges to allow their analysis by TLC and other methods [1]. However, although several aspects of the macroreticular resins of the Amberlite XAD series have been investigated, including their chromatographic properties [2–4], use for the separation of phenols [5] and other compounds [6,7], and for the isolation of polyphenols [8,9], their use to purify polyphenolic plant extracts by solid-phase extraction has not been reported.

Pietrzyk and Chu [6] pointed out that for stripping applications the stronger XAD adsorbent might be preferred. In accordance with this, McRae *et al.* [4] found that Amberlite XAD-8, a polar acrylic ester resin, was useful for the separation of polar solutes from aqueous extracts, while Amberlite XAD-2, a non-polar copolymer of styrene–divinylbenzene, was not satisfactory. On the other hand, Vian et al. [9] did not find the acrylic ester-type Amberlite suitable for the retention of carbohydrates. This indicates the applicability of this resin to deprive adsorbable polyphenols of sugars.

Polyphenols containing phenylpropanoid, coumarin and flavonoid structures have been reported in the roots of cassava (*Manihot esculenta*, Crantz) and the flour prepared from them [10–13]. Coumarins are by far the main component; the other polyphenols, *e.g.* catechins, are minor, and proven to be present in the experimentally injured root's parenchyma [11–13]. These polyphenols have not been assayed on Amberlite XAD resins.

For the continuation of our studies on cassava root discoloration [14,15] a method to purify the polyphenols extracted from cassava root that would permit their analysis by TLC, UV–Vis spectroscopy and other methods was needed. A

0021-9673/93/$06.00
SSDI 0021-9673(93)E1003-I

successful process using Amberlite XAD-8 was developed and is reported here.

EXPERIMENTAL

Chemicals

The solvents and reagents used were of analytical grade, and from either Fisher Scientific (Fair Lawn, NJ, USA) of Merck (Darmstadt, Germany). Polyphenols and other standards were from Sigma (St. Louis, MO, USA). Amberlite XAD-8 (Rohm & Haas) was also obtained from Sigma.

Resin preparation

Amberlite XAD-8 was thoroughly washed before use as follows: 10 g of resin were poured into 300 ml of 0.1 *M* sodium hydroxide in a filtering flask, degassed under the vacuum of a water jet pump, and stirred. Excess sodium hydroxide was washed off with 300 ml of water, 300 ml of 0.1 *M* hydrochloric acid added and the resin shaken. After discarding the acid the resin was washed with water in a büchner funnel until the filtrate was neutral (universal indicator paper). Excess water was removed with ethanol and the resin was extracted in a Soxhlet apparatus for 7 h with the following solvents, leaving the resin immersed in the same solvent overnight: toluene, acetone, ethanol and methanol. The resin was rinsed with the new solvent whenever there was a change of solvent.

The washed resin was ground when dry with a porcelain mortar and pestle, and the 0.250 mm fraction (dry) collected. The fines of the XAD-8 resin had to be removed with organic solvents [methanol–water or acetone–water, 7:3 (v/v) would do] since water was found to be unable to eliminate all the fines. Keeping the unused resin in organic solvents is not advisable.

Column packing and operation

For the processing of crude cassava root extracts, an Econo-Column (Bio-Rad, Richmond, CA, USA) glass column 10 cm × 0.7 cm I.D., with a polypropylene tip and polyethylene bed support, was packed with a water suspension of the XAD-8 resin. Afterwards, the resin was washed with methanol–water (7:3) and reversed to water. A final bed volume of 1 ml (approximately 0.3 g of dry XAD-8 resin) was used. A Pasteur pipette plugged with glass wool was substituted for the Econo-Column for the purification of TLC-resolved polyphenols to be analysed by UV–Vis spectroscopy, otherwise the organic parts of the Econo-Column and tubing contribute interfering substances.

Prior to the application of the sample, the column was rinsed with 10 ml of methanol–water (7:3) followed by 10 ml of water, then the sample was loaded, the non-polyphenolic material was washed out with 10 ml of water, and the polyphenols eluted with 10 ml of methanol–water (7:3). Flow-rates between 0.2 and 1 ml/min were used. The methanolic eluates were taken to dryness under a stream of nitrogen at 35°C, and the residue dissolved in 1 ml of methanol–water (7:3).

When performing the above procedure, the washings and eluates were collected as 1-ml fractions for further analysis.

Extraction of cassava

Fresh cassava root cv. Algodona (a sweet, white cultivar with small roots) of 10 months was purchased from a producer. Samples of fresh roots that included only the uninjured parenchymatous cylinder were extracted as previously reported [14] followed by extraction with two 100-ml portions of acetone–water (7:3) in an Omni-Mixer (Omni, Waterbury, CT, USA). The acetone extract was mixed with the polar phase of the previous extraction, and ten-fold concentrated under vacuum in a rotary evaporator at 35°C. Any deposit that formed was removed by centrifugation at low speed. Aliquots of the aqueous extracts, concentrated as indicated above, which had a pH of about 5 and a dry mass of the order of 7 mg, were percolated down with XAD-8 resin column.

TLC and spectroscopy

To check the nature of the compounds in the fractions collected from the XAD-8 resin column during the development of the solid-phase extraction system, these fractions were subjected to TLC on microcrystalline cellulose with butanol–acetic acid–water (4:1:5, v/v/v) [16] as solvent

system, and on silica gel G developing with both toluene–ethyl formate–formic acid (5:4:1, v/v/v) or ethyl acetate–methyl ethyl ketone–formic acid–water (5:3:1:1, v/v/v) [17]. The layers were visualized with 366-nm UV light, before and after exposure to ammonia vapours, and by spraying with 1-naphthol (for sugars), ninhydrin and arabinose–aniline (for organic acids [18]) reagents.

To verify that the purification process had rendered the polyphenols susceptible to analysis by TLC and UV–Vis spectroscopy, aliquots of the polyphenolic fraction were streaked on 0.5-mm-thick preparative silica gel G (Merck) layers and developed three times, once for 15 cm and twice for 12 cm, with the solvent system chloroform–methanol–acetic acid–water (170:25:25:6, v/v) [14]. The bands were localized by exposing the plates to 366-nm UV light, their positions marked, the silica gel scraped off the plates, the compounds extracted with three 1-ml portions of ethanol–formic acid–water (8:1:1, v/v), taken to dryness, and dissolved in methanol. The procedures given by Markham [19] were followed to obtain the UV–Vis spectra of the eluted bands. A Perkin-Elmer (Norwalk, CT, USA) Model Lambda 3B dual spectrophotometer was used.

Analytical methods

For total phenols a method using Folin and Ciocalteau reagent was used [20]. For catechins the vanillin methods of Price *et al.* [21] and of Butler *et al.* [22] were followed. Column elution was monitored by manually measuring the absorbance of the fractions at several wavelengths and/or by chemical analysis [20,23–26].

RESULTS AND DISCUSSION

In order to further our studies on cassava root discoloration, the analysis of the polyphenols allegedly responsible for this process [11–13] became essential. The analysis of crude polyphenol extracts was hampered by the high concentration of other compounds, so purification of the extracts was required.

Standards of the kind of compounds reported in cassava root [10–13,15] or similar tissues were assayed in the Amberlite XAD-8 solid-phase extraction system devised, to determine the feasibility of this system for the purification of cassava extracts. The results for some of these compounds are given in Table I. Other substances assayed (data not shown) exhibited behaviours similar to those of their chemical analogues in Table I, among them the organic acids citric, succinic, shikimic and quinic, the amino acids tryptophan and histidine, and the coumarins esculetin and esculin. Rutin and (+)-catechin were eluted with methanol–water (7:3), while chlorogenic acid required acetone–water (7:3).

The results show that the interaction with Amberlite XAD-8 of the non-polyphenolics tested is weak enough to permit their complete displacement with water, including aromatic amino acids, even though, like polyphenols, they contain a benzene ring.

On the contrary, none of the polyphenols assayed was eluted by water; they required either methanol–water (7:3) or acetone–water (7:3), depending on their structure. Scopoletin, esculin and (+)-catechin, which are reportedly found in cassava root [11–13], where all eluted in the same fraction. These polyphenols are completely recovered from the resin, *e.g.* scopoletin, the main polyphenol in cassava [11,13], was 98 ± 6% (standard deviation, $n = 3$) recovered, on average, when loading the system with 2–50 μg of scopoletin. The behaviour of these standards in isolation is maintained when in admixture, as demonstrated by the separation of a mixture of tyrosine, rutin and quercetin (Table I). The results indicate that the system is capable of separating the polyphenols found in cassava root from other widely distributed substances, including intermediates of polyphenol metabolism.

The data for the elution of the cassava root extracts are included in Table I, where it can be seen that most of the acids and carbohydrates, and all the ninhydrin-reactive substances, were eluted with water. Methanol–water (7:3) eluted one peak of material measurable with Folin and Ciocalteau reagent [20]. This material gave a feeble response with reactives for total sugars and acidic groups. The separation of the polyphenols from other compounds was verified with four TLC systems, which showed that methanol–

TABLE I

ELUTION OF STANDARD COMPOUNDS AND CASSAVA ROOT EXTRACT FROM AMBERLITE XAD-8 RESIN

A 1-ml volume of wet, 0.250 mm Amberlite XAD-8, flow-rate 0.2–1 ml/min, 1-ml fractions, gravity flow.

Sample	Absorbance																	
	Eluent/fraction number																	
	Water						Methanol–water (7:3, v/v)						Acetone–water (7:3, v/v)					
	1	2	3	4	5	10	11	12	13	14	15	20	21	22	23	24	25	30
Glucose[a] (260 nm)	1.52	1.84	0.13	0.16	0.18	0.00												
Malic acid[b] (470 nm)	0.13	1.58	0.26	0.06	0.07	0.00												
Ascorbic acid[c] (297 nm)	0.95	2.13	0.07	0.02	0.02	0.00												
Tyrosine[d] (280 nm)	0.06	0.66	0.15	0.05	0.05	0.00												
Scopoletin[e] (280 nm)	0.01	0.01	0.01	0.00	0.00	0.01	0.01	0.17	0.36	0.16	0.04	0.00						
Caffeic acid[f] (470 nm)	0.00	–	–	–	–	0.00	0.00	–	–	–	–	0.00	0.34	0.21	0.00	–	–	0.00
Quercetin[g] (350 nm)	0.00	–	–	–	–	0.00	0.00	0.03	0.06	0.08	0.09	0.11	0.15	1.01	0.47	0.07	0.01	0.00
Mixture of[h] standards (280/350 nm)	0.02	0.03	0.61	0.16	0.00	0.00	0.00	0.67	0.58	0.31	0.23	0.14	0.19	1.29	0.48	0.09	0.02	0.00
Cassava extract																		
(470 nm)[i]	0.00	0.86	1.13	0.08	0.00	0.00	0.00	0.01	0.00	0.08	0.01	0.01	0.00	–	–	–	–	0.00
(560 nm)[j]	0.01	1.69	2.53	0.18	0.05	0.01	0.01	0.04	0.01	0.00	0.00	0.01	0.01	0.10	0.00	–	–	0.00
(570 nm)[k]	0.01	1.11	1.14	0.06	0.03	0.03	0.03	0.03	0.04	0.04	0.03	0.05	0.01	–	–	–	–	0.00
(725 nm)[l]	0.01	0.27	0.31	0.14	0.12	0.04	0.15	0.41	0.11	0.05	0.02	0.00	0.01	0.03	0.02	0.01	0.01	0.00

[a] A 0.25-ml aliquot of 1 mg/ml aqueous glucose, measured by the method of Agranoff *et al.* [24].
[b] A 0.25-ml aliquot of 1 mg/ml aqueous malic acid, fractions titrated with sodium ortho-nitrophenol [25].
[c] A 0.20-ml aliquot of 1 mg/ml aqueous ascorbic acid, direct absorbance reading.
[d] A 0.25-ml aliquot of 0.4 mg/ml aqueous tyrosine, direct absorbance reading.
[e] A 0.25-ml aliquot of scopoletin aqueous saturated solution, direct absorbance reading.
[f] A 0.10-ml aliquot of caffeic acid aqueous saturated solution, fractions titrated with sodium ortho-nitrophenol [25].
[g] A 12.5-μl aliquot of 4 mg/ml ethanolic quercetin, loaded in 1 ml of water, direct absorbance reading.
[h] A 0.25-ml aliquot of 0.4 mg/ml aqueous tyrosine, plus 0.25 ml of rutin aqueous saturated solution, plus 12.5 μl of 4 mg/ml ethanolic quercetin; water eluates direct reading at 280 nm, others at 350 mm.
[i] Fractions titrated with sodium ortho-nitrophenol [25].
[j] Fractions analysed for sugars [23].
[k] Fractions reacted with ninhydrin [26].
[l] Fractions analysed for Folin and Ciocalteau reactive substances [20].

water (7:3) eluates did not produce any band for free sugars, organic acids (arabinose–aniline visualization [18]) or amino group-containing compounds, but gave bands positive for polyphenols. Conversely, water eluates failed to produce bands of polyphenols, but bands were visualized for all the other components. This shows that the methanol–water (7:3) eluates contain the polyphenolic fraction in pure form.

The recovery for cassava extracts was 91.2 ± 7% (S.D., $n = 7$) on average, through a range of load of 63–188 μg (as scopoletin); 20–30% of the loaded material was adsorbed depending on the root extracted.

Overloading, or fouling with repeated use, of the XAD-8 resin with cassava extracts could cause acetone–water (7:3) to remove a small amount of material from the resin (see Table I).

TLC analysis showed that this material was similar to that eluted by methanol–water (7:3).

After their purification, the polyphenols were neatly resolvable by TLC. A maximum of eight intense plus two weak bands were observed. The compound in the main band, after its extraction and cleaning with the all-glass system described, gave UV–Vis spectra [19] equivalent to those for scopoletin. Processing cassava extracts with the solid phase extraction system reported permitted verification of the absence of polyphenols with a flavonoid nucleus in extracts prepared from sound root's parenchyma, excluding any injured surface; three cassava cultivars were used. In contrast, this type of polyphenol has been detected with histochemical techniques [12] and measured in extracts prepared from experimentally injured root [11–13].

The Amberlite XAD-8 solid-phase extraction procedure reported has proven to be reproducible through 2 years of use, with both standards and different cassava extracts, which together with the above results —effective purification and high recovery, and the stability, sustained usability and economy of the resin— makes it an efficient method to render cassava polyphenol extracts susceptible to further analysis. The performance of the method suggests that it could be used successfully on other plant extracts.

ACKNOWLEDGEMENT

This work was partially financed by CONICIT Project S1-1909.

REFERENCES

1 H.A. Stafford and H.H. Lester, *Plant Physiol.*, 66 (1980) 1085.
2 D.J. Pietrzyk, and C. Chu, *Anal. Chem.*, 49 (1977) 757.
3 E.M. Thurman, R.L. Malcolm and G.R. Aiken, *Anal. Chem.*, 50 (1978) 775.
4 T.G. McRae, R.P. Gregson and R.J. Quinn, *J. Chromatogr. Sci.*, 20 (1982) 475.
5 J.S. Fritz and R.B. Willis, *J. Chromatogr.*, 79 (1973) 107.
6 D.J. Pietrzyk and C. Chu, *Anal. Chem.*, 49 (1977) 860.
7 E.P. Kroeff and D.J. Pietrzyk, *Anal. Chem.*, 50 (1978) 502.
8 E.M. Thurman and R.L. Malcolm, *Environ. Sci. Technol.*, 15 (1981) 463.
9 A. Vian, E. Castro and J.J. Rodríguez, *Separation Sci. Technol.*, 20 (1985) 481.
10 S. Sefa-Dedeh and V.F. Rasper, *Cereal Chem.*, 54 (1977) 746.
11 J.E. Rickard, *Trop. Sci.*, 23 (1981) 235.
12 J.E. Rickard and P.B. Gahan, *Ann. Bot.*, 52 (1983) 811.
13 Y. Tanaka, E.S. Data, S. Hirose, T. Taniguchi and I. Uritani, *Agric. Biol. Chem.*, 47 (1983) 693.
14 F. Lalaguna and M. Agudo, *J. Am. Oil Chem. Soc.*, 65 (1988) 1808.
15 F. Lalaguna and M. Agudo, *Phytochemistry*, 28 (1989) 2059.
16 J.B. Harbone, *Phytochemical Methods*, Chapman & Hall, London, 1973, p. 33.
17 E. Stahl and P.J. Schorn, *Hoppe-Seyler's Z. Physiol. Chem.*, 325 (1961) 263.
18 M. Bourzeix, J. Guitraud and F. Champagnol, *J. Chromatogr.*, 50 (1979) 83.
19 K.R. Markham, *Techniques of Flavonoid Identification*, Academic Press, New York, 1982, p. 36.
20 T. Swain and W.E. Hillis, *J. Sci. Food Agric.*, 10 (1959) 63.
21 M.L. Price, S. Van Scoyoc and L.G. Butler, *J. Agric. Food Chem.*, 26 (1978) 1214.
22 L.G. Butler, M.L. Price and J.E. Brotherton, *J. Agric. Food Chem.*, 30 (1982) 1087.
23 A.W. Devor, *J. Am. Chem. Soc.*, 72 (1950) 2008.
24 B.W. Agranoff, R.M. Bradley and R.O. Brady, *J. Biol. Chem.*, 23 (1958) 1077.
25 L. Kesner and E. Muntwyler, *Anal. Chem.*, 38 (1966) 1164.
26 S. Moore and W.H. Stein, *J. Biol. Chem.*, 211 (1954) 907.

Journal of Chromatography A, 657 (1993) 450–454
Elsevier Science Publishers B.V., Amsterdam

CHROM. 25 660

Short Communication

Separation of condensed phosphates using capillary zone electrophoresis with indirect UV detection

Frederick S. Stover* and Sherry S. Keffer

Performance Products Technology, Chemical Group of Monsanto Company, 800 N. Lindbergh Boulevard, St. Louis, MO 63167 (USA)

(First received August 10th, 1993; revised manuscript received October 19th, 1993)

ABSTRACT

A capillary zone electrophoresis (CZE) separation of ortho-, pyro- and tripolyphosphate anions using a phthalate buffer and indirect UV detection is described. Advantages of a CZE method for phosphates include speed, efficiency and unique selectivity. Quantitative parameters and application to the analysis of a commercial sample are presented.

INTRODUCTION

Orthophosphate and condensed phosphate compounds are important industrial chemicals used in many applications including cleaning formulations and as food acidulants. Instrumental analysis of ortho-, pyro- and tripolyphosphate species is commonly done using ion chromatography [1,2], paper chromatography [3] and ^{31}P NMR [4]. We and others have shown the utility of capillary isotachophoresis (ITP) for the separation and quantitation of condensed phosphate species [5,6]. A newer electrophoretic method, capillary zone electrophoresis (CZE), is gaining in popularity for the quantitative analysis of small ionic compounds [7,8] due to its high speed, resolution and the commercial availability of automated instruments. However, few applications of CZE for the analysis of polyvalent, inorganic anions have appeared.

We present here the initial separations of ortho-, pyro- and tripolyphosphate using CZE. The separation can be accomplished in 5 min using pH 4.2 phthalate buffer with indirect UV detection. Calculated mobilities of phosphate ions, example separations and the analysis of phosphate species in commercial food processing samples are presented.

EXPERIMENTAL

Apparatus

A Spectra-Physics (now Thermo Separation Products, San Jose, CA, USA) SpectraPHORESIS 500 capillary electrophoresis instrument was used for all CZE experiments. A 45 cm long separation capillary was fabricated from 75 μm I.D. × 365 μm O.D. fused silica (Polymicro Technologies, Phoenix, AZ, USA). The capillary window was made by scraping off *ca.* 2 mm of polyimide coating prior to mounting in the cassette. The UV detector was operated at

* Corresponding author.

0021-9673/93/$06.00
SSDI 0021-9673(93)E1101-5

250 nm using a rise time of 1 s. Electrophoresis was performed at a constant applied voltage of −20 kV (resulting current = −13 μA) and at 25°C. An applied vacuum of 1.5 p.s.i. (1 p.s.i. = 6894.76 Pa) for 1 s was used for all injections.

Ion chromatography (IC) was performed on a Dionex (Sunnyvale, CA, USA) series 2000i IC equipped with an AS5 column, a CDM-II conductivity detector, an AMMS micromembrane suppressor with 25 m*M* H_2SO_4 regenerant, and a 50-μl injection loop. Data from both IC and CZE experiments were acquired and integrated using a Dionex AI-450 chromatography data system.

Chemicals

Potassium acid phthalate (KHP), ACS certified grade, monosodium phosphate monohydrate, reagent grade, and 50% sodium hydroxide were obtained from Fisher Scientific (Pittsburgh, PA, USA). Reagent-grade tetrasodium pyrophosphate decahydrate was obtained from Mallinckrodt (St. Louis, MO, USA) and technical-grade pentasodium tripolyphosphate, anhydrous, was obtained from Monsanto (St. Louis, MO, USA). Dodecyltrimethylammonium bromide (DTAB) was obtained from Sigma (St. Louis, MO, USA). IC regenerant was prepared from concentrate (Dionex, Sunnyvale, CA, USA). Water used to prepare buffers and dilute standards and samples was purified using a four-bowl Plus analytical Milli-Q system (Millipore, Bedford, MA, USA).

Methods

One mg/ml (as anion) stock phosphate standards were prepared by diluting appropriate masses of the sodium salts with deionized water. Mixed standards in the range 5–300 μg/ml for CZE or 5–100 μg/ml for IC were prepared by further diluting aliquots of the stock standards. Phthalate buffer was prepared by diluting 0.102 g KHP and 6.2 ml of 2.5 mg/ml DTAB in water to 100 ml with deionized water. The resulting buffer (5 m*M* KHP/0.5 m*M* DTAB) pH was found to be 4.2 as measured using a glass electrode. No pH adjustment of the buffer was performed.

The following daily washing procedure (using vacuum) was found to give reproducible migration behavior: 15 min with 1 *M* NaOH, 5 min with 0.1 *M* NaOH, 5 min with water, 10 min with 0.25% DTAB and 10 min with running buffer. Between runs, a 2-min wash with buffer was performed.

IC was performed using 50 m*M* NaOH eluent pumped isocratically at 1 ml/min. The eluent was prepared by diluting 4 g 50% NaOH to 1 l. Potato bath samples were diluted 100- or 1000-fold in deionized water.

RESULTS AND DISCUSSION

Our previous experience with ITP separations of condensed phosphates showed that differences in electrophoretic mobilities are effective in providing separations of these species. Prior to attempting a CZE separation, effective mobilities of ortho-, pyro- and tripolyphosphate were calculated and the results are given in Fig. 1.

Calculations were based on the normal equations for effective mobility [9]. Values for pK_a and absolute mobilities were taken from the literature [10,11]. Absolute mobilities for tripolyphosphate were estimated from ITP data generated in our laboratories [5].

The plot of mobility *vs.* pH indicates that electrophoretic separations of ortho-, pyro- and tripolyphosphate are fairly robust, since mobility differences vary little with pH. The plot includes the calculated mobility curve for phthalate, a common buffer used for indirect UV detection of anions in CZE. To minimize electrodispersion

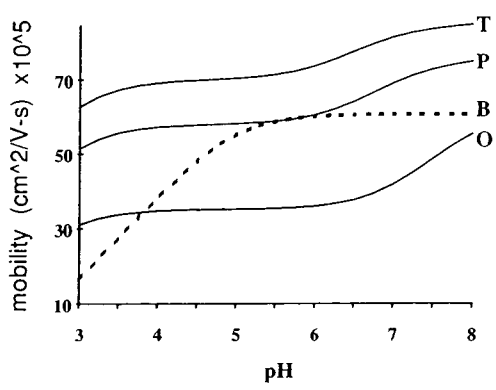

Fig. 1. Calculated mobilities of ortho- (O), pyro- (P), tripolyphosphate (T) and phthalate (B) *vs.* pH.

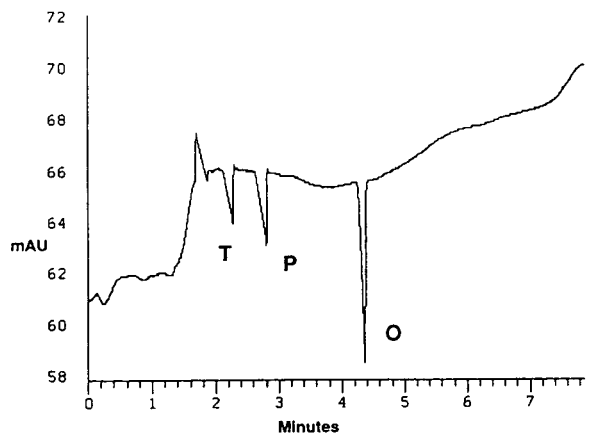

Fig. 2. Typical separation of ortho- (O), pyro- (P) and tripolyphosphate (T) in 5 m*M* KHP/0.5 m*M* DTAB, pH 4.2; 100 μg/ml of each anion injected. For details of the separation, see Experimental section.

[12], a buffer pH of 4.2 was chosen, which makes phthalate's mobility intermediate to those of the phosphates of interest. Another advantage of operating at this pH is that no pH adjustment of a 5 m*M* KHP solution is necessary. DTAB was added to the buffer to ensure anodic electroosmotic flow and rapid separations.

A typical separation of phosphates in 5 m*M* KHP/0.5 m*M* DTAB is shown in Fig. 2. The mobility order of the three phosphate species is consistent with calculated mobilities shown in Fig. 1. Significant baseline shifts are seen during the course of electrophoresis, a phenomenon we have observed consistently with indirect detection of phthalate buffers with different pH, concentration and additive content.

While the speed and efficiency of the separation shown in Fig. 2 are acceptable, pyro- and tripolyphosphate peaks are small relative to that for orthophosphate. To investigate the quantitative potential of this system, calibration curves were constructed using triplicate injections of mixed standards over the concentration range 5–300 μg/ml. Results of the calibration are given in Table I. All precisions stated in Table I are within-day precisions.

TABLE I

CALIBRATION STATISTICS

Concentration (μg/ml)	Area relative standard deviation (%) $n = 3$		
	Ortho	Pyro	Tripoly
5	13	–	–
10	8	–	–
50	0.5	4	40
100	2	1	10
300	1	1	3

Peak areas showed good reproducibility at 10–300, 50–300 and 100–300 μg/ml for ortho-, pyro- and tripolyphosphate, respectively. Calibration curves were linear as seen from the correlation coefficient. Of particular interest were the slopes and intercepts obtained for the three phosphates. From pK_a data, effective charges on the phosphates are *ca.* -1, -2 and -3 at pH 4.2. Slopes can be corrected for migration time (t_m) and effective ionic charge by

$$\text{corrected slope} = [\text{slope}(\text{area}\mu\text{g}^{-1}\text{ml})\text{F.M.}]/[\text{charge} \cdot t_m] \quad (1)$$

where F.M. = formula mass of the anion and the term (F.M./charge) converts the slope from a mass-based to an equivalents-based measure. Normalization of areas using migration time corrects for differing velocities of ions past the detector. Corrected slopes are given in Table II, and they should be equal for 1:1 displacement of buffer ions using indirect detection [13]. The approximately equal slopes indicate that the low sensitivities seen with pyro- and tripolyphosphate arise primarily from the large negative intercepts. Possible causes of these large intercepts, including interaction with surfactant and/or online hydrolysis, are under investigation.

As a further check on quantitation using this method, commercial samples were analyzed by CZE and results compared with those obtained by IC. Samples were taken from solutions of sodium acid pyrophosphate used for the treatment of potatoes. Results of the analyses are given in Table III, and typical separations are shown in Fig. 3. Good agreement is seen between the two techniques. Somewhat higher migration times and different baselines seen in Fig. 3 *vs.* Fig. 2 are typical of day-to-day variations with this system.

TABLE II

SENSITIVITY AND REPRODUCIBILITY PARAMETERS

	Ortho	Pyro	Tripoly
Slope (area μg^{-1} ml)	300	190	154
Corrected slope	6360	5930	5690
Intercept (area)	−4520	−1746	−510
r^2	0.9995	0.9995	0.9960
Average t_m (min)	4.4	2.7	2.28
t_m R.S.D. (%)	1.8	3.3	3.0

TABLE III

CZE *VS.* IC ANALYSIS OF POTATO BATH SAMPLES

	% Pyro (S.D., $n = 3$)		% ortho (S.D., $n = 3$)	
	CZE	IC	CZE	IC
Sample A	6.98 (0.19)	6.92	0.79 (0.13)	0.76
Sample B	0.39 (0.002)	0.53	<0.1	<0.1

Analysis of phosphate in potato baths appears accurate despite the complex matrix. To check for interferences from common inorganic anions, sulfate, chloride and nitrate standards were analyzed in the present system. All three anions migrate ahead of tripolyphosphate, in agreement with previous ITP data [10]. Organic acids extracted from the potatoes should migrate well behind the phosphate species. The early-eluting peaks seen in Fig. 3b are likely organic acids (*e.g.* ascorbic) with migration times greater than 7 min in the CZE system.

The above results show that CZE is a viable alternative for quantitative determination of

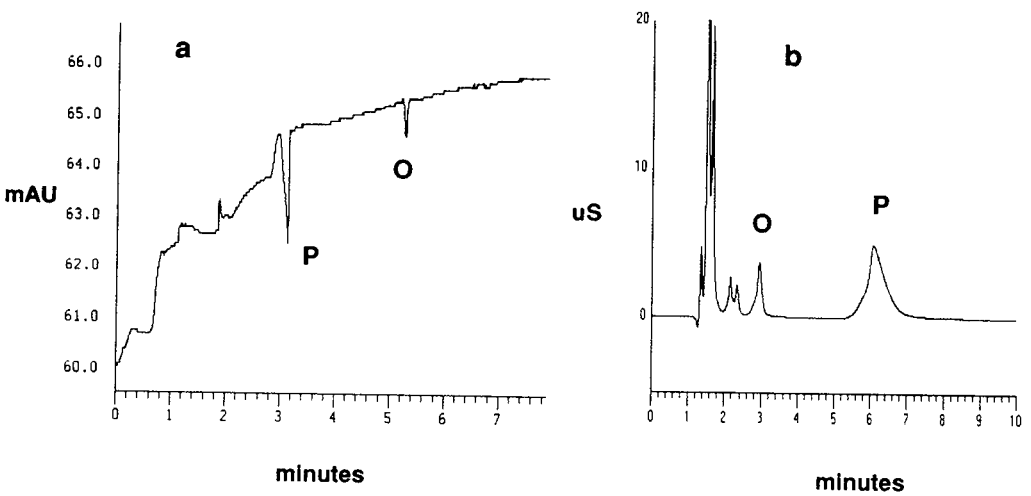

Fig. 3. Analysis of potato bath samples by (a) CZE and (b) IC. O = ortho- and P = pyrophosphate peaks.

phosphate speciation. While the present system is not fully optimized in terms of baseline stability and day-to-day reproducibility, quantitative separations are demonstrated. Investigations into improved buffer systems for phosphate analyses, including improved stability, sensitivity and possible extension to other condensed phosphates, are continuing.

REFERENCES

1 R.D. Rocklin, C.A. Pohl and J.A. Schibler, *J. Chromatogr.*, 411 (1987) 107.
2 M. Chino and H. Sato, *Bull. Coll. Agr. Vet. Med. Nihon Univ.*, 47 (1990) 197.
3 Y. Kiso, M. Kobayashi and Y. Kitaoka, in M. Halmann (Editor), *Analytical Chemistry of Phosphorus Compounds*, Wiley-Interscience, New York, 1972, Ch. 3, p. 124.
4 D.R. Gard, J.C. Burquin and J.K. Gard, *Anal. Chem.*, 64 (1992) 557.
5 F.S. Stover, *Electrophoresis*, 11 (1990) 750.
6 T. Yagi, K. Kojima, H. Nariai and I. Motooka, *Bull. Chem. Soc. Jpn.*, 55 (1982) 1831.
7 J. Romano, P. Jandik, W.R. Jones and P.E. Jackson, *J. Chromatogr.*, 546 (1991) 411.
8 B.F. Kenney, *J. Chromatogr.*, 546 (1991) 423.
9 F.M. Everaerts, J.L. Beckers and Th.P.E.M. Verheggen, *Isotachophoresis —Theory, Instrumentation and Applications*, Elsevier, Amsterdam, 1976, p. 32.
10 T. Hirokawa, M. Nishino, N. Aoki, Y. Kiso, Y. Sawamoto, T. Yagi and J.-I. Akiyama, *J. Chromatogr.*, 271 (1983) D1.
11 J.A. Dean (Editor), *Lange's Handbook of Chemistry*, McGraw-Hill, New York, 14th ed., 1992, Ch. 8, p. 16.
12 V. Sustacek, F. Foret and P. Bocek, *J. Chromatogr.*, 545 (1991) 239.
13 Y. Ma and R. Zhang, *J. Chromatogr.*, 625 (1992) 341.

Journal of Chromatography A, 657 (1993) 455–456
Elsevier Science Publishers B.V., Amsterdam

CHROM. 25 567

Book Review

Principles and practices of solvent extraction, edited by J. Rydberg, C. Musikas and G.R. Choppin, Marcel Dekker, New York, Basle, Hong Kong, 1992, 592 pp., price US$ 185.00 (US$ 55.00 on orders of five or more copies, for classroom use only), ISBN 0-8247-8668-8.

This book was written for third- to fourth-year undergraduate and postgraduate chemistry and chemical engineering students and for researchers in the chemical industry, according to the authors.

Contrary to the well known books on extraction (*e.g.*, *Handbook of solvent extraction* by Lo, Baird and Hanson), this book discusses the chemistry of the extraction in detail.

In the first chapter, an introduction is given, the history and modern trends of extraction are discussed and IUPAC References, General References and Proceedings of Extraction Conferences are listed.

The book is divided into two main parts: Fundamental principles and Applied solvent extraction.

The first part consists of six chapters. The second chapter deals with the principles of solubility and solutions, especially with solute–solvent interactions, solution thermodynamics, aqueous electrolyte and organic solutions and solubilities of binary and ternary systems. Complexation of metal ions is treated in the third chapter, where stability constants, models of complex formation, thermodynamics of complexation and synergism are discussed. The fourth chapter deals with solvent extraction equilibria, especially with solvent properties, extraction of metal and non-extractable complexes and the determination of equilibrium constants. Chapter 5 investigates solvent extraction kinetics: rate-controlling steps, diffusion process, rate laws and reaction mechanisms in addition to liquid–liquid interfaces, rate-controlling regimes and experimental techniques. Systematics of solvent extraction, relationships between extraction parameters and extractant structure are considered in Chapter 6.

The second part consists of seven chapters. Chapter 7 deals with the principles of industrial solvent extraction, especially with single- and multi-stage extraction, stripping equipment for continuous contact, extraction efficiency and solvent losses. Engineering design and calculation of extractors for liquid–liquid systems is the subject of Chapter 8, which includes droplet formation, pulsated, agitated, centrifugal and gravitational extractors, separation of phases and scale-up of extractors. Extraction of organic compounds is the topic of Chapter 9, which covers design criteria, phase equilibria, industrial applications in the petrochemical, pharmaceutical and biotechnological industries and environment engineering. It also deals with supercritical fluid extraction. In the tenth chapter, hydrometallurgy and the extraction of different metals with various extracts are investigated. Solvent extraction in nuclear science and technology is the subject of the eleventh chapter. Chapter 12 deals with the development of industrial solvent extraction processes with different solvents and operating modes. In addition to small-scale testing, it also deals with pilot- and full-scale plant operations, solvent recovery, environmental problems and economics of extraction. The thirteenth chapter is most relevant for the readers of this journal, giving a review on analytical and other applications of solvent extraction. This chapter deals with preconcentration by extraction for chemical analysis and discusses analytical procedures involving extraction, liquid–liquid partition chromatography and liquid membranes as ion-selective electrodes.

SSDI 0021-9673(93)E1039-3

All the chapters are written by international leading experts in this field. The book gives a good physico-chemical foundation of extraction and covers a broad range of its applications in various fields of industry. It is recommended for students of chemistry and chemical engineering and for scientists and engineers interested in extraction.

Hannover (Germany) Karl Schügerl

Journal of Chromatography A, 657 (1993) 457
Elsevier Science Publishers B.V., Amsterdam

CHROM 25 572

Book Review

Diode array detection in HPLC (*Chromatographic Science Series*, Vol. 62), edited by L. Huber and S.A. George, Marcel Dekker, New York, 1993, 392 pp., price US$ 150.00, ISBN 0-8247-8947-4.

This text covers the specific application of UV–visible diode array detection in liquid chromatography. The first two chapters cover the technical aspects of diode array detection, both from an historical perspective, as well as more current developments. Advantages of diode array detection to the chromatographer are covered in a separate chapter, with an additional lengthy chapter on spectral matching and peak purity. This chapter is followed by a shorter section on more advanced chemometric approaches for the analysis of diode array data. The remaining chapters are devoted to various application areas, including pharmaceuticals, clinical and toxicological applications, food and beverages, environmental samples, and polymer analysis.

The editors and all but one of the authors of this book are from Hewlett-Packard, and although other vendor's instrumentation is mentioned, the focus is on the Hewlett-Packard detector. The level of the book is relatively introductory, so that it should be useful to someone who has a diode array in their laboratory, but does not really know what to do with it. In terms of advanced and more recent applications, the book is not as useful.

The lengthy chapter on peak purity and spectral matching explains in detail the different types of match parameters used, and the relationship between them. One difficulty with this book that becomes apparent upon reading this chapter is that many of the figures are difficult to interpret, without a very close reading of the text. The captions are not very clear or informative. The figures and captions in the subsequent chapter on chemometrics are much clearer.

Overall, however, this book will probably be useful for those who are just starting to use diode array detection, and are looking for more information how to get the most out of their instrument.

Richmond (VA, USA) Sarah Rutan

SSDI 0021-9673(93)E1016-S

Journal of Chromatography A, 657 (1993) 458
Elsevier Science Publishers B.V., Amsterdam

CHROM 25 533

Book Review

Voltammetric determination of molecules of biological significance, by W.F. Smyth, Wiley, Chichester, 1992, VIII + 134 pp., price £ 35.00, ISBN 0-471-93345-7.

This book might well have been titled "Electrochemical determination of organic molecules —a literature survey." There is no introduction to electrochemical methodology and not a single mathematical expression or electrochemical cell is depicted! This will be a relief to many. On the other hand, the text is liberally illustrated with organic structures, electrochemical reactions, voltammograms, useful tables, and chromatograms. There is good coverage of applications for liquid chromatography with electrochemical (amperometric) detection.

The eight chapters are organized according to compound type. Nitrogen-, sulfur-, oxygen- and halogen-containing substances are covered as well as unsaturated hydrocarbons, organophosphorous compounds, organometallics and a few inorganic substances.

The reference list is selective rather than exhaustive and the index is quite helpful. Overall, this is a good survey of the potential utility of electroanalytical approaches to a variety of substances. The book will be especially useful to those chemists who are unfamiliar with the scope of modern electroanalysis.

Peter T. Kissinger
West Lafayette, IN (USA)

SSDI 0021-9673(93)E0957-V

Author Index

Erratum

J. Chromatogr., 644 (1993) 11–16

Page 13, Figs. 1 and 2 should be interchanged (the captions are correct).

Instructions to Authors

JOURNAL OF CHROMATOGRAPHY A

INCLUDING ELECTROPHORESIS AND OTHER SEPARATION METHODS

(incl. SYMPOSIUM VOLUMES)

JOURNAL OF CHROMATOGRAPHY B: BIOMEDICAL APPLICATIONS

INCLUDING ELECTROPHORESIS AND OTHER SEPARATION METHODS

Editorial Office *Journal of Chromatography A* and *B*
P.O. Box 681, 1000 AR Amsterdam, Netherlands
Sara Burgerhartstraat 25, 1055 KV Amsterdam, Netherlands
Tel. +31-20-5862794
FAX +31-20-5862304
e-mail chrom-eo @ elsevier.nl

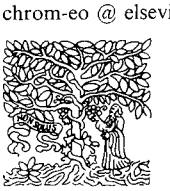

ELSEVIER

AMSTERDAM – LONDON – NEW YORK – TOKYO

General

The *Journal of Chromatography A* publishes papers on all aspects of **chromatography, electrophoresis** and related methods. Contributions consist mainly of research papers dealing with chromatographic and electrophoretic theory, instrumental developments and their applications. In the *Symposium Volumes*, which are under separate editorship, proceedings of symposia on chromatography, electrophoresis and related method are published.

Journal of Chromatography B: Biomedical Applications. This journal, which is under separate editorship, deals with the following aspects: developments in and applications of chromatographic and electrophoretic techniques related to clinical diagnosis or alterations during medical treatment; screening and profiling of body fluids or tissues related to the analysis of active substances and to metabolic disorders; drug level monitoring and pharmacokinetic studies; clinical toxicology; forensic medicine; veterinary medicine; occupational medicine; results from basic medical research with direct consequences in clinical practice.

Types of contributions

The following types of papers are published in the *Journal of Chromatography A* and *Journal of Chromatography B: Biomedical Applications:* Regular research papers (full-length papers), Review articles, Short Communications and Discussions. Review articles are invited or proposed in writing to the Editors, who welcome suggestions for subjects. An outline of the proposed Review should first be forwarded to the Editors for preliminary discussion prior to preparation. Short Communications are usually descriptions of short investigations, or they can report minor technical improvements of previously published procedures: they reflect the same quality of research as full-length papers, but should preferably not exceed five printed pages. Discussions (one or two pages) should explain, amplify, correct or otherwise comment substantively upon an article recently published in the journal.

Submission of an article is understood to imply that the article is original and unpublished and is not being considered for publication elsewhere.

Upon acceptance of an article by the journal, the author(s) will be asked to transfer the copyright of the article to the publisher. This transfer will ensure the widest possible dissemination of information.

Submission of papers

Manuscripts in English (***four*** copies, as well as a set of reproducible figures, are required) should be submitted to:

Editorial Office
JOURNAL OF CHROMATOGRAPHY (A or B)
P.O. Box 681
1000 AR Amsterdam, Netherlands

Manuscripts for the SYMPOSIUM VOLUMES section (*three* copies are required) should be submitted during the symposium concerned. After the symposium, correspondence should be sent by *regular air mail (NOT by registered, special delivery of private mail services)* to the Editor handling the corresponding proceedings, *i.e.*, either:

Dr. E. Heftmann
Editor of
JOURNAL OF CHROMATOGRAPHY A,
SYMPOSIUM VOLUMES
P.O. Box 928
ORINDA, CA 94563-0818, USA

or

Dr. Z. Deyl
Editor of
JOURNAL OF CHROMATOGRAPHY A,
SYMPOSIUM VOLUMES
Institute of Physiology
Czech Academy of Sciences
Videnská 1083
14220 PRAGUE 4-Krc
Czech Republic

English linguistic improvement, if appropriate, is provided as part of the normal editorial process.

Every paper must be accompanied by a letter from the senior author, stating that he/she is submitting the paper for publication in the *Journal of Chromatography A* or *B*.

Manuscripts

Manuscripts should be typed in ***double spacing*** on one side of consecutively numbered sheets of paper of uniform size. A 2-cm margin should be left on each side, an easily readable font (12 pt.) should be chosen, and (in case of computer-processed manuscripts) a letter-quality printer or equivalent should be used. The manuscript should be preceded by a sheet of manuscript paper carrying the title of the paper and the name, full postal address and FAX number of the author to whom correspondence is to be addressed. As a rule, papers should be divided into sections, headed by caption (*e.g.* Abstract, Introduction, Experimental, Results, Discussion). All illustrations, photographs, tables, etc. should be on separate sheets. ***Four*** copies of the complete manuscript (with illustrations and tables attached to each copy) should be submitted (for *Symposium Volumes* only: *three* copies).

Electronic manuscripts

Electronic manuscripts have the advantage that there is no need for the rekeying of text, thereby avoiding the possibility of introducing errors and resulting in reliable and fast delivery of proofs.

The preferred storage is a 5.25- or 3.5-in. disk in MS-DOS format, although other systems are welcome, *e.g.*, Macintosh (in this case, save your file in the usual manner, do not use the option "save in MS-DOS format"). Your disk and (**exactly matching**) printed version (printout, hardcopy) should be submitted together to the accepting editor or Editorial Office **according to their request**. Please specify the type of computer and word-processing package used (do not convert your textfile to plain ASCII). Ensure that the letter "l" and digit "1" (also letter "O" and digit "0") have been used properly, and format your article (tabs, indents, etc.) consistently. Characters not available on your word processor (Greek letters, mathematical symbols, etc.) should not be left open but indicated by a unique code (*e.g.* gralpha, ⟨α⟩, #, etc., for the Greek letter α). Such codes should be used consistently throughout the entire text. Please make a list of such codes and provide a key. Dot not allow your word processor to introduce word splits and do not use a "justified" layout. Please adhere strictly to the general instructions on style/arrangement and, in particular, the reference style of the journal. Further information may be obtained from the Publisher.

Title

The title of the paper should be concise and informative. Since titles are widely used in information retrieval systems, care should be taken to include the key words. The title should be followed by the authors' full names, academic or professional affiliations, and the address of the laboratory where the work was carried out. If the present address of an author is different from that mentioned, it should be given in a footnote. Acknowledgements of financial support are not to be made in a footnote to the title or name of the author, but should be included in the Acknowledgements at the end of the paper.

Abstract

All articles should have an abstract of 50–100 words which clearly and briefly indicates what is new, different and significant. No references should be given.

Introduction

Every paper must have a concise introduction that mentions what has been done before on the topic, with appropriate references, and that states clearly what is new in the paper now submitted.

Experimental

The Experimental section should contain sufficient information for others to repeat the Experiments. Whereas general conditions can usually best be specified in the Experimental section, it is often better to give specific details in the figure captions. Appendix 1 lists what should typically be specified.

Tables and illustrations

Although appropriate tables and illustrations contribute to a clear and concise presentation of results, they should not merely repeat data already given in the text.

Tables should be typed (in double spacing) on separate pages, and numbered in Roman numerals according to their sequence in the text. A brief descriptive heading should be given above each table. Below the heading the experimental conditions should be described. The layout of the tables should be given serious thought, so that the reader can grasp quickly the significance of the results.

Figures should be submitted in a form suitable for reproduction, either drawn in Indian ink on drawing or tracing paper, or as sharp prints [either photographic (glossy) prints or prints from a high-resolution laser printer]. All axes of graphs and chromatograms should be clearly labelled, with full quantitative data, or equivalent information should be provided in the legend. Please note that any lettering should also be in a form suitable for reproduction. Lettering (which should be kept to a minimum) and spacing on axes of graphs should be such that numbers, etc., remain legible after reduction in size. One reproducible copy and three photocopies are required. The figures should preferably be of such a size that the same degree of reduction can be applied to all of them. The size of the figures should preferably not exceed the size of the text pages. Simple straight-line graphs (such as calibration lines) are not acceptable, because they can readily be described in the text by means of an equation or a sentence. Claims of linearity should be supported by regression data that include slope, intercept, standard deviations of the slope and intercept, standard error and the number of data points; correlation coefficients are optional. Standard symbols should be used in line drawings; the following are available to the typesetters and can also be used in the legends:

○ ● □ ■ △ ▲ ◇ ◆ + × ▽ ▼

Photographs should have good contrast and intensity. Sharp, glossy photographs are required to obtain good halftones. References to the illustrations should be included in appropriate places in the text by Arabic numerals and the approximate position of the illustration should be indicated in the margin of the manuscript. Each illustration should have a caption, all the *captions* being typed (with double spacing) together on a *separate sheet.*

If structures are given in the text, the original drawings should be provided.

Coloured illustrations are reproduced at the author's expense, the cost being determined by the number of pages and by the number of colours needed.

The written permission of the author and publisher must be obtained for the use of any figure already published. Its source must be indicated in the legend.

Nomenclature, symbols, abbreviations and units

Widely accepted symbols, abbreviations and units (SI) should be used. If there is any doubt about a particular symbol or abbreviation, the full expression followed by the abbreviation should be given the first time it appears in the text. Abbreviations used in tables and figures should be explained in the captions. In general, the recommendations of the International Union of Pure and Applied Chemistry (IUPAC) should be followed and attention should be given to the recommendation of the Analytical Chemistry Division in the journal *Pure and Applied Chemistry* [Nomenclature for Chromatography, *Pure Appl. Chem.*, 65 (1993) 819–872]. Appendix 2 gives a conversion table for the non-SI units most frequently used and in Appendix 3 the abbreviations and symbols that may be used without definition are given. Decimal points should be indicated by full stops. All decimal numbers smaller than unity should include a leading zero (*e.g.* 0.11).

References

References should be numbered in the order in which they are cited in the text, and listed in numerical sequence on a separate sheet at the end of the article. The numbers should appear in the text at the appropriate places in square brackets. In the reference list, periodicals [1], monographs [2], multi-author books [3], and proceedings [4] should be cited in accordance with the following examples:

1 D. P. Ndiomu and C. F. Simpson, *Anal. Chim. Acta*, 213 (1988) 237.
2 T. Paryjczak, *Gas Chromatography in Adsorption and Catalysis*, Wiley, Chichester, 1986.
3 M. Saito, T. Hondo and Y. Yamauchi, in R. M. Smith (Editor), *Supercritical Fluid Chromatography*, Royal Society of Chemistry, London, 1988, Ch. 8, p. 203.
4 F. I. Onushka and K. A. Terry, in P. Sandra, G. Redant and F. David (Editors), *Proceedings of the 10th International Symposium on Capillary Chromatography, Riva del Garda, May 1989*, Hüthig, Heidelberg, 1989, p. 415.

Abbreviations for the titles of journals should follow the system used by *Chemical Abstracts*. Articles not yet published should be given as "in press" (journal should be specified), "submitted for publication" (journal should be specified), "in preparation" or "personal communication".

Vols. 1–651 of the *Journal of Chromatography; Journal of Chromatography, Biomedical Applications* and *Journal of Chromatography, Symposium Volumes* should be cited as *J. Chromatogr.* From Vol. 652 on, *Journal of Chromatography A* (incl. Symposium Volumes) should be cited as *J. Chromatogr. A* and *Journal of Chromatography B: Biomedical Applications* as *J. Chromatogr. B.*

Dispatch

Before dispatch of the manuscript please check that the envelope contains four copies of the paper complete with references, legends and figures. One of the sets of figures must be the originals suitable for direct reproduction. Please also ensure that permission to publish has been obtained from your institute.

Proofs

One set of proofs will be sent to the author to be carefully checked for printers' errors. Only type-setter's errors may be corrected. No changes in, or additions to, the edited manuscript will be accepted.

To ensure the fastest possible publication, proofs are sent to authors by *air mail* and must be returned to the publisher also *by air mail*. If this is not done, the article will be passed for publication with house correction only. Proofs may also be returned by FAX; the FAX number of *Journal of Chromatography* is: 31 (Netherlands) -20 (Amsterdam) -5862459.

Reprints

Fifty reprints of Full-length papers, Reviews, Short Communications and Discussions will be supplied free of charge. Additional reprints can be ordered. The order form containing price quotations will be sent to the authors together with the proofs of their article.

Subscription orders

Subscription orders should be sent to Elsevier Science Publishers B.V., P.O. Box 211, 1000 AE Amsterdam, Netherlands. The *Journal of Chromatography A* and the *Journal of Chromatography B: Biomedical Applications* can be subscribed to separately. Indexes can also be ordered separately. Write to the Marketing Manager, Chemistry, at the above address for more details.

Appendix 1: Experimental conditions to be specified

Experimental conditions should preferably be given on a *separate* sheet, headed "Conditions". These conditions will, if appropriate, be printed in a block, directly following the heading "Experimental".

General

Chemicals. Supplier (+ city/town, state, country) and degree of purity of all less common chemicals; EC number of enzymes; optical purity of enantiomers.

Equipment. Model and manufacturer (+ city/town, state, country) of commercial instruments (*e.g.* chromatographs and detectors). For instruments that are not commercially available, sufficient detail (or a reference) should be given to allow others to construct their own instrument. Detection parameters (*e.g.* type, wavelength, attenuation, linearity range, limit of detection at a specified signal-to-noise ratio).

Sample preparation. Application papers should contain full details (or a reference) of the method of sample preparation. For centrifugation steps, give details of g value and time. Injection device and volume and concentration of the injected sample should be specified.

Column liquid chromatography

Column. Column dimensions (length × internal diameter), manufacturer and location, packing material (for non-commercial columns or columns that are not widely used the chemical composition should be specified), particle diameter, pore diameter, column temperature.

Mobile phase. Complete and unambiguous description of the mobile phase composition or procedure for its preparation; pH; flow-rate; gradient programme.

k' values. When reporting k' values, the method for determining the hold-up time (t_0) must be described.

Gas chromatography and supercritical fluid chromatography

Column. In addition to the parameters mentioned for column liquid chromatography, specify type of column (packed, capillary, etc.) support material, film thickness of the stationary phase, and surface modification, if applicable.

Carrier gas. Type, purity, flow-rate or inlet pressure (bar or MPa).

Temperature. All relevant temperatures (or temperature programmes) should be detailed.

Planar chromatography

Chamber. Internal dimensions, manufacturer and location, saturation, temperature, humidity.

Thin layer or paper. Manufacturer and location, material, dimensions, type (laboratory-prepared or commercially precoated) and thickness of layer, additives (fluorescent indicator, binder), position of starting line, development mode, method of activation.

Solvent. Composition of solvent, monophasic or upper or lower phase of two-phase mixture, total volume.

Sample. Application method, size of spot or streak, solvent and amount of solute and volume of solution applied.

Detection. Spray reagent, wavelength, details of colours, R_F values.

Electrophoresis

Matrix. For example, cellulose acetate, agarose, polyacrylamide; gel concentration; percentage cross-linker; dimensions and material of tube, sheet, etc., surface modification, length between column inlet and detector, temperature.

Buffers. Complete and unambiguous description of buffers used, pH and how the pH was set or adjusted.

Other. Injection method, voltage, current. In electropherograms, anode and cathode should be indicated.

Appendix 2: Conversion table for the non-SI units most frequently used

The use of some non-SI units has been accepted for practical reasons; to this category belong units for time (min, h), volume (l), pressure (1 bar = 10^5 Pa), temperature (°C), energy (1 eV ≈ 160 219 · 10^{-21} J), mass (1 u ≈ 1.66053 · 10^{-27} kg) and activity (1 Ci = 3.7 · 10^{10} Bq). This journal also accepts Å (= 0.1 nm). Concentration should formally be expressed in mol dm^{-3} or mol l^{-1}, but the symbol M is accepted; normality (N) should not be used, however. The frequently used "daltons" are not compatible with the SI system —the relative molecular mass (M_r) should be given as a value only (dimensionless). Gravitational force must be expressed in g; rpm is not allowed for centrifugation (but it is, *e.g.*, for Vortex mixing). The table below summarizes some conversion factors; to obtain the value in SI units, the value in non-SI units should be multiplied by the factor.

Physical quantity	Type of conversion	Factor
Length	in. → cm	2.54
	ft. → cm	30.4801
Area	$in.^2$ → cm^2	6.451626
Mass	lb. → kg	0.45359237
Volume	gallon (USA) → l	3.785332
	gallon (UK) → l	4.54609
Pressure	atm → Pa	101 325
	mmHg or Torr → Pa	133.322
	mmH_2O → Pa	9.80665
	kp cm^2 → Pa	98 066.5
	lbs. $in.^{-2}$ or p.s.i. → Pa	6894.76

Other frequently used non-SI "units" are ppm, ppb and ppt. When used in this journal, the American billion (10^9) and trillion (10^{12}) are meant. The use of ppm, ppb and ppt is *only* permitted if they refer to mass/mass or volume/volume ratios; they should **not** be used for mass/volume ratios. The first time such a "unit" appears in an article, it should be indicated whether it refers to mass/mass or to volume/volume.

Appendix 3: Abbreviations and symbols that may be used without definition

Abbreviations and symbols should not be used in article titles. Please note that most abbreviations should only be used in combination with a value, or in structural formulae.

Abbreviations

A, C, G, T	adenine, cytidine, guanine, thymine
Ac, OAc	acetyl, acetate
A/D	analog-to-digital
ADP, AMP, ATP, and similar nucleoside phosphates	adenosine 5′-di-, -mono-, triphosphate, etc.
a.c.	alternating current
amino acids	standard 3- and 1-letter codes
AU	absorbance units
BET	Brunauer–Emmett–Teller
b.p.	boiling point
Bu	butyl
cpm	counts per minute
CE	capillary electrophoresis
d, m, p, r, t (in nucleosides/ nucleotides/ nucleic acids)	deoxy, messenger, phosphate, recombinant/ribosomal, transfer
d.c.	direct current
DDD, DDT, DDE	di-, trichloro-bis(chlorophenyl)ethane, -ethylene
DEAE	diethylaminoethyl
DNA, DNase	deoxyribonucleic acid, deoxyribonuclease
Dns, dansyl	5-dimethylaminonaphthalene-1-sulphonyl
DOPA	3,4-dihydroxyphenylalanine
dpm	desintegrations per minute
EC	enzyme commission numbering system
EDTA	ethylenediaminetetraacetate, -acetic acid
equiv.	equivalent
Et	ethyl
FS	full scale
FT	Fourier transform
GC, GLC, GSC	gas chromatography, gas–liquid chromatography, gas–solid chromatography
HP...	high-performance...
I.D.	internal diameter
IgG	immunoglobulin G
i.p.	intraperitoneal
IR	infrared
I.S.	internal standard
I.U.	international unit
i.v.	intravenous
LC	liquid chromatography
LD	lethal dose
Me	methyl
m.p.	melting point
MS	mass spectrometry
NAD, NADH (NADP, NADPH)	nicotinamide–adenine dinucleotide (phosphate)
NMR	nuclear magnetic resonance
O.D.	outer diameter
Ph	phenyl
Pr	propyl
PTFE	poly(tetrafluoroethylene)
RNA, RNase	ribonucleic acid, ribonuclease
RP....	reversed-phase....
rpm	revolutions per minute
R.S.D.	relative standard deviation (preferred over coefficient of variation)
S.D.	standard deviation
TLC	thin-layer chromatography
Tris	tris(hydroxymethyl)aminomethane
u	atomic mass units (reference to mass of ^{12}C; preferred over a.m.u./amu: reference to mass of ^{16}O)

UV	ultraviolet
vol., v/v	volume, volume/volume
Vis	visible
wt., w/w	weight, weight/weight

Symbols

A	absorbance
α	separation factor
d_p	particle diameter
ε	molar asorptivity
ΔG^0	standard Gibbs free energy
ΔH^0	enthalpy
H	plate height
J	coupling constant
K	equilibrium constant
k' or k	capacity factor or retention factor
λ	wavelength
M_r	(relative) molecular mass
N	number of plates
n	number of determinations
η	viscosity
p, P	probability or pressure
p...	negative logarithm of... (as in pH, pI, pK_a)
r	correlation coefficient
R	molar gas constant
R_F	distance travelled by spot / distance travelled by solvent front
R_M	log $(1/R_F - 1)$
R_s	resolution
ΔS^0	entropy
S/N	signal-to-noise ratio
T	temperature
t	time
t_0	retention time of unretained compound
t_R (t'_R)	(corrected) retention time
V_0	retention volume of unretained compound
V_R (V'_R)	(corrected) retention volume

PUBLICATION SCHEDULE FOR THE 1994 SUBSCRIPTION

Journal of Chromatography A and *Journal of Chromatography B: Biomedical Applications*

MONTH	O 1993	N 1993	D 1993	J	F	
Journal of Chromatography A	652/1 652/2 653/1	653/2 654/1 654/2 655/1	655/2 656/1 + 2 657/1 657/2	658/1 658/2 659/1 659/2	660/1 + 2 661/1 + 2 662/1 662/2	The publication schedule for further issues will be published later.
Bibliography Section						
Journal of Chromatography B: Biomedical Applications				652/1	652/2 653/1	

INFORMATION FOR AUTHORS

(Detailed *Instructions to Authors* were published in Vol. 657, pp. 463–469. A free reprint can be obtained by application to the publisher, Elsevier Science Publishers B.V., P.O. Box 330, 1000 AH Amsterdam, Netherlands.)

Types of Contributions. The following types of papers are published: Regular research papers (Full-length papers), Review articles, Short Communications and Discussions. Short Communications are usually descriptions of short investigations, or they can report minor technical improvements of previously published procedures; they reflect the same quality of research as Full-length papers, but should preferably not exceed five printed pages. Discussions (one or two pages) should explain, amplify, correct or otherwise comment substantively upon an article recently published in the journal. For Review articles, see inside front cover under Submission of Papers.

Submission. Every paper must be accompanied by a letter from the senior author, stating that he/she is submitting the paper for publication in the *Journal of Chromatography A* or *B*.

Manuscripts. Manuscripts should be typed in **double spacing** on consecutively numbered pages of uniform size. The manuscript should be preceded by a sheet of manuscript paper carrying the title of the paper and the name and full postal address of the person to whom the proofs are to be sent. As a rule, papers should be divided into sections, headed by a caption (*e.g.*, Abstract, Introduction, Experimental, Results, Discussion, etc.) All illustrations, photographs, tables, etc., should be on separate sheets.

Abstract. All articles should have an abstract of 50–100 words which clearly and briefly indicates what is new, different and significant. No references should be given.

Introduction. Every paper must have a concise introduction mentioning what has been done before on the topic described, and stating clearly what is new in the paper now submitted.

Experimental conditions should preferably be given on a *separate* sheet, headed "Conditions". These conditions will, if appropriate, be printed in a block, directly following the heading "Experimental".

Illustrations. The figures should be submitted in a form suitable for reproduction, drawn in Indian ink on drawing or tracing paper. Each illustration should have a legend, all the *legends* being typed (with double spacing) together on a *separate sheet*. If structures are given in the text, the original drawings should be supplied. Coloured illustrations are reproduced at the author's expense, the cost being determined by the number of pages and by the number of colours needed. The written permission of the author and publisher must be obtained for the use of any figure already published. Its source must be indicated in the legend.

References. References should be numbered in the order in which they are cited in the text, and listed in numerical sequence on a separate sheet at the end of the article. Please check a recent issue for the layout of the reference list. Abbreviations for the titles of journals should follow the system used by *Chemical Abstracts*. Articles not yet published should be given as "in press" (journal should be specified), "submitted for publication" (journal should be specified), "in preparation" or "personal communication".

Vols. 1–651 of the *Journal of Chromatography*; *Journal of Chromatography, Biomedical Applications* and *Journal of Chromatography, Symposium Volumes* should be cited as *J. Chromatogr.* From Vol. 652 on, *Journal of Chromatography A* (incl. Symposium Volumes) should be cited as *J. Chromatogr. A* and *Journal of Chromatography B: Biomedical Applications* as *J. Chromatogr. B.*

Dispatch. Before sending the manuscript to the Editor please check that the envelope contains four copies of the paper complete with references, legends and figures. One of the sets of figures must be the originals suitable for direct reproduction. Please also ensure that permission to publish has been obtained from your institute.

Proofs. One set of proofs will be sent to the author to be carefully checked for printer's errors. Corrections must be restricted to instances in which the proof is at variance with the manuscript. "Extra corrections" will be inserted at the author's expense.

Reprints. Fifty reprints will be supplied free of charge. Additional reprints can be ordered by the authors. An order form containing price quotations will be sent to the authors together with the proofs of their article.

ANABIOTEC 94

5th International Symposium on Analytical Techniques, Systems & Strategies in Biotechnology

31 October — 2 November 1994

Minneapolis Hilton & Towers, USA

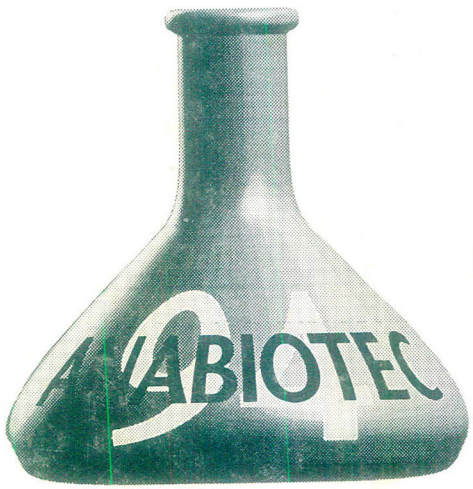

Learn of the new instruments and techniques for analytical chemistry
Improve monitoring of industrial scale processes
Update your strategies for clinical diagnosis
Meet international colleagues and contacts

The analytical chemistry of complex matrices involving species of a biological origin is a rapidly developing research frontier.

ANABIOTEC 94 — consisting of plenary sessions, selected original papers, posters and an exhibition — will address the wide array of research issues involved in this field. This symposium is the ideal forum for information exchange between the fields of analytical chemistry, biochemistry, clinical chemistry and biotechnology: you need to be there!

For further information send a copy of this advert, complete with your address details to:

Anabiotec 94 Conference Secretariat, Elsevier Science Ltd,
PO Box 150, Kidlington, Oxford OX5 1AS, UK.
Tel: +44 (0) 865 512242
Fax: +44 (0) 865 310981

anabiota.3d (2) 12/93

0021-9673(19931231)657:2;1-Q